S. Wagner • A. Bode • H. Satzger • M. Brehm *EDITORS*

High Performance Computing

in Science and Engineering Garching/Munich 2014

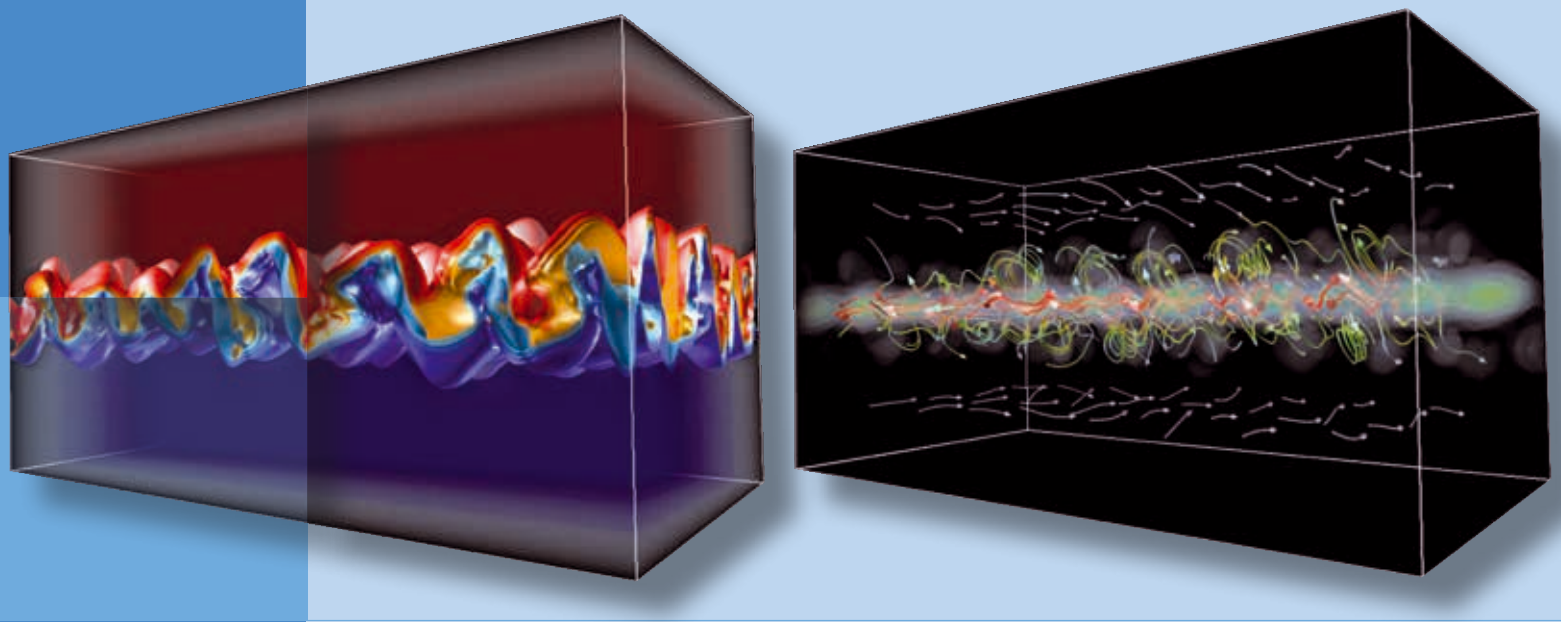

KONWIHR III

GCS Gauss Centre for Supercomputing

Bayerische Akademie der Wissenschaften

lrz

Impressum:

Bayerische Akademie der Wissenschaften
Alfons-Goppel-Str. 11, D-80539 München
info@badw.de, www.badw.de

Leibniz-Rechenzentrum (LRZ)
Boltzmannstraße 1, D-85748 Garching bei München
lrzpost@lrz.de, www.lrz.de

Herausgeber: Siegfried Wagner, Arndt Bode, Helmut Satzger, Matthias Brehm
Redaktion: Helmut Satzger
Gestaltung: Tausendblauwerk, Schleißheimer Straße 21, 85221 Dachau, www.tausendblauwerk.de
Druck und Bindung: bonitasprint gmbh, Max-von-Laue-Straße 31, 97080 Würzburg

Titelbild entnommen aus dem Artikel von Jorge Vieira, L.D. Amorim, Paulo Alves, Anne Stockem, Thomas Grismayer, and Luis Silva (LRZ Project ID: pr89to), „Plasma acceleration: from the laboratory to astrophysics". Visualisierung der Elektrondichte Wirbel (links) und Magnetfelder (rechts) aufgrund der Kelvin-Helmholtz Instabilität. Weitere Informationen im Artikel ab Seite 62.
Bilder des SuperMUC (Vorwort, Seite 8/9, sowie Umschlag-Rückseite) von Helmut Satzger.

Bezugsadresse:

Leibniz-Rechenzentrum (LRZ)
Boltzmannstraße 1, D-85748 Garching bei München

ISBN 978-3-9816675-0-9

S. Wagner • A. Bode • H. Satzger • M. Brehm *EDITORS*

High Performance Computing

in Science and Engineering Garching/Munich 2014

Bayerische
Akademie der Wissenschaften

Table of contents

Preface

Chapter 01 – Astrophysics and Plasma Physics

Chapter 02 – Earth and Environmental Sciences

Chapter 03 – Engineering and Computational Fluid Dynamics

Chapter 04 – High Energy Physics

Chapter 05 – Life and Material Sciences

Chapter 06 – Extreme Scaling on SuperMUC

Appendix

The First Experiences with the Petaflop System SuperMUC

On July 20th, 2012, the Leibniz Supercomputing Centre (LRZ) inaugurated the new high performance computer in Bavaria. The system, called SuperMUC, has a peak performance of more than three Petaflop/s. This book presents reports of the projects that have used the system from 2012-2014.

SuperMUC uses a new, revolutionary form of direct warm water cooling developed by IBM. Active components like processors and memory modules are directly cooled with water that can have an inlet temperature of up to 40 degrees Celsius. The innovative design uses free-air cooling without chillers and makes SuperMUC one of the most energy efficient supercomputers in the world.

SuperMUC was specifically designed as a general purpose machine and does not contain any form of accelerators. The compute nodes consist of Intel x86 Sandy Bridge processors, which are connected by InfiniBand. This means that most stages of program development and testing can be done on any x86 based cluster or desktop and can easily be ported to SuperMUC. The system was over-booked from the start of operation; therefore an upgrade (Phase 2) will be performed in early 2015, which will double the performance of the system.

The Gauss Centre for Supercomputing (GCS) combines the three national supercomputing centres High Performance Computing Center Stuttgart (HLRS), Jülich Supercomputing Centre (JSC), and Leibniz Supercomputing Centre (LRZ) into Germany's foremost supercomputing institution. GCS is jointly funded by the German Ministry of Education and Science and the corresponding ministries of the states of Bavaria, Baden-Wuerttemberg and North Rhine-Westphalia. GCS massively contributes to European large-scale scientific and engineering research by its involvement in the Partnership for Advanced Computing in Europe (PRACE). Several European projects report about their work in this book.

The main research areas studied using SuperMUC are astrophysics and plasma physics, earth and environmental sciences, life and material sciences, engineering and computational fluid dynamics, and high energy physics – which is also reflected in the ordering of the chapters of this book. LRZ created dedicated application labs for astrophysics, earth and life sciences, where application experts from the LRZ work closely with scientists on optimization and scalability of the relevant applications. LRZ also initiated the partnership initiative πCS to address the special requirements of computational scientists. The primary goal is to provide individual and tailored support for scientists with complex IT questions in addition to the regular support structures.

The variety and high quality of the submitted papers demonstrate that SuperMUC is a huge success. The largest resource consumption on SuperMUC comes from the area of astrophysics. Federrath et al. simulated the world's largest supersonic turbulences with grid resolutions of $4{,}096^3$. The simulation used 7.2 mio CPU-hours and ran on 32,768 CPU cores, producing 115 TByte of data. Another simulation of warm dark matter by Maccio et al. performed simulations with $1{,}024^3$ particles – again, one of the highest resolution work ever done in this field. Indeed, there are several projects in the field of astrophysics and plasma physics, as well as in the Life Sciences and Earth Sciences, that efficiently use 2 or 4 islands of SuperMUC (16,384 or 32,768 CPU cores – the largest job class available during regular user operation).

Picture of SuperMUC in the server room. The yellow cable trays on top of the racks contain the cables for the Infiniband interconnect.

Computational fluid dynamics has traditionally a strong request for supercomputing time. Holzäpfel et al. simulated wake vortices of landing aircraft which help to gain better insight into the turbulences created by landing aircraft and are thus directly relevant for aviation safety. Pitsch et al. work in the field of combustion research with their own application code CIAO that showed good scaling up to 65,536 cores on SuperMUC.

The field of Life Science and Chemistry gained strong momentum over the last five years, becoming the third largest user group of SuperMUC. Bungartz et al. developed the code ls1 mardyn that allowed a record-breaking molecular dynamic simulation of 4 trillion particles. Many other examples of outstanding scientific work are presented in the book.

SuperMUC offers a 40-times increased computing performance as compared to its predecessor, HLRB II. Whereas, on HLRB II, half of the compute time was used by jobs larger than 256 cores, this dramatically increased on SuperMUC, where now more than half of the compute time is used by jobs larger than 2,048 cores. Application experts from LRZ and TU Munich spend a lot of effort on improving the scalability of applications. This led to the idea of dedicated testing time in special block operation periods and the installment of extreme scaling workshops. A last chapter of this book summarizes the results from the first extreme scaling workshop, held in June 2013. The workshop showed that six applications scale to the full machine. As a result of the lessons learned during the workshop, in early 2014, the geophysical application SeisSol managed to achieve the impressing performance of 1.4 PFLOP/s on 18 islands, which corresponds to 48% of peak performance.

Acknowledgments

We gratefully acknowledge the continued support of the State of Bavaria, The Bavarian Competence Network for Technical and Scientific High Performance Computing (KONWIHR), the Gauss Centre for Supercomputing, the German Research Foundation (DFG), the German Federal Ministry of Education and Research (BMBF), the Partnership for Advanced Computing in Europe (PRACE), and many other institutions promoting high performance computing. We thank the reviewers and the Steering Committees of GCS and SuperMUC for the reviews of the projects, their insights and helpful remarks. Without their efforts it would not have been possible and will not be possible in the future to sustain the high scientific quality we see in the projects.

Garching bei München, Juni 2014
Siegfried Wagner
Arndt Bode
Helmut Satzger
Matthias Brehm

Astrophysics and Plasma Physics

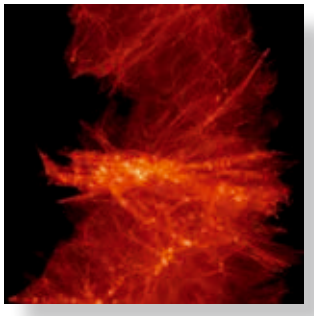

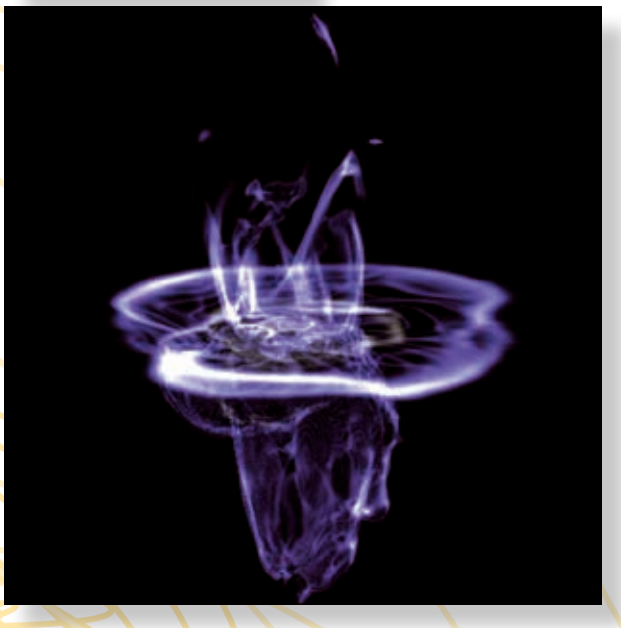

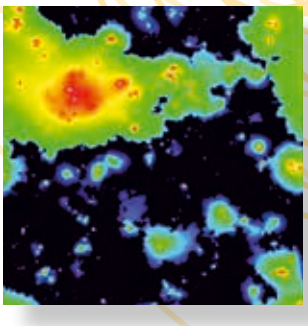

Local Supercluster Simulations

1

Research Institution
Leibniz-Institut für Astrophysik Potsdam

Principal Investigator
Stefan Gottlöber

Researchers
M. Abadi, A. Benitez-Llambay, Y. Hoffman, J. Navarro, M. Steinmetz, G. Yepes

Project Partners
IATE Cordoba, HU Jerusalem, U Victoria, UAM Madrid

LRZ Project ID: h009z

Introduction

Our Local Group consists of two massive galaxies – Andromeda and the Milky Way - and a few dozens smaller ones. Within the Local Group and the surrounding Local Volume, even very small objects can be observed. Understanding how the small-scale structure forms in the Universe is a major challenge to the standard model of structure formation. This model overpredicts the number of galactic satellites and dwarf galaxies compared to what is observed locally, in and around the Local Group of galaxies. This and other problems have prompted cosmologists to turn into 'archeologists' looking for fossils and clues from the early formation phase in the present day structure of the Local Group, practicing the so-called near field cosmology. We have followed astronomers and extended the near field cosmology to numerical cosmology. This is done by performing Constrained Local UniversE Simulations (CLUES), designed to reproduce the structure of the nearby universe, within a few tens to hundreds of million light years and in particular the Local Group. We use observational data from which we construct the initial conditions for our constrained simulations, namely the distribution of matter about 13.5 billion years ago and follow then numerically the formation of structures [1].

Results

Within our project at LRZ Munich we have performed a series of constrained simulations within a box with a size of about 300 million light years. This box contains the Local Supercluster with the Virgo cluster. The numerical counterpart of our Local Group is situated in the center of the simulation box. These simulations have been performed with 8,589,934,592 particles so that both the large-scale structure in the Local Universe as well as the dark matter halos which host galaxies and their satellites can be resolved. Using this simulation, the relationship between halo spin and the relevant directions that characterize the large-scale structure has been studied. We found an alignment of halo spin with the vorticity, and the tendency of the vorticity to be orthogonal to the axis of the fastest collapse of the velocity shear tensor [2].

In order to study the formation of the Local Group in more detail we have performed a series of zoomed high-resolution simulations. Within a smaller volume (a sphere with a radius of almost 10 million light years) we have increased the mass and force resolution by a factor of 64 while we have decreased the resolution in the remaining parts of the simulation. Figure 1 shows the dark matter distribution within the high resolution region at early times, revealing a very complex filamentary structure from which the simulated Local Group is formed.

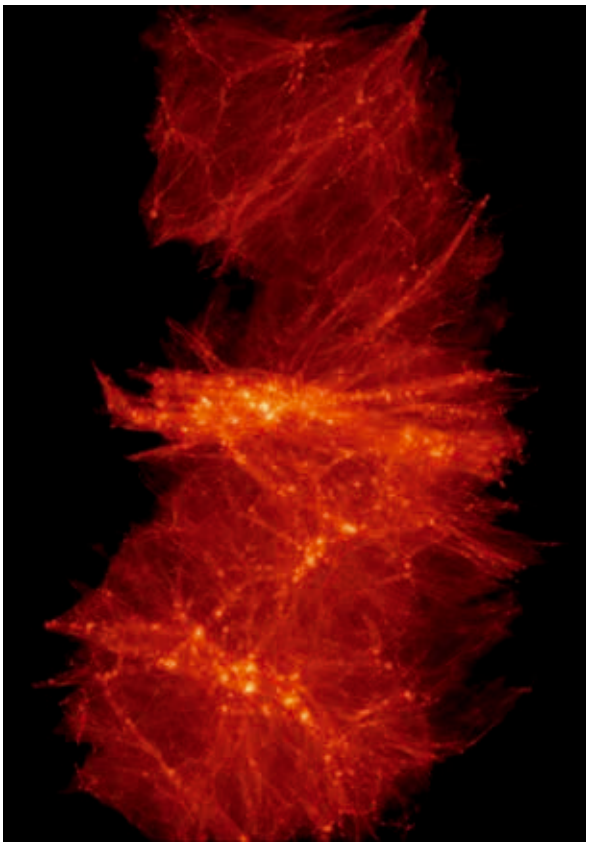

Figure 1: Dark matter moves towards the filament in the center of the figure (3.5 billion years after the Big Bang).

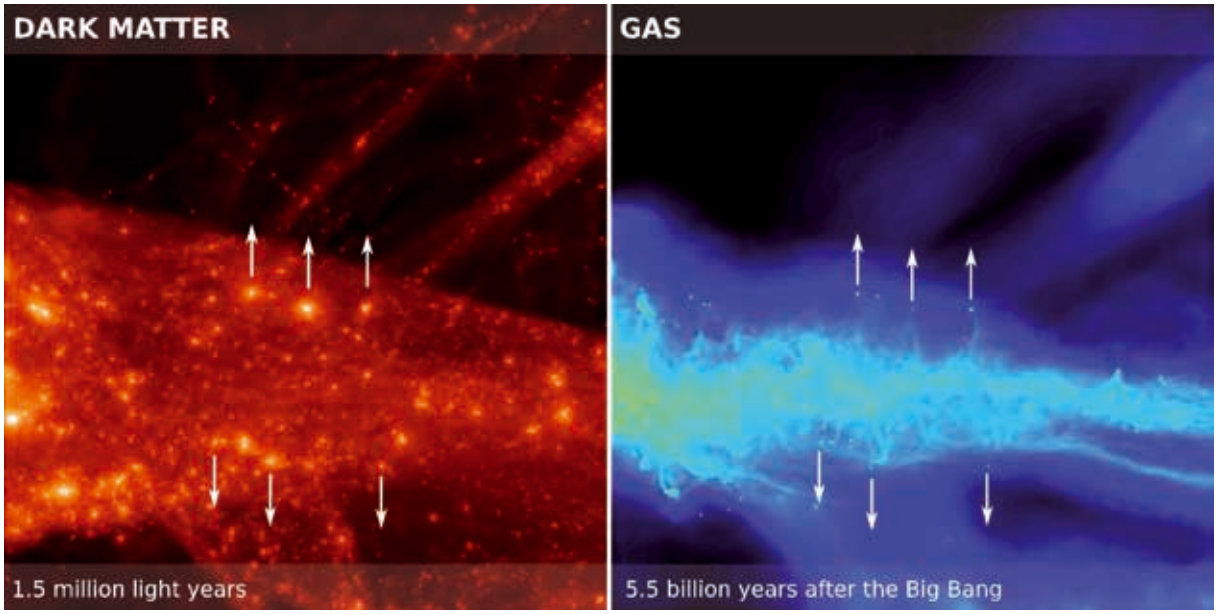

Figure 2: The clumps of dark matter (left) and gas (right) move with high velocity through the filament. Just as an example, a few objects are marked with arrows pointing to the direction they move.

The simulations described so far are dark matter only simulations. In such simulations we can study the formation of dark matter halos within which the observed galaxies are expected to form. The number of low mass dark matter halos in the simulation is much higher than the number of observed dwarf galaxies. Simulations and observations could be reconciled if not all low mass dark matter halos contain a dwarf galaxy that could be observed. In a second step we have added baryons to the simulation in order to follow also the gas-dynamical processes, the cooling of the gas, the formation of stars and the feedback of the newly formed stars on the gas.

We use such high resolution hydro-dynamical simulations of the local universe as a laboratory for testing the models of structure formation and theories of galaxy formation in particular on small scales and for low mass objects which can be observed only in the local universe. We have shown that ram-pressure stripping may operate on isolated low-mass halos as they travel through the cosmic web [3]. The loss of baryons is the main reason why these galaxies have stopped forming stars. The origin of these baryon-poor, non-star-forming galaxies can be seen in the right panel of Fig. 2. The objects marked with the arrows move very fast through the filament shown in horizontal direction. The lost gas can be seen as tiny gas tails behind them, but there are no signals of this when looking at the dark matter distribution on the left panel. The importance of cosmic web stripping on isolated low mass halos has not been recognized before because it is a purely hydro-dynamical effect that requires simulations of a sufficient large volumes able to resolve properly both the cosmic web and the internal halo properties. This demands numerical resources that are only now becoming available.

Outlook

We will use the new CosmicFlow2 dataset of Brent Tully and Helene Courtois to construct initial conditions for constrained simulations in larger volumes. These initial conditions will be constructed with codes developed within the CLUES project, namely ICeCoRe and Ginnungagap and using the Reverse Zeldovich Approximation [4].

References and Links

[1] G. Yepes, S. Gottlöber, Y. Hoffman, New Astronomy Reviews 58 (2014), 1
[2] N. I. Libeskind, Y. Hoffman, M. Steinmetz, S. Gottlöber, A. Knebe, S. Hess, ApJ 766 (2013), L15
[3] A. Benitez-Llambay, J. F. Navarro, M. G. Abadi, S. Gottlöber, G. Yepes., Y. Hoffman, M. Steinmetz, APJ 763 (2013) L41
[4] J.G. Sorce, H.M. Courtois, S. Gottlöber, Y. Hoffman, R. B. Tully, MNRAS 437 (2014) 3586

The home page of the CLUES project is http://www.clues-project.org

A set of movies demonstrating the web-stripping can be found in: http://www.clues-project.org/movies/cosmicwebstripping.html

Physics of Galactic Nuclei

1

Research Institution
Max-Planck-Institute for extraterrestrial Physics / University Observatory

Principal Investigator
Marc Schartmann

Researchers
Christian Alig, Alessandro Ballone, Manuel Behrendt, Andreas Burkert, Katharina Fierlinger, Marc Schartmann

Project Partners
Excellence Cluster Universe, Priority Programme 1573

LRZ Project ID: h0075

In this ongoing project, we are interested in simulating physical processes in galactic nuclei and the onset of nuclear activity cycles. We will present two highlights from our recent work with SuperMUC in the following, concentrating on the Galactic Centre of our Milky Way.

The Galactic Centre Cloud G2: a mass-losing source?

Introduction

Recently, a gas and dust cloud has been found on an eccentric orbit around the massive black hole in our own Galactic Centre (GC) [1], which has already started its roughly one year long peri-centre passage. Integral field spectroscopy allowed to determine the position as well as line of sight velocity of the cloud for various epochs. These so-called position-velocity (PV) diagrams clearly showed the signature of a tidally disrupting gas cloud within the last few years. With the help of hydrodynamical simulations with the PLUTO [2] code, we have investigated the possible origin of the cloud and its near future evolution using the HLRB II supercomputer and

concentrating on a scenario of a diffuse cloud initially in pressure equilibrium. The latter might be the result of stellar wind interactions. Here, we report on recent SuperMUC simulations of an equally promising scenario, namely a mass-losing source on the observed orbit of G2, which might be connected to a stellar wind of a low-mass star or a photo-evaporating proto-planetary disc.

Results

The problem at hand is determined by two parameters: (i) the mass loss rate of the source and (ii) the ejection velocity of the wind. In order to scan this two-dimensional parameter space, we use axisymmetric PLUTO simulations. First of all, we find differences in the structure of the winds in the extreme environment of Galactic Nuclei compared to stellar winds in our solar neighbourhood. Due to the high pressure atmosphere in the direct vicinity of the central black hole, only a weak and very wide outer shock forms and the densest part of the built up cloud is given by the shocked wind itself. The latter is confined by the external thermal pressure in the beginning and shaped by ram pressure interaction due to the motion of the cloud through the dense atmosphere during the course of its orbital evolution. At this stage, the contact discontinuity forms Rayleigh-Taylor fingers (Fig.1, upper panel), which get stripped due to the interaction with the dense atmosphere and form a filamentary envelope and tail. In the late time evolution (Fig.1, lower panel) – close to the currently observable state of the cloud – tidal disruption is the dominant process for shaping the simulated

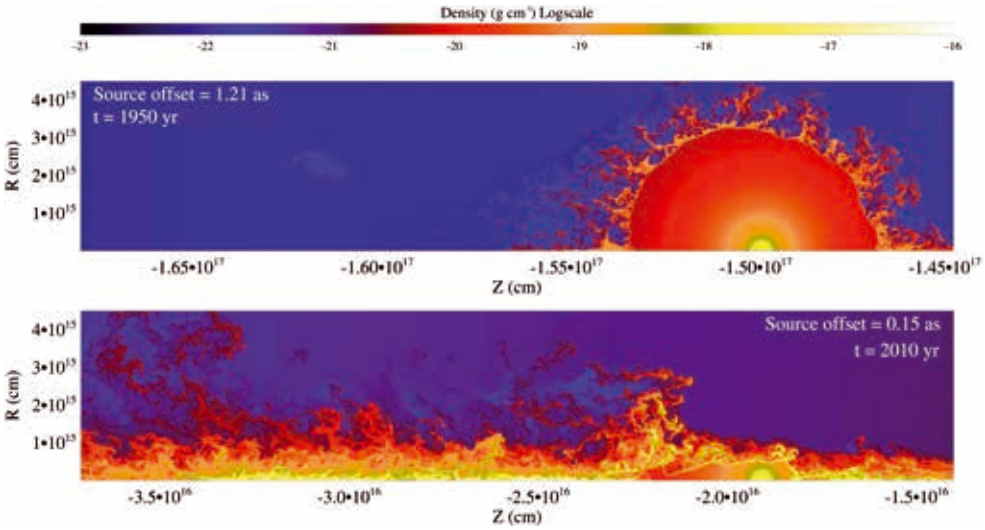

Figure 1: Time evolution of the density distribution of the compact source scenario for the G2 cloud [3].

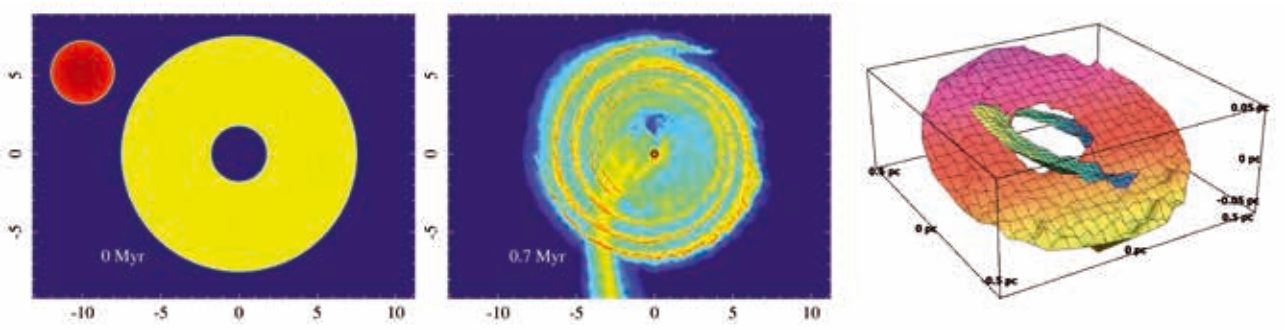

Figure 2: Surface density of the initial configuration with the cloud approaching from the left and the disc rotating counter-clockwise (left panel), the large-scale view at the stage when the most massive disc has formed (middle panel) and the final configuration of the two inclined and counter-rotating discs (right panel) [5].

cloud in agreement with what is seen in the observations. The dense, stretched out filaments yield the largest contribution to the observable Brackett Gamma line emission, which helps us to constrain our two parameters. Additionally, we calculate PV diagrams from the simulation data and compare them to the observations as detailed above, breaking the remaining ambiguity. This procedure yields a best-fit simulation with a wind mass loss rate of 8.8×10^{-8} solar masses per year and a velocity of 50 km/s for our assumed atmosphere, which places it in the observed range for young T-Tauri stars. The results of this study are published in [3].

These PLUTO-simulations were typically run on 400 cores using the Message Passing Interface (MPI). A total number of 20 simulations have been necessary in order to sample the parameter space accurately enough, leading to a consumption of roughly 200.000 CPU-h for this sub-project. Approximately 5.000 files have been produced requiring 1 TB of disk space.

On-going Research / Outlook

Building up on the parameter study mentioned above, we are currently running 3D AMR simulations employing the PLUTO code. This will be done for both, the compact source as well as the diffuse cloud scenario, enabling us to make a thorough comparison of the predictions for the near future evolution of the G2 cloud, which can then be observationally tested.

The Formation of two counter-rotating discs in the Galactic Centre

Introduction

On a similar scale as the G2 cloud, the GC harbors two young, inclined, counter-rotating sub-parsec scale stellar discs around the supermassive black hole Sgr A*. Due to the harsh environment close to the black hole, they cannot be formed in-situ by standard star formation (SF) processes, as molecular clouds would be torn apart by tidal torques on short time scale. Additionally, the observed stars are too young to be the result of standard inward migration. This is the so-called "Paradox of Youth". The currently favoured solution is to replace the standard mode of SF by a two-stage process: (i) the formation of an accretion disc, which in a second step (ii) fragments and forms stars.

Results

Inspired by the currently observed circum-nuclear gas disc, we investigate a formation mechanism via a collision of a molecular cloud (with parameters as observed in the GC region) and such a pre-existing disc (Fig.2, left panel). This collision leads to multiple streams of gas flowing towards the black hole and finally to the formation of sub-parsec scale gas discs with angular momenta depending on the ratio of cloud and circum-nuclear disc material. In the simulation shown in Fig.2, two major gas discs form, whereas one of them predominantly contains molecular cloud gas and the other one predominantly disc gas, which leads overall to counter rotation (see right panel in Fig.2 for the final state). A time difference of 1 Myr between the formation of the discs leaves ample time for them to fragment into stars and getting dispersed, before the following disc builds up.

The simulation was run with the Gadget code [4] on 400 cores and used a total of 400.000 CPU-h. For a more detailed description of the results we refer to [5].

On-going Research / Outlook

From one of the simulations of a larger parameter study we find a very similar gas morphology as is currently observed in the so-called "mini-spiral" in the Galactic Centre, which might be an indication that a similar process is happening right now again. To get a better understanding and to do a more detailed comparison to the currently observed state is the subject of our future research within this sub-project.

References and Links

[1] Gillessen et al. 2012, Nature, 481, 51
[2] Mignone et al. 2007, ApJS, 170, 228
[3] Ballone et al. 2013, ApJ, 776, 13
[4] Springel et al. 2005, MNRAS, 364, 1105
[5] Alig et al. 2014, ApJ, 771, 119

http://www.usm.lmu.de/CAST/
http://www.mpe.mpg.de/642947/pgn

Dynamics of binary neutron star systems

1

Research Institution
Friedrich Schiller University Jena

Principal Investigator
Bernd Brügmann

Researchers
S. Bernuzzi, T. Dietrich, D. Hilditch, N. K. Johnson-McDaniel, N. Moldenhauer, M. Ujevic Tonino, A. Weyhausen

Project Partners
–

LRZ Project ID: h1021

Introduction

In our project we are interested in spacetimes containing strong gravitational fields and the numerical tools necessary for the accurate simulation of such systems. In particular, we have a well-developed program investigating the final stage of the evolution of binary neutron star systems. Double neutron star binaries (including the famous Hulse-Taylor pulsar) provide some of the best laboratories to test the predictions of General Relativity (GR), including providing indirect evidence for the existence of gravitational radiation, the gravitational analogue of electromagnetic radiation. Gravitational radiation carries away energy and angular momentum from the binary, and one observes the effects of these losses on the binary's orbit. Eventually, these losses drive the binary to coalescence, by which time the orbit will have circularized in all but a few exceptional cases. The last phases of the binary's evolution are highly relativistic and the theoretical predictions that are the focus of our project can only be made using numerical techniques that solve the full field equations of GR.

One of the primary reasons we model these systems is to study their gravitational wave signals: Coalescing neutron star binaries are a prominent source for ground-based gravitational wave detectors such as LIGO and Virgo. Because of the huge distance between Earth and the systems one observes, the gravitational wave signals reaching Earth are very weak. One therefore needs numerical modeling to develop accurate templates for the radiation from such systems in order to be able to detect them in the detector's noise and infer their properties from the detected waveform. In particular, the properties of cold, dense matter are imprinted on the gravitational wave signal through their influence on stellar structure. Our binary neutron star simulations have focused on simulating tidal and spin effects. We have also shown that a new formulation of GR we proposed is well-suited for compact binary simulations.

Results

Computational Setup
We perform our simulations with the BAM code, which combines state-of-art methods to deal with black hole spacetimes and general relativistic hydrodynamics.

The code is written in C and based on the method of lines. It uses high-order finite difference stencils for the spatial discretization of the geometric variables, while high resolution shock capturing methods are used for the hydrodynamic variables. The time integration is done with an explicit Runge-Kutta method. The BAM infrastructure also supplies adaptive mesh refinement via a combination of fixed and moving boxes, as well as cubed spheres.

The code is hybrid OpenMP/MPI parallelized. The fundamental parallelization strategy is as follows: when N MPI processes are used, each box on each refinement level is divided into N equally sized sub-boxes with added ghostzones, whose sizes depend on the applied stencil. Each of the sub-boxes is owned and evolved by a single MPI process. The ghostzones are synchronized after each evolution step. In this way, each MPI process owns exactly one sub-box of every mesh refinement box, which optimizes load balancing, because each processor works on the same number of grid points. Additionally, each MPI process can launch an equal number of OpenMP threads using shared memory, which increases our memory efficiency compared to single MPI parallelization.

For our simulations, we have to span a reasonable range in the parameter space to see the influence of individual quantities (e.g., eccentricity, spin, equation of state) on the inspiral and post-merger dynamics. Additionally, we are forced to simulate at least a few physical setups with different resolutions to (i) show consistency, (ii) compute the convergence order, and (iii) give proper error bars for the physical quantities. Thus the individual simulation of one physical setup using one resolution is meaningless and we can only make a meaningful scientific statement using a bundle of jobs. Each individual simulation is run on up to ~512 cores, depending on the resolution. Additionally, we run several (approximately 5) of those setups in parallel to span a reasonable range in the parameter space. In total, we have used ~5 million CPUh on SuperMUC. We produced ~25 million files and used a maximum of ~22TB of storage.

Scientific results
Over the last years we moved from simulating binary black hole systems to systems involving matter, mainly binary neutron stars. We focused on the gravitational

waves emitted by those systems in different portions of parameter space and developed a new formalism of GR well suited for numerical simulations.

Accurate simulations of tidal effects for quasi-circular orbits: As the starting point for our investigation of binary neutron star systems, we performed simulations of nine to ten orbits before merger with the goal of quantifying signatures of tidal deformation in the gravitational radiation emitted [1,2]. These simulations enabled us to study for the first time the errors in the extracted gravitational wave signal. These signals convey unique information about tidal interaction in the strong-field regime, and are crucial for the development of analytic and semi-analytic models for the construction of GW template banks. We compared the numerical data with the most modern tidal models, assessing these models' robustness and possible nonlinear amplification effects.

Spinning binary neutron star simulations: Recently, we presented the first simulation of binary neutron star systems with astrophysical spins using consistent and constraint satisfying initial data [4]. We compared the dynamics of binary neutron star systems and binary black holes for the first time in this context. We extracted the spin-interaction contributions from our numerical data with a novel approach. A preliminary analysis of the waveform indicated the importance of including spin when building GW templates for binary neutron stars.

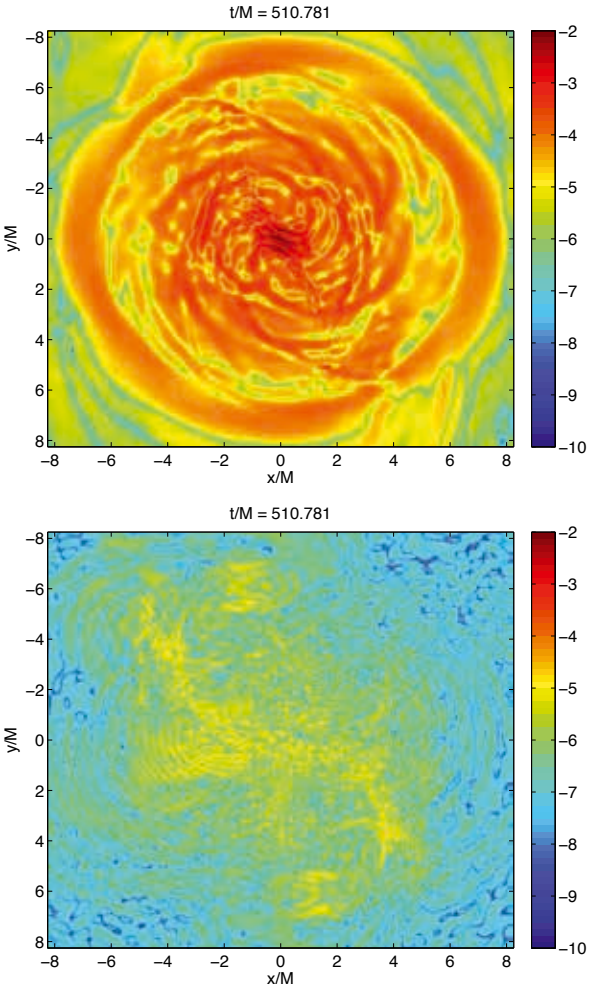

Figure 1: Illustration of the significant improvement in constraint violation for a binary neutron star system between the BSSN formulation (upper panel) and the Z4c formulation (lower panel), taken from [5].

The Z4c formulation: We have introduced a new formulation of GR, known as Z4c, which combines the advantages of two commonly used formulations. We completed the development by deriving constraint-preserving boundary conditions and performing three-dimensional tests for binary black hole and binary neutron star spacetimes [5]. One sees smaller constraint violations, cleaner convergence, and better conservation of the energy compared to other formulations.

Outlook

In the future we plan to extend our work on binary neutron star systems and have already made major improvements, e.g., the implementation of conservative mesh refinement. We have also developed a new method to construct constraint solved and consistent binary neutron star initial data including eccentricity, allowing us to improve upon our initial evolutions of highly eccentric neutron star binaries – the first in full GR [3]. Additionally, we are now able to simulate quasicircular binary neutron stars with realistic equations of state and unequal masses.

Even more important is the development of a new pseudospectral code, BAMPS. This code will be the next-generation successor to BAM. Currently, BAMPS only solves the vacuum Einstein equations with relatively simple grid setups (not yet applicable to binaries). However, we have started to develop the more complicated grids necessary to simulate binaries and are also beginning to develop discontinous Galerkin methods to allow us to tackle matter. Thus, in the next few years we plan to have a gradual transition from BAM to BAMPS. We are presently applying BAMPS to the problem of critical collapse on SuperMUC.

To further pursue our binary neutron star simulation program and studies of critical collapse, and help achieve this code transition, we recently applied for the follow-up project pr87nu "The dynamics of strong gravity: neutron star mergers and critical collapse".

References and Links

[1] S. Bernuzzi, M. Thierfelder, B. Brügmann. Accuracy of numerical relativity waveforms from binary neutron star mergers and their comparison with post-Newtonian waveforms. Phys. Rev. D 85, 104030 (2012)
[2] S. Bernuzzi, A. Nagar, M. Thierfelder, B. Brügmann. Tidal effects in binary neutron star coalescence. Phys. Rev. D 86, 044030 (2012).
[3] R. Gold, S. Bernuzzi, M. Thierfelder, B. Brügmann, F. Pretorius. Eccentric binary neutron star mergers. Phys. Rev. D 86, 121501(R) (2012).
[4] S. Bernuzzi, T. Dietrich, W. Tichy, B. Brügmann. Mergers of binary neutron stars with realistic spin. arXiv:1311.443 (submitted to Phys. Rev. D)
[5] D. Hilditch, S. Bernuzzi, M. Thierfelder, Z. Cao, W. Tichy, B. Brügmann. Compact binary evolutions with the Z4c formulation. Phys. Rev. D 88, 084057 (2013).

https://www.tpi.uni-jena.de
http://wwwsfb.tpi.uni-jena.de

Ionization Feedback in Massive Star Formation

Research Institution
Institut für Theoretische Astrophysik, Universität Heidelberg

Principal Investigator
Dr. Thomas Peters

Researchers
Prof. Dr. Ralf Klessen, Prof. Dr. Robi Banerjee, Prof. Dr. Mordecai-Mark Mac Low

Project Partners
Universität Zürich, Universität Hamburg, American Museum of Natural History

LRZ Project ID: h1343

Introduction

Understanding massive star formation is a key problem in modern astrophysics. High-mass stars, which are a factor of 10 to 100 more massive than our Sun, dominate the matter cycle and the energy budget in galaxies by their strong radiative and mechanical feedback. They also produce heavy elements, which are then released into the interstellar medium via strong stellar winds and during supernova explosions. Progress in modeling galaxy formation and evolution therefore requires knowledge of how such objects form and how their feedback impacts their surroundings.

With this SuperMUC project, we extend our previous work on ionization feedback during massive star formation with HLBR II in several directions. In this intermediate report, we focus on our simulations on molecular cloud scales and describe our efforts to include an additional feedback process in our simulations, the mechanical feedback by protostellar outflows. We describe how the new findings are related to our previous work on massive star formation and how they help us to better understand high-mass protostellar outflows.

Results

We use the adaptive mesh refinement code FLASH [1] for our numerical simulations. Our previous collapse simulations of high-mass star formation already included feedback by ionizing and non-ionizing radiation [2]. When the mass of the growing protostar exceeds approximately 10 solar masses, a region of ionized hydrogen forms around it. Because the ionized gas has a two to three orders of magnitude higher temperature than the surrounding molecular gas, these H II regions tend to explosively expand once they have formed. Since the density in the accretion disk around the massive protostar is particularly high, the H II region preferentially grows perpendicular to the disk plane. However, the accretion flow from which the massive protostar accretes material can become gravitationally unstable and form dense filaments that subsequently shield the ionizing radiation efficiently. When this happens, the expanding ionized gas recombines and cools down again. An example of such a molecular fountain flow is shown in Figure 1.

These ionization-driven molecular outflows have energies at the lower limit of observed high-mass outflows [3]. Furthermore, our simulations with magnetic fields suggest that magnetic launching of massive outflows via magneto-centrifugal acceleration and magnetic tower flows is difficult because fragmentation destroys the coherent azimuthal velocity structure in the disk and the ionization feedback further disrupts the magnetic field structure [4].

However, the fragmentation also results in the formation of lower-mass companions around the central high-mass star [5]. We have therefore hypothesized that magnetically-driven outflows around these companion stars could be the origin of observed high-mass outflows [3].

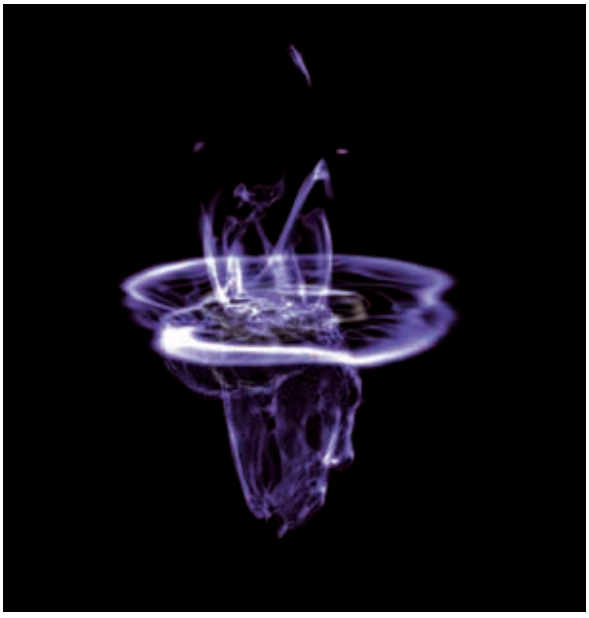

Figure 1: Volume rendering of an ionization-driven molecular outflow. The figure shows the accretion disk surrounding the growing massive star and the bipolar molecular fountain driven be the thermal pressure of the ionized gas. A single star in the center of the disk is launching the outflow.

To test this proposal, we have repeated our simulation with a subgrid-scale model for the injection of protostellar outflows [6]. This subgrid model is necessary since we cannot spatially resolve the accretion disks around the

low-mass stars in our simulation and self-consistently form an outflow. At each timestep, we inject a fraction of the accreted material into a cone centered on the protostar and aligned with its rotation axis. The launching speed is set to depend on the Keplerian velocity at the outflow footpoint and thus increases with protostellar mass. At the current stage of the simulation, a small cluster of four stars has formed, all of which will soon become massive enough to start ionizing their surroundings. So far, this simulation has consumed 1.73 million CPU hours and produced more than 20 TB of data. A single snapshot contains up to 487 million grid cells on 10 FLASH refinement levels. Without the generous allocation of computing time and disk space at LRZ, and in particular the very efficient tape archiving system, conducting this simulation up to this stage would have been impossible. The availability of compute nodes with a large amount of shared memory on SuperMUC was also crucial.

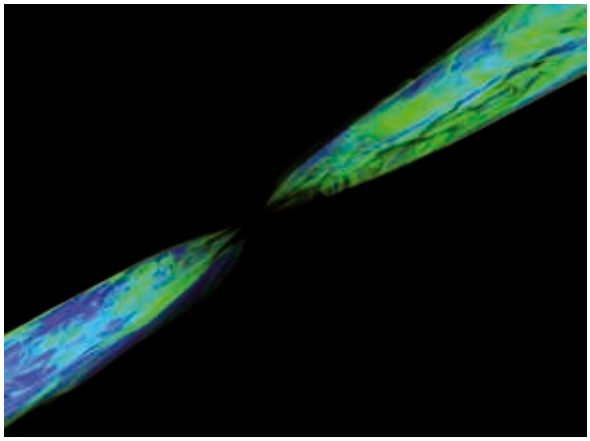

Figure 2: Volume rendering of the collective outflow from a small stellar cluster. The protostellar outflows are launched with a subgrid-scale model from four stars that form in a common accretion flow and thus have aligned angular momentum vectors. We thank Herwig Zilken for his support with this visualization.

Figure 2 shows a snapshot from this simulation. Since all four stars form within the same rotationally-flattened accretion flow, their spin axes are all aligned. Thus, their individual outflows overlap and form a single collective outflow. The energetics of this collective outflow are in good agreement with observed values for high-mass outflows. Since the four stars form very close to each other, it is possible that they and their individual outflows could not be distinguished observationally. Thus, such a collective outflow could be mistakenly interpreted as driven from a single central, massive protostar.

Besides the energetics, the morphology of the outflow also agrees well with observed high-mass outflows. As the protostars in the simulation grow in mass, their angular momentum vectors start to diverge. As a result, the collective outflow widens and looks less collimated. This agrees with the observation that high-mass outflows appear to be less collimated than outflows from low-mass stars. Synthetic observations of the collective outflow reproduce many features seen in Cepheus A and DR 21, two of the closest sources in which high-mass outflows can be observed. Thus, our initial results support the idea that massive outflows may be driven by the lower-mass companions of the central massive star. They substantiate our model of massive star formation in which high-mass stars form in gravitationally unstable accretion flows [5].

On-going Research / Outlook

Additional investigations are necessary to further test our theory. In particular, we want to continue our new simulation until H II regions form around the massive stars. We want to study how the protostellar outflows and the H II regions will interact. We expect additional low-mass stars to form very soon [2-5]. It will be interesting to see how their feedback will affect the morphology of the collective outflow, and if we will obtain a realistic stellar mass spectrum at the end of the simulation.

Once we have understood our highly idealized simulations, we can start to make them more realistic. One important step will be to add turbulent velocity fluctuations to our setup. Turbulence is currently not included in our initial conditions to avoid the computational complexity of fragmentation on molecular cloud scales, but such fragmentation is present in real clouds. With turbulence, we expect to form smaller and less massive accretion disks. An important question will then be whether the stars forming in these disks are still close enough and have sufficiently well aligned spin axes to produce collective outflows.

Such simulations will likely require higher numerical resolution to resolve these smaller-scale disks. Moving towards smaller spatial scales is not only a computational challenge, but it also requires substantial improvements on our simulation methodology. In particular, the gas will become optically thick in the infrared wavelength regime in these small, but very dense accretion flows. Our current approach to radiation hydrodynamics is not applicable to such situations. We will therefore use a new radiative transfer scheme, which is currently in the final testing phase, to propagate the stellar radiation in these optically thick media. The new scheme will further allow us to add another important feedback process to our simulations, the radiation pressure by non-ionizing radiation on dust grains. With radiation pressure included, our simulations will be among the most complete and comprehensive studies of massive star formation feedback on molecular cloud scales. They will certainly significantly improve our understanding of this important process.

References and Links

[1] Fryxell et al. 2000., Astrophys J Suppl S, 131, 273
[2] Peters et al. 2010, Astrophys J, 711, 1017
[3] Peters et al. 2012, Astrophys J, 760, 91
[4] Peters et al. 2011, Astrophys J, 729, 72
[5] Peters et al. 2010, Astrophys J, 725, 134
[6] Schrön 2012, Diploma Thesis, University of Heidelberg

http://www.ita.uni-heidelberg.de
http://www.ics.uzh.ch/ics/live/index.html

The world's largest simulation of supersonic turbulence

1

Research Institution
Zentrum für Astronomie der Universität Heidelberg, Institut für Theoretische Astrophysik,
Monash Centre for Astrophysics, School of Mathematical Sciences, Monash University

Principal Investigator
Christoph Federrath & Ralf S. Klessen

Researchers
R. Banerjee, D. Schleicher, W. Schmidt, A. Ginsburg, P. Girichidis, L. Konstandin, J. Schober, T. Tricco, D. Vlaykov

Project Partners
Hamburger Sternwarte, Georg-August-Universität Göttingen, Max-Planck-Institut für Astrophysik in Garching,
European Southern Observatory

LRZ Project ID: pr32lo, pr89mu (PRACE project)

Introduction

The aim of this study is to determine the properties of supersonic, compressible and magnetized turbulence. This kind of turbulence is relevant for the highly compressible interstellar medium [1], because it controls the rate an efficiency of star formation triggered by gas compression in shocks [2] and determines the mass distribution of stars when they are born [3]. Supersonic turbulence has an important effect on the gravitational instability of galaxies. Even the early Universe was likely dominated by supersonic turbulence when the first cosmic haloes started to contract to form the first galaxies. Analytic models of star formation are based upon the probability distribution function (PDF) of the gas density and the scaling of the velocity power spectrum of supersonic turbulence. It is thus crucial to determine the PDF and the power spectrum with high precision, in order to test whether these are universal properties of supersonic turbulent flows and/or whether they depend on how the turbulence is driven.

With the advent of supercomputers combining thousands of compute cores in one large-scale parallel application, it has only recently become possible to measure the velocity spectrum of supersonic turbulence with high precision. Such studies find a velocity spectrum $P(v) \sim k^{-2}$, which is much steeper than the Kolmogorov spectrum and closer to Burgers turbulence. Burgers turbulence consists of a network of discontinuities and shocks, which can only form in supersonic flows. However, previous numerical studies were limited to 1024^3 grid cells. Here we present the world's largest simulations of supersonic turbulence with an unprecedented grid resolution of 4096^3 cells. We focus on the most compressible type of turbulent clouds in the Milky Way and compare two extreme modes of driving the turbulence: solenoidal (divergence-free) driving and compressive (curl-free) driving, in order to test the influence of different driving patterns. We find a significant influence on the statistics of supersonic turbulence exerted by the driving, with important implications for earlier models of supersonic turbulence and analytic theories of star formation.

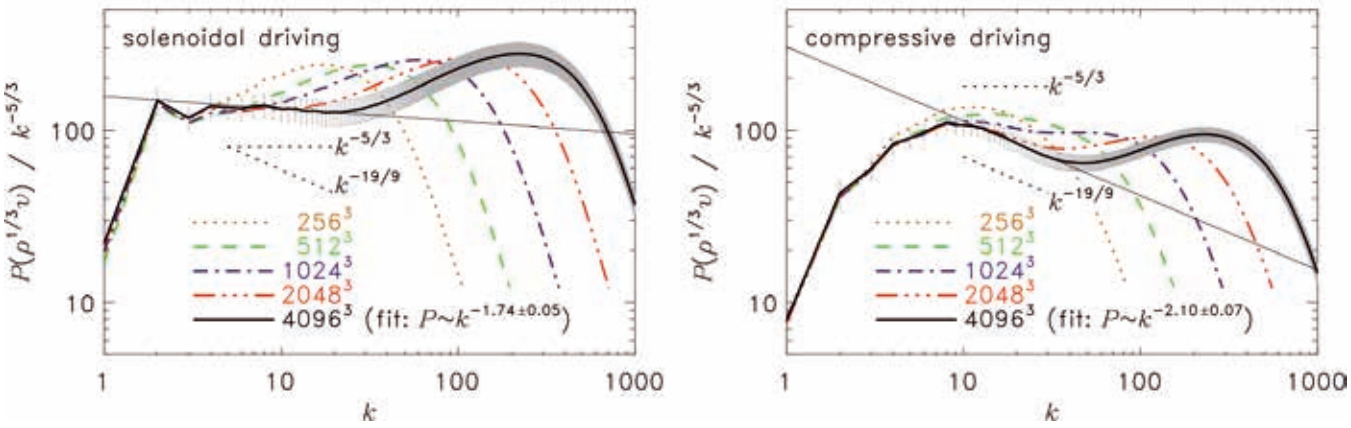

Figure 1: Shows the density-velocity hybrid power spectrum for supersonic turbulence for solenoidal driving (left) and compressive driving (right) at a maximum grid resolution of 40963 cells. Supersonic turbulence is not universal!

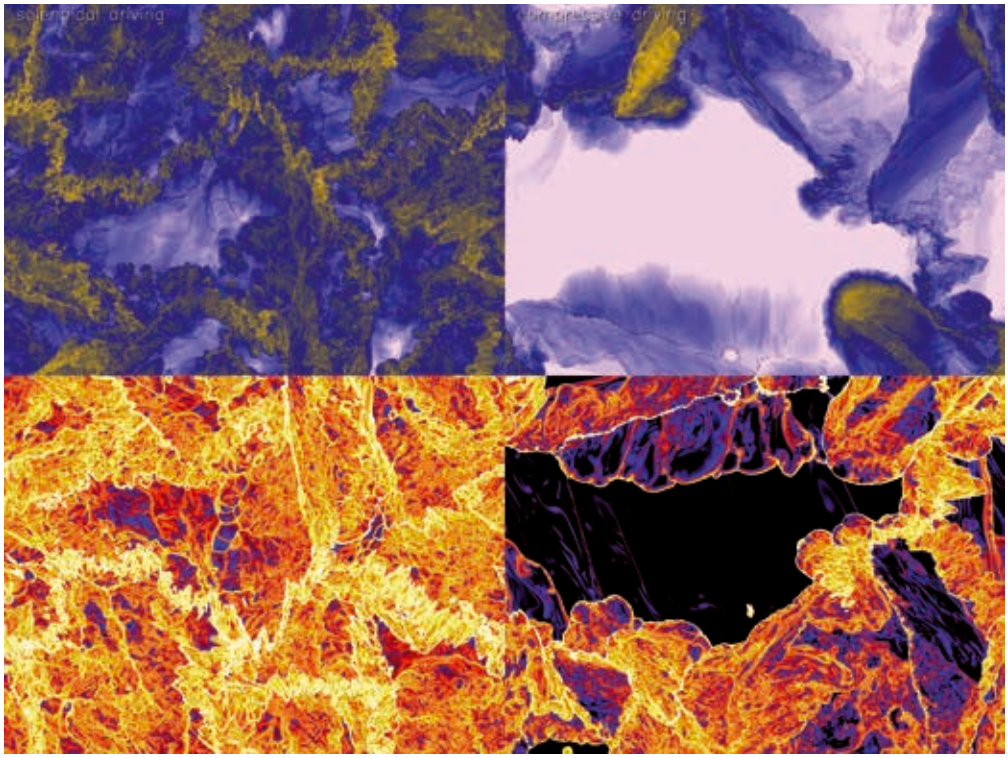

Figure 2: Slices through the three-dimensional gas density (top) and vorticity (bottom) in the world's largest simulations of supersonic turbulence with a grid resolution of 4096³ cells. Left shows solenoidal driving and right shows compressive driving of the turbulence, exhibiting vastly different statistical properties.

Results

We focus on comparing two simulations with solenoidal (divergence-free) and compressive (curl-free) driving, each with a grid resolution of 4096^3 points, which is currently the world's largest data set of supersonic turbulence [4]. Each simulation was evolved for about 44,000 time steps on 32,768 compute cores running in parallel on SuperMUC. The simulations consumed about 7.2 million CPU hours. Each run produced 115 TB of data in 51 double-precision snapshots of the three-dimensional turbulent density and velocity, stretched over six turbulent turnover times. In order to study resolution effects, we compare each 4096^3 model with the respective lower-resolution versions consisting of 2048^3, 1024^3, 512^3, and 256^3 compute cells. Figure 1 shows a resolution study of the hybrid density-velocity power spectrum of supersonic turbulence. We find that this type of spectrum is not universal for supersonic turbulence, contrary to previous suggestions. The spectrum depends on the driving of the turbulence and is not always compatible with the density-weighted extension of the Kolmogorov power spectrum ($P \sim k^{-5/3}$). We find that the spectrum for compressive driving is much steeper with $P \sim k^{-2.1}$, in excellent agreement with the new theoretical model by Galtier & Banerjee [5]. The resolution study in Figure 1 shows that we would not have been able to identify this scaling at any lower resolution than 4096^3 cells.

Figure 2 displays the unprecedented level of detail in density and velocity structures achieved with our 4096^3 simulations. This visualization demonstrates the significant differences between the two extreme driving modes of the turbulence. Simulation movies are available online (see links below). This work is published in the Monthly Notices of the Royal Astronomical Society [4] and was selected as the SAO/NASA ADS paper of the year 2013.

On-going Research / Outlook

In order to generate this huge dataset of supersonic turbulence, we pushed towards the technical limit of what is currently feasible on any supercomputer in the world. Increasing the resolution by another factor of two would require a machine about twice as powerful as SuperMUC. Turbulence has many important applications in science and engineering, including the exponential amplification of magnetic fields, which we are currently studying. We hope to get closer to solving the riddles of supersonic, magnetized turbulence in the near future, with the aid of increasingly fast and world-leading high-performance computing systems provided by the LRZ.

References and Links

[1] McKee & Ostriker 2007, ARAA 45, 565
[2] Federrath & Klessen 2012, ApJ 761, 156
[3] Padoan & Nordlund 2002, ApJ 576, 870
[4] Federrath 2013, MNRAS 436, 1245
[5] Galtier & Banerjee 2011, PRL 207, 134501

http://www.gauss-centre.eu/gauss-centre/EN/Projects/Astrophysics/federrath_astrophysics_weltrekord.html?nn=1345700
http://www.ita.uni-heidelberg.de/~chfeder/pubs/supersonic/supersonic.shtml

Numerical Simulation of Binary Black Hole and Neutron Star Mergers

1

Research Institution
Albert Einstein Institut

Principal Investigator
W. Kastaun, L. Rezzolla

Researchers
R. Ciolfi, K. Dionysopoulou, I. Hinder, S. Hopper, D. Siegel, K. Takami

Project Partners
–

LRZ Project ID: pr32pi

Introduction

One of the last predictions of general relativity that still awaits direct observational confirmation is the existence of gravitational waves. Those fluctuations of the geometry of space and time are expected to travel with the speed of light and are emitted by any accelerating mass. Only the most violent events in the universe, such as mergers of two black holes or neutron stars, produce gravitational waves strong enough to be measured. Even those waves are extremely weak when arriving at Earth, and their detection is a formidable technological challenge. In recent years sufficiently sensitive detectors became operational, such as GEO600, Virgo, and LIGO. They are expected to observe around 40 events per year.

To interpret the observational data, theoretical modeling of the sources is a necessity, and requires numerical simulations of the equations of general relativity and relativistic hydrodynamics. Such computations can only be carried out on large scale supercomputers, given that many scenarios need to be simulated, each of which typically occupies hundreds of CPU cores for a week.

Our main goal is to predict the gravitational wave signal from the merger of two compact objects. Comparison with future observations will provide important insights into the fundamental forces of nature in regimes that are impossible to recreate in laboratory experiments. The waveforms from binary black hole mergers would allow one to test the correctness of general relativity in previously inaccessible regimes. The signal from binary neutron star mergers will provide input for nuclear physics, because the signal depends strongly on the unknown properties of matter at the ultra high densities inside neutron stars, which cannot be observed in any other astrophysical scenario. Besides mergers, we also want to improve the theoretical models of close encounters between black holes.

A gravitational wave detector with even higher sensitivity, the Einstein Telescope, is already in the planning stage. It is natural to ask what could be learned from the expected observations. Particularly intriguing is the possible detection of sources at cosmological distances. The fact that observed frequencies will be reduced due to the expansion of the universe could be used to determine the distance, but only if the original frequency is known. As it turns out, numerical modeling of the source might provide this information. Independent distance measures are very valuable for cosmology, improving estimates of the past expansion rate of the universe and predictions of its future fate.

Another goal of our project is to shed some light on the mystery of so called short gamma-ray bursts, intense and sudden bursts of gamma radiation that puzzled astronomers since decades. Previous simulations indicated that they are caused by neutron-star mergers. The exact emission mechanism is however unknown, and many features were completely unexplained, for example the X-ray afterglows which often accompany the main burst.

Results

To achieve the project goals, we made use of a large collection of software modules based on the CACTUS com-

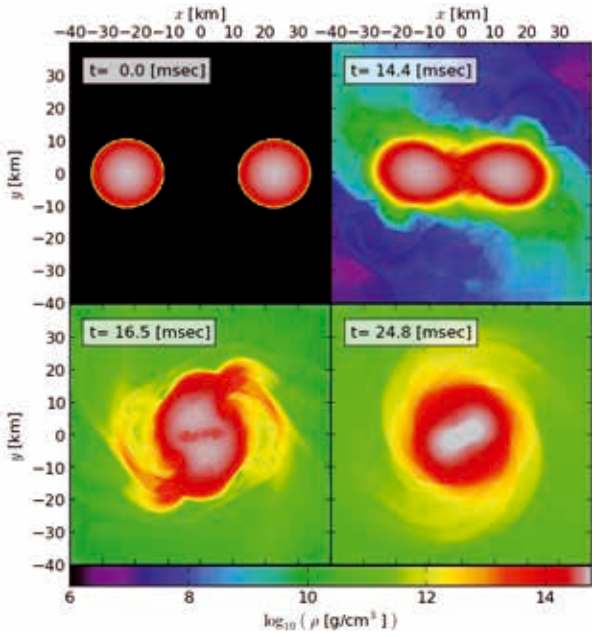

Figure 1: Snapshots of a binary neutron star merger, from late inspiral (top left), touching (top right), merging (bottom left) to the formation of a metastable hyper-massive neutron star (bottom right). The colors represent the mass density in the orbital plane.

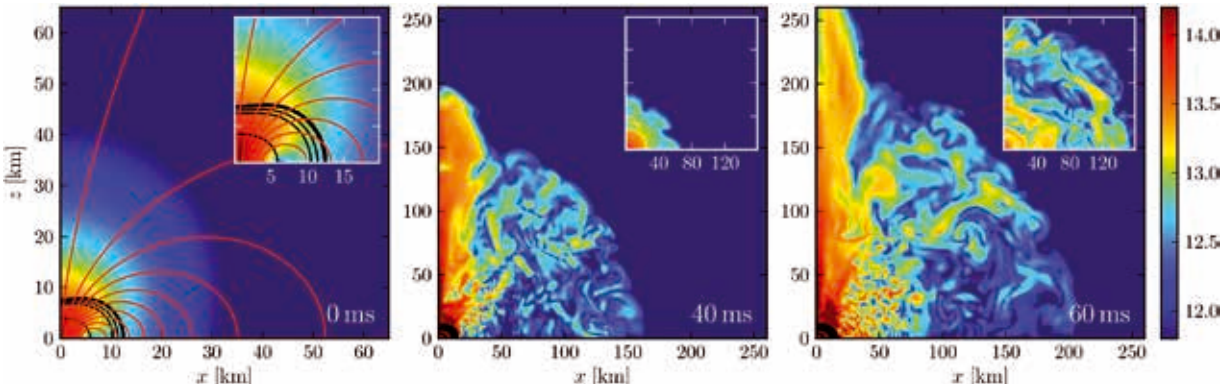

Figure 2: Evolution of a differentially rotating and strongly magnetized neutron star as produced in a neutron star merger. A dense and magnetized outflow is powered at the expense of rotational energy and generates electromagnetic emission that is compatible with the observed X-ray afterglows of short gamma-ray bursts. The panels show the color-coded magnetic field strength in Gauss (log scale) and indicate the initial magnetic field (red lines) as well as the neutron star (black lines).

putational toolkit, which provides infrastructure for large scale simulations, including MPI parallelization, mesh refinement (provided by the CARPET driver), memory management, and data storage. The equations of general relativity are integrated using the McLachlan module from the Einstein Toolkit, which is based on high order finite differencing methods.

The (magneto-)hydrodynamic equations are evolved using the Whisky code. It employs modern finite volume methods for conservation laws in conjunction with various approximate Riemann problem solvers and a piecewise parabolic reconstruction algorithm. Initial data for binary neutron stars was generated using the LORENE code, a solver for elliptic PDEs based on spectral methods.

In total, we used 14 million core hours for simulations of binary neutron star mergers, magnetized hyper-massive neutron stars, binary black hole mergers and close encounters. A typical run required around 200-500 cores over several days up to several weeks. The resulting data occupies more than 19 TB permanent disk storage, contained in around 1 million files.

Binary neutron star mergers
Using the above codes, we computed the inspiral and merger of binary neutron stars with 5 different masses, assuming a simple analytic model (gamma-law equation of state) for the properties of matter at high densities. An example is shown in Figure 1. For each model, we extracted the gravitational wave signal. The corresponding power spectrum contains contributions from the inspiral phase and the hyper-massive neutron star stage. It is also shifted to lower frequencies with increasing distance to the source. We demonstrated that these features could be combined to infer the absolute distance and total mass, assuming a particular equation of state of the neutron star matter [1]. We have shown that such observations of sources at cosmological distances with sufficient signal to noise ratio should be possible with the proposed Einstein Telescope.

Hypermassive neutron stars
A large part of our simulations was devoted to hyper-massive neutron stars formed during binary neutron star mergers. Besides the gravitational wave signal, the evolution of the magnetic field is of astrophysical interest. We therefore performed general relativistic magneto-hydrodynamics simulations of such models, in the limit of infinite conductivity (ideal MHD). Here, we could show that differential rotation causes magnetically driven outflows, carrying substantial amounts of energy [1]. Those winds might well be the source of the X-ray afterglows which often accompany short gamma-ray bursts. Figure 2 depicts the development of the wind.

Further, we studied the effect of large magnetic fields on the so called bar-mode instability. This instability develops only for rapidly rotating neutron stars, such as those formed in mergers, and converts rotational energy into gravitational waves, also accelerating the collapse of the star to a black hole. We found that only very high magnetic field strengths exceeding 1016 Gauss can delay or even suppress the instability [3].

Binary black hole systems
In contrast to binary black hole mergers, which are well investigated by now, little was known on the dynamics of close encounters. We performed numerical simulations of such encounters with different impact parameters and compared the results with existing analytic estimates, thus determining the accuracy of such predictions in different regimes [4]. Besides physics runs, a fraction of our resources was used to further test and develop the codes used for simulating binary black hole mergers, also with regard to numerical optimization.

On-going Research / Outlook

Currently, we are expanding our results mainly in three directions. One is the influence of the matter properties at high densities. Another is the influence of resistive effects on the evolution of magnetic fields. Finally, we are including the effects of neutrino cooling into merger simulations.

References and Links

[1] http://arxiv.org/abs/1312.1862, "Host redshifts from gravitational-wave observations of binary neutron star mergers"
[2] http://arxiv.org/abs/1401.4544, "Magnetically driven winds from differentially rotating neutron stars and X-ray afterglows of short gamma-ray bursts"
[3] Phys. Rev. D 88, 104028, "Dynamical bar-mode instability in rotating and magnetized relativistic stars"
[4] http://arxiv.org/abs/arXiv:1402.7307 "Strong-Field Scattering of Two Black Holes: Numerics Versus Analytics"

Simulating the life cycle of molecular clouds

Research Institution
Max-Planck-Institute for Astrophysics/ University of Cologne/ ITA Heidelberg

Principal Investigator
Stefanie Walch

Researchers
S. Walch, T. Naab, P. Girichidis, A. Gatto, R. Wünsch, R. Klessen, S. Glover, P. Clark, C. Baczynski, T. Peters

Project Partners
–

LRZ Project ID: pr45si (Gauss Large Scale project)

Introduction

Star formation takes place in the densest and coldest gas in a galaxy, in so-called molecular clouds (MCs). MCs do not evolve in isolation but are highly dynamical objects, which are born, fed, heated, and stirred from their turbulent environment into which they eventually dissolve. They form in regions where the hot or warm, ionized and atomic interstellar medium (ISM) condenses into cold (T< 300K), molecular gas. Often concentrated to the midplane of galactic disks, this process involves metallicity-dependent, non-equilibrium chemistry and molecule formation, heating and cooling, turbulence, self-gravity, and magnetic fields. Once formed, MCs further collapse to form stars and star clusters. Less than 1% of all new-born stars are more massive than 8 solar masses, but these are particularly important for galaxy evolution. The life and death of massive stars differ intriguingly from those of their low-mass counterparts. Such stars affect their environment dramatically through their strong UV radiation, their energetic stellar wind, and their final explosion as a supernova (SN). These 'feedback' processes generate turbulence in the parental molecular cloud, dissociate, ionize, and eventually destroy them from within, thereby preventing further star formation. Stellar feedback is thus thought to regulate the star formation efficiency in molecular clouds leading to a self-regulation of star formation on galactic scales. In the framework of the Gauss project "SILCC" on SuperMUC, we model representative regions of disk galaxies using adaptive, three-dimensional simulations at unprecedented resolution and with the necessary physical complexity to follow the full life-cycle of molecular clouds. These simulations include self-gravity, magnetic fields, heating and cooling at different gas metallicities, molecule formation and dissociation, and stellar feedback in form of stellar winds and supernovae. The ultimate goal of the SILCC project is to provide a self-consistent answer as to how stellar feedback regulates the star formation efficiency of a galaxy, how molecular clouds are formed and destroyed, and how galactic outflows are driven. Here we discuss first results of the SILCC project.

Results

With a European team of experts from Cologne, Garching, Heidelberg, Prague and Zurich we have performed the first simulations of the turbulent ISM in a galactic environment including self-gravity and the self-consistent formation of H_2 and CO.

The simulations are being carried out with the massively MPI-parallel, Eulerian, adaptive mesh refinement code FLASH 4.0.1 [1]. FLASH includes ideal MHD, an external gravitational potential, and recently also a Barnes & Hut tree method for self-gravity, in the standard release. However, much more physics is required in order to carry out the proposed simulations. For this project, we further implemented a chemical network that includes non-equilibrium ionization effects as well as H_2 and CO formation [2]. It also computes radiative heating and cooling. The heating and cooling terms, and also the chemical source and sink terms, are operator split from the advection and PdV work terms and are solved implicitly using the DVODE solver. In order to treat the formation of molecules, we implemented TreeCol [3] to compute shielding and self-shielding of H_2 and CO as well as dust attenuation and temperature. TreeCol is a cost-efficient way to treat diffuse radiation. TreeCol defines a set of HealPix rays from every cell within the computational domain. During the self-gravity tree walk, we compute the column densities necessary for solving the radiation transport along each ray.

Furthermore, we include Supernova and stellar wind feedback. Supernovae can be placed randomly with a given Supernova rate (SNR). Alternatively, the explosions might be launched from gas density peaks within molecular clouds or from sink particles. Each Supernova injects 10^{51} erg and a few solar masses of gas into the ISM. The temperature within the injection region typically rises to ~10^7 K, and therefore the hydrodynamic timestep is recomputed and limited accordingly. Stellar winds are implemented in a similar way. We simulate representative regions of disk galaxies (500 pc x 500 pc x ± 5 kpc) with different gas surface densities, i.e. Σ_{gas} = 10, 30, 100, and 500 M_{sun}/pc^2, to mimic the conditions of star-forming galaxies in their centers and at large radii, as well as at low and high redshift. The initial density distribution of the gaseous disk is Gaussian. The boundary conditions are periodic in x- and y-, and allow for outflow in z-direction. To account for the aforementioned physical processes on spatial and temporal scales ranging from

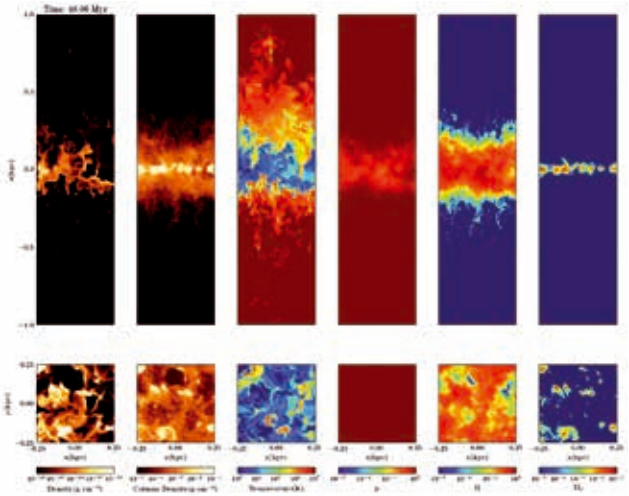

Figure 1: Projections and slices through the y=0 (top) and z=0 (bottom) planes of a disk with 30 M_{sun}/pc^2, which was stirred by randomly placed SNe for 40 Myr. The SNR is 19 Myr^{-1}. From left to right we show a density slice, the total column density, and slices of gas temperature, and the fractional abundances of ionized hydrogen, atomic hydrogen, and molecular hydrogen.

several 100 AU and 10 years to kpc-scales and 10^7 years, each run requires more than 5 million CPU hours, runs on more than 1000 cores, and occupies more than 5 TB of scratch storage.

A disk galaxy similar to the Milky Way has an average gas surface density of 10 - 30 M_{sun}/pc^2. We present results from simulations at an intermediate resolution, where we include turbulence driving from randomly placed Supernova explosions (see Fig. 1). The random positions are weighted with a Gaussian with a scale height of 60 pc. The mean SNR for such a disk can be derived from the observed star formation rate – gas surface density relation.

Typically, a significant fraction of molecular gas forms after > 10 Myr and accumulates in the form of clouds in the disk mid-plane. Clouds can be disrupted by SNe that explode within or near them. Within the MCs the abundances of H_2 and CO are well correlated. However, there is H_2 at higher altitudes, which is not well traced by CO. This gas, which has been driven out of the molecular clouds by SNe, is CO-dark and cannot be seen in observations. CO does not survive at higher altitudes as it requires a higher column density to shield itself from the interstellar (ultraviolet) radiation field. Simulations of disks with higher gas surface density show that the mass fraction of molecular gas is higher with increasing surface density, even though the SNR is correspondingly higher in high surface density disks. In Figure 2, we show the molecular gas mass fraction as a function of time for four different initial disk surface densities: Σ_{gas} =10, 30, 100, and 500 M_{sun}/pc^2.

For the highest gas surface density of 500 M_{sun}/pc^2, the H_2 mass fraction rapidly approaches values of up to 90%. At 100 M_{sun}/pc^2 the H_2 mass fraction saturates at 70 – 80%. This result is in good agreement with observational estimates of the molecular gas mass fraction in centers of local galaxies as well as gas-rich high redshift disks. For lower initial gas surface densities the molecular fractions are respectively lower and it takes longer to reach the saturation values. The Milky Way value of roughly 50% (interior to the Sun's galactic orbit) agrees well with the 10 M_{sun}/pc^2 disk simulation, for which peak values of 40% are achieved.

We have performed the first synthetic observations of the simulations for direct comparison with observational H∝ and CO surveys with e.g. SINFONI, IRAM and ALMA.

On-going research

Even though most of the mass is in cold and molecular gas, the fractional volume filled by this gas component is small. Therefore, simulating the life-cycle of MCs in more detail and e.g. resolve the internal turbulent structure of the MCs, requires simulations with higher spatial resolution. We have now started the second phase of the SILCC project, in which we carry out simulations that run at a higher spatial resolution, to follow the self-consistent formation of star clusters. With these runs we resolve the relevant spatial scales to investigate the relative importance of the different forms of stellar feedback. We will e.g. be able to formulate new constraints on the amount of CO-dark molecular gas. In addition, we perform simulations with different magnetic field strengths to study the impact of magnetic fields on the turbulent multi-phase structure of galactic disks and the formation of molecular gas. At the same time we are preparing the data for public access via the Galformod-Millenium data portal at MPA.

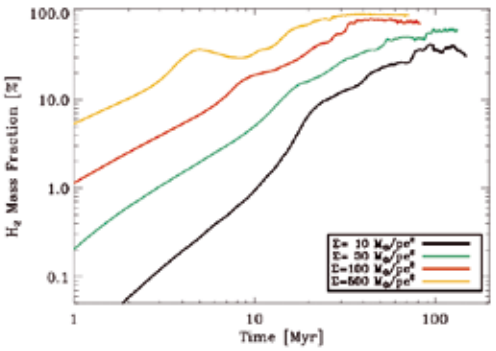

Figure 2: Mass fraction of H_2 as a function of time for four different disk surface densities.

We have made immense progress since the upgrade from HLRBII with respect to both, code development as well as the size of the simulations we were able to run. Therefore, we could gain new and significant insight into the physics of the turbulent ISM. The limiting factor for our runs was the amount of memory per node. We have optimized the code to overcome this issue and we will continue to do so in the future. This project will continue, so please stay tuned! [4]

References and Links

[1] Fryxell et al. 2000, ApJS, 131, 273
[2] Glover et al. 2011, MNRAS, 412, 337
[3] Clark et al. 2012, MNRAS, 420, 745
[4] https://www.astro.uni-koeln.de/node/794

1 Adaptively refined large eddy simulations of disk galaxies

Research Institution
Institut für Astrophysik, Georg-August-Universität Göttingen

Principal Investigator
Dr. Wolfram Schmidt

Researchers
Prof. Dr. Jens C. Niemeyer, Harald Braun

Project Partners
Computational Cosmology Center at Lawrence Berkeley National Laboratory

LRZ Project ID: pr47bi

Introduction

We performed simulations of isolated disk galaxies with the adaptive mesh refinement (AMR) code Nyx [1]. A rotating gaseous disk of uniform temperature in hydrostatic equilibrium is used as initial condition. Since galaxies are embedded in massive dark-matter halos, the disk is bound by a spherically symmetric gravitational potential in addition to its self-gravity. We apply the CLOUDY package for the radiative cooling of the gas, which causes the initial disk to collapse into a thin disk. The disk fragments due to gravity and cooling instabilities. Since the resulting multi-phase structure of the interstellar medium (ISM) cannot be fully resolved in galaxy simulations, we use a simple model [2]. Basically, small clouds of cold, dense gas are assumed to be embedded in a warm phase. The cold-gas clouds contain a certain fraction of molecular hydrogen, from which stars can form. The star formation rate, which specifies how much gas mass is converted into stars per unit time, depends on the density of the molecular hydrogen, the free-fall time scale in the cold gas, and the star formation efficiency. The latter is not a fixed free parameter, as in most simulations of galaxy evolution, but varies with the local turbulent Mach number and virial parameter on the length scale associated with star-forming clouds. To calculate these parameters, we apply a subgrid scale (SGS) model for the numerically unresolved turbulence energy, which can be interpreted as non-thermal pressure [3]. In addition to turbulence energy production due to the shear of the numerically resolved flow, we incorporated small-scale processes such as supernova feedback as sources into the SGS model.

Results

We produced a suite of disk galaxy simulations to investigate the influence of different model assumptions and numerical resolutions. For the runs with the highest resolution (30 pc at the maximal refinement level for a box size of 500 kpc), we used 128 MPI processes running on 64 nodes with 8 OMP threads per process. Each run consumed between 0.25 and 1.0 Mio. CPU-h. We used mainly SCRATCH to store between 10 and 30 TB of output data per run for post-processing. The maximal total data volume was about 300 TB.

Various parameterizations of the local star formation efficiency in terms of the Mach number of turbulence and the virial parameter of the star-forming cloud have been suggested [4,5]. Since the clouds are not numerically resolved in our simulations, we utilize the SGS model to estimate the local turbulent Mach number (ratio of turbulence energy to thermal energy) and virial parameter (ratio of turbulence energy to potential energy). This allows us to calculate the dynamical star formation efficiency with some parameterization or other, depending on local conditions. Typically, the resulting efficiencies in our simulations are of the order 1 % relative to the total gas density, which is the expected value in agreement with observations [2]. The global star formation rate settles around two solar masses per year for most parameterizations, as shown in Figure 1. For the comparison shown in this figure, we restarted our reference run after 1 Gyr (billion years) of evolution (at this point the disk has reached a quasi equilibrium)

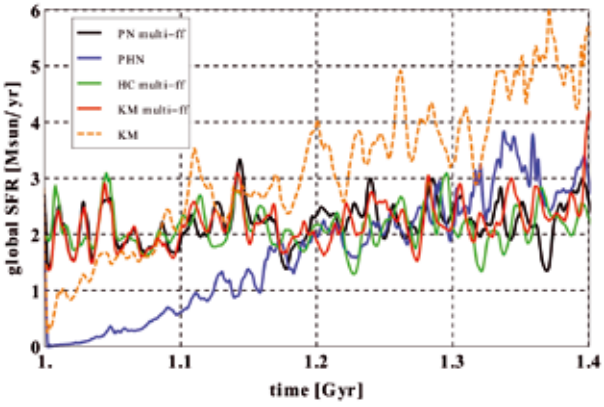

Figure 1: Global star formation rate as a function of time for different parameterizations of the star formation efficiency in terms of the turbulent Mach number and virial parameter (PN: Padoan-Nordlund, HC: Hennebelle-Chabrier, KM: Krumholz-McKee [4]; PHN: simple star formation law [5]).

with different star formation laws. In particular, the multi-freefall formulations of the star formation laws proposed in [4] produce very similar behavior. If a single freefall time is assumed, which is given by the local cold-gas density, we find significant deviations from the reference run (as an example, see the orange line in Figure 1 for the Krumholz-McKee model). Also for the recently proposed simple star formation law, where the efficiency is solely a function of the virial parameter [5], the disk undergoes a process of restructuring (see blue line in Figure 1). This results in concentrations of stars in much larger clumps than in the reference run.

Stars increase the thermal and non-thermal pressures via feedback. While a relatively small fraction of the supernova energy is converted into SGS turbulence energy, most of the energy heats up the gas to very high temperature. We assume that the hot gas is initially confined in bubbles and cannot cool efficiently. However, the energy of the bubbles decays exponentially into the warm phase, which can cool. As a result, the cooling of the hot gas produced by feedback is suppressed over a time scale of the order 1 Myr (million years). This is similar to the commonly used numerical technique of delayed cooling in galaxy simulations. The importance of the supernova bubbles becomes clear by comparing the disk structure in runs with and without bubbles. In our reference run, we obtain a strongly fragmented gaseous disk (see top panels in Figure 2), where star formation is spread out over the disk. In contrast, the distributions of gas and stars tend to become unrealistically clumpy without supernova bubbles (bottom panels in Figure 2). This is caused by overcooling of the gas if the feedback is too inefficient. Turbulent feedback partially alleviates this problem, but supernova bubbles are nevertheless required to avoid an overly clumpy disk (middle panels in Figure 2).

We also obtained a plethora of results about the local star formation rate, the correlations with gas surface densities, turbulence driving in the ISM, etc. These results are going to be published in Monthly Notices of the Royal Astronomical Society.

On-going Research / Outlook

The architecture of SuperMUC is very well suited for our code (Nyx successfully run on roughly 100 000 cores during the Extreme Scaling Workshop last year). We didn't encounter any particular difficulties or limitations related to SuperMUC for the simulations in the current project. For new applications, however, some further performance tuning might be necessary. For example, we encountered performance bottlenecks when running cosmological simulations with zoom-ins into particular regions with a large number of refinement levels. This would be relevant for simulations of galaxy formation, which is a potential follow-up project. Cosmological simulations with unconstrained AMR, on the other hand, work very well with Nyx. This could be the subject of a medium or big project in the near future.

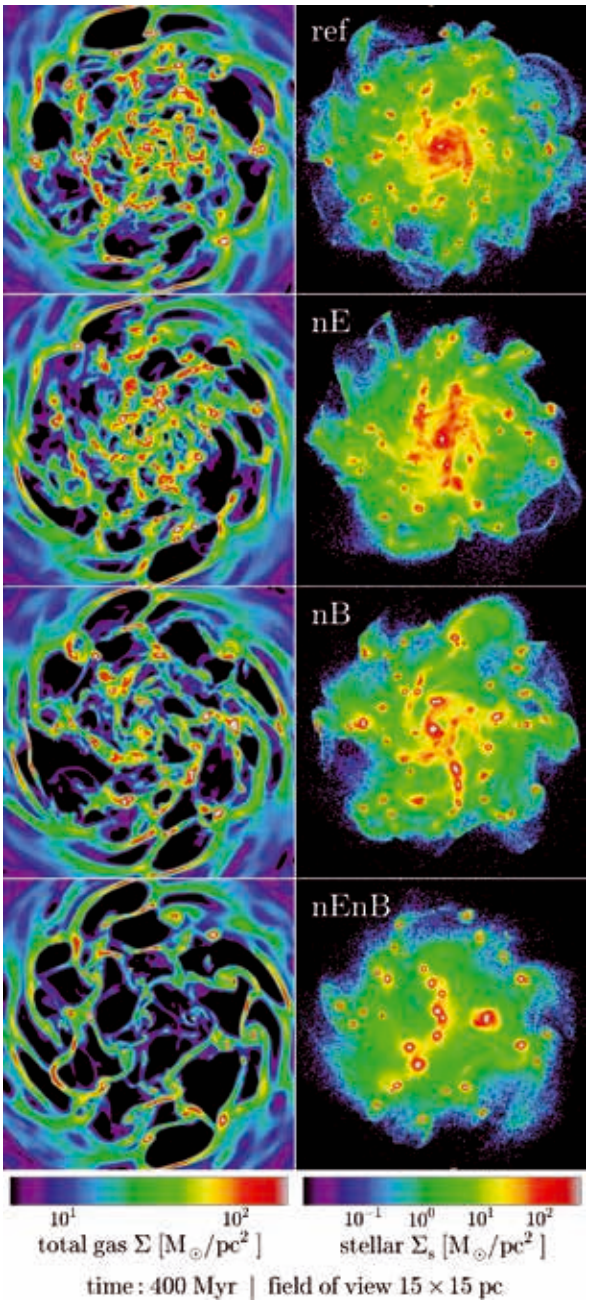

Figure 2: Surface densities of the gas (left) and stars (right) for four different runs (ref: reference run, nE: no turbulent feedback, nB: no supernova bubbles, nEnB: neither turbulent feedback nor bubbles).

References and Links

[1] Almgren et al. 2013, ApJ 765, 39
[2] Braun & Schmidt 2011,MNRAS 421, 1838
[3] Schmidt & Federrath 2011, A&A 528, A106
[4] Federrath & Klessen 2012, ApJ 761, 32
[5] Padoan et al. 2012, ApJ 759, L27

Turbulence and its effect on protostellar disk formation

1

Research Institution
Hamburger Sternwarte, Universität Hamburg

Principal Investigator
Daniel Seifried

Researchers
Daniel Seifried, Robi Banerjee, Ralf Klessen

Project Partners
Institut für theoretische Astrophysik, Universität Heidelberg; McMaster University, Hamilton, Canada

LRZ Project ID: pr47pi

Introduction

In our research we investigate the formation of protostars and their associated protostellar disks, the early precursors of planetary systems.

During the last decade simulations of collapsing molecular cloud cores have revealed the so-called catastrophic magnetic braking problem: Magnetic fields are able to transport angular momentum by means of toroidal Alfven waves. Modeling the collapse of rotating molecular cloud cores, simulations have shown that in the presence of magnetic fields with strengths comparable to observational results, the formation of rotationally supported (Keplerian) protostellar disks is largely suppressed. This is due to the fact that angular momentum is removed very efficiently from the interior of the core by the magnetic field. In previous works we could confirm this effect for the collapse of massive (100 solar masses), molecular cloud cores. This key result of the suppression of Keplerian disk formation during the earliest stages of star formation is in contrast to recent observational results which state that protostellar disks should be present already in the Class 0 stage.

Results

The results described before show up in case that highly idealized initial conditions are used for the simulations. In particular the lack of turbulent motions - frequently observed in molecular cloud cores – could have a significant effect on the formation of protostellar disks and outflows. For this reason, in our research we recently focused on the influence of turbulence on the formation of protostellar disks and outflows.

In our work we have performed a number of simulations on SUPERMUC. Each of the simulations required a computational time of a few 100 000 CPU-hours with a simultaneous use of up to 1000 CPUs per simulation. A few hundreds of files were produce for each simulation requiring a disk space of a few TB in total. The simulations are performed with the hydrodynamics code FLASH[1] written in Fortran 90. The code solves the 3-dimensional, discretized magnetohydrodynamical equations on a Cartesian grid. Making use of the adaptive-mesh-refinement (AMR) technique, only those regions which are of particular interest for us are resolved with the highest possible spatial resolution whereas other regions of minor interest are resolved more coarsely. This significantly reduces the number of calculations to be performed and hence the computational time required, thus allowing us to perform the simulations over long physical timescales.

Initial conditions
Observations of the birth places of stars show a wide range of physical quantities, in particular in their initial mass. As we do not simulate a particular region observed by astronomers but rather aim to understand the systematic influence of the initial conditions, we have to perform a number of simulations in our work covering a wide range of masses and turbulence strengths. This allows us to draw conclusions about the effect of the initial conditions on the formation mechanism of stars. We modeled the collapse of molecular cloud cores with masses ranging from about 2 solar masses up to 1000 solar masses. The cores are threaded by a strong magnetic field along the z-axis and have an additional supersonic, turbulent velocity field as indicated by observations.

Turbulence-induced disk formation
We examine our simulations focusing on the question of how turbulence affects the formation of Keplerian disks[2,3]. An example result is shown in Fig. 1 showing the protostellar disk in a representative run with a core of 100 solar masses. As can be seen, in the presence of turbulence rotationally supported disks are re-obtained again, which is in contrast to the previous simulations with comparable magnetic field strengths but no turbulence. This suggests that the efficiency of the magnetic braking, which is responsible for removing angular momentum from the midplane, is reduced significantly in the turbulent case. Analyzing the surroundings of the disks we can show that this indeed the case. The turbulent surroundings of the disk exhibit no coherent rotation structure (compare Fig. 1). Therefore, an efficient

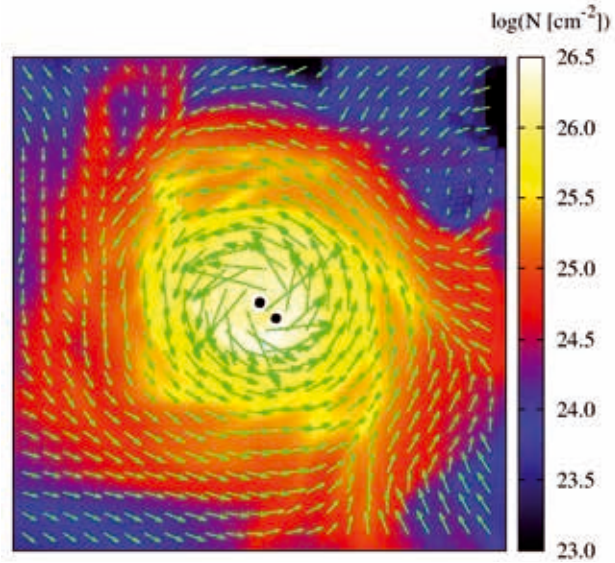

Figure 1: Protostellar disk seen from top-on. Black dots represent protostars, green arrows the velocity field.

build-up of a strong toroidal magnetic field responsible for angular momentum extraction is hampered. Moreover, the turbulent motions lead to a strongly disordered magnetic field which further reduces the magnetic braking efficiency. Since simultaneously the angular momentum inwards transport remains high due to the presence of local shear flows in the vicinity of the disks, there is a net inwards angular momentum transport towards the center of the disk. The combination of these effects results in the observed build-up of Keplerian disks as expected from observations. Varying the core masses (2.6 - 1000 solar masses) and the turbulence strengths does not change our findings. This clearly demonstrate that the turbulence-induced disk formation mechanism works for a wide range of initial conditions. In particular, we could show that the formation of Keplerian disks does not require an uniform rotation of the core – turbulent motions alone lead to the build-up of Keplerian disks. Moreover, we showed that even for subsonic turbulence, which is usually present in low-mass protostellar cores, the turbulence-induced formation mechanism still holds.

In Fig. 2 we show the 3-dimensional structure of the magnetic field and the gas motions around a protostellar disk in one of our simulations. The magnetic field lines clearly reveal a highly complex structure being far off from well-ordered. The anisotropy of the accretion towards the disk is represented by the colored regions in the figure.

On-going Research / Outlook

For our future research we intend to study the self-consistent ejection of protostellar outflows from the Keplerian disks formed in our turbulence simulations. In order to reach this goal we will have to redo some of our simulations with increased spatial resolution, which will require further large amounts of computing power in the future. Furthermore, we plan to produce so-called synthetic observations. These synthetic observations will allow us to directly compare our simulation results with real observations. Such comparisons allow us to assess what can be inferred from observations - in particular how reliable parameters obtained from real observations are.

References and Links

[1] Fryxell, B., Olson, K., Ricker, P., et al. 2000, ASTROPHYS. J. SUPPL. S., 131, 273
[2] Seifried, D., Banerjee, R., Pudritz, R. E., & Klessen, R. S. 2012a, MNRAS, 423, L40
[3] Seifried, D., Banerjee, R., Pudritz, R. E., & Klessen, R. S., 2013, MNRAS, 432, 3320

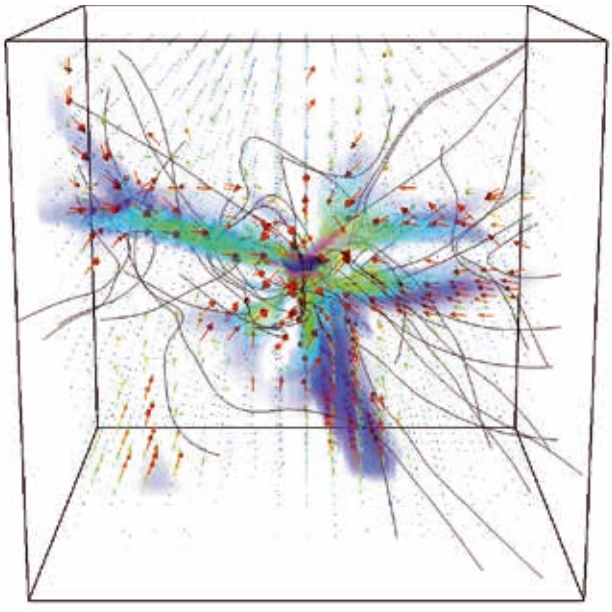

Figure 2: 3-dimensional structure of the magnetic field and gas motions around a Keplerian disk in one of our simulations.

Some like it warm

1

Research Institution
Max Planck Institute for Astronomy

Principal Investigator
Andrea V. Macciò

Researchers
Aurel Schneider, Juerg Diemand, Donnino Anderhalden

Project Partners
University of Zurich, University of Sussex

LRZ Project ID: pr58fa

Introduction

It is now a day well established that more than 80% of the matter content of the Universe is not made by ordinary matter (e.g. protons, electrons, neutrons, etc.). This new type of matter does not emit any electromagnetic radiation and has been dubbed Dark Matter. The nature of Dark Matter is one of the key questions of modern physics and the answer to this question can open completely new scenarios for future research in fundamental physics.

Most of the past research has focused on the assumption that the putative dark particle should be thermally cold and massive. However there are some observational clues that this model has shortcomings on small scales. One possible solution from particle physics is for the dark particles to be lighter and retain some thermal velocity. This scenario is dubbed Warm Dark Matter (WDM). In our project we have explored cosmic structure formation in the WDM scenario with unprecedented precision via extremely high-resolution Nbody simulations.

These simulations have allowed us to uncovering the details of how structure formation behaves from the very largest scale structure, down to the free-streaming mass scale. We have considered models with just one Warm dark matter component and models where both a warm and cold components coexist (usually called mixed models). In the following we will summarize our main findings on the impact of warm dark matter component on structure and galaxy formation.

Results

We have started our research program by studying the effect of WDM on the properties of collapsed dark matter haloes. For this first project we have run several large-scale simulation each of them with different masses for the warm component, plus a simulation in the usual cold dark matter scenario, to be used as a test ruler.

Each simulation has been run using the highly parallelized Nbody code PKDGRAV, originally written by J. Stadel at the University of Seattle. This code has shown very efficient scaling and has been used to perform simulations with up to 10 billions particles. For this first part we have started with a series of 4 simulations with 1024^3 particles each. This represented one of the highest resolution work ever done on the subject. The computational load was shared between the LRZ and the computer facilities at the University of Zurich employing more than 3 millions cpu hours in total.

This first study [1] is now published on the Monthly Notice of the Royal Astronomical Society, one of the major journal in the field of astrophysics and it is now the standard reference for large simulations in WDM. A nice map of the density field in the different models is shown in figure 1.

After this first work we decided to concentrate our efforts in simulating single dark matter haloes similar to the one of our own galaxy (the Milky Way) with very high numerical resolution. The aim of this second stage of our project

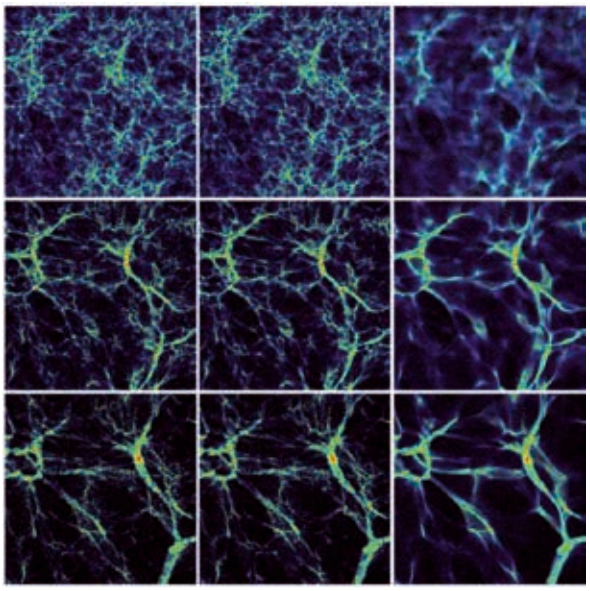

Figure 1: Density maps from the $N=1024^3$ particle simulations. Each box has a length of 50 Mpc and a depth of 2.5 Mpc. From left to righ, Cold DM, Warm Dark Matter with mass of 1 keV and 0.25 keV. Redshift changes from 0 to, 1 and 4 from top to bottom.

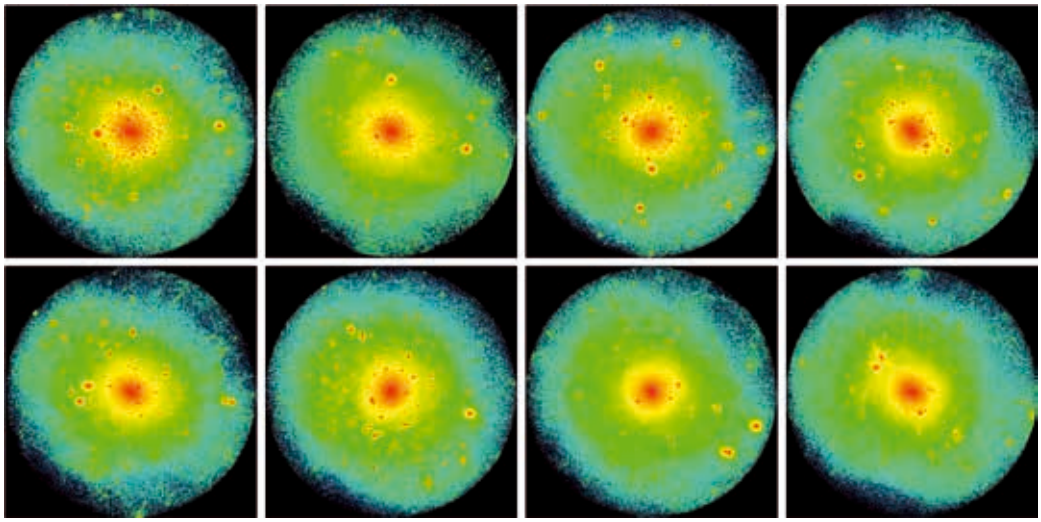

Figure 2: Projected density map of the high resolution realization of the dark matter halo of a Milky way like galaxy. The top left picture is for the CDM scenario, while the others are for different mixture of cold and warm dark matter. Each panel contains more than 10 millions resolution elements.

was to see whether cold and mixed (warm+cold) models could actually solve some of the problems faced by the standard cold dark matter paradigm at galactic scales.

For this second project we concentrated more than 50 millions of dark matter elements in one single dark matter halo, performing the highest resolution suite of simulations ever run in Warm and Mixed cosmologies. All together these simulations have used more than 15 millions CPU hours, most of them from the resources allocated to our project at the LRZ. Thanks to our extremely high spatial resolution we have been able to characterize the properties of the dark matter distribution with extremely high precision and at very small scales. In the first part of this second project we have used a combination of different observational data to learn about the nature of dark matter and the possible impact of a mixture of cold and warm components.

We have used three different direct constraints coming from observations of the Milky Way satellite population, namely the abundance of satellites, their radial distribution and the dark matter distribution within the satellites (coming from their internal kinematics). We have demonstrated in [2] that by combining all these different observational evidences we can obtain tight constraints on the nature of dark matter, and we made possible to rule out some scenarios that were previously proposed.

In a third publication [3] we have implemented new observational limits on the mass of the dark matter particle, recently obtained from analysis of the large scales structure of the Universes. We then ask ourselves the question if, when restricted to these limits, the Warm dark matter scenario was still to be preferred to the standard cold one. We have clearly demonstrated that this is not the case and that WDM does not perform better than CDM on small scales IF the new limits are correct. While more exotic models of Warm Dark Matter (e.g. models where the decoupling does not happen in thermal equilibrium) can still save the WDM scenario, a classical thermal approach to WDM does not provide any advantages with respect to Cold Dark Matter.

On-going Research / Outlook

Numerical simulations are at the present the best tools to unveil the nature of Dark Matter and to make clear and testable predictions on the distribution of DM within galaxies like our own Milky Way.
Thanks to the resources allocated to use by the LRZ we have made one of the first thorough analysis of the impact of a possible Warm Dark Matter component on the whole process of structure formation.

We have now pushed to the limits the capabilities of Nbody (pure gravitational) simulations and reached scales where the effects of gas dissipation and star formation start to be very significant.

We are ready now to move to the next step and to start to add the physics of gas and stars self consistently in our simulations. We plan to use the hydro-dynamical extension of the PKDGRAV code (called GASOLINE) to run a new series of simulations in both the cold and warm scenario in a forthcoming project (soon to be submitted for approval to the LRZ).

We hope that we will be able to achieve a self-consistent picture of galaxy formation, where dark matter, gas and stars all contribute to shape the properties of the galaxy we observe today.

References and Links

[1] Aurel Schneider, Robert Schmidt, Andrea V. Macciò and Ben Moore. 2012. Non-linear evolution of cosmological structures in warm dark matter models. MNRAS, 424, 684.

[2] Donnino Anderhalden, Aurel Schneider, Andrea V. Macciò, Juerg Diemand, Gianfranco Bertone. 2013.
Hints on the Nature of Dark Matter from the Properties of Milky Way Satellites. JCAP, 03, 014A.

[3] Aurel Schneider, Donnino Anderhalden, Andrea V. Macciò, Juerg Diemand. 2014. Warm dark matter does not do better than cold darkmatter in solving small-scale inconsistencies. MNRAS in press.

Magnetorotational Instability in Core-Collapse Supernovae

1

Research Institution
Max-Planck-Institut für Astrophysik

Principal Investigator
Ewald Müller

Researchers
Tomasz Rembiasz, Martin Obergaulinger, Pablo Cerdá-Durán

Project Partners
Universidad de Valencia

LRZ Project ID: pr58xi

Introduction

The possible influence of magnetic fields on the dynamics of core-collapse supernovae and the evolution of nascent proto-neutron stars is largely unknown. As pointed out by [1], one of the most promising agents amplifying the magnetic fields in a core-collapse supernova explosion is the magnetorotational instability (MRI) [2]. The MRI has been studied intensively in accretion disks where it excites turbulence and provides the effective viscosity required for the accretion of the gas. Nevertheless, the saturation level of the instability is still not fully understood. It was suggested that the MRI growth is terminated by secondary parasitic instabilities (Kelvin-Helmholtz and resistive tearing-mode instabilities) growing on top of MRI modes [3,4]. Hence, the saturation level of the MRI is determined by the interplay between the MRI and the parasites. Extending our previous set of local simulations [5], we study this interplay in three-dimensional, non-ideal magnetohydrodynamics (MHD) simulations. Our final goal is the formulation of a simple model connecting the initial magnetic field strength, the resistivity and the viscosity of matter with the termination and saturation of the MRI.

Results

Our (mostly) 3D and (some) 2D simulations are performed with a Newtonian grid based flux-conservative finite-volume MHD code Aenus written in Fortran 95. The code employs a domain decomposition method and is hybrid parallelized (MPI + OpenMP). It has an excellent weak MPI scaling and a very good OpenMP speed up on both the FAT and THIN nodes of the SuperMUC. The computational costs and the number of cores used depend on resolution. The smallest 3D simulations were performed with 320 CPUs and they required ≈ 3,000 CPUhs. The largest simulations on the FAT and THIN nodes were run with 4,096 (512 MPI x 8 OpenMP) and 16,384 (1024 MPI x 16 OpenMP) CPUs, respectively. The computational cost of the latter simulation is ≈ 1,800,000 CPUhs. In total, we have performed over fifty 3D simulations (not including additional auxiliary tests) for which ≈ 4,000,000

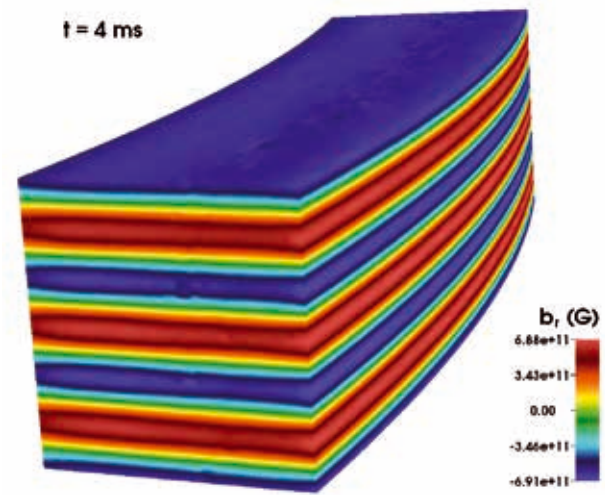

Figure 1: Radial component of the magnetic field in a 3D simulation performed in a box of a size 1 km x4 km x1 km in (r, φ, z) direction, respectively, and a resolution of 100 zones/km. 4 ms after introducing perturbations, three MRI channels are visible. The time evolution of the box aver- aged Maxwell stress component $|b_r b_\varphi|$ is shown in Fig. 4.

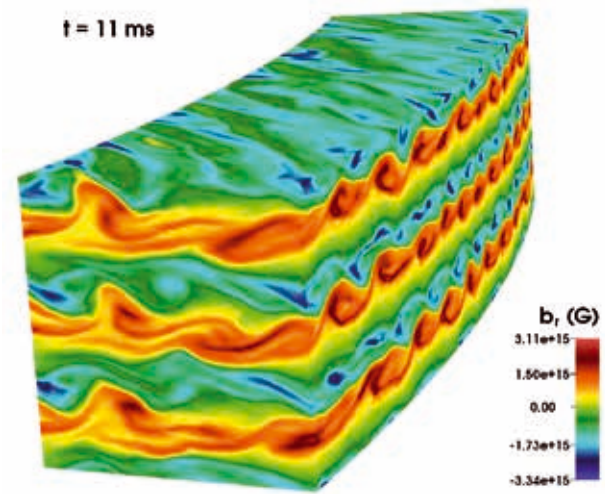

Figure 2: On top of the MRI channels shown in Fig.1, the Kelvin-Helmholtz instability develops.

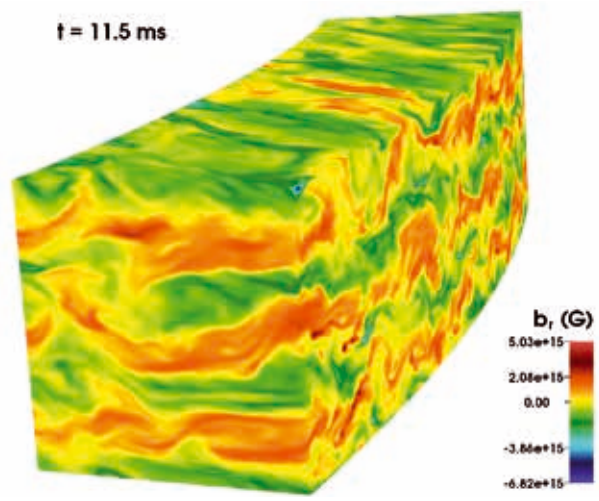

Figure 3: Kelvin-Helmholtz instability disrupts the MRI channels and the turbulent phase sets in.

CPUhs were used. Over 810,000 files and directories were generated, which occupy 3.8 TB in our PROJECT directory.

Our 3D simulations confirm that the MRI in core-collapse supernovae is terminated by the Kelvin-Helmholtz instability (see Figures 1-3). In 2D simulations, because of the assumed axial symmetry, this secondary instability cannot develop and the MRI growth is terminated by more slowly developing tearing modes. As a result, MRI-driven magnetic field amplification is overestimated (see Fig. 5). We conclude that the MRI termination process can be properly studied bonly in 3D simulations.

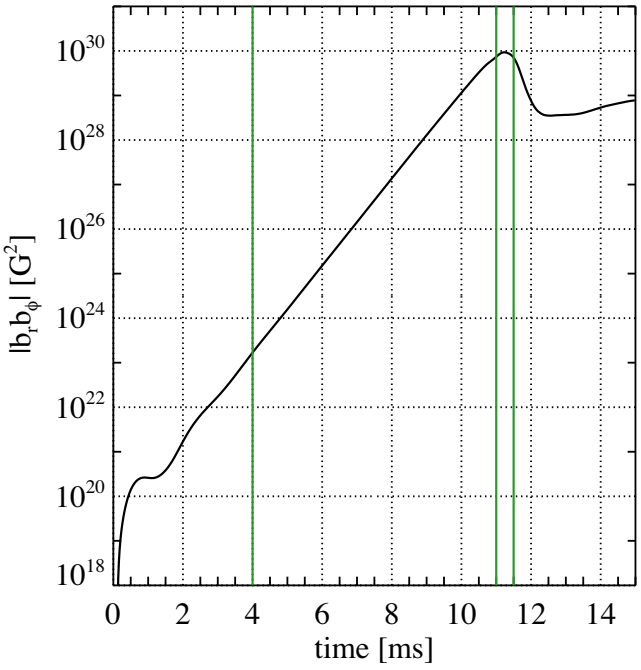

Figure 4: Time evolution of the box averaged Maxwell stress component $|b_r b_\varphi|$ in the simulation presented in Figs. 1-3. From ≈2 ms to ≈10 ms, the MRI is fully operational and the magnetic field is amplified exponentially. At ≈11 ms, the MRI is terminated by the Kelvin-Helmholtz instability and the turbulent phase sets in. The green vertical lines indicate the times at which the snapshots in Figs. 1-3 are taken.

The 3D simulation results also allowed us to formulate a hypothesis on the dependence of the MRI termination amplitude on the initial magnetic field strength. Should our hypothesis be true, we will be able to give an upper limit on the magnetic field amplification by MRI in core-collapse supernovae – a very interesting result for the whole supernova community.

On-going Research

We are still running additional simulations, which will help us to verify our hypothesis. The estimated computational cost is ≈ 3,000,000 CPUhs (we were granted this extra time in January 2014).

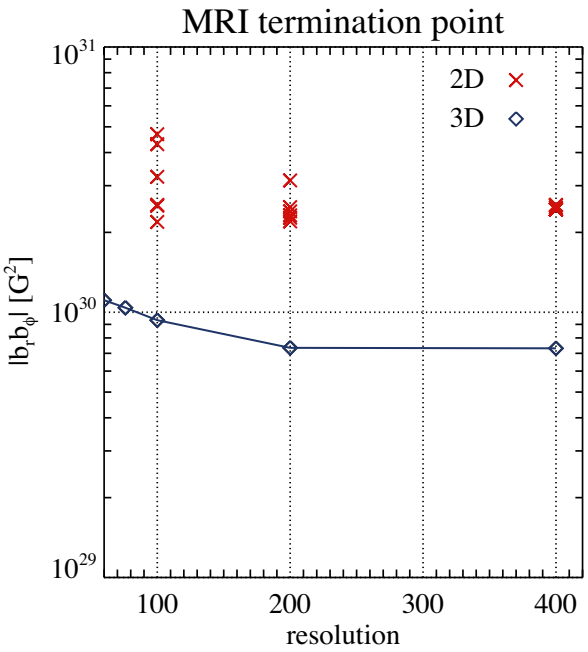

Figure 5: Box averaged Maxwell stress component $|b_r b_\varphi|$ at MRI termination in 2D (red crosses) and 3D (blue diamonds) simulations. The abscissa gives the number of grid zones per kilometer.

Simulations performed on the FAT nodes in the period from April 2012 to February 2013 would randomly crash when more than 10 OpenMP threads per MPI process were used. This issue was reported to the LRZ computational support. However, despite our joint efforts, this problem was not solved (until February 2013). We do not know whether after recent software/hardware updates, the problem is still there, because currently we are using only the THIN nodes, where such crashes do not occur. Because our simulation require very high resolutions and many iterations, they can be performed only on large supercomputers such as SuperMUC. We would like to thank the LRZ for the good cooperation.

References and Links

[1] Akiyama, S., Wheeler, J. C., Meier, D. L., & Lichtenstadt, I., Astrophys. J., 584 (2003), 954
[2] Balbus, S. A. & Hawley, J. F., 1991, Astrophys. J., 376 (1998), 214
[3] Goodman, J. & Xu, G., Astrophys. J., 432 (1994), 213
[4] Pessah, M. E. 2010, Astrophys. J., 716 (2010), 1012
[5] Obergaulinger, M., Cerdá-Durán, P., Müller, E., & Aloy, M. A., Atron. Astrophys., 498 (2009), 241

Molecular Cloud Evolution Driven by Colliding Streams with Feedback

1

Research Institution
Hamburger Sternwarte, Universität Hamburg

Principal Investigator
Bastian Körtgen

Researchers
Robi Banerjee, Daniel Seifried

Project Partners
–

LRZ Project ID: pr85ga

Introduction

Stars form within the densest regions of the interstellar medium (ISM), namely molecular clouds, due to the gravitational collapse of unstable clumps and cores. During their lifetime they reinject energy and momentum in the form of radiation and stellar winds into the surrounding medium. These feedback processes are known to be a main agent in controlling the star formation process and its efficiency. Especially the high mass end of the stellar distribution function is of great importance to understand the star formation within galaxies and molecular clouds, since it is these stars that create huge bubbles of hot, ionised gas and finally end their (short) lives with a powerful explosion, known as supernova. During a supernova, a huge amount of energy is injected into the surrounding ISM, within only a short amount of time.

Since turbulence and magnetic fields control the formation and evolution of molecular clouds, especially in the first stages prior to star formation, localised gravitational collapse can induce the formation of massive stars in a still globally contracting cloud. Thus, massive stars should influence their birthplaces in a strong fashion as soon as they are born.

Here, we investigate the question, whether the feedback from supernova explosions alone is able to disperse or even disrupt entire molecular clouds. Further, we aim at understanding how the feedback influences the dynamics of the gas and how the star formation process proceeds after the first massive stars have exploded.

Results

The molecular cloud is formed by the compression of two converging flows of warm, neutral interstellar matter, which undergo thermal instability and thus condense into a cold, dense phase [1]. The dense phase is embedded in a warm, diffuse component, and is restricted to a gravitationally bound and pressure confined filamentary network. The filaments contain clumps and cores, which

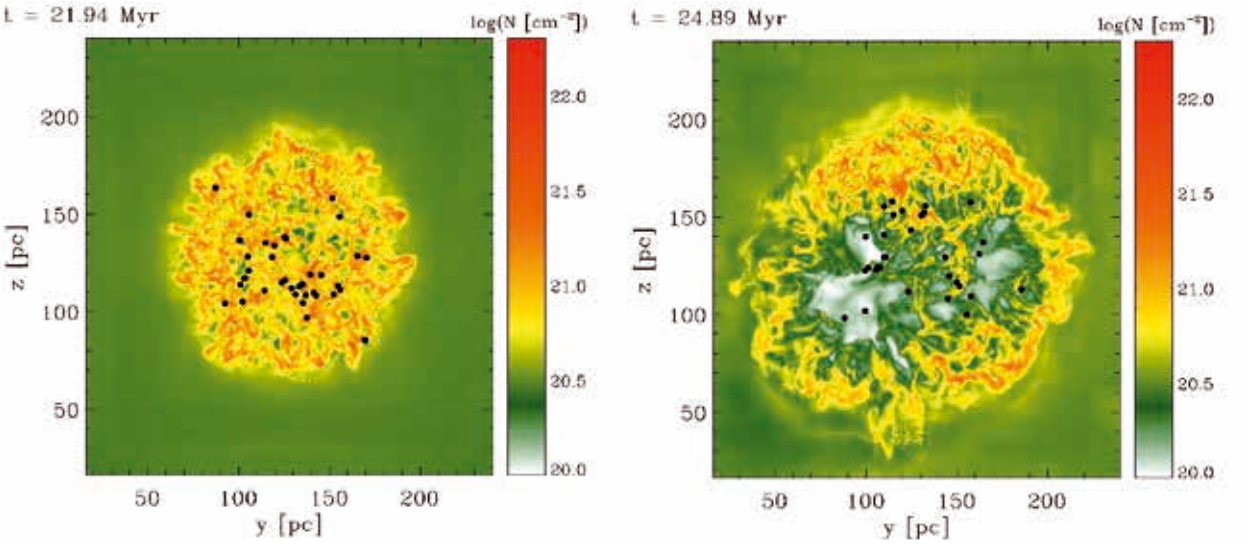

Figure 1: Face on view of the molecular cloud. Left: Simulation without feedback. Right: The same setup including supernovae feedback. At the time shown in the right panel, already two stars have exploded in a violent event, thereby shaping the major parts of the molecular cloud by disintegrating the inner regions.

are prone to gravitational collapse and subsequently the formation of stars (denoted by the black dots). These stars can then feed back onto the surrounding clump and the whole cloud by means of supernova explosions. Fig. 1 shows the column density along the flows, i.e. perpendicular to the collision plane. The left panel shows the control run with no stellar feedback. Stars form in the densest regions within the molecular cloud, which is globally in a state of collapse. If massive stars form, they can go off as a supernova (see fig.1, right). The injection of energy heats and accelerates the surrounding gas and the inner regions of the cloud are being dispersed. At the time shown, two massive stars have exploded. The shock waves travel through the whole cloud medium and finally reach the regions of the warm neutral medium. Since the shocks evacuate the inner regions of the molecular cloud, where most of the stars are residing, the accretion rates are decreased by orders of magnitude, giving rise to large groups of low-mass stars.

The temporal evolution of the cloud's mass, as well as the total stellar mass is shown in fig. 2. The masses grow with time due to accretion from the immediate environment. As soon as stellar feedback is initiated, the supernovae expel the gas, yielding a strong decrease in the total cloud mass. The resulting molecular cloud now contains only roughly 1/3 of its initial mass and its shape becomes arc-like.

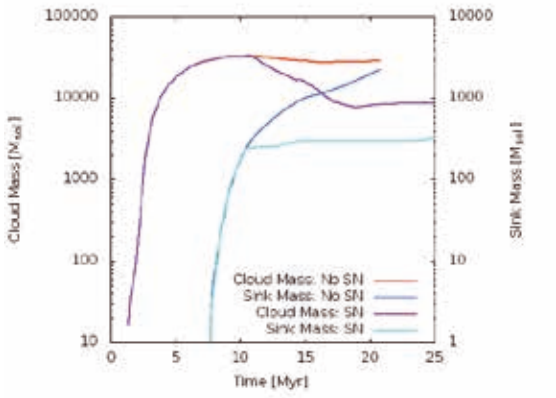

Figure 2: Cloud mass (red, purple) and total stellar mass (blue, cyan) as function of time. As supernovae go off, the cloud is disrupted and its mass decreases by roughly a factor of three.

During the supernovae 65% of the energy is released in the form of thermal energy, according to the Sedov-Taylor blastwave solution. This gives rise to strong thermal pressures within the supernova bubble (in addition to the kinetic motions), which further drive the remnant until the remnant cooled down sufficiently due to adiabatic expansion and radiative cooling. The evolution of the temperature in the midplane is shown in fig. 3. The filaments are embedded in a diffuse, warm gas and become even colder as time advances due to efficient cooling. The supernovae then heat the gas, where the less dense regions are subject to more efficient heating. The denser filaments and clumps are initially compressed by the shock wave and then dispersed as these waves strongly interact with the inter-filament and inter-clump media. As soon as the blastwaves from the supernovae reach the regions surrounding the molecular cloud, they are shock heated and compressed. This, in turn, enables very efficient cooling, which leads to overcooled and slightly overdense regions in the post-shock regions.

Since the shock speed depends on the density of the medium it travels through, different regions are affected at different times, yielding a very inhomogeneous temperature distribution. In the end of the simulation, the molecular cloud with its dense, cold regions is replaced by a hot, diffuse phase which is more likely to be a typical non-star forming region of the ISM, where gravitational interactions are negligible. Only a few 'cloudlets' are left, which look quite similar to isolated objects like Bok globules, immersed in a tenuous gas.

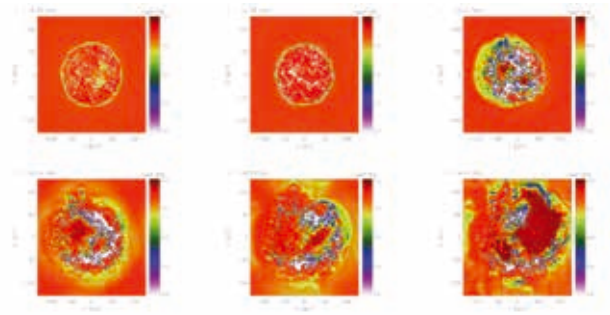

Figure 3: Temporal evolution of the temperature in the midplane, i.e. the plane where the two flows initially collide. The molecular cloud complex is entirely disrupted by the feedback from the massive stars. Note that the shock compression initiate overcooling of the compressed ISM, as seen in the outer parts of the domain. Maximum temperatures can reach millions of Kelvin and thus hypersonic

On-going Research / Outlook

The results shown here were quite unexpected and look very promising. Our on-going research therefore focuses on the influence of different initial conditions. We vary the initial velocity of the two colliding streams, as well as the magnitude of the turbulent fluctuations. Varying initial magnetic field strengths will help us to approach more realistic scenarios and to probably match observations.

Preliminary case studies show that the fate of molecular clouds seems to be the entire disruption by massive star feedback. The difference lies, at the moment, only in the time when the feedback occurs and its subsequent duration, since it is closely linked to the star formation rate in the parental cloud.

Finally we seek to increase the numerical resolution by a few refinement levels to resolve small scale structures in greater detail. The outcome of this study will also help to assess, how interstellar turbulence may be driven – either solenoidal or compressive.

References and Links

[1] Vazquez-Semadeni E., Gomez G. C., Jappsen A. K., Ballesteros-Paredes J., Gonzalez R. F., Klessen R. S., 2007, ApJ, 657

1 Forming disk galaxies in magneto-hydro-dynamical simulations of the Universe

Research Institution
Heidelberg Institute for Theoretical Studies

Principal Investigator
Volker Springel

Researchers
Rüdiger Pakmor, Federico Marinacci, Mark Vogelsberger, and further collaborators

Project Partners
Institute for Theory and Computation, Harvard-Smithsonian Center for Astrophysics

LRZ Project ID: pr85je (Gauss Large Scale project)

Introduction

Our Universe is permeated with magnetic fields – they are found on the Earth, in and around the Sun, as well as in our home galaxy, the Milky Way. Often the magnetic fields are quite weak: for example, the magnetic field on Earth is not strong enough to decisively influence the weather on our planet. In galaxies like the Milky Way, the field is however so strong that its pressure on the interstellar gas in the galactic disc is of about the same size as the gas thermal pressure. Astrophysicists hence conclude that magnetic fields could play an important role here although their origin still remains mysterious. Current hypotheses argue that they either already existed directly after the Big Bang and were then greatly amplified with time, or that the field was produced by the first stars and has then been dispersed in the Galaxy.

In principle, computer simulations that follow the formation and evolution of galaxies starting at the Big Bang ought to be able to answer these questions. However, they have thus far mostly failed because the predicted galaxies did not agree with astronomical observations. In fact, the formation of disk galaxies has long been a puzzling conundrum for cosmologists: computer simulations produced typically far too massive and too small disks, a problem that persisted for decades. Also, the simulations have not been able to follow the dynamics of magnetic fields within the full cosmological context. Treating the latter is mathematically and numerically considerably more challenging than the plain gas dynamics, which has typically been employed for computing galaxies so far.

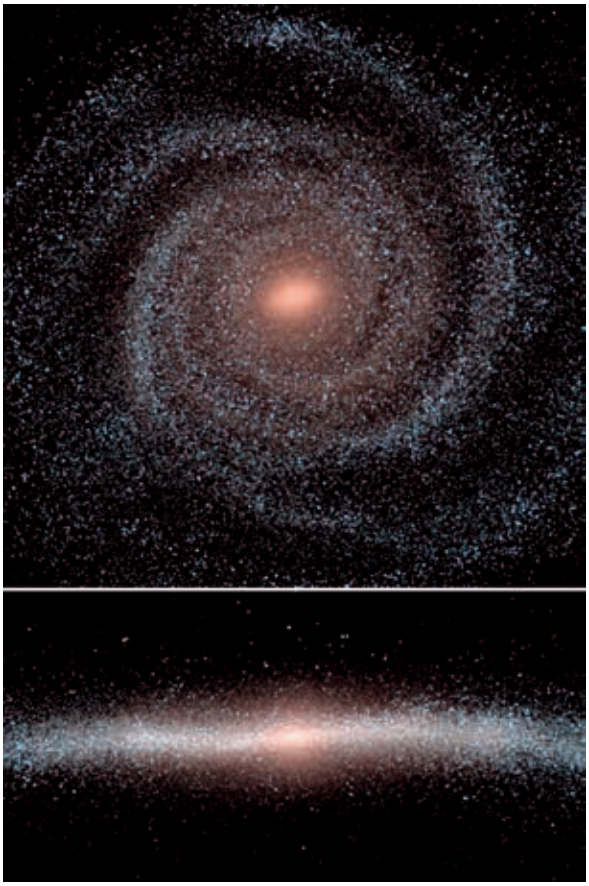

Figure 1: Stellar structure of a Milky Way-like galaxy formed in one of our magneto-hydrodynamical cosmological simulations after 13 billion years of evolution. The face-on projection on top nicely reveals spiral structure in the disk.

Results

Within our project pr85je on SuperMUC, we use the massively parallel simulation code AREPO, developed at the Heidelberg Institute for Theoretical Studies, to study galaxy formation within a fully cosmological setting, using a comprehensive treatment of the physics and much higher numerical resolution than ever used before. AREPO is a so-called „moving mesh code". What distinguishes it form other astrophysical codes is that AREPO does not partition the simulated universe with a fixed mesh but rather uses a movable and deformable mesh, which allows a particularly accurate processing of the vastly different size and mass scales occurring in individual galaxies. Thanks to the very low advection errors of the method, it is particularly well suited to the

highly supersonic flows occurring in cosmology, and to treating subsonic turbulence within the gas of virialized halos. These properties make it superior to smoothed particle hydrodynamics and adaptive mesh refinement codes that use a stationary Cartesian mesh. AREPO also follows the dynamics of dark matter with high accuracy, as required to compute cosmic structure growth far into the non-linear regime.

In our recent work, we have succeeded in including additional physical processes such as magnetic fields in the simulations, thereby improving them in a decisive way. In fact, with the help of our novel numerical methods and the progress on parallelization achieved, we could leverage the power of SuperMUC to form a virtual galaxy that closely resembles our own Milky Way. It has the right stellar mass for its dark matter halo mass of about 1012 solar masses, forms a disk of the right scale length, and the relation between mean age of stars and the total stellar mass of the disk is consistent with observations, too. Also, the predicted content of metals in the gas synthesized in stars and stellar explosions is consistent with observational data. This represents a major success over previous attempts to form disk galaxies, and demonstrates that the futile attempts in the past to do so were not due to an inherent flaw of the underlying cosmological ΛCDM paradigm.

In addition, we were for the first time able to predict the expected structure of the magnetic field in a spiral galaxy directly from the initial conditions left behind after the hot Big Bang. It turns out that already an extremely tiny magnetic field left behind by the Big Bang is sufficient to explain the orders of magnitude larger field strengths observed today. We were able to show that the magnetic field first grows exponentially for about 1 billion years due to gas motions in the early Universe, before the field reaches a stationary average value that is independent of its initial strength at the beginning. Once the first disk galaxies have formed (ca. 2.5 billion years after the Big Bang), the rotational motion of the disk further amplifies the field linearly with time, yielding field strengths at the micro-Gauss level. The revolving flow of the gas in the disk also pulls the magnetic field lines and directs them tangentially along this motion. Interestingly, the magnetic field strength found in the simulation does not only agree very well with the values measured for the Milky Way and neighboring galaxies, it also reproduces the observed vertical and horizontal profiles. This is remarkable given that there are no free parameters that could be tuned to influence the final field strength.

The successful formation of disk galaxies with a small bulge-to-disk ratio constitutes a long sought breakthrough in the intricate problem of the formation of galaxies in hydrodynamical cosmological simulations. It is fascinating that this can at the same time explain the formation of typical magnetic field found in galaxies like the Milky Way. These findings also promise to help in understanding the deflection of cosmic ray particles in the magnetic field of the Milky Way, and in providing clues for tracking down the sources of these particles, which is still an unsolved problem in observational astronomy.

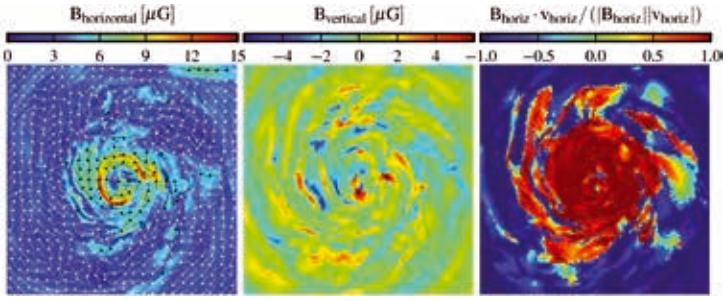

Figure 2: Structure of the magnetic field in one of our simulated Milky Way-sized galaxies. The left and center panels show the strength of different components of the magnetic field. The right panel shows the pitch angle, illustrating that the field develops a large-scale orientation in the disk where it is aligned with the rotational motion.

On-going research

SuperMUC has played a decisive role in making the present simulations possible. Within our project, we are currently working on substantially scaling up the numerical resolution and dynamic range achieved in our simulations of the formation of Milky Way-sized galaxies, thereby allowing a treatment of the small-scale physics that is more faithful to the processes of the interstellar medium than possible in past work. In particular, we aim to carry out the first cosmological hydrodynamic simulation of galaxy formation with more than one billion resolution elements within the virialized region of a single Milky Way-sized halo, thereby advancing the state-of-the-art by about two orders of magnitude. The resulting Milky Way models will contain more than 100 million star particles alone. This should facilitate predictions of transformative quality for the stellar and metallicity structure of the disk, and the bulge and halo components.

For example, previous isolated galaxy models had problems to reproduce the long-lived spiral arms that rotate about the Galaxy with a constant pattern speed. Instead, spiral arms in previous simulation models appear to be very short-lived transient features that co-rotate with the stars. Evidence against density wave theory has also been presented in several extragalactic observational works that report that the spiral arms rotate with radially decreasing pattern speed. Therefore, the time has come to reassess how spiral arms form. Our currently prepared high-resolution cosmological simulations of the Milky Way's formation will have for the first time a large enough number of star particles in their disks to allow these questions to be meaningfully studied within a proper cosmological setting.

References and Links

[1] V. Springel, MNRAS 411 (2010) 1525
[2] R. Pakmor, F. Marinacci, V. Springel, ApJL 783 (2014) L20
[3] F. Marinacci, R. Pakmor, V. Springel, MNRAS 437 (2014) 1750
[4] R. Pakmor, V. Springel, MNRAS 432 (2013) 176
[5] M. Vogelsberger, S. Genel, D. Sijacki, P. Torrey, V. Springel, L. Hernquist, MNRAS 436 (2013) 3031

http://www.h-its.org/english/press/pressreleases.php – *A Milky Way out of the Supercomputer*
http://www.cfa.harvard.edu/itc/research/movingmeshcosmology
http://www.mpa-garching.mpg.de/~volker/arepo

Transport of energetic particles in the heliosphere

1

Research Institution
Julius-Maximilians-Universität Würzburg

Principal Investigator
Cedric Schreiner

Researchers
Felix Spanier

Project Partners
North-West University Potchefstroom

LRZ Project ID: pr85li

Introduction

Although the Sun has been subject to scientific studies over centuries, there are still many open questions concerning the properties of the Sun itself and the mechanisms related to it and the space around it – the so-called heliosphere. One topic that has come up mostly in recent years is the research on the dynamics of the solar wind. Especially the acceleration and transport characteristics of extremely energetic charged particles in the solar wind are of major interest. The detection of such particles can often be related to space storms, which present a threat to the ever increasing number of satellites circling Earth. It is, therefore, important to understand the mechanisms, which lead to space storms and to be able to model the transport of fast particles to predict the effects of such energetic events.

Figure 1 depicts the way of energetic particles from their source to the observer: Particles are originating at the Sun (a) and accelerated in coronal mass ejections (CMEs) (b). These large scale structures reach out into the solar wind and create shock fronts, where a few particles are accelerated to relativistic speeds (c). On its way through interplanetary space the solar wind becomes turbulent and electromagnetic radiation is emitted (d). While the dynamics of the solar wind as a whole can be described magneto-hydrodynamically, the transport of single, energetic particles (e) has to be analyzed on microscopic scales. However, direct measurements can only be attempted close to Earth (f) and it is impossible to track the particles during their long journey.

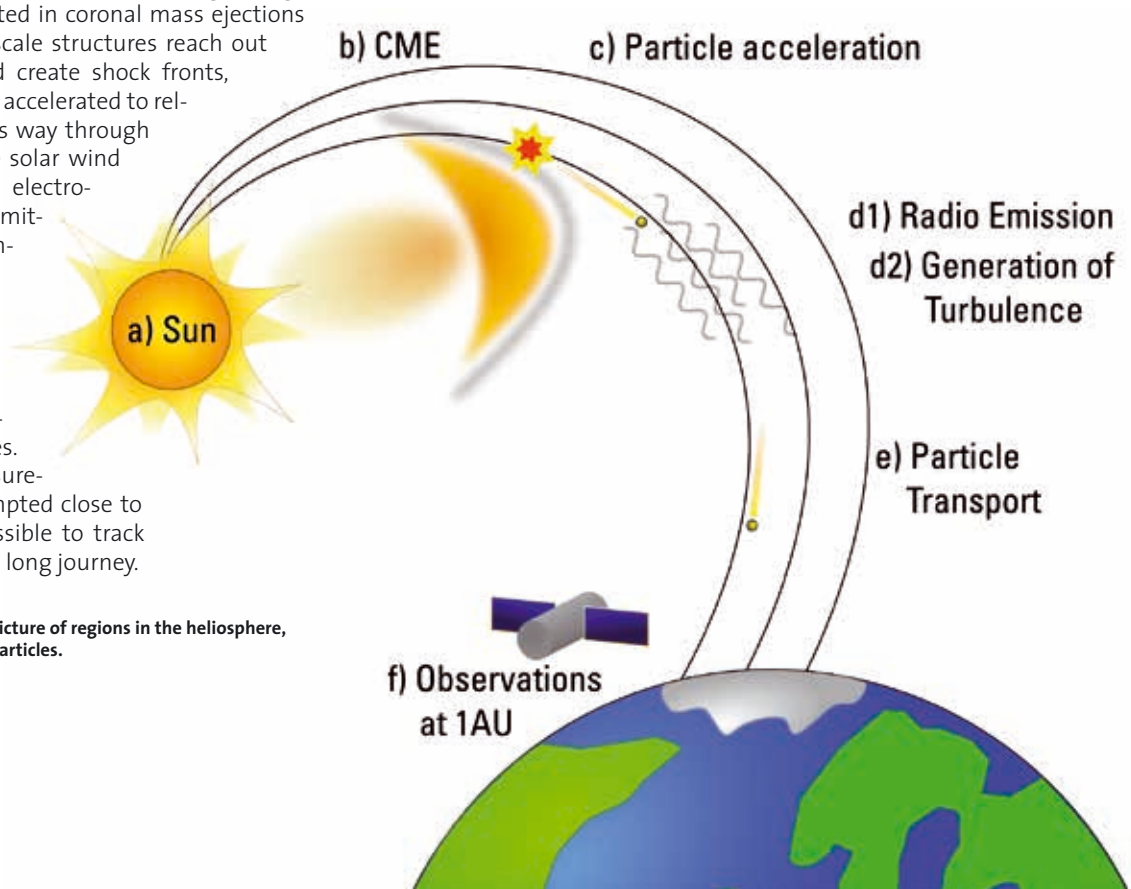

Figure 1: Schematic large scale picture of regions in the heliosphere, which are related to energetic particles.

The missing possibility of in-situ measurements has brought forth a whole discipline of astrophysical studies using numerical models to describe the heliosphere and the plasma within it. However, none of these models can describe all aspects at once and different numerical approaches have to be chosen for different physical problems.

With our project pr85li we aim at a better understanding of the micro-physical properties of particle transport in the heliosphere. Looking at the large scale picture in figure 1 again, that means that we are modeling a small fraction of region (e), where we simulate the solar wind plasma by means of a kinetic particle-in-cell (PIC) approach.

PIC codes – such as our code ACRONYM – basically reproduce plasma behavior by modeling the interaction of single particles with electromagnetic fields and yield high

resolution of micro-physical processes in both time and space. Particles can be tracked separately throughout the simulation, which makes it possible to resolve their trajectories.

Using a basic model for the solar wind, consisting of a small number of highly energetic test particles moving through a thermal background plasma, PIC simulations allow new insights into the transport characteristics of charged particles moving at relativistic speeds.

The huge drawback of PIC simulations is that the high resolution of micro-physical processes comes at the cost of a large amount of computational effort. In order to be able to model particle transport as described above, both the microscopic scales of single particle motion and the relatively large scales of magnetic field fluctuations and plasma waves have to be resolved – again in both time and space. PIC simulations are, therefore, bound to very small time steps and grid cells, but have to describe time intervals and spatial volumes much larger than these basic numerical units. This results in simulation setups with up to half a million time steps and a few hundred to a few thousand grid cells in each of the three spatial dimensions.

The computational effort for such simulations can only be met by supercomputers, such as SuperMUC.

Results

Our explicit PIC code ACRONYM is fully relativistic, parallelized and three-dimensional [1] and it proved to be well suited for the use on SuperMUC. First tests suggested that the performance of the code scales well with the number of CPUs used in a simulation. In fact, we were able to run our code efficiently on up to 16384 CPUs. So far, the main effort we were engaged in were parameter studies, where we ran simulations with different problem sizes and physical parameters. A typical amount of CPUs, CPU-hours or storage and RAM usage per job is, therefore, not applicable here. Job sizes and durations lay between 30,000 CPU-hours on 2048 cores with about 170 GB of RAM required and 1.5 million CPU-hours on 16384 cores with about 500 GB of RAM.

Beside these purely technical numbers, our simulations contained up to 83 million grid cells including more than 1.4 billion simulated particles. For our analysis of particle transport we tracked the positions and velocities of 1.2 to 80 million test particles, depending on the individual problem size.

The physical results obtained so far serve as a proof of concept, showing that PIC simulations are capable of modeling the interaction of fast particles with the electromagnetic fields of waves in a thermal background plasma, which leads to typical transport characteristics.

In order to validate our findings we reproduced the setup used in MHD simulations, which deal with the same physical problem [2]. Comparing the results produced by the two different numerical approaches, we find consistency in the outcome of both. Although a PIC simulation requires a larger amount of computing time compared to an equivalent MHD simulation, there are certain advantages of the new approach. The most important one is that PIC simulations can be applied to a wider range of physical parameters, allowing the probing of physically possible setups, which simply do not have an MHD equivalent. Such situations occur, when energetic particles interact with dispersive wave modes, such as Whistler modes. Since the MHD approach can only access the dispersionless regime of low frequency Alfvén waves, the transport of fast electrons for example, which interact with Whistlers, cannot be studied in an MHD model.

Until now we have not run any jobs modeling this specific case, but again we could establish a proof of concept with one of our simulations, which includes a dispersive wave that interacts with test particles.

Parallel to our simulation runs on SuperMUC we have repeated each run in two-dimensional and one-dimensional setups, using a modified version of the ACRONYM code. In this version, electromagnetic field vectors and particle velocities are still treated as three-dimensional vectors, but the spatial coordinates are reduced. This is a common technique used with PIC codes to reduce the computational effort for the simulations. While in some cases a reduction of spatial dimensions does not lead to major defects in the physical processes modeled in the simulation, we have found that the interaction of fast particles with plasma waves has to be treated fully three dimensional. Although the interaction involved in the scattering process can theoretically be described as a two-dimensional problem, our simulations showed that certain artifacts will occur in low-dimensional simulations. This means that physically reliable results can only be obtained with computationally expensive three-dimensional PIC simulations.

On-going Research / Outlook

With most of our simulations being numerically very expensive, we were able to run only a few different setups. The overall conclusion we have drawn so far is that our code – or PIC codes in general – is suitable for studies of particle transport characteristics on a microscopic scale. However, simulation runs and physical setups have to be chosen carefully, in order not to waste computing time.
We are planning follow-up simulations, which will be run either within our current project pr85li or in a successional project. Especially the above mentioned scenario of electrons scattering off of Whistler modes will be a point of interest, since it is a relevant process in the solar wind.

References and Links

[1] P. Kilian, T. Burkart, F. Spanier, in: W. E. Nagel, D. B. Krner, M. M. Resch (Eds.), High Performance Computing in Science and Engineering '11, Springer, 2012, p. 5
[2] S. Lange, F. Spanier, M. Battarbee, R. Vainio, T. Laitinen, Astronomy and Astrophysics 553 (2013) A129

Our Neighbourhood in the Universe: From the First Stars to the Present Day

1

Research Institution
University of Sussex

Principal Investigator
Ilian Iliev

Researchers
Stefan Gottloeber, Gustavo Yepes, Garrelt Mellema, Keri Dixon,Paul Shapiro,Pierre Ocvirk,et al.

Project Partners
AIP Potsdam, UA Madrid, Stockholm University, University of Strasbourg, UTexas at Austin

LRZ Project ID: pr86be (PRACE project)

Introduction

Reionization is believed to be the outcome of the release of ionizing radiation by early galaxies. Due to the complex nature of the reionization process it is best studied through numerical simulations. Such simulations present considerable challenges. The tiny galaxies which are the dominant contributors of ionizing radiation must be resolved in volumes large enough to derive their numbers and clustering properties correctly. The ionization fronts expanding from these galaxies into the surrounding neutral medium must then be tracked with a 3D radiative transfer method. The combination of these requirements makes this problem a formidable computational task [1].

The aim of this project was to perform several beyond current state of the art constrained simulations of the cosmic structures in the neigbourhood of our Galaxy, the Milky Way and use the rich observational data available on them to study reionization. Our main goals are to: 1) simulate the complete star formation and galaxy formation history of our local volume, from the very First Stars to the present day; 2) derive the complete reionization history of the Local Group (the Milky Way, Andromeda and their satellite galaxies) with focus on internal (by own sources) vs. external (by nearby proto-clusters) scenarios and their observable consequences; 3) model in detail the effects of reionization on the number, distribution and star formation histories of the Local Group satellite galaxies and globular clusters; and 4) do cosmic archaeology: find the expected distribution of the surviving low-mass metal-free stars by tracking their parent halos to the present day. Our simulations are the first ever to achieve these goals, thereby are expected to result in significant breakthroughs in our understanding of the young Universe, unavailable by any other means.

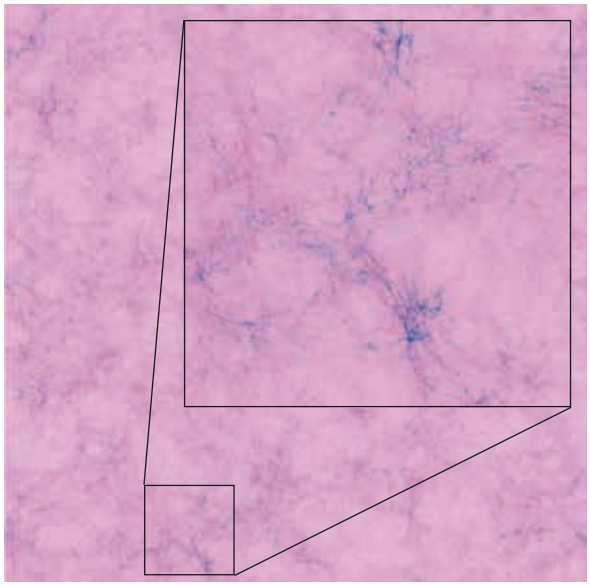

Figure 1: Our neighbourhood in the Universe, as reproduced by our high-resolution constrained-realization simulation with volume of 91 Mpc per side and 69 billion particles and (inset) zoom of a region 14 Mpc per side. Shown are the density of the cosmic web (pink) and the halos hosting the First Stars (blue).

Achieving this required performing some of the largest cosmological N-body simulations ever attempted, with up to 69 billion particles, based on a constrained realisation of the Gaussian field of initial density perturbations. This technique allows imposing available observational data as constraints on the initial conditions and thereby yielding large-scale structures which closely mimic the actual nearby universe. In particular, constrained simulations reproduce the key structures of the local cosmic web of structures like the Local Group, Virgo and Coma clusters with sizes and relative positions which closely resemble the actual ones [3]. We then used radiative transfer simulations to follow in detail the reionization of this volume. Preliminary work on this, based on lower-resolution simulations was done in [4].

Results

We have completed four structure formation N-body simulations, two at intermediate resolution (8.6 billion particles) and two at high-resolution (69 billion particles), all having the same volume of 91 Mpc per side. In each pair of simulations the first uses the special constrained initial conditions, and a second one with uncon-

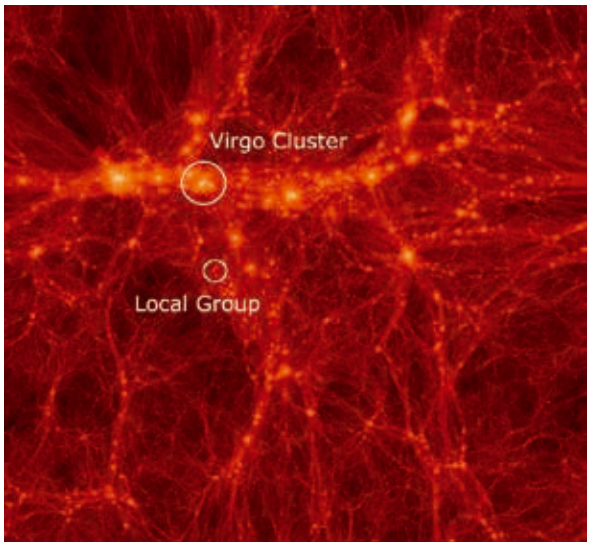

Figure 2: Cosmic Web of structures in the local neighbourhood at present (redshift zero). Indicated are the Local Group and theVirgo cluster of galaxies [2].

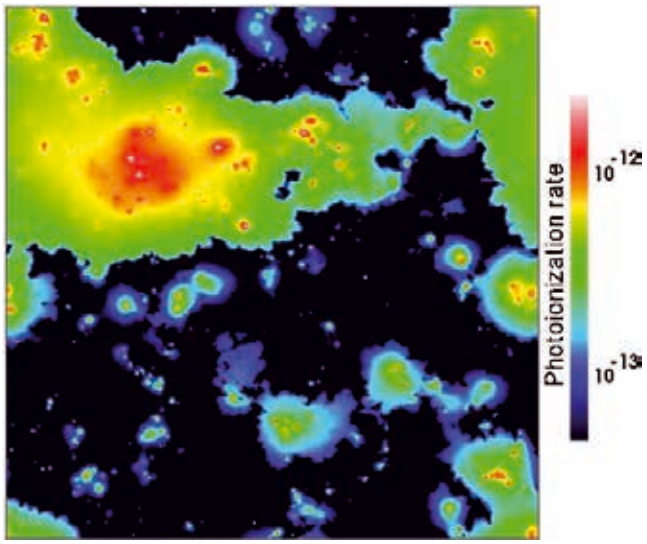

Figure 3: Photoionization rates distribution during reionization (redshift 6.7) from one of our radiative transfer simulations with 512^3 computing cells.The (proto) Virgo cluster reionizes significantly earlier than the progenitors of the Local Group.

strained, random-realization initial conditions. This approach is taken in order to enable detailed head-to-head comparison analysis of the differences between the constrained realization and a random one. Furthermore, by having two independent realizations of the Gaussian random noise initial conditions we double the number of objects of any given mass and thus significantly decrease the sampling variance of various statistical measures.

Based on this constrained-realization cosmic structure formation data we have completed a large series of radiative transfer simulations which allows us to study the effect of cosmic reionization in our neighbourhood. These simulations explore different models for the efficiency of star formation in dwarf galaxies and its suppression due to Jeans-mass filtering in the ionized regions. This allows us to address the problem of the effect of reionization on the satellite galaxies of the Local Group, by tracing our reionization results to the present (redshift z=0). The latter step will be done by matching our high-resolution high-redshift results to previously-completed lower-resolution runs which reach all the way to the present time. At lower redshifts our high resolution is no longer necessary since the reionization process rises the temperature of the intergalactic medium, thus the lowest-mass halos (minihalos and low-mass atomically-cooling halos) cannot infall gas and form stars. The same tracing of our reionization results to low redshift will be used for cosmic archaeology, as it will allow us to track any surviving First Stars to the present. Sample results from our reionization simulations are shown in Figure 3, with the corresponding present-day structures shown in Figure 2.

The simulations were ran on between 2,048 and 8,192 computing cores (N-body) and between 4,000 and 30,000 cores (radiative transfer). Each individual simulation required between few hundred thousand and few million computing core-hours to complete, for a total of the full 26 million core-hours awarded for our project. Overall, several hundred Terabytes of data were generated, subsequently reduced to few tens of Terabytes and stored off-site for further analysis.

On-going Research / Outlook

These simulation results allow us to study the 'memories' of reionization remaining in our Local Group, for comparison with observations. We are currently working on tracking the reionization history of different individual present-day structures by tracing their contents back in time. Separately, the simulations done at different resolutions need to be matched and halo merger trees build. We will then use these merger trees for semi-analytical modelling of the formation of galaxies in our volume through cosmic time.

During this project we had to overcome a number of software and code performance issues, which were mostly resolved satisfactorily with the help of LRZ staff, which allowed us to successfully complete our project. The planned future expansion/upgrade of SuperMUC could be very useful for our work, particularly if we manage to make good use of the planned Intel Phi multi-core co-processors. We are currently working on developing our codes to make effective use of this new architecture.

References and Links

[1] Iliev, I. T., Mellema, G., Ahn, K., Shapiro, P. R, Mao, Y., Pen, U.-L. "Simulating cosmic reionization: how large a volume is large enough?", 2014, MNRAS, 439, 725
[2] http://www.clues-project.org/
[3] Gottloeber, S., Hoffman, Y., Yepes,G., Constrained Local UniversE Simulations (CLUES) (arXiv:1005.2687)
[4] Iliev, I.T.,Moore, B., Gottloeber, S., Yepes,G., Hoffman, Y., Mellema, G. "Reionization of the Local Group", 2010, MNRAS, 413, 2093

1 Evolution of the corona above an emerging active region

Research Institution
Max Planck Institute for Solar system research

Principal Investigator
Hardi Peter

Researchers
Sven Bingert, Feng Chen

Project Partners
–

LRZ Project ID: pr86bi (PRACE project)

Introduction

he corona is the hot and dynamic outer atmosphere of the sun seen brilliantly during solar eclipses. Since it became clear in the 1940s that the corona consists of dilute million K hot plasma, the question what heats the corona is one of the most intriguing problems in (stellar) astrophysics. When observed in X-rays of the extreme UV (EUV), the corona is dominated by stunning loops that follow the magnetic field like iron filings around a magnet. While numerous theoretical concepts exist to explain the hot temperatures of coronae, only few numerical experiments have been conducted to test these suggestions in a realistically complex three-dimensional and time-dependent model of the corona. These are three dimensional magnetohydrodynamical (3D MHD) models that solve an induction equation for the magnetic field together with the mass, momentum and energy balance.

With the help of the numerical simulations on SuperMUC we could conduct the first experiment to see how the corona above an emerging active region on the Sun does evolve. In this process new magnetic field rises from the solar interior through the solar surface to form the sunspots. The strong magnetic field in these, up to 0.3T, emerges into the corona and forms the basis for the coronal structures that appear. Graphically speaking, in our models motions at the surface braid magnetic field-lines. This induces currents in the upper atmosphere, which are dissipated and subsequently heat the plasma. Based on the results of the 3D numerical models run on SuperMUC, we synthesize the coronal emission that would emerge from the computational domain and compare this with actual EUV observations from space-based solar observatories.

With this model we could produce a realistically evolving corona above an emerging active region and could pinpoint the energy source and transport that leads to the appearance of the coronal loops. This provides a major step forward in our understanding what determines the structure, dynamics and heating of the solar corona.

Results

Model setup
We couple our numerical experiment to another simulation that described the rise of magnetic flux through the interior until it appears at the surface, forming a pair of sunspots [1]. We extracted four horizontal layers near the surface of the flux emergence model and use these as a time-dependent bottom boundary of our coronal model. Consequently, the coronal dynamics is driven by the flux emergence process.

We conducted two major simulations. The first was a low-resolution preparatory run, which resolved a 147x74x74 Mm^3 domain with a 256x128x256 grid. The horizontal grid spacing is about 600 km, which is not really sufficient to resolve the small-scale magnetic fields and convective motions near the surface. The second simulation is the high-resolution run based on the same model setup but with four times the grid points in each horizontal dimension. With a 150 km grid spacing, we can now resolve the small-scale structures near the surface, which are important for the energy input and structuring of the corona. The preparatory run was considered as a test only, but turned out to produce valuable scientific results.

Numerical methods
Both numerical experiments are done using the Pencil Code [2], which uses a 6th order finite difference scheme for spatial derivatives and a 3rd order Runge-Kutta scheme for the time integration. We typically used 256 cores for the setup of the preparatory run, and 4096 cores for the high-resolution run. At the end of the project, we consumed 8.6 million CPU-hours to finish the preparatory run after about 7 hours solar time and to evolve the high-resolution run for about 1.5 solar hours. We finally generated more than 2 TB of data. We will further advance the high-resolution run in a new project accepted by PRACE.

Coronal loops forming with an active region
In our numerical experiment coronal loops start to appear self-consistently after the appearance of the sun-

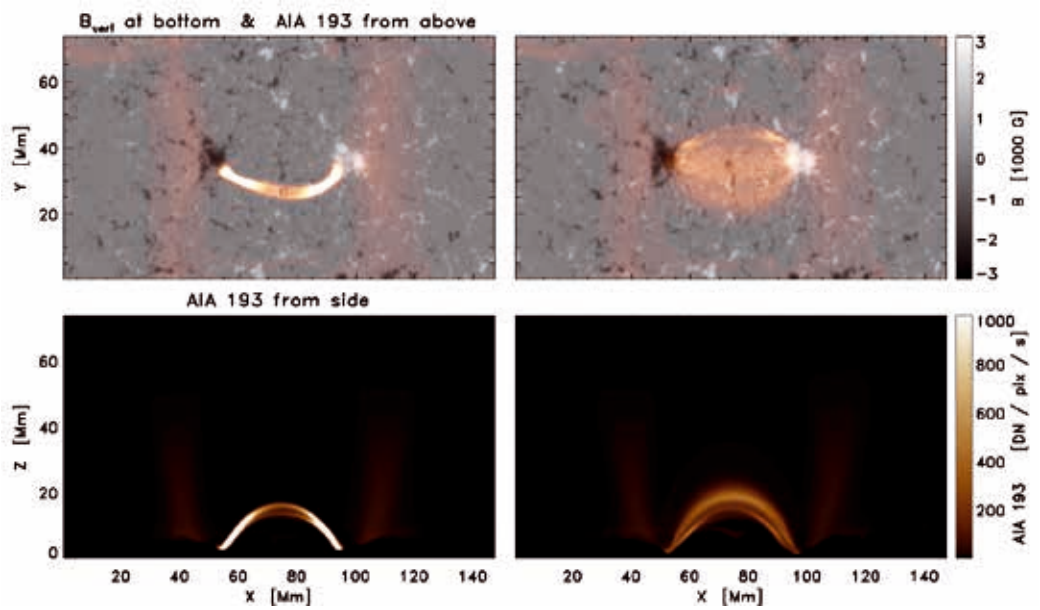

Figure 1: Evolution of synthesized coronal emission and magnetic field in the preparatory run. The top panels show the vertical magentic field in the photosphere, overlaid with the synthesized coronal emission as it would be seen in the 193 Å channel of the Atmospheric Imaging Assembly (AIA) on NASA's Solar Dynamics Observatory (SDO). This mainly shows plasma at temperatures of about 1.5 MK. The bottom panels show synthesized 193 Å images as seen from the side along the y direction. The synthetic emission is integrated along the line of sight, comparable to what is seen at disk center (top) or at the limb (bottom). The left column shows the situation when the loop forms, the right column displays a state 20 minutes later when the active region has fully formed. From [3].

spots at the surface. At one footpoint of the loop at the solar surface we find an upward-directed Poynting flux, i.e., a flux of (electro-)magnetic energy up into the loop. We found that the magnetic disturbances then propagate along the magnetic fieldlines with Alfvén speed and reach after about half a minute the other side of the loop. This finally triggers an energy flux into the corona on the other side of the loop, too. In addition to this, the emerging magnetic field interacts with the weak pre-existing coronal magnetic field. The resulting currents are dissipated and add significantly to the energy input into the emerging loops. The plasma gets heated to a million K and the loop appears bright in the synthesized EUV emission (see left panels of Fig. 1). This provides us with a self-consistent description on how and why emerging loops seen in EUV and X-rays do form [3].

During its further evolution the loop fragments, or more precisely, the coronal emission gets weaker along some fieldlines and brighter along others (right panels of Fig. 1). This is driven by the near-surface convective motions that shuffle around the footpoints of the fieldlines: the location of increased currents changes in time and thus different areas light up in sequence. This apparent fragmentation is of high interest to interpret the constantly evolving structures observed in solar EUV and X-ray observations.

The high-resolution run shows a much finer structure and more dynamics than the preparatory run, just as expected (see Fig. 2). Turning to a more detailed analysis of the high resolution run reveals not only more details, but also new physical effects, such as oscillations of loops. These await an investigation to check and improve the interpretation of observations of the Sun.

On-going Research / Outlook

Without the use of high-performance computing facilities these results would not have been possible. It is only now that three-dimensional models allow us to study coronal loops embedded in a magnetically complex environment that brings us closer to an understanding of the heating, structure and dynamics of the solar corona. We expect more of this interaction in the later stages of the evolution high-resolution run, which is supported in a new PRACE project. Future work will include the investigation of other solar structures of various levels of solar activity. Pushing the simulations to a the activity level of more active stars will lead to a better understanding of the relationship between coronal emission and stellar activity in a more general context.

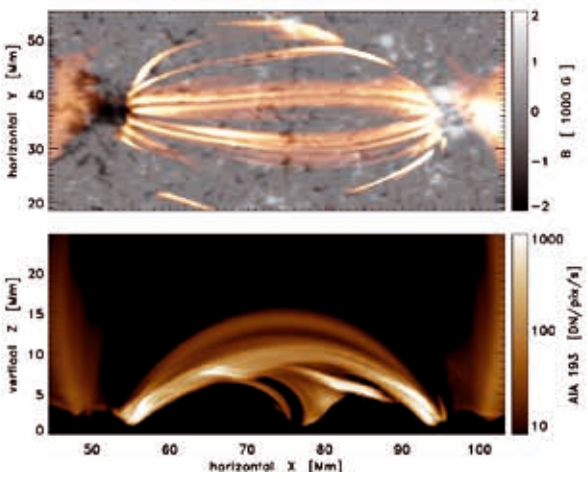

Figure 2: Similar to Fig. 1, but for the high resolution run at a four times higher spatial resolution. This snapshot is taken at roughly the same time as the snapshot shown in the left column of Fig. 1.

References and Links

[1] Rempel, M. & Cheung, M.C.M., 2014, Astrophys. J., in press, http://arxiv.org/abs/1402.4703
[2] Brandenburg, A. & Dobler, W. 2002, Computer Physics Communications, 147, 471
[3] Chen, F, Peter, H., Bingert, S. & Cheung, M.C.M., 2014, Astron. Astrophys., in press, http://arxiv.org/abs/1402.5343

Mocking the Universe:

Large Volume Simulations for galaxy surveys

1

Research Institution
Universidad Autónoma de Madrid

Principal Investigator
Gustavo Yepes

Researchers
S. Gottlöber[2], A.Klypin[3], F. Prada[4], S. Hess[2]

Project Partners
[2]Leibniz Astrophysical Institute Potsdam, [3]New Mexico State University, [4]Instituto Física Teórica-UAM/CSIC

LRZ Project ID: pr86bu (PRACE project)

Introduction

More than 96% of the total energy content of the universe consists of an still unknown form of dark energy and dark matter. Understanding the physical nature of these two components is one of the great challenges for the (astro)physics of the 21st century. Both dark energy and dark matter are only detectable through their gravitational interaction. Together they give rise to the observed large scale structure in the universe. Thus understanding large scale structure formation is a prerequisite to understand dark energy and dark matter. Due to the non-linear nature of gravitational clustering computer simulations play a very important role in cosmology. Research in computational cosmology started four decades ago with the first N-body simulations having a few hundred or thousand particles. Nowadays, large simulations with billions of particles are rather easy to do. They are used to address numerous aspects of the evolution of fluctuations and formation of structures on the vast range of relevant scales. Meanwhile numerical simulations provide extraordinary accuracy for important statistics such as the mass function and the correlation function of objects, the biases between dark matter and luminous matter distribution. Thus large dark matter simulations are an essential tool to interpret the observational data. In the next years there will be a substantial number of observational projects that will be gathering photometric and redshift data from galaxies at different epochs in the universe and covering a large area of the sky (e.g BOSS, DES, KIDS, DESI, LSST, Euclid, eROSITA, etc). Galaxies and the matter distribution on larger scales will be mapped more accurately and, consequently, this will put strong limits on the cosmological model of the Universe. But, in order to derive cosmological constraints from these data, they must be compared with the theoretical predictions of the different cosmological scenarios. Due to the intrinsic non-linear nature of the physics behind the formation and evolution of galaxies and larger structures, the only reliable tool to perform this task is the numerical simulation of the gravitational evolution of fluctuations in computational boxes large enough to accommodate the sampled volumes of the different observational surveys. State of the Art N-body simulations are now dealing with hundreds of billions of particles, and very soon would go over trillions (1012) particles. Moreover, these large volume simulations would need to be created for different models of dark energy (i.e. Cosmological constant, dynamical dark energy with an evolving equation of state, dark energy coupled with dark matter, etc) and also in other alternative cosmological scenarios such as those with modified gravity, non-homogeneous or isotropic models, non-gaussian initial conditions or non standard particles such as sterile neutrinos. All these alternatives to the standard cosmological model would need to be properly modelled numerically in order to produce mock catalogues to the different observational surveys, so their predictions on clustering, abundance of galaxies, etc can be reliably compared with their observational counterparts

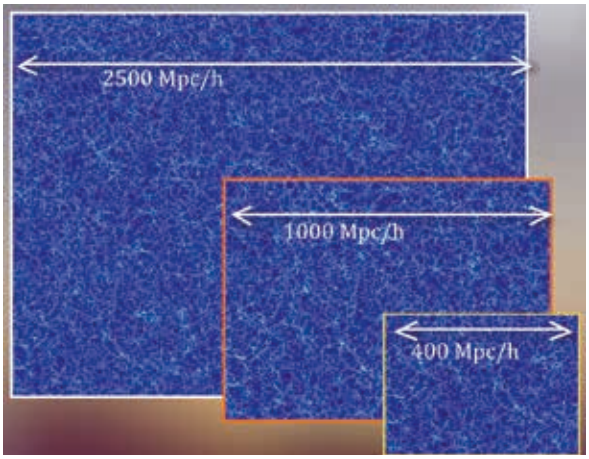

Figure 1: A representation of the density of dark matter in the 3 different boxes simulated within the PRACE Multidark project. Each box contains the same number of particles, 56.6 billion (38403).

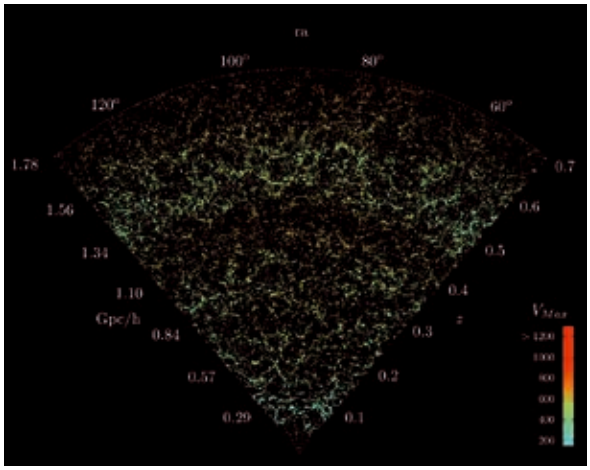

Figure 2. A mock galaxy redshift catalogue derived from the PRACE simulations with box size 2500 Mpc. The colour code represents the maximum circular velocity of the dark matter halos hosting the galaxies, which is a very good proxy of the stellar mass and thus, for the luminosity of the galaxies.

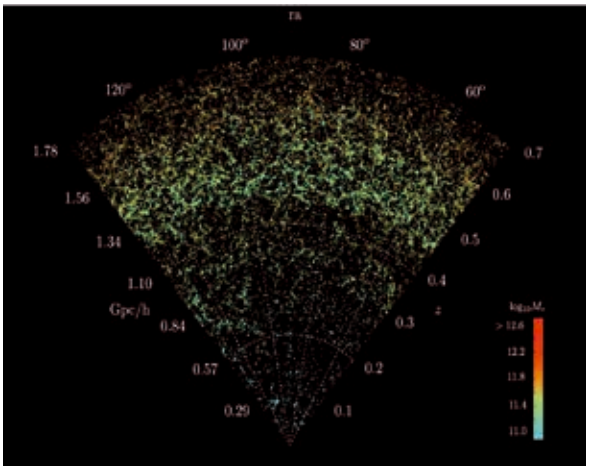

Figure 3. Distribution of galaxies in the BOSS galaxy redshift survey. The colour code represents the stellar mass of each galaxy.

Simulations

The PRACE project that we have been running in Supermuc aims at producing a set of N-body simulations in sufficiently large volumes to accommodate the volume sampled by the recently finished BOSS [1] redshift survey with enough resolution to be able to resolve all the dark matter halos which host the same galaxies as those detected in the survey. This imposes a severe constraint in the minimum number of particles that has to be used in the simulations [2]. A total of more than 56 billion (3840^3) were used in the various runs performed at LRZ. We also simulated several boxes of different sizes to achieve more resolution and for convergence studies [2]. In Figure 1 we show the different box sizes that we have used in this project, all of them run with the same number of particles. We also run several boxes with different cosmological parameters, including those recently derived from ESA's Planck satellite. In total, we produced more than 2 PBYTES of raw data that had to be analysed in order to derive galaxy catalogues which mimic those from the BOSS survey. This is a very time consuming process due to the large amount of data that has to be processed. In the end, we want to generate a distribution of object in redshift which closely resembles those from the observed galaxies. In Figures 2 and 3 we present an example of a mock catalogue derived from our simulation and the real one from the BOSS data. From these 3D datasets, we can then compare their clustering properties and derive conclusions about the nature and content of the dark matter and dark energy components of the universe.

Our simulations are also being used to produce weak lensing maps, that is, to simulate the bending of the light emitted from early galaxies due to the intervening dark matter distribution. Observational projects like KIDS [3] and CHFTLens [4] are going to measure the galaxy distortions due to this effect. To compare with the predictions of cosmological models, it is only possible though these kind of large volume simulations.

All the mock catalogues and other deliverables from our simulation dataset are going to be publicly available through the MULTIDARK database [5]

Future work

We plan to continue the analysis of the dataset of the simulations performed in the course of the PRACE project pr86bu. There is still a fair amount of work to do until we finish the production of halo catalogues and the derivation of light-cone samples (see figures [2]). On the other hand, we would like to perform new, larger (4000 Mpc) simulations with the same mass resolution (i.e. $> 6000^3$ particles). Our goal is to use them to generate again mock catalogues that will be used for making predictions for the upcoming larger surveys such as DESI [6] and Euclid [7]. This will be the purpose of the next PRACE projects we are currently preparing.

References and Links

[1] http://cosmology.lbl.gov/BOSS/
[2] Klypin, et al., 2013, arxiv/1310.3740
[3] http://www.astro-wise.org/projects/KIDS/
[4] http://www.cfhtlens.org/
[5] http://www.multidark.org
[7] http://desi.lbl.gov/
[8] http://sci.esa.int/euclid/

1 Star formation in extreme conditions: Shock heating, thermal cooling and turbulent dissipation in Stephan's Quintet

Research Institution
CEA-Saclay, Direction des Sciences de la Matière

Principal Investigator
Frederic Bournaud

Researchers
Florent Renaud, Pierre-Alain Duc, Katarina Kraljic, Romain Teyssier, Eric Emsellem

Project Partners
CEA Saclay, University of Zurich, ESO Garching

LRZ Project ID: pr86di (PRACE project)

Introduction

Understanding galaxy formation is severely limited by our lack of knowledge about star formation (SF). SF is governed by the chaotic parsec-scale physics of the interstellar medium (ISM), and the link between this small-scale physics and SF on galactic scales is still poorly understood. In the densest gas clouds, on scales of a few parsecs, SF is probably a relatively universal process. But the conversion of low-density galaxy-wide gas reservoirs into molecular clouds and dense substructures may be a non-universal process. The transition between SF physics on small scales and the scaling relations for the rate of SF on large scales is hence a highly debated topic of fundamental importance in galaxy formation.

The connection between the actual formation of individual stars on small scales and the properties of SF in entire molecular clouds and entire galaxies is governed by the structure and properties of the Interstellar Medium (ISM). Numerical simulations of galaxies are a major tool to study the properties of the ISM in various conditions. Only recently, simulations became capable to accurately describe the global structure and dynamics of galaxies and resolve supersonic turbulence in the cold phases of the ISM at the same time. This typically requires a very high resolution (around one parsec) in boxes of tens of kilo parsec: adaptive-resolution techniques such as AMR hydro-codes are a powerful tool for this.

To date, the properties of ISM turbulence have been explored in details in isolated galaxies, like our Milky Way – our own PRACE project is enabling major progress in this direction, by developing a new predictive model of the interaction between newly formed stars and the surrounding gas (the so-called « feedback » processes).

Galaxy formation, however, often proceeds in violent phases during which galaxies accrete mass very rapidly, collide and merge with each other – not just in calm isolation as is the case for the Milky Way. The properties of ISM turbulence and ISM structures are likely different in such systems. Observationally, these systems often undergo strong bursts of very rapid star formation. But whether these bursts are only a large-scale property with a universal efficiency of SF on small scales, or whether there could be locally-enhanced, or locally-suppressed SF in molecular clouds at some intermediate scale, is still unknown.

In this project, we model ISM physics and SF in such extreme events with bursts of star formation. We performed simulations of colliding/interacting galaxies with a resolution sufficient to capture the turbulent cascade in the ISM, down to scales of about one parsec and explicitly resolving high gas densities (above 10^5 atoms per cm^3) in which SF can reasonably be supposed to be a locally universal process. We also developed a thorough and accurate modeling of stellar feedback.

We performed simulations of Stephan's Quintet at parsec-scale resolution. This is a well-known group of galaxies in mutual interaction/collision. This system is very rich in various types of features that can have different efficiencies of SF (active nuclei, supermassive star clusters, a large-scale shock rich in molecular gas, many tidal tails, etc). Observations indeed suggest that locally-enhanced and locally-suppressed SF are present in this system on intermediate scales, but whether the stabilization of relatively dense gas against SF results from thermal heating in shocks, or from tidally-triggered, slowly-dissipating turbulence, or some other process is still unknown.

Results

The simulation used about 9 million CPU-hours on SuperMUC and run on 4,096 cores, with typical runtimes of 20-24 hours, distributed over several months. The total amount of data generated was 36 TB.

We have performed the highest-resolution simulation of galaxy interactions to date, and can properly describe the turbulence of fragmentation of interstellar gas, and the formation of proto-stars in dense gas clouds.

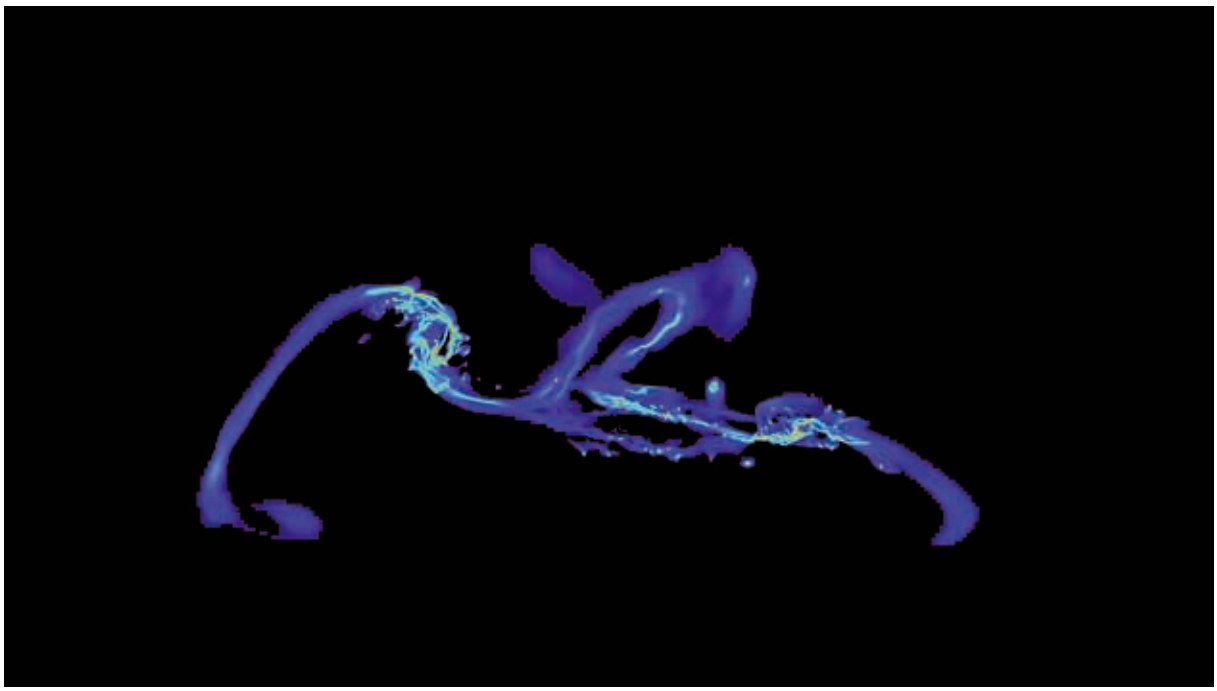

Gas density distribution in a system of interacting galaxy. The actual resolution of the simulation is 512 times higher than the pixel size on this figure. Note the strong fragmentation of the gas into dense clouds where new stars form rapidly, under the effect of interaction-induced turbulent fragmentation.

Compared to previous simulations, the linear resolution in each direction is 10 times better, which means that volumes 1,000 times smaller have been resolved, and fragments of interstellar gas several thousands of times less massive are describe in this simulation. In fact, it is the first time that the dense gas clouds that form star clusters one by one are really resolved. We could also resolve the feedback from young stars on the gas clouds in which they were born, including supernovae explosions, radiation pressure, photo-ionization

The preliminary results are as follows:

- modelling the global star formation activity in interacting galaxies requires a resolution of ~4 parsec, but between 4 and 1pc the results seem to largely converge.
- The bursts of star formation ("starbursts") triggered by galaxy interactions are stronger and last longer then previously thought. This is because old models could resolve only the global compression of the global gas content by tidal forces, while we can now resolve the local compression of small pieces of gas through turbulent fragmentation – the latter appears to be a more efficient starburst triggering mechanism. The Mach number of interstellar turbulence increases by a factor 3 to 5 under the effect of galaxy interactions.
- Star clusters formed in galaxy mergers follow a "Main Sequence" (Figure 2 below) between the mass and size much tighter than in isolated spiral galaxies. Our preliminary results support that this is because turbulent fragmentation dominates star cluster formation.
- For the specific case of the Antennae galaxies (one of the most observed system of this type) we conclude that the system is mostly in a pre-starburst phase but its so-called overlap region (an infrared-bright region) is locally in a post-starburst phase. This result is key to understand new ALMA data and is stable with respect to the possible variations in the initial conditions used to model the system.

We have established a milestone with a realistic interstellar gas structure in interacting galaxies, and demonstrated convergence of our model with resolution.

With this we should be able to study the role of other physical processes in starburst galaxies, in particular the role of feedback from supermassive black holes (active galactic nuclei) in quenching the star formation activity of galaxies after their starburst phase.

References and Links

[1] Renaud F., Bournaud F., Emsellem E., et al. MNRAS 436, 1836, 2013. *A sub-parsec resolution simulation of the Milky Way: global structure of the interstellar medium*

[2] Kraljic K., Renaud F., Bournaud F., et al., Astrophysical Journal, 2014. in press. *The role of turbulence in star formation laws and thresholds.*

1 Full-f gyrokinetic simulation of edge pedestal in Textor

Research Institution
Aalto University

Principal Investigator
Timo Kiviniemi

Researchers
Paavo Niskala, Susan Leerink, Salomon Janhunen, Tuomas Korpilo, Jukka Heikkinen

Project Partners
VTT, Finland

LRZ Project ID: pr86go (PRACE project)

Introduction

In order to invest in a sustainable energy mix and avoid CO_2 emissions, new energy sources such as fusion energy need to be developed. Understanding turbulent transport is needed for further optimization of fusion reactors but realistic transport time scale simulations of plasma turbulence are computationally very demanding. The aim of the present project is to increase the understanding of the mechanisms behind the sudden improvement in confinement observed in experiments. The research activities carried out on GCS supercomputer SuperMUC of LRZ Garching shed some light on the possible role of the radial derivative of a time-varying electric field in triggering this transition using the ELMFIRE turbulence simulation code [1] which investigates these phenomena with a so-called first principal computer model. This model tracks individual particles providing information on the complex interplay between the magnetic field, the electric field and the particle trajectories.

ELMFIRE is even more computationally demanding than other turbulence codes as it does not assume a Maxwellian distribution of particles but instead simulates the full distribution of electrons and ions. While this approach enables more realistic simulations especially near the plasma edge, a very large number of simulation particles is needed for good statistics. So far excellent results for the small FT-2 tokamak have been obtained and the GCS supercomputing resources, made available through the Partnership for Advanced Computing in Europe (PRACE), were used to investigate phenomenology of confinement improvement in the mid-sized tokamak TEXTOR.

Results

The main effort in the project was a scan over local parameters like temperature and density starting from experimental Textor parameters. Most of the runs were run with 4096 cores as it was noticed that scaling got worse after that. Each of the cases took about 400 000 CPUh and produced about 200 GB data of results and 120 temporary snapshop files, which were used to continue the runs. At the end of the project overall storage used was totalling up to 10TB of which 4TB was transferred to our local computer for future analysis. According to the counter, we used only 80 % of our allocated 30MCPUh time. However, counting did not start immediately at the beginning of the project.

From the data obtained, we have managed to interpret old Textor experiments and also cross-validate a recent sophisticated analytic theory of radial wave length of radial electric field oscillation [2] as shown in Figure 1. With the present data we were also able to investigate the parametric dependence of the amplitude of the oscillation. Example of this oscillation is shown in Figure 2. From these three quantities one can derive an equation for the contribution of time varying electric field on turbulence suppression which can be one important part in understanding the sudden improvement in confinement. As confinement improves when building larger fusion devices, theoretical understanding of optimizing confinement helps to build cheaper reactors in the future. Part of the resources was also used to finish similar work for FT-2 [3] which were included in doctoral thesis of S.Leerink [4] and presented in several conferences (together with first Textor results).

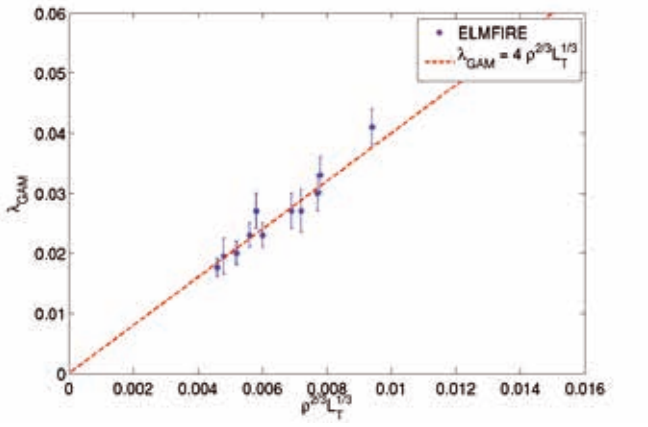

Figure 1: Radial wave lengths of electric field oscillations show good agreement with recent analytic theory.

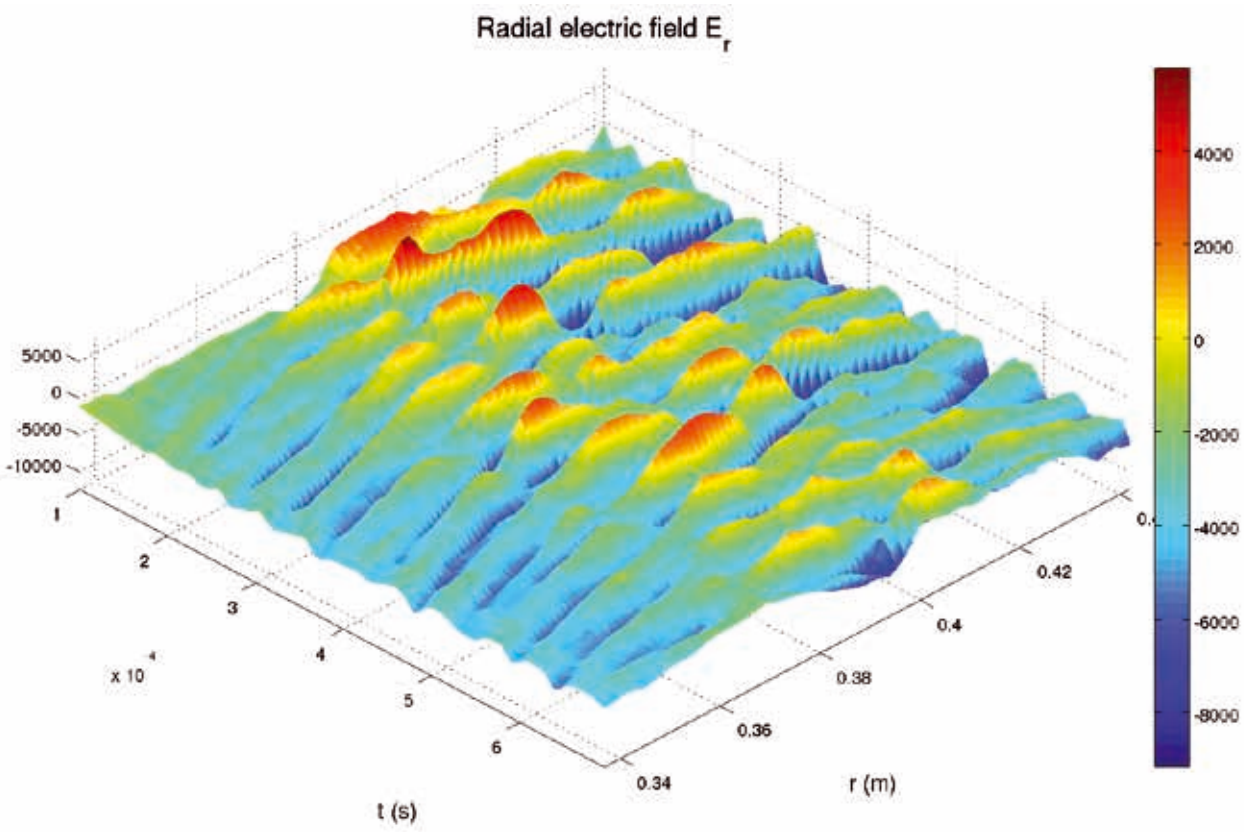

Figure 2: Clear oscillations in radial electric field are seen in the data and were compared to experimental values and analytic estimates.

From allocations we have received via others we have got excellent results for small (diameter d=1.1 m) FT-2 tokamak including first ever multi-scale benchmark of gyrokinetic simulations to experimental measurements. With the present PRACE resources we are able to investigate phenomenology of confinement improvement in TEXTOR (d=3.5 m), which is one of the largest tokamaks in Europe. With PRACE resources our group is the only one in Europe which is able to do direct comparison of first principles simulations to multi-scale experimental data for a tokamak close to reactor relevant size. Present PRACE project is a highly important and necessary step on a way towards simulating ITER (d = 12 m).

On-going Research / Outlook

Even the present database (about 20 cases and some 4TB of data) can be further explored. Most of the results seen so far can be seen from flux surface average quantities and analyzing the temporal and spatial structures and parameter dependencies from 3D data will take more time (including visualizations). We plan to also study the tilting angle of turbulence and difference in phase in correlation between Er and transport coefficients which may be consistent with predator-prey model. Plans for new simulations runs include e.g. the effect of the SOL flows and impurities on the modes and meso-scale variations of the radial electric field.

References and Links

[1] J.A. Heikkinen, S.J. Janhunen, T.P. Kiviniemi and F. Ogando, Journal of Computational Physics 227 (2008) 5582.
[2] T.P. Kiviniemi, P.Niskala, S.Leerink, J.Heikkinen, S.Janhunen and T.Korpilo, Gyrokinetic simulation of GAMs in Textor plasma edge, P2.187, in Proceedings of 40th EPS Conference on Plasma Physics 1 - 5 July 2013, Espoo, Finland.
[3] S. Leerink, V. V. Bulanin, A. D. Gurchenko, E. Z. Gusakov, J. A. Heikkinen, S. J. Janhunen, S. I. Lashkul, A. B. Altukhov, L. A. Esipov, M. Yu. Kantor, T. P. Kiviniemi, T. Korpilo, D. V. Kuprienko, and A. V. Petrov, Phys. Rev. Lett. 109, 165001 (2012).
[4] S.Leerink, doctoral dissertation, Aalto University http://www.elmfire.eu

1 Non-radial Instabilities During the Violent Birth of Neutron Stars

Research Institution
Max Planck Institute for Astrophysics

Principal Investigator
Hans-Thomas Janka

Researchers
Florian Hanke, Andreas Marek, Tobias Melson, Bernhard Müller

Project Partners
Rechenzentrum Garching (RZG)

LRZ Project ID: pr86la (PRACE project), pr85ja (Gauss Large Scale project)

Introduction

Stars with more than roughly eight times the mass of our sun end their lives in gigantic explosions, so-called supernovae. These spectacular events belong to the most energetic and brightest phenomena in the universe and can outshine a whole galaxy for weeks. Supernovae are the cosmic origin of chemical elements like carbon, oxygen, silicon, and iron, which the earth and our bodies are made of. These heavy elements are bred in the evolving stars over millions of years or they are freshly fused during the supernova to be expelled into the surrounding space with enormous power by the stellar explosion.

While supernovae eject most of the material of the dying star, the stellar core of iron collapses under the influence of its own gravity within fractions of a second to an extraordinarily exotic, compact remnant, a neutron star. Such an object contains about 1.5 times the mass of our Sun, compressed into a sphere with the diameter of Munich. The central density of a neutron star exceeds that in atomic nuclei, gargantuan 300 million tons in the volume of a sugar cube.

But how can the implosion of the stellar core be reversed to an explosion? The exact processes are still a matter of intense research, in which supercomputer simulations like the ones in this project play a crucial role. Neutrinos, mysterious elementary particles, which are produced in tremendous numbers in the extremely hot and dense interior of the newly formed neutron star, are believed to play a decisive role for the fate of the collapsing star. Like the thermal radiation of a heater they pump energy into the gas surrounding the hot neutron star and thus can initiate the explosion by building up pressure until an outgoing shock wave ultimately disrupts the star in the supernova. A successful explosion can take hundreds of milliseconds of quasi-static evolution of the blast-wave shock, which is launched at the moment when the collapse of the stellar core is abruptly stopped at nuclear-matter density and the infalling plasma begins to assemble into the nascent neutron star. Because of this considerable time delay, the neutrino trigger of the supernova outburst was termed "delayed neutrino-driven mechanism." Because of the complexity of the involved physics, a final confirmation of the viability of this mechanism is still missing and requires three-dimensional (3D) numerical simulations.

Computer models in 3D are indispensable because the neutrino-driven mechanism is accompanied and crucially assisted by violent hydrodynamical instabilities, i.e., by powerful non-radial fluid motions in the supernova core. On the one hand neutrino heating causes the gas to become buoyant such that strong convective overturn helps accelerating the shock front. On the other hand, the shock wave was found to be naturally unstable against non-spherical deformation modes, the so-called "standing accretion shock instability" or SASI [1], which leads to large-amplitude dipolar and quadrupolar asymmetries and phases of violent sloshing and spiral motions of the neutrino-heated matter around the nascent neutron star.

Results

In this project stellar core collapse, neutron star formation, and the onset of the supernova explosion are studied with the PROMETHEUS-VERTEX code for multi-dimensional hydrodynamical simulations including a highly sophisticated description of three-flavor neutrino transport and neutrino-matter interactions in full energy dependence. While the former is treated with an explicit, higher-order Godunov-type scheme, the latter is solved by an implicit integrator of the neutrino energy and momentum equations, supplemented by a state-of-the-art set of neutri-

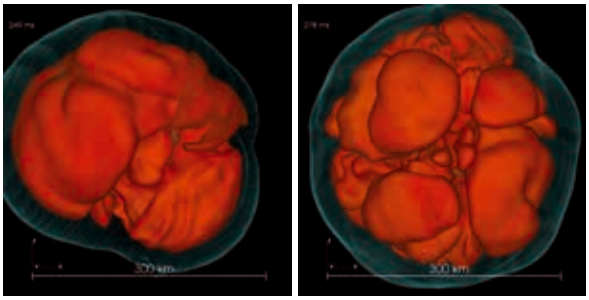

Figure 1: Dipolar and quadrupolar SASI asymmetry (left) compared to higher-mode convective asymmetry (right) of the turbulent flow between supernova shock (transparent bluish surface) and central neutron star (invisible) [2].

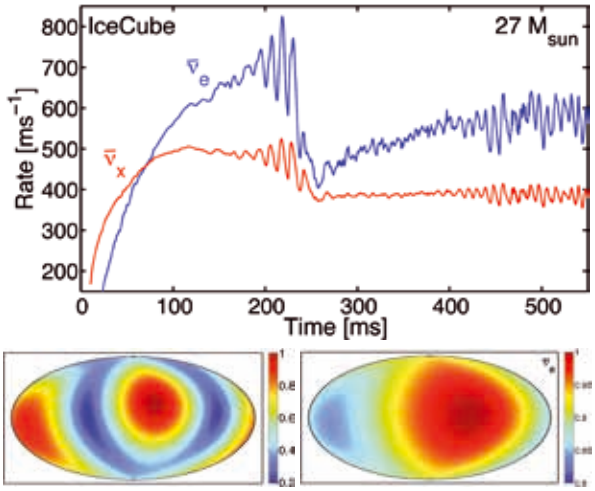

Figure 2: Predicted time-dependent neutrino count rate in the IceCube detector for a future galactic supernova at 10 kpc distance (top; [4]). Full-sphere images of quadrupolar neutrino-emission asymmetry during SASI (bottom left) and dipolar lepton-emission asymmetry during convection-dominated phases (bottom right; [5]).

no-reaction kernels and a closure relation computed from a simplified model-Boltzmann equation. Consistent with the basically spherical geometry the equations are discretized on a polar coordinate grid, and the computational efficiency is enhanced by the use of an axis-free Yin-Yang implementation and a time- and space-variable radial grid. The thermodynamics and changing chemical composition of the stellar medium are determined by high-dimensional equation-of-state tables and nuclear burning at non-equilibrium conditions.

Employing mixed MPI-OpenMP parallelization, our ray-by-ray-plus approximation of multidimensional transport allows for essentially linear scaling up to tested processor-core numbers of more than 130,000. In production applications we are granted access to nearly 15,500 cores (allowing for two degrees angular resolution) and the code typically reaches 10–15% of the peak performance. The computational load is strongly dominated by the complexity of the neutrino transport. A single supernova run for an evolution period of roughly half a second takes several months and up to 50 million core hours. PRACE and GAUSS contingents on SuperMUC of 48.9 and 64 million core hours, respectively, allow for typically three to four model runs and yield several hundred Tbytes of data.

Simulating the collapse of iron cores of stars with 20 and 27 solar masses, we could – for the first time – confirm the development of violent SASI sloshing and spiral motions of the accretion flow around the newly formed neutron star in full-scale supernova models that include all relevant microphysics [2,3]. Previous studies of this hydrodynamic instability considered only artificial, highly idealized and simplified set-ups [1]. Before the explosion sets in, in phases when the supernova shock front stagnates at sufficiently small radii or retreats, the growth of dipolar and quadrupolar SASI asymmetry modes dominates the growth of the convective overturn (Rayleigh-Taylor) instability, whose higher-order multipole pattern consisting of buoyant plumes, separated by narrow downdrafts, is distinctively different (left and right panels of Figure 1). Based on our models we predict that the SASI mass motions lead to quasi-periodic modulations of the neutrino emission that will be well measurable by the cubic-kilometer IceCube detector at the south pole for a future galactic supernova even at distances of 10–15 kpc (Figure 2, top; [4]). SASI shock sloshing and spiraling induce variations of the mass-accretion flow to the neutron star mainly in a randomly selected plane, for which reason the variation amplitude of the neutrino signal for different observer directions exhibits a quadrupolar pattern (Figure 2, bottom left).

Moreover, during SASI-quiet, convection-dominated phases we discovered a completely novel phenomenon, namely a long-lasting dipolar asymmetry of the lepton emission from the nascent neutron star (Figure 2, bottom right; [4]). This self-sustained global asymmetry of the emission of electron neutrinos and antineutrinos, which we named LESA, is caused by a dipolar asymmetry of the accretion flow to the neutron star as a consequence of anisotropic neutrino heating and postshock convection, which lead to a persistent deformation of the stalled supernova shock (Figure 3; [5]). The outer asymmetry is linked to hemispheric differences in the electron distribution and convection inside the neutron star. This neutrino-emission asymmetry could be important for supernova nucleosynthesis and neutrino oscillations.

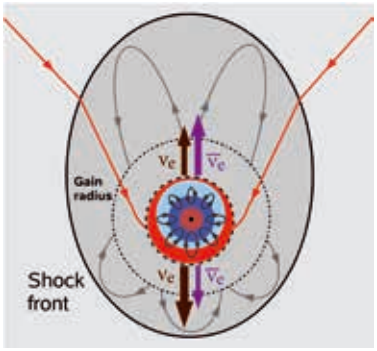

Figure 3: Self-sustained dipolar lepton-emission asymmetry (LESA). The cartoon summarizes the physics components of the new non-radial instability [5].

On-going Research / Outlook

Despite interesting and exiting discoveries achieved so far, our 3D simulations have not (yet) provided successful supernova explosions, different from corresponding 2D models. Higher grid resolution is therefore demanded to reduce the still worrisome influence of numerical viscosity. Stellar core rotation, even on a low level, can play an important role for the growth rate of the spiral SASI. Also uncertain microphysics like the high-temperature, high-density equation of state of neutron star matter need to be tested for their impact on the development of the explosion. More computer time for a larger number and for better resolved models is therefore urgently needed!

References and Links

[1] J.M. Blondin, A. Mezzacappa, Nature 445 (2007) 58
[2] F. Hanke et al., ApJ 770 (2013) 66
[3] http://www.mpa-garching.mpg.de/mpa/institute/news_archives/news1306_ddd/news1306_ddd-en.html
[4] I. Tamborra et al., PRL 111 (2013) 121104
[5] I. Tamborra et al., submitted to ApJ; arXiv:1402.5418

Extreme Star Formation Modeling: From the Galactic Fountain to Single Stars in One Run

1

Research Institution
ICREA & Institute for Cosmos Sciences, University of Barcelona

Principal Investigator
Paolo Padoan

Researchers
Troels Haugbølle, Åke Nordlund

Project Partners
Star and Planet Formation Center & Niels Bohr Institute, University of Copenhagen

LRZ Project ID: pr86li (PRACE project)

Introduction

The objective of this PRACE proposal was to study star formation as a multi-scale process, using simulations with an unprecedented dynamic range (seven orders of magnitude in linear scale).

The ISM goes through a complex life cycle known as the Galactic fountain: Massive stars explode as supernovas (SNs), sending hot gas out of the disk into the halo, where it cools, condenses, and then falls down on the disk again. Because of computational limitations, star formation simulations to date were based on unphysical initial conditions and artificial driving forces that can only mimic this energy injection from large-scale processes. We proposed to overcome these limitations using numerical simulations of unprecedented size and complexity, which can resolve the collapse of individual protostellar cores while simultaneously modeling the Galactic fountain. These simulations were possible thanks to the specific combination of our unique OpenMP/MPI hybrid version of the public adaptive-mesh-refinement code Ramses and large-node supercomputers such as SuperMUC.

Results

In this project, we carried out the first simulations to date describing the full Galactic fountain while resolving at the same time the formation of individual stars. Previously, the best simulations of the Galactic fountain had only achieved a resolution of order 1 pc, which is not even sufficient for a satisfactory description of the formation of giant molecular clouds. Star formation could not be studied in such runs. Different types of simulations, where the formation of individual stars was modeled, were based on periodic boxes and random forcing (hence artificial boundary conditions and turbulence driving), or isolated clouds with decaying turbulence (hence artificial initial conditions and unrealistically low turbulence after a decay time), using an outer scale typically of order 1-10 pc.

In this SuperMUC project we covered an unprecedented range of scales, from 0.07 pc to 32 kpc, more than two orders of magnitude larger than that of previous Galactic fountain simulations. In our main simulation, Fountain1, we simulated a region of 1x1x32 kpc, driving the turbulence with supernova (SN) explosions of Type II and Type Ia. Although less frequent, SNae of Type Ia release the same thermal energy as SNae of Type I, but on a much smaller mass, resulting in a less efficient cooling and the generation of hot gas feeding the Galactic fountain. They are also distributed with a larger scale-height above the Galactic plane, which further help the initiation of the fountain flow. They are therefore essential to reproduce a correct fraction of very hot gas in the ISM. On the other hand, the role of the very hot gas in the dynamic of the cold and dense gas, and thus on the star formation process, has never been established. In order to address this point, we also started a simulation, Fountain2, on a region of the same size as Fountain1, but without SN explosions of Type Ia. As a further test of the role of hot fountain gas in the star formation process, we started a third simulation (Fountain3) on a smaller region (0.25x0.25x1 kpc), without SN of Type Ia. The smaller size and much smaller aspect ratio (4 instead of 32) of the Fountain3 run allows also a better description of the SN-driven turbulence.

The comparison between the Fountain2 and 3 runs with the main simulation has not been carried out yet, so here we mention only our preliminary results from Fountain1. These results were obtained after developing the SN-driven turbulence in the cold gas for over 20 Myr,

Figure 1: Square root of projected density of the mid-plane region of the main galactic fountain simulation of this project. The computational volume has a size of 1 x 1 x 32 kpc, perpendicular to the Galactic plane, and a maximum resolution of almost 1000 AU. This image is extracted to a resolution of 0.2 pc, and show only a very limited fraction of the vertical extension of the computational volume, within a distance of ±150 pc from the Galactic plane. This is the largest Galactic fountain simulation to date (*Padoan, Haugbølle and Nordlund, in preparation*).

which involves the explosions of approximately 1,000 SNs (according to current estimates of the Galactic SN rate). The process of star formation was then followed for several more Myr. As shown in Figure 1, the cold gas in the midplane of the simulation shows a complex filamentary structure, consistent with images from the Herschel and Planck satellites. Overdensities on the scale of ~10-50 pc have properties similar to those of observed molecular clouds, including a realistic value of the star formation rate. The global star formation rate is ~10-2 Msun/yr/kpc2, consistent with values found in disk galaxies at a comparable total gas surface density (~13 Msun/pc2), and only 2-3 times larger than estimates for the Milky Way. As shown by Figure 2, the SFR is also nearly constant in time. The small discrepancy from the Milky Way may be real, because the small-scale turbulence in the simulation may be slightly underestimated. This is the first time that a realistic star formation rate is achieved, using realistic boundary and initial conditions and SN driving.

An important goal of our experiment was to achieve a realistic mass distribution of massive stars, because, at a later phase, we want the turbulence to be driven by SNs resulting directly from the evolution of stars (sink particles) formed in our simulation. Figure 3 shows the mass distribution based on approximately 4,000 stars from the Fountain1 run. This is by orders of magnitude the largest sample masse stars in any star formation simulation to date. It is also the first time that a statistically significant mass distribution of massive stars is achieved. The result is in striking agreement with the observed Salpeter slope of the stellar initial mass function. The mass distribution is a power law down to approximately 5 solar masses. We also have preliminary evidence that, at later times, the power law continues down to 2 solar masses. Because the smallest stellar mass to explode as a SN is approximately 7 solar masses, our Fountain1 simulations contain a complete census of SN progenitors, besides their correct mass distribution.

On-going Research / Outlook

The PRACE project has resulted in approximately 20 TB of data, which are being transferred to our storage and data analysis centers in Barcelona and Copenhagen. Our group will work on the data analysis for approximately one more year, and the results will be published in a number of papers and presented at conferences. We are also preparing a web portal [1] to share the data more effectively within our group, and with the scientific community at large. The runs of this project will also be continued using other resources, in order to follow the further development of the star formation process in the galactic fountain.

One of our current projects is to study the properties of the giant molecular clouds formed in the galactic fountain simulations. We will investigate their formation process, their lifetime and the nature of their turbulence with respect to the magnetic field strength found in the clouds. A great advantage of our dataset, relative to previous simulations, is that it provides a large sample of giant molecular clouds, so we will be able to obtain reliable statistical distributions of cloud properties.

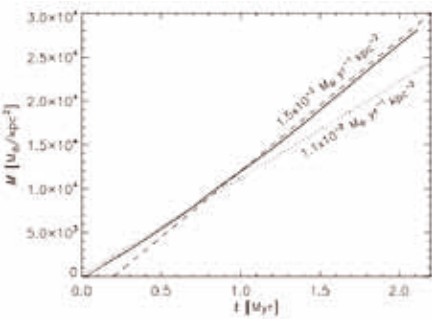

Figure 2: Total mass in stars versus time in the Fountain1 simulation. The dotted and dashed lines show the value of two constant star formation rate. These values are consistent with those found disk galaxies with comparable total gas surface density as in this simulation. (*Padoan, Haugbølle and Nordlund, in preparation*).

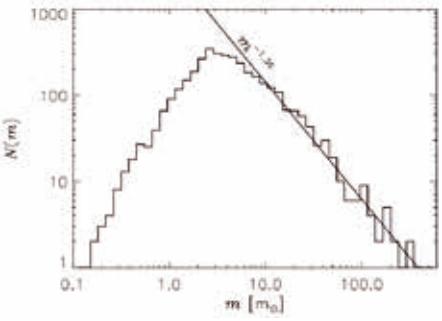

Figure 3: The mass distribution of approximately 4,000 stars from the Fountain1 simulation. Massive stars follow an almost perfect power law, with slope nearly identical to the observed Salpeter value. The power law covers the full range of masses of stars that end their lives as SNae. (*Padoan, Haugbølle and Nordlund, in preparation*).

We will also correlate the cloud properties with their local star formation rate, in order to test analytical models of star formation, and the results of existing numerical parameter studies [2,3]. Such studies have shown that the SFR is a sensitive function of the virial parameter (the ratio of turbulent to gravitational energy in the star-forming sites), and much less dependent on the sonic and Alfvenic Mach numbers. Because of the large number of star formation regions in our simulations, we can directly tackle this problem using a single simulation. The result will also be more reliable than in the current parameter studies, because of the realistic large scale environment in our fountain runs, which was completely missed in parameter studies that were based on idealized turbulence simulations.

In future simulations, we will also study the effect of driving the turbulence with the SN explosions resulting from the stars (sink particles) formed in the fountain simulations. This will be the first time that the turbulence driving in a simulation is controlled self-consistently by the star formation process itself, as it happens in nature. With such simulations we will study the ability of the star formation process to self-regulate in galactic disks.

This project allows us to study the origin and the nature of interstellar medium turbulence as well. We want to compare our realistic SN driving with that of more idealized star formation simulations adopting a random, large-scale force, with varying fractions of compressible power. It has been shown that the compressible fraction of the random force controls the gas density pdf and the star formation rate. We will thus study the fraction of compressible to solenoidal energy resulting from SN driving, its spatial variations, and the correlation of such variations with the local star formation rate.

References and Links

[1] http://icc.ub.edu/~ppadoan/Site/SF_Portal.html
[2] Padoan, P., Haugbølle, T., Nordlund, Å. 2012, ApJL, 759, L27
[3] Padoan, P., Nordlund, Å. 2011, ApJ, 730, 40

http://www.lrz.de/services/compute/supermuc

1 Comprehensive ab initio simulations of turbulence in ITER-relevant fusion plasmas

Research Institution
Max Planck Institute for Plasma Physics

Principal Investigator
Frank Jenko

Researchers
Daniel Told, Tobias Görler, David Hatch, Stephan Brunner, Tilman Dannert

Project Partners
Ecole Polytechnique Federale de Lausanne (CRPP), RZG

LRZ Project ID: pr86lu (PRACE project)

Introduction

The development of a better understanding of turbulent transport mechanisms in plasmas poses a crucial step on the way to fusion power plants – a technology that would offer a sustainable and ecologically sensible energy supply once matured. However, even the description of comparatively simple fluid-type turbulence is considered to be one of the most challenging problems in classical physics – here it is further complicated by the need for a reduced kinetic theory coupled to Maxwell's equations. With virtually no analytical solution at hand, theoretical studies of turbulent fluctuations can only be based on massively parallelized numerical simulations as performed within the project at hand.

With major progress regarding the implemented physics effects in the last decade, such simulations have been found to be not only qualitatively but even quantitatively comparable to experimental data in many cases. One obvious application is thus to revise previous finite-size effect studies in a more realistic manner as such investigations are vital for scalings from the current small- to medium-size experiments to future large-scale fusion devices. They furthermore allow for the evaluation of the validity of reduced simulation domain approaches (so-called flux tubes) which substantially reduce the computational effort and hence allow for much more sophisticated parameter scans.

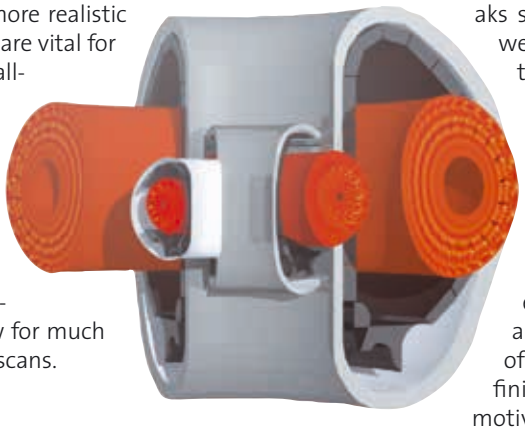

Fig. 1: Comparison of ASDEX-Upgrade, JET and ITER-size plasma simulation volumes and vessels. Studies regarding the scaling from present-day to future devices like ITER represent a crucial task for turbulence investigations and can only be performed in HPC environments as provided by SuperMUC.

Results

Two approaches have been pursued within this project. On the one hand, a feasibility study directly aiming at realistic simulations for the future flagship of fusion experiments, the ITER tokamak currently being built in Cadarache, Southern France, has been launched. In a pioneering effort, global simulations covering a large part of an ITER plasma were carried out in an unprecedentedly realistic framework, i.e., retaining kinetic electrons, collisional effects, electromagnetic fluctuations, and profiles and a magnetic equilibrium consistent with the ITER coil design [1]. Studying finite-size effects in reactor-size plasmas with realistic physics is an extremely challenging task due to the large size of the numerical problem. However, although the simulation could only be carried over a limited extent of the steady state phase and should be extended in follow-up work, no significant meso-scale effects have been found so far. This is consistent with the so-called gyro-Bohm scaling where characteristic sizes of the turbulent structures are predominantly found on a scale of a few ion gyroradii and which would support the validity of flux tube simulations for this kind of scenario.

To shed more light on the transition to such large devices affected weakly by finite-size effects, further global and local studies on medium-sized tokamaks such as ASDEX Upgrade and DIII-D were performed in the framework of the project. As a particular subject of these studies, so-called L-mode type discharges have been selected where previous investigations [2] had found order-of-magnitude discrepancies between the heat transport levels predicted by gyrokinetic simulations and the experimentally inferred values. As a possible explanation, the neglect of turbulence spreading (an effect of finite machine size) was put forward, motivating global simulations of such cases. Both for DIII-D and ASDEX Upgrade, global and local simulations were thus carried out [3,4], finding finite-size effects to be negligible even in these cases. Assured by these results, comprehensive tests varying the input parameters within the experimental error bars could

be run in the local limit. With these, the experimental transport levels could be reconciled with the GENE results, suggesting that the previously observed discrepancies are likely related to subtleties occurring in the numerical treatment of such parameter regimes. Indeed, it was necessary to use both large resolution as well as a complete set of physics (requiring in some cases also the inclusion of impurity physics) to obtain agreement with experimental results.

A further issue occurs specifically in the examined discharge of the DIII-D tokamak, where it was found that a significant amount of the heat transport carried by electrons cannot be explained based on ion-scale turbulence, but instead requires also a treatment of turbulence driven by the electron temperature gradient, which occurs at much smaller spatial scales. Initial simulations focusing on these electron-gyroradius scales have indeed confirmed this expectation. However, such simulations necessarily neglect any interaction between both scales and thus will have to be complemented by future multi-scale simulation efforts which treat turbulence at both scales self-consistently.

All simulation results discussed above are based on the nonlinear gyrokinetic GENE code (http://gene.rzg.mpg.de) which has now been developed and maintained for more than a decade at IPP, Garching, and more recently by an international team of developers. Here, the discretized nonlinear gyrokinetic equations are solved on a fixed, five-dimensional (three spatial and two velocity space dimensions) grid which is aligned with the magnetic field lines in order to reduce the computational requirements describing highly anisotropic plasma turbulence structures. Furthermore, a so-called δ f-splitting technique consistent with the ordering used in the derivation of the gyrokinetic theory is employed so that only the fluctuating parts of each distribution function are propagated in time. The phase space and time operators are treated separately, following the so-called method of lines. While the time stepping is typically done with a fourth-order explicit Runge-Kutta scheme in the initial value solver mode, the numerical schemes in the spatial directions are mainly employing finite difference and pseudo-spectral methods. Considering collisions with a linearized Landau-Boltzmann operator furthermore requires finite volume methods in one of the two velocity space dimensions.

For an efficient use of high-performance architectures, the Fortran-based GENE code typically relies on the MPI paradigm – other approaches like OpenMP/MPI hybrid parallelization have been tested but have not been found to be superior yet. The MPI parallelization is achieved through domain composition in the species, in the velocity space directions and in two of the three spatial directions (all three in the nonlocal code, respectively). At present, the code has demonstrated a good to excellent scaling behaviour on up to 262k cores.

On SuperMUC, about 18 MCPUh have been invested in the aforementioned project tasks. While up to 16,384 cores have been used in some occasions, on average, the individual simulations were based on a series of 24h jobs with about 4800 cores, the latter representing a compromise between queue waiting time and the parallel potential for the parameters at hand. The number of files written during these investigations is on the order of 40,000 requiring up to 6TB of disk space.

On-going Research / Outlook

The astonishing improvements achieved in supercomputing capabilities over the past two decades have allowed groundbreaking new insights into the physics of plasma turbulence. Even though much has been learned already, fundamental challenges related to predicting the performance of future fusion reactors still remain.

In particular, today's fusion experiments routinely achieve a transition to a high-confinement mode (H-mode) with a strong transport barrier at the plasma boundary. Understanding the formation conditions of this barrier and its characteristic size and height are crucial to predicting the efficiency of future fusion reactors, but a fully consistent numerical treatment has still been lacking up to now. A main challenge in the treatment of such barriers is their extreme profile variation, implying their susceptibility to finite-size effects. Global simulation capabilities such as demonstrated within the framework of the present project are thus essential in order to understand the dynamics of the edge transport barrier. Both present and future projects employing the GENE code will build on the experience established within this SuperMUC project and tackle this challenging issue.

Another increasingly important field relates to turbulence studies in stellarators, which represent an alternative machine design for future fusion applications. With its newly developed capability of studying turbulence in stellarator geometry (i.e. retaining magnetic geometry variations within a magnetic surface), the GENE code is uniquely suited for this problem. With the new German stellarator experiment Wendelstein 7-X nearing completion, existing predictions already made with GENE for stellarator turbulence will be put to the test, and possibilities for validation will emerge. Due to the complex magnetic geometry, stellarator turbulence simulations have extreme computational requirements and will thus continue to challenge the available supercomputing capabilities also in the foreseeable future.

The transition from HLRBII to SuperMUC, however, has already greatly influenced the possible problem complexity which has roughly increased by one order of magnitude since then and enabled the presented studies.

References and Links

[1] "Self Consistent Simulations of Plasma Scenarios for ITER: Final Report", F4E-GRT-255 (PMS-PE), (2012)
[2] C. Holland et al., Phys. Plasmas 16, 052301 (2009)
[3] D. Told, F. Jenko, T. Görler et al., Phys. Plasmas 20, 122312 (2013)
[4] T. Görler, F. Jenko, D. Told et al., to be submitted to Phys. Plasmas (2014)

SuperCAST: Simulating the Universe

1

Research Institution
University-Observatory Munich, LMU Munich

Principal Investigator
Klaus Dolag

Researchers
Lisa Bachmann, Maximilian Brunner, Andreas Burkert

Project Partners
Computational Center for Particle and Astrophysics, Excellence Cluster Universe

LRZ Project ID: pr86re

Introduction

It is now well accepted that the observed structure of our universe is best reproduced in the presence of cold dark matter and dark energy, within the framework of LCDM cosmology, in which structures form in a hierarchical bottom up fashion. In such hierarchical picture of structure formation, small objects collapse first and then merge in a complex manner to form larger and larger structures. Astronomical instruments nowadays have opened the so-called era of precision cosmology, where we need to understand the formation of structures in the universe with high precision, e.g. it requires that we understand the complex, non-gravitational, physical processes, which determine evolution of the cosmic baryons. The evolution of each of the underlying building blocks – where the baryons fall into the potential well of the underlying dark matter distribution, cool, and finally condense to form stars – within the hierarchical formation scenario will contribute to the state and composition of the inter-galactic and intra-cluster media (IGM and ICM, respectively), and are responsible for energy and metal feedback, magnetic fields, and high-energy particles. Depending on their origin, these components will be blown out by jets, winds or ram pressure effects and finally mix with the surrounding IGM/ICM. Some of these effects will be naturally followed within hydrodynamic simulations (like ram pressure effects), others have to be included in simulations via effective models (like star formation and related feedback and chemical pollution by supernovae). Further components like black holes and their related AGN feedback need additional modeling of their formation and evolution processes, and must also be self consistently coupled with the hydrodynamics.

SuperCAST

Research in the Computational Astrophysics Group (CAST) at the University Observatory Munich ranges from the theoretical investigation of star formation up to cosmological scales. A variety of different, well known numerical codes (like RAMSES, GADGET, PLUTO, SEREN) are used. Primary investigations regard the relation between turbulence and phase transitions in the multiphase interstellar medium (ISM), energetic feedback processes, molecular cloud and star formation in galaxies as well as cosmological structure and galaxy formation and the interplay between feedback processes, AGN and galaxy evolution and their imprint on the intergalactic medium (IGM) or intercluster medium (ICM). It is now clear that small-scale processes like the condensation of molecular clouds into stars and large-scale processes like gas infall from the cosmic web into galaxies are intimately coupled and have to be investigated in a concerted effort. The various projects cover a link between the various scales and contribute to our understanding of crucial aspects of the formation and evolution of star-forming regions and the ISM, galaxies and their IGM as well as galaxy clusters and the ICM. It also drives the continuous effort to develop and to apply new numerical methods and the next generation of multi-scale codes within the framework of numerical astrophysics through our group of students and young PostDocs.

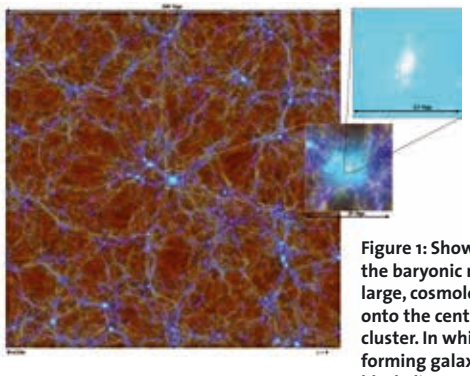

Figure 1: Shown is a visualization of the baryonic matter distribution of a large, cosmological box with a zoom onto the central region of a galaxy cluster. In white the stellar component, forming galaxies are shown, while the black diamonds are showing the AGNs within the simulation.

Simulating the Universe

Hydrodynamical cosmological simulations are needed to interpret data from upcoming astronomical surveys and current instruments like PLANCK, South Pole Telescope (SPT), eROSITA and many more. Such simulations need to follow simultaneously the growth of galaxies and their associated components in detail (like stellar population and central black hole) with their interplay with the large scale environment they are embedded in. Upcoming surveys will map large volumes of the Universe as well as record the birth of the first structures, especially galaxies and even progenitors of massive galaxy clusters at high

redshift. In fact, their large potential of determining the nature of dark matter and dark energy comes from being able to map the content and geometry of the universe over most time in cosmic history. Figure 1 shows the result of the largest, currently available simulation with the role as a theoretical counterpart. So far it was used to compare the structure of the ICM as seen by PLANCK [1] as well as to study the growth and evolution of black holes [2] and many more projects are on their way.

Accretion and star-formation in a Galaxy

Understanding the physics of the ISM is essential for many different areas of astrophysics, from the formation of stars to galaxy evolution and galactic nucleosynthesis. New high-resolution observations show that the ISM is a complex web of cold, molecular filaments and clouds, embedded in diffuse, hot gas phases, driven by super-sonic turbulent flows. Stars form within cold clouds, heat their gaseous environment, drive turbulence and generate new clouds in regions of converging and cooling gas flows. Here we simulated an isolated galactic disc, where our studies focus on the interaction between the accretion of extragalactic baryonic material and the resulting star formation within the galactic disc. Since both the accretion of hydrogen onto the discs as well as the details of stellar formation are not yet completely determined by neither theory nor observation we are performing simulations of different models for several plausible scenarios and parameters describing them. These simulations also have to run for long time spans due to the different timescales of the processes involved, which are governing the evolution of galactic discs as well as the star-formation process itself. Coupled with our desire to push the limits of numerical resolution our simulations are computationally quite demanding. Figure 2 shows the result of such simulation after evolving a galaxy over 1.7 billion of years, assuming a cosmic depletion rate of 5 solar masses of gas per year. So far we could verify a toy model, which in our work describes the connection between hydrogen accretion and global star formation rates by a set of differential equations. Yet more simulations have to be run to determine the effects of various model parameters and to determine a more robust model to predict the evolution of the galactic disc coupled to the external environment.

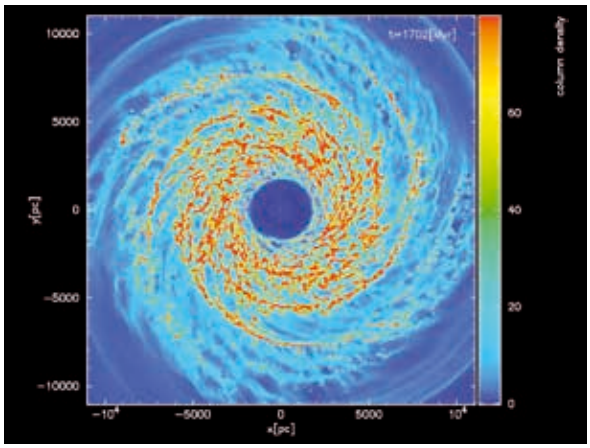

Figure 2: Shown is the column density of Hydrogen in a simulated galactic disk after an evolution of 1.7 billion years.

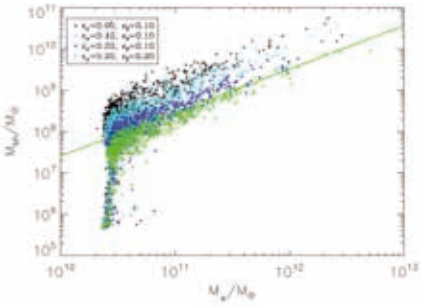

Figure 3: Shown is the predicted relation between the stellar mass of host galaxies and the mass of the black hole within their centre obtained from cosmological simulations with different feedback settings [3]. The best fit relation obtained from observations is shown as line.

Simulating black holes in the universe

Active galactic nuclei (AGNs) do not evolve in isolation but are strongly linked to their galactic environment which provides the gas (fuel) to drive activity cycles in the center of these galaxies and feed their super massive black hole. The galactic environment, in turn, is strongly affected by energetic feedback from the nucleus. We are following the evolution of black holes within cosmological simulations using an effective sub grid model, where black holes are treated as sink particles which accrete material from their surrounding following the Bondi-Hoyle-Littleton formulation. Such black hole sink particles are placed on the fly in forming galaxies and release energy to their environment related to their growth by accretion. This so called AGN feedback has been recently realized to be a key ingredient to understand the chemo-energetic evolution of galaxies within cosmological context. However, these effective sub-grid models still depend on various simplified assumptions and nuisance numerical parameters, describing our incomplete knowledge of the physical processes on scales much below the resolution of current, cosmological simulations. We therefore performed various simulations of moderate resolution simulations of a $(68\ \mathrm{Mpc})^3$ cosmological box, sampled by 20 million particles. This allowed us to study the impact of the exact values of several of these model parameters on the growth, evolution and the imposed feedback of black holes within these simulations. Figure 3 shows the predicted relation between the stellar mass of the host galaxy and the black hole mass for simulations where the energy feedback efficiency is varied, compared with the best fit value obtained from observations. Such numerical experiments allows us also to improve the underlying sub-grid models by adapting the parameterization of the models to recent observational findings, which for the first time shed some more light on the underlying physical processes.

On-going Research / Outlook

Results from such detailed simulations will help us to improve and refine the subscale models used in cosmological simulations and will be crucial to improve the realism of the next generation of structure formation simulations.

References and Links

[1] Planck Collaboration, 2013, A&A, 558, 2
[2] Hirschmann, Dolag, Saro, Bachmann, Borgani & Burkert, 2013, MNRAS submitted, astro-ph:1308.0333
[3] Lisa Bachmann, Mastrarbeit

Modeling gravitational wave signals from black hole binaries

1

Research Institution
Universitat de les Illes Balears

Principal Investigator
Sascha Husa

Researchers
Michael Pürrer, Mark Hannam, Sebastian Khan, Alejandro Bohé, Bernd Brügmann, Francisco Jimenez Forteza, Nathan Johnson-McDaniel, Denis Pollney, Christian Reisswig, Milton Ruiz, Patricia Schmidt, Marcus Thierfelder

Project Partners
Cardiff University, University of Jena, California Institute of Technology, Rhodes University

LRZ Project ID: pr86va (PRACE project)

Introduction

Until now, our knowledge of the cosmos has been limited to what we could learn from observations of electromagnetic waves. Our work on SuperMUC contributes to the emerging field of gravitational wave (GW) science, which will soon open a new window to the universe. GWs are ripples in spacetime, generated by massive compact objects such as black holes and neutron stars, as predicted by Einstein's theory of general relativity, which explains gravitation as a phenomenon arising from the curvature of spacetime. The most promising source for the first detections of such waves are binary systems of dead stars – black holes or neutron stars – which coalesce as a consequence of their energy loss to GWs. Their observations will answer key questions in astrophysics, and provide the most stringent test of Einstein's theory of general relativity to date. An international network of GW observatories has been constructed in the form of km-scale interferometers in the US and Europe [1,2], and will come online again in 2015 after an upgrade that will expand the volume of the observable universe by a factor of 1000 in the next five years. The detection, identification, and accurate determination of the physical parameters of the sources rely on the availability of template banks of theoretical waveforms, which are filtered against the detector data. For the last orbits and merger, where the fields are particularly strong, and where one has the best chances of discovering entirely new physics, perturbative post-Newtonian expansion techniques break down and the full Einstein equations have to be solved numerically.

In our work we solve Einstein's equations as a system of 21 coupled nonlinear partial differential equations, using finite-difference methods [3]. A variant of Berger-Oliger mesh refinement is used to resolve the different scales of the problem with 12-14 refinement levels. Parallelization is based on domain decomposition and MPI. The combination of aggressive mesh refinement with high-order finite differencing (6th- and 8th-order) makes the code communication intensive, and we typically use all the memory available per core, tuning the sizes of mesh-refinement boxes and number of cores for each run.

Our simulations cover the last 10 orbits of black-hole binaries with the aim of synthesizing from our numerical results and analytical perturbative methods a waveform model that is accurate enough to detect and identify the first such signals ever to be observed. We face a seven-dimensional parameter space of the mass ratio and two spin vectors, where a single numerical simulation may require several hundred thousand CPU hours. Spanning the parameter space may thus not seem feasible at first, but a judicious strategy of proceeding along the principal directions of parameter dependence and exploitation of degeneracies has allowed us to progress in steps from initially non-spinning black holes to the recent breakthrough that allows us to construct approximate precessing-binary waveforms from non-precessing ones [4,5], with the potential to model the essential features of observable signals with not more than a few hundred simulations. This will be feasible on European Tier-0 machines before routine detections will be made.

Results

Our previous work was limited to mass ratios up to 4, which has proven rather limiting for GW data analysis purposes. The focus of our new work on SuperMUC have been simulations at mass ratios 8–18, which should be sufficient to connect to analytical calculations of the extreme-mass-ratio case, thus yielding a description of the whole parameter space. However, solving the Einstein equations for such mass ratios is computationally very challenging due to the difference in spatiotemporal scales determined by the masses of the individual black holes. Overcoming the difficulties we describe below, we were able to use our 37-million-hour PRACE allocation to complete simulations at different resolutions of 12 binary configurations at mass ratios 8, 10, 15, and 18, and different spin configurations. These include the most expensive numerical relativity simulations to date that we are aware of, running between 768 and 1536 cores for up to four calendar months each, involving numerous restarts from checkpoints.

In order to maximize our throughput we have developed a strategy to bundle several individual simulations into larger jobs. After each job step bundles can be flexibly reconfigured. In some cases jobs for single simulations had to be submitted to run the last few hours of such long simulations. Initial robustness problems at job startup were solved by restricting jobs to a single island. Several problems had to be overcome to carry out our work plan. The first problems were of a scientific nature: both the methods we had used previously to adapt our coordinate gauge conditions to different mass ratios and spins, and the perturbative methods we had used to construct our initial data parameters, proved insufficient for high mass ratios. In parallel to eventually solving these problems, we faced a software issue: in the first half-year of our allocation it was not possible to bundle together smaller simulations to larger jobs with satisfactory performance, due to a bug in the IBM parallel environment at SuperMUC. LRZ staff helped us to analyze the problem and provided us with a workaround, which we have been using in the last few months to go through our work plan with increased speed. During the last ~4 months we used more than 20 million hours of our 37-million-hour allocation. This was possible by recording detailed job statistics, and configuring our job bundles accordingly. The number of cores in "queued" and "running" states is shown in Fig. 1, along with the total number of cores in queued or running jobs. The maximum and the mean number of cores per job are shown in Fig. 2. As can be seen, toward the end of our allocation we needed to reduce job sizes to increase throughput, but running large bundles of roughly the size of a single island over several months has not caused significant problems in robustness or performance.

Our code writes three files per core: a "physics log file," a performance-statistics log file, and a checkpoint file, plus several hundred files that accumulate science data during the run, plus a few files every few time steps, which are used for visualizations. The greatest quantity of data are in checkpoint files, which are typically overwritten every 8-12 hours, and amount to several hundred GByte in total per simulation. In order to safeguard against corruption of checkpoints during the month-long simulations, backups were created in the TSM archive system and partially in the PROJECT directory. Due to the fact that most of our simulations were running side by side for several months, our peak SCRATCH usage was about 40TByte.

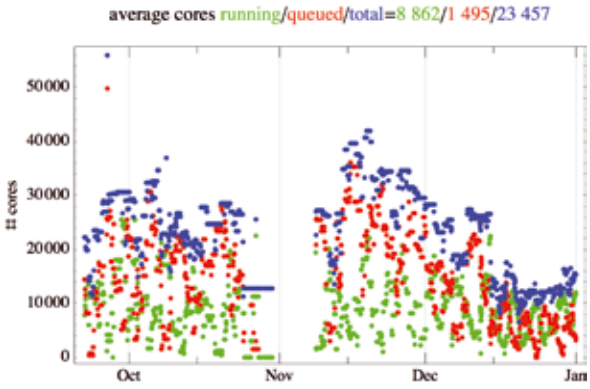

Figure 1: Cores in running and queued states. The ~1 week "hole" is due to downtime and SuperMUC reconfiguration that required changes to our monitoring code.

We are currently analysing our data set in order to extend our waveform models for the 3-dimensional non-precessing parameter space of binaries to large mass ratios in the next months. In addition, we have also performed several series of less expensive simulations, mapping out the parameter space for non-precessing unequal-spin cases up to mass ratio 4 at low resolution, and performing dozens of precessing simulations to prepare systematic high-resolution surveys of this region of the parameter space in the future. While most of our previous work has been focused on modeling only the dominant quadrupolar spherical harmonic mode of GW emission, our new simulations performed on SuperMUC will also allow us to extend our models to subdominant harmonics, which will be most relevant to accurately identify the heaviest black-hole binaries we will observe.

On-going Research

Quantitatively understanding the parameter space of black-hole binaries to the level of detail that will be observed through gravitational waves in the next five years is an undertaking that will require several tens of millions of CPU hours. In our project we have used SuperMUC to demonstrate for the first time that it is feasible to manage many individual simulations requiring several hundred cores each, as well as the required sustained high throughput. We have overcome a number of scientific and software obstacles as detailed above, and are now in an excellent position to complete our program to develop an analytical waveform model across the astrophysically expected parameter space on SuperMUC, which we plan to explore in follow-up projects. A next generation computer would make it possible to keep up with the increasing accuracy requirements of GW detectors and to also study the more complicated physics of neutron stars in much more detail than what is currently possible.

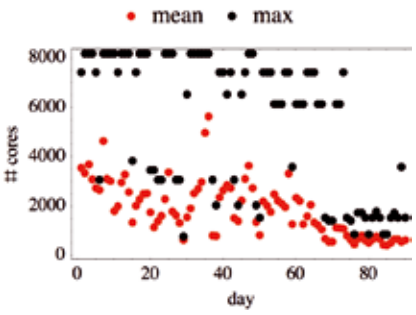

Figure 2: Maximum and mean job sizes during the last ~100 days of our allocation.

References and Links

[1] LIGO Scientific Collaboration, http://ligo.org
[2] European Gravitational Observatory, http://www.ego-gw.it
[3] S. Husa, J.A. Gonzalez, M. Hannam, B. Brügmann, U. Sperhake, Classical and Quantum Gravity 25, 105006 (2008).
[4] http://www.gw-models.org (includes a complete list of related publications of our collaboration).
[5] P. Schmidt, M. Hannam, S. Husa, Phys. Rev. D 86, 104063 (2012).

Multi-scale, Multi-physics Plasma Simulations

1

Research Institution
University of Pisa

Principal Investigator
Francesco Califano

Researchers
Pierre Henri, Matteo Faganello, Dario Borgogno, Francesco Pegoraro

Project Partners
Institute for Practical Computation, LMU Munich

LRZ Project ID: pr89ma (PRACE project)

Introduction

The understanding of the coupling between the solar wind and the magnetosphere is of crucial importance in the context of space weather modeling and forecasting. This coupling strongly depends on the solar wind properties and their variability, in particular on the direction of the solar wind magnetic field. When the solar wind (SW) and magnetosphere (Msph) field lines are nearly parallel, the so-called northward conditions, the system becomes unstable against the Kelvin-Helmholtz instability (KHI) at low latitudes (equatorial plane). The instability, driven by the velocity shear between the SW plasma flow and the Msph plasma at rest, eventually generates large scale, fully rolled up MHD vortices of typical size of the order of many ion kinetic scale length, as shown by satellite observations [1]. The vortices are in turn unstable against vortex pairing and various secondary instabilities [2] leading to the formation of a mixing layer responsible for the entry of SW plasma into the Msph. The competition between vortex pairing and secondary instabilities has been deeply investigated in the last ten/twenty years mainly using a 2D fluid modeling. However, a 2D approach cannot take into account the global magnetic field topology where the lines are connected on one side to the Earth and, on the other side, to the open space. A second aspect requiring a fully 3D model is that the KHI is stabilized at high/low altitude thus requiring a fully 3D configuration. Here we present our investigations of the plasma dynamics driven by the KHI at the Msph flanks carried out in the framework of an European FP7 project SWIFF [3]. Our physical model is based on the Hall-MHD set of equations in 3D slab geometry with open boundary conditions along the x-axis (perpendicular to the magnetopause) and periodic along the northward direction (z-axis) and the SW direction (y-axis) [4]. All quantities are normalized to ion scales, the ion skin depth d_i, the Alfven velocity V_a, the ion cyclotron frequency Ω_{ci}. We impose an initial velocity shear that generates large-scale vortices only around the equator by adopting a 2D analytical equilibrium able to retaining the high-latitude stabilization for the KHI, which is considered as a key ingredient for the modeling of the "3D real" system. Our main result has been to demonstrate that in a 3D configuration the standard 2D vortex dynamics developing in the equatorial plane, as studied in the last ten years, is no longer the leading mechanism able to set-up a mixing layer responsible for the entry of SW into the Msph. In particular, we have identified a new, fully 3D mechanism, which we conjectured as driven by a magnetic reconnection (MR) process arising at mid-latitude and not in the equatorial plane [4]. As an example, in Fig. 1 we show five planes corresponding to the equator (middle), high-latitude planes (bottom and upper) and mid-latitude (in between). Blue/red colors (except that at mid-latitude) represent a passive tracer of the Msph/SW plasma, respectively, moving at $\pm^1/_2 V_{SW}$ velocity. Fig. 1 shows that KH vortices are generated in the equatorial plane while the KHI is stable at higher and lower latitudes. In the frame where vortices are at rest, the magnetic field lines, frozen in the Msph and SW (blue and red) plasmas are bent and arched because of the vortex rolling-up and because of the motion of the field lines anchored in the moving plasmas at high/low mid latitude with respect to their anchoring in the vortices. As a result of such bending and stretching of the field lines, extended current sheets

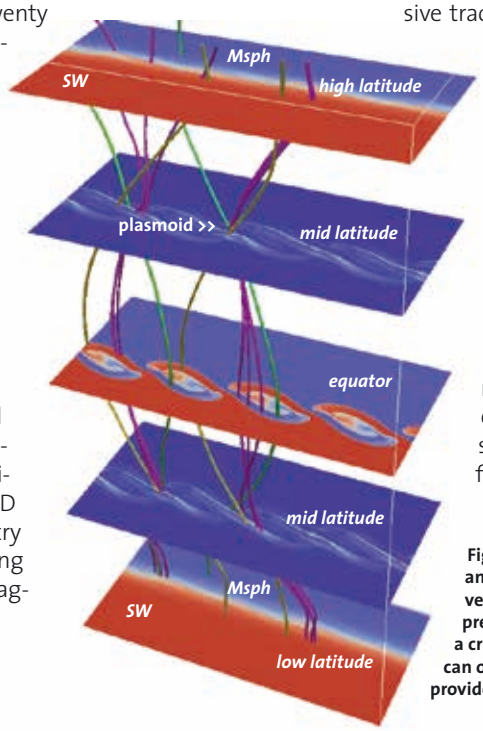

Fig. 1: Comparison of ASDEX-Upgrade, JET and ITER-size plasma simulation volumes and vessels. Studies regarding the scaling from present-day to future devices like ITER represent a crucial task for turbulence investigations and can only be performed in HPC environments as provided by SuperMUC.

are generated at mid-latitudes. By a careful inspection of the mid latitude regions, we have demonstrated the onset of a MR process and the formation of plasmoid-type structures at mid-latitude [5]. The plasmoid structure is illustrated in Fig. 2. We underline that this spontaneous onset of reconnection will proceed, in general, in both hemispheres on a similar time scale, thus creating magnetic flux tubes topologically connected to the Earth at both poles but, at the same time, embedded in the SW when crossing the low-latitude region. This point could explain the entry of SW plasma into the Msph. A direct comparison of 3D numerical simulations with satellite data has been recently performed and allowed us to support the validity of the mid-latitude reconnection process [6].

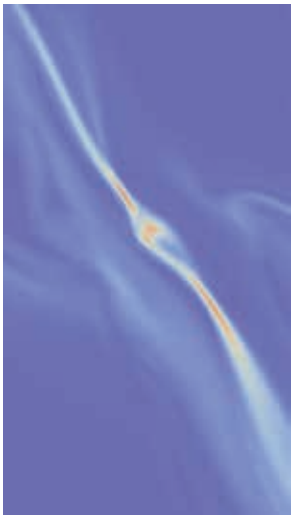

Fig. 2. The plasmoid at mid-latitude

A second topic developed in the context of our super-computing project on Supermuc at LRZ is the analysis of the magnetofluid turbulence induced by the non-linear evolution of the KH vortices in the 2D plane perpendicular to the ambient magnetic field. The analysis of the turbulence is important, on one side, for the understanding of the transport properties of the mixing layer at the Msph flanks and, on the other side, for direct comparison with satellite data that we intend to perform in the next period after the end of this PRACE project. Here we present preliminary results obtained from 2D numerical simulations using the two-fluid model in the presence of a guide magnetic field along z, perpendicular to the (x,y) plane of the simulation. We impose an intial shear flow along y representing the direction of the solar wind which generates two MHD size vortices that are completely disrupted by the development of secondary fluid and magnetic instabilities. A constant magnetic field of the order of the 2% of the guide field is present at the initial time and parallel to the flow direction. The magnetic tension associated to this in-plane magnetic field is very small and unable to inhibit the development of the KHI. In Fig. 3 we show the z-component of the magnetic fluctuations δB_z in the (x,y) plane. We see that after the development of fluid and magnetic secondary instabilities that have disrupted the primary KH vortices, the system has reached a fully turbulent state. We can define this regime as a multi-scale plasma regime where the large scales, $5 < L < 100$ (in d_i units) corresponding to the size of the initial vortices, evolve following an MHD dynamics, while the small scales, $L < 1$, follow a faster EMHD-like dynamics. In Fig. 4 we show the magnetic and electric energy spectrum of the fluctuations taken in the middle of the shear layer, $x \sim 200$ (see Fig. 3), versus k_y (we recall that y is the direction of the SW flow). The blue and red color represents the magnetic and the electric spectrum, respectively. We see that the spectrum is characterized by two distinct power low slopes, -5/3 at large scales for $k < k_i$, and -2.8 at large wave numbers for $k > k_i$. Here $k_i \sim 1$ represents the wave number corresponding to the d_i ion scale length. The slope change around $k \sim k_i$ is the typical signature of the change of the physical regime, from single-fluid to two-fluid and has been also observed by satellite measurements.

The simulations presented here have been performed using typical grid size of the order of 1024^3 in 3D and of 8192^2 in 2D. Future development of this work will address direct comparison with satellite data, in particular with those obtained by the Cluster and Themis missions.

All the simulations have been performed on Supermuc at LRZ. The research on the physics of the Magnetosphere flanks by means of a two-fluid model leading to these results has received funding from the European Commission's Seventh Framework Programme (FP7/20072013) under the grant agreement SWIFF (Project No. 263340, www.swiff.eu).

References and Links

[1] H. Hasegawa et al., Nature **430**, 755, 2004
[2] P. Henri et al, Phys. Plasmas **19**, 072908, 2013
[3] Space Weather Integrated Forecasting Framework; http://www.swiff.eu
[3] M. Faganello et al., Plasma Physics and Controlled Fusion **54**, 124037 (2012)
[4] M. Faganello et al., Europhys. Lett. **100**, 69001, 2012
[5] D. Borgogno et al., in preparation
[6] M. Faganello et al., *submitted* to Europhys. Lett.

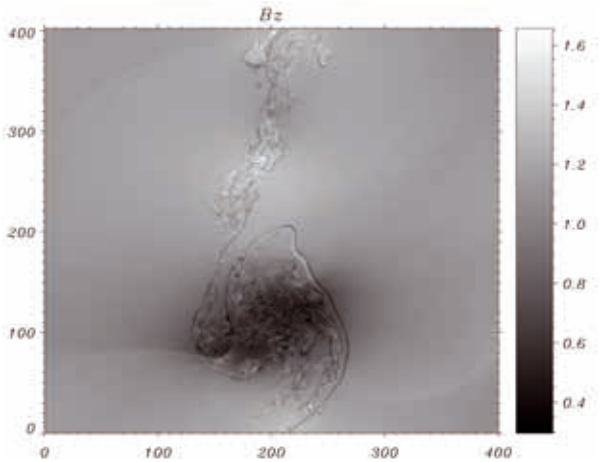

Fig.3 The parallel magnetic fluctuations in the plane perpendicular to the guide field

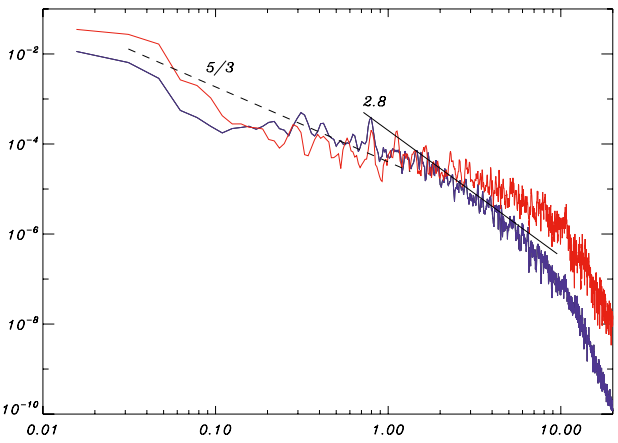

Fig.4 The magnetic (blu) and electric (red) energy spectrum vs ky in the plane perpendicular to the guide field

Plasma acceleration: from the laboratory to astrophysics

1

Research Institution
GoLP/IPFN, Instituto Superior Técnico

Principal Investigator
Jorge Vieira

Researchers
L.D. Amorim, Paulo Alves, Anne Stockem, Thomas Grismayer, Luís Silva

Project Partners
–

LRZ Project ID: pr89to (PRACE project)

Introduction

The study of novel particle acceleration and radiation generation mechanisms can be important to develop advanced technology for industrial and medical applications, but also to advance our understanding of fundamental scientific questions from sub-atomic to astronomical scales. For instance, particle accelerators are widely used in high-energy physics, and in the generation of x-rays for medical and scientific imaging. Although extremely reliable, conventional particle accelerator technology is based on radio-frequency fields, which can lead to very long and very expensive machines. For instance, the LHC at CERN is several tens of kilometers long and costed several billions of Euros. Thus, investigating new more compact accelerating technologies can be beneficial for science and applications. Plasmas are interesting for this purpose, because they support nearly arbitrarily large electric fields, and thus lead to a future generation of more compact accelerators. Plasma acceleration experiments, for instance, succeeded in doubling the energy of electron beams accelerated for several kilometers at SLAC in less than a one-meter long plasma.

Most of the matter in the known universe is also plasma. Hence, plasma based particle acceleration and radiation generation mechanisms may also play a key role in some of the astrophysical mysteries that remain unresolved, such as the origin of cosmic rays and gamma ray bursts through collisionless shocks and magnetic field generation and amplification mechanisms. Using computing resources at SuperMUC we have explored several questions with impact on the development of plasma acceleration technology and improving on our understanding of the mechanisms that may lead to particle acceleration and radiation in astrophysics. This report will describe some of the highlights that were achieved during our present allocation in these topics.

Results

Plasma acceleration in the laboratory: towards plasma-based linear colliders

As conventional particle acceleration techniques are hitting their technological limits, plasma based acceleration is emerging as a leading technology in future generations of higher energy, compact particle accelerators. Although initially proposed more than 30 years ago [1], the first ground breaking plasma acceleration experimental results appeared in 2005. Plasma acceleration is presently an active field of research, being pursuit by several leading laboratories (e.g. SLAC, DESY, RAL, LOA, LBNL). Electron or positron acceleration in plasma waves is similar to sea wave surfing. Plasma accelerators use an intense laser pulse or particle bunch (boats on water) as driver to excite relativistic plasma waves (sea waves for surfing). Accelerating structures are sustained by plasma electrons and are not affected by physical boundary effects as in conventional accelerators. The plasma accelerator only lasts for the driver transit time through the plasma. The resulting plasma wavelength is only a few microns long (<10 m for sea waves), and support accelerating electric fields up to 3 orders of magnitude higher conventional particle accelerators. These accelerating fields can then accelerate electrons or positrons (as surfers in sea waves) to high energy in short distances (<1 m).

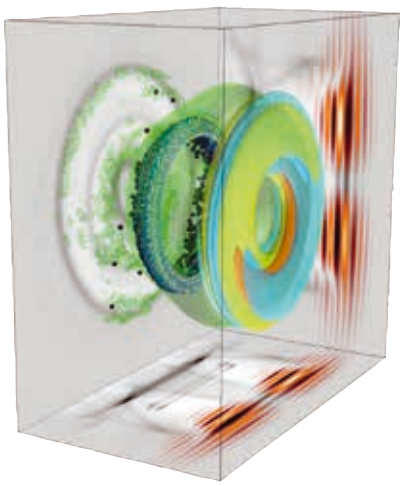

Figure 1: 3D simulation of a plasma wakefield excited by a doughnut shaped laser.

One of the challenges associated with the design of a plasma based linear collider is positron acceleration. Most important plasma based acceleration experimental results were performed in strongly nonlinear regimes, enabling to optimize the quality of accelerated electron bunches. It has been recognized, however, that these strongly non-linear regimes, are not suitable for positron

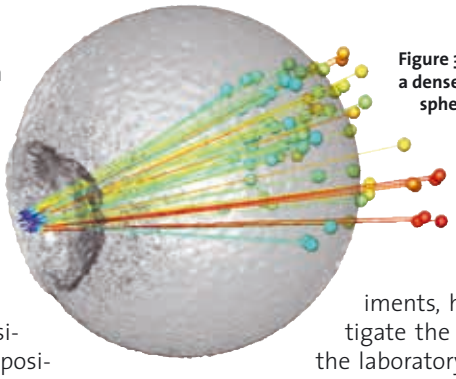

Figure 3: 3D simulation result showing the irradiation of a dense hydrogen target by a high intensity laser. Colored spheres represent accelerated protons.

acceleration. Using SuperMUC we then explored novel configurations for positron acceleration in strongly non-linear regimes. We investigated plasma acceleration driven by narrow particle bunch drivers and by doughnut shaped Laguerre-Gaussian lasers. Although the work using narrow particle bunch drivers is still in progress, we found that the wakefields driven by Laguerre-Gaussian beams can have good properties for positron acceleration in the strongly non-linear. Figure 1 is simulation result showing a doughnut plasma wave. Typical simulations require $4x10^4$ (doughout wakefields) – $2x10^5$ (narrow drivers) core-hours, pushing $2.5\ x10^9$ – $1.6x10^{11}$ particles for more than $4x10^4$ time-steps.

We also performed simulations to clarify important physical mechanisms associated with a future plasma based acceleration experiment at CERN using proton bunches from the Super Proton Synchrotron (SPS) at the Large Hadron Collider (LHC) [2,3]. In this experiment, the proton bunch will drive plasma waves through a beam plasma instability called the Self-modulation Instability or SMI. The SMI modulates the bunch density profile radially. A fully self-modulated beam then consists of a train of shorter uniformly spaced bunches. Each of them will excite a plasma wave that grows through the beam, thereby producing acceleration gradients that grow through the beam. A long proton bunch will also be subject to the hosing instability or HI. The HI can lead to beam break up. Hence, HI suppression is required for successful experiments. SuperMUC simulations unraveled a new HI instability suppression mechanism, establishing the conditions for stable plasma wakefield generation in future experiments at CERN. Figure 2 illustrates a fully self-modulated particle bunch propagating stably in the plasma, without HI growth. Typical simulations ran for roughly $5x10^4$ core-hours, pushing $6.4x10^8$ particles for more than $2x10^5$ time-steps.

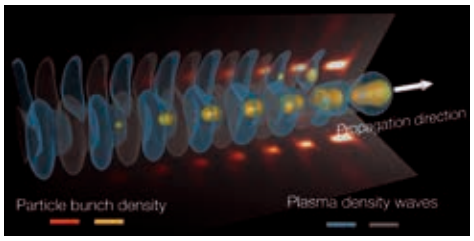

Figure 2: 3D simulation of a long particle bunch in a plasma leading to stable accelerating fields.

Particle acceleration in the universe: mimicking astrophysical conditions in the laboratory

The origin of cosmic rays and gamma ray bursts are fundamental mysteries for our understanding of the universe. These questions are closely related to particle acceleration in shocks and to strong magnetic field generation. Collisionless shocks have been studied since decades in the context of space and astrophysics due to their potential of efficient particle acceleration to energies larger than 10^{15} eV. Large-scale magnetic fields are also important for particle acceleration in astrophysics, but also allow for non-thermal radiation processes to operate. Exploring these extreme scenarios is complex, since astronomical observations are limited. Recent experiments, however, have started to investigate the onset of collisionless shocks in the laboratory resorting to high power laser pulses. There are distinct shock types according to the energy transfer to the plasma. We performed simulations in SuperMUC that enabled to explore the transition between different shock types. Our simulations showed that electrostatic shocks, which lead to the formation of strong electric fields, can be used to efficiently accelerate plasma ions or protons (see Fig.3). Electromagnetic shocks, which lead to the formation of intense magnetic fields, can lead to particle acceleration in astrophysics through Fermi-like acceleration mechanisms. Magnetic field generation also occurs in electromagnetic shocks, due to the Weibel or Current Filamentation Instability (WI or CFI). These instabilities can grow when counter-streaming plasma flows interpenetrate. Magnetic field generation and amplification is important in astrophysics as they can lead to stron bursts of radiation. Thus, in addition to magnetic field amplification in collisionless shocks, simulations at SuperMUC enabled the discovery of a novel mechanism driving large-scale magnetic fields in shearing counter-streaming plasma flows. Velocity shear flows lead to the development of the Kelvin-Helmholtz Instability or KHI. We found that the KHI is an important dissipation mechanism, capable to efficiently transform plasma kinetic energy into electric and magnetic field energy [4]. Fig. 4 shows the development of the characteristic KHI vortices and associated magnetic field in conditions relevant for astrophysics. Each simulation took $2x10^4$ core-hours pushing 10^{10} particles for more than 10^6 iterations.

On-going Research / Outlook

SuperMUC enabled to make important advances to plasma acceleration in the laboratory and in astrophysics in conditions for which purely analytical models are currently unavailable. We managed to perform very large simulations, which would not have been possible in smaller supercumputers.

References and Links

[1] T. Tajima and J. Dawson, Phys. Rev. Lett. 43 267 (1979).
[2] A. Caldwell et al, Nat. Physics 5, 363 (2009).
[3] http://awake.web.cern.ch/awake/
[4] T. Grismayer et al Phys. Rev. Lett. 111 015005 (2013).

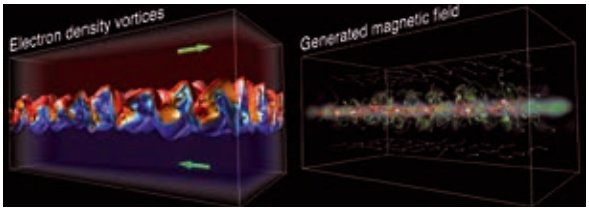

Figure 4: 3D simulation result showing electron density vortices and magnetic field due to the KHI.

Earth and Environmental Sciences

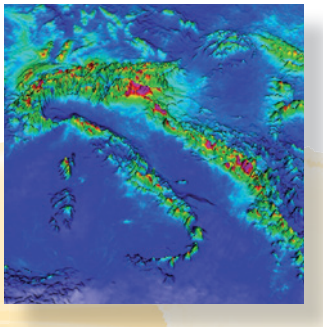

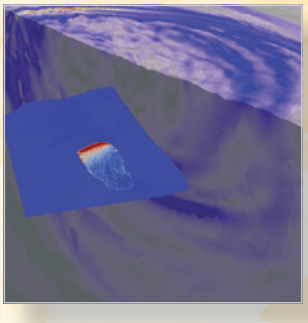

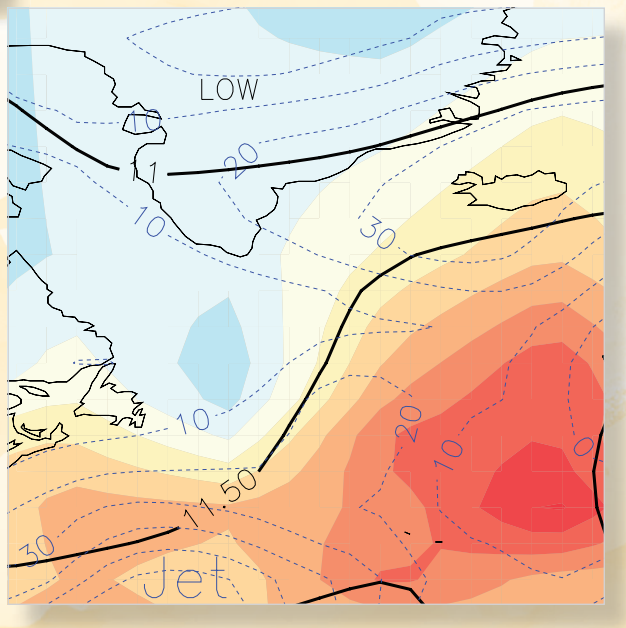

Advancements in Seismic Tomography and Seismic Source Analysis

Research Institution
Department of Earth and Environmental Sciences

Principal Investigator
Heiner Igel

Researchers
Christian Pelties, Alice Gabriel, Martin Käser, Stefan Wenk, Alan Schiemenz, Moritz Bernauer, Lion Krischer, Simon Stähler

Project Partners
KAUST, ETH Zürich, Caltech, TUM

LRZ Project ID: h019z (KONWIHR project), pr63qo (KONWIHR project)

Introduction

The computational seismology group at LMU Munich is focused on the development and application of numerical modeling and analysis software to study the accumulation, release and propagation of seismic energy in the Earth. Moreover, tomographic techniques are advanced to enhance the illumination of the Earth's internal structure and material composition.

In particular, we investigated full waveform inversions for industrial and academic research. In fact, we optimized setup parameters as well as workflows and performed forward simulations to analyze seismic wave propagation in complex geological 3D media with respect to kinematic and dynamic source descriptions.

Besides the established standard processing of translational ground motions we further incorporate rotations in our investigations to extend the available data space and are therefore able to reduce the non-uniqueness of finite source inversions.

We made use of modern state-of-the-art modeling software based on the high-order accurate Spectral-Element (SE) and Discontinuous Galerkin (DG) methods.

Results

3-D full-waveform inversion using simultaneously encoded sources
We developed a method of simultaneously encoded sources to perform computationally inexpensive full-waveform inversion (FWI) on fixed-spread, marine seismic data. A workflow is proposed whereby both data- and model-based preconditioning strategies are enforced to mitigate the non-linearity of the seismic inverse problem. Artificial crosstalk, introduced by the false correlation of forward and adjoint wave fields of simultaneously simulated sources, is minimized by simulating super-shots of random linear combinations of data with iteration-varying encoding (Fig. 1).

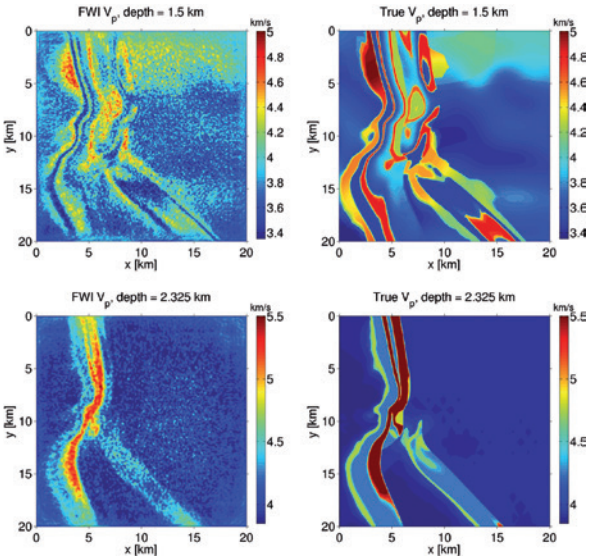

Fig. 1: True horizontal Earth models (seismic velocities) are given in the right, inversion results in the left column. Key features of the true model can be reconstructed by inverting a single "supershot" resulting in a speed-up of 500 for the inversion.

We choose simple and robust strategies that are suitable for the inversion of relevant (low) frequency bands. We preconditioned the gradient search direction during inversion via an absolute threshold given as a function of depth. Simulations were carried out with the SpecFEM3D code based on the Spectral-Element method. The key feature of the inversion scheme is the many calculations of the forward problem. A typical forward solution run on approx. 200 cores required 20 min wall-clock time.

Reducing non-uniqueness in finite source inversion using rotational ground motions
The detailed knowledge of earthquake rupture processes is essential for a comprehensive management of seismic hazard. The kinematic description of earthquake sources, i.e. the evolution of the rupture process in space and time on a finite fault, is one key for understanding earthquake mechanics. However, earthquake source inversion

is an ill-posed inverse problem with multiple solutions. To reduce the non-uniqueness in finite source studies we included rotational ground motion measurements in addition to conventional strong translational ground motion data. We demonstrated that synthetic earthquake scenarios combining both, translational and rotational ground motion provide substantially more information on earthquake source parameters compared to scenarios exclusively based on velocity seismograms. Accounting for the ill-posedness of the inverse problem and the difficulties in combining distinct data types we applied a Bayesian, i.e. probabilistic, approach in this study. The demands on computational resources concerning probabilistic inverse algorithms can be challenging. However, the simulations in this initial study took on the order of 10h on 1000 cores. Based on the Bayesian approach we will expand the application of this novel observations to investigate both structural and earthquake source parameters at the same time, which will substantially increase the computational costs.

Investigating the generation of Love waves in secondary microseisms

Secondary microseismic noise can be attributed to oceanic disturbances causing non-linear, second-order pressure perturbations at the ocean bottom. This mechanism can be considered as a seismic source acting normal to the ocean bottom. In an isotropic, layered half-space with flat interfaces vertical forces generate only longitudinal and vertical polarized, transversal particle motions. This way, so called Rayleigh waves are excited at the surface. However, several real data observations show significant Love wave contributions in the secondary microseismic frequency band (0.1-0.25 Hz). But, Love waves are caused by the interference of horizontally polarized shear waves, which cannot be explained by the aforementioned source mechanism.

We applied point and extended force sources acting, delayed in time, on the dipping sea-floor topography to study the generation of Love waves. Further, the effect of variations in the shape of the bathymetry is investigated (Fig. 2), which can cause the conversion of Rayleigh into Love waves. We found a strong influence of sea-floor roughness in the source region on the amount of the generated Love wave energy, whereas surface wave conversion has a minor effect. Simulations were performed with SeisSol (DG method) on 1600 cores of SuperMUC using an average wall-clock time of 10h.

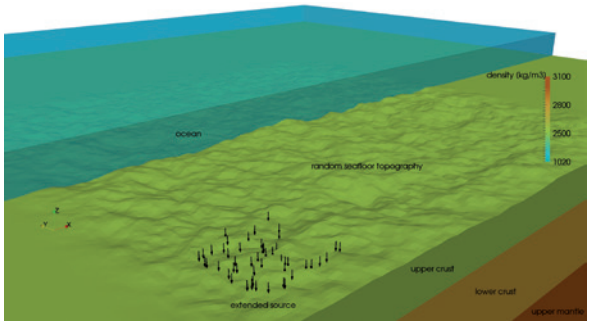

Fig. 2: Ocean model with irregular bathymetry. The black arrows indicate a random distribution of force sources.

We will further investigate and quantify the effects of internal material scattering on the Love to Rayleigh wave energy ratio depending on statistical properties like the magnitude of perturbation, correlation length and fractal dimension.

A 3D dynamic rupture scenario for the curved Northridge 1994 fault

The 1994 Northridge event was felt over 200,000 km² in US and Mexico, left sixty killed, more than 7,000 injured, 40,000 buildings damaged and caused a loss of 44 Billion US$. Its ground shaking involved high accelerations (~1g) exceeding the building codes at many instances. In the year of the 20th anniversary of the 1994 Northridge earthquake a fresh look with today's state-of-the-art modeling capabilities on its source dynamics is performed on SuperMUC. In a large-scale dynamic rupture scenario conducted with SeisSol (DG method) and constrained by observations we find that the effect of realistic fault geometries on the source dynamics and excited ground motions may be dominant (Fig. 3). The scenario required the incorporation of geological velocity structures, topography, and fault shape data and enables us to study different representations of natural fault zone complexities and their impact on earthquake dynamics and seismic hazard assessment. The study reveals the potential of modern dynamic rupture simulation methods to further bridge the gap between earthquake source physics and seismological observations in the long term. For generating and testing the model for frequencies up to 1.5 Hz, tens of simulations on 500 cores required 4h wall-clock time each. Computational costs of earthquake scenario simulations scale with the complexity of the setup and the resolved frequencies of the wave field.

We will extend the application of SeisSol to realistic scenario settings, e.g. by considering plastic material deformation and tackling the challenge of resolving high-frequency ground motions relevant for engineering and hazard assessment.

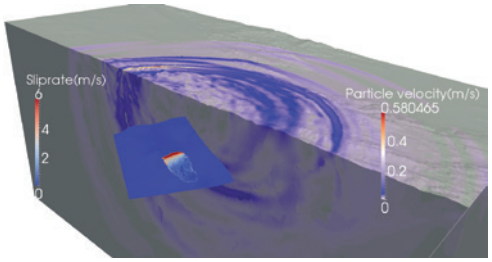

Fig. 3: Snapshot of the rupture evolution, which is pulse-like due to fault geometry effects, and the corresponding 3D wave field for the 1994 Northridge scenario.

References and Links

[1] Schiemenz, A., and Igel, H., Accelerated 3-D full-waveform inversion using simultaneously encoded sources in the time domain, *Geophys. J. Int.* (2013) 195, 1970–1988

[2] Bernauer, M., Fichtner, A., and Igel, H., Reducing non-uniqueness in finite source inversion using rotational ground motions, submitted to Journal of Geophysical Research, 2014.

[3] Wenk, S., Hadziioannou, C., Pelties, C., and Igel, H., Investigating the generation of Love waves in secondary microseisms using 3D numerical simulations, *EGU 2014 General Assembly*, Vienna, Austria, 2014.

[4] Gabriel, A.-A., Pelties, C., Atanasov, A., Sachdeva, V., Passone, L., Jordan, K. E., Ely, G., Mai, P. M., Large-Scale Earthquake Dynamic Rupture Simulations with the ADER-DG Method, Oral presentation, 2013 SIAM Conference on Mathematical and Computational Issues in the Geosciences, Padova, Italy, 2013.

Modelling the impact of transport on the climate

Research Institution
DLR – Institut für Physik der Atmosphäre

Principal Investigator
Robert Sausen

Researchers
Sabine Brinkop, Duy Cai, Simone Dietmüller, Roland Eichinger, Veronika Eyring, Christine Frömming, Hella Garny, Klaus-Dirk Gottschaldt, Phoebe Graf, Volker Grewe, Johannes Hendricks, Patrick Jöckel, Christopher Kaiser, Sigrun Matthes, Mariano Mertens, Michael Ponater, Mattia Righi, Eleni Tsati

Project Partners
MESSy-Consortium (http://www.messy-interface.org)

LRZ Project ID: h1112

Introduction

The transport sectors (land-based transport, shipping and aviation) are major sources of atmospheric pollution. Due to increasing world population, economic activities and related mobility, the emissions from these sectors are growing faster than other human activities and this growth is projected to continue in the future. Quantifying the impact of these sources on atmospheric composition and climate is therefore of primary importance not only from a scientific point of view, but also for providing support to policy makers. This is the main task of our research activity at SuperMUC, which focuses on the simulation of the Earth system, in particular on the interactions between climate, atmospheric chemistry and aerosol particles, as well as on the impact of external perturbations on the atmosphere, its composition and dynamics.

Our model system is ECHAM5/MESSy Atmospheric Chemistry (EMAC), based on the atmospheric general circulation model ECHAM5 [1] and coupled to sub-models simulating atmospheric chemistry and aerosol dynamics, in the framework of the Modular Earth Submodel System (MESSy) [2]. EMAC supports different horizontal and vertical resolutions, and a wide range of possible configurations, with various parameterisations for the simulated processes. We work to continuously improve and expand the model, including more sophisticated representations of physical and chemical atmospheric processes. Complementary to that, the model is being regularly evaluated to test its ability to reproduce observational data.

Our model studies contribute to national and international projects, including the global assessments of the Intergovernmental Panel on Climate Change (IPCC) and the World Meteorological Organization (WMO).

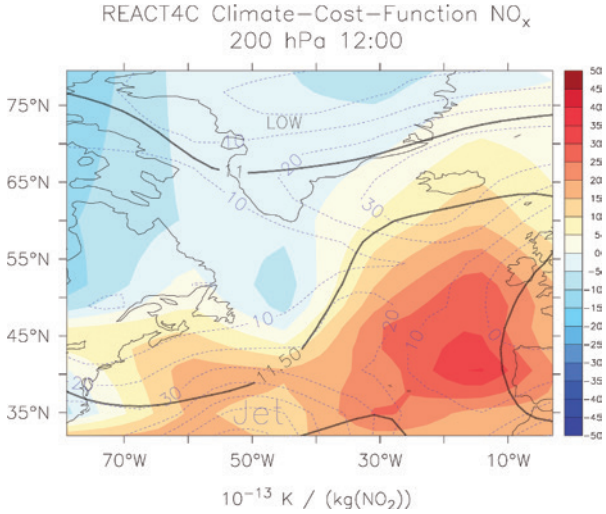

Figure 1: Climate-cost function: The coloured area shows the average temperature response over 20 years in a weather pattern with the characteristic "strong tilted jet". Black and blue lines represent the geopotential height (in km) and the wind velocity (in m/s), respectively.

Results

Climate-cost functions for climate-optimal flight planning
Within the EU-project REACT4C (Reducing Emissions from Aviation by Changing Trajectories for the benefit of Climate), EMAC has been extended with a Lagrangian tracer transport model, in which air traffic emissions are released at well-defined points in the North Atlantic region and at selected times of the day.

The model allows the explicit calculation of the contribution of aircraft emissions to the atmospheric concentrations of nitrogen oxides, ozone and methane.

In addition to chemical processes, also micro-physical processes (e.g., the development of contrail-cirrus clouds) are simulated on the trajectories. A typical weather pattern in the North Atlantic, which is charac-

terized by a strong tilted jet stream, was selected and the typical strength of air traffic emissions was considered. But instead of using an air traffic inventory, the emissions in the model were released in a region covering the North-Atlantic flight corridor, in order to estimate the potential impact of air traffic flying at that specific location and time. The resulting climate-cost functions (Figure 1) form the basis for an optimisation of aircraft routing.

Atmospheric and climate impacts of changing aircraft cruise altitudes

Simplified mitigation studies have been performed as part of a multi-model analysis in REACT4C. The objective is to identify the major processes and mechanisms for the aviation impact on atmospheric chemistry and climate. For this study, EMAC has been used in nudged Quasi Chemistry Transport Model (QCTM) mode [3], in order to calculate the impacts of alternative routing strategies. By comparing the effects of different aircraft-related nitrogen oxides emission scenarios (a reference base case, a "flying higher", a "flying lower" and a "no aircraft" scenario) a quantitative estimate of aviation contribution to chemical impacts and climate effects has been derived. The comparison with four participating Chemistry-Transport models showed that large differences in the chemical perturbation exist (more than 50%). The radiative impact of different routing scenarios in all models showed consistent signs when evaluating mitigation impact: the "flying higher" case shows increased ozone contributions and a higher radiative forcing, while the "flying lower" leads to less short-lived ozone forcing.

TAGGING: attributing chemical changes to emission categories

Simulations with EMAC have been performed to diagnose the impact of various emissions, such as nitrogen oxides and carbon monoxide, from different sources, such as road traffic, biomass burning, lightning, etc. on the atmospheric composition. The underlying method has been implemented in the EMAC sub-model TAGGING and allows to tag emitted species and to follow them through their reaction pathways. Thereby ozone budgets are calculated in a complete way and the contribution of the emissions to secondary species are determined. This procedure enables, for the first time, the calculation of a closed ozone budget and the comparison of the natural and anthropogenic origin of ozone. Results show that lightning contributes by around 20%, methane and stratospheric intrusions by around 15% each and all anthropogenic emissions by around 30% to the tropospheric ozone concentration.

The isotopic signature of the atmospheric hydrological cycle

A new sub-model has been implemented in EMAC containing a second hydrological cycle, including the water isotopologues HDO and $H_2{}^{18}O$. Additionally, it comprises a simple parameterisation for the treatment of the methane isotopologue CH_3D and its effect on the stratospheric budget of HDO. The comparison of the isotopic ratios in precipitation of the model results with data from the GNIP measuring survey of the IAEA-WMO stations and the ECHAM5-wiso model shows good agreement, considering the horizontal resolution of the simulation. A simulation with specified dynamics (i.e., using EMAC in nudged mode) and with high vertical resolution has been used to investigate the ratio of the simulated HDO isotopologue in the stratosphere. Stratospheric 'tape-recorder' signals in HDO and $\delta D(H_2O)$ were detected, which to a certain degree are similar to those from satellite measurements from the ACE-FTS and the MIPAS instrument. Investigations of the 'tape-recorder' signal in $\delta D(H_2O)$ reveal a high correlation with the strength of the Western Pacific Monsoon.

Atmospheric Chemistry and Climate Model Intercomparison Project (ACCMIP)

In the framework of the model evaluation activity, we participated in the ACCMIP project [4], an international model intercomparison project designed to provide input to the Fifth Assessment Report of the IPCC. The main goal is to analyse and evaluate changes in atmospheric composition and Earth's radiative balance from the pre-industrial times (1850) to the future (2100), according to different scenarios for future emissions. The project involved 16 global models from all over the world, including EMAC. The results from all models have been thoroughly evaluated using new and updated observational dataset and specifically focusing on processes related to atmospheric chemistry and climate. Together with the efforts of the other participating models, the EMAC results allowed to assess the future trends of tropospheric ozone and the related climate impacts, the changes in atmospheric OH and in methane lifetime, as well as an extensive assessment on global air quality and climate.

On-going Research / Outlook

We are currently developing simplified models to allow a more efficient assessment of transport impacts under different future scenarios. We are also continuously working to develop and improve our model system. One aim of this development work is to simulate chemical processes at higher spatial resolution, at least on a regional scale. For this, the global EMAC model has been complemented by the on-line nested regional model COSMO/MESSy. This approach will furthermore allow for a more detailed model evaluation based on observational data from aircraft-based measurement campaigns. Moreover, we plan to further investigate the role of methane for climate, its impact on the atmospheric self-cleansing capacity and its contribution to the stratospheric water vapor. And last but not least, we aim to improve even further the assessment of climate mitigation options through aircraft rerouting, by refining and improving our Lagrangian-technique-based methodology.

References and Links

[1] Roeckner et al., 2006. Sensitivity of simulated climate to horizontal and vertical resolution in the ECHAM5 atmosphere model, Journal of Climate, 19, 3771-3791.
[2] Jöckel et al., 2010. Development cycle 2 of the Modular Earth Submodel System (MESSy2), Geoscientific Model Development, 3, 717-752.
[3] Deckert et al., 2011. A quasi chemistry-transport model mode for EMAC, Geoscientific Model Development, 4, 195-206
[4] Lamarque et al., 2013. The Atmospheric Chemistry and Climate Model Intercomparison Project (ACCMIP): overview and description of models, simulations and climate diagnostics, Geoscientific Model Development, 6, 179-206.

Seismic Signature and Dynamics of Earth's Mantle

Research Institution
Geophysics Section, Dept. of Earth and Environmental Sciences, Ludwig-Maximilians-Universität München

Principal Investigator
Bernhard Schuberth

Researchers
Lorenzo Colli, André Horbach

Project Partners
Géoazur (Observatoire de la Côte d'Azur, Université de Nice Sophia-Antipolis, CNRS, France)
Institute de Physique du Globe de Strasbourg (Université de Strasbourg/EOST, France)

LRZ Project ID: pr32mu

Introduction

In this project, we address fundamental questions in the deep Earth sciences on the dynamics of the mantle, the related upward heat transport as well as the associated seismic structures. Understanding the dynamic behaviour of Earth's mantle is important as the flow drives plate tectonics and controls the way the Earth loses its heat. Thus, mantle convection provides boundary conditions - thermal and mechanical - to other key elements of the Earth system (e.g., geodesy, geomagnetism, plate tectonics). A major goal of our project is to shed light on the connection between lower and upper mantle flow patterns. In particular, we want to better understand the role of the multiple phase transitions that take place in that region together with the subsequent expected change in rheological parameters. Here, we present results from one part of the project that focused on the seismic structure in the upper mantle. New tomographic images of the mantle under the South Atlantic were obtained based on full waveform inversions.

The South Atlantic is a region of great geological and geophysical interest. It is characterized by an anomalous residual bathymetry going from the highly elevated African superswell to the abnormally deep Argentine basin, and it has been speculated that the cause of this trend in the residual bathymetry lies in upper mantle flow. Unfortunately, upper mantle structure in the South Atlantic is poorly known, mainly because of the scarcity of seismic data for this region, and thus testing of this hypothesis is particularly difficult. Also of particular interest is the feeding mechanism of the Tristan hotspot and the potential link to the African superplume in the deep lower mantle as its ultimate source. Along with its Pacific counterpart, this large seismic anomaly has received considerable attention in seismological and geodynamic studies, but its connection to the upper mantle still remains elusive.

Most of our knowledge on deep Earth structure and flow comes from the analysis of recordings of seismic waves that travel through the Earth after large earthquakes. Similar to medical tomography, seismic tomography allows us to "see" the present day elastic structure of Earth's mantle in 3-D. Traditional methods of seismic imaging based on ray theory – although computationally inexpensive – rely on strong assumptions that we now know are not satisfied in the solid Earth. Traditional methods are not able to account for so-called finite-fre-

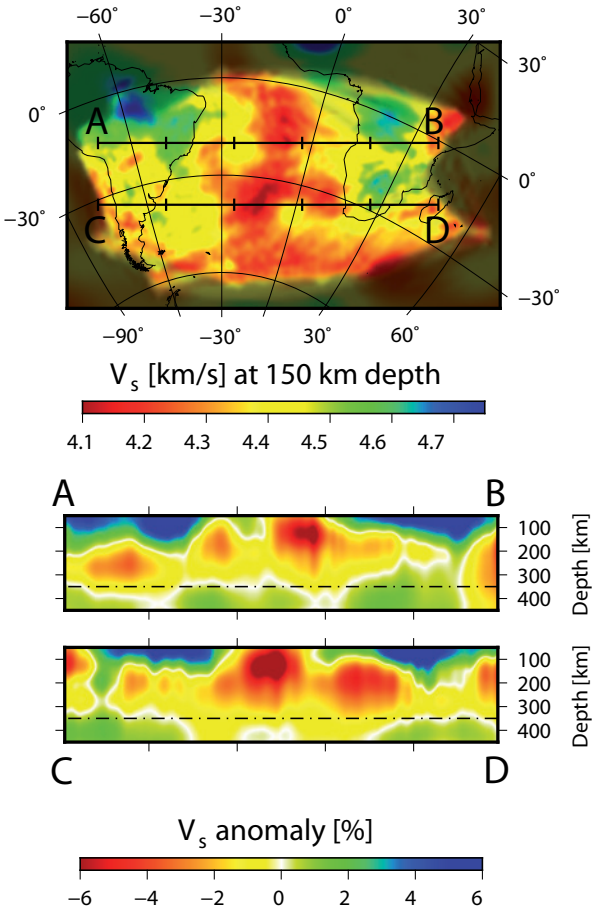

Figure 1: Tomographic images of variations in shear-wave velocity in the South Atlantic region obtained with the full waveform inversion based on the adjoint method [1].

quency effects, such as wave scattering and wavefront healing, that bear significantly on the behaviour of seismic waves, leading to potential artefacts in the final tomographic models. To properly account for the full physics of the system, one must compute the propagation of the full wavefield in a three-dimensional heterogeneous Earth model, and an inversion procedure has to be used that allows us to account for finite-frequency effects.

Full waveform tomography, made possible by the dramatic gain of computational resources in recent years, takes advantage of a numerical solution of the wave equation to account for the effects of 3-D heterogeneous seismic structures on wave propagation. The numerical solution allows one to treat simultaneously all direct, reflected and scattered body and surface waves, thus considerably increasing the exploitable information carried by each seismogram. The inverse problem is solved iteratively using an efficient adjoint method. The adjoint technique is a general and versatile method to compute partial derivatives with respect to model parameters, and has been implemented for a range of geophysical applications that include, in addition to seismic tomography, lithosphere, mantle and core dynamics. The adjoint method exploits the fundamental fact that the change in the observed quantity generated by a change in the model parameters is governed by the physics of the system. In the case of seismology, a change in the elastic properties of some part of the model causes the wavefield passing through that region to be reflected, refracted and diffracted differently, leading to a variation in the synthetic seismograms. This perturbation of the wavefield is still a wavefield itself, and propagates in accordance to the constraints of the wave equation. It is possible to backtrack the place of origin of the perturbation by solving for a subsidiary wavefield subject to a set of equations, called adjoint equations that are derived from the original wave equation. The adjoint equations are still of the wave type, and the source term in the adjoint equation is derived from the misfit between observed and synthetic seismograms.

Results

We have successfully obtained a seismic tomography for isotropic upper-mantle structure in the South Atlantic (Figs. 1 and 2). By employing the full waveform methodology and thanks to a careful choice of the misfit function and the use of the adjoint method, we have been able to avoid the artefacts generated by common simplifying approximations and to extract the maximum amount of information from each seismogram, thus compensating for the paucity of data.

As mentioned before, it is important to compute the propagation of the full wavefield through the 3-D heterogeneous seismic model. Since this is beyond an analytical solution, the elastic wave equations and their adjoint equations are solved numerically in a regional domain with the code SES3D [2]. The similarity between the original and adjoint equations implies that the same code used to solve for the forward wavefield can be used, with only minor changes, to solve for the adjoint wavefield. SES3D is based on the spectral-element method and operates in a spherical section. We employ a spherical section of 140° x 80° x 1440 km (longitude x latitude x depth) going from the surface to the mid-mantle, divided into nearly 650,000 elements that are 0.8° x 0.9° x 40 km (longitude x latitude x depth). Inside each element the dynamic fields are approximated by degree 4 Lagrange polynomials, for a total of about 40 million grid points. Around 160 CPU-hours are needed for the simulation of a single earthquake, and one single iteration of the adjoint method needs around 100,000 CPU-hours. To obtain the final tomographic model, five iterations were necessary, thus requiring a total of around half a million CPU-hours.

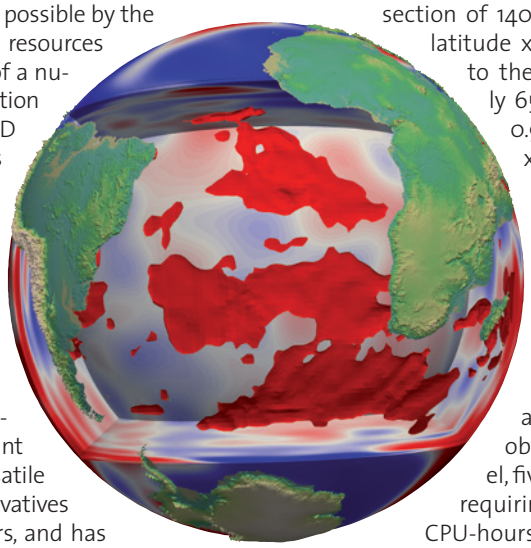

Figure 2: 3-D rendering of the tomographic model. Red iso-surface shows the 2.5% contour.

On-going Research

The tomographic model in Figures 1 and 2 shows a broad region in the shallow upper mantle characterized by particularly low velocities that may reflect the dynamics of a thin and very mobile asthenosphere. In addition, our results also point towards a change in characteristic length-scale of seismic structures at a depth of ~350 km. This may potentially be interpreted as an indication for a change in the direction of flow from vertical in the lower mantle to horizontal in the upper mantle, a geodynamic scenario that we are currently starting to explore using global mantle circulation simulations. However, as a first step to better assess the spatial extension of this region and its geodynamical significance we plan to extend the tomographic inversion and increase the frequency window up to 33 mHz (30 s period). This will allow us not only to use seismic waves characterised by a different spatial sensitivity, but also to exploit a larger number of seismograms, thanks to the more favourable signal-to-noise ratio at these higher frequencies. Each iteration of the tomographic inversion at these higher frequencies will need around 300,000 CPU-hours. Given that at least three to four iterations are needed to obtain a suitable solution, around 1–1.5 million CPU hours are thus necessary to perform this next step.

References and Links

[1] Colli, L., Fichtner, A., and Bunge, H.-P., Tectonophysics 604, 0 (2013), 26–40.
[2] Fichtner, A., Kennett, B. L. N., Igel, H., and Bunge, H.-P., Geophys. J. Int. 179, 3 (2009), 1703–1725

Combined high-resolution gravity field modeling

Research Institution
Institute of Astronomical and Physical Geodesy, TU München

Principal Investigator
Thomas Gruber

Researchers
Thomas Fecher, Roland Pail

Project Partners
–

LRZ Project ID: pr32qu

Introduction

The exact knowledge of the Earth's gravity field is a key parameter for several Earth oriented science disciplines, such as geodesy, oceanography or geophysics. It is usually represented as an equipotential surface corresponding, in a first approximation, to the mean global ocean surface. This surface is called the geoid. It can be described by geoid heights, which are the deviations of this surface from a regular Earth ellipsoid. Another way to represent the Earth gravity field are gravity anomalies, which represent the deviation of the Earth gravitational acceleration from those of the Earth ellipsoid (see figure 1).

As the geoid heights represent the physical shape of the Earth, they serve as reference surface for the determination of sea level rise or the modeling of geostrophic currents. Also for the unification of height systems the knowledge of this reference surface is a key parameter. Gravity anomalies, which are mainly linked to the geoid heights by a radial differentiation, directly provide insight into the Earth's interior. Besides the Earth's topography, like mountainous regions as the Andes or the Himalaya, deep-sea trenches or subduction zones are clearly visible (compare figure 1).

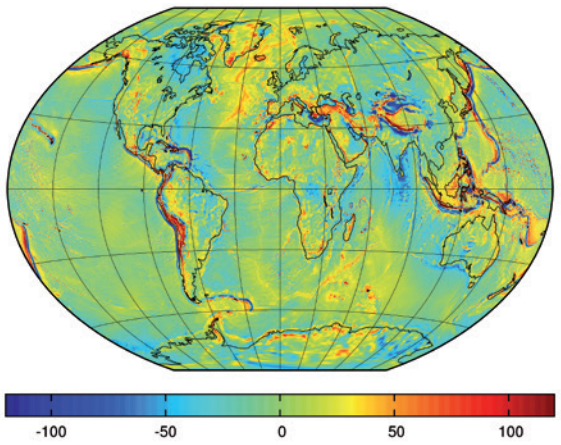

Figure 1: Gravity anomalies [10-5 m/s²] provide insight into geophysical structures of the Earth.

Due to its importance for a multiplicity of applications, there is a need for high accurate global modeling of the Earth's gravity field, which is the issue for LRZ's SuperMUC project pr32qu. In the framework of this project, different kind of observations of the Earth gravity field shall be combined together ideally to achieve a global high resolution gravity field model.

Results

The global Earth gravity field is represented by spherical harmonic functions, which are a generalization of the Fourier series on the sphere. The main goal of global gravity field modeling is the determination of the spherical harmonic coefficients up to highest possible degree and order (higher degree and order corresponds to finer spatial resolution). They are estimated in a least-squares adjustment based on a general Gauß-Markov model, where different kind of gravity field measurements enter as observations. The Earth's gravity field can be measured by different means. The satellite missions GRACE and GOCE observe the gravity field from space. They achieve high accurate measurements of the gravity field in the spectral range between spherical harmonic degree and order (d/o) 2 and 200, but due to Newton's law, which says that the signal is damped at satellite height, they are not sensitive to signals above. Gravity signal in the short wavelengths can only be observed by terrestrial gravity field measurements at the continents, or by satellite altimetry over the oceans. For this reason, for many areas of the world (South America, Africa, Asia) no high accurate or free accessible data sets are available. Nevertheless, to achieve the best possible and highest resolution gravity field model, different kind of gravity field observations have to be combined (c.f. figure 2).

The combination of the different kind of observations is carried out in terms of full normal equations systems. Solving of these normal equation systems delivers the spherical harmonic coefficients, i.e. the gravity field model. By propagating the variance-covariance information to geoid heights, the accuracy of the model can be assessed. If this is done separately for the combined model and for the satellite information, the impact of

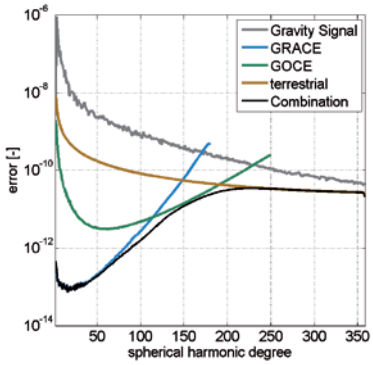

Figure 2: Error [–] per spherical harmonic degree for different kind of gravity field observables compared to the gravity signal (grey line)

the satellite information can be quantified (c.f. figure 3). The contribution of the satellite information of GRACE and GOCE can be clearly seen worldwide, but mainly areas where no high accurate terrestrial data is available strongly benefit from it (e.g. South America, Asia, Africa). A detailed description of the calculation process, and of the results and an elaborate validation of the results can be found in [2]

From HLRBII to SuperMUC

As full normal equation systems, due to the huge number of parameters and due to the independent stochastic modeling of all data sets and observations, can become very large, there is a need for using supercomputing resources. In the framework of this project, we gained experience in the field of supercomputing through the usage of SuperMUC's predecessor, LRZ's HLRB-II [1]. While HLRB-II was an important step on our way to determine high resolution gravity field models, SuperMUC enabled us to increase the number of parameters significantly such that we are at the forefront of research in this area. On HLRB-II an approach was implemented, which could be applied to calculate gravity field models based on full normal equation systems up to spherical harmonic d/o 600, corresponding to 360000 parameters and a normal equation size of almost 1 TByte. SuperMUC allowed us to perform calculations up to d/o 720, corresponding to 520000 unknowns and a normal equation size of 2TByte. This means, with SuperMUC the number of estimated parameters could be quasi doubled. The processing chain is based on several FORTRAN 90 routines. The most important routines are the programs which assemble normal equation systems from individual observations, which combine the different normal equations systems, which solve and invert the normal equations systems and which propagate the variance-covariance information of the inverted normal equation system to different functionals of the gravity field.

Next to FORTRAN90, the most important software used in our programs is BLACS for organizing the process grids, Intel's Math Kernel Library for the normal equation accumulations and SCALAPACK for solving and inversion of the normal equation systems. Besides the computational power of SuperMUC, another factor allowed to double the computational effort on the way to a gravity field model up to d/o 720. This factor is SuperMUC's General Parallel File System (GPFS). Due to the GPFS, reading and writing of the large normal equation systems has not only become stable, but also very fast. As we had to use own I/O programs on HLRB-II, MPI-IO2 on SuperMUC performs much better in combination with the general parallel file system.

For the assembling of the normal equations, we use between 3000 and 5000 cores, depending on the number of observations of the corresponding gravity field data set. This takes depending on the observation type between 6 and 18 hours. The combination of two 2TByte normal equations systems can be done with approximately 3500 cores in less than one minute, what is a quantum leap compared to the normal matrix combination process on HLRB-II. Solving and inversion of the normal equation

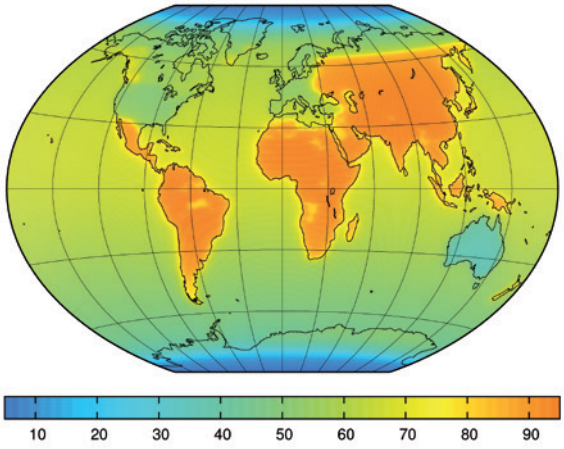

Fig. 2: Ocean model with irregular bathymetry. The black arrows indicate a random distribution of force sources.

system is performed in less than 5 hours with 3500 cores. As very helpful for our work it turned out, that SuperMUC's file systems allow storage of several normal equation files. In the average, between 10 and 20 TByte are stored on $WORK as well as $SCRATCH. Temporarily the number of storage can be significantly higher.

The only inconvenience in connection with the use of SuperMUC is, that sometimes the queuing time can be very long. Especially time consuming is, if the queuing time for test jobs is quite high, as this decelerates the development process of a program.

Outlook

For the future we plan to enhance the spherical harmonic resolution of our models to even higher degrees and orders corresponding to more parameters. Several new data sets shall be included in our calculations when they become available. Errors and in-accuracies in the existent data sets shall be eliminated prior to normal equations setup.

References and Links

[1] Fecher T; Gruber T; Pail R: The gravity field – an important parameter for Earth observation; inSIDE, Vol. 9, Nr. 2, pp 26-31, Gauss Centre for Supercomputing, 2011

[2] Fecher, T.; Pail, R.; Gruber, T.: Global gravity field modeling based on GOCE and complementary gravity data; International Journal of Applied Earth Observation and Geoinformation; ISSN (Online) 0303-2434, DOI: 10.1016/j.jag.2013.10.005 , 2013

EXtreme PREcipitation and Hydrological climate Scenario Simulations (EXPRESS-Hydro)

Research Institution
Leibniz-Rechenzentrum, Garching bei München, Germany

Principal Investigator
Dieter Kranzlmüller

Researchers
Jost von Hardenberg[1], Antonio Parodi[2], Alexandre Pieri[1], Antonello Provenzale[1]

Project Partners
(1) Institute of Atmospheric Sciences and Climate - National Research Council (ISAC-CNR) and
(2) CIMA Research Foundation, Italy

LRZ Project ID: pr45de (Gauss Large Scale project)

Introduction

Predicting weather and climate and its impacts on the environment, including hazards such as floods, droughts and landslides, continues to be one of the main challenges of the 21st century with significant societal and economic implications. At the heart of this challenge, lies the ability to have easy access to hydrometeorological data, to share predictive models, and to facilitate the access to High Performance Computing facilities supporting leading edge hydro-meteorological simulations. Advances in the science and observation of climate change are providing a clearer understanding of the inherent variability of Earth's climate system and its likely response to human and natural influences. Extensive uncertainties exist in future forcings of the climate system and in human responses to climate change, suggesting the use of different future scenarios to explore the potential consequences of different response options. Numerical simulations at the global scale of future climate in different emission scenarios, produced in the framework of the fifth climate model intercomparison project (Coupled Model Intercomparison Project Phase 5, CMIP5), have been typically obtained using hydrostatic global climate models (GCM) and are available only at quite coarse spatial resolutions which do not allow an accurate representation of intense precipitation events over complex topography areas such as Europe.

An improved generation of regional climate models (RCM) is being developed and applied in the framework of the CORDEX (COordinated Regional climate Downscaling Experiment; Giorgi et al. 2009) initiative, with the aim to produce regional climate change projections world-wide for input into impact and adaptation studies, considering multiple forcing GCMs from the CMIP5 archive. Recent results for the European branch of the CORDEX initiative (Kotlarski et al. 2014) confirm, with simulations on grid-resolutions up to about 12 km (0.11 degree), the ability of RCMs to capture the basic features of the European climate for the period 1989-2008, but also show non-negligible deficiencies of the simulations

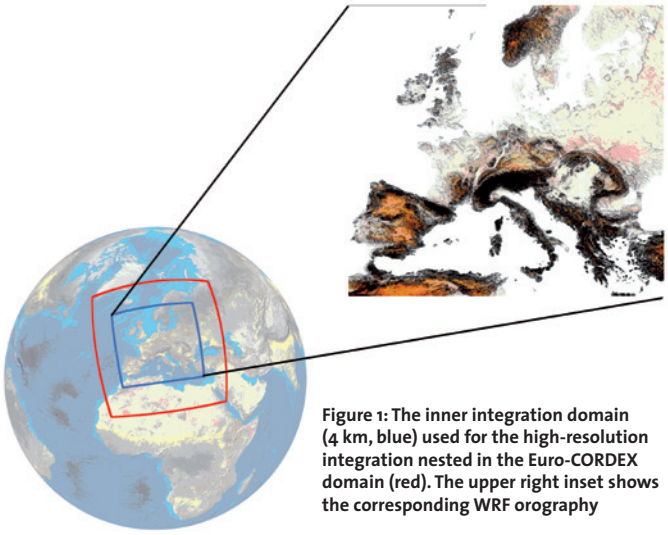

Figure 1: The inner integration domain (4 km, blue) used for the high-resolution integration nested in the Euro-CORDEX domain (red). The upper right inset shows the corresponding WRF orography

concerning selected metrics, certain regions and seasons: for example seasonally and regionally averaged temperature biases are mostly smaller than 1.5 °C, while precipitation biases are in the ±40% range.

Recent literature (Rasmussen et al. 2011) has shown that a reduction of the overestimate in precipitation over orography can be achieved avoiding convective parameterizations and resolving convection explicitly at high enough spatial resolutions. Starting from these findings, in this project we move one step further, performing very high-resolution regional dynamical downscaling of historical climate scenarios produced by the ERA-Interim reanalysis and of climate change scenarios produced by a global climate model (the EC-Earth model), using the state-of-the-art non-hydrostatic Weather Research and Forecasting (WRF) regional climate model. To the best knowledge of the authors, we are performing for the first time long climate simulations over the European domain at a very fine cloud-permitting resolution of about 4 km (0.037°) with explicitly resolved convection and a sharp representation of orography (figure 1).

Results

Using nested RCMs still presents issues such as the influence of boundary conditions, the best size of the nested domains and the choice of adequate parameterizations, all of which can severely affect the simulated precipitation and temperature outputs. Therefore, a careful analysis of the sensitivity of the model to different parameterizations, such as microphysics, planetary boundary layer (PBL) and convective schemes, and to spatial resolution, especially when approaching the cloud-permitting range (4-10 km) has been performed as an essential preliminary step (Pieri et al. 2013). To this end, we ran a set of dynamical downscaling WRF control runs, forced by ERA-Interim for the period 1979-2008, applied to the European area, at different spatial resolutions and with different physics schemes. We compared the model results with the observed precipitation and 2 m temperature properties provided by a number of available observational and reanalysis datasets.

The resulting optimized WRF model setup used in this project for high-resolution simulations consists of 2 domains (figure 1): the external domain corresponds exactly to the standard Euro-CORDEX area, resolved with spatial resolution 0.11°, corresponding to about 10^7 grid points; two-way nested model simulations have been performed with an innermost domain covering most of continental Europe with spatial resolution 0.037° (about 4 km), corresponding to about $4 \cdot 10^7$ grid points. The simulations used Thompson microphysics and the Yonsei University (YSU) scheme for the PBL and a Kain-Fritsch convective closure in the external domain. This setup was used to perform the main model experiment, for the period 1979-2008 with ERA-Interim forcing at the boundaries. This experiment has required the production of 750TB of output and restart data, temporarily stored in the SuperMUC Archive System, making PR45DE belonging to the TOP 10 projects regarding the usage of the SuperMUC Archive System. The raw output has been post-processed to extract important selected variables in a format agreeing with internationally defined standards.

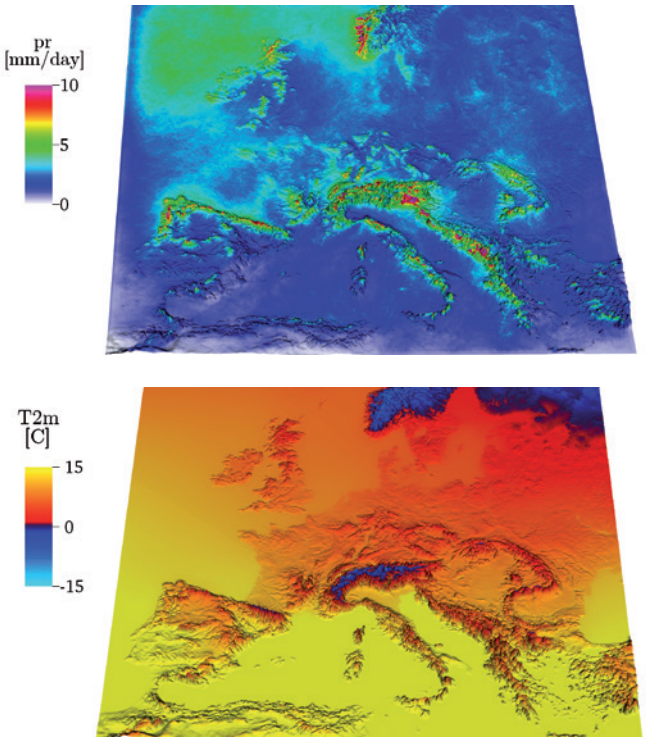

Figure 2: Annual average of simulated total precipitation (a) and 2m temperature (b) for a sample model year (1979) at 4 km resolution, with ERA-Interim forcing

We performed an analysis of the model climatology (see e.g. figure 2), particularly in terms of its ability in reproducing observed precipitation extremes, over Europe and in detail over the Greater Alpine Region, comparing with available high-resolution gridded data sets, in particular ERA-Interim, MERRA and CFSR reanalyses, GPCP, GPCC, EOBS and CRU datasets and the Alpine datasets HISTALP and EURO4M-APGD (Pieri et al 2014). Overall our results indicate that increased resolution with explicitly resolved convection helps to obtain a closer representation of the precipitation field, reducing the overestimation of precipitation (about 25% on average over the European domain) and allowing to better reproduce the distribution and the statistics of the rainfall rate, particularly over the Alps.

On-going Research

We are complementing our simulation of the present climate with a future scenario projection at high-resolution, in which the WRF model is forced with CMIP5 output from the EC-Earth global climate model, with RCP4.5 greenhouse gas and aerosol concentrations, for the period 2030 to 2050. The post-processed datasets produced in this project will be used as inputs for regional impact studies, in particular forcing hydrological models and ecosystem dynamics models over selected study areas. The data will be distributed in the framework of major international projects such as DRIHM, DRIHM2US, SCIHM and the Italian Project of Interest NextData.

References and Links

[1] Giorgi F., C. Jones, G.R. Asrar: Addressing climate information needs at the regional level: the CORDEX framework. WMO Bulletin 58 (3) (2009)

[2] Kotlarski, S., K. Keuler, et al.: Regional climate modeling on European scales: a joint standard evaluation of the EURO-CORDEX RCM ensemble, Geosci. Model Dev. Discuss., 7, 217-293 (2014).

[3] Pieri, A.B., J. von Hardenberg, A. Provenzale, A. Parodi. Impact of different microphysics parameterizations on dynamical downscaling with WRF for the EURO-CORDEX domain, International Conference on Regional Climate - CORDEX 2013, Brussels, Belgium (2013).

[4] Pieri A.B., J. von Hardenberg, A. Parodi A., A. Provenzale. Do precipitation rates from non-hydrostatic simulations agree with data? A view from the WRF model over Europe. To be submitted to Journal of Hydrometeorology (2014).

[5] Rasmussen, R., C. Liu, K. Ikeda, D. Gochis, et al. High-Resolution Coupled Climate Runoff Simulations of Seasonal Snowfall over Colorado: A Process Study of Current and Warmer Climate. J. Climate, 24, 3015–3048 (2011).

http://www.drihm.eu
http://www.drihm2us.eu
http://www.scihm.org
http://www.nextdataproject.it

SHAKE-IT: Evaluation of seismic shaking in Northern Italy

Research Institution
Istituto Nazionale di Geofisica e Vulcanologia, Italy

Principal Investigator
Andrea Morelli

Researchers
Irene Molinari, Piero Basini, Paride Lagovini, Peter Danecek, Andrea Berbellini

Project Partners
Toronto University, Toronto, Canada

LRZ Project ID: pr86vo (PRACE project)

Introduction

Ground shaking due to an earthquake not only depends on the energy radiated at the source but also on propagation effects and amplification due to the response of geological structures. A further step in the assessment of seismic hazard, beyond the evaluation of the earthquake generation potential, requires then a detailed knowledge of the local Earth structure and of its effects on the seismic wave field. The simulation of seismic wave propagation in heterogeneous crustal structures is therefore an important tool for the evaluation of earthquake-generated ground shaking in specific regions, and for estimates of seismic hazard. Current-generation numerical codes, and powerful HPC infrastructures, now allow for realistic simulations in complex 3D geologic structures. We apply such methodology to the Po Plain in northern Italy, a region with relatively rare earthquakes but with a large property and industrial exposure — as it became clear during the recent events of May 20-29, 2012. The region in characterized by a deep sedimentary basin: the 3D description of the spatial extent and structure of sedimentary layers is very important, because they are responsible for significant local effects that may substantially amplify the amplitude of ground motion. Our goal has been to produce estimates of expected ground shaking in northern Italy through detailed deterministic simulations of ground motion due to possible earthquakes.

Results

We started the work with the implementation of a 3D description of the sub-surface geological units of the sedimentary Po Plain basin, plus neighbouring Alps and Northern Apennines mountain chains. Once the spatial characters of the structure have been set by merging detailed information from scientific literature and databases, the elastic parameters and density of the different units had to be adjusted. Our strategy consisted of defining an a priori plausible space of model parameters, and exploring it following a metaheuristic procedure based on a Latin hypercube sampling. This strategy was chosen to direct the trial-and-error procedure, as it provides a more uniform coverage of the subspace of interest than a random sampling. Each model has been tested for its ability to reproduce observed seismic waveforms for recent events. Best models were those providing the best fit. We have extensively simulated and independently compared in performance three different models for the Earth's crust — ranging from a simple 1D

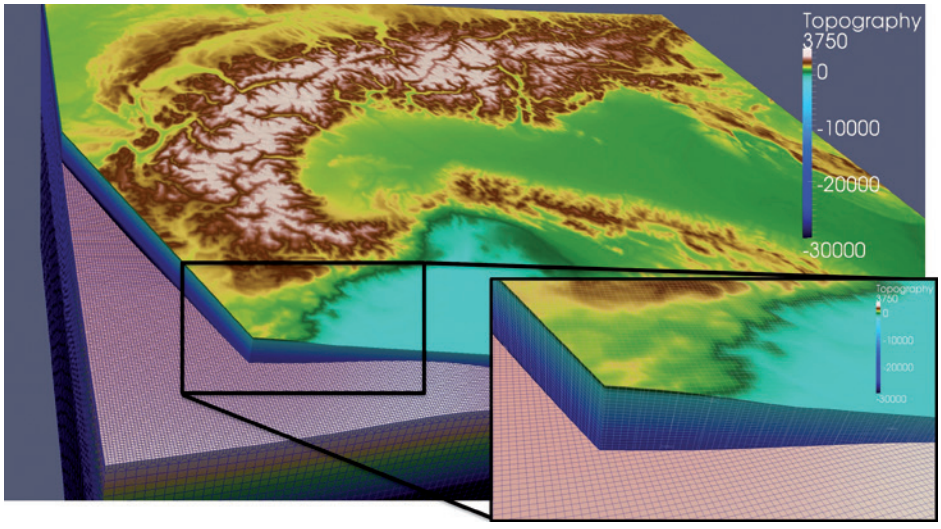

Figure1: Mesh of the crust and the mantle, coloured as a function of topography. The mesh honours the topography of free surface and crust/mantle boundary.

model, to a 3D large-scale reference model, to our new "optimal" high resolution 3D model — to gauge their ability to fit observed seismic waveforms for a set of 20 recent earthquakes occurred in the region. We observe a strong improvement of the fit to observed data by the wave field computed in our new detailed 3D model of the plain. Specifically, the new model has shown to be able to reproduce the long so-called 'coda' of the signals — late-arriving energy, due to reverberations and scattering. A 1D model, as expected, cannot account for the waveform complexity due to the effect of the sediments, while the high-resolution 3D model does a very good job in fitting the envelope of the seismograms. For the local earthquakes for which high-quality seismograms were available, the new 3D model can reproduce well the peak ground acceleration at periods longer than 2 s, and the overall duration of the shaking — two parameters of highest relevance engineering purposes, as they are of great consequence to model the response of high-rise buildings and soil liquefaction effects. The new high-resolution model shows therefore significant improvement with respect to both the 1D and the large-scale 3D models. Understandably, the differences are most evident for propagation paths crossing the sedimentary basin.

Having verified that we now have a model (and a reliable computational framework), able to reproduce the gross characters of seismically-induced ground motion, we can then put them to work to infer the ground shaking that would be caused by seismic sources deemed plausible for the region. Seismic hazard assessment is built on the knowledge of past activity derived from historical catalogues and geological evidence. We can legitimately reason that some event of the past will repeat itself with very similar characters in the future, and the numerical framework (that we have verified on recent events) permits to reconstruct the ground shaking that will ensue. We have therefore considered in detail two specific cases. One refers to the earthquake that struck the city of Ferrara in 1570, an event very similar to the one occurred in May, 2012; the other to a series of historical events, with similar characters, located along the same linear geological structure roughly comprised between the cities of Modena and Parma. The uncertainty in the knowledge of source parameters — quite relevant in the case of knowledge deriving from historical catalogs — has been explicitly considered by generating suites of source parameters spanning the uncertainty ranges of hypocentral coordinates and geometrical parameters. For each earthquake, we represent the uncertainty regions by 200 instances generated through Latin hypercube sampling, and analyse the statistical properties of the resulting ensemble of wave fields generated. We may thus address the minimum, maximum, or median of the suite of peak ground accelerations, for all the geologically acceptable source models, in all possible locations. We can also explore the dependence of shaking parameters on source parameters — such as hypocentral depth or fault plane orientation. Different geological settings (i.e. hard rock, vs. consolidated sediments, or water-saturated sediments) in fact show a quite different response.

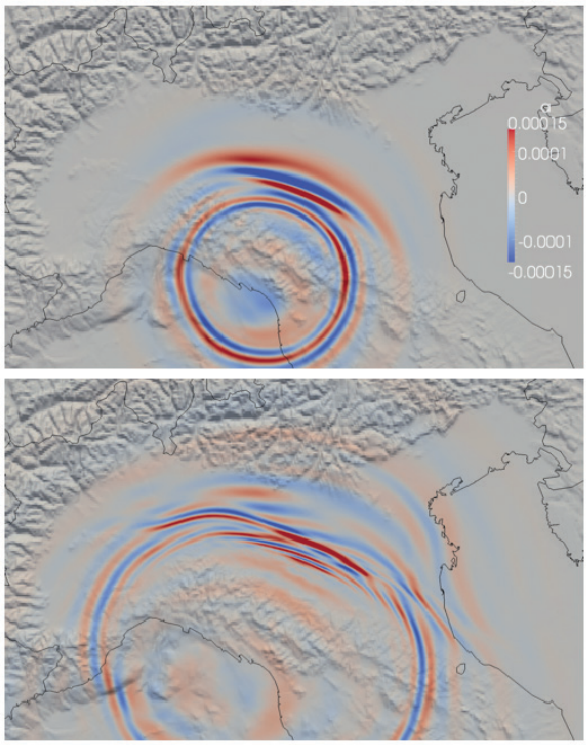

Figure 2: Snapshots at 30s and 70s of the simulation of the Mw=5.2 June 21, 2013, earthquake. The effect of the basin structure is clearly apparent when the wave front passes the ESE-WNW-trending boundary with the mountain front.

On-going Research / Outlook

This study builds the basis for a physics-based approach to seismic hazard estimates in Northern Italy. We will need, on one side, to increase the resolution of the geological model, in some critical locations, to slightly increase the highest significant frequency. We are currently limited to relatively low-frequency ($f < 0.5$ Hz) and more efforts are needed to go to higher frequency. A more detailed description of the geological structure may permit to increase to $f \sim 1$ Hz. Stochastic synthesis is required to reach further high frequencies – $f > 1$ Hz, with engineering interest for low-rise residential buildings – so a hybrid deterministic-stochastic approach must be used.

References and Links

[1] Molinari I., and A. Morelli, 2011. Geophys. J. Int., 185, 352-364, doi: 10.1111/j.1365-246X.2011.04940.x
[2] Morelli A., I. Molinari, P. Basini, P. Danecek, 2012. Abstract S32B-02 presented at 2012 Fall Meeting, AGU, San Francisco, Calif. (USA), 3-7 Dec.
[3] Molinari I., A. Morelli, P. Basini, A. Berbellini, 2013. Abstract S32B-03 presented at 2013 Fall Meeting, AGU, San Francisco, Calif. (USA), 9-13 Dec.
[4] Tondi, R., C. Cavazzoni, P. Danecek, and A. Morelli, 2012. Computers & Geosciences, 48, 143-156, DOI: 10.1016/j.cageo.2012.05.026
[5] Gualtieri L., P. Serretti, and A. Morelli, 2013. Geochemistry, Geophysics, Geosystems, DOI:10.1002/2013GC004988

Engineering and Computational Fluid Dynamics

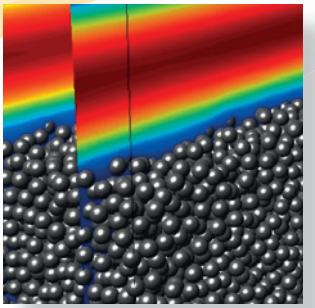

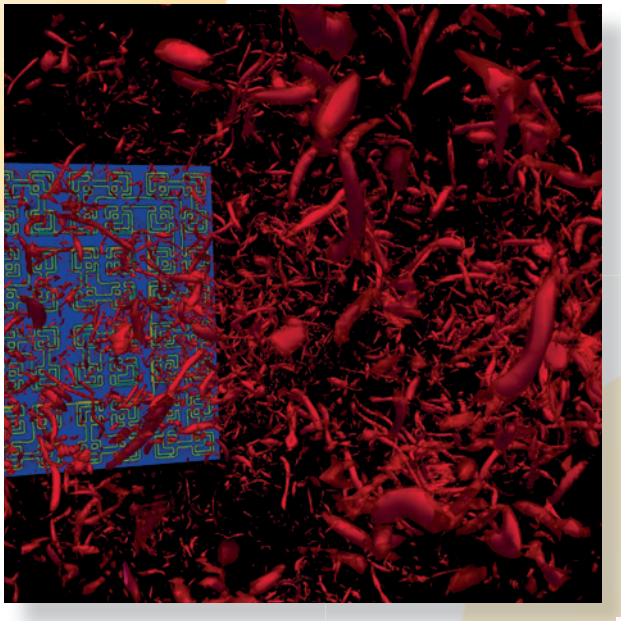

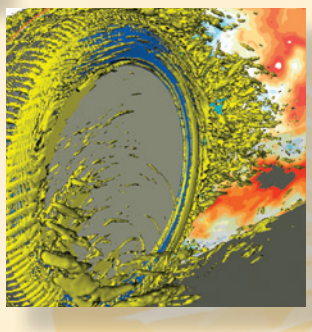

Direct Numerical Simulation of Turbulent Flows in Consideration of Microstructure by Monte-Carlo-Methods

Research Institution
Fachgebiet Hydromechanik, Technische Universität München

Principal Investigator
Michael Manhart

Researchers
Sheema Kooshapur, Wolfgang Schanderl, Tao Zhu, Amin Moosaie

Project Partners
–

LRZ Project ID: h0022

Introduction

Turbulent flows are of intrinsic complexity due to the non-linear character of the governing equations which leads to a complex interaction of flow structures with a continuous spectrum of scales. With increasing Reynolds number, the range of the involved scales increases. As a consequence, realistic technical or geophysical flows can only be predicted by the use of simplified models. Computer simulations have emerged as a powerful tool to improve understanding of such flows and to develop simplified models which allow for a prediction of complex turbulent flows with a largely reduced effort.

The flows considered within this projects are complex flows in which the complexity is introduced by (i) the geometrical configuration and/or (ii) by interactions of the flow with a micro-structure that is beyond of what can be geometrically represented in a reasonable way. Two examples for the former are the turbulent flow over topography (hills) [1] and the flow around a bridge pier in a sandy river bed. Two examples of the latter which have been treated within this project are turbulent particulate flow and turbulent flow of fiber suspensions [4]. A special case combining geometrical complexity and interactions with micro-structure is the interaction of a turbulent flow with sediment transport during scouring of a bridge pier. This case will be discussed in this report.

The main goals of the project are
1. to develop methods for a detailed simulation of complex turbulent flows that are beyond the reach of currently available standard simulation tools
2. to perform simulations of such flows which can be used as reference for model development
3. to analyze flow behavior and develop models for a reduced order description of such flows.

Within this project, the flow solver MGLET is being employed [2,3,5]. It uses a Finite Volume method to solve the incompressible Navier Stokes equations. A Cartesian grid with staggered arrangement of the variables enables an efficient formulation of the spatial approximations. An explicit third order low storage Runge-Kutta time step is used for time integration. Geometrically complex surfaces, arbitrarily curved, can be represented by an Immersed Boundary Method. Like other academic research codes, MGLET is being under constant development and improvement.

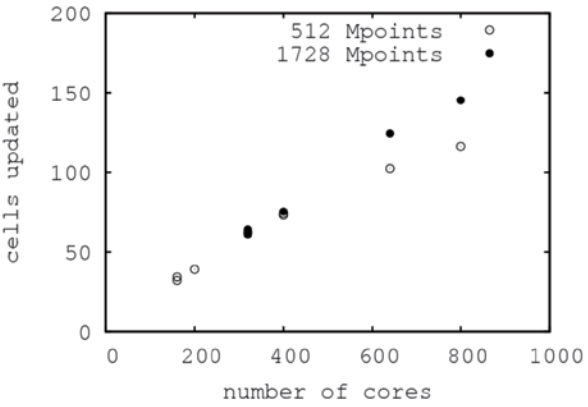

Figure 1: Total number of cells (in million) updated by one time step during one second as function of number of cores. Two problem sizes, $512x10^6$ and $1,7x10^9$ cells, are considered.

Results

MGLET is parallelized by a domain decomposition method using MPI as a framework. For simple rectangular domains, the code has been tested so far for up to 8192 cores. As the purpose of the code is doing long runs, gathering statistics of the flow field, the applications are designed for maximum throughput on a number of cores as small as possible. Here the key number is the number of grid cells to be advanced by one time step within a CPU second. In Figure 1, this measure is plotted in terms of total number of grid points per second as a function of the number of cores on the SuperMUC. Figure 1 shows, that in one core-second, about 200000 grid points can be advanced in time by one time step. The problem sizes used for these benchmarks are 512 million and 1728 million points, respectively. The figure demonstrates that MGLET is well scalable for these number of cores and

problem sizes. It has to be noted, however that this scalability is obtained in a regular one-block grid and with the basic second order solver. The scalability suffers, if multi-block grids are used, such as in the prediction of the flow around a cylinder on a flat plate which is described below.

In this report, we discuss the flow around a cylinder on a flat plate, which is the first step in a detailed analysis of the flow field around a bridge pier developing a local scour hole in a sandy river bed. This project is currently being funded as a combined numerical/experimental study by the DFG. Parallel to the simulations performed at HLRB, experiments are performed at the Hydromechanics Laboratory at TUM. The experiments will be used for validation and to obtain complementary data to the numerical simulations, such as longtime records and high Reynolds number flow data. While the experiments have just started, first simulation results are already available and have been accepted for presentation at conferences.

The main scientific questions of this project are (i) how does the flow around the cylinder change with Reynolds number and scour development; (ii) which simulation strategy and models can best be used to predict this flow; (iii) which flow quantities and events determine the initiation and the rate of erosion; (iv) which modeling strategy is best suited to model the erosion rates around the cylinder?

First results of turbulent flow around a cylinder on a flat plate have already been obtained. This configuration represents the initial state. We use MGLET to perform a highly resolved LES of the flow at a Reynolds number of Re=39000 based on cylinder diameter and oncoming bulk velocity. The subgrid scale stresses are parameterized by the Wall-Adapting Local Eddy-Viscosity model (WALE). A free surface channel flow at a low Froude number is approximated by a free-slip condition at the upper wall. A fully turbulent boundary layer flow is set as inflow condition. It is generated by a so-called precursor simulation which is run in parallel to the main flow simulation, see Figure 2.

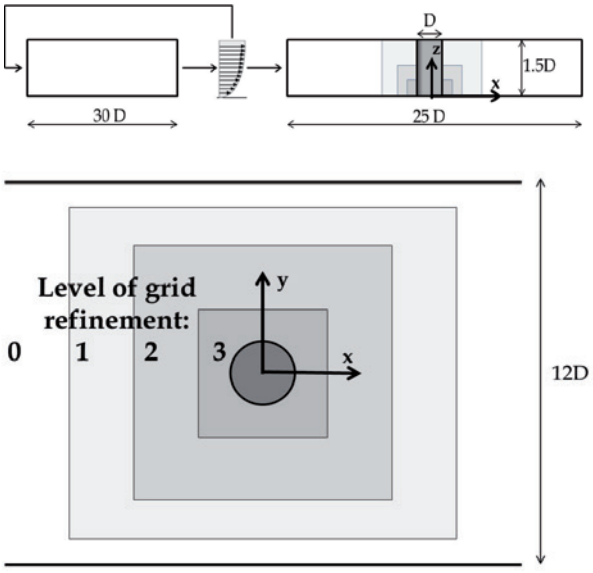

Figure 2: Side and top views of the setup. The outflow of the precursor is set as inflow boundary condition of the grid containing the cylinder. The grid around the cylinder is refined with three locally embedded grids.

The region of interest around the cylinder/plate junction is resolved by three zonally embedded grids which give a total refinement by a factor of eight with respect to the global basic grid. The configuration including the precursor simulation is documented in Figure 2 and Figure 3. In total three different grids have been investigated which differ in the number of refinement levels around the cylinder. The finest configuration, using in total a number of 250 million grid cells, can be run on 288 cores with about 10 seconds per time step and on 768 core with about six seconds per time step (SuperMUC). Compared to the Benchmark given in Figure 1, this is about a factor of 2-3 slower than a configuration with a single block grid. Considering the complex communication patterns that arise from the zonally embedded grids, this can still be regarded as satisfying.

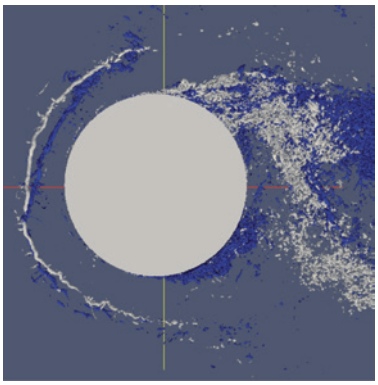

Figure 4: Isosurfaces of the Q-criterion (second invariant of the velocity gradient tensor) rendering strong vortices. The flow is coming from left, top view. Two different instances in time are displayed by blue and grey isosurfaces.

While the flow is dominated by the von Karman vortex street behind the cylinder, in front of the cylinder a so-called horse-shoe vortex develops that wraps around the cylinder at the bottom plate. A correct description of the horse-shoe vortex system including its space-time dynamics can be considered as the key point in predicting the wall shear stress underneath, which is responsible for the erosion around the cylinder. Figure 4 displays an overlay of two instantaneous snapshots of the Q-criterion which renders strong vortices in the flow. One can see that at the two different instances in time (grey and blue isosurfaces) the position of the horse-shoe vortex differs considerably. This leads to bi-modal velocity and wall shear stress distributions in the zone in which scouring is largest. Note that this particular dynamics of the horse-shoe vortex can only be seen in the simulation with the finest grid.

References and Links

[1] M. Breuer, N. Peller, Ch. Rapp, and M. Manhart. Flow over periodic hills – numerical and experimental study over a wide range of Reynolds numbers. Computers and Fluids, 38(2):433–457, February 2009.

[2] A. Hokpunna and M. Manhart. Compact fourth-order finite volume method for numerical solutions of Navier-Stokes equations on staggered grids. Journal of Computational Physics, 229:7545–7570, 2010.

[3] M. Manhart. A zonal grid algorithm for DNS of turbulent boundary layers. Computers and Fluids, 33(3):435–461, March 2004.

[4] A. Moosaie and M. Manhart. Direct Monte Carlo simulation of turbulent drag reduction by rigid fibers in a channel flow. Acta Mechanica, 224(10):2385–2413, 2013.

[5] N. Peller, A. Le Duc, F. Tremblay, and M. Manhart. High-order stable interpolations for immersed boundary methods. International Journal for Numerical Methods in Fluids, 52:1175–1193, 2006.

Large Scale CFD For Complex Flow

Research Institution
Institute of Aerodynamics and Fluid Mechanics

Principal Investigator
Christian Stemmer

Researchers
Bernd Budich, Nikolaus A. Adams

Project Partners
–

LRZ Project ID: h0983

Passive Flow Control of Shock-Wave/Turbulent Boundary Layer Interactions using Micro-Vortex Generators

During the course of this project, also the complex flow of an oblique shock, interacting with a supersonic boundary layer has been investigated. Shock-wave/turbulent boundary layer interactions (SWBLI) can be encountered in virtually every high-speed application, including engine intakes, turbo–machinery or rocket engines. It is well known that shock induced flow separation is followed by severe energy losses and flow distortion degrading overall system performance [1,2]. Additionally, substantial thermal as well as pressure loads result from the interaction. In conjunction with their highly unsteady nature, SWBLI are of major concern also for the structural integrity and lifetime of high-speed vehicles. In order to address these issues, flow control devices can be deployed which allow for influencing the dynamic behavior of the SWBLI and mitigating their detrimental influences. A promising class of control devices are micro-vortex generators (μVGs) [2,3], which are placed upstream of the interaction region. Being completely submerged within the boundary layer, they induce a pair of counter-rotating longitudinal vortices that energize the boundary layer within their wake. By this mechanism, flow separation is effectively delayed and the dynamic behavior, i.e. thermal and pressure fluctuations within the interaction region can be controlled.

With only few numerical investigations available, these flow devices have mostly been investigated experimentally up to now. During the course of this project, implicit large-eddy simulations of the flow around micro-vortex generator have been conducted. The The considered flat plate turbulent boundary layer is characterized by a free-stream Mach number $Ma_\infty = 2.31$ and Reynolds number $Re_\delta = 67.4 \cdot 10^3$, based on the reference boundary layer thickness $\delta_{ref} = 12.64$ mm, located at $8\delta_{ref}$ upstream of the theoretical inviscid impingement point. The incident shock deflects the undisturbed flow by β=9.5°. The employed wedge-shaped μVGs, see Fig. 1, possess an opening angle of 24°. The device's tip is located within the logarithmic region of the TBL ($h_{VG} = 0.2\delta_{ref} \approx 180^+$), spanwise spacing is $s_{VG} = 1.6\delta_{ref}$.

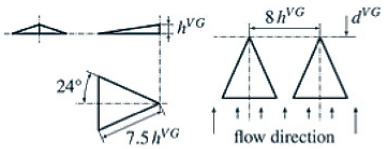

Fig. 1: Geometry of the utilized μVGs.

Detailed analysis of the flow field has been carried out, whereas four different distances of the control devices to the interaction region were considered ($d_{VG} = \{10, 5, 2.5, 0\}\ \delta_{ref}$), in order to investigate the effect of possible off-design conditions. Exemplarily, the vertical flow around the control device placed immediately upstream of the interaction as well as the shock system is shown in Fig. 2. Iso-contours of the Q-criterion $Q = 1.5$, colored by axial vorticity ω_x, highlight how the two distinct, counter-rotating vortices develop on either side of the wedge. While lifting away from the wall, they are consecutively convected towards the shock system, which is visualized by iso-surfaces of $\partial p/\partial x = 0.17$.

It has been found that a significant reduction of the interaction's spatial extent by up to 18% can be achieved. This can be accredited to a combined positive effect of energizing the logarithmic region of the TBL, a reduction of upstream propagation of the adverse pressure

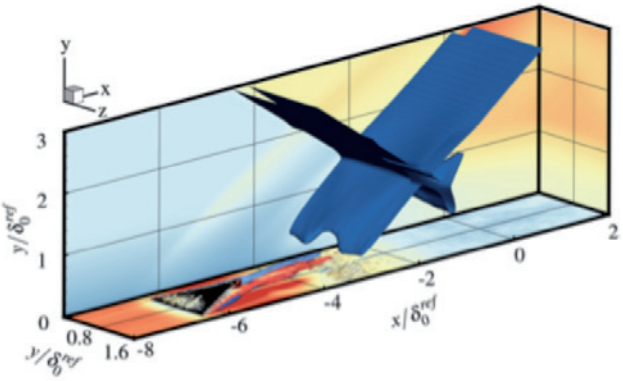

Fig. 2: Visualization of the interaction region controlled by a μVG placed at $d_{VG} = 5\delta_{ref}$.

gradient and an increase of turbulence intensity. In contrast, a misalignment of the shock system only leads to a restricted separation growth. It can be concluded that overall system performance is not excessively deteriorated at off-design conditions. Furthermore, the freestream is only slightly changed and almost no additional loss in total pressure is introduced into the system.

Moreover, control also alters the shock oscillations, regarding their frequency content, amplitude and excursion area. Clearly being connected to material stress and fatigue, μVGs can thus be employed to address these aspects.

References and Links

[1] Babinsky, H., Li, Y. & Pitt Ford, C.W. 2009 Microramp Control of Supersonic Oblique Shock-Wave/Boundary-Layer Interactions. *AIAA Journal* 47 (3), 668–675.
[2] Lin, J.C. 2002 Review of research on low-profile vor- tex generators to control boundary-layer separation. *Progress in Aerospace Sciences* 38 (4-5), 389–420.
[3] Délery, J.M. 1985 Shock Wave/Turbulent Boundary Layer Interaction and its Control. *Progress in Aerospace Sciences* 22, 209–280.

Large-Eddy Simulation of Turbulent Trans- and Supercritical Mixing

Research Institution
Institute of Aerodynamics and Fluid Mechanics, Technische Universität München

Principal Investigator
Christian Stemmer

Researchers
Christoph A. Niedermeier, Stefan Hickel

Project Partners
Institute for Thermodynamics, Universität der Bundeswehr München

LRZ Project ID: h0983

Introduction

Injection and mixing processes at elevated pressures play a key role in combustion engines, such as internal-combustion engines for automotive applications or liquid-propellant rocket engines for space transportation systems. The operating pressure in modern rocket combustion chambers using a gas generator cycle typically exceeds 10 MPa. Because this is significantly above the critical pressures of common propellants like hydrogen and oxygen, these fluids are in a trans- or supercritical thermodynamic state at injection, depending on whether the temperature is below or above the pseudo-boiling temperature. The molecular interactions in this high-pressure environment significantly affect the fluid properties. Therefore, a real-gas equation of state and suitable relations for the transport properties have to be used to correctly describe the fluid physics.

Computational Fluid Dynamics (CFD) has become more and more important for the design and optimization process of new engines that satisfy the increasing requirements in terms of rocket performance and reliability despite decreasing budgets and the request for short development cycles. Large-Eddy Simulation (LES) appears to be the most suitable CFD method, because the process of the propellant injection into a rocket combustion chamber is strongly three-dimensional and unsteady. However, the subgrid-scale (SGS) turbulence models of all well-established LES methods were originally designed and calibrated for incompressible or ideal-gas flows. Therefore, they have to be validated and possibly adjusted for the simulation of flows at supercritical pressure to ensure that they correctly account for effects of real-gas thermodynamics.

In this context, the Technische Universität München (TUM) and the Universität der Bundeswehr München (UniBw) started a joint effort in developing numerical tools that can predict trans- and supercritical injection, mixing and combustion processes.

Results

While the UniBw extends the capabilities of the open-source CFD program OpenFOAM® (pressure-based) and mainly relies on its own computational resources, the TUM promotes the software INCA (density-based) and uses the SuperMUC for computations. Both codes have been extended by a sophisticated thermo-physical modeling of fluids in trans- and supercritical state.
The INCA code employs the Adaptive Local De-convolution Method (ALDM) for solving the compressible Navier-Stokes equations on adaptive Cartesian grids. ALDM is a nonlinear Finite Volume method for implicit LES based on a holistic approach to physical and numerical modeling of under-resolved flow features, such as small-scale turbulence and discontinuities.

INCA employs domain decomposition where the mesh is split into a number of sub-domains, which are then allocated to separate processors. The MPI protocol is used for communication between the different sub-domains. For the present LES of trans and supercritical jet injection, 3.9 million grid cells distributed over 40 cores of the Fat Node Island were used. Long integration times were required for converging statistics of the relevant quantities. Therefore, a total amount of about 27,000 core hours has been used for each case.
We use the data of fully turbulent, trans- and supercritical nitrogen jet experiments performed by Mayer et al. [4] to successfully validate our methodology and to compare our results with previous simulations. The setup of the experiments, where cold nitrogen at a temperature near the critical temperature is injected into nitrogen at supercritical temperature and pressure, resembles the situation in a real rocket combustion chamber in terms of injection and mixing processes. Three different operating conditions from the experimental database [4] at different temperatures and pressures were used as a reference for validation.

Figure 1 shows the instantaneous temperature distribution on an x-y plane for all three cases. It is clearly visible that the cold and therefore dense core region is much

longer in the transcritical cases 3 and 7 (top and bottom) than for the supercritical case 4 (middle), where the density of the injected nitrogen is much lower. This means that the main mixing process between the injected, cold nitrogen and the surrounding, warm nitrogen takes place at a later stage than in the supercritical case. The decreased mixing for the transcritical cases also leads to a lower spreading angle. This is the expected behavior due to the higher, liquid-like density in the core region for the transcritical cases, as the injection temperature is below the pseudo-boiling temperature here.

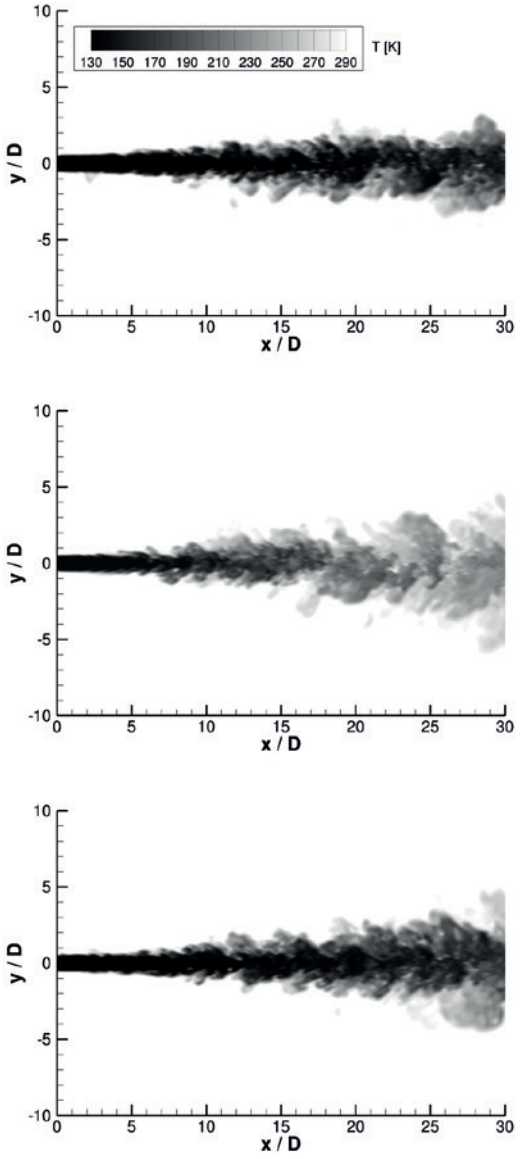

Figure 1: Instantaneous temperature distribution [K] in the central x-y plane for case 3 (top), case 4 (middle) and case 7 (bottom).

The heat capacity significantly increases when the temperature of the fluid passes the pseudo-boiling temperature during heat-up, slowing down the heat transfer between the warm surrounding and the cold jet core. This further stabilizes the jet, delays the mixing process and moves the jet break-up further downstream.

Although the grid is rather coarse, fine structures of cold and warm fluid packets that mix with each other can be seen for all cases. This illustrates that we were able to correctly reproduce such flow patterns already with a rather low grid resolution. When we compare our results to flow visualizations of other simulations of the same experiments, which used a grid resolution that was more than three times higher than ours, we can see that the main features nonetheless are very similar.

Mean density profiles along the jet centerline (not shown) are also in very good agreement with the experimental data. Analyzing our LES data and previously published simulations by other groups, we found that proper thermodynamic modeling is the crucial ingredient needed for accurately predicting the mixture-density evolution and that our choice works very well for all three test cases.

On-going Research / Outlook

In the future, we will conduct a series of Direct Numerical Simulations (DNS) to serve as an additional reference for the validation of LES methods for trans- and supercritical fluid flows in terms of higher-order correlations, as suitable experimental data for such a comparison does not exist. Therefore, we will simulate fully turbulent, temporally evolving mixing layers and channel flows comprised of different binary species combinations.

As no modeling is included in DNS, all relevant length and time scales of the turbulent flow have to be resolved, leading to a very high demand in computational power and computing time. The grid sizes will be several 100 million cells for each simulation, a challenge we can reasonably face by using one full Thin Node Island of SuperMUC for each single simulation in the future.
Additionally, we will use our extended thermodynamic modeling for LES of multi-component coaxial injection and the subsequent mixing and combustion process of different species like Oxygen and Hydrogen or Oxygen and Methane. Our final goal is to provide an LES methodology suitable for the design and the predictive analysis of future rocket combustors.

References and Links

[1] Niedermeier, C.A., Müller, H., Jarczyk, M., Hickel, S., Adams, N.A., Pfitzner, M. (2013). Large-Eddy Simulation of Turbulent Trans- and Supercritical mixing. AIAA paper 2013-2950. 21st AIAA Computational Fluid Dynamics Conference, San Diego, CA, USA. doi: 10.2514/6.2013-2950

[2] Müller, H., Niedermeier, C.A., Jarczyk, M., Pfitzner, M., Hickel, S., Adams, N.A. (2013). Large-Eddy Simulation of Trans- and Supercritical Injection. In Progress in Propulsion Physics Volume 7, EDP Sciences. (in press)

[3] Niedermeier, C.A., Hickel, S., Adams, N.A. (2013). Assessment of Implicit Subgrid-scale Modeling for Turbulent Supercritical Mixing. In Direct and Large-Eddy Simulation IX, Springer. (in press)

[4] Mayer W., Telaar J., Branam R., Schneider G. and Hussong J. (2003). Raman Measurements of Cryogenic Injection at Supercritical Pressure. Int. J. Heat Mass Transfer, Vol. 39, pp. 709-719.

www.sfbtr40.de
www.aer.mw.tum.de/abteilungen/large-eddy-simulation
www.inca-cfd.org

Aeroacoustic Analysis of Ducted Helicopter Tail Rotor

Research Institution
Institute of Aerodynamics and Fluid Mechanics, Technische Universität München

Principal Investigator
Christian Stemmer

Researchers
Jae Hun You, Christian Breitsamter

Project Partners
Bavarian Research Foundation, Eurocopter Deutschland GmbH

LRZ Project ID: h0983

Introduction

TA conventional helicopter configuration with single main rotor has a tail rotor providing the necessary anti-torque. There are two design concepts of helicopter tail rotors: conventional open tail rotor and ducted tail rotor (DTR). The DTR such as Eurocopter-Fenestron is a multi-bladed fan embedded in a helicopter vertical fin. In this way, rotor blades are protected against collisions with ground obstacles thus achieving significant safety enhancement in flight operation. In contrast to the open tail rotor, the DTR reveals significant advantages in terms of low noise emission. Primarily, the duct-fairing provides an acoustic masking effect, especially, in the plane of blade rotation. The multi-blade configuration also leads to low noise power emission as a result of reduced tangential velocity of the blade tip. In addition, the rotor blades are unevenly circumferentially distributed to avoid acoustic repetition thus reducing annoying tonal noise at the blade passing frequency (BPF).

However, the duct-fairing also has its drawback. First of all, it interacts with the incoming flow. Thereby, undesirable flow phenomena (e.g. inlet distortion) occur inside the duct fairing, which in turn interacts with the rotating blades. Consequently, it leads to a negative impact on the DTR acoustic properties. Thus, a detailed understanding of both aerodynamic and aeroacoustic phenomena of the DTR is still required in order to improve the aeroacoustic characteristics of the Fenestron.
In this context, the present research, which is initiated by the Bavarian research project FORLärm, addresses the numerical analysis of Fenestron aeroacoustic properties for more in-depth understanding of flow induced noise in cruise flight. Thereby, a hybrid methodology is employed for the acoustic noise analysis. First, the aerodynamic noise sources of the Fenestron are captured with CFD (Computational Fluid Dynamics) approach by using the Unsteady Reynolds Averaged Navier-Stokes (URANS) method. Two different turbulence models, the Shear Stress Transport (SST) model and the Scale Adaptive Simulation (SAS) model, are employed and compared to assess the noise-prediction capabilities of the hybrid approach applied herein.

The source information from the flow analysis is then used to calculate the radiated far-field sound by using the Ffowcs Williams and Hawkings (FW-H) surface integral method.

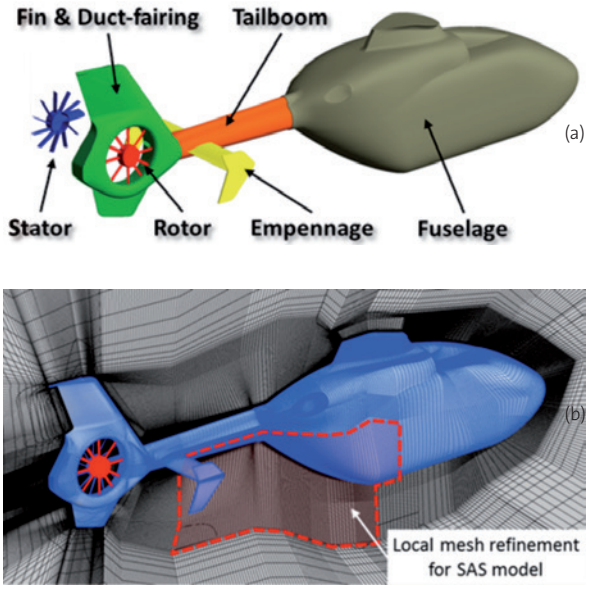

Figure 1: (a) Investigated helicopter configuration; (b) block structured mesh topology.

Results

Based on the detail helicopter configuration (Fig. 1 (a)), a multi-block structured mesh are generated by using ANSYS ICEMCFD (Fig. 1(b)). An O-grid topology with y^+ <1 is applied to improve the accuracy of flow prediction in the boundary layer on the fuselage, as well as on the blade of the ducted tail rotor. Overall, 3400 blocks and approximately 26.3 million nodes are created around the helicopter geometry.

*) Providing of simulation software CFX by ANSYS, Inc. is gratefully acknowledged.

The commercial flow simulation software ANSYS CFX*) has been used to perform URANS simulations. The rotation of the blades is modelled by applying the sliding mesh method. Hereby, the rotor blade rotates one degree per numerical time step Δt (360 time steps for a single fan revolution).

Two different turbulence models, the k-omega SST model and the SAS model, are used to assess the noise-prediction capabilities of the hybrid approach applied here with respect to the approximation order of turbulent flow modelling. The SAS model is a second generation URANS turbulence formulation which can resolve spectral contents of unstable flow up to almost grid limitation. Consequently, it can provide a LES-like resolution of turbulent eddies in the unsteady flow region.

All simulations have been conducted on the high performance computers (HLRB II / SuperMUC) of the Leibniz-Supercomputing center (LRZ). A number of 40 to 160 processors per run have been used to compute totally 15 fan revolutions.

In Fig. 2 (a) and (b), turbulent structures around the helicopter fuselage, predicted with the SST and the SAS simulations are visualized by means of isosurfaces of the Q-criterion ($Q=\Omega^2-S^2$, where Ω is the absolute value of vorticity and S is the absolute value of shear strain rate).

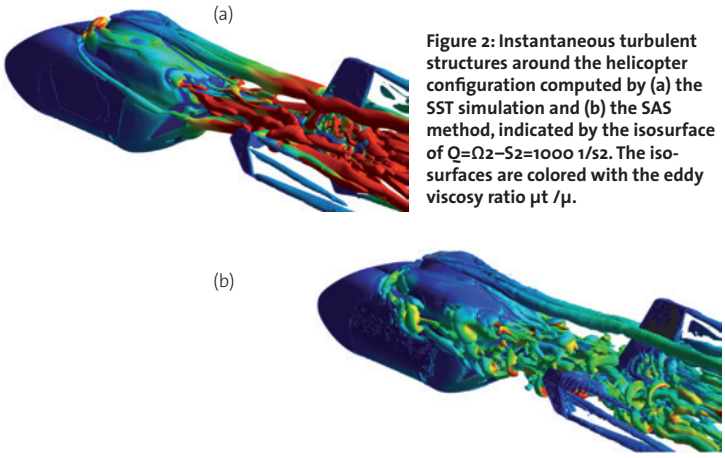

Figure 2: Instantaneous turbulent structures around the helicopter configuration computed by (a) the SST simulation and (b) the SAS method, indicated by the isosurface of Q=Ω2–S2=1000 1/s2. The isosurfaces are colored with the eddy viscosy ratio µt /µ.

Additionally, the isosurfaces are colored with the ratio of the modelled turbulent viscosity µt to the molecular dynamic viscosity, µ, denoted as eddy viscosity ratio, $\mu t / \mu$. As illustrated in Fig. 2 (a) and (b), the wake region of the helicopter fuselage reveals a highly disrupted flow field in cruise flight. It is provoked by a massive flow separation occurring at the different parts of the fuselage (lower fuselage aft body, sealed engine inlet, engine exhaust and rotor mast fairing). Thus, the Fenestron operates under highly perturbed flow conditions. Comparing the turbulent structures in the region of separated flow reveals that the SAS approach produces resolved scales of vortical structures with significantly lower ratios of $\mu t / \mu$, whereas the SST simulation predicts comparably large scale vortical structures with remarkable higher ratios of $\mu t / \mu$.

Based on the information gathered from the CFD task, aeroacoustic calculations were carried out by using an In-house FW-H code. As shown in Fig. 3 (a), the SPL calculated for the SAS model is higher than that of the SST simulation over a wide frequency range. The deviation is especially larger at higher frequencies, which underlies the capability of the SAS model capturing small scale eddies. In Fig 3 (b), the predicted SPL is compared to aeroacoustic flight test results obtained by Deutsche Zentrum für Luft- und Raumfahrt (DLR).

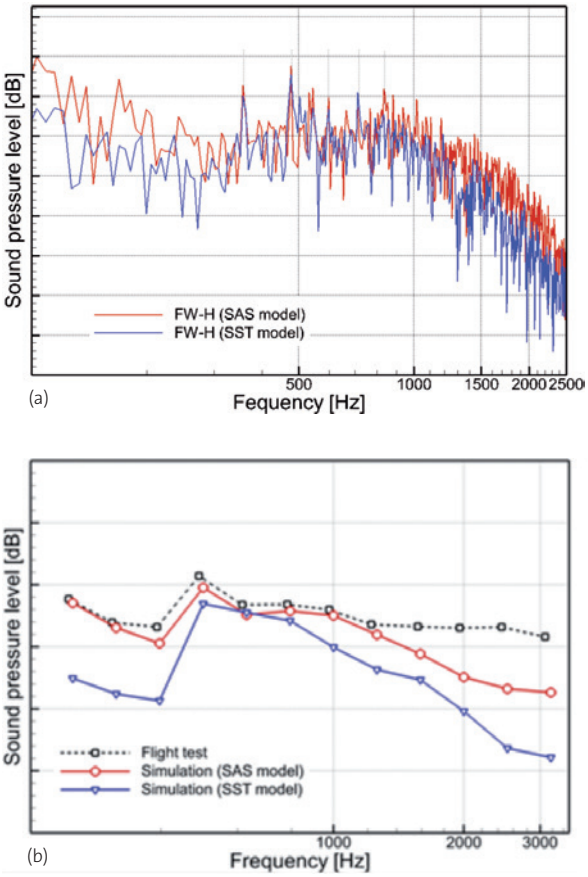

Figure 3: The Fenestron noise spectra predicted by the coupled CFD-CAA method for totally 10 fan revolutions; (b) Comparison of the FW-H results with the measured noise spectra [1] for forward flight condition.

On-going Research / Outlook

Further work will be performed to correlate the noise sources with the far-field sound pressure levels applying DES (Detached Eddy Simulation) and/or Zonal-LES (Large Eddy Simulation).

References and Links

[1] P. Spiegel, F. Guntzer, A. Le Duc and H. Buchholz, Aeroacoustic Flight Test Data Analysis and Guidelines for Noise-Abatement-Procedure Design and Piloting, Proceedings of 34th European Rotorcraft Forum, Liverpool, UK, Sept. 16-19, 2008.

Numerical Simulation of Wing and Nacelle Stall

Research Institution
Institut für Strahlantriebe, Universität der Bundeswehr München

Principal Investigator
Reinhard Niehuis

Researchers
Sebastian Barthmes, Andreas Lesser

Project Partners
TU Braunschweig, DLR-Institut für Aerodynamik und Strömungstechnik, TU Darmstadt, Rolls-Royce Ltd.

LRZ Project ID: h1101

Introduction

Modern transport airplanes are highly efficient in terms of operational costs, environmental friendliness and overall performance. Further optimization is only possible by gaining detailed knowledge of the safe operating range of each vital part of the aircraft. The research unit "Simulation of Wing and Nacelle Stall" (FOR1066) funded by the DFG, Airbus and Rolls Royce Deutschland, investigates new numerical methods to simulate wings in high lift configuration, modern nacelles and highly loaded compressors coupled in one simulation environment with the meteorological simulation of wind gusts. The part of FOR1066 presented in this report deals with the simulation of nacelle compressor interaction at high angles of attack [1]. The challenge in simulating such a configuration consists in coupling two specialized CFD codes – TAU for the external flow around the nacelle, and TRACE for the internal flow through the compressor. Both solvers are developed by the DLR and are used in a wide range of academic and industrial applications.
TAU is a finite volume solver for unstructured and hybrid meshes, whereas TRACE is specialized on block-structured and rotationally periodic meshes. Both solve the Reynolds Averaged Navier-Stokes equations (RANS) and are capable of simulating both steady and unsteady flows. Second-order discretization schemes in time and space as well as a variety of advanced turbulence and transition models are available in both solvers.

Results

In the first period of the project, fundamental research on compressors with non-uniform and distorted inflow is done to gain further knowledge of the relevant features and time scales of flow phenomena within the compressor stage [2], [3]. These simulations were conducted with the TRACE solver on both HLRBII and the Supzero using parallelization with up to 1000 cores and approximately 1 TB of memory.

After the first investigations, which were presented in the report of 2012, further studies were conducted with a new test setup, which was designed especially for the research on rotor distortion interaction. In Fig. 1 the test rig is shown, which is located at the TU Darmstadt. Depicted in red is the transonic high pressure compressor stage, which is designed to feature strong secondary flow phenomena and a distinctive tip vortex [4]. The inflow is distorted by an obstacle (shown in green), which generates similar

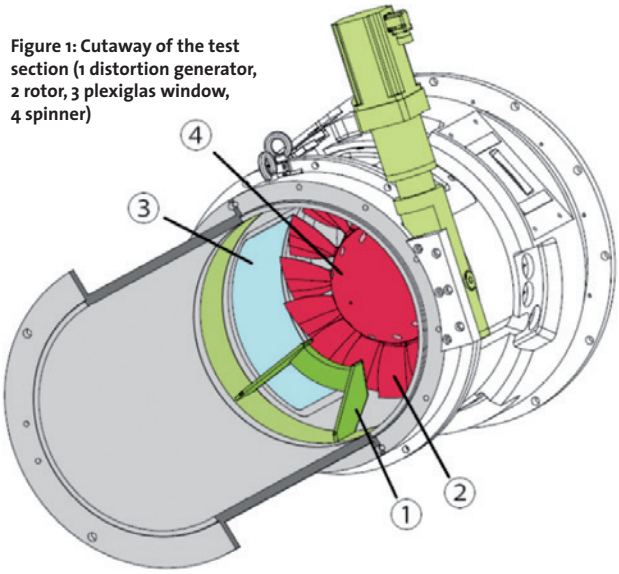

Figure 1: Cutaway of the test section (1 distortion generator, 2 rotor, 3 plexiglas window, 4 spinner)

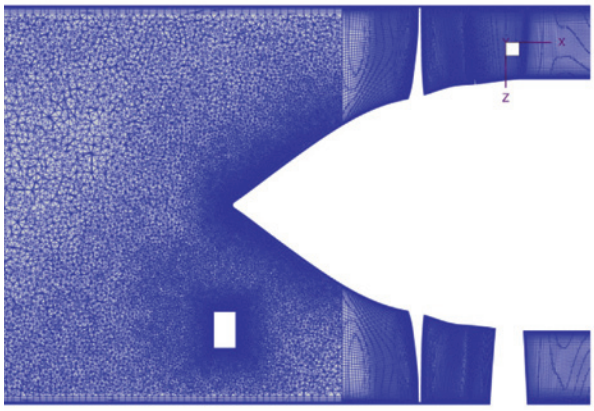

Figure 2: Computational domain of the test rig for TRACE simulations

flow phenomena like a stalling nacelle intake [2]. Due to some delay in the development of the code coupling, the numerical simulations of this test setup were as a start conducted with TRACE only, using the new unstructured TRACE option for the intake part. The entire computational domain consists of about 120 million cells (Fig 2).

Comparing experimental and numerical results, a good data match was found concerning total pressure distribution between distortion generator and compressor inlet, see Figure 3. For the peak efficiency operation point at 100% speed the total pressure directly downstream of the distortion generator is about 20% lower than in the undisturbed flow. Latest results will be presented at the upcoming ASME conference in June 2014 [5].

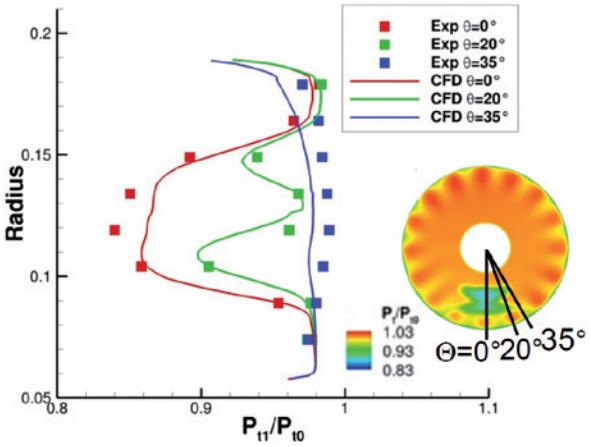

Figure 3: Radial total pressure distribution downstream of distortion generator at different circumferential positions

In addition to the big advance in understanding the flow phenomena in compressors with distorted inflow, also important experience was achieved in handling and post-processing of big amounts of data. The solution file size for one time step is approximately 17 GB. One rotor revolution was resolved with 3000 time steps, which would yield 51 TB of data. Hence the knowledge to distinguish important from derivable or insignificant data also is an important outcome of this research. The needed data could successfully be broken down to a few TB which allowed an efficient data analysis.

On-going Research / Outlook

The current focus of on-going research is to gain experience in coupling TAU and TRACE. Due to delays in code development, it was not possible yet to use the

SuperMUC Cluster for a highly parallelized coupled compressor simulation. Currently, the coupling module - which was developed in collaboration with DLR AT - is in its final validation steps before it is applied to the test setup measured at TU Darmstadt. The work flow of the TAU TRACE coupling is basically depicted in Figure 4. It uses TCP socket and MPI communication to exchange the needed mesh and flow values and is therefore prepared for massively parallelized computing environments.

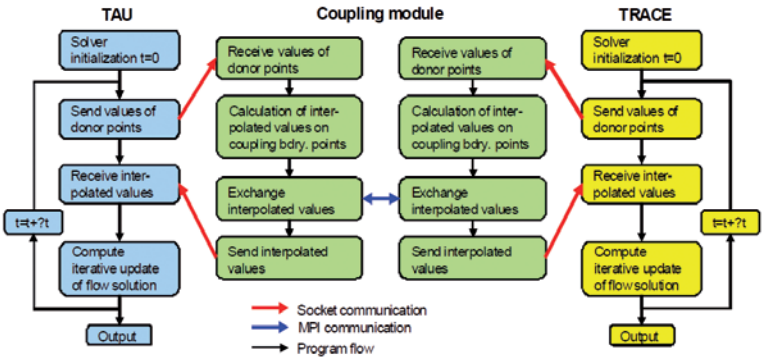

Figure 4: Data interpolation and exchange between TAU and TRACE during iterative time stepping

After successfully coupled simulations of the TUD test rig the final objective is to simulate a generic nacelle compressor configuration, concluding the research work of FOR1066.

References and Links

[1] R. Niehuis, A. Lesser, A. Probst, R. Radespiel, S. Schulze, C.J. Kähler, F. Spiering, N. Kroll, F. Wartzek, H.-P. Schiffer: „Simulation of Nacelle Stall and Engine Response“, Proceedings of the XXI. International Symposium on Air Breathing Engines (ISABE), ISABE-2013-1402, Busan, Korea, 2013

[2] J.P. Lieser, C. Biela, C.T. Pixberg, H.-P. Schiffer, S. Schulze, A. Lesser, C.J. Kähler, R. Niehuis: „Compressor Rig Test with Distorted Inflow using Distortion Generators“, Paper DGLRK2011-241449, 2011

[3] A. Lesser, S. Barthmes, R. Niehuis: “Numerical Investigation of the Effect of Inflow Distortions on Transonic Axial Compressor Stages with 2D and 3D Calculations”, 28th International congress of the Aeronautical Sciences (ICAS), Brisbane, Australia, 2012

[4] R. Ciorciari, A. Lesser, F. Blaim, R. Niehuis: “Tip Clearance Investigation for an Axial Transonic Compressor”, Proceedings of the 10th International Symposium on Experimental Computational Aerothermodynamics of Internal Flows, ISAIF10-018, Brussels, Belgium, 2011

[5] A. Lesser, R. Niehuis: “A Study about Transonic Axial Compressors with Total Pressure Inlet Flow Field Distortions”, Proceedings of ASME Turbo Expo 2014, GT2014-26627, June 16-20, Düsseldorf, Germany, 2014

Simulation of the unsteady flow around the Stratospheric Observatory For Infrared Astronomy SOFIA

Research Institution
Deutsches SOFIA Institut (DSI), University of Stuttgart

Principal Investigator
Christian Engfer

Researchers
Sebastian Illi, Philipp Gansel, Thorsten Lutz, Ewald Krämer

Project Partners
Institute of Aerodynamics and Gas Dynamics, University of Stuttgart

LRZ Project ID: h1142

Figure 1: View of the SOFIA aircraft during a test flight with open door

Introduction

The Stratospheric Observatory For Infrared Astronomy SOFIA, a joint project between NASA and DLR, is a 2.5m reflecting telescope housed in an open cavity on board of a Boeing 747SP aircraft (see Figure 1). SOFIA operates in the stratosphere at an altitude above 12km to observe objects in the universe in the infrared region of the electromagnetic spectrum. The flow over the open port during the observation flights presents challenging aerodynamic and aero-acoustic problems. In general, the flow over cavities such as the SOFIA telescope port is characterized by unsteady flow phenomena associated with prominent self-sustained pressure fluctuations caused by amplified acoustic resonances. In the present case, these phenomenon cause unwanted vibrations of the telescope structure and deteriorates the image stability [1].

Numerical approach and computational details

To investigate the pressure fluctuations in the cavity, CFD simulations using the Detached Eddy Simulation (DES) approach were performed with the Finite-Volume solver TAU that was developed by the Institute of Aerodynamics and Flow Technology of DLR [2]. The code solves the unsteady, compressible, three-dimensional Reynolds-Averaged Navier-Stokes (RANS) equations on unstructured or hybrid grids. In general, DES is characterized by a hybrid length scale that splits the flow field in a RANS and Large Eddy Simulation (LES) domain. The idea is to entrust the calculation of the attached boundary layers to a RANS model and only the separated and wall-distant regions to LES. In the LES zone large scales are resolved directly in space and time down to a defined spatial filter width. For meaningful LES, 80% of the turbulence spectrum should be resolved which requires a finely spaced hexahedron block in the shear layer zone over the cavity opening.

The fine spatial resolution of the SOFIA shear layer leads to significant mesh sizes of more than 50 million cell elements (half model) that can only be calculated efficiently on supercomputers such as SuperMUC at LRZ. In the following Figure 2 is shown the scaling performance of the TAU solver on the SuperMUC architecture.

The present SOFIA computations were carried on 1312 processor cores in parallel. A typical CFD simulation using the Improved Delayed DES (IDDES) approach consisted of 12000 physical time steps (simulated time of 1.6s) with 80 inner iterations per time step. The physical time step size was chosen to 100µs. The computational cost for one IDDES run was about 150.000CPUh.

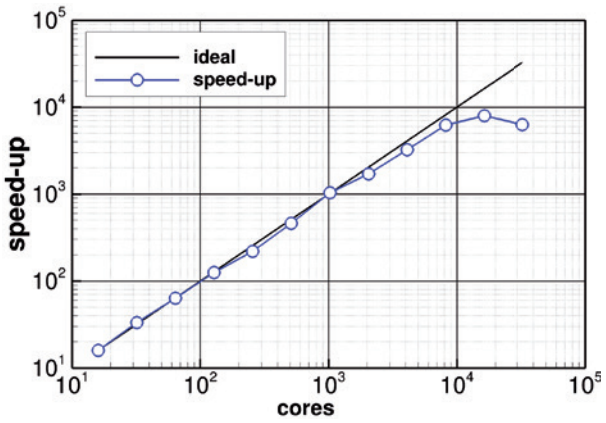

Figure 2: Scaling performance of the TAU solver on the supercomputer SuperMUC for a hybrid grid with 45 million points (using the TAU standard partitioner)

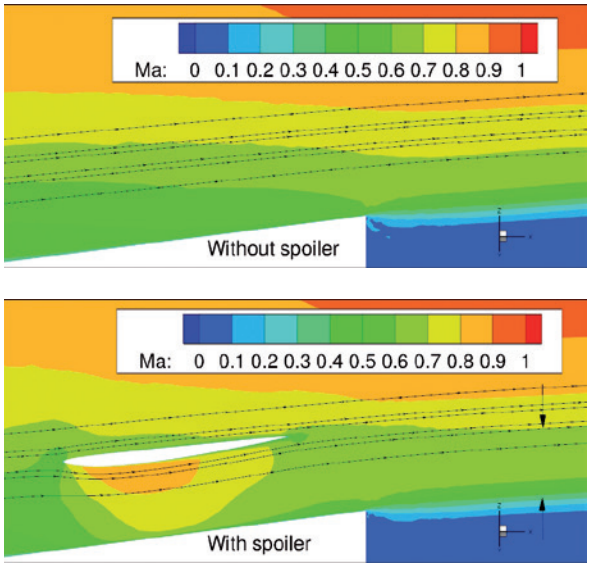

Figure 3: Instantaneous plot of the Mach number in a cut through the cavity at 40° elevation without spoiler (upper) and with a spoiler upstream of the cavity leading edge (lower picture) [3]

Results

Next to the understanding of the highly complex flow phenomena that occur under baseline conditions (Mach number 0.85, 12.5km altitude, 40° telescope elevation), the objective of the CFD simulations was to investigate passive flow control concepts that are capable of improving the observatory´s performance by mitigating the aerodynamic excitation acting on the telescope. The simulation of a spoiler concept installed upstream of the cavity leading edge and situated in the attached aircraft boundary layer shows a high potential to improve the telescope´s pointing stability while preserving the aero-optical properties of the shear layer [3].

The basic idea of the spoiler installed upstream of the cavity leading edge is to displace high energetic flow upwards as it is illustrated in Figure 3 by means of a comparison of the instantaneous Mach number plotted in a cut through the cavity at 40° elevation. It can be observed that the green Mach number zone (indicated by the two black arrows in the lower picture) downstream of the spoiler is thicker compared to the baseline configuration without spoiler.

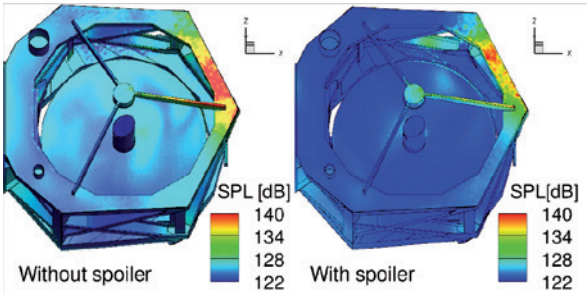

Figure 4: Comparison of the Sound Pressure Level (SPL) plotted over the telescope surface without (left) and with a spoiler installed upstream of the cavity leading edge (right picture) [3]

The impact of the spoiler on the pressure amplitude on the telescope surface is shown by means of a comparison of the Sound Pressure Level (SPL) plotted over the telescope surface in Figure 4.

The comparison in Figure 4 reveals that the upstream spoiler yields to a reduced pressure amplitude over the entire telescope surface. A Fourier analysis of the pressure fluctuations on the telescope surface shows that the pressure amplitude drops over a large frequency

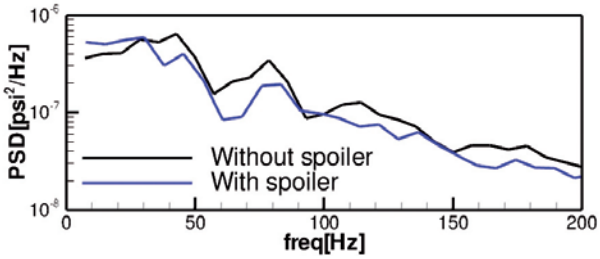

Figure 5: Spoiler impact on the spectral distribution of the pressure fluctuations by means of the PSD average over all 56 pressure sensor locations on the telescope [3]

band as it can be seen in the comparison of the PSD average over all 56 pressure sensor locations on the telescope (Figure 5).

On-going Research / Outlook

Thanks to the computing power of SuperMUC and the calculation resources provided by Leibniz Rechenzentrum (LRZ), a detailed description of the SOFIA cavity aeroacoustics was possible by means of state of the art DES simulations. The performed computations allowed in addition the investigation of passive flow control concepts capable of mitigating the aero-acoustic and aerodynamic loading on the telescope under baseline conditions.

Acknowledgements

SOFIA, the "Stratospheric Observatory for Infrared Astronomy", is a joint project of the Deutsches Zentrum für Luft- und Raumfahrt e.V. (DLR; German Aerospace Centre, grant: 50OK0901) and the National Aeronautics and Space Administration (NASA). It is funded on behalf of DLR by the Federal Ministry of Economics and Technology based on legislation by the German Parliament, the state of Baden-Württemberg, and the Universität Stuttgart.

References and Links

[1] Sven Schmid, Thorsten Lutz, Ewald Krämer and Timo Kühn: Passive Control of the Flow Around the Stratospheric Observatory for Infrared Astronomy, *Journal of Aircraft*, Vol. 46, No. 4, July-August 2009

[2] Gerhold T., "Numerical Flow Simulation for Aircraft Design, chap. Overview of the Hybrid RANS Code TAU", pp. 81–92. Springer-Verlag 2005

[3] Christian Engfer, Thorsten Lutz, Ewald Krämer: Spoiler Concept to Reduce the Aerodynamic Loading on the SOFIA Airborne Telescope, submitted to *Journal of Aircraft* in January 2014

http://www.dsi.uni-stuttgart.de/
http://www.nasa.gov/mission_pages/SOFIA/

DNS of Gas Transfer across the Air-Water Interface

Research Institution
Institute for Hydromechanics, Karlsruhe Institute of Technology (KIT), Germany

Principal Investigator
H. Herlina

Researchers
H.Herlina, J.G. Wissink

Project Partners
School of Engineering and Design, Brunel University London, UK

LRZ Project ID: pr28ca

Introduction

The present numerical work considers the case of gas transfer across the air-water interface driven by isotropic turbulence diffusing from below. Applications include, for example, the transfer process of oxygen from the atmosphere into natural water bodies, which is an essential pathway for e.g. rivers to overcome dissolved-oxygen deficits. Oxygen and many other atmospheric gases have low-diffusivity (high Schmidt number) in water. For such gases, the interfacial mass transfer is marked by a very thin concentration boundary layer and occurrences of steep concentration gradients in other regions of the fluid domain. To accurately resolve the physical mechanisms of the turbulent mass transfer at high Schmidt (*Sc*) numbers, an extremely fine grid resolution is needed. To mitigate this, we employ a specifically-designed numerical scheme [1] capable of resolving details of the mass transfer on a computationally feasible mesh size while avoiding spurious oscillations of the scalar quantity. In the code, a 5^{th} order WENO scheme [2] for scalar convection combined with a 4^{th} order central method for scalar diffusion was implemented on a staggered and stretched mesh. For the fluid flow the incompressible Navier-Stokes equations were solved using 4^{th} order discretisations of convection and diffusion.

Because the diffusion coefficient of the scalar is much smaller than the diffusion coefficient of the ambient fluid, the resolution requirements for the scalar are much higher. Thus, to further save computing time, a dual-meshing strategy is employed in which the scalar field is solved on a finer mesh than the flow-field. The setup of the present simulations was similar to the gas transfer experiments driven by grid-stirred turbulence performed at KIT [3]. Despite the advanced measurement techniques used in the experiments, they still faced accuracy limitations when elucidating the Batchelor sublayer as well as capturing minute fluctuations of the turbulent transport in the deeper bulk region. Compared to previous simulations that were limited to low Schmidt numbers, the present DNS-s allow us to obtain high quality data for Schmidt numbers that are typical for environmental gases like oxygen (Sc=500). In this way, many experimentally inaccessible aspects of the gas-transfer problem can now be addressed.

Results

Simulations were performed for three different turbulent Reynolds (R_T) numbers. Compared to the size of the experimental domain (50cm x 50cm x 45cm), only a small part near the water surface was numerically modeled to save computing time. In the experiments the turbulence was generated by an oscillating mesh in the lower part of the tank. In the DNS, the incoming turbulence was generated in a separate but concurrently running simulation of isotropic-turbulence. At each time step a cross-sectional snapshot from this isotropic-turbulence simulation was introduced at the bottom of the main DNS computational domain (Dirichlet boundary condition). The free-surface at the top was modeled using a free-slip boundary condition. Periodical boundary conditions were employed at the sides to account for the much larger horizontal sides. The transfer of the diffused substance into the liquid was forced by keeping the concentration c at the surface at saturation, while at the bottom $\partial c/\partial z = 0$. The initial condition for the simulation was c=0 in the entire computation domain, except at the upper interface.

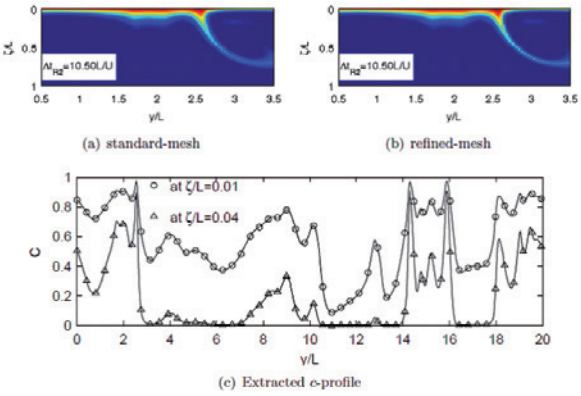

Figure 1: Verification of scalar grid spacing (case GS500). Blue and red color scaling indicate regions with low and high scalar concentration, respectively.

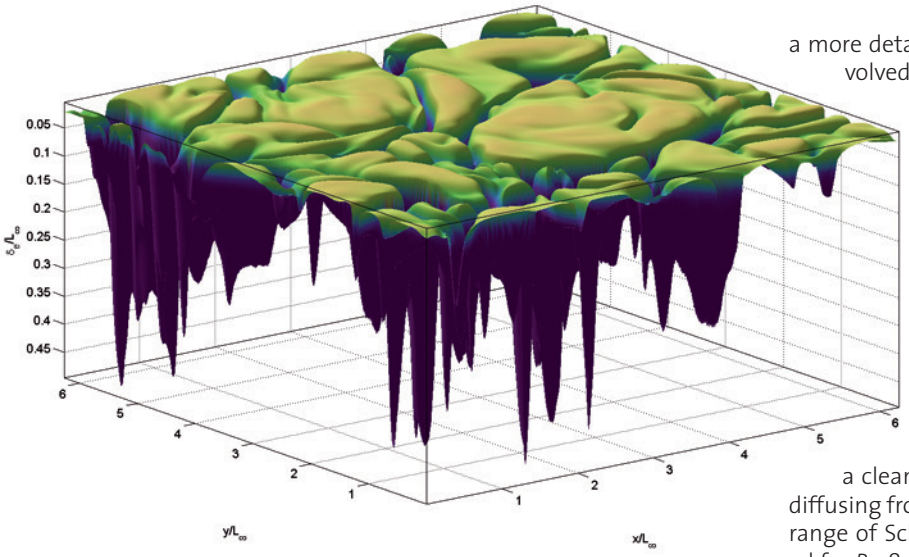

Figure 2: Isosurface of scalar concentration (Sc=8) for case GS500 (R_T=507). *The* color coding indicates the thickness of the concentration boundary layer.

To fully resolve the problem 3.5 x 10^6 to 79 x 10^6 grid points were used. The computational domain was subdivided into about 300 and 900 blocks on previously Supzero and now SuperMUC, respectively. Communication between blocks happened through the standard MPI protocol.

On SuperMUC we could efficiently perform the grid refinement studies to verify the choice for the grid resolution. The tests were conducted both for the velocity and scalar concentration fields using refinement factors 1.4 and 2, respectively. The results of the scalar refinement test, shown in Fig. 1, were obtained by

starting both the unrefined and refined simulations from the same initial scalar field and the same background turbulent flow-field. Both simulations were allowed to evolve for a period of time Δt_{R2}=10.5 time-units and the snapshots show a very good agreement between the unrefined and refined meshes. It can be seen that the numerical code is capable of capturing steep gradients in the scalar distribution without introducing any spurious oscillations (under/overshoots) as further evidenced by the extracted concentration profiles in Fig. 1c. The extracted 2D snapshot also shows the mass transport mechanisms driven by the isotropic turbulence. The upper saturated concentration boundary layer is constantly being disturbed by the turbulence coming from below. The upwelling motion of unsaturated fluid causes the concentration boundary layer to become thinner, thereby increasing the concentration gradient and enhancing the interfacial scalar flux.

Downwelling motions transport a portion of the highly-saturated upper layer into the bulk where it is intensely mixed by the turbulence. While in the experiments at KIT only 2D snapshots were recorded, in the DNS instantaneous 3D information of the flow-field and scalar concentration distribution could be obtained allowing a more detailed examination of the physical process involved. For example, Fig. 2 shows an isosurface of the concentration. It is shown that the top surface is dominated by divergence areas separated by narrow downwelling areas. When compared to the lower RT=84 case (not shown here), at higher RT not only the largest eddies but also smaller structures managed to clearly affect the concentration boundary layer. Further statistical analysis can be seen in [4].

On-going Research / Outlook

DNS-s of interfacial mass transfer across a clean flat- surface driven by isotropic-turbulence diffusing from below have been performed. While a wide range of Schmidt numbers (Sc=2 to 500) were simulated for R_T=84 and 195, at R_T=507 the Sc=500 case was not simulated yet because of the excessively high demand for computational resources. This should become feasible on SuperMUC. For comparison, on the older Supzero machine the flow-field simulation of case GS500 when using 288 processors required 6.7 CPUh per t^* (t^*=simulation time-unit) whereas on SuperMUC – where usage of more blocks is not an issue- the same case required 3.8 CPUh/t^* (using 800 blocks). Furthermore when activating the scalar solver (Sc=8 and 32) using a scalar-mesh refinement factor of 2 the computing resources needed increases from 6.7 CPUh/t^* to 26.3 CPUh/t^*. To fully resolve the R_T=507 at Sc=500 case a refinement factor of 5 for the scalar mesh is needed so that at least 32000 blocks would be required. So far we used the standard MPI protocol for parallelization. This is fine when dealing with only O(1000) blocks but for a larger number of blocks the amount of data to be exchanged each time step becomes excessive. Currently, the aim is to implement a hybrid OpenMP / MPI method and use more than one processor per block, which significantly reduces the total number of blocks.

In addition, our long term plan is to perform simulations of interfacial mass transfer driven by a combination of isotropic-turbulence with a buoyant-convective instability.

References and Links

[1] Kubrak B., Herlina H., Greve F., Wissink J.G. 2013. Low-diffusivity scalar transport using a WENO scheme and dual meshing. J. Comput. Phys. 240, 158-173.
[2] Liu X., Osher S., Chan T. 1994. Weighted essentially non-oscillatory schemes. J. Comput. Phys. 115, 200–212.
[3] Herlina and Jirka G.H. 2008. Experiments on gas transfer at the air-water interface induced by oscillating grid turbulence. J. Fluid Mech. 59, 183-208.
[4] Herlina H. and Wissink J.G. 2014. Direct numerical simulation of turbulent scalar transport across a flat surface. Accepted in J. Fluid Mech.

http://www.ifh.kit.edu
http://www.brunel.ac.uk/~mestjgw

Numerical investigation of complex multiphase flows with Lagrangian particle methods

Research Institution
Institute of Aerodynamics and Fluid Mechanics, TU Munich

Principal Investigator
X.Y. Hu

Researchers
M. Ellero, S. Litvinov, S., Adami, S.

Project Partners
–

LRZ Project ID: pr32ma

Introduction

Polymer solutions are widely used in industrial applications; oil refinery, medical diagnostics, micro-injection devices in printing are only few examples. In this project we focus on computational investigation of rheological properties of polymer solutions.

One obvious difference between water and polymer solutions is viscosity: polymer solutions are much more resistant to the gradual deformation. But also everyone who tried to get ketchup out of a bottle observed that properties of polymer solutions depend on the history of deformation. In general, how the polymer solution reacts to the deformation dependents on shear rate and shear rate history. These are so-called non-Newtonian properties are caused by inter- and intro-molecular interaction of polymers. Polymer chains are long and heavy objects and they can interact with each other up to the point they are tangled up; inter-molecular effects are also complex, examples are viscous drag, entopic elasticity, Brownian forces, hydrodynamic interactions, excluded-volume effects. All of these make theoretical predictions for polymer solutions rheology very difficult.

A straightforward simulation approach to model polymer solutions is to build up a detailed model with all atomistic phenomena taken into account. But the computational capacity required to perform a full atomistic simulation is very high and methods based on mesoscopic theories, which connect the microscopic and macroscopic descriptions of the systems, are a promising alternative. By applying mesoscopic methods one expects to capture only essential microscopic parameters and relationships and to omit details which are not important for the phenomena under investigation.

In this project we use Lagrangian particle methods with explicit solvent model: we represent the solutions as a whole using particles (discretization elements to represent a "packet" of liquid). The polymer chain is embedded into a number of special particles (denoted as polymer beads) which represent the segments of the polymer chains. Polymer beads interact hydrodynamically and with additional forces due to the chemical bond between the polymer segments (Figure 1). These additional forces are taken into account by simple elastic potentials. The polymer chain is immersed in a domain full of Lagrangian particles (solvent). Many particles methods are developed recently and their advantages and drawbacks are an area of active investigation. Hence the part of this project is concerned with the method development and validation.

Results

First, we performed transient simulations of a semi-dilute polymer solution in a microchannel following extensional flow by dissipative particle dynamics (DPD). This is the most mature explicit solvent method which takes thermal fluctuations into account. The simulation setup is shown in Figure 4. Preliminary extended polymers are entering the channel at the inlet and eventually relax downstream. This relaxation is affecting the flow profile. In experiments only the macroscopic flow measurements are available and our results allow deducing the information on polymers configuration. [1]

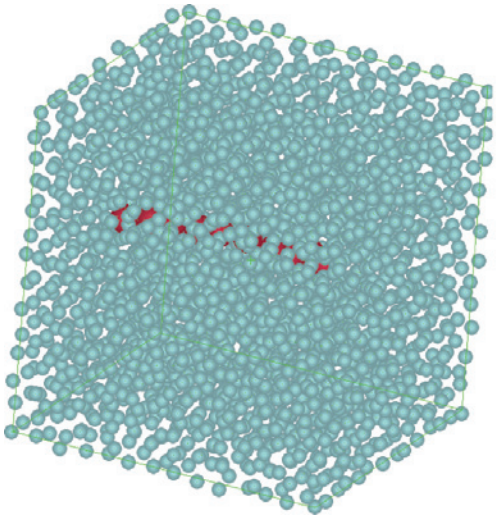

Figure 1: Polymer chain is immersed in "an ocean" of solvent particles.

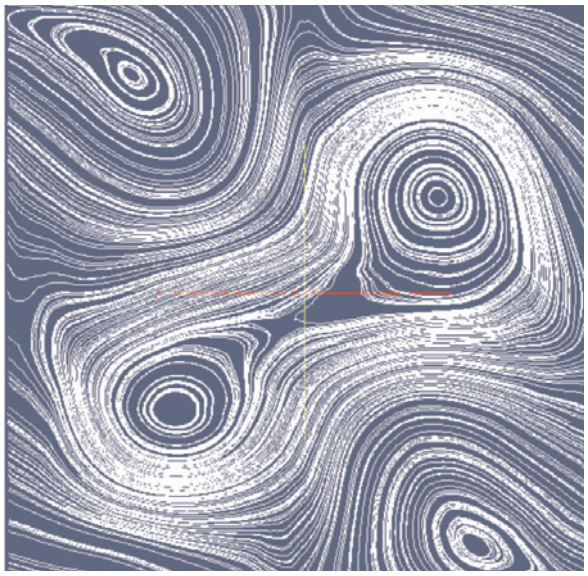

Figure 2: Streamlines (lines tangent to the velocity vector) of four-roll mill flow simulation. For Newtonian liquid four symmetric vertices are expected. Presence of the polymers leads to instability.

The second part of the project is dedicated to the study of elastic instabilities or elastic turbulence. Traditionally turbulence is associated with high Reynolds number (low viscosity) but the instabilities in polymer solutions can arise even for almost zero Reynolds number. The source of such behavior is elastic stress created by polymers. In this case Brownian motion is dominated by mechanical forces in the system and we used Smoothed Particle Hydrodynamic (SPH) method which does not include thermal fluctuations but is very good to represent incompressible media. We performed two dimensional simulation of four-roll mill flow. For lower elastic stresses four identical vertices are seen, with increasing elastic stresses vertices are destabilized and at even higher level of elastic stresses the flow becomes chaotic. In Figure 2 streamlines of the flow for intermediate level of stress are shown.

The third sub-project continues our previous work and develops a new particle method Smoothed Dissipative Particle Dynamics (SDPD) witch borrows advantages of both DPD and SPH: it includes thermal fluctuations, correctly represents hydrodynamic, and can deal with high pressure gradients [2,3]. We investigated the static and dynamic properties of single polymer and polymer solution in 3D. For polymer solution a typical simulation snapshot is shown in Figure 3. We found that the SDPD model captures the steady shear rheological properties of typical polymer melts. For the polymer solution with 50% polymer concentration the method qualitatively reproduces the cross-stream migration phenomena reported in previous experimental and numerical works.

Outlook

We found that Lagrangian particle methods with explicit solvent are very promising and robust tools but the obvious disadvantage is a big number of discretization elements and hence high computational cost. So the access to faster supercomputers immediately widens the area of possible applications.

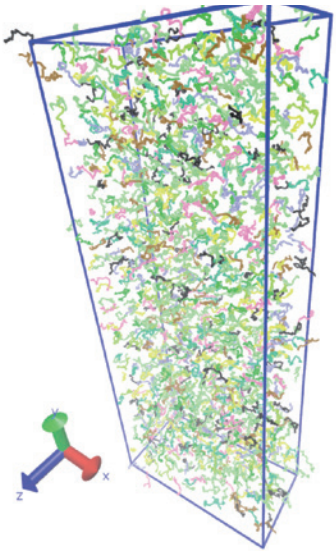

Figure 3: Snapshot of the polymer solutions simulation: x is a direction of the external force; y is a direction of the velocity gradients. Solvent particles are not shown.

References and Links

1. Litvinov S., Ellero M, Hu X.Y, and Adams *N.A.Microfluid. Nanofluid.* 16.1-2 (2014)
2. Litvinov S., Ellero M., Hu X.Y., and Adams N.A., *Phys. Rev. E*, 77(6):66703, 2008
3. Litvinov S., Hu X. Y., and Adams N. A., *J. Phys: Condensed Matter* 23.18 (2011): 184118.

A pool filled with Non-Newtonian fluid
http://www.youtube.com/watch?v=f2XQ97XHjVw
An article on elastic turbulence by Prof. Steinberg:
www.scholarpedia.org/article/Turbulence:_elastic

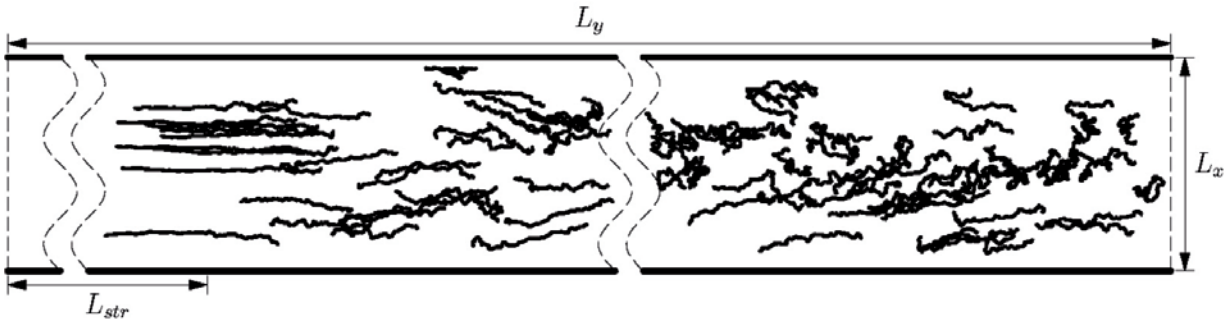

Figure 4: Simulation snapshots: domain is periodic in y and z directions; in the x direction straight wall boundaries are used; a constant body force is applied in the y direction; polymers are stretched by means of an additional force in the region $y<L_{str}$ and let relax in the region $y>L_{st}$

Spatially resolved flame transfer function of a swirl stabilized flame

Research Institution
Leherstuhl für Thermodynamik, Garching

Research Area
Combustion, thermo-acoustics, flame stabilization.

Principal Investigator
Robert E. Leandro, leandro@td.mw.tum.de

Researchers
Ahtsham Ulhaq, Wolfgang Polifke

Project Partners
CERFACS (France)

LRZ Project ID: pr42ku

Abstract

In the current work we do a Large Eddy Simulation (LES) of a fully premixed, swirl stabilized flame, to which experimental data is available. Detailed input data is provided by the current project for a one dimensional (1D), thermoacoustic distributed flame model, that will allow to assess the impact of distributed heat release on combustion system instabilities. This data includes mean temperature and density fields, as well the local dynamic response of the flame to an imposed velocity fluctuation, i.e. a local flame transfer function FTF(x). A specific code was developed in order to extract and pre-process the binary LES data fields, and due to libraries access and the large amount of data involved, it runs exclusively at LRZ/ Supermuc. The local nature of a distributed flame model required an optimized System Identification (SI) method, that allowed us to obtain an axially discretized FTF, for a broad range of frequencies and from only one LES run. Furthermore a non-trivial wall temperature profile is seen to be required, in order to better match the LES mean heat release distribution to the experiments.

Introduction

With the development of lean- premixed combustion technologies thermoacoustic combustion instabilities have become a recurrent problem. In low order modelling of such instabilities [1] the Flame Transfer Matrix (FTM) relating the acoustical properties upstream and downstream of the flame is obtained starting from a Flame Transfer Function (FTF), that relates the acoustic fluctuations of velocity at the burner with the heat release rate of the flame, with the assumption that the flame is an acoustically compact element. This compactness assumption is only valid for Helmholtz numbers $He = k.L_{flame} << 1$, where k is the wave number and L_{flame} the flame length. Previous results [4] have a) extended the applicability of low-order models to non-compact conditions, and b) evaluated the damping potential of distributed heat release on the thermoacoustic stability of a combustion system. The low order model approach proposed in [4] can handle any heat release distribution, and the current numerical study should provide realistic and detailed input flame data to access the damping potential of distributed heat release under realistic conditions.

The Large Eddy Simulations (LES) are done using the AVBP code (CERFACS/ France), for the geometry and conditions of Kim et al. [2] experiment. Their experimental work dealt specifically with an acoustical non-compact flame.

Goals of the project

- Stabilization of realistic flame Experiments providing spatial distributed data of heat release and flame frequency response, i.e FTF(x), are relatively scarce. We chose to study the 70kW, fully premixed flame of Kim et al. [2], as in their experimental work it is stated that acoustical non-compactness is relevant.
- Detailed flame response The potential of the LES simulations, coupled to an efficient excitation at the flow inlet is explored. The output data of the simulations, i.e. full 3D fields of fluctuating heat release and thermoacoustical variables, is processed using a signal/ response correlation method. The result is the spatially and frequency resolved response of the fluctuating heat release FTF(x), that together with the average temperature and density fields, provide the data for spatially distributed thermoacoustical models.

HLRB computational work

LES/SI
The large eddy simulations (LES) flow solver used on the current work is AVBP [3], developed by CERFACS. AVBP can be optimally adapted to any kind of processor architecture and initial tests have shown that it can be highly parallelized with an optimal load per CPU, especially if high performance network interconnections are available. Additionally this code can be restarted from a previous result file, allowing splitting the calculation in different runs. As AVBP is provided without license or parallelization limitations and is already available at Supermuc, an efficient use of the computing resources was ensured.

The LES/ System Identification (SI) method [1] involves both producing the CFD data and a latter, two level, data processing. After a statistical stabilized solution is obtained, the system is excited at the inlet with broadband noise superimposed on the mean flow velocity. These broadband perturbations a) propagate to the flame front and create a response in the heat release of the flame and b) reach the boundaries of the computational domain. In order to correctly identify the response of the flame, the reflection of acoustical waves at the boundaries need to be suppressed. These reflected waves would would affect both with the inlet excitation signal and the flame response, deteriorating the identification quality. Therefore evolved non- reflecting boundary conditions are used at both inlet and outlet of the domain. Identification of the flame response requires time series of both the velocity fluctuations at a reference position and the heat release field. Due to practical aspects of data storage and processing, these variables are exported only every 100th time step. Even after this down- sampling, the very small CFD time step of 1E-7s, allow us to have a maximum resolved frequency of 100 kHz, well above the ones that we are interested in (~1 kHz). The 3D heat release fields are then pre-processed to 1D axially resolved data and, together with the reference velocity, processed using the SI method, with which the spatially resolved flame response is finally obtained.

Pre-processing of CFD data
A pre-processing routine FLUCT1D on FORTRAN was developed in collaboration with CERFACS (France) to allow extraction of specific thermo-acoustic variables from the raw, 3D, time series. The interest of the thermoacousticall model developed on this project becomes evident at this early stage: as only 1D fields of the thermo-acoustical variables are required, the amount of data that needs to be stored/ transferred outside of the LRZ network is largely reduced by appropriate pre-processing of the 3D raw data. As access to the binary raw data is done through closed source code/ libraries, compiled specifically for SuperMuc, a specific pre-processing routine was developed in this project. Written in Fortran and running on SUPMUC as well, Fluct1d extracts time series of velocity at a reference position and of 1D, axially resolved and transversally averaged, instantaneous and time averaged properties such as heat release or temperature. The final pre-processed data, now in an ASCII format, is typically smaller then 100 Mb (instead of the initial 12 Tb) and easily transferred from Supermuc/ LRZ to an external network or personal computer.

Resources used
The intrinsic nature of LES (full three-dimensional resolution of the unsteady Navier Stokes equations) makes it very expensive, requiring massive computing resources not available at the Lehrstuhl für Thermodynamik, TUM. Preliminary runs done on the Linux-Cluster (LRZ) have shown that the amount of processors available and the duration of each job were not sufficient for the amount of time steps required in this work. Therefore access to high performance computing Supermuc resources was necessary.

The LES mesh used on the current project consists of ~11 million cells that, for tracking of the acoustical waves, requires a computational time step of 1.0e-7 s. Furthermore, the overall simulation length is 0.3 seconds to identify low frequency oscillations (Nyquist criterion). Then a LES/SI simulation would need at least 2.0e6 iterations. Indeed previous works using only global heat release with a high level of turbulent noise, similar to the present configuration, concluded that 3e6 iterations were necessary for a correct identification.

Therefore on the SI production phase the data for a given working condition consists of around 3E6 time steps, with each time step solution having a size of ~400MB. These 3D full solutions are then saved every 100th iteration, resulting on 30.000 files with ~12 Tb of raw data. As shown if Table 1 such a simulation would take around 10 days using 50 nodes with 16 tasks per node to complete in the current Supermuc configuration. However it was seen that AVBP would only support a maximum of 200.000 consecutive iterations. As a result the run had to be split into 15 jobs/ individual sets, that, accounting with resubmission/ queueing times increased the simulation time from ~10 days to ~20 days.

The pre-processing of these CFD data, even if not CPU intensive, was carried out at Supermuc. This was necessary as access to the binary data required copyrighted libraries only compiled for Supermuc. Furthermore, local data pre-processing was in this case very convenient due to the large data sets involved (typically up to 12 Tb of data).

Table 1: Typical LES/SI run

Time step [s]	1.50E-07
Number of iterations/simulation	3.00E+06
CPU time per iteration [s]	240
CPU time per simulation [h]	7.96E+03
Number of CPUs (50 nodes x 16 Tasks per node)	800
Simulation time [h] (stops not incl.)	250

Results

Stabilization of a realistic flame

In these work we chose to simulate a 70Kw, swirl-stabilized flame [2]. The round cross-section combustor burn a fully premixed and preheated (400K) methane/ air mixture, at a lean equivalence ratio of 0.7. A side view of both combustor and flame is show in Fig. 1.

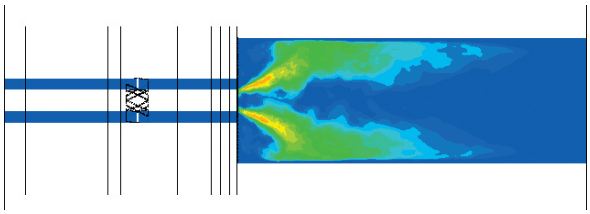

Figure 1: Side view of the round cross section combustor, showing a contour of the average heat release,the central bluff body (white inner section) and swirler (left). Vertical lines correspond to acoustical probe locations.

Combustor wall temperature: Initial runs with adiabatic or uniform temperature combustor walls resulted in flames that did not compare well with the experimental heat release distributions. As experimental temperature measurements were not available, a series of non trivial temperature profiles were tested and used to modulate the average heat release distribution along the flame axis. A small subset of these test runs are shown in Fig. 2. Fine tuning of the temperature of two combustor wall sections, covering about half of the flame length and centred at the maximum heat release location, provided a good match to the experimental data. Additionally, the chosen temperature profile insured a flame with the non-reacting outer shear layer, next to the dump plane (cf. Fig. 1), seen on the experiments.

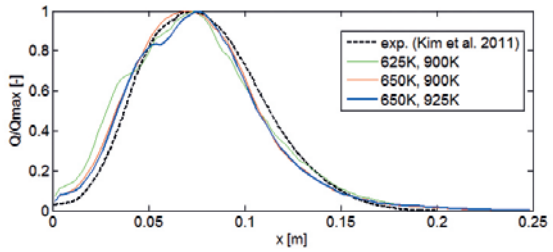

Figure 2: Comparison between axial mean heat release profiles o tained in experiments and in the current work, showing the temperature influence of two combustor wall sections.

Flame response

An advanced identification signal was applied to the inlet of the combustor. The results shown on the remaining of this paper correspond however to the uniform wall temperature runs, and not yet to the optimized mean heat release profile shown in Fig. 2. The use of specific Characteristic Based non- reflecting boundary conditions allowed to minimize the inward reflections from the inlet and outlet, providing an improved signal to noise ratio for the frequencies of interest (f > 50Hz). For the above mentioned wall temperature tests, these non reflecting boundary conditions were able to cope with local differences on temperature, axial velocity and pressure at the outlet plane. However, during the System Identification runs, the 6% inlet velocity excitation further increased the outlet fluctuations, causing partial flow reversal (at the outlet) and forcing computations to stop. For this reason a 1mm thick plane with artificial, high viscosity was added at the outlet. This artificial viscosity patch produced a more uniform flow profile without outlet flow reversal, and did not affect the performance of the acoustical non-reflecting boundary condition nor the overall heat release profile.

Global and local FTFs

The high spacial resolution of the current LES simulations combined with the SI method and a broadband excitation signal, allow us to obtain the local flame response, for a range of frequencies, and with only one simulation. Making use of the Fluct1D pre-processing tool, the excitation and multiple response signals are fed into a modified version of the SI tool. Through a Single Input/ Multiple Output (SIMO) correlation, the spatially resolved heat release response to the reference velocity excitation, i.e. the FTF, is obtained. Figure 3 shows the local FTFs, function of both frequency and a 25 sections,10mm spaced, axial discretization. It is interesting to note that the amplitude of the flame response shows, contrary to the mean heat release distribution with one clear maximum (cf. Fig. 2), several local fluctuation maximums for a given frequency. The region Furthermore the location of these amplitude maximums is not fixed as frequency changes: note the downstream shift of these peaks as frequency increases from 100 to 200Hz. As to the angle of the local FTF, it shows the expected smooth decrease with increase of the distance to the (upstream) reference position. This phase change is seen on both laminar and turbulent flames and is usually described by a heat release model with a linear time delay distribution [4].

We have further included on the SI tool a lumping routine, that allows coarsening the original output signals to a user defined axial resolution. This proved particularly interesting in both finding a balance between larger signal/noise ratios and finer resolutions, while providing a mean to crossvalidate the global FTF against local FTFs:

$$FTF_{global} = \sum_{i=1}^{n} FTF_i$$

Indeed by lumping all the axially discritized heat release fluctuations (amplitude and phase) in one global value, the identification is reduced to a Single Input/ Single Output (SISO) system. Figure 4 shows this cross-validation, i.e. SISO versus Σ(SIMO), for a 25 sections flame region. Even though the frequency of the maximum FTF amplitude is still ~75Hz lower that the experimental data, the exact superposition of both amplitude and phase plots allow us to attest the correct implementation of the SIMO identification procedure.

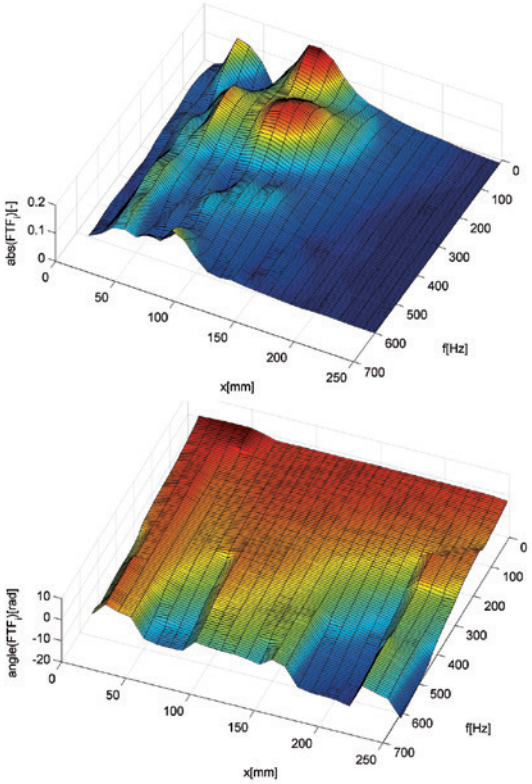

Figure 3: Axially resolved flame transfer functions FTFi, obtained from identification of the LES data. Combustor dump plane located at x = 0.

Conclusions / work in progress

Results have shown the ability of the LES simulations to produce realistic flame data and the SI method to reasonably capture the global FTF and the respective local FTFs. The shift of ~75Hz to a lower frequency of the maximum FTF amplitude when compared to the experiments are probably caused by the poor simulation of the mean heat release rate, i.e. the mean position of the flame inside the combustor. The improved wall temperature profile (cf. Fig. 2) is expected to correct this frequency shift. Furthermore recent developments on the WHI tool seem to indicate that an improved signal identification might be possible using Wavelet based signals [5]. Such signals were generated and contrary to the currently used white noise signals, they show a uniform spectral content on the frequencies of interest (cf. Fig.5). Results are expected to be both physically and statistically more accurate then previous identification results, and closer to the experimental data.

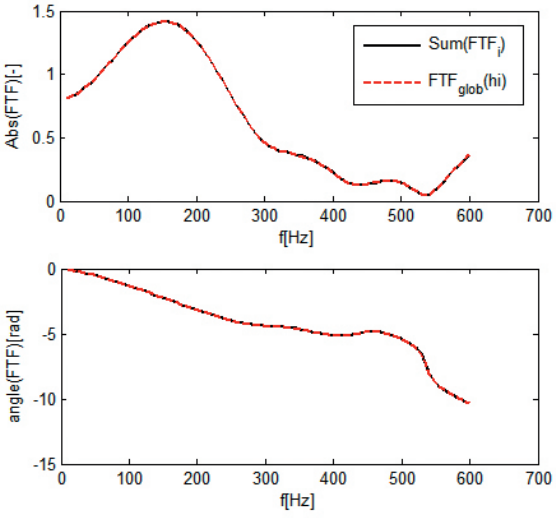

Figure 4: Cross-validation of identified flame transfer functions: global FTFglob vs. ∑(FTFi), i=1,2,...,25.

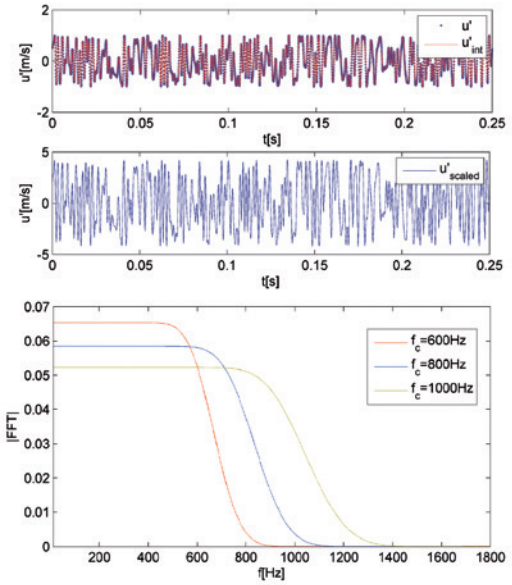

Figure 5: Wavelet based excitation signals: time series of original, interpolated and amplitude scaled signal (fc=600Hz), with frequency spectra (bottom).

References and Links

[1] Polifke W., Numerical techniques for identification of acoustic multi-ports. Advances in Aeroacoustics and applications, VKI lecture series, 2004.

[2] Kim K., Lee J., Quay B. and Santavicca, D. Spatially distributed flame transfer functions for predicting combustion dynamics in lean premixed gas turbine combustors, Combust Flame 157 (2010) 1718 – 1730.

[3] Giauque A., Selle, L., Poinsot, T., Buechner H., Laufmann P. and Krebs W. System identification of a large scale swirled partially premixed combustor using LES and measurements. J. of Turb. 6, 21, 1-20, 2005.

[4] Leandro, R.E. and Polifke, W. Low-Order Modelling of Distributed Heat Release. 19th International Congress on Sound and Vibration (Vilnius, Lithuania), 2012.

[5] Foeller, S., Polifke, W. Advances in Identification Techniques for Aero-Acoustic Scattering Coefficients from Large Eddy Simulation; 18th International Congress on Sound & Vibration (Rio de Janeiro, Brasil), 2011.

http://www.td.mw.tum.de/tum-td/de/forschung/themen/non- compact-flames

Bubbles in turbulent flows

Research Institution
Institut für Strömungsmechanik, Technische Universität Dresden, Germany

Principal Investigator
Jochen Fröhlich

Researchers
Claudio Santarelli

Project Partners
Bavarian Research Foundation, Eurocopter Deutschland GmbH

LRZ Project ID: pr42no

Introduction

Bubbly flows occur in many industrial and environmental applications, like power plants and chemical reactors, and much effort has been devoted in the last decades to analyze the phenomena involved. In more recent years, numerical simulations have proven to be a valuable tool to get insight into such flows, beside experimental investigations. This has been possible due to constantly increasing computer resources and substantial algorithmic advances.

This report describes the employed methods, the computational strategies and a selection of the acquired results in the framework of the project "Bubbles in turbulent flows". The goal of the project is to investigate the bubble dynamics and to get insight into fundamental phenomena such as bubble-bubble and bubble-turbulence interaction.

Numerics

All simulations presented have been performed with the in-house code PRIME (Phase Resolving sIMulation Environment) employing an Euler-Lagrange approach for disperse multiphase flows. The Navier-Stokes equations (NSE) for an incompressible fluid are solved with a direct numerical simulation (DNS) approach, such that all flow scales, both spatial and temporal, are resolved on a very fine grid. This avoids the use of any model for the smallest turbulent scales. The bubbles are considered as objects of fixed shape and are introduced by means of an immersed boundary method (IBM). The phase coupling is realized by means of additional forces which are located at the Lagrangian points on the phase boundary and which are introduced in the NSE, see Fig. 1. This method is extensively described in [1]. The code employs the highly efficient Hypre and Petsc libraries: the former is used for the solution of linear systems which arise from the discretization of the NSE, while the latter ensures a suitable domain decomposition and a fast, parallel communication between different processes based on the MPI protocol.

Configuration

The simulations have been conducted for a channel between two unbounded vertical walls at distance H in the wall-normal (y) direction. The flow is driven by an instan¬taneously adjusted volume force which ensures the desired mass flux.

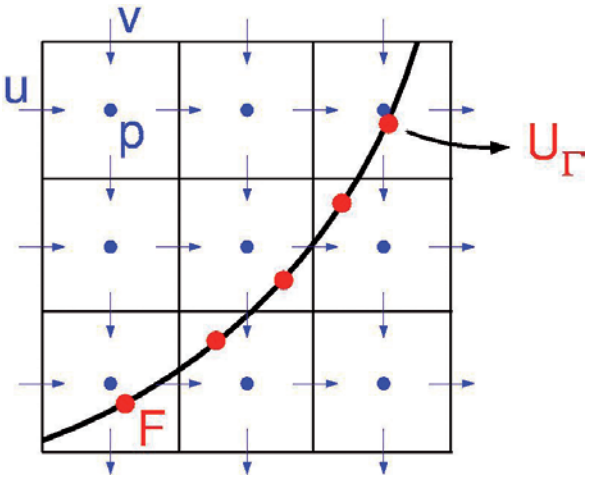

Figure 1: Eulerian grid and Eulerian quantities (blue); Lagrangian quantities at forcing points (red).

In the numerical configuration the flow is modelled as periodic in the streamwise (x) and in the spanwise (z) direction and a zero-velocity condition is applied at the walls. The flow is directed upwards, so that bubbles ascending in upwards direction travel faster than the fluid. A repulsive force is introduced to model bubble-bubble and bubble-wall collisions.

Two sets of simulations were performed so far: four simulations with spherical bubbles and three with ellipsoidal bubbles, varying the bubble size, the form and the global void fraction. Additionally, a single-phase simulation was conducted to be used as reference. For the range of physical parameters chosen in this study, characterized by low-to-middle Reynolds number and low Eötvös number, the assumption of fixed spherical shape is justified. The simulations with a fixed ellipsoidal shape was undertaken to analyze the influence of the bubble

shape only, keeping all other parameters constant. This is motivated by the fact that for larger Eötvös number (i.e. larger diameters), bubbles tend to assume an ellipsoidal shape, possibly also varying in time.

For the simulations with spherical bubbles the domain sizes are 4.43 H x H x 2.21 H in x-, y- and z-direction, respectively. An Eulerian, equidistant grid with 1024 x 232 x 512 ≈ 120 Million points was employed. In the cas of ellipsoidal bubbles, a smaller domain but a finer mesh was used: 2.27 H x H 1.13 H in x-, y- and z-direction, respectively, with 1024 x 450 x 512 ≈ 236 Million grid points. This choice was a compromise between available computational time and the finer mesh required for ellipsoidal bubbles. The latter was the outcome of a preliminary mesh refinement study, where the grid had been successively refined until target quantities converged.
For all the simulations presented here, a typical run on the SuperMuc machine requires 512 to 1024 tasks over 48 hours and is carried on for several months.

Considering for all simulations the time needed for the computation to reach a stationary state, the time needed to collect fluid and bubble statistics and the post-processing, the total amount of CPU-hours used was around 3 Million, during a period of three years, including also the runs performed on the old HLRB-II machine.

Results

In this report we focus only on the most recent outcomes of our analyze concentrating on a novel technique for the detection and characterization of bubble clusters in the framework of Euler-Lagrange simulations developed in this project. This method is based on the definition of an Eulerian quantity, the smoothed void fraction (SVF), which depends only on the instantaneous bubble positions [2]. Two different approaches were introduced: the Eulerian approach defines clusters as flow regions where the SVF is above a given threshold. With the second approach, a Lagrangian one, clusters are defined as groups of bubble fulfilling some distance-related criterion. Each of the two complementary approaches allows to evaluate different quantities of interest: cluster size and cluster-related fluid quantities for the Eulerian approach; cluster velocity and orientation for the Lagrangian approach to mention just a few. Fig. 2 displays an instantaneous snapshot of the simulation with 2880 spherical bubbles of radius equal 0.02586H. The clusters, detected by means of the Eulerian approach, are represented as red iso-surfaces of the SVF. Among other results, the cluster analysis allowed to extend previous knowledge regarding bubble interaction: the preferential horizontal alignment was confirmed not only for bubble pairs but also for larger groups of bubbles, [2].

Outlook

In the near future, simulations are planned where bubbles are allowed to deform as a result of the bubble-fluid interaction. This is possible by minimizing the potential displacement energy of the bubble surface and by an analytical representation of the bubble shape by means of spherical harmonics [4]. The simulation of deformable bubbles will allow to complete the present research study with the comparison of spherical, ellipsoidal and deformable bubbles. Additionally, simulations are under way to investigate the influence of bubbles on the heat-transfer at the walls of the channel. To this end, a thermal energy equation has to be solved and integrated in the NSE, requiring particular attention concerning the thermal boundary condition at the phase boundary [3].

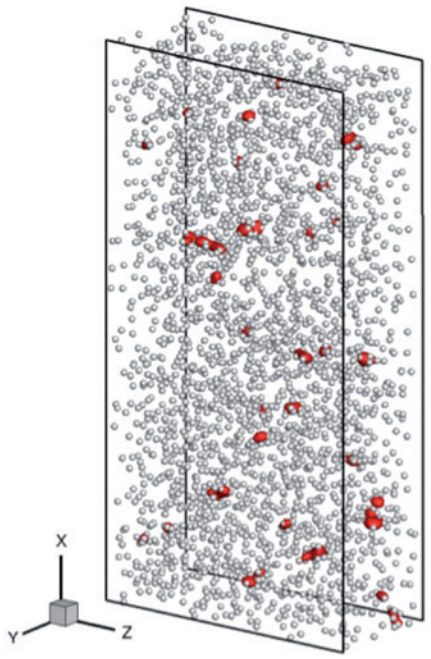

Figure 2: Geometry, snapshot of bubble positions and instantaneous Eulerian clusters from the simulation with 2880 small, spherical bubbles.

References and Links

[1] Kempe T., Fröhlich J., An improved immersed boundary method with direct forcing for the simulation of particle laden flows. Journal of Computational Physics, 2012, 231: 3663 – 3684.

[2] Santarelli, C., Hashimoto, K., Fukagata, K., Fröhlich, J., A smoothed void fraction approach for the detection of bubble clusters, *submitted for the* Proceedings of the ASME 2014 4th Joint US-European Fluids Engineering Division Summer Meeting, August 3-7, 2014, Chicago, Illinois, USA.

[3] Santarelli C., Kempe T., Fröhlich J., An immersed boundary method and a ghost cell method for the simulation of heat transfer problems, *accepted for the* Proceedings of the 3rd International Conference on Computational Methods for Thermal Problems, June 2-4, 2014, Lake Bled, Slovenia.

[4] Schwarz S., Fröhlich J., Representation of deformable bubbles by analytically defined shapes in an immersed boundary method. Paper in Proceedings ICNAAM, American Institute of Physics Conference Series, edited by T.E. Simos, G. Psihoyios, C. Tsitouras and Z. Anastassi, 1479 (1): 104-108, 2012.

Unsteady CFD for Automotive Aerodynamics

Research Institution
Institute of Aerodynamics and Fluid Mechanics, Technische Universität München

Principal Investigator
Thomas Indinger

Researchers
Bastian Schnepf, Angelina Heft, Martin Peichl, Patrick Nathen

Project Partners
BMW Group, AUDI AG

LRZ Project ID: pr42re

Introduction

The importance of aerodynamic optimization in road vehicle development has increased over recent years. Most effort is put into the reduction of aerodynamic drag which is one of the major driving resistances defining fuel consumption. There are two main reasons for this trend. Most importantly, the need of reducing CO_2 emissions in combination with customers asking for larger and more powerful vehicles are conflicting goals for the automotive industry. Furthermore, electric vehicle concepts face the issue of achieving long ranges despite limited battery capacities. Among the different vehicle areas, wheels and wheel houses are responsible for approx. 25 percent of the total drag. Together with the complex nature of the flow mechanisms in this area this has put a high level of attention on wheel aerodynamics recently. Investigating the unsteady flow topology at rotating geometries such as the rim spokes or the tire tread is, however, difficult. Using computational fluid dynamics (CFD), computational resources needed for local and temporal discretization as well as limitations of the physical models are the key challenges. In this report, approaches for the aerodynamic assessment of rim and tire influences using unsteady CFD are presented.

Results

Numerical Method
The numerical simulations presented in this report were conducted using the commercial solver Exa PowerFLOW, Release 4.4. Its computations are based on the Lattice-Boltzmann method which derives the macroscopic flow variables like density, momentum and energy from microscopic particle distributions following the Boltzmann kinetic theory. This method is inherently transient and discretizes the particles' motion both in velocity and direction on an equidistant, cubic lattice. The resulting equations are of coupled, algebraic nature and flow quantities are computed by simple summations. Thus, parallelization is easier than in the case of a finite volume method which uses coupled, partial differential equations instead.

Since the spectrum of turbulent time and length scales is very large in the case of industrially relevant flows a direct numerical simulation is not possible with today's computational resources. Instead, the smallest turbulent scales are modeled using an enhanced two-equation RNG k-epsilon model. The boundary layer is modeled according to the logarithmic law of the wall, additionally taking into account the effect of pressure gradients on flow separation.

Computational Setup
For the full vehicle simulations the detailed geometry of a 2012 BMW 3 Series sedan consisted of 10M surface elements. At the inlet and on the moving floor a velocity of 38.9 m/s was prescribed leading to a Reynolds number of 7M, calculated using the wheelbase. The finest voxel size was 1.5 mm around the wheels, wheel spoilers and grills and 3 mm around the rest of the model. In total, the discretization of the domain resulted in 90M voxels and 20M surfels (fine equivalent, i.e. volume and surface elements which participate in the computation of every time step). The time step was set to 6 x 10-6 s resulting in 250k time steps to be calculated for 1.5 s of physical time. The wheel rims and vented brake discs were included inside sliding mesh regions, thus effectively rotating during the simulation. The tires were laser scanned at a load of 4200N and 38.9 m/s in the wind tunnel thus including both static and centrifugal deformation. Being scanned in a rotating state the resulting tire section was rotationally averaged thus only including the longitudinal main grooves. Since the tires were deformed they could not be included inside sliding mesh regions and had to be modeled as rotating walls instead. This means that the tangential velocity at the tire surface was prescribed.

The case setup for the isolated wheel simulations was created by Gillard [2] and included fully detailed, finite element analysis deformed tires. At that, the deformation took account of both vertical load and rotational speed, using the same values as in the experiments by Schnepf et al. [1]. Using a smallest voxel size of 1 mm close to the tire surface and a maximum expected velocity of 70 m/s the time step was set to 3.3×10^{-6} s.

Similarly to the full vehicle simulations, a sliding mesh interface included the rim whereas a rotating wall BC was applied on the tire. The results for a tire with de-

tailed tread pattern, however, turned out to be unsatisfactory because of the limitations of the rotating wall BC. Therefore, in following simulations it was tested to lift an undeformed, but still detailed tire model 10mm above the ground and to include the whole geometry in a cylindrical sliding mesh interface. In doing so, the influence of the rotating grooves could be evaluated in the numerical simulation. The near ground behavior, however, could not be assessed due to the unrealistic gap between tire and ground and due to the missing contact patch deformation. Including both tire and rim in the sliding mesh interface resulted in an increase of 75% of computational effort. This was caused by the large amount of high resolution surfels created on the interface between rotating and stationary grid regions. At the end, 50M voxels and 5M surfels (fine equivalent) were discretized. Both full vehicle and isolated wheel cases took 13k core hours on 128 cores for a single simulation run.

Full Vehicle Simulation Results

Focusing on the influence of different rim designs on the flow around the wheels at a full vehicle, the simulation results agreed well with experimental data from the wind tunnel. In figure 1 the total pressure distribution and its downstream development is shown in three slices as an average of the last second. The most important structure is the ground vortex which evolves from the flow around the contact patch. The magnitude of total pressure loss (and thus energy loss) caused by it correlates well with the drag coefficients obtained for different rim designs. The same trend was observed in the wind tunnel when analyzing flow topology measurements, recorded using a five-hole probe, and force data from the balance. Altogether, the drag deltas between different rim designs from the simulation showed a deviation of approx. 1% (of total vehicle's drag) from the drag deltas measured in the wind tunnel.

Isolated Wheel Simulation Results

Testing different tires of the same nominal size (e.g. 225/55 R17) at a passenger car, the best and worst drag values differ by approx. 2% of the vehicle's total drag. This is due to differences in shoulder curvature, tread pattern and rim protection edges. Capturing these differences calls for a very detailed tire simulation. Applied on a full vehicle, it would take more computational resources than what is acceptable for productive use at the moment. Hence, in a first step, the authors investigated an isolated wheel

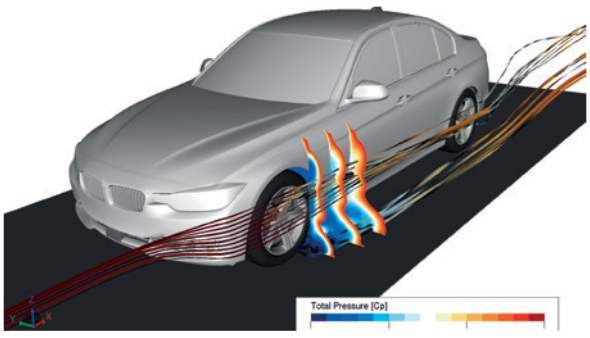

Figure 1: Streamlines and flow slices at the left front wheel colored by total pressure.

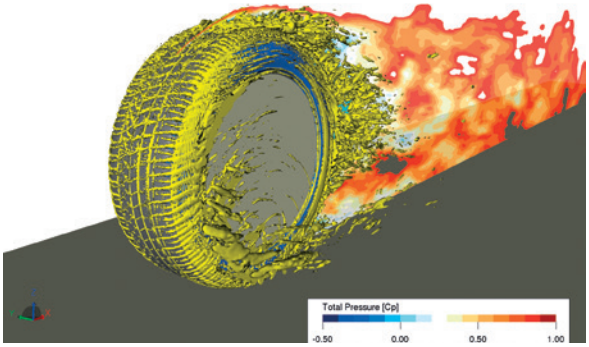

Figure 2: Vortex cores visualized using a Lambda2 isosurface and total pressure distribution in the tire's wake from a transient snapshot.

to reduce both computational effort and complexity (see Gillard [2] and Schnepf et al. [1]). Evaluating the vortex structures in the tire's wake a significantly better agreement between experimental and numerical results could be achieved when including the whole tire in a rotating sliding mesh region. Although a voxel size of 1mm is not small enough to fully resolve the small grooves they affect the flow by transporting fluid upwards in the wake. Thus the flow separates earlier at the top and the wake's height increases. This effect can only be captured using unsteady CFD as it naturally requires the geometry's rotational motion. Taking a closer look into the transient structures in figure 2, the complexity of the flow becomes obvious. The wake's nature is inherently unsteady including a wide spectrum of turbulent structures. Using the Lambda2 criterion small vortex cores are visualized in the transient snapshot. The evolution of vortices through the tread pattern affects the separation behavior and thus aerodynamic drag and lift.

On-going Research / Outlook

The example of a tire's tread pattern shows that the spatial resolution would have to be increased by one order to reproduce the finest geometrical details in the simulation and to fill them with enough cells to compute the flow correctly. At the moment this is possible for an isolated wheel at acceptable costs but not for a full vehicle. The physically correct model would include a contact patch at the ground and have the tread rotating at the same time. A possible solution would be to run a coupled simulation of fluid and finite element analysis solvers and to update the geometry at every time step. The computational effort, however, would be beyond today's acceptable limits for an industrial application. Therefore, enhanced methods for moving geometries are also needed. Another aspect is the physical time which is computed in a simulation. Due to numerical stability reasons the time step decreases with increasing spatial resolution in the case of explicit methods. Combining a smaller time step and longer total physical simulation time for improved accuracy consequently results in a significant increase of computational effort.

References and Links

[1] Schnepf, B., Tesch, G. and Indinger, T. 2013. Investigations on the Flow Around Wheels Using Different Road Simulation Tools. In "On Progress in Vehicle Aerodynamics and Thermal Management", Proceedings of the 9th FKFS Conference (Stuttgart, Germany, October 01-02, 2013). Expert Verlag.

[2] Gillard, J. 2012. Numerical simulation of an rotating, isolated wheel using a Lattice-Boltzmann method. Master's thesis. TU München.

http://www.aer.mw.tum.de/

Large-Scale Simulations and Modeling of Pollutant Emissions in Turbulent Premixed Flames

Research Institution
Institut für Technische Verbrennung, RWTH Aachen University

Principal Investigator
Heinz Pitsch

Researchers
Philipp Trisjono and Konstantin Kleinheinz

Project Partners
The University of New South Wales, Sydney, Australia

LRZ Project ID: pr45di (Gauss Large Scale project)

Introduction

Within the Sonderforschungsbereich (SFB 686), we are developing LES (Large-Eddy Simulation) models for turbulent premixed combustion that will be used for the design of future gas turbines. Recent reviews highlight the potential of LES of turbulent combustion [1]. In particular, we focus on strategies to accurately model pollutants such as NO_x and CO. Models developed in our group are based on the flamelet concept [1], and have been successfully applied to experiments of laboratory-scale flames and devices of industrial relevance. However, predictions of NO_x are still challenging, especially for low temperature combustion, where not only thermal, but also more complex formation pathways are NO_x important.

Rapid advances in supercomputing and numerical methods make DNS (Direct Numerical Simulation) a powerful tool in combustion science and enable the simultaneous simulation of turbulence and chemistry as well as the analysis of their interaction. A majority of existing DNS from the literature are carried out for simple hydrogen flames only. However, the lack of even simple NO_x and CO chemistry prevents these simulations to be used for the analysis of the complex, yet not well understood, formation of pollutants in premixed flames. Therefore, we have performed large-scale DNS of turbulent premixed lean methane flames including comprehensive chemistry of pollutant formation. An instantaneous snapshot of this simulation is shown in Fig. 1, where the isocontour represents the flame surface and streamlines indicate the flow pattern. The level of detail with respect to complex pollutant formation makes DNS performed by our group on SuperMUC unique and a strong method to unravel the interaction of turbulence and pollutant chemistry and guide the development of high-fidelity models for LES of turbulent premixed combustion.

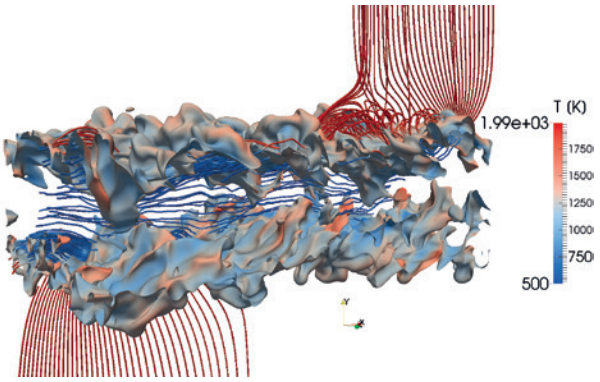

Figure 1: Petascale simulation of turbulent premixed combustion on SuperMUC. The isocontour represents the flame surface and the streamlines indicate the flow pattern.

Numerical approach

The computational challenge of DNS of turbulent reacting flows stems from a wide scale separation, since all scales ranging from the smallest scales associated with the fastest reactions up to large integral scales of the turbulence must be resolved.

In this project, we tackle this challenge with our in-house code CIAO. CIAO is a second order, semi-implicit finite-difference code, which solves the reacting Navier-Stokes equations in the low-Mach number limit [2]. The time integration of the chemistry is based on a symmetric operator splitting and computationally efficient and robust algorithms to advance a set of ODEs describing the chemistry.

In the course of this project and during the Extreme Scaling Workshop 2013 at LRZ and special block operations of the entire SuperMUC system, the scaling of CIAO was analyzed and continuously improved. Nearly all communication time is devoted to the solution of the elliptic Poisson equation, which, however, is only a small portion of the overall CPU time. Since the main portion of the CPU time is consumed for the time inte-

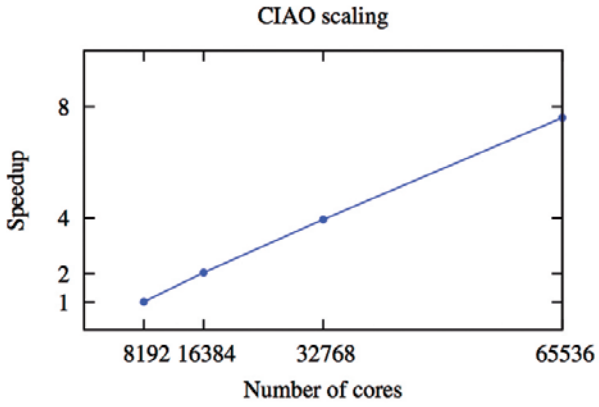

Figure 2: Strong scaling test of CIAO of SuperMUC.

gration of the chemistry, which does not require communication, CIAO features excellent scalability. A representative scaling plot of CIAO is illustrated in Fig. 2, where excellent scaling up to 65536 cores is observed.

Results

One of the project highlights is an international collaboration with Prof. Hawkes of the University of New South Wales in Sydney on the assessment and validation of LES models for the turbulent burning velocity [3,4], which is based on a DNS of Hawkes at al. [4]. Many LES models for turbulent premixed rely on models for the turbulent burning velocity, which is a conceptual quantity ensuring the correct mass conversion rate. Accordingly, reliable and accurate models are needed for high-fidelity simulations of industrial combustion systems.

This project consists of three parts, which the analysis of the flame displacement speed, an *a priori* analysis of turbulent burning velocity models, and an a *posteriori* validation study, where the same configuration is simulated in LES.

The flame displacement analysis revealed insight into the local flame speed, its contributions, and its dependencies on other quantities. Interestingly, the highly turbulent flame characterized by the thin reaction zones regime locally propagates slower than its laminar counterpart. An analysis of the effect of flame stretch showed that strain is responsible for the local decrease of the flame displacement speed.

This finding directly translates to the a *priori* analysis, where the correlation between subfilter velocity fluctuations and the turbulent burning velocity is investigated. In the analysis, the turbulent burning velocity is evaluated from a local mass balance. It is found that the mass balance formulated as an area ratio yields a turbulent burning velocity which is higher than the model predictions. If the mass balance is formulated with the actual flame displacement speed, good agreement is found between the DNS data and the model predictions.

Finally, in the *a posteriori* analysis LES of the DNS configuration is performed in order to rigorously assess the model performance. Before comparing the flame statistics of the LES to DNS data, the jet spreading is compared. It is found that the LES does not only capture the jet spreading due to heat release, but also the intrinsic jet spreading, indicating the high quality of the LES. A comparison of the global heat release rate shows that the LES and the investigated models predict global heat release and mass conversion with excellent accuracy, as seen in Fig. 3. This means that the quality of assessed models is very good and supports the applicability in more complex LES such as LES of combustion engines and gas turbine engines.

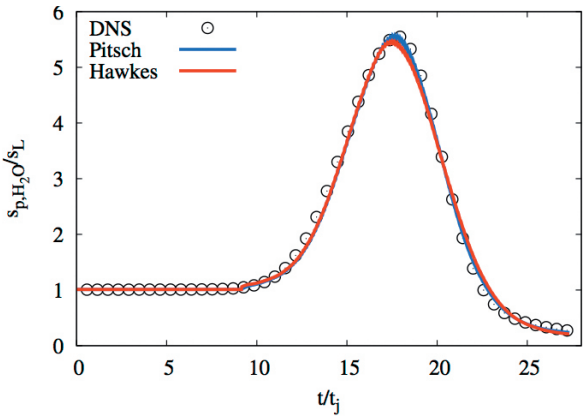

Figure 3: Comparison of the global heat release rate between DNS and LES with two different models.

On-going Research / Outlook

In a subsequent project, the data generated in this project will be used to study CO formation. In the future, our high performance code CIAO will also be used for other DNS of turbulent combustion.
These may include non-premixed and auto-igniting flames as well as the extension to other multi-physics phenomena. We also intent to further develop CIAO for the use on future Exascale systems.

References and Links

[1] Pitsch, H, 2006 Large-eddy simulation of turbulent combustion. *Ann. Rev. Fluid Mech.* **38**, 453-483
[1] Desjardins, O., Blanquart G., Balarac G. and Pitsch, H, 2008 High order finite difference scheme for variable density low Mach number turbulent flows. *J. Comput. Phys.* **227**, 7125-7159
[3] Pitsch, H, 2005 A consistent level set formulation for large-eddy simulation of premixed turbulent combustion. *Combust Flame.* **38**, 453-483
[4] Hawkes, E. R., Chatakonda O., Kolla H., Kerstein A. R., Chen J. H. 2012 A petascale direct numerical simulation study of the modelling of flame wrinkling for large-eddy simulations in intense turbulence. *Combust Flame.* **159**, 2690-2703

LES of premixed combustion for assessment of combustion noise

Research Institution
Lehrstuhl für Thermodynamik

Principal Investigator
Camilo Silva

Researchers
Ahtsham Ulhaq, Wolfgang Polifke

Project Partners
Ecole Centrale Paris

LRZ Project ID: pr45ru

Introduction

In recent years noise generated by combustion has received a lot of attention from the combustion community. Not only because of the modern restrictive policies about noise emission, but also because its understanding and correct estimation is crucial for a reliable characterization of flames. Combustion noise of enclosed systems is considered complex due to all different physical mechanisms that may interact with the sources of noise and, by the time, there is not any validated procedure to decompose the noise that is directly produced by combustion from the noise that is originated by the coupling of external acoustic sources with the turbulent flame. In this work Large Eddy Simulation (LES) is used together with advanced System Identification techniques (SI) in order to understand and differentiate these two types of noise generation. The dynamic response of the flame will be computed simultaneously with the turbulent combustion noise spectrum.

The present study aims to perform highly reliable Large Eddy Simulation of combustion noise. In order to achieve this general goal, different tasks must be accomplished. Summarizing, they can be listed as:

- Computational Fluid Dynamics (CFD) Simulation of a two-dimensional laminar flame exposed to external acoustic fluctuations.
- Large Eddy Simulation (LES) of turbulent combustion in a confined swirled burner. Here the design of acoustic non-reflecting boundary conditions is of great relevance. Assessment of `pure' combustion noise is aimed at this point.
- Addition of external acoustic perturbations to previous LES.
- Recognition of the system structure in terms of inputs and outputs. If the acoustic scattering of the system is aimed, inputs and outputs are considered to be the incoming and outgoing acoustic waves, respectively. Methodologies for extraction of these quantities must be validated. It should be noted that outgoing acoustic waves contain high levels of noise related to combustion, a fact that makes difficult the assessment of the scattering matrix due to the flame. As a final step, the source vector of noise is extracted.

As observed, production and propagation of acoustic waves play a major role in this study. Consequently, the computational domain is required to be of high resolution (tens of millions of cells), which in turn signifies that a good performance of the numerical tools used for High Performance Computing (HPC) is compelling.

Large Eddy Simulation will be carried out by means of the AVBP solver [1]. AVBP resolves the complete set of Navier Stokes equations of reacting flows on 3D complex geometries with second order spatial and temporal accuracy. It is based on a finite volume discretization with a cell-vertex approach combined to a numerical scheme derived from the Lax-Wendroff scheme. Subgrid scales are described by the dynamic Smagorinsky or Wale model. The flame/turbulence interactions are modeled by the Dynamic Thickened Flame (DTF) model. AVBP has been satisfactorily used in several applications considering, among others, premixed and diffusion flames on turbulent combustion chambers associated to phenomena like ignition, blow-off, flashback and also combustion instabilities.

The code AVBP is written in standard FORTRAN 77 which is actually the predominant language in High Performance Computing (HPC) in industry. Nevertheless, standard FORTRAN 77 does not permit dynamic allocation of memory. As a consequence, AVBP has been upgraded in a gradual manner to FORTRAN 90/95 in order to enhance the portability of these packages to different machines architectures. In a parallel code, the computational domain is partitioned into several sub-domains. This partition is performed in AVBP by following different algorithms based on standard recursive bisection methods such as recursive inertial (RIB)- the default method-, recursive coordinate (RCB) or recursive graph bisection (RGB). Message passaging between processors is based in the standard MPI libraries. It should be noted that in

the cell-vertex data environment of AVBP the grid is split along the cell edges and hence certain nodes are duplicated at partition interfaces. This results in a slight increase of the total number of grid points with a growing number of processors. Regarding portability, the AVBP package, on the one hand, is available for various hardware architectures and is currently installed on the following platforms: Compaq Alpha Server, Silicon Graphics, SUN, IBM SP3/4, PC LINUX clusters.

Scientific and technical results

First, an academic case based on the Kornilov's burner [2] is studied with the main purpose of setting up all the `machinery' LES/SI. It consists of a laminar conical flame confined in a rectangular cavity. Figure 1 illustrates the academic configuration. A stoichiometric mixture of methane and air is injected upstream at 1 m/s of mean velocity.

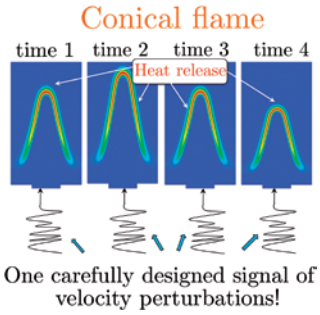

Figure 1: 2D Laminar premixed flame

In order to correctly resolve the flame, it is important to discretize the reactive layer by at least six nodes. Since a methane flame with an equivalence ration equal to 0.8 is considered, the flame thickness is estimated to be of the order of some tenths of a millimeter. As a result, the size of one cell in the reactive region must be of the order of hundredths of a millimeter. Considering this a mesh containing 2 million of cells is used. Once the flame reached the steady state, it was excited by a broadband acoustic signal at the inlet. It was noticed that a small addition of artificial viscosity was necessary in order to avoid strong gradients of the thermodynamic quantities through the flame front. It was assumed that the addition of this small quantity of artificial viscosity would not influence the response of the flame due to external acoustic perturbations. Several computations were necessary to adjust the relaxation of at both inlet and outlet, so that the technique of Wave Masking was optimal used. Accordingly, acoustically non-reflecting boundary conditions were assured: only 1% of a given outgoing acoustic wave was reflected to the domain.

Results, plotted in Fig. 2, show a very good agreement between experimental measurements of the flame transfer function and the corresponding numerical simulation. It should be noted that similar results had already been obtained by Duchaine et al. (2011) [3]. In such a study, tens of simulations were necessary to obtain the flame response at punctual frequencies. In the present work, only one simulation was necessary to recover the whole FTF spectrum with very high frequency resolution. This accomplishment is achieved thanks to the extremely careful design of the input acoustic signals and to the advanced SI tools that include polynomial models that are far more complete that the classical Finite Impulse Response (FIR) model for linear time invariance systems.

In addition to the acoustic inlet excitation, which is indeed the classical procedure used in experiments and today numerical simulations, acoustic excitation at the outlet and at both inlet-outlet was carried out. Results, which indeed are not obvious, show that the FTF is indeed well characterized by the upstream velocity perturbations and is independent from the acoustically excited boundary. In addition to prove the direct dependence of heat release rate to upstream velocity perturbations, post-treatment of results, based on correlation of residuals, show, nevertheless, that the relation heat release rate-upstream velocity perturbations is indeed not causal. Further on, preliminary studies show that a close loop between these quantities is present and, sometimes, even instability may appear. This is a novel concept recently introduced in the literature and is recognized as intrinsic flame instability. This topic is currently been investigated in the framework of the present project.

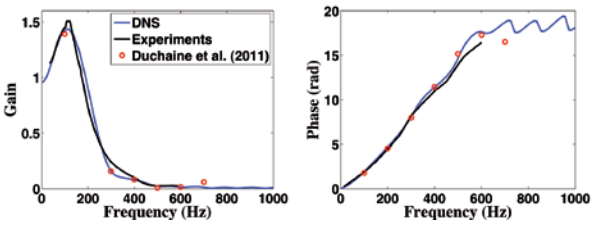

Figure 2: Flame Transfer function

On-going Research / Outlook

Currently LES of a turbulent premixed flame with totally non-reflecting boundary conditions is being performed without external acoustic excitation. A transverse acoustic mode is present and deteriorates significantly the output acoustic signals and the signal associated with the global heat release rate. A technique to add an artificial dissipation at the combustion chamber walls is being studied so that acoustic dissipation is enhanced mainly on high frequency acoustic modes. Once this step accomplished, acoustic excitation at both inlet and outlet will be added. Results of this study will show the feasibility of extracting simultaneously combustion noise, Flame Transfer Function, and Scattering matrix of a generic turbulent combustor.

References and Links

[1] www.cerfacs.fr/4-26334-The-AVBP-code.php
[2] V. N. Kornilov, R. Rook, J.H.M. ten Thije Boonkkamp and L.H.P. de Goey. 156(2008) 1957-1970
[3] F. Duchaine, F. Boudy, D. Durox and T. Poinsot. Combustion and Flame. 158(2011) 2384-2394.

Numerical investigation of pseudo-shock systems in Laval nozzles

Research Institution
Institute of Aerodynamics and Fluid Mechanics, Technische Universität München

Principal Investigator
S. Hickel

Researchers
J.F. Quaatz, M. Giglmaier

Project Partners
School of Engineering and Design, Brunel University London, UK

LRZ Project ID: pr45tu

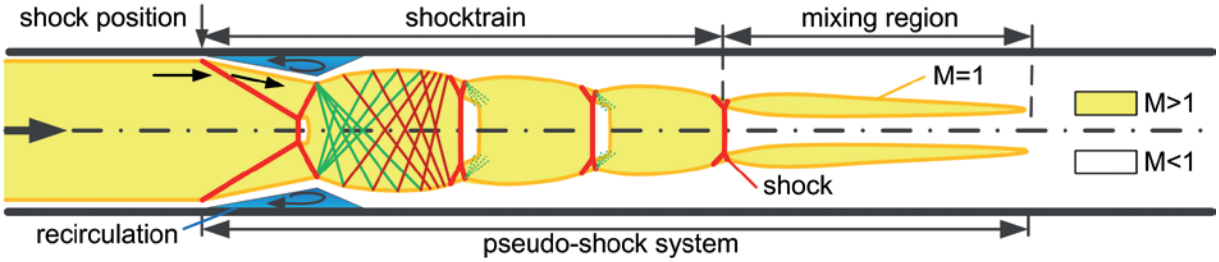

Fig. 1: Sketch of a pseudo-shock system in a constant area duct consisting of shocktrain and mixing region. Supersonic regions with M>1 are colored yellow, shocks are indicated by red lines.

Introduction

Shock/boundary-layer interaction is a particularly challenging subject of enduring fluid dynamics research. A shock wave is the most common way by which a supersonic fluid flow can be compressed and decelerated to subsonic speeds. In internal flows, such as nozzles and channels, the adverse pressure gradient imposed by a sufficiently strong normal shock will cause flow separation upon interaction with the wall boundary layers. Flow separation and reattachment then result in complex 3-D system of interacting oblique shocks, compression and expansion waves. *Fig. 1.* shows a sketch of a pseudo-shock system, which develops if the re-acceleration due to expansion waves locally leads to supersonic speeds such that secondary shocks can form.

We perform highly resolved Large-Eddy Simulations (LES) with the flow solver INCA to investigate the topology and real-time dynamics of pseudo-shock systems in the divergent part of a double chocked Laval nozzle system based on the setup of a recent experiment of Gawehn et al. [1]. Our LES incorporate, for the first time, the full 3-D geometry of the rectangular Laval nozzle duct including parallel sidewalls, such that effects of secondary flow features and flow separation at all channel walls can be analyzed. Preliminary simulations showed that a reduction of the computational costs by considering only one half of the domain is not possible without affecting the overall structure of the pseudo-shock system. Sophisticated numerical techniques such as adaptive grids, an immersed boundary method and the recycling-rescaling method at the domain inlet are employed to facilitate these unprecedented, computationally challenging simulations. Comprehensive statistical data is generated that will help to validate and further improve simpler approaches such as Reynolds-averaged simulations. Within this paper we present the recent state of the investigation. A detailed review of the results is given by [4].

Results

We solve the compressible Navier-Stokes equations for viscid ideal-gas flows with the LES-code INCA on a Cartesian multi-block grid consisting of 384 million finite vol-

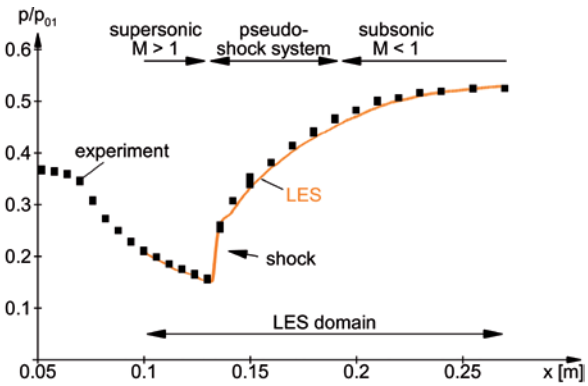

Fig. 2: Comparison of experiment and numerical simulation by normalized pressure distribution measured at the divergent channel wall.

umes. The unresolved scales of turbulence are modeled by ALDM [2, 3], which efficiently combines sub-grid scale modeling and shock-capturing numerical discretization. The simulation covers about 35 x 10-3 s of physical time and was performed on 500 Thin Node Islands of the LRZ SuperMUC. Due to the high amount of memory necessary for fluid dynamics simulations, only 2500 parallel MPI tasks were used. So far, this numerical study consumed about 15 million CPUh. For the post-processing of the huge amount of result data, we use SuperMUC's Fat Node Island.

To proof the reliability and accuracy of the numerical results, we performed a detailed analysis and validation against the corresponding experiment conducted by Gawehn et al. [1]. The measured wall pressure distribution is in excellent agreement with the time-averaged LES data (*Fig. 2*). The confined LES domain starts within the supersonic part of the nozzle. Initially, the flow is further accelerated due to the divergent channel cross section. The acceleration is accompanied by a static-pressure reduction till the primary shock, which visible as an instant pressure jump in *Fig. 2.* Note that the experimental shock position is exactly captured by the LES. Downstream, the flow is further decelerated and the static pressure increases monotonically. The subsequent shocks of the shocktrain do not appear in this graph because they do not reach close enough to the wall.

The shape of the shocktrain can be analyzed through schlieren pictures, which visualize density variations within the flow (*Fig. 3*). Dark regions correspond to compressions, such as shocks, and bright regions to expansions. The numerical simulation is able to reproduce all important flow features that govern the shape of the shocktrain. The primary shock is bifurcated and a small section normal to the flow direction (Mach reflection) is developed at the centerline of the channel. The subsequent shocks are slightly curved. Detailed analyses showed that also the numerical simulation outstandingly reproduces the experimental shock angles and the spacing.
The LES gives detailed information about the flow variables at every point of the domain, which is not available from the experiments. *Fig. 4* shows the time-averaged 3-D flow pattern within the pseudo-shock system. Statistical data is collected for more than one flow through

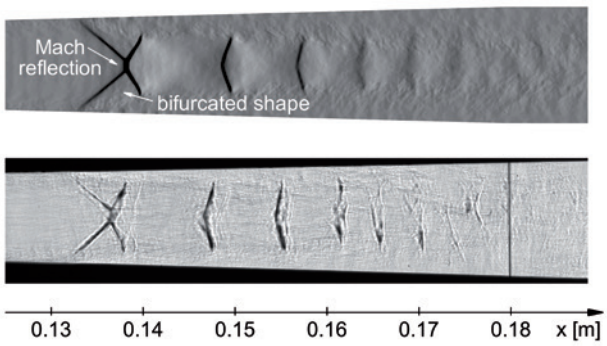

Fig. 3: Numerical and experimental schlieren pictures showing a snapshot of the axial density gradient spatially averaged along view direction through the channel.

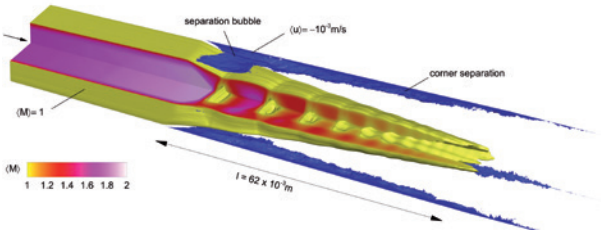

Fig. 4: Time-averaged 3-D structure of the pseudo-shock system predicted by the LES. The picture is adopted from [4]. The yellow surface corresponds to M=1 and blue regions depict reversed flow by a slightly negative axial velocity u.

time of the LES domain. The yellow iso-surface corresponds to Mach number M=1. One quarter of the channel is cut out to allow for an insight into the shocktrain. The supersonic regions of the cut interface are colored by the Mach number distribution. After passing the primary bifurcated shock, the re-accelerated supersonic core flow is bent to the channel center. A distinct shear layer develops between supersonic core flow and subsonic surrounding flow regions. The shocktrain consists of 5 subsequent shocks and is followed by a mixing zone where shock-free recompression of the supersonic core flow takes place. The total length of the pseudo-shock system can be evaluated to about 62 x 10^{-3} m. The blue regions in *Fig. 4* visualize reversed flow. There is a stable separation bubble at the diverging channel walls downstream of the first oblique shock that extends over the complete channel depth. In contrast, statistically no separation can be found at the parallel side walls. Moreover, we observe separation at the channel corners downstream of the primary shock that extend over the full length of the pseudo-shock system.

Summary and outlook

We showed by this extensive numerical simulation that it is possible to predict the highly complex flow within the pseudo-shock system LES. We performed a detailed investigation of the mean shock structure and validated the results against experimental data. For more details on recent results we refer to [4].

The next steps will cover an analysis of the transient behavior of the pseudo-shock system. Therefore, snapshots of the shape and time-series of local pressure data will be investigated. The turbulent flow variables will be analyzed and consulted to validate RANS turbulence models. Moreover, mixing of a passive scalar passing the pseudo-shock system will be simulated and analyzed.

References and Links

[1] Gawehn, T., Gühlhan, A., Giglmaier, M., Al-Hasan, N. S., Quaatz, J. F., and Adams, N. A. 2010. Analysis of Pseudo-Shock System Structure and Asymmetry in Laval Nozzles with Parallel Side Walls. In *19th International Shock Interaction Symposium (ISIS19)*, Moscow, Russia.
[2] Hickel, S., Adams, N. A., and Domaradzki, J. A. 2006. An adaptive local deconvolution method for implicit LES. *Journal of Computational Physics* 213, 1, 413–436.
[3] Hickel, S. and Larsson, J. 2009. On implicit turbulence modeling for LES of compressible flows. In *Advances in Turbulence XII*, B. Eckhardt, Ed. 132. Springer, Berlin, Heidelberg, 873–875.
[4] Quaatz, J. F., Giglmaier, M., Hickel, S., and Adams, N. A. Large-eddy simulation of a pseudo-shock system in a Laval nozzle. *International Journal of Heat and Fluid Flow* submitted 2013.

www.aer.mw.tum.de/abteilungen/large-eddy-simulation
www.inca-cfd.org

On the Richtmyer-Meshkov instability evolving from a deterministic multimode planar interface

Research Institution
Institute of Aerodynamics and Fluid Mechanics

Principal Investigator
V. K. Tritschler

Researchers
S. Hickel, X. Y. Hu, N. A. Adams

Project Partners
Stanford University, Lawrence Livermore National Laboratory

LRZ Projec tID: pr45wa

Introduction

The Richtmyer-Meshkov instability [1,2] is a hydrodynamic instability that occurs at the interface separating two fluids of different densities. In the limit of an impulsive acceleration of the interface, e.g., by a shock wave, the instability is referred to as Richtmyer-Meshkov instability (RMI). In RMI, baroclinic vorticity production at the interface is caused by the misalignment of the pressure gradient (∇p) associated with the shock wave and the density gradient ($\nabla \rho$) of the material interface. The baroclinic vorticity production term $(\nabla\rho \times \nabla p)/\rho^2$ is the initial driving force of RMI.

So far, research mainly focused on the identification and quantification of parameters that affect the evolution of Richtmyer-Meshkov unstable flows. The investigations have assumed, based on standard arguments such as empirical resolution criteria, that the marginally and non-resolved scales have a negligible effect on the resolved scales, and therefore on the evolution of the instability. Uncertainties introduced by the numerical method, i. e., the subgrid-scale regularisation and truncation errors, have not yet been investigated systematically. There is, however, strong evidence that numerical model uncertainty can significantly affect the linear and non-linear stages of evolution, and in particular the mixing measures. In fact, it is unclear how subgrid-scale regularisation and dispersive or dissipative truncation errors can affect the resolved scales and thus the important turbulent mixing measures.

In the present investigation, two independently developed and essentially different numerical methods (Miranda and INCA) are employed to study the prediction uncertainties of RMI simulations. Miranda is the numerical method that has been developed at Lawrence Livermore National Laboratory, whereas INCA is the research code of the Institute of Aerodynamics and Fluid Mechanics at TUM. The first method has a dominantly dissipative truncation error at the non-resolved scales, whereas the second one exhibits a more dispersive behaviour. At the marginally resolved scales the numerical truncation error is not small and the particular character of the truncation error is essential for the implicit modelling capabilities of the method, and thus also affects the resolved-scale solution. For the purpose of investigating this effect integral and spectral mixing metrics as well as probability density functions are analysed on four computational grids with resolutions ranging from *1562µm* to *195µm*, see also [3]. It is important to point out the significance of quantifying the influence of subgrid-scale regularisation and truncation errors in order to better understand previous works and the uncertainties associated with under-resolved simulations of RMI. This investigation is a joint effort together with Prof. Sanjiva Lele from Stanford University and Dr. Britton Olson from Lawrence Livermore National Laboratory and this report is only an excerpt taken from a full paper [3,4].

Results

The three-dimensional compressible Navier-Stokes equations are solved in a shock tube with constant square cross section. The fine-grid domain extends in the y- and z-direction symmetrically from $-L_{yz}/2$ to $L_{yz}/2$ and from $-L_x/4$ to L_x in the x-direction. An inflow boundary condition is imposed far away from the fine-grid domain in order to avoid shock reflections. To reduce computational costs a hyperbolic mesh stretching is applied between the inflow boundary and $-L_x/4$. L_x is set to *0.4m*, and $L_{yz} = L_x/4$, see Fig. 1.

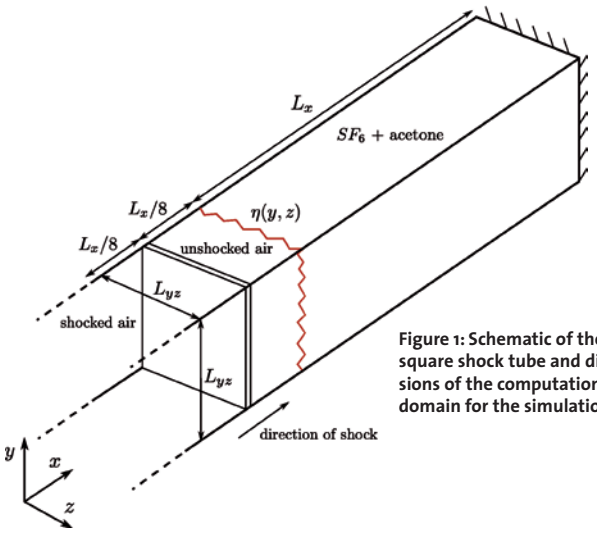

Figure 1: Schematic of the square shock tube and dimensions of the computational domain for the simulations.

The fine-grid domain is discretised by four different homogeneous Cartesian grids with planar resolutions of 64^2, 128^2, 256^2 and 512^2 cells resulting in cubic cells of size $1562\mu m < \Delta_{xyz} < 195\mu m$. The total number of cells in the fine-grid domain amounts to $\approx 1.3 \cdot 10^6$ for the coarsest resolution and to $\approx 670 \cdot 10^6$ for the finest resolution. The fine-grid simulation consumed approximately *1.5* million-CPUh running on *5248* cores.

For illustration we show the three-dimensional contour plots of species mass fraction of the heavy gas, consisting of SF_6 and acetone (Ac), $Y_{HG} = Y_{SF6} + Y_{Ac}$ obtained with Miranda and INCA, respectively, see Fig. 2. Similarities at the large scales are clearly visible after re-shock, but also differences exist at the fine scales, more clearly visible from the inset.

The mixing width plotted in Fig. 3 shows that data from both numerical methods converge to a single solution throughout the entire simulation time. Furthermore, it was observed that even with very-high-order models a minimum resolution of $\sim 400\mu m$ appears to be necessary for an accurate prediction of the mixing zone width. Coarser grids tend to overpredict the growth of the mixing zone and also molecular mixing.

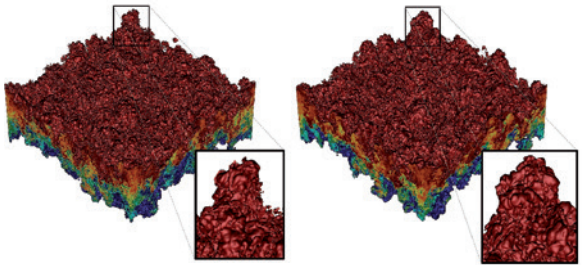

Figure 2: Three-dimensional contour plots of species mass fraction of the heavy gas Miranda (left) and INCA (right) data. Data are from the finest grid at t=2.5 ms that contours of the heavy gas mass fraction from 0.1 (blue) to 0.9 (red). Note that although large scale features remain consistent between codes, small and intermediate scales are different at this stage.

The radial power spectra of density are plotted in Fig. 4, which shows the spectra after re-shock at $t=2.5ms$. Before re-shock, the dominant initial modes slowly break down and redistribute energy to smaller scales. Re-shock causes additional baroclinic vorticity production with inverse sign that results in a destruction process of the pre-shock structures. This process in conjunction with a vorticity deposition that is one order of magnitude larger than the pre-shock deposition leads to rapid formation of complex disordered structures, which eliminates most of the memory of the initial interface perturbation as can be seen in Fig. 4. The spectra demonstrate a broad range of resolved scales which are in very good agreement.

However, data also show that differences do exist in the fine scales. The frequency dependence of the density fluctuations shows the existence of an inertial subrange and that the two numerical approaches agree at lower frequencies. The observed spectral scalings were consistent among the methods but had slightly steeper slopes than the classical Kolmogorov scaling.

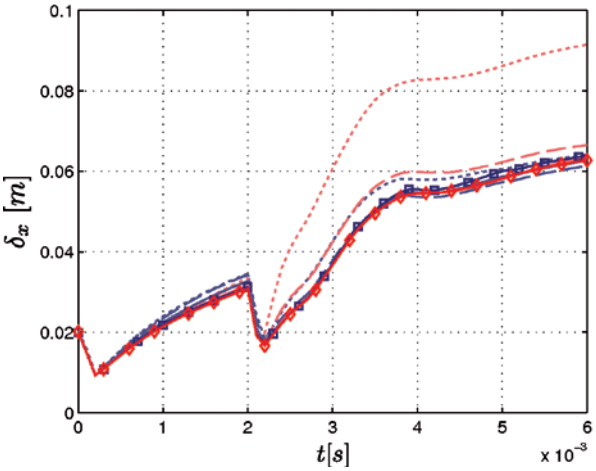

Figure 3: Time evolution of the mixing zone width from Miranda (blue/dark grey) and INCA (red/light grey). The different resolutions are represented as dotted line (64^2), dashed line (128^2), solid line (256^2) and solid line with open squares for Miranda and open diamonds for INCA (512^2).

On-going Research / Outlook

At the moment we are extending INCA for reacting flows. Simulating the reacting RMI (rRMI) requires approximately 10 times the computational resources compared with the inert RMI. Therefore, we are eagerly awaiting the next extension of SuperMUC.

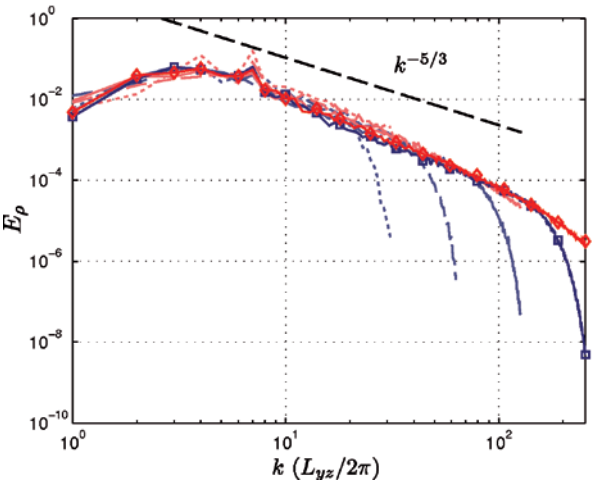

Figure 4: Power spectra of density from Miranda (blue) and INCA (red) after re-shock at t=2.5ms. The different resolutions are represented as dotted line (64^2), dashed line (128^2), solid line (256^2) and solid line with open squares for Miranda and open diamonds for INCA (512^2).

References and Links

[1] R.D. Richtmyer 1960 Taylor instability in shock acceleration of compressible fluids. *Communications on pure and applied mathematics* 13, 297.

[2] E.E. Meshkov 1969 Instability of the interface of two gases accelerated by a shock wave. *Fluid Dyn.* 4, 151.

[3] V.K. Tritschler, B.J. Olson, S.K. Lele, S. Hickel, X.Y. Hu and N.A. Adams 2014 On the Richtmyer-Meshkov instability evolving from a deterministic multimode planar interface. *Under review J. Fluid. Mech.*

[4] http://arxiv.org/abs/1402.1433

Numerical Investigation of the Flow Field about the VFE-2 Delta Wing

Research Institution
Institute of Aerodynamics and Fluid Mechanics, Technische Universität München

Principal Investigator
Stefan Hickel

Researchers
Christian Zwerger

Project Partners
–

LRZPproject ID: pr47bu

Introduction

The industrial application of delta wings is manifold and reaches from classical aerospace engineering, e.g., high-agility aircraft, aerodynamic devices or control surfaces, to unique environmental technologies, such as snow fences. Common to all these cases is the exploitation of leading edge vortices (see Figure 1).

Steadiness and stability of these leading edge vortices is of paramount importance, notably for the controllability of high-agility aircraft. Given that vortices can undergo a sudden expansion often related to vortex breakdown, and considering that the occurrence of this phenomenon is critical for aircraft and not yet physically fully understood, a further investigation leading to a profound insight is required. A detailed understanding of vortex formation and breakdown necessitates a comprehensive insight into the entire unsteady flow. This insight can only be obtained from time-accurate high-fidelity simulations accompanied by experiments. The ongoing investigation is funded by the DFG project "Numerische Untersuchung der instationären Strömung um generische schlanke Deltaflügel". The international Vortex Flow Experiment 2 (VFE-2) delta wing is employed as a generic aerodynamic configuration, see Fig. 1.

A complete description of fluid flows is given by the Navier-Stokes equations, which govern the evolution of momentum, mass, and energy in a viscous fluid. Solving the Navier-Stokes equations requires very high spatial and temporal resolution. A Direct Numerical Simulation (DNS), which resolves the whole range of temporal and spatial scales, is still not feasible for complex turbulent flows in real industrial applications due to the required tremendous computational resources.

RANS (Reynolds Averaged Navier-Stokes) simulations with appropriate statistical turbulence models are widely used in industry. However, this simplified approach often fails to accurately predict flow separation and reattachment. In the case of the VFE-2 delta wing, results obtained by RANS simulations poorly resemble existing experimental results.

One expects significantly better results from Large Eddy Simulation (LES). In LES, the large flow structures are resolved, while small structures are modeled by subgrid-scale (SGS) turbulence models. In implicit LES (ILES), the truncation error of the discretization of the convective terms is carefully tailored to act as a SGS model. In this project the Adaptive Local Deconvolution Method (ALDM) for implicit LES is used. ALDM has been derived from spectral turbulence theory [3] and has shown considerable potential for the efficient representation of physically complex flows in generic configuration.

Numerical Method

The Adaptive Local Deconvolution Method (ALDM) [3] turbulence model is incorporated in a solver for the compressible Navier-Stokes equations. The equations are discretized on a collocated Cartesian mesh and bounding surfaces of the flow that are not aligned with the grid are accounted for by the Conservative Immersed Interface (CIIM) approach [4]. For time advancement, an explicit third-order Runge-Kutta scheme is used. The diffusive terms are discretized by a second-order scheme.

An efficiency improvement is achieved by modeling the turbulent boundary layer with a wall model [1] based on

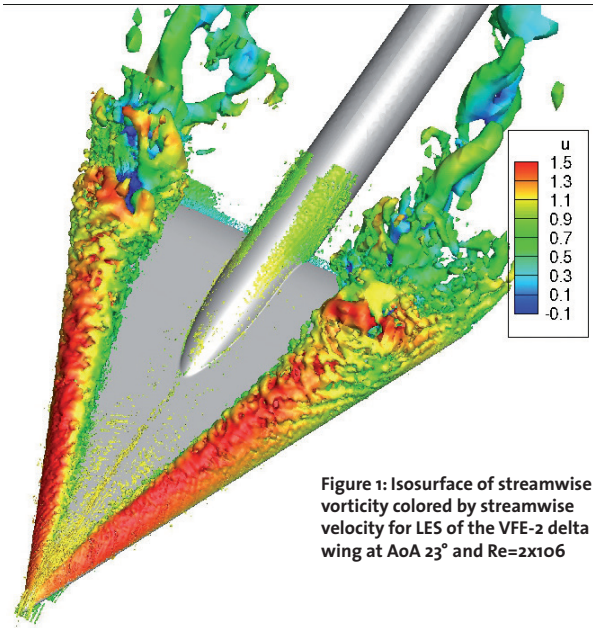

Figure 1: Isosurface of streamwise vorticity colored by streamwise velocity for LES of the VFE-2 delta wing at AoA 23° and Re=2x106

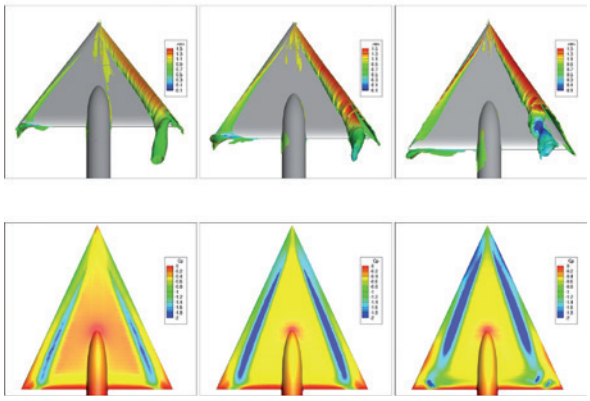

Figure 2: Top row: visualization of primary and secondary vortex. Bottom row: Cp distribution on upper surface of the wing. AoA 13° (left), 18° (middle), and 23° (right).

the Turbulent Boundary Layer Equations (TBLE) and by locally adapting the mesh resolution with local mesh refinement.

As a result of the high grid resolution and the requirement to catch the unsteady behavior, which necessitates small time steps, high-performance computing power is necessary for the investigation of the complex three-dimensional flow field. To date, the simulations have been mainly run on the fat node island of SuperMUC, which are equipped with Intel Xeon E7-4870 10C processors and provides 6.4 GByte of memory per core. Tests have shown that our MPI parallelized FORTRAN code INCA has very good scaling properties on the fat node island.

Results

The results in 2013 have been obtained for a Reynolds number (Re) of 2 x10^6 based on root chord length (cr) and angles of attack (AoA) of 13°, 18°, and 23° (see Table 1).
The simulations show good qualitative agreement with the experimental results of Furman and Breitsamter [2] for all angles of attack considered - vortex formation at approximately half chord length for an AoA of 13°, fully developed leading edge vortex for an AoA of 18°, and asymmetric vortex breakdown over the wing for an AoA of 23°, which results in the characteristic pressure coefficient distributions on the upper surface of the wing, shown in Figure 2. Our LES correctly predict the formation of the counter-rotating secondary vortices below the leading edge vortices (see Figures 2 and 3).

LES results for the wall-pressure coefficient are in good agreement with the experimental data (see Figure 4).

Table 1: Overview of conducted simulations

Angle of attack [°]	Number of grid cells [-]	Number of cores [-]	Number of CPUh
13	~50x10^6	(up to) 2080	5.3 x 10^6
18	~54x10^6	(up to) 2080	5.7 x 10^6
23	~56x10^6	(up to) 2080	6.0 x 10^6

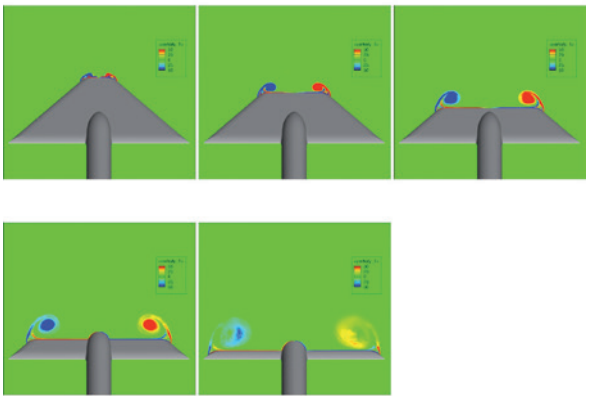

Figure 3: Distribution of streamwise vorticity at different cross sections for AoA 23°. Vortex breakdown observable at last cross section.

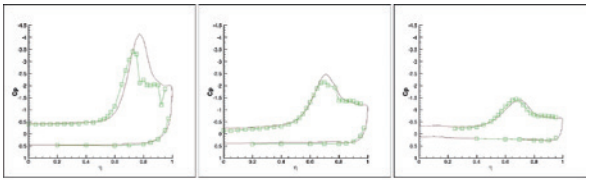

Figure 4: Cp distribution at x/cr=0.4 (left), 0.6 (middle), and 0.8 (right) for AoA 23°. LES data is shown in red, experimental data in green.

Outlook

Given these promising results, future work will consist in investigating leading edge devices helping to influence and prevent the vortex burst. Mechanisms considered will be oscillating control surfaces and possibly periodic blowing through slots. Simulations shown in Table 2 are under way and expected to be completed in 2014. Due to the higher complexity of these simulations, the computational resources required will presumably be larger than in 2013.

Table 2: Overview of planned simulations.
OCS – oscillating control surfaces; Per. Blow. – periodic blowing;

Angle of attack [°]	Description	Number of cores [-]	Number of CPUh
18	**OCS**	2080	~8.0 x 10^6
23	**OCS**	2080	~8.5 x 10^6
23	**Per. Blow.**	2080	~8.5 x 10^6

References and Links

[1] Chen, Z.L., Hickel, S., Devesa, A., Berland, J., Adams, N.A. 2014 Wall-modeling for implicit large-eddy simulation and immersed-interface methods. Theoretical and Computational Fluid Dynamics 28: 1-21.
[2] Furman, A. and Breitsamter, C. 2008 Experimental Investigations on the VFE-2 Configuration at TU Munich, Germany. RTO-TR-AVT-113,21,1-47.
[3] Hickel, S., Adams, N.A. & Domaradzki, J.A. 2006 An adaptive local deconvolution method for implicit LES. J.Comput.Phys.213(1),413-436.
[4] Meyer, M., Devesa, A., Hickel, S., Hu, X.Y. & Adams, N.A. 2010 A Conservative Immersed Interface Method for Large-Eddy Simulation of Incompressible Flows. J.Comput. Phys.229(118),6300-6317.

www.aer.mw.tum.de/abteilungen/large-eddy-simulation
www.inca-cfd.org

Coupling kMC and CFD in Heterogeneous Catalysis

Research Institution
Department Chemie – Technische Universitaet Muenchen

Principal Investigator
Karsten Reuter

Researchers
Matteo Maestri, Sebastian Matera, Stefano Rebughini

Project Partners
–

LRZ Project ID: pr47ma

Introduction

The worldwide rapidly growing demand for more efficient and sustainable exploitation of energy and material resources puts catalysis higher and higher up on the research agenda. New and improved catalysts are needed to deliver security of supply and industrial competitiveness. The required extreme targets on activity, selectivity and stability under very demanding operating conditions represent a formidable challenge and require the ability to nano-design catalytic materials well beyond our present capabilities. In this respect, it is pivotal to distinguish between the intrinsic catalytic properties of the catalyst material and its macroscopic observed functionality. The intrinsic properties are related to the ability of making/breaking chemical bonds when interacting with molecules and are ultimately determined by the electronic structure at the atomic scale. The macroscopic functionality, instead, is the actual observed behavior of the catalyst material in the reactant environment (chemical reactor) and is ultimately determined by the interplay among the rates of all the chemical and physical phenomena involved in the transformation. Consequently, its rigorous understanding requires to address a wide range of phenomena at different time and length scales (Fig. 1). In particular, in order to reach a rational understanding of the mechanisms underlying the observed functionality, an increased level of scientific understanding is required at each scale.

With reference to Fig. 1, this entails:

- At the microscale, ab-initio - i.e. first-principles - electronic structure theory calculations are used to unravel the making and breaking of chemical bonds at the surface, by explicitly treating the electronic degrees of freedom;
- At the mesoscale, statistical simulations explicitly account for the interplay among all the chemical events, largely improving upon effective formulations that inherently rely on uncontrollable averagings;
- At the macroscale, energy, mass and momentum conservation equations are employed to model transport phenomena in the reactor and in the catalyst support, fully integrating the first-principles based reactive surface chemistry unraveled at the lower scales.

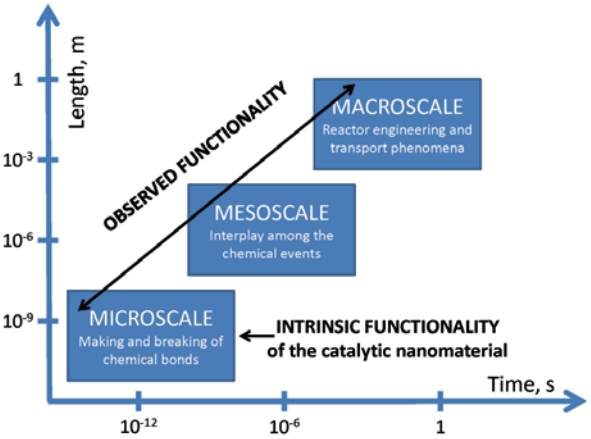

Figure 1: Time and length scales in heterogeneous catalysis.

In the first two-years of the project pr47ma (2010-2012), we have successfully demonstrated how first-principles calculations and semi-empirical models can be used for the estimation of kinetic constants for complex reaction networks [1,2]. In the extension period (2012-2014) – subject of the present report – we have focused our attention on the coupling of the microscale to meso- (kinetic-Monte-Carlo simulations, kMC) and macro-scales (Computational Fluid Dynamics, CFD). The developed approach establishes an accurate, well formalised, and fully integrated multiscale framework that roots in a first-principles description of the nanomaterial and includes all larger-scale aspects to the full reactor.

Results

The integration of the kMC simulations into the fluid dynamic framework has been achieved using the interpolated kMC method [3]. For the computational solution of the fluid-dynamics we have used the recently developed solver catalyticFOAM, that allows for the solution of Navier–Stokes equations for complex and general geometries for reacting flows at surfaces, based on a detailed microkinetic description of the surface reactivity [4,5]. The catalyticFOAM solver exploits the op-

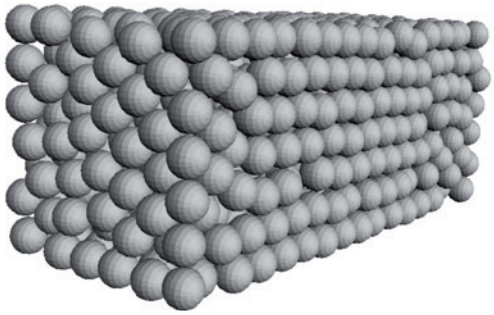

Figure 2: Packed bed of spheres generated with the DEM algorithm. Mesh: 2,000,000 cells.

erator-splitting technique, based on the separation of transport and reaction terms.

The project on superMUC consisted in two main phases:
1) Testing of catalyticFOAM on complex geometries and meshes under mean-field assumptions at the meso-scale.
2) Development and test of the interface between the interpolated kMC method and catalyticFOAM.

1. Testing of catalyticFOAM on complex geometries
In this phase we have tested the capability of the code in managing complex computational domains. At this scope, we have restricted our analysis only to mean-field microkinetic models for the surface reactivity.

Random geometries for the computational tests were built using the Discrete Elements Method. A typical example of a computational domain used for the analysis is reported in Figure 2.
Our tests on superMUC clearly showed that the combination of the domain decomposition technique and operator splitting algorithm enable the simulation of very complex geometries along with a microkinetic description of the surface reactivity. The most time consuming part of the run was always the solution of the catalytic chemistry, which, by the combination of the operator splitting algorithms with the domain decomposition technique, was easily parallelized on superMUC. Nevertheless, differently from homogeneous (gas-phase) reactors (e.g., combustors/flames), we found that the efficient application of the domain decomposition technique for heterogeneous reactors strongly depends on the distribution of the catalytic cells in the different sub-domains. In fact, in heterogeneous reactors, the reaction occurs only at the interface between the solid and gas. As a consequence, depending on the geometry of the reactor, the parts of the domain which are characterized by high surface to volume ratio requires higher computational time. Therefore, in order to enable good scalability, we found it crucial to perform the domain decomposition by keeping constant the ratio between the number of catalytic cells per processor in each sub-domain. We tested several systems (H2 oxidation, CH4 partial oxidation, water-gas-shift on Rh [2]) on different structured and random geometries. Very good scaling properties were found for all the investigated cases. For instance, the mesh reported in Figure 2, which consists of about 2,000,000 cells, was found to scale almost linearly up to 1024 processors (2000 cells/core).

On the whole, through the granted computational time, we were able to prove that the proposed numerical algorithm makes possible the simulation of multidimensional systems with complex and detailed kinetic mechanisms, overcoming the unfeasible computational effort (especially in terms of memory) that would be required by fully-coupled algorithms.

2. Interface between the interpolated kMC method and catalyticFOAM
The second part of the projects dealt with the efficient integration of kMC simulations in the framework of CFD for very general and complex geometries. This is crucial to efficiently integrate the microscopically correct account of the spatial arrangements and interactions of the adsorbed chemicals with the fundamental description of fluid-dynamics and transport at the catalyst interface. From a numerical point of view, a direct coupling between kMC and CFD was unfeasible especially for complex and realistic geometries, given the huge difference in characteristic times. In order to overcome this, we applied the interpolated kMC method of Matera and Reuter [3] to efficiently integrate the kMC simulations into the fluid dynamic framework. Since this interpolated kMC method enables an effective decoupling between the scales, its implementation in the catalyticFOAM environment did not affect the very good scaling properties that we found during phase 1 of the project.

In particular, using the CO oxidation at RuO_2 (110) as a prototypical example, we analyzed several cell configurations typical of UHV set-ups. Thanks to the simulations performed on superMUC, we illustrated that the peculiarities of the thin single-crystal reactor geometry can readily lead to heat dissipation and mass transport limitations that severely affect the observable catalytic function. If these limitations are not appropriately accounted for in both experiment and theory, wrong mechanistic conclusions about the atomic-scale surface kinetics at technologically relevant gas-phase conditions may easily arise, with detrimental effects on envisioned rational design of future improved catalysts [4].

On-going Research / Outlook

Our on-going activity mainly deals with the extension and testing of the kMC-catalyticFOAM algorithm to more complex chemistry, especially in terms of number of steps and intermediates (WGS, steam reforming) and description of the catalyst active sites (multifacets, dynamic of nanoparticles, ...). Such extensions will require further applications for computational time at supercomputers.

References and Links

[1] M. Maestri, K. Reuter, Chem. Eng. Science, 74 (2012) 296
[2] M. Maestri, K. Reuter, Angew. Chemie Int. Ed. 50 (2011) 1194
[3] S. Matera, K. Reuter, Catal. Letters, 133 (2009) 156
[4] M. Maestri, A. Cuoci, Chem. Eng. Science, 96 (2013) 106
[5] www.catalyticfoam.polimi.it
[6] S. Matera, M. Maestri, A. Cuoci, K. Reuter, in preparation

Fluid-Structure Interaction of Thin Structures in Turbulent Flows

Research Institution
Department of Fluid Mechanics, Helmut-Schmidt-University, Hamburg, Germany

Principal Investigator
Michael Breuer

Researchers
Guillaume De Nayer

Project Partners
Chair of Structural Analysis, TU Munich (Prof. Bletzinger)

LRZ Project ID: pr47me

Introduction

Fluid-Structure Interaction (FSI) is a topic of major interest in many engineering fields. The significant growth of the computational capabilities allows solving more complex coupled problems, whereby the physical models get closer to reality. The long-term objective of the present research project is to simulate practically relevant lightweight structural systems in turbulent flows (for example outdoor tents as shown in Figure 1). In order to do that a cooperation between the University of Erlangen, the University of Technology Munich and the Helmut-Schmidt University Hamburg was established. An original computational methodology has been developed and implemented especially for thin flexible structures in turbulent flows [1].

Figure 1: Outdoor giant tent (Khan Shatyr in Astana, Kazakhstan, www.khanshatyr.com)

In order to reach the final objective to tackle civil engineering FSI applications, it was decided to use highly advanced solvers for both subtasks (fluid and structure mechanics). A coupling program does the required exchange of data between both codes. Therefore, the resulting FSI scheme is partitioned and divided into three parts:

- The fluid solver FASTEST-3D is a highly parallelized finite-volume 3D CFD solver, written in FORTRAN and relying on MPI. To simulate turbulent flows, eddy-resolving schemes such as large-eddy simulations (LES) is chosen.
- The structure solver Carat++ [4] developed at TU Munich is a 3D finite-element C++ solver specialized in the prediction of thin structure deformations based on shell or membrane elements.
- The coupling program, CoMA [5], developed at TU Munich is responsible for the mapping between the non-matching meshes and for the exchange of data between the solvers. Like Carat++, CoMA is an object-oriented program using C++.

To get suitable and stable results in FSI a "strong" coupling procedure is highly recommended. For partitioned solution algorithms this means that a subiteration process is required at each time-step in order to guarantee dynamic equilibrium between the fluid and the structure. One of the big challenges of this research project are the CPU-time requirements. To reduce the CPU-time consumption a special procedure for eddy-resolving schemes was developed using an explicit time-marching scheme [1].

In order to assure reliable numerical simulations for complex configurations, the present methodology and the FSI code needs to be validated at first on simpler test cases. For laminar flows several reference test cases (such as FSI3 from Hron and Turek, 2006) are available in the literature and the present methodology was validated based on this test case using HLRB2 [1]. However, for the turbulent regime the test cases are rare and often too challenging. Therefore, the short-term goal of the current project is to provide reasonable benchmark case for the FSI community. For this purpose complementary experimental-numerical investigations on a variety of test cases involving thin flexible structures in turbulent flows were carried out.

Results

A first test case, denoted FSI-PfS-1a, is already released [2]. A thin flexible rubber plate behind a fixed cylinder interacting with the turbulent flow is considered. The structure exposed to a sub-critical flow (Re=30,470) leads to the formation of alternating vortices shedding behind the cylinder. Oscillating forces are generated on the plate. Consequently, the flexible structure deforms in

the first swiveling mode with moderate displacements. All the simulations were carried out on SuperMUC. Between 84 and 144 processors were used. Around 1 Tera bytes of data were generated per simulation in order to have enough files to obtain phase-averaged results for the comparison with measurements. A detailed study including experimental PIV data and numerical LES predictions can be found on the ERCOFTAC Knowledge Base Wiki in the category 'Flow around Bodies' as case UFR 2-13 under this link:
http://qnet-ercoftac.cfms.org.uk/w/index.php/UFR_2-13

Based on this first test, a second experiment was conducted under the same flow conditions using a similar geometry as before [3]. This leads to a the test case, denoted FSI-PfS-2a. A thin plate clamped behind a cylinder is still used. However, a rear mass is added to the extremity of the structure and the material is less stiff.

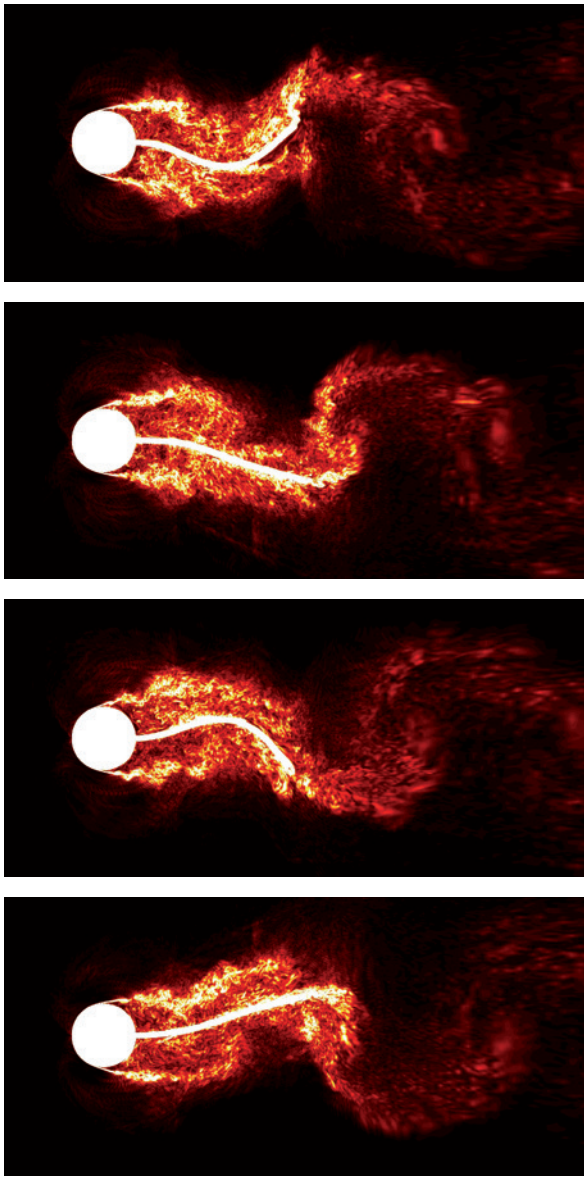

Figure 2: Instantaneous vorticity magnitude at different instants in time of the FSI period of FSI-PfS-2a: flexible plate deforms in second swiveling mode.

As a consequence large deformations of the structure in the second swiveling mode result. Again, all FSI-PfS-2a simulations are performed on SuperMUC applying 93 processors. One second in physical time is simulated in about 500 CPU-hours wall-clock. The amount of data for each FSI-PfS-2a run is similar to FSI-PfS-1a.

The first numerical results of FSI-PfS-2a are very encouraging. The frequency of the FSI phenomenon is found in close agreement with the experiment (f=11.25 Hz). The displacement maxima of the flexible structure are predicted with about 10% errors for the moment. Figure 2 depicts four important instants in time of the FSI period. As visible on this figure the present numerical methodology using LES is able to resolve different scales of vortices in the turbulent flow.

Outlook

Thanks to the experience collected during the FSI-PfS-1a investigation, the FSI-PfS-2a study is making fast progress and shows encouraging results. However, additional simulations have to be started to improve the present results. This requires a lot of CPU-time and storage space. SuperMUC provides enough resources for combined LES and FSI data. Moreover, the use of the energy tags permits to get the results quicker.

The next step of the project is to investigate a more complex thin flexible structure. In order to get stronger three-dimensional effects the flow around an hemisphere has been chosen. Preliminary CFD tests are currently conducted on SuperMUC with a rigid hemisphere to investigate the turbulent flow structures. The pure CFD simulations are already very expensive due to a grid consisting of 30 million cells. This very fine mesh implies small time-steps, necessary to resolve the turbulent flow in time.

References and Links

[1] Breuer, M., De Nayer, G., Münsch, M., Gallinger, T., Wüchner, R.: *Fluid-Structure Interaction Using a Partitioned Coupled Predictor-Corrector Scheme for the Application of Large-Eddy Simulation*, J. of Fluids and Structures, 29, 107-130, (2012).

[2] De Nayer, G., Kalmbach, A., Breuer, M., Sicklinger, S., Wüchner, R.: *Flow past a Cylinder with a Flexible Splitter Plate: A Complementary Experimental-Numerical Investigation and a New FSI Test Case (FSI-PfS-1a)*, Int. Journal of Computers and Fluids, submitted (2014).

[3] Kalmbach, A. and Breuer, M.: *Experimental PIV/V3V Measurements of Vortex-Induced Fluid-Structure Interaction in Turbulent Flow - A New Benchmark FSI-PfS-2a*, J. of Fluids and Structures, 42, 369-387, (2013).

[4] Fischer, M., Firl, M., Masching, H., Bletzinger, K.-U.: *Optimization of Nonlinear Structures based on Object-Oriented Parallel Programming*, ECT2010: 7th Int. Conf. Eng. Computational Techn., Valencia, Spain, (2010).

[5] Gallinger, T., Kupzok, A., Israel, U., Bletzinger, K.-U., Wüchner, R.: *A Computational Environment for Membrane-Wind Interaction*, Int. Workshop on Fluid-Structure Interaction. Kassel Univ. Press, 283-294, (2009).

Numerical simulation of the primary breakup of a generic airblast atomizer

Research Institution
Fachgebiet Energie- und Kraftwerkstechnik, TU Darmstadt

Principal Investigator
Johannes Janicka

Researchers
Benjamin Sauer

Project Partners
Rolls-Royce Germany

LRZ Project ID: pr47ve

Introduction

New core concepts are required to lower the emissions and the fuel consumption of future aircraft engines. The integration of lean combustion technologies is required to enter this next technology level. Lean combustion has a high demand to fuel atomization and thus demands an efficient fuel preparation prior to the ignition. An improved understanding of the breakup processes in two-phase flows is essential to effectively control the fuel atomization in all possible conditions of the flight envelope. A detailed insight into the phenomena of primary breakup is a major limitation in understanding these flow systems.

Aircraft engines are equipped with airblast atomizers to assure the liquid fuel injection (figure 1). The geometry of these atomizers is complex, the Reynolds and Weber number range varies over several orders of magnitude. Due to the complexity of the flow, experimental and numerical investigations are challenging. Experiments utilizing an airblast atomizer at realistic flight engine conditions seem out of sight in the near future. Numerical experiments are a potential alternative to cope with these problems.

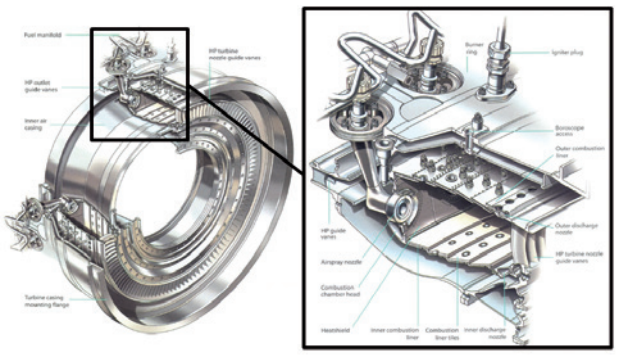

Figure 1: An annular combustion system and a section through the combustor showing the airspray nozzle (adapted from Rolls-Royce, The Jet Engine, 6th ed. 2005)

Methodology

The embedded Direct Numerical Simulation (eDNS) methodology is introduced to cope with these problems. The eDNS approach consists of three major steps [1].

First, the complex airblast atomizer geometry is simplified to a generic planar prefilming airblast atomizer. This geometry enables the experimental validation at atmospheric conditions. It also has been confirmed that the dynamic behavior of planar and annular liquid sheets are equivalent.

Second, the embedded domain requires inlet boundary conditions for the coflowing air streams. These boundary conditions are gained from a single-phase zonal Large Eddy Simulation (LES) of the turbulent channel flow. This

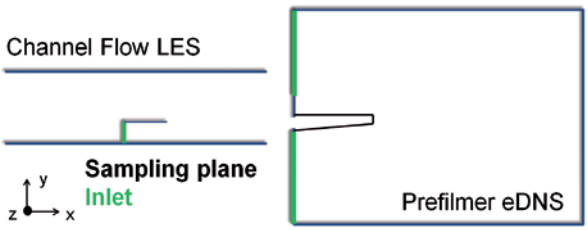

Figure 2: Mapping of transient data from the turbulent channel flow LES to the air inflow of the prefilmer eDNS

flow configuration is simple and DNS data exist for a variety of Reynolds numbers in order to validate the inflow fields. The data are sampled inside the channel domain and mapped to the inlet planes of the eDNS as seen in figure 2. A linear interpolation in space and time is performed.

Third, the breakup is computed applying a two-phase DNS using the Volume-of-fluid method. Within this domain, the liquid fuel is injected and is transported along the prefilmer lip to the prefilmer trailing edge. The liquid film is subjected to high shear due to the coflowing air streams which eventually leads to the fragmentation and the breakup of the continuous sheet.

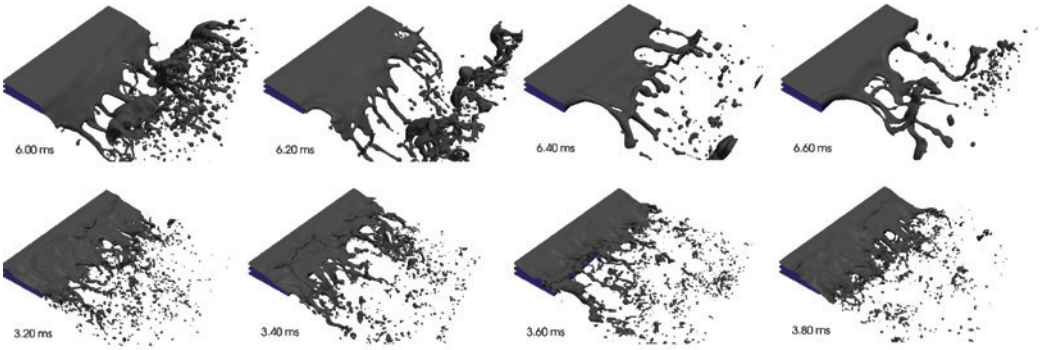

Figure 4: Prefilming airblasted sheet evolution for OP 2 (top) and OP 5 (bottom)

Results

This project aims to understand the primary breakup under aircraft engine operating conditions. The operational range of an engine covers idle, start, take off, cruise, landing and altitude relight. Six different operating points are covered in this numerical investigation, thereby approaching cruise conditions in terms of the Reynolds and Weber number range [2]. The first three operating points are computed at atmospheric conditions. The liquid parameters correspond to Shellsol D40, which was utilized in the prefilmer experiment [3]. This setup enables a validation of the primary breakup with the experimental study. A second set of three operating points is simulated at elevated pressure conditions. The liquid properties correspond to kerosene at higher temperatures where the surface tension force is reduced.

The qualitative assessment of the results focuses on the primary breakup appearance. All atomization mechanisms are identified depending on the Weber number of the flow: the stretched ligament breakup at low Weber numbers, the torn-sheet breakup at medium Weber numbers and the membrane breakup at high Weber numbers. The dominating liquid deformations distinguish the denotation of the primary atomization mechanism. These regimes were previously defined in experiments.

Figure 3 visualizes the different primary atomization mechanisms depending on the Weber number. An additional regime is introduced in this project to confine the torn-sheet from the membrane breakup. Due to the dominant longitudinal structures, this mechanism is denoted as *thin ligament breakup*.

The evolution of the airblasted liquid sheet is illustrated in figure 4 contrasting OP 2 and OP 5. The air bulk velocity is equal at 50 m/s. OP 2 within the torn-sheet breakup regime is dominated by the generation of longitudinal streamwise ligaments. The continuous sheet and the longitudinal ligaments both collapse into big irregular shaped bulgy droplets accompanied by small droplets.

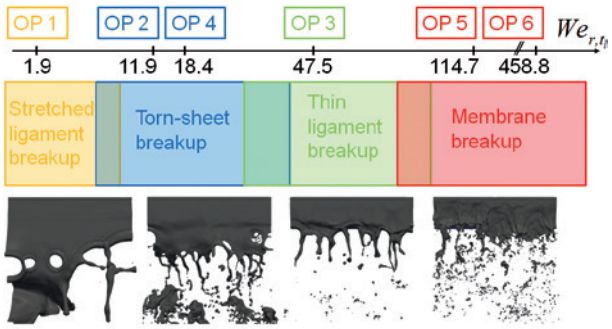

Figure 3: Primary atomization mechanism evolution scaling with the Weber number

At OP 5, the reduced surface tension force leads to increased instabilities on the liquid film surface. The breakup time and length scales are significantly smaller compared to OP 2. Characteristic membranes are formed at the edge of the continuous sheet without dominating streamwise or spanwise ligaments. The primary breakup regime is denoted as *membrane breakup*. Numerous small structures and droplets are separated from the sheet.

In the quantitative evaluation of the simulations, three main aspects are covered: the feasibility of the grid in resolving turbulence and small scale structures, the analysis of characteristic parameters such as ligament length, breakup length and Sauter diameter, and the investigation of the droplet distributions resulting from the primary breakup.

The qualitative and quantitative investigations prove the agreement to experimental results within the low Reynolds and Weber number range. These findings confirm the applicability of the embedded DNS concept for predicting the primary breakup of prefilming airblast atomizers.

On-going Research / Outlook

For the continuation of the project, a further reduction of the equidistant grid spacing is intended. A reduced grid spacing would improve the resolution of the smallest scales especially at high Reynolds and Weber numbers, where only a limited number of separated droplets can be considered as resolved using the existing grid. The second research direction is the expansion of the embedded DNS approach to a realistic annular Rolls-Royce airblast atomizer. In order to handle the computational demand of such a complex geometry, only a segment of the main prefilmer is computed. This segment is embedded inside the full airblast atomizer geometry.

References and Links

[1] Sauer, B., A. Sadiki and J. Janicka: Embedded DNS for Simulating the Primary Breakup of an Airblast Atomizer. Atomization and Sprays, submitted.

[2] Sauer, B., A. Sadiki and J. Janicka: Embedded DNS of the primary breakup of a prefilming airblast atomizer at aircraft engine operating conditions. European Conference on Liquid Atomization and Spray Systems, Chania, Greece, 1-4 September 2013.

[3] Gepprth, S., A. Müller, R. Koch and H.-J. Bauer: Ligament and Droplet Characteristics in Prefilming Airblast Atomization. International Conference on Liquid Atomization and Spray Systems, Heidelberg, Germany, 2-6 September 2012.

http://www.ekt.tu-darmstadt.de

The effect of the cell aspect ratio dependency on the heat transport

Research Institution
DLR Göttingen

Principal Investigator
Olga Shishkina

Researchers
Kai Leong Chong, Matthias Kaczorowski, Olga Shishkina

Project Partners
–

LRZ Project ID: pr47vi

Introduction

THow to efficiently remove heat from the heat source is important for many practical applications, for example, indoor ventilation. Usually, there is treatment on the heated surface, e.g., to extend the surface area by using fin array, to increase the efficiency for cooling down the surface. However, the finned channel might inhibit the fluid motion such that the convective heat transfer finally becomes poor. It is therefore essential to study the behavior of thermal convection in highly confined space.

To study the thermal convection, we use a model so-called Rayleigh-Bénard (RB) convection, which is a simplified physical framework that a fluid layer is heat from below and cooled from above by the horizontal isothermal plates. This model has been studied extensively over the past decades (for details we refer to reviews Ahlers, Grossmann & Lohse 2009; Lohse, Xia 2010). Our focus is on the effect of geometrical confinement, which is described by aspect-ratio Γ, on the global heat transfer efficiency. Recent experiments by Huang *et al.* (2013) show that simple geometrical confinement on the convection cell can significantly enhance the heat transport despite that the flow is slowed down due to wall shear. The experiments span Γ down to 0.1, but it is technically challenging to control heat loss if one would like to explore even smaller Γ by experiments.

Therefore the objective of our studies is to investigate thermal convection in highly confined convection cell with Γ down to 1/32 by means of direct numerical simulations (DNS). It on one hand complements the experiments with wider aspect-ratio range. On the other hand, the simulation can provide the complete information of both temperature and velocity in the domain that helps to understand how changes in flow dynamics and flow structures can lead to the enhancement in heat transport..

Numerical method

We carry out the simulations of RB convection with a well-tested, fourth-order, finite-volume code FLOWSI [3]. The code solves the incompressible Navier-Stokes equations under Boussinesq approximation with Cartesian geometry. The sidewalls are precisely assigned to be adiabatic and all walls are no-slip in our simulations. The speed-up of the code on Supermuc thin node island behaves almost perfectly up to 1024 CPUs (figure 1).

In all simulations, it is necessary to use very fine meshes to resolve the dissipative scale in turbulent flow, which are the Kolmogorov and the Batchelor length scales (a). Close to the boundary, there are even stricter requirements on the resolutions [5]. Thus non-equidistant meshes are adopted for the simulations where the grid spacing is uniform in the bulk and much denser near the boundary.

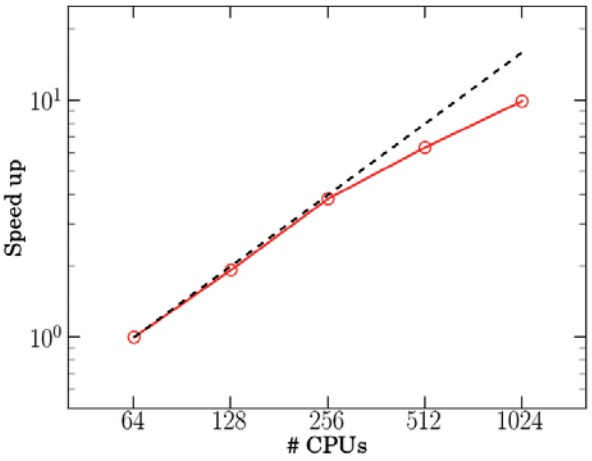

Figure 1: Speed-up of Flowsi relative to the case of using 64 CPUs with 512x512x512 grid points tested on Supermuc thin node island. The black dash line indicates the ideal speed-up.

In our study, we focus on water (Pr = 4.38) at Ra=1x10^9 and Ra=1x10^{10}. The aspect–ratio Γ spans from 1 (cube) to 1/32. Among all simulations, the case at Ra=1x10^{10} with Γ=1 is the most computational expensive which requires 1040x1040x1040 grid points for reliable simulation. This simulation totally takes about 1.5x10^6 CPU hours (more than two months by using 1024 CPUs). In order to save

enough snapshots of temperature and velocity field for statistical analysis, it totally costs 2TB for disk storage. Results

Results

The heat transfer efficiency is characterized as Nusselt number *Nu* in our system. It is interesting to know how Nu varies with Γ. Thus $Nu/Nu_{\Gamma=1}$ is plotted against Γ in figure 2. Figure 2 reveals the significant enhancements in global heat transfer efficiency with decreasing Γ at both Rayleigh numbers, where the results agree with the experiments [2]. This result is non-trivial as one might think that the two lateral walls would suppress the vertical movement of fluid under confinement and therefore a reduction in the heat transfer efficiency should be resulted. With wider range in Γ, one could also find that the increase in heat transfer efficiency becomes significant once Γ is sufficiently small. Under our explored parameter range, the maximum enhancement can be as large as 17.2% at Ra=1x1010 with Γ=1/32.

In RB convection, the flow is usually organized globally as large scale circulation (LSC). Another typical feature in RB convection is the formation of thermal plumes detaching from the heated surface (see figure 3). These thermal plumes are driven by LSC such that hot plumes carry a large fraction of heat to colder region on one side and there is supplement of colder fluid to cool down the heated surface on the other side. From the snapshots of simulations (figure 4), we find that this typical picture has been changed under confinement. First, the velocity fields reveal that the global wind is weakened under confinement. Then the temperature fields reveal that the thermal plumes become more coherent (more broad) in the case of smaller Γ such that thermal plumes can better retain their temperature and hot plumes can carry more heat upwards.

On-going Research / Outlook

A reliable DNS of turbulent convection requires strongly on both computational power and disk storage. We gratefully acknowledge the computational resources supported by Leibniz-Rechenzentrum Munich. We so far

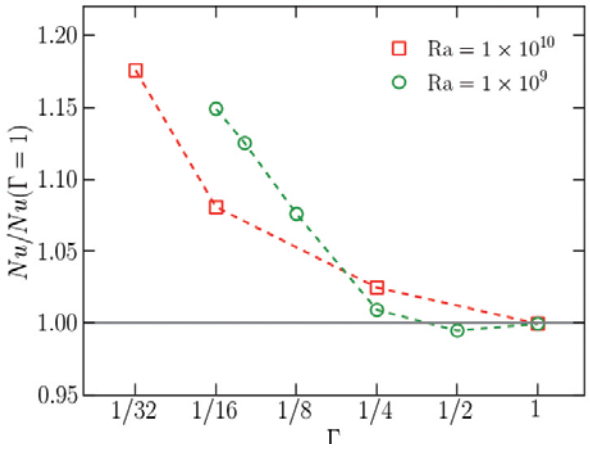

Figure 2: Normalized *Nu* versus Γ at *Ra*=1x10⁹ and 1x10¹⁰

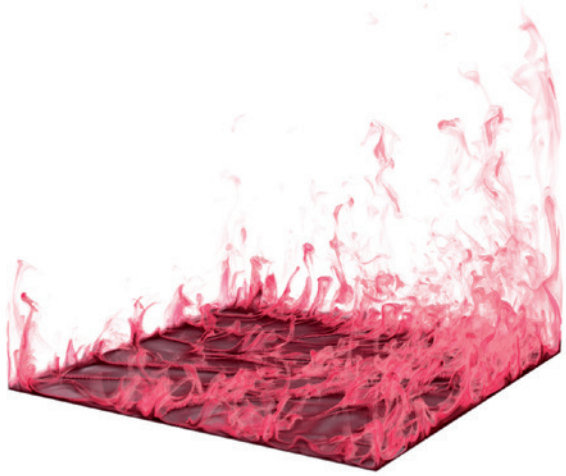

Figure 3: Volume render of instantaneous temperature field at Ra=1x10¹⁰ and Γ=1. The hot fluid is represented in red and the detachment of hot plumes from the heated bottom plate is visualized.

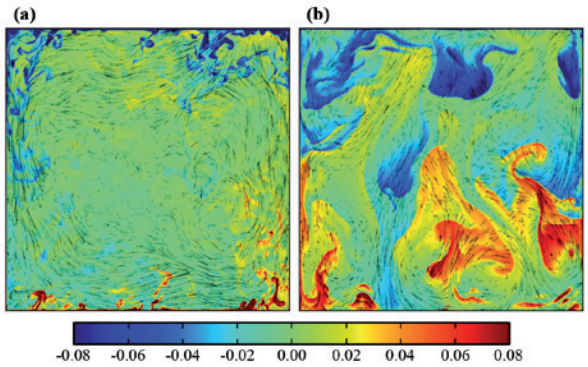

Figure 4: Snapshots of temperature and velocity fields taken at the vertical plane midway between the lateral walls with cases (a) *Ra*=1x10¹⁰ at Γ=1, (b) *Ra*=10¹⁰ at Γ=1/32. The color scale represents the non-dimensional temperature.

investigated how simple geometric confinement can significantly enhance heat transport in water (*Pr*=4.38) at Ra=1x10⁹ and Ra=1x10¹⁰. Our next step is to push up to higher Ra, where it is usually the situation in daily applications. It will be expensive in supercomputing power as the necessary grid points will grow tremendously with *Ra*. With different Ra explored, we expect to capture the trend for the heat transport enhancement due to confinement.

References and Links

[1] Ahlers, G., Grossmann, S., Lohse D. 2009. Heat transfer and large scale dynamics in turbulent Rayleigh-Bénard convection. *Rev. Mod. Phys.* 82: 503–537.

[2] Huang, S.-D., Kaczorowski, M., Ni, R., Xia, K.-Q. 2013. Confinement-induced heat-transport enhancement in turbulent thermal convection. *PRL.* 111 (104501)

[3] Kaczorowski, M., Shishkin, A., Shishkina, O., Wagner, C. 2008. Development of a numerical procedure for direction simulations of turbulent convection in a closed rectangular cell. New Results in Numerical and Experimental Fluid Mechanics VI. 96:381–388.

[4] Lohse, D, Xia, K.-Q. 2010. Small-scale properties of turbulent Rayleigh-Bénard convection. *Annu. Rev. Fluid Mech.* 42: 335–364.

[5] Shishkina, O., Stevens, R. J. A. M., Grossmann, S., Lohse, D. 2010. Boundary layer structure in turbulent thermal convection and consequences for the required numerical resolution. New J. Phys. 12 (075022)

Direct numerical simulation of gravitational settling of finite-size particles in homogeneous flow

Research Institution
Institute for Hydromechanics, Karlsruhe Institute of Technology

Principal Investigator
Markus Uhlmann

Researchers
Todor Doychev

Project Partners
–

LRZ Project ID: pr58cu

Introduction

Particle-laden flows are found in a large number of environmental natural and technical processes. Examples include pollution dispersion in the atmosphere, raindrop formation in clouds, sediment transport, fluidized bed reactors and combustion devices. Thus, the accurate prediction of such flows is of great importance. This naturally leads to the necessity of reliable theoretical description of the mechanisms that take place in such flows. Despite the progress made in the past, there is still a large scatter of the available data. A recent review on the subject can be found in [1].

In the present project we consider the sedimentation of finite-size particles (size of the particles is comparable or larger than the smallest flow structures) in an initially ambient fluid under the influence of gravity. The particles under consideration in the present work have a particle Galileo (Reynolds) number of the order of $O(100)$. For single particle, the Galileo number and the particle-to-fluid density ratio characterize the regime of particle settling and in particular the particle wake. Depending on the Galileo number a variety of particle motion patterns can be identified, from straight vertical to oblique and to fully chaotic paths, for which the fluid motion in the near field around the particles play a dominant role [2].

The interaction between the solid particles and the (turbulent) carrier flow can lead to a number of hydro-dynamical coupling phenomena which are most prominently manifested by the following open questions: (*a*) Do finite-size particles exhibit clustering or not? (*b*) How does the flow field and/or particle clustering affect the settling rate of the particles? (*c*) What are the characteristics of the wake-induced turbulence?

Despite the importance and the range of applications of particulate flows, the fundamental mechanisms involved in such flows are far from completely understood.

Objectives
The richness of applications and complexity of dispersed multiphase flows has caused a lot of difficulties in the process of their study over the years. Moreover, a study of the literature revealed a lack of high-fidelity data covering a wide range of parameters. This has lead to a poor theoretical and statistical description of such flow systems. The present work will try to address some of the topics involved in the dynamics of finite-size particles settling under the influence of gravity, as well as the characteristics of the flow field induced by the settling particles and its impact upon the dispersed phase. Furthermore, this study aims at improving the understanding of the fundamental processes that take place in such flows and also aims at providing a deep and new insight into this processes by trying to isolate the effects of different key parameters. In order to do so, the problem is simplified by eliminating influences due to wall effects, while allowing to focus solely on the fundamental physics involved in the particle-particle and particle-fluid interactions. Moreover, one of the main objectives of the present project is to provide a high-fidelity data-set which covers a wider range of parameters than previous studies.

The present objectives are tackled by performing a direct numerical simulation (DNS) with immersed boundary method for the representation of the fluid-solid interface. This allows the generation of high-fidelity data which describes all relevant flow and particle scales involved in such flow configurations.

Results

Numerical method
We employ an efficient and precise formulation of the immersed boundary method for the simulation of particulate flows as proposed by [4]. This method employs direct forcing approach by adding localized volume force term to the momentum equation. The force term is formulated in such way, as to impose a rigid body motion upon the fluid at the locations of the solid particles. A detailed description of the numerical methods can be found in [4].

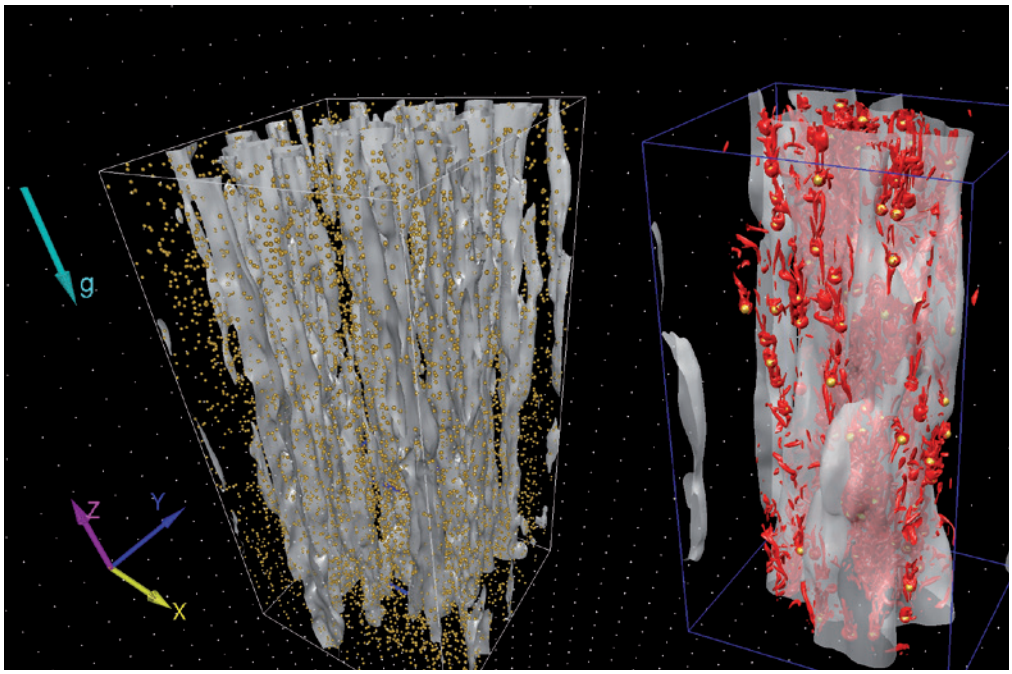

Figure 1: Left: Iso-surfaces of the negative vertical fluid velocity fluctuations at one instant in time in the statistically steady regime. The velocity has been box-averaged with a filter width of five particle diameters. Right: iso-surfaces of the vortex eduction criterion proposed by [3] showing a sub-volume of size 16x16x30 particle diameters.

The computational domain in all simulations performed in the present project is a box elongated in the vertical direction extending several hundred particle diameters. In all three directions a periodic boundary conditions are applied. The simulated systems are dilute and include large number of freely settling spherical particles. The various simulations were performed on large number of processor cores ranging from 640 to 8192. Until present a total of approximately 5·10^6 CPU-hours were consumed and an approximately 200 TB data was produced.

In the following results for one of the performed simulations are presented. Here we consider the sedimentation of finite-size particles with Galileo number of 180 in an initially ambient fluid under the influence of gravity. The particles are placed randomly in the computational domain and simulation is initialized by releasing the particles to move freely. The computational grid was set to 2048x2048x4096 grid points and a total of 11867 particles were considered. The simulation was performed on a 8192 processor cores.

Figure 1 shows an instantaneous three-dimensional snapshot of the flow field and the particle positions in the statistically steady regime. As can be seen the particles are clearly distributed in a non-homogeneous manner, forming vertically oriented columnar-like clusters. The flow field experiences coherent structures corresponding to the particle agglomerations. The right side of figure 1 depicts a small sub-volume showing that the particle-induced vortex structures corresponding to the particle wakes are mainly concentrated in the strong downward currents shown on the left side. It can be observed that in this regions complex interactions between the particle wakes take place. On the other hand, in the void regions surrounding the downward current the particle wakes are observed to be close to the double-threaded wake of an isolated sphere at the same Galileo number.

A detailed analysis of the particle settling velocity revealed that due to the particle clusters the particles located inside such agglomerations settle on average faster than particles located outside.

On-going Research / Outlook

We have performed various DNS simulations of finite-size particles settling in an initially ambient flow. The computational resources available on SuperMUC allowed us the generation of unique data-set which will contribute substantially to the understanding of the processes involved in particulate flows.

The agglomeration of particles into cluster was observed. The formation of clusters solely due to the particle-induced fluid motion as well as the exact processes and the parameters controlling the formation of the clusters needs further investigation. Moreover, the influence of turbulence upon the clustering process is to our knowledge not fully understood and further work is required. The present results are currently submitted for publication in the J. Fluid Mech [5].

References and Links

[1] Balachandar, S., Eaton, J.K., 2010. Turbulent Dispersed Multiphase Flow. Annual Review of Fluid Mechanics. 42, 111-133
[2] Ern, P., Risso, F., Fabre, D., Magnaudet, J., 2012. Wake-Induced Oscillatory Paths of Bodies Freely Rising or Falling in Fluids. Annual Review of Fluid Mechanics 44, 97–121.
[3] Jeong, J., Hussain, F., 1995. On the identification of a vortex. J. Fluid Mech., 285:69-94.
[4] Uhlmann M. 2005. An immersed boundary method with direct forcing for the simulation of particulate flows. J. Comput. Phys, 209(2):448-476.
[5] Uhlmann M., Doychev, T. 2014. Sedimentation of a dilute suspension of rigid spheres at intermediate Galileo numbers: particle motion and clustering

Direct numerical simulation of the formation of subaqueous sediment patterns

Research Institution
Institute for Hydromechanics, Karlsruhe Institute of Technology (KIT)

Principal Investigator
Markus Uhlmann

Researchers
Aman G. Kidanemariam

Project Partners
–

LRZ Project ID: pr58do

Introduction

The formation of sediment patterns is a common occurrence in river and marine flows as well as in various technical applications involving shear flow over a bed of mobile sediment particles. The erosion of particles from the sediment layer and their deposition at certain preferential locations often leads to bed shapes which are commonly described as ripples or dunes. From an engineering point of view it is highly desirable to be able to predict the occurrence and the nature of this phenomenon, since the bedform significantly influences flow characteristics such as resistance, mixing properties and sediment transport.

Experiments show that at low flow rates small-scale undulations of the sediment bed appear, having no clear-cut shape [1]. When increasing the flow rate in a given experiment, these ripples give way to the much larger dunes, which have an asymmetric shape with a steeper slope on the downstream side of the crests, where flow separation and recirculation occurs, and which propagate downstream.

Most of the previous theoretical work on the formation of ripples is based upon the notion that a flat bed is unstable with respect to perturbations of sinusoidal shape. Over the years a number of researchers have studied this stability problem for a variety of flow conditions, in the laminar and turbulent regime. The hydrodynamic stability problem is complemented by an expression for the particle flux at a given transversal section of the flow [2-3]. Compared to experimental observations current stability results can be broadly described as unsatisfactory, sometimes predicting ripple wavelengths which are off by an order of magnitude. The reason for this disagreement can be linked to a poor description of the dynamics of particle motion near the mobile bed.
The objective of the present project is to contribute to the understanding of the physical mechanisms involved in the formation of sediment patterns driven by (turbulent) shear flow by providing a complete description of the flow field as well as particle-related quantities for idealized flow configurations at relatively low Reynolds numbers.

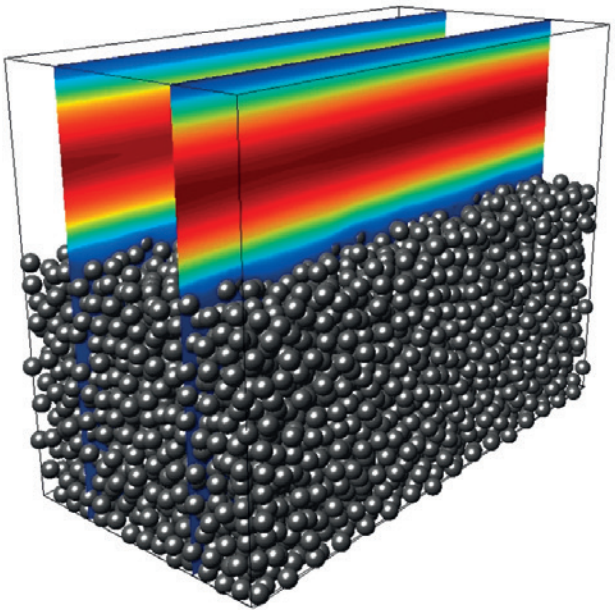

Figure 1: Instantaneous three-dimensional snapshot of the flow field and particle positions.

Results

Numerical method
The numerical method employed is a formulation of the immersed boundary method. The incompressible Navier-Stokes equations are solved throughout the entire domain comprising the fluid domain and the domain occupied by the suspended particles while adding a force term which serves to impose the no-slip condition at the fluid-solid interface. A detailed account of the method can be found in [4]. The numerical method employs domain decomposition for parallelism and has been shown to run on grids of up to 8192^3, using up to of the order of 105 processor cores in scaling tests [5]. In order to accurately treat inter-particle contacts, a discrete element model (DEM) which mimics the basic collision dynamics between the immersed particles is incorporated into the DNS code. The DEM is developed

by adopting a soft-sphere model which is based on a linear mass-spring-damper system to model the collision forces. Here we include a normal repulsive force (proportional to the overlap distance), a normal dissipative force (proportional to the normal component of the relative velocity) and a tangential damping force (equal to the minimum of either the Coulomb friction or a force which is proportional to the tangential component of the relative velocity).

Small-scale validation-purpose simulations
Validation of the adequacy of the numerical method for such four-way-coupled flows is necessary. To this end, we have performed a number of small-scale simulations of the movement of a large number of spherical particles as bedload transport subjected to erosion in a closed laminar channel flow at various values of the control parameters and compared obtained results with reference experimental observations. Figure 2 gives an impression of the extents of the domain adopted in these validation simulations. An established flow field shearing a mobile bed made up of spherical particles is shown in selected wall-perpendicular planes.

Medium-scale simulations of pattern formation
In this phase of our simulation, we have performed direct numerical simulations (DNS) of the formation of subaqueous patterns in a statistically uni-directional channel flow configuration both in the laminar and turbulent regimes.

A very large number of freely moving spherical particles (of the order of 10^5) are considered which make up an initially flat, mobile sediment bed. All the relevant length and time scales of the (turbulent) flow, even in the vicinity of the particles, have been accurately represented by resolving the fluid-solid interface. The Reynolds number of the flow, based on the bulk velocity and the half-channel height, was set at a value $Re_b \approx 350$ for the laminar case and at a value $Re_b \approx 3000$ for the turbulent case. The spherical particles considered are mono-dispersed with a diameter approximately 25 times smaller than the half-channel height and a density 2.5 times larger than that of the fluid. The value of the Galileo number, which is the ratio of gravity forces to viscous forces, is chosen such that the value of the Shields number, which is a non-dimensional basal shear stress, is above the critical value for incipient particle motion.

As a result of the net effect of the driving hydrodynamic force, gravity force as well as forces arising from inter-particle contacts, particle erosion and transport is observed to take place. The continued process of erosion from certain preferred regions and deposition at other downstream regions, introduces small perturbations to the initially flat sediment bed which ultimately leads to the organization and formation of the patterns as is shown in figure 2.

So far, for performing the small- and medium-scale simulations mentioned above, we have consumed about 7.5 million of CPU hours.

On-going Research / Outlook

Within the scope of this project, we plan to perform additional medium-scale simulations to pinpoint the most unstable initial wavelength by successively minimizing the streamwise length of the computational box.

References and Links

[1] Coleman S. E. and Melville B. W. 1994. Bedform development. *J. Hydraul. Engng*, 120(4):544-560.
[2] Sumer B. M. and Bakioglu M. 1984. On the formation of ripples on an erodible bed. *J. Fluid Mech.*, 144:177-190.
[3] Charru F. 2006. Selection of the ripple length on granular bed sheared by a liquid flow. *Phys. Fluids*, 18:121508.
[4] Uhlmann M. 2005. An immersed boundary method with direct forcing for the simulation of particulate flows. *J. Comput. Phys*, 209(2):448-476.
[5] Uhlmann M. 2010. Jülich Blue Gene/P Extreme Scaling Workshop 2010. Technical report FZJ-JSC-IB-2010-03.

http://www.ifh.kit.edu

Figure 2: An instantaneous three-dimensional snapshot of the flow field and particle positions corresponding to the turbulent regime. Vortical structures are visualized by means of the λ_2 criterion. The particles are colored based on the wall-normal location of their center.

Investigation of Dynamics of Technically Premixed Flames Using LES

Research Institution
Lehrstuhl für Thermodynamik Technische Universität München,85747, Garching

Principal Investigator
Ahtsham Ulhaq

Researchers
Ahtsham Ulhaq, Wolgang Polifke

Project Partners
–

LRZ Project ID: pr58gi

Introduction

In order to meet stringent emissions regulations, modern gas turbines use lean premixed combustion systems. It has been found that lean premixed flames are more sensitive to combustion instabilities. Combustion instability arises from the interaction of acoustic waves and fluctuating heat release, resulting in self-sustained, large amplitude oscillations of pressure and velocity in the combustor. These instabilities can be predicted by performing a stability analysis, which requires information about the flame response to the perturbations. The dynamic response of premixed flame to upstream perturbations can be represented by its flame transfer function. Practically premixed combustion is characterized by inhomogeneous lean premixed conditions, where fuel is injected at one or multiple locations relatively close to the flame. For practically premixed combustion, velocity fluctuations caused by acoustic waves also lead to equivalence ratio fluctuations, so the overall flame dynamics is affected by both velocity and equivalence ratio fluctuations.

The overall objective of the present proposal is to develop the LES/SI approach for turbulent swirl burners in the "practical premix" configuration, where fuel injection is influenced by acoustic perturbations, such that mixture in-homogeneities contribute in an essential manner to the overall flame dynamics. This approach has already been successfully used by Luis Tay [1] for full lean premixed flames.

Results

For the present work, the LES solver AVBP based on Finite Volume methods has been used. The full compressible multispecies Navier-Stokes equations are solved on unstructured meshes.

AVBP code is developed by Cerfacs, France. It solves the laminar and turbulent compressible Navier-Stokes equations in two and three space dimensions. For the prediction of unsteady turbulence various Large Eddy Simulation (LES) sub-grid scale models have been developed. AVBP is written in standard FORTRAN 77. The solver produces the grid partitions using standard algorithms like the recursive inertial method. The aim is to minimize the interfaces generated by the partitioning process. It uses the Message Passing Interface (MPI) for the communication between the processes; and for the application, a Master-Slave parallelization scheme is chosen. Apart from the generation of complete output files, an interval of iterations can be selected after which the master process collects certain data from the slave processes and writes it to an output file, in order to provide e.g. convergence data. This process was modified in order to collect acoustic information at certain predefined monitor planes [2]. Additionally, as already used in [2] , a domain integrated reaction rate is written out "on the fly", allowing to collect the necessary time series data during the calculations and saving in this way a huge amount of disk space.

The AVBP package is available for various hardware architectures and is currently installed on the following platforms: Compaq Alpha Server, Silicon Graphics, SUN, IBM SP3/4, PC LINUX clusters.

In first step, steady state simulations are carried out for technically premixed combustor. In this step it is ensured that perfect mixing of air fuel and right flame shape are achieved. The results presented below are for U= 40 m/s and phi= 0.65. Figure-1(a) presents a comparison of experimentally and numerically computed flame structures and figure-2(b) presents a comparison of nor-

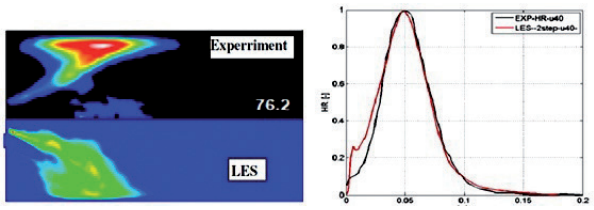

Figure-1:(a) Mean Heat Release from LES and OH* Chemiluminescence from Experiments (b) Comparison of Mean Axial Heat Release Distribution for LES and Experiments

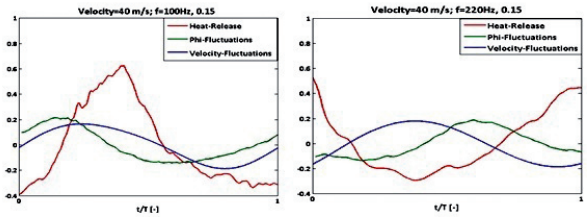

Figure-2: Complete Cycle of Modulation for Velocity, Equivalence Ratio and HR fluctuations (a) f=100 Hz. (b)= 220 Hz.

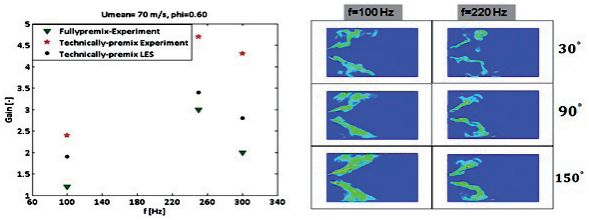

Figure-3:(a) Comparison LES and Experimental Gain of FTF U= 70 m/s, Phi= 0.6 (b) Phase-averaged HR plot U= 40 m/s, Phi= 0.65

malized spatial heat release distribution for technically premixed case. This shows that the results of LES are in very good agreement with experimental results. In order to compare the results of LES and experiment, it is important to get the right flame shape because a different flame shape can affect the flame transfer functions.

Figures-2(a) and 2(b) present the fluctuations of velocity, equivalence ratio and heat release fluctuations for one complete cycle of oscillations at two different forcing frequencies. The modulation amplitude is 15% of mean velocity and equivalence ratio fluctuations are also caused by velocity fluctuations. This shows that changing the harmonic frequency leads to variation of phase and amplitude among these fluctuations. Once the phase and amplitude of these fluctuations is changed, it will lead to variations of flame dynamics. The corresponding phase-averaged images of heat release in figure-3(b) show that flame responds differently for both the frequencies.

In technically premixed combustion systems, in addition to magnitude of harmonic frequency, the phase and magnitude among these fluctuations are modified by the mean flow velocity, fuel injection location and location of the swirler. The effects of magnitude of frequency of modulation and mean flow velocity have already been computed and analyzed. In order to analyze the effects of fuel injection location and swirler position on flame dynamics are in process. Figure-3(a) represents the comparison of gain of FTF from numerical simulations with experimental data. It shows the predicted gain from LES has small magnitudes than the measured data. The possible reasons can be the presence of noise in simulation data.

For this study the number of computational resources used are summarized in the following table:

Table 1: Details of Computations run on SuperMUC

Type of run	# of runs	# of steps/ Run	Wall time per step [hours]	# CPU cores	Total core hours
LES steady	4	$1x10^6$	$5x10^{-5}$	800	**$0.2x10^6$**
LES/SI	6	$4x10^6$	$5x10^{-5}$	800	**$1.2x10^6$**
LES Sin.	5	$1x10^6$	$5x10^{-5}$	800	**$0.3x10^6$**

Outlook

While performing the LES of technically turbulent premixed flames, very fine meshes are required in order to capture the proper air fuel mixing and also to resolve the flame front. The typical size of the overall mesh used for this study consists of 1.5 million cells and with a corresponding time step of order 1e-07.

Indeed without the availability of SuperMUC facility it was not possible to perform these simulation and to get the results in reasonable amount of time. Furthermore, the effects of fuel injection location and swirler position for technically premixed flames are in progress. The results obtained from these simulations will be used to perform stability analysis using 1D acoustic Network approach.

References and Links

[1] L. Tay Wo Chong, S. Bomberg, A. Ulhaq, T. Thomas Komarek, W. Polifke, Comparative Validation Study on Identification of Premixed Flame Transfer Function GT2011-46342

[2] R. Kaess , W. Polifke , T.Poinsot , N. Noiray ,D. Durox ,T. Schuller and S. Candel (2008) CFD based mapping of the thermo-acoustic stability of a laminar premix burner. In: Proceedings of the Summer Program CTR, Stanford

http://www.cerfacs.fr

PaTriG – Particle Transport Simulation in Grids

Research Institution
Department of Informatics (Technische Universität München), School of Engineering and Computing Sciences (Durham University)

Principal Investigator
Tobias Weinzierl

Researchers
Philipp Neumann, Kristof Unterweger, Bart Verleye, Roland Wittmann

Project Partners
Technische Universität München (TUM), University of Leuven (KU Leuven), Durham University

LRZ Project ID: pr63no

Introduction

Mesh-based discretisations of parabolic partial differential equations (PDEs) are the predominant strategy to tackle computational fluid dynamics (CFD) on the continuum scale. At home in many application areas, successful on supercomputers, there are nevertheless good reasons also to study particle-based descriptions on this scale: particles running along the flow profile can represent real particles suspended in the liquid or, correctly coupled, they can inject Brownian fluctuation or the impact of almost negligible tiny bodies into the fluid's behaviour. A particle model here is not an algorithmic gimmick on top of the CFD challenge. It allows us to work around (computationally) harder setups such as fluid-structure interaction or a volume coupling to molecular dynamics codes. Particles in the cells bring along their own particularities. Besides an accurate and fast mesh-based CFD solver and the particle physics, they demand for algorithms sorting the bodies into the CFD grid such that we are able to evaluate mesh-particle and particle-mesh interactions efficiently. Once the particles are sorted into the mesh, we also need adequate ways to move them across the grid. Needless to say, all this has to integrate into domain decomposition approaches for adaptive grids, as the serial or regular case is trivial.

Spacetree mesh-based CFD solvers

Spacetree-based meshes interplaying with the construction scheme of space-filling curves [1] are a powerful technique to realise dynamically adaptive Cartesian meshes. Their underlying recursive traversal automaton with a code full of branches however typically yields a rather low performance if the computational workload per mesh cell is low. In the present fluid dynamics schemes – based upon Lattice-Boltzmann discretisations [2], low order finite elements or low order finite volume stencils for hyperbolic equations – spacetree formalisms face exactly this problem. As a consequence, we augment the spacetree structure and embed regular Cartesian grids into the adaptive (meta) mesh.

The size of the embedded patches plays a crucial role to obtain reasonable MFlop rates per node. Too small patches hinder us to exploit vector registers and cannot hide the spacetree's administrative overhead. Too big patches prevent the solver to resolve the physics with an accurate, low cell count mesh and suffer from cache capacity effects as soon as the patches leave a cache hierarchy.

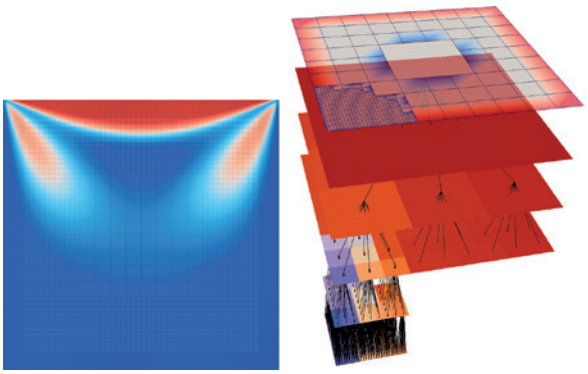

Figure 1: Lattice Boltzmann driven cavity flow (left) from [2] based upon a spacetree (right) into which regular Cartesians grid is embedded [3].

Empirical studies reveal that there is a sweet spot for the patch sizes. They reveal that XeonPhi systems or other accelerator boards benefit from the fact that the spacetree's patch decomposition allows us to deploy whole patches to different cores. In contrast, they reveal that SuperMUC's per-node memory subsystem plays the memory game in a different league. In our experiments, our low-overhead patch decomposition was outperformed by simple parallel for loops where all cores process one single patch at a time (cf. [3] for results on hyperbolic problems, e.g.). With proper case studies, that insight, and an algorithm merging small patches into more efficient assemblies on demand, we were able to make our computational patch kernels hit the roofline model's best-case thresholds; also on dynamically adaptive grids.

The size of the embedded patches plays a crucial role to obtain good time-to-solution once local adaptive time stepping enters the stage. As a computationally demanding time step adaption per mesh cell is not feasible for our problems, we stick with one time step size per patch that can alter on the patch-level – a formalism well-known for hyperbolic PDEs, straightforward for parabolic PDEs, and inherently built into adaptive Lattice Boltzmann schemes. Again, too small patch sizes introduce a high administrative overhead and lead to a global discretisation where only few work units can be advanced in time at once. Too big patch sizes reduce the speedup resulting from local time stepping.

Once a proper patch size is found, empirical studies reveal that local time stepping has a disadvantageous impact on the parallel efficiency of the overall algorithm if the mesh's refinement structure is not reasonably balanced. Even using the time stepping decisions to determine whether data along partition boundaries have to be sent via mpi could not render this impact small. For future work, we have to anticipate this fact in the load balancing or find communication-avoiding or communication-reducing strategies. For the time being, our text-book load balancing algorithms are too static.

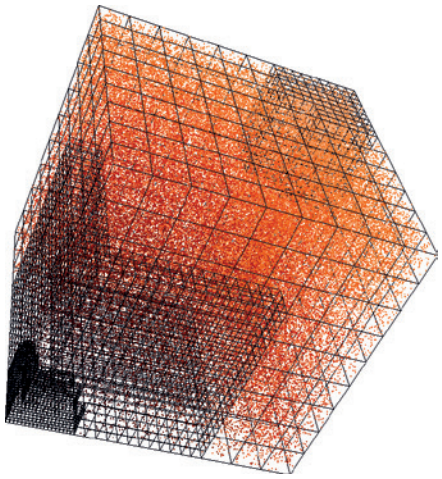

Figure 2: Particles are embedded into the spacetree. Its cells are the finer the slower and denser the particles in a region (from [3]).

Particle sorting and parallelisation

Spacetree-based particle sorting is a well-established, powerful technique to distribute huge particle counts according to their spatial position among a parallel computer. Most algorithms start from the list of particles and impose a spacetree on top of this list. Our setup differs slightly, as we have a spacetree at hand already – it represents either the mesh or a meta-mesh – and have to sieve the particles into this mesh. We have to bucket sort the particles. A per-particle brute force sieving from scratch, i.e. from the root of the spacetree, is a poor idea once the particles are held in the spacetree, as they do not jump dramatically. However, different to many other codes, our physical models allow tunneling, i.e. that particles more more than one spacetree cell. The latter case occurs sporadically.

The multiscale nature of the spacetree allows us to assign the spacetree nodes links to the individual particles. As soon as the particles have moved, we can check whether they reside inside a cell. If not, we exploit the spacetree's multiscale structure and move them to the next coarser mesh. A final postprocessing step then sieves the particles back into finer levels. This sieve is significantly faster than making each particle run down the whole tree per particle movement. On SuperMUC, such an approach can handle up to 108 particles per node and achieve around 27,8 percent of the stream benchmark throughput. Our multiscale tree sorting is outperformed by classical linked-list algorithms as found in molecular dynamics if the particles never move more than one cell per time step. Passing them between neighbouring particles is a process with a high concurrency level that requires per spatial movement solely the geometric data of few cells.

Empirical studies [4] reveal that a hybrid variant – though more complex to realise than a pure multiscale approach – outperforms the latter if the characteristic particle speed to cell size ratio is reasonably small, if many parallel nodes are involved, and if the particle density is significant. As rule of thumb, hybrids do not pay off for rank counts below 1000. In contrast, the fact that the particles are already (pre-)sorting by the previous time steps, i.e. all particles have resided in the right spacetree cell prior to a particle time step, implies that we can process individual spacetree cells in parallel. Synchronisation is only required for those particles that tunnel. The multicore hence depends on the particle velocity profile and the grid structure, but again, eight cores per mpi rank have proven to be a reasonable parallelisation strategy.

Outlook

The present project's focus shifts from solving PDEs with only a handful of particles to mesh-based solvers with millions of particles embedded. Algorithmic questions how to handle such huge systems then are subject of the present work, and well-suited algorithmic building blocks were developed, benchmarked and tailored to the particular hardware. While the project allows us to illustrate that SuperMUC's cores and vector registers can fully be utilised by today's PDE solver kernels and high particle counts per node are doable, it also highlights that requirements such as local time stepping and sorting particles globally along the machine can not be realised straightforwardly. They raise severe load balancing and communication challenges that are, besides a transfer of the algorithms into applications, to be tackled next.

References and Links

[1] T. Weinzierl: A Framework for Parallel PDE Solvers on Multiscale Adaptive Cartesian Grids, Verlag Dr. Hut, 2009
[2] P. Neumann: Hybrid Multiscale Simulation Approaches For Micro- and Nanoflows, Verlag Dr. Hut, Munich. 2013.
[3] T. Weinzierl et al: Hardware-aware grid blocking on spacetrees, Parallel Processing Letters, submitted.
[4] B. Verleye et al: Two Particle-in-Cell Realisations on Spacetrees, to be submitted.

http://www.peano-framework.org

DNS of the turbulent Poiseuille flow with wall transpiration

Research Institution
Chair of Fluid Dynamics, TU Darmstadt

Principal Investigator
Martin Oberlack

Researchers
Victor Avsarkisov

Project Partners
–

LRZ Project ID: pr63qu

Introduction

In the classical non-transpirating plane turbulent channel flow all statistical quantities are symmetric or antisymmetric with respect to the channel centerline. This includes symmetric distribution of the mean velocity, the normal Reynolds stresses, and point symmetric distributions of viscous and turbulent shear stresses including values of shear stresses at the walls. These results are consistent with zero total shear stress and zero mean velocity gradient in the center of the channel. In the presence of uniform wall transpiration all these

symmetries are broken. Furthermore, the occurrence of an additional term in the streamwise component of the mean momentum equation modifies the classical universal scaling laws (linear viscous sublayer and law of the wall) for non-transpirating wall-bounded flows.

In comparison to the other wall-bounded flows with specific, non-standard boundary conditions, turbulent channel, i.e. Poiseuille flow with wall transpiration is a relatively new subject of investigation.

The objective of this project is the analysis of a fully developed, turbulent Poiseuille flow with wall transpiration, i.e. uniform blowing and suction on the lower and upper walls correspondingly, as it may be taken from Figure 1. We used Lie symmetry analysis to find symmetry transformations and to derive invariant solutions of the set of two-point correlation equations, while DNS is used to simulate turbulent channel with wall-transpiration at different Reynolds numbers and transpiration velocities. Both tools are used to find new mean velocity scaling laws. Consequently, it is shown that the transpiration velocity is a symmetry breaking, which implies a logarithmic scaling law in the core region of the channel.

Numerical Details and Conducted Simulations

In the present numerical study we were using the code developed in the School of Aeronautical Engineering,

Technical University of Madrid. The code integrates the Navier-Stokes equations for an incompressible fluid in the velocity-vorticity formulation, in the form of two evolution equations for the Laplacian of the wall-normal velocity and for the wall-normal vorticity, so pressure is not computed during the run. The remarkable property of the formulation is that it is independent whether or not the frame of reference is inertial, i.e. non-inertial effects are present only in initial and boundary conditions. Numerics and the main ideas are based on the original code made by [2], but presently none of the original code subroutines remain in it.

Figure 1: (a) Volume rendering of the positive part of the instantaneous streamwise velocity field. Yellow areas represent the region of the maximum velocity. (b) Instantaneous field of vorticity magnitude colored with streamwise component of vorticity. Yellow reddish structures are hairpin vortices and packets of hairpins. On both plots blowing is applied at the bottom wall and suction at the upper one. Visualizations were performed on the RZG (MPG & IPP) cluster.

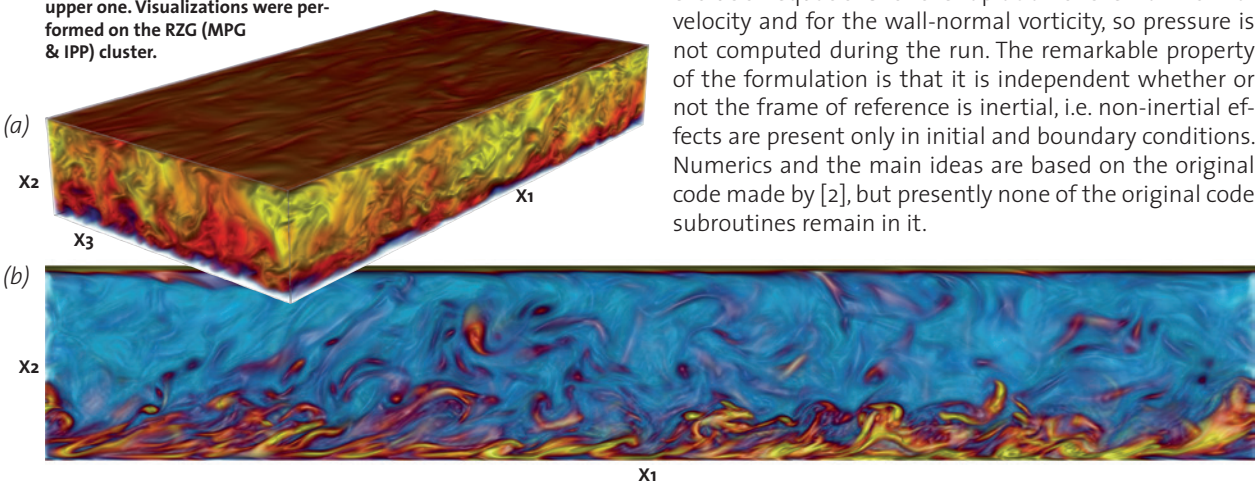

For the intended DNS a CFD algorithm employing a Fourier-Compact Finite Difference method to solve the Navier-Stokes equations was used. In the streamwise and spanwise directions it uses a spectral formulation (Fourier series), while in the wall-normal direction, a seven-point compact finite difference scheme with fourth-order consistency and extended spectral-like resolution is applied. For the time discretization, a third-order semi-implicit Runge-Kutta (R-K) algorithm is implemented.

The code is written in Fortran77, MPI parallelized and does compile and run on different machines and compiler (IBM and Intel). It has planes-lines parallelization scheme.

The code demonstrates excellent speed-up for a large amount of processors. In order to save time and memory, the code computes only a few statistics and spectra during the run. Many other quantities are computed in the post-process stage, using images of the fields saved each few hundred time steps. The cost of computing almost any imaginable (and useful) quantity is of the same order of magnitude that computing just one time-step advance, providing that a parallel post-process code is available. In order to keep a forcing constant during the run a fixed mass-flow rate is employed in the code.

Table 1: Summary of the simulations. v_o/u_r is the transpiration rate. L_{x_1} and L_{x_3} are respectively the periodic dimensions of the numerical. N_{x_1}, N_{x_2} and N_{x_3} are numbers of collocation points in streamwise, wall-normal and spanwise directions. T is the computational time spanned by statistical fields.

Re_τ	vo/u_τ	L_{x_1}/h	L_{x_3}/h	N_{x_1}	N_{x_2}	N_{x_3}	$u_\tau T/h$
Turbulent Poiseuille flow with transpiration							
480	0.05	8π	6π	768	386	768	41
480	0.1	8π	6π	768	385	768	40
480	0.16	8π	6π	768	385	768	25
480	0.26	8π	6π	768	385	768	30
850	0.05	8π	6π	3072	471	3072	26
850	0.16	8π	6π	3072	471	3072	22

Performed production runs can be conditionally divided into two sets depending on the friction Reynolds number. Re_τ=480 set consists of four cases for the different transpiration rates, while Re_τ=850 set consists of only two simulations. A complete summary of the flow and the numerical parameters are given in Table 1.

All the simulations presented in the Table 1 were conducted on the SuperMuc cluster. Each Re_τ=480 simulation case took 20.000-25.000 CPU hours, simulations were running on 16-64 processors and were finished within 4 months.

For the largest simulations we were using 1024 processors and it took 1.2-1.3 million CPU hours each case to run the code for 10 wash-outs. Both Re_τ=850 simulations were finished within 5 months.

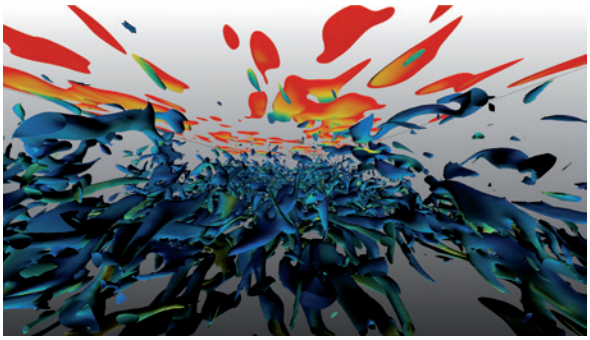

Figure 2: Mid-plane view of the coherent vortical structures in the channel flow with blowing from the bottom and suction from the top. Visualization was performed on the RZG (MPG & IPP) cluster.

Scientific results

In the present project we combined Lie symmetry analysis of the TPC equations and DNS to investigate the statistical characteristics of the turbulent channel flow with wall transpiration. Lie symmetry analysis revealed a new mean velocity logarithmic type of scaling law that, afterwards, has been confirmed in the center of the channel and studied in detail by DNS [1]. For the derivation of the new log-law we used symmetry transformations which have been previously derived in the two- and MPC equations [3][4].

Visualizations of the instantaneous velocity and vorticity fields have shown that ejections dominate at the blowing wall, where the big amount of hairpin-type vortical structures have been found, while at the suction wall have only found sweep motions towards the suction wall. It was found that hairpin packets (LSM structures), are affected by blowing (see Figure 1b). In particular, vertical and spanwise growth angles were increased. As a result, these structures grow faster and penetrate into the core region of the flow, as it can be taken from Figure 2.

On-going Research / Outlook

Presently we are planning to perform DNS of the turbulent plane Couette flow at high Reynolds numbers. For the DNS of a turbulent Couette flow the box has to be extensively larger compared to the one for a turbulent Poiseuille flow as in the central region of the flow very large streamwise elongated structures were observed. Due to extremely large amount of the grid points this DNS was impossible to perform earlier.
We are planning to extend the present project for one year to perform another plane turbulent Couette flow computation at Re_τ=950 with N=2.5–3.5·10^{10}grid points.

References and Links

[1] V. Avsarkisov, M. Oberlack, S. Hoyas. New Scaling Laws for Turbulent Poiseuille Flow with Wall Transpiration. *Accepted in J. Fluid Mech.* 2014.
[2] J. Kim, P. Moin and R. Moser. Turbulence statistics in fully developed channel flow at low Reynolds number. *J. Fluid Mech.* **177**, 133–166. 1987.
[3] M. Oberlack. A unified approach for symmetries in plane parallel turbulent shear flows. *J. Fluid Mech.* **427**, 299–328. 2001.
[4] M. Oberlack, A. Rosteck. New statistical symmetries of the multi-point equations and its importance for turbulent scaling laws. *Dis. and Cont. Dyn. Sys. S* **3** (3). 2010.

Numerical Simulations of natural thermal convection at high Rayleigh numbers

Research Institution
Deutsches Zentrum für Luft- und Raumfahrt, Göttingen

Principal Investigator
Olga Shishkina

Researchers
Susanne Horn, Olga Shishkina

Project Partners
–

LRZ Project ID: pr63ro

Introduction

Turbulent flows driven by thermal convection are not only ubiquitous in astro- and geophysics, as for example in the convective zone of stars, the interior of gaseous planets and the Earth's atmosphere and oceans, but they are also important for engineering applications, as crystal growth, ventilation of buildings and aircrafts and other different technological heating/cooling processes. These phenomena are often accompanied by a rotational force. To study the underlying fundamental processes it is convenient to study rotating Rayleigh-Bénard convection, which is one of the classical problems of fluid dynamics. The setup is rather simple: It consists of a fluid confined between a heating plate at the bottom and a cooling plate at the top. Despite its simplicity, the occurring buoyancy driven flows are highly complex and we are still far away from a complete understanding. Thus, it kept on being an active field of research for over a century now. Nonetheless, little is known so far about the impact of the Coriolis force on natural thermal convection with Prandtl numbers smaller than one. The Prandtl number Pr is the ratio of the kinematic viscosity to the thermal diffusivity, and gases like air or sulfur hexafluorid (SF_6), have Prandtl numbers around 0.7 and 0.8.

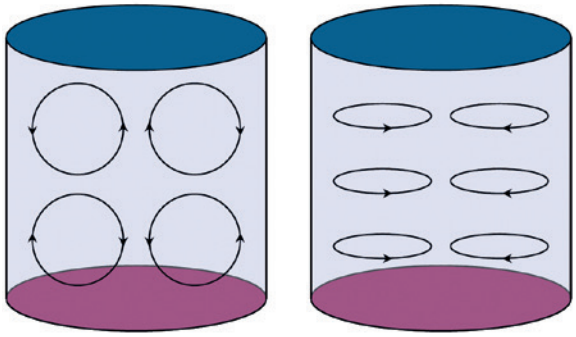

Figure 2: Sketch of the poloidal (left) and toroidal (right) field in a cylindrical geometry.

One important question asked, is, when the flow is dominated by buoyancy and when by rotation.

Results

We try to answer this question by means of direct numerical simulations (DNS) using a finite volume method for cylindrical domains [1]. We simulate rotating Rayleigh-Bénard convection in a cylindrical cell with a diameter-to-height aspect ratio of one half filled with

Figure 1: Instantaneous temperature fields in the non-rotating case. Shown are isosurfaces for ten equidistantly distributed values between the top and bottom temperature, blue corresponds to temperatures below the arithmetic mean temperature and pink to temperatures above it. The Rayleigh number increases from left to right from 10^5 to 10^{10}.

Figure 3: Instantaneous temperature fields for Ra = 10^8 in the rotating case, similar as in figure 1. The rotation rate increases from left to right (from Ro = 10. to Ro = 0.05).

SF6. Apart from the Prandtl number and the aspect ratio, the system is determined by the Rayleigh and the Rossby number. The Rayleigh number Ra characterises how vigorous convection is, as visualised in figure 1. The higher the Rayleigh number the more efficient heat is transported and the smaller are the structures. The Rossby number Ro is is inversely proportional to the rotation rate. If Ro is much larger than one, then the system is buoyancy dominated, when Ro is much smaller than one, the system is dominated by rotation. However, this does not mean that the transition occurs when Ro equals one.

From a computational point of view, there are two challenges. On the one hand, reaching high Ra requires very fine meshes and small time steps [2,3], on the other hand, finding transitions, means that a series of DNS with varying Ro and varying Ra has to be performed. As a compromise, we performed DNS up to Ra = 10^9, using typically 64 to 128 CPUs. Each simulation runs for several weeks to months to achieve statistical convergence and reliable results.

To determine the transition point we analyse the contribution of the poloidal and toroidal energy to the total kinetic energy. For this purpose we decomposed the incompressible, hence, solenoidal, velocity field into its toroidal and poloidal part. This is sketched in figure 2. The poloidal energy is associated with cellular motion, or a large-scale circulation and multiple roll states, as can be found in the non-rotating or weakly rotating case. The toroidal energy, on the other hand, is associated with the vertical vorticity, and hence with plumes and even more with the columnar vortex structures, typical for rotating convection and as presented in figure 3.

Hence, the toroidal energy increases with increasing Rayleigh number, where more plumes emerge, that are torn apart due to the higher toroidal energy. However, in the rotating case the toroidal energy can also have a stabilising effect. It increases with the rotation rate, i.e. decreasing Ro, and the flow becomes two-dimensional in the horizontal plane. The poloidal energy, on the other hand, decreases, and finally the large-scale roll structures break down [4,5]. Thus, we argue, that at a critical Rossby number the transition occurs, which is induced by the dominance of the toroidal energy over the poloidal energy [6], as shown in figure 4.

For smaller Rayleigh numbers, however, none such crossover occurs. Instead, convection is suppressed completely and heat is transported by conduction alone. But also for moderate Ra, rotation reduces turbulent fluctuations, thus, we only obtain a truly rotation dominated regime, if the Rayleigh number is high enough. In this case, one speaks of geostrophic turbulence.

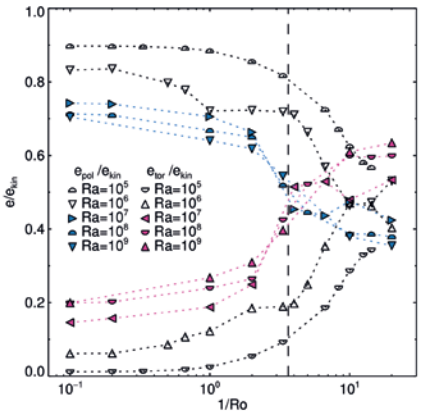

Figure 4: Toroidal and poloidal energy normalised by the kinetic energy at the same rotation rate. The vertical line corresponds to the transition point.

On-going Research / Outlook

Further numerical simulations are planned for higher Ra and small Ro to further explore thermal convection in the regime of geostrophic turbulence, which is thought be most relevant for rotating convective flows occurring in nature.

References and Links

[1] Shishkina, O. & Wagner, C. CR Mecanique 333 (2005).
[2] Shishkina, O., Stevens, R.J.A.M., Grossmann, S., & Lohse, D. New J. Phys. 12 (2010)
[3] Shishkina, O., Wagner, S. & Horn, S., Phys. Rev. E (accepted)
[4] Kunnen, R.P. J., Clercx, H.J.H. & Geurts, B.J.. EPL 84 (2008)
[5] Stevens, R.J.A.M., Clercx, H.J.H. & Lohse, D., Phys. Rev. E (2012)
[6] Horn, S. & Shishkina, O., J. Fluid. Mech (submitted)

Wake Vortices of Landing Aircraft

Research Institution
Deutsches Zentrum für Luft- und Raumfahrt, Institut für Physik der Atmosphäre

Principal Investigator
Frank Holzäpfel

Researchers
Anton Stephan, Tobias Heel

Project Partners
–

LRZ Project ID: pr63zi

Introduction

As an unavoidable consequence of lift aircraft generate a pair of counter-rotating and long-lived wake vortices that pose a potential risk to following aircraft. The prescribed aircraft separations during landing to avoid wake vortex hazards contribute significantly to capacity restrictions of large airports. Severe encounters of wake vortices have also been reported during cruise. Wake vortex behavior is largely controlled by the prevailing meteorological conditions and the interaction with the ground. The most important meteorological parameters are ambient wind, wind shear, turbulence, and temperature stratification.

The Deutsches Zentrum für Luft- und Raumfahrt (DLR) develops wake vortex advisory systems for airports and en route which aim at optimizing the air traffic with respect to the measured and predicted wake vortex behavior. As part of such systems simple probabilistic wake vortex prediction models are required that predict wake vortex behavior accurately, robust, and fast. Highly resolving large eddy simulations (LES) conducted on the SuperMUC supercomputer provide valuable insights in the physics of wake vortex behavior under various atmospheric conditions. These LES contribute indispensable guidance for the development of the real-time/fast-time wake vortex models.

Results

A particular risk prevails during final approach, where the vortices cannot descend below the flight path, but tend to rebound due to the interaction with the ground. Moreover, the possibilities of the pilot to counteract the imposed rolling moment are restricted due to the low flight altitude of aircraft above ground. Numerical simulations and field measurements indicated that approaching aircraft frequently fly close to or even through not fully decayed wake vortices in ground proximity. We got several steps further in understanding the physics, leading to unexpectedly save landings, with the help of numerical simulations.

The wake vortex evolution depends not only on environmental conditions such as atmospheric turbulence, temperature stratification and wind shear, but also on the specific aircraft geometry and the configurations for cruise, take-off or landing. A novel wake initialization approach, where a realistic aircraft wake is generated in an LES domain by sweeping a high-fidelity Reynolds-Averaged Navier-Stokes (RANS) flow field through the domain, was applied to an A340 aircraft in high lift configuration. Using this approach a simulation was performed from the wake roll-up until the vortex decay.

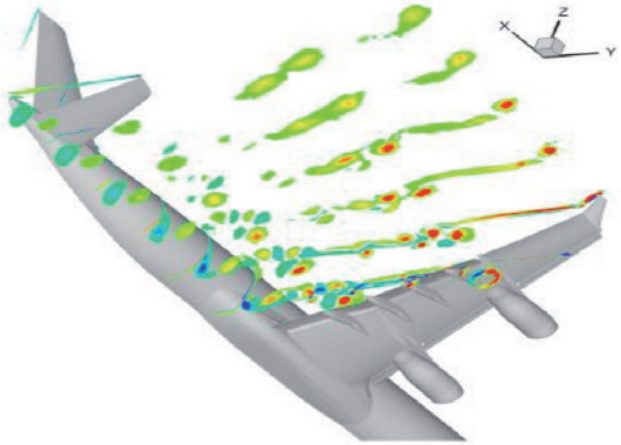

Figure 1: Near-field vorticity distribution around AWIATOR long range aircraft model obtained from RANS simulation.

Figure 1 shows near-field vorticity distributions obtained from the RANS simulation. The contours in blue and red represent axial vorticity in clockwise and counter-clockwise directions, respectively, viewed from the tail. The vorticity distribution is complex just after the main wing in high-lift configuration. Nevertheless, only a few vortices remain at the position of tail wings, i.e., wing- and flap-tip vortices as well as vortices from the wing-fuselage junction. Only the vortex from the wing-fuselage junction has opposite rotation direction among the vortices at the position of the tail wings.

With this novel method we simulated the complete landing phase including final approach, flare, touchdown, and vortex decay. Figure 2(a) shows the roll-up process of the aircraft wake. The tracer is initialized at certain vorticity levels, depicting the vortex structure behind the aircraft. Wing-tip and flap-tip vortices as well as a vortex from the engine pylon and from the wing fuselage junction remain at the tail wing position, as strong coherent structures. Wing-tip and flap-tip vortices merge in the mid-field constituting the so-called wake vortices.

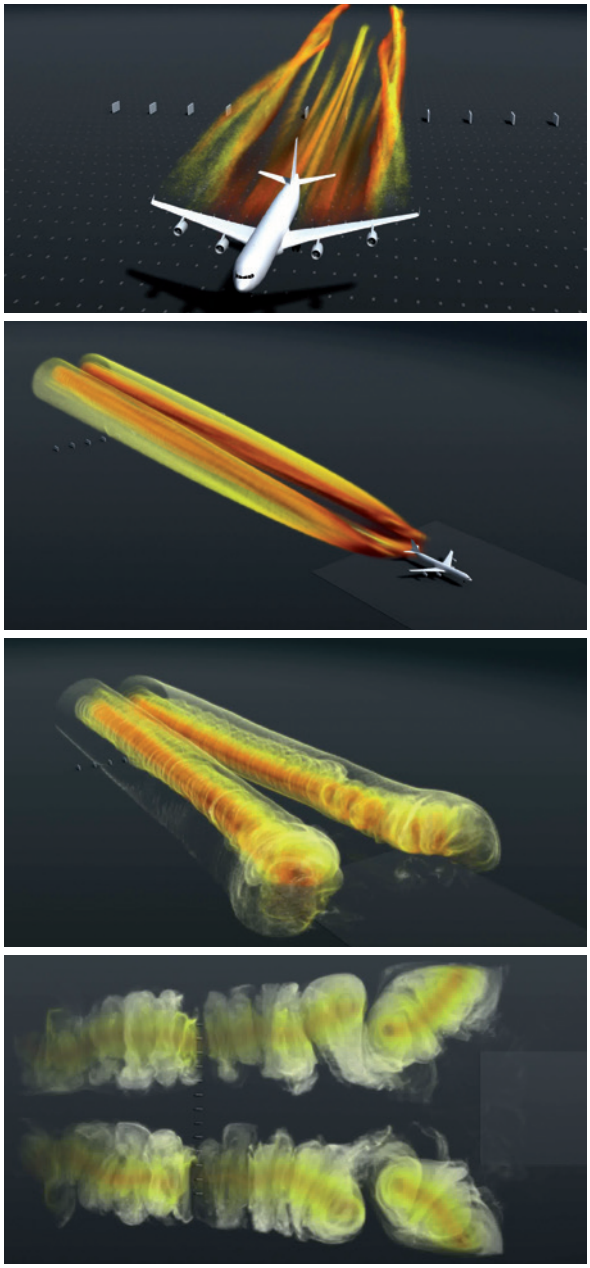

Figure 2: Spatial LES of landing with plate line (a) final approach, tracer initialized inside the wake vortex (b)-(d) touchdown and vortex decay, tracer initialized behind the aircraft wing, velocity of the tracer color coded.

Figure 2(b) depicts the instant of touchdown. The wake is initialized incorporating the approach and the lift reduction after touchdown. Regions of high velocities (red color), particularly dangerous for following aircraft, are around the vortex cores. After touchdown, Figure 2 (c), the vortices remain freely in space for a short time. At this instant so-called end effects appear from the touchdown zone, propagating against flight direction, weakening the wake vortex strength.

Figure 2(d) depicts the vortex decay phase of the wake vortices. Multiple ground linkings can be observed.

The introduction of a plate line at the ground surface substantially accelerates vortex decay [2] in the critical area close to the threshold where most vortex encounters occur, as shown in Figure 2(d). The reddish fraction of the vortices, indicating the potentially hazardous region, dissolves quickly. Figure 3 shows the reduction of vortex circulation along the final approach path. In flight experiments at the Airport Oberpfaffenhofen it was confirmed that the obstacles effectively accelerate vortex decay, see Figure 4 [3].

On-going Research / Outlook

The capabilities of SuperMUC enabled to reveal valuable insights into wake vortex physics in cruise and approach to airports. The results have been validated with flight measurement campaigns. Field experiments have shown that the number of plates should be sufficiently large to achieve a maximum efficiency of the plate line. In an ongoing study we aim to optimize the plate line design. For this purpose the flight tests have to be simulated as accurate as possible. In future aircraft landings will be investigated in even substantially increased computational domains.

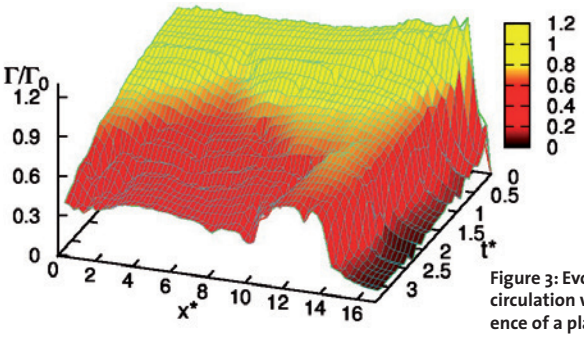

Figure 3: Evolution of vortex circulation with the influence of a plate line.

References and Links

[1] Misaka, T., Holzäpfel, F., Hennemann, I., Gerz, T., Manhart M., Schwertfirm, F., "Vortex Bursting and Tracer Transport of a Counter-Rotating Vortex Pair", Physics of Fluids, 2012

[2] Stephan, A., Holzäpfel, F., Misaka, T., "Aircraft Wake Vortex Decay in Ground Proximity -Physical Mechanisms and Artificial Enhancement," Journal of Aircraft, 2013

[3] Holzäpfel, F., Stephan, A., Körner, S., Misaka, T. "Wake Vortex Evolution during Approach and Landing With and Without Plate Lines", AIAA Paper 2014-0925

http://www.pa.op.dlr.de/wirbelschleppe/

Figure 4: Flight experiments at Oberpfaffenhofen airport, confirming the efficiency of plate lines.

Simulation of Turbulent and very Anisothermal Flow

Research Institution
CEA Grenoble DEN/DANS/DM2S

Principal Investigator
Benoit Mathieu

Researchers
CNRS-PROMES laboratory, Rambla de la thermodynamique, Perpignan France

Project Partners
–

LRZ Project ID: pr86bo (PRACE project)

Introduction

At the PROMES laboratory, we study the effect of very strong temperature gradients on the turbulence of wall bounded flows. This study is motivated by the flow characteristics inside solar receiver of concentrated solar power tower plants. As an example, PEGASE (Production of Electricity from GAs turbine and Solar Energy) is a technology of solar plant that uses pressurized air at very high temperature.

In the situation of high temperature gradients, the interaction between energy and momentum equations are strong and classical models are not valid anymore. The temperature gradient can be considered as a strong external agency that modifies the turbulence properties. In the case of low speed flow, only very few studies are dedicated to this coupling. In particular, there is no reference data that concerns subsonic flow without low Reynolds number effect and with dilatational effect due to strong thermal gradient.

Trio_U is a fluid mechanic c++ code designed for HPC with a natural MPI parallelization that allows to run over 10 000 cores. With a specific module developed for this project, the operator and pressure solver use SEE vectorization, IJK structured grid and a cache optimized multigrid solver that give us a speed up of 3 from the previous version of Trio_U.

Using Trio_U code, we run a large Direct Numerical Simulations (DNS). With this DNS, we will be able to study the thermal boundary layer in the case of dilatational flows. Furthermore, it can help to better understand the coupling between the dynamic and the thermal part in low Mach flows.

Results

In solar receiver air flows, the velocity dilatational effect is negligible and the thermal dilatation has strong effect. Consequently, we use the low Mach flow assumption (Ma<0.3). This implies that continuity, momentum and energy conservation equations are coupled. For the numerical point of view, the equations are coupled using a fully conservative algorithm that ensures local and global conservation mass and energy independently of the mesh.

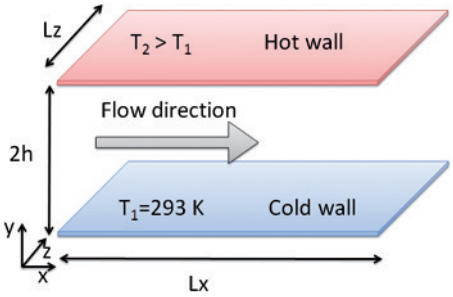

Figure 1: Channel flow configuration, thermal gradient is applied between the two walls.

Simulation set up
The time integration is done using a Runge-Kutta third-order scheme. The convective operators are centered fourth order for velocity and third order QUICK for mass.

We use a suitable geometry for the study of wall-fluid interaction: the bi-periodic channel flow (figure 1). The lengths of the channel are Lx=4πh, Ly=2h, and Lz=2πh. We apply a ratio between the two walls Tr=T2/T1=2. The turbulent Reynolds number (based on friction velocity) is 395.

The mesh is regular in periodic directions (1536 for x and 1536 for y) and hyperbolic in wall-normal direction (896 cells). The dimensionless first cell size is y+=0.125.

In total, the 2.1 billion cells are divided between 8192 cores (one whole island). This simulation has run over 500 k time step for a total time of 6 000 000 cpuhours. The multigrid solver uses 6 grid levels and a mixed precision method (3 simple precision iterations followed by a double precision iteration) consequently the domain is splited only on eight parts in wall normal direction (respectively 32 and 16 in x and y directions). The amount of data generated is around 8 To.

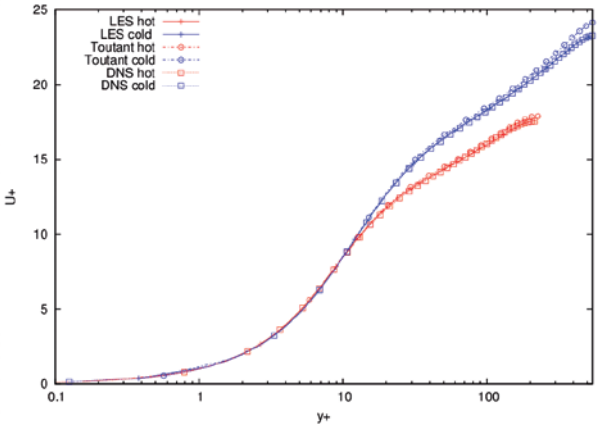

Figure 2: Normalized longitudinal mean velocity, cold side in blue, hot side in red. (Toutant curves represent the old algorithm DNS). Anisothermal channel flow at Re_τ = 395 and thermal rate T2/T1 =2.

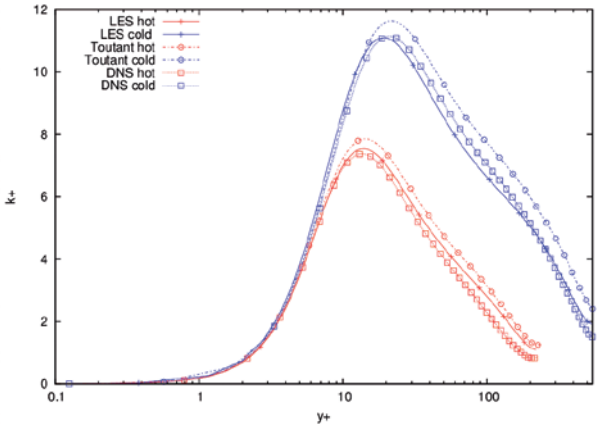

Figure 4: Normalized turbulent kinetic energy, cold side in blue, hot side in red. (Toutant curves represent the old algorithm DNS). Anisothermal channel flow at Re_τ = 395 and thermal rate T2/T1 =2

Simulation profiles

We have compared the results from the new DNS with an older DNS (5 times less cells and older algorithm) made by Toutant et al. [1] and a fine LES (100 times less cells and this study algorithm) computed on JADE cluster.

Figure 2 represents the mean longitudinal velocity. One can see only slightly differences between the two DNS and the LES. Represented on figure 3, the mean vertical velocity profile has a similar behavior than the LES simulation but the magnitude does not match. The magnitude of vertical velocity is directly linked with mesh accuracy and can explain the differences between DNS and LES. In the same time, the behavior and the magnitude are different between the DNS realized with the previous algorithm and with the new algorithm. This implies that the new algorithm modifies the behavior of vertical velocity in the channel.

For the root mean square profiles, we find that the DNS realized with the previous algorithm and with the new one match on streamwise and spanwise velocity and differ on vertical velocity and temperature. In the same way, the correlations including vertical velocity or temperature are slightly different between the two DNS. From these profiles, the LES has the same behavior than the new DNS with a magnitude error near to 5% on each component. The figure 3 represents the turbulent kinetic energy. It shows these differences.

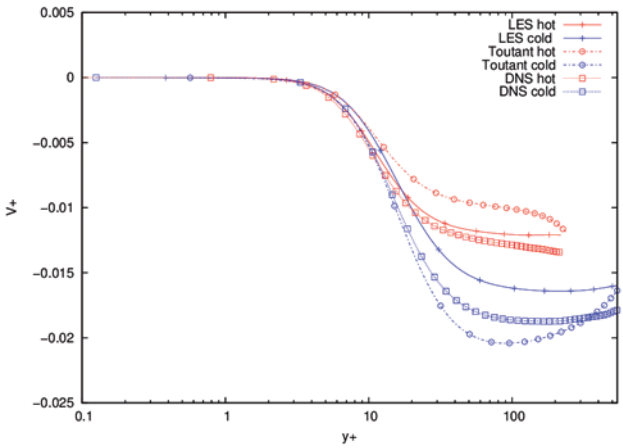

Figure 3: Normalized vertical mean velocity, cold side in blue, hot side in red. (Toutant curves represent the old algorithm DNS). Anisothermal channel flow at Re_τ = 395 and thermal rate T2/T1 =2.

On-going Research / Outlook

This very fine simulation constitutes a very interesting database. We will compare the DNS results with other LES and DNS. In the case of very anisothermal flows, the variations of fluid properties are important. It creates specific subgrid terms. It can be interesting to compute these terms usually neglected in subgrid models (like viscosity-velocity gradient correlation). With these terms, we should be able to improve thermal subgrid models for LES. Furthermore, we can study the turbulent kinetic energy equation in physical and spectral space. In addition, by comparisons to other setup (thermal rate, friction number, boundary conditions, geometry...) we will be able to understand the effects of the interaction between turbulence and temperature and propose some geometry modifications for solar receivers.

Finally, this academic work has for goal to improve the understanding on the coupling between turbulence and thermal gradient in low-Mach flows using numerical simulations. Following, this work is used to propose new innovative heat exchanger designs. Implemented in solar tower power plant, these exchangers will decrease the cost of electricity production by a better efficiency.

References and Links

[1] A. Toutant, F. Bataille, "Turbulence statistics in a fully developed channel flow submitted to a high temperature gradient", International Journal of Thermal Sciences, 74, 0, 104-118, December 2013.

Trio_U project web site:
http://www-trio-u.cea.fr/
Promes Laboratory web site:
www.promes.cnrs.fr

DNS of boundary layer transition in channel flow

Research Institution
Laboratoire de Mécanique des Fluides et d'Acoustique

Principal Investigator
Marc Buffat

Researchers
Anne Cadiou, Lionel Le Penven, Julien Montagnier

Project Partners
Université Lyon I, CNRS, Ecole Centrale de Lyon, INSA de Lyon, Villeurbanne, France

LRZ Project ID: pr86du (PRACE project)

Introduction

Since the famous Reynolds' 1883 experiment, the interest for stability of wall shear flows (boundary layers, plane channel or pipe flows) and their transition to turbulence has not weakened (Schmid and Henningson, 2001). Progress has come from new refined theories, often based on linearized theory and mathematical analysis, and their confrontation to reality. In this process, the use of computing has become essential, the simulations of Navier-Stokes equations having now raised to the status of numerical experiments (Durbin and Wu (2007), Wu and Moin (2010), Schlatter, Brandt, deLange and Henningson (2008)), sometimes more flexible than their physical counterparts. Accurate prediction of transition and turbulence however require highly resolved simulations to take into account the spatial development of the flow and analyze the transition scenario associated to nonlinear mechanisms that cannot be taken into account by linear stability theory. Therefore, such simulations need very large computational resources and the use of massively parallel supercomputer facilities.

The present project is focused on simulation of the transitional flow developing in the entrance region of a plane channel. The stability of the asymptotic plane Poiseuille flow (emerging far downstream) has been widely studied (Schmid and Henningson, 2001).

Entrance flows however significantly differ from the asymptotic Poiseuille flow. For uniform inlet flow conditions and at high enough Reynolds numbers, the turbulent transition actually takes place inside the boundary layers and relatively near the entrance and well before the fully developed regime. Since the boundary layers are distant, the nature of their transition and of their initial development is expected to have some similarity to the free-stream Blasius boundary layer case. For Blasius flow, the linear stability theory gives a critical Reynolds number at Re_x = 92 000 (Schmid and Henningson, 2001), but for entrance flows the boundary layers are modified, in particular because of the small favorable pressure gradient existing inside the plane channel. This is known to have a stabilizing effect on the boundary layers (Corbett and Bottaro, 2000). Another aspect of the entrance flows that differs from the Blasius case is linked to the fact that two boundary layers are actually co-existing in the velocity profiles. This raises the question of their mutual interaction in the transition scenario of the flow.

Results

The computational domain starts at a small distance x0 downstream from the channel entry . A set of 5 subcritcal values of the Reynolds number $Re_h = hU_o/nu$ has been explored in this project (from Re_h = 1250 to Re_h = 20000) for which the entrance flow is linearly stable in the channel entry zone. This was possible thanks to an allocation of 20.2 millions of core-hours. For all simulations, the Reynolds number $Rex = xU_o/nu$ is 40000 at the domain inlet, so that decreasing the Reynolds number Reh is equivalent to narrowing the walls of the channel.

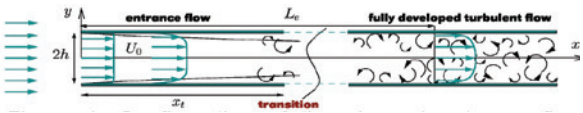

Figure 1: Configuration of the channel entrance flow, transition and evolution towards a fully-developed turbulent state.

The simulation of such a geometry for turbulent transition is a computational challenge because of the high-accuracy required by the physics and the very elongated domain needed to recover the fully turbulent regime. With a spectral accurate method, it typically takes from 1 to 2 billions of modes. For example, at Re_h=5000, the computational domain size of 150h x 2h x 3.2h require 17280 x 192 x 384 modes per velocity components (~ 1.3 billions of modes).

Spectral method has been widely used for turbulent transition studies since the past two decades. It has numerous attractive features such as accuracy, exponential convergence, vectorized computational efficiency or conservative properties, that matches the computational

requirements of transition and turbulence simulations. However, the parallelization of spectral method is inherently difficult because it requires global and non-local communications. As a result, efficient implementation of spectral methods on petaflopic high-performance distributed-memory computers is much more difficult than with local lower order method.

In our team, we have developed an efficient code, NadiaSpectral, based on a spectral Fourier-Chebychev Galerkin method and an orthogonal decomposition of the divergence-free velocity field into two orthogonal solenoidal velocity fields (Buffat, Le Penven and Cadiou, 2011). The parallelization is classically based on a bi-dimensional domain decomposition and uses MPI for message-passing among nodes and is fairly portable. An original explicit coarse grain parallelism using OpenMP for core shared-memory computation allows to get similar performances with pure MPI and hybrid parallelization on more than 65536 cores. Optimization has been done by implementing tasks parallelizations and overlapping communication and computation.

The simulations performed with this project have required about 16384 cores and contributed to the analysis of the transition at the entrance of the plane channel. They helped to characterize the stability of the flow evolving downstream from the channel entry at sub-critical Reynolds number. The transition is triggered by imposing inlet perturbations/, consisting of an optimal mode derived from the linear stability analysis and a white noise of smaller amplitude. The optimal mode consists of steady pairs of contra-rotating longitudinal vortices inside the boundary layers on the upper and lower walls, with a spanwise wavenumber of the order of the boundary layer thickness and zero streamwise wavenumber. It generates elongated streaks that reach sufficiently high amplitude during the transient phase to sustain secondary instabilities leading to turbulence. This scenario has been largely discussed in the literature for a Blasius boundary layer, where it is also described that the secondary instability of the streaks is either sinuous or varicose.

In our simulations, perturbations are imposed at the inlet of the computational domain, which is very close to the edge of the boundary layers. By doing so, it can be seen that even for very small amplitudes of the perturbation (less than 1% of the inlet free-stream velocity), very large amplitude of streaks can be reached very rapidly thereby strongly modifying the laminar base flow.

It has been found that for large amplitude of the optimal perturbation, streaks are subjected to a varicose secondary instability whose wavenumber is about $2\pi/h$. For smaller amplitudes of the optimal perturbation, the secondary instability is a sinuous instability whose wavenumber is half the optimal perturbation wavenumber.

For small Reynolds number Re_h, the optimal perturbation consists as expected in steady pairs of contra-rotating longitudinal vortices inside the boundary layers, but with a 180° phase shift between the upper and lower walls, that disappear at higher Reynolds number. This shows a coupling between the walls, the staggered placement of the vortices being favorable to a larger growth of the resulting streaks inside the boundary layers.

It has also been observed that the amplitude of the optimal perturbation scales with $1/Reh$. Moreover, the secondary sinuous instability is dominant at large Reynolds number, whereas for small Reynolds number, the transition is triggered by a varicose secondary instability.

Finally, the characteristics of the developing turbulence towards a fully developed state has been investigated. Once the transition is complete, the boundary layers merge at some distance downstream and the turbulence invades the whole channel width. If the Reynolds number is sufficiently high, the flow tends slowly to a fully turbulent state, statistically independent on the streamwise coordinate. Time statistics have been accumulated during the simulations to get the spatial evolution of the turbulent quantities and budget. These simulations could simply not have been run on the Tier-1 platforms. Their analysis is not finished yet.

On-going Research / Outlook

Massively parallel simulations generate increasing volumes of large data, whose exploitation requires large storage resources, efficient network transfer rates and increasingly large post-processing facilities. With the imminent arrival of exascale computers, there is an emerging need for new data analysis and visualization strategies. One solution consists in coupling analysis with simulation, so that both are performed simultaneously. In this perspective, we have set up a client-server in-situ analysis for massively parallel time-evolving simulations. On local Tier-2 resources, it is shown to have a low impact on computational time with a reasonable increase of resource usage, while enriching data exploration. Within a future Tier-0 project, we would be interested to migrate the analysis and explore how computational steering could be performed with real-time adjustment of the simulation parameters, in order to get closer to a numerical experiment process.

References and Links

[1] M. Buffat, L. Le Penven., A. Cadiou, and J. Montagnier. "DNS of bypass transition in entrance channel flow induced by boundary layer interaction", European Journal of Mechanics-B/Fluids, doi:10.1016/j.euromechflu.2013.06.009, June, 2013.

[2] A. Cadiou, M. Buffat, L. Le Penven, J. Montagnier, "DNS of Turbulent By-Pass Transition at the Entrance of a Plane Channel", Progress in Turbulence V, p59-64, 2013.

[3] J. Montagnier, A. Cadiou, M. Buffat, L. Le Penven, "Towards petascale spectral simulations for transition analysis in wall bounded flow", *Int. J. Numer. Methods Fluids,* doi:10.1002/fld.3758, December, 2012.

[4] M. Buffat, L. Le Penven, A. Cadiou, "An efficient spectral method based on an orthogonal decomposition of the velocity for transition analysis in wall bounded flow", Comput. Fluids, 42, 62-72, doi:10.1016/j.compfluid.2010.11.003, 2011.

High-fidelity simulations of multiscale-generated turbulence

Research Institution
Imperial College London, UK

Principal Investigator
J.C. Vassilicos

Researchers
Sylvain Laizet, Ning Li, Eric Lamballais

Project Partners
P' Institute, Poitiers, France and National Algorithms Group, UK

LRZ Project ID: pr86lo (PRACE project)

Introduction

After more than a century of exhaustive research on the aerodynamics and hydrodynamics of geometrically simple shapes, whether streamlined as in wings or bluff as in spheres/cylinders, it is blindingly natural to expect much of the future in fluid mechanics to lie in the aerodynamics and hydrodynamics of geometrically complex, and thereby multiscale, shapes. There has of course been work over the past decades on how to model and simulate complex turbulent flows, but the emphasis here is on working out rules for the design of multiscale objects so as to obtain desired flow effects beneficial for particular applications. The simplest cases of multiscale shapes are fractal, which is why they have been a good start. Multiscale/fractal generation/design is about using multiscale/fractal objects (grids, fences, profilers etc) to shape the nature of the resulting turbulent flow over a broad range of scales for a broad range of applications, such as:

1. Fractal mixers: fractal grids can be used to design turbulent flows with low power losses and high turbulence intensities for intense yet economic mixing over a region of designed length and location.
2. Fractal combustors: the fractal design of a long region of high turbulence intensity and its location are of great interest for premixed combustion and may pave the way for future fractal combustors particularly adept at operating at the lean premixed combustion regime where NOx emissions are the lowest. In fact results recently obtained at Imperial College 's Mechanical Engineering Department suggest that fractal design seems to generate turbulent flame speeds which increase by even more than the increase in turbulence intensities!
3. Fractal spoilers and airbrakes can have significantly reduced sound pressure levels without degrading the lift and drag characteristics of the wind system.
4. Fractal wind breakers and fractal fences: a fractal fence, for example, can have increased resistance, yet be an effective fence by modifying the momentum profilesin its lee and thereby forcing deposition of particulates, snow etc where desired.

Results

PRACE allocated 5,475,000 core hours on SuperMUC to this project and we managed to run six large simulations to investigate the turbulence generated by six grids (see figure 1) but also the stirring of a passive scalar in the presence of a mean scalar gradient.

To solve the incompressible Navier-Stokes equations that can predict fluid motions and the scalar transport

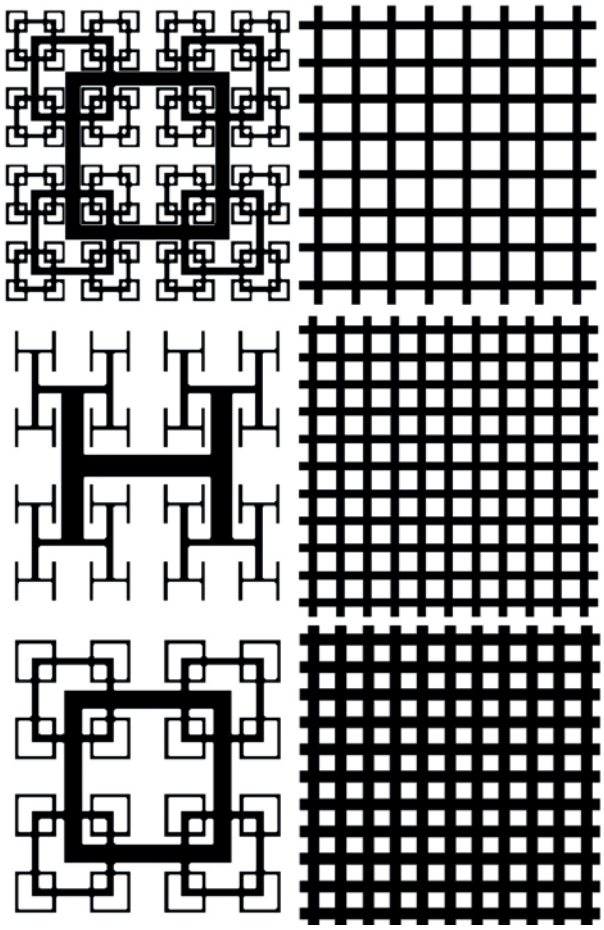

Figure 1: Diagrams of the six grids used in this study. More details about those grids can be found in [4].

equations, we use the in-house finite difference code **Incompact3d** [1] which is based on sixth-order compact schemes for spatial discretisation on a Cartesian mesh and a third-order Adams-Bashforth scheme for time advancement. To treat the incompressibility condition, a fractional step method requires to solve a Poisson equation. The main originality of this code is that this equation is fully solved in spectral space via the use of relevant 3D Fast Fourier transforms (FFT) which allows different sets of boundary conditions in each spatial direction for the velocity field and the scalar field. With the help of the concept of modified wavenumber, the divergence free condition is ensured up to machine accuracy. The modeling of the turbulence-generating grids is performed with an Immersed Boundary Method (IBM). The present IBM is a direct forcing approach that ensures the no-slip boundary condition at the wall of the grid. The idea is to force the velocity to zero at the wall and inside the grids as our mesh is Cartesian and therefore conforms with the geometry of the grids because they consist of right angles and are placed normal to the mean flow. Finally, the pressure mesh is staggered from the velocity one by half a mesh to avoid spurious pressure oscillations introduced by the IBM. More details about the present code and its validation, especially the original treatment of the pressure in spectral space, can be found in [2]. Because of the size of the simulations with up to 370 millions mesh nodes, the parallel version of the code has been used for this numerical work. Based on a highly scalable 2D decomposition library and a distributed FFT interface, it is possible to use the code on thousands of computational cores. More details about this efficient parallel strategy can be found in [3].

The unique simulations of unusual size gave us very valuable insight on the way turbulence develops. Those simulations showed us how turbulence is generated from three different fractal grids and three different regular grid. The simulations with the fractal grids revealed that the celebrated -5/3 energy spectrum famously predicted by Kolmogorov in 1941 [2] appears well before the flow is fully turbulence in the sense of vortex and strain dynamics. These develop further downstream as the -5/3 law progressively fades. The consequences of the results of these simulations on fundamental theory have the potential to be very far reaching as they will force a re-appraisal of turbulence dynamics. The post-processing of all the data gathered from these rare simulations has of course not finished yet and further results are expected to do, in particular, with interscale transfers. This post-processing is multifaceted and includes quite complicated post-processing codes to do, for example, with aeroacoustic predictions which will need some further time to come to fruition. Hence the full impact of the present simulations will not be complete for a few years to come, not only in terms of the data they have generated.

About the passive scalar investigation, the simulations shown that the pressure drop is about the same across grids of same blockage ratio irrespective of whether they are fractal or not (with the proviso that the pressure recovery is longer for the fractal grids). Even so, the fractal grids enhance turbulent scalar transfer by up to an order of magnitude downstream of the grid and they also greatly enhance the streamwise growth of the fluctuating scalar variance. The presence of such growth results from the persistence in time and space of the mean scalar gradient. Such fractal grids can be seen as an alternative to current static in-line mixers for fluid mixing and can also be used for mixing a fluid and a gas to create homogeneous end products. Target applications include the petrochemical industries for additive mixing; in waste and water treatment for aeration, sludge mixing and chemical addition as well as for generating powders in the pharmaceuticals industry.

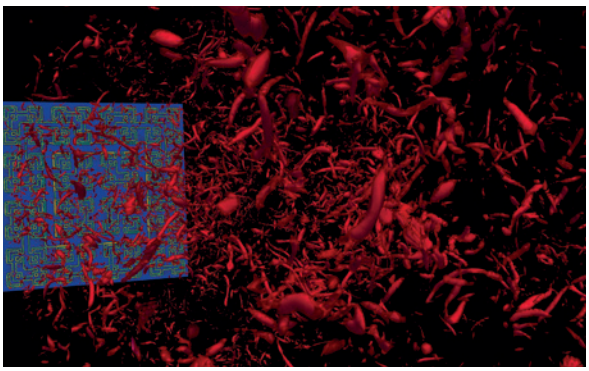

Figure 2: Turbulent flow generated by a fractal square grid in our virtual wind tunnel using 8,100 computational cores.

On-going Research / Outlook

Future works include experiments and simulations about turbulence interscale dynamics in non-equilibrium and equilibrium regimes with various types of turbulence cascade and interscale exchanges and evolutions, dissipation, vortex and strain-rate dynamics; related statistics of the multiscale topology within the turbulence; two-point and one-point turbulent theories and modelling and related turbulent flow profiles, self-similarity and self- preservation, and conservation laws; mixing and heat transfer by a new class of fractal/multi-scale stirrers which also define new canonical flows; aerodynamic forces and their fluctuations on ractal/multiscale objects and new types of wakes, jets and plumes. Both boundary-free and wall flows will be considered with a preference for spatially developing turbulent flows as well as interactions of different turbulent flows. Both fundamentals and applications will be considered, the latter including wind tunnel simulations of atmospheric flows, wind turbines, mixers and heat transfer devices.

References and Links

[1] http://code.google.com/p/incompact3d/
[2] Laizet S. & Lamballais E., 2009, High-order compact schemes for incompressible flows: a simple and efficient method with the quasi-spectral accuracy, J. Comp. Phys., 228(15), pp 5989--6015
[3] Laizet S. & Li N., Incompact3d, 2011, A powerful tool to tackle turbulence problems with up to o(10^5) computational cores, Int. J. of Numerical Methods in Fluids, 67(11), pp1735—1757
[4] Laizet S. & Vassilicos J.C., 2014, Stirring and scalar transfer by grid-generated turbulence in the presence of a mean scalar gradient, Submitted to J. of Fluid Mechanics

waLBerla – A massively parallel framework for fluid simulations

Research Institution
Chair for System Simulation (Informatik X), Friedrich-Alexander-Universität Erlangen-Nürnberg

Principal Investigator
Harald Köstler, Ulrich Rüde

Researchers
R. Ammer, D. Bartuschat, M. Bauer, C. Godenschwager, K. Pickl, F. Schornbaum

Project Partners
–

LRZ project ID: pr86ma (KONWIHR project)

Introduction

Injection and mixing processes at elevated pressures play Development of the waLBerla software framework [1] (widely applicable lattice Boltzmann solver from Erlangen) started almost 10 years ago as a joint effort of several researchers at the University of Erlangen-Nürnberg to provide a common basis for fluid simulation codes using the lattice Boltzmann method [2]. Over the years, the capabilities and the number of contributors also from other universities and institutes have grown and recently waLBerla became Open Source. Main applications of the software are

- blood flow in arteries,
- free surface liquid-gas flows such as bubbly flows or foams,
- particle suspensions like sedimentation processes, fluidization or colloids,
- potentials and charged particle agglomerates in flows,
- transport phenomena in porous media and complex geometries.

In order to be able to simulate real-world scenarios waLBerla relies on using an immense compute power only available on modern supercomputers. This is reflected in the architecture of waLBerla that was designed systematically in every step to run efficiently on massively parallel architectures like CPU or GPU clusters.

Results

In the last months we used SuperMUC for scaling experiments and production runs within several projects that are realized within waLBerla.

Blood flow in complex geometries [3]: Scaling experiments were conducted on regular and complex geometries obtained from medical data sets, where we achieved excellent weak and strong scaling results on SuperMUC performing up to 0.99 trillion lattice cell updates per second on the full machine (see fig. 1), currently the fastest LBM implementation that we are aware of.

Local refinement: Data structures and algorithms of waLBerla have been extended to support grid refinement for the lattice Boltzmann method. This new implementation was designed for massively parallel simulations and shows excellent scalability up to 147,456 cores of SuperMUC. Based on these algorithms, a study of flow in the vocal fold geometry was performed (see fig. 2). Due to refinement, the workload of this simulation was reduced by a factor of 98.6 compared to a simulation that uses a uniform grid. The simulation of the vocal fold runs for 864,000 time steps and performs 95.5 time steps per second (both on the finest grid level). Due to refinement, the simulation only requires 4,300 processes (instead of more than 100,000) and makes use of 10^8 fluid cells (instead of 5.5×10^9). Several runs for slightly different geometries and Reynolds numbers have been executed. Depending on the necessary post-processing, the output

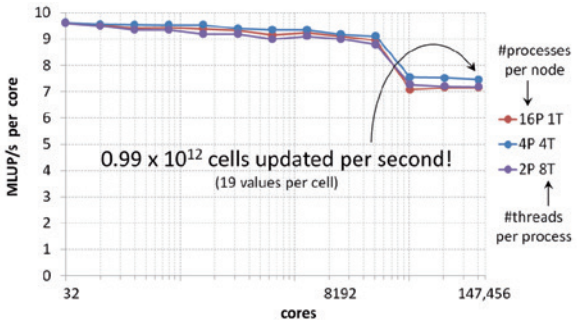

Figure 1: Weak scaling using a TRT lattice Boltzmann kernel on 3.43 million cells per core. Pure MPI as well as hybrid (MPI/OpenMP) approaches are compared.

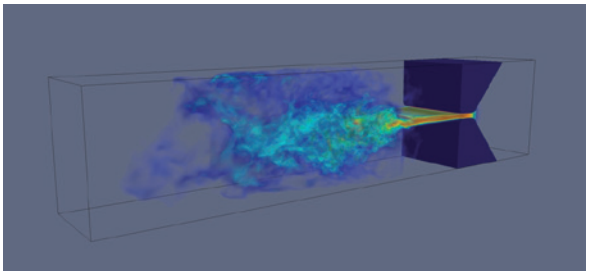

Figure 2: 3D direct numerical vocal fold simulation with a Reynolds number of 1000 and local refinement.

generates 1,000 to 1,000,000 files (on SCRATCH), ranging from just a few gigabytes up to 100 gigabytes.

The following applications couple waLBerla with the physics engine pe, a software package that is developed at LSS to simulate rigid multibody dynamics on massively parallel supercomputers.

Simulation of microscopic swimmers: The four-way coupling of waLBerla with the physics engine pe is used to simulate microscopic active swimmers. The latter are realized as three rigid particles connected by spring-like pair wise interactions. In particular the scalability of a new algorithm capable of handling spring-like pair wise interactions extending over more than one process domain was investigated [4]. A weak scaling of a setup of 2x8x8 swimmers per process from 4 to 2048 nodes was performed. We used an energy tag resulting in 2.5 GHz per core. A single run can take several hours due to the large number of time steps required for a realistic scenario, what leads to an amount of approximately 100,000 core hours for the total weak scaling.

Electron Beam Melting: A better understanding of the beam-powder interaction and improving building strategies by 3D lattice Boltzmann simulations are the most relevant target objectives of the EU Project FastEBM (High Productivity Electron Beam Melting Additive Manufacturing Development for the Part Production). Here, we simulated different hatching strategies (see fig. 3) of the electron beam gun with varying scan velocities and beam powers in order to find the best parameter set.

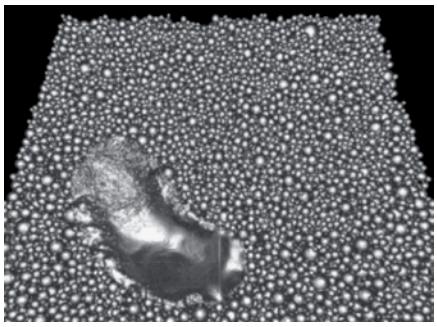

Figure 3: Simulation of melting metal powder by the electron beam.

Systematic weak and strong scaling tests of our thermal LBM software on SuperMUC have been conducted as well as numerous production runs to explore and develop improved technological process strategies. For these simulations we used approximately 100,000 core hours.
Charged particles in Poiseuille flow: *For performing a multiphysics simulation of charged particles in Poiseuille flow (see fig. 4), where the particles with a radius of 60µm are attracted by the oppositely charged surface and deposit there, a parallel geometric multigrid solver was included in waLBerla to solve a finite volume discretized Poisson equation for the electric potential. To resolve fluid-particle interaction, simulated with the momentum exchange method, the physics engine pe was coupled to waLBerla as well. On SuperMUC, weak scaling experiments were performed, showing good parallel scaling on up to 32,768 cores (4 thin-node islands). The experiments were executed several times on varying numbers of nodes and took about 6 minutes per run. Additionally, several simulation runs were performed to find parameters, such as the optimal number of coarsest-grid CG iterations, for all problem sizes. For these runs, about 10,000 core hours were used.*

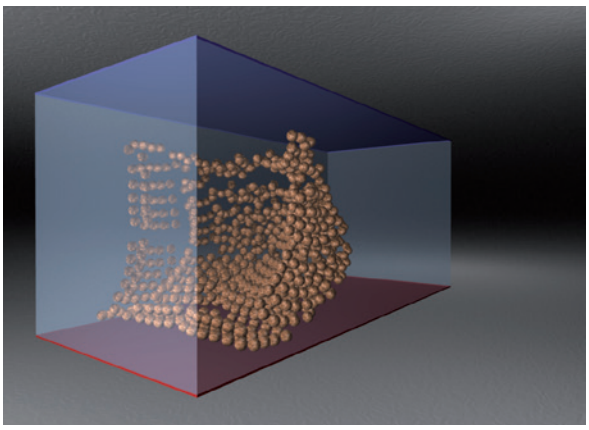

Figure 4: Multiphysics simulation of charged particles in Poiseuille flow subject to an electric field.

On-going Research / Outlook

SuperMUC allowed us to develop and test our code on one of the largest x86-based systems in the world. Scalability of our framework was only limited by the communication network's design, when using more than two islands (see fig. 1). Here the SuperMUC architecture exhibits an unfortunate bottleneck that limits its designated use as a top 10 supercomputer.

Besides application oriented projects outlined above, we are currently researching dynamic load balancing strategies and new algorithms that shall be incorporated into the waLBerla framework. In the future, we would like to integrate these in our applications and run them on SuperMUC. At this stage, an increasing number of production runs will be performed. For example, the swimmer scenario is now systematically explored in order to investigate collective hydrodynamic interactions resulting in swarm like-behavior. For this, the run time of a single run increases and additional file-I/O is necessary.

Furthermore, we currently put much effort into making all waLBerla features Open Source in order to increase its user base.

References and Links

[1] http://walberla.net
[2] Köstler, Rüde. 2013. The CSE software challenge – covering the complete stack. it – Inf. Techn. Meth. und innov. Anwendungen der Inf. und Inf.Techn., 55(3):91–96
[3] Godenschwager et al. 2013. A framework for hybrid parallel flow simulations with a trillion cells in complex geometries. In Proc. of SC13: International Conference for High Performance Computing, Networking, Storage and Analysis
[4] Pickl et al. 2013. Parallel simulations of self-propelled microorganisms. Advances in Parallel Computing, accept.
[5] Ammer et al. 2014. Simulating fast electron beam melting with a parallel thermal free surface lattice Boltzmann method. In Proc. of ICMMES-2012: Mesoscopic Methods for Engineering and Science, 67(2):318-330

http://www10.informatik.uni-erlangen.de

Computational acoustics of supersonic turbulent free round jets

Research Institution
Institute for Fluid Mechanics and Engineering Acoustics

Principal Investigator
Jörn Sesterhenn

Researchers
Juan José Peña Fernández

Project Partners
Institute for Fluid Mechanics and Engineering Acoustics, TU Berlin

LRZ project ID: pr86po (Gauss Large Scale project)

Introduction

Noise prediction is one of the most relevant topics for Computational Fluid Dynamics due to the fact that noise optimization, energy saving and pollutant emission minimization complement each other. In this project headed by Professor Jörn Sesterhenn of the Technische Universität Berlin, numerical simulations of a supersonic jet were performed on HPC system SuperMUC of LRZ, focusing on the research of the acoustic field.

The most accurate method to simulate this problem is based on Direct Numerical Simulation. However, this kind of simulation requires a huge amount of computational resources which to date are not available to most of the researchers or the industry. To overcome these limitations, a feasible approach to said problem is based on Large Eddy Simulations (LES). The downside of LES, however, is that only the large scales of the problem are solved whilst the small structures created by the turbulence are modeled with a mathematical algorithm. This is due to the fact that the small structures show universal behavior for high Reynolds numbers in which the large scales are decoupled of the small ones.

Of special interest in this project was the so called *'near to intermediate field'* in which the acoustic properties can be directly related to the fluid structures that generate these acoustic waves.

The main objective of this project is to describe the noise generation mechanisms that take place in the supersonic jet case. The so called *'turbulent mixing'* noise is created in both subsonic and supersonic jets. Turbulent mechanisms in the shear layer of the jet are the main reason for noise generation. This kind of noise is mainly radiated downstream of the jet. If a supersonic jet is not in adapted condition, a quasi-periodic structure with shock-waves is generated. These shock-cell structures generate some additional noise, which shows two different characteristics depending on the generating mechanism. *'Broadband shock-associated'* noise radiates mainly in upstream direction and is generated by the present shock-cell structure. The other mechanism is the one that is being referred to as *"screech"*. This is a single frequency tone which is the result of a feedback loop at the nozzle exit. The generated noise and the eddies which are detached from the shear layer generate a single frequency tone. Depending on the relative velocity of the jet to the speed of sound, different large coherent structures are present in the flow field, and the noise mechanism change. Examples of such structures are single or double helical modes and toroidal modes.

Results

For free round jets focusing the near to intermediate field, a simulation should be performed in a box of dimensions 25**D** x 15**D** x 15**D** (while **D** is the diameter of the nozzle exit). In our case, a grid of 2048 x 1024 x 1024 = 2.1 billion cells was necessary. To perform the needed statistics, we had to run the simulation for a minimum of 30.000 time steps. This means that 2.1 billion points and the governing equations had to be solved at every individual time step. Taking all these factors into account, this simulation required at least 22.9 million CPU hours which means this project would have taken more than 2614

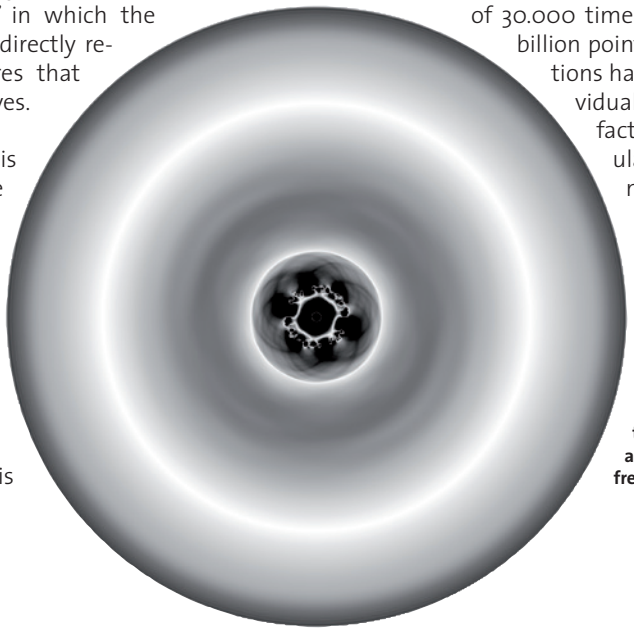

Figure 1: In the first stage of the jet, the first acoustic wave is shown over a plane normal to jet axis. In addition, the shear layer can be seen and the turbulent structures that in the shear layer are generated. The region in which the acoustic phenomena are radiated can be also perceived. Direct Numerical Simulation of a free round jet with Reynolds number 10.000.

years to compute if executed on a single CPU system. Thanks to now available petascale HPC systems like SuperMUC of the LRZ, though, projects of this magnitude can be tackled. Due to the fact that on SuperMUC more than 8000 CPUs simultaneously computed the numerical solution, we were able to execute this project within the time frame of just one year.

The simulations were performed with a self developed code, written in FORTRAN language, that solves the compressible Navier-Stokes equations in characteristic formulation with finite differences. For this case is especially important to have a high order numerical code in order not to damp the acoustic waves that we try to investigate. Our code is sixth order and compact in space, and through a Runge-Kutta time integration routine we have fourth order in time.

In this project, both Direct Numerical Simulations (DNS) and Large Eddy Simulations (LES) are performed. The DNS are essentially the reference of the problem in which we are interested. With them we infer the physical phenomena that are occurred and we get more information about the noise generation process. The Large Eddy Simulations are the feasible solution for the current industry problems. Today DNS are not affordable for the industry, and therefore only the academia is able to perform this kind of simulations. The problems that the industry have to face, the academia is not able to solve, but in this context the Large Eddy simulations are the wire that connect both of them. In order to run enough accurate LES, the mathematical models behind have to be developed and validated, and this is exactly the aim of this part of the project, the validation of two LES models.

The most important finding of this project is the difference between the structures that are generated in the shear layer in a turbulent jet in comparison with a laminar one. The spatio-temporal evolution of these structures, and more specifically the effect that these structures have in the radiated noise is under detailed investigation. In figure 1 the shear layer has a hexagonal shape in which different noise sources can be identified. Around the shear layer a ring can be identified. This ring is the region in which the noise generated has been radiated, but due to the early stage of the fluid flow, the noise has not yet reached the whole domain. The big circle shown in figure 1 is the first acoustic wave that is generated when the jet starts.

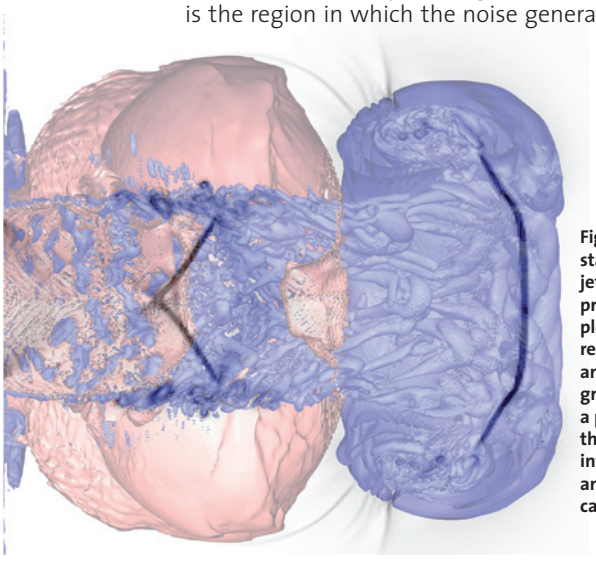

Figure 2: In the starting stage of the free round jet, Q-criterion and pressure isosurfaces are plotted in blue and red, respectively. In black and white the density gradient is presented as a pseudo-schlieren over the mean plane. Here the interaction between flow and acoustic phenomena can be observed.

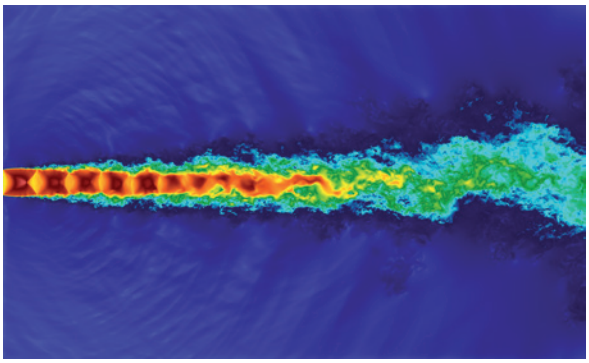

Figure 3: Continuous stage of the free round jet. Contour of velocities in logarithmic color scale. The flow phenomena as well as the acoustic ones can be clearly seen in this dual image.

Of special interest is also the first vortex ring that is generated because of the expansion when the first stage of the jet passes through the nozzle exit. In figure 2 an isosurface of the Q-criterion has been plotted in blue. In this figure a lot of structures that belong to the vortex ring can be identified.

Another relevant finding is that strong pressure perturbations are attached to the rear part of the vortex ring and this is the reason why some slots are formed in this region of the vortex ring. In figure 2 one can see how the center of the pressure perturbations, plotted in this figure as red isosurface, have their center on the shear layer, and more specifically where the shock-waves are present. In a supersonic jet, both the shear layer and the shock-cell structure contribute to the noise generation process. In this project we expect to identify more accurate the process of noise generation by investigating in detail the structures of the shear layer and the acoustic field.

On-going Research

The most important limitation of this project has been the WORK disk space. In order to investigate the statistically steady regime of the jet, more than 30000 time steps have to be taken into consideration. This problem was overcome by doing the statistics during the simulation take place. In the close future, an extensive post-processing of all the generated data will be done. Special focus on the present structures of the shear layer will be made and the global objective of the post-processing stage is the deep understanding of the involved phenomena of the noise generation process.

References and Links

[1] Sesterhenn, J. 2000. A characteristic-type formulation of the Navier-Stokes equations for high order upwind schemes. *Computers and Fluids.*

[2] Schulze, J and Sesterhenn, J. 2011. Adjoint based noise minimization of a round supersonic jet. *Journal of Physics: Conference Series*

LES of cavitating turbulent flow in fuel injection systems

Research Institution
Institute of Aerodynamics and Fluid Mechanics, Technische Universität München

Principal Investigator
Christian Egerer

Researchers
Felix Örley, Matthias Thalhamer, Steffen Schmidt, Stefan Hickel, Nikolaus Adams

Project Partners
–

LRZ project ID: pr86ta, pr95ma

Introduction

Cavitation occurs when the liquid fuel is accelerated through throttles or valves and the static pressure drops below the vapor pressure. Closing of valves, for example, results in a collapse-like recondensation of vapor. During this process, high-momentum liquid jets and strong shock waves are generated which can damage material surfaces and lead to failure of the injection device.

The present research project focuses on the prediction of cavitation erosion in fuel injection systems. Wave dynamics, interaction of cavitation and turbulence as well as flow transients due to moving geometries need to be investigated in order to account for all effects related to cavitation erosion.

Results

All results presented below have been computed with our in-house code INCA [1] which solves the compressible Navier-Stokes equations for a homogeneous mixture of liquid and vapor by means of a 3D finite volume method on adaptive Cartesian grids. Complex geometries are represented by a conservative immersed interface method [2]. Parallelization is achieved by domain decomposition and communication by the MPI standard.

Turbulent Cavitating Flow in a Generic Throttle
Large-eddy simulations of turbulent cavitating flow in a generic throttle [3] have been performed. Two different operating points which can be discriminated by their pressure difference (300 to 115 bar, and 300 to 55 bar), have been investigated. The main goal of this study was to investigate the influence of turbulence on cavitation and vice versa. The locally refined computational mesh consists of roughly 30 million cells decomposed into 1290 blocks. The computations were run on 832 CPUs on SuperMUC's thin nodes. Code testing, grid sequencing, and development of the flow field until statistics could be computed consumed roughly 1 Mio CPUh per operating point. Gathering of statistical quantities consumed another 0.5 Mio CPUh per operating point.

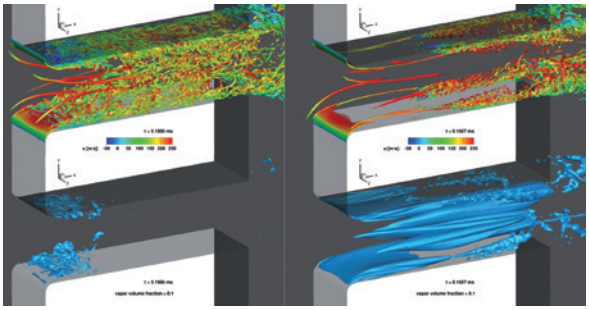

Figure 1: Instantaneous turbulence (top) and cavitation structures (bottom) in a generic throttle valve. Pressure difference 300 to 115 bar (left) and 300 to 55 bar (right).

At low pressure difference, we observe periodic formation of vapor in the vortex cores of the detached shear layer at the throttle inlet, see left side of Fig. 1. When the pressure difference is increased, right side of Fig. 2, a stable vapor sheet develops at the throttle inlet. Furhtermore, cavitation is observed in the corner vortices of the throttle. In the center of the throttle, cavitation in vortices originating from roll-up of the oncoming boundary is observed. By comparing both operating points, the change in flow topology by cavitation is illustrated: while turbulence and vortex dynamics play a dominant role at low pressure differences, the formation of a stable sheet cavity and cavitating vortices suppress turbulence at high pressure differences.

Cavitating Flow in Moving Geometries
Current studies on components of Diesel injection systems focus on cavitation effects at single operating points within the static nozzle. Andriotis et al. [4] investigated different, but static, needle positions, thus controlling the effect of both flow rate and geometrical configuration. They showed that including the region upstream of the injector holes leads to a highly unsteady flow behavior and conclude that the actual flow rate through the injection nozzles can largely vary due to the occurrence of cavitation strings, which sensitively respond to the needle lift and the nozzle geometry.

Since the geometry of injection systems largely varies during one cycle, it can be assumed that the flow characteristics inside the nozzles is significantly affected by interactions with the moving needle surface as well as the complex geometry change during one injection cycle. Therefore, the full system including a moving injection needle with a prescribed motion should be taken into account when investigating the performance of diesel injection systems.

In a first step, our immersed interface method was supplemented with the ability to treat moving geometries. Hereby, the geometrical properties (face-apertures, volume fractions...) oft he cut cells are directly computed from a user-defined STL-geometry file, which is a necessary upgrade from the previous method based on a level-set field [2]. The implementation was validated against common test cases, such as a cylinder oscillating in a resting fluid at Re=40 or the flow over an inline-oscillating cylinder at Re=100.

Towards the long-term goal of simulating a full injector geometry, we first put a focus on the simulation of a simplified ball valve. This case was chosen for assessing the ability of the method to capture cavitation structures on moving interfaces. The fluid domain was initialized as a Riemann-problem causing an expansion wave travelling to the left into the inflow-domain creating a steady liquid flow through the gap. The valve is then closed with different closing velocities. Results for the iso-contour of vapor fraction (left column) and Q-criterion colored by axial velocity (right column) is shown in Fig. 2. The figures show the flow conditions at a ball position of x = 0.09 mm for a stationary ball (top), a closing velocity of 1 m/s (center) and 5 m/s (bottom). Clearly the velocity of the ball plays a significant role in the turbulence transition process, which in turn causes a different behavior of the vapor sheet.

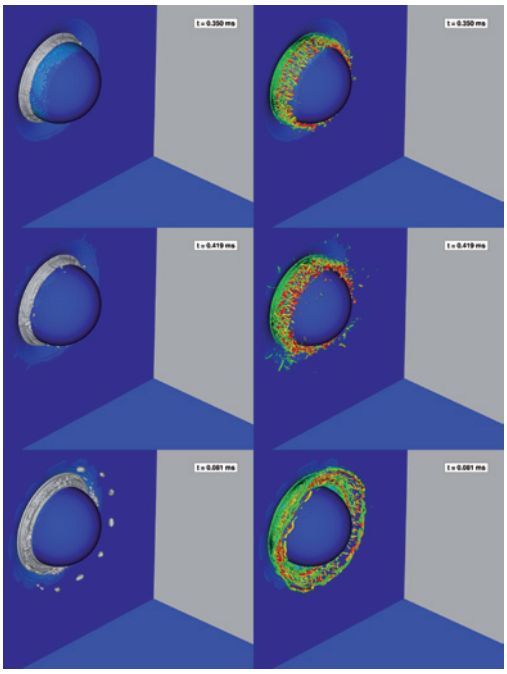

Figure 2: Simplified ball valve. Iso-contours of vapor volume fraction and Q-criterion colored by axial velocity for stationary case (top), 1 m/s (center), and 5 m/s closing velocity (bottom).

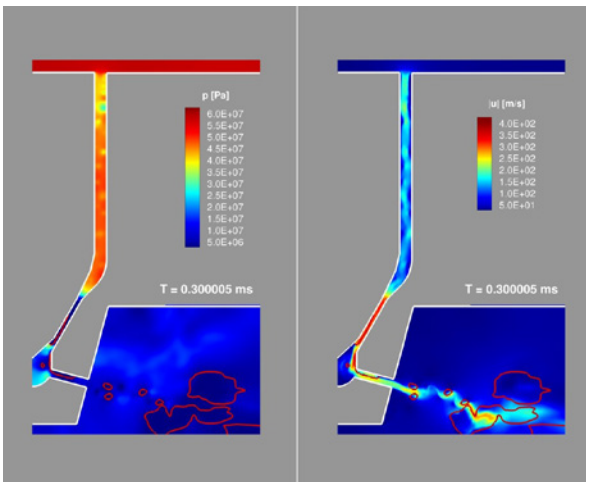

Figure 3: Pressure (left) and velocity magnitude (right) at fully opened needle position.

As a next step we moved towards realistic injector geometries. We first consider a 2D model with reduced complexity. The problem is initialized with an initial pressure difference from 600 bar to 26 bar and a fully closed needle. From the initially closed state, we apply a forced body motion of a realistic opening process of a high-pressure diesel injector. Up to now, we are using a relatively coarse mesh to save computational time while evaluating important aspects of our numerical method, such as opening or closing of gaps and correct computation of geometrical parameters in cut cells. The demonstrator test case shows the ability of our code to treat small gaps between stationary and moving obstacles up to a full closing and suppressing of flow.

The fully opened state is shown in Fig. 3. Shortly after the opening phase a stationary flow is obtained in the channel. The flow is dominated by growing and collapsing vapor sheets, which goes hand in hand with compression- and shock-waves that interact with the formation and shedding of vapor in a complex way. During the injection phase, we observe a periodic shedding behavior of the vapor sheet in the nozzle, which is characteristic for this kind of application.

On-going Research / Outlook

In the future, we will move towards realistic three-dimensional injector geometries and compare the results to experimental observations and findings.

References and Links

[1] S. Hickel, M. Mihatsch, and S. Schmidt. 2011. Implicit Large Eddy Simulation of Cavitation in Micro Channel Flows. In *Proceedings of WIMRC 3rd International Cavitation Forum*. Warwick, UK.

[2] M. Meyer, A. Devesa, S. Hickel, X. Y. Hu, and N. A. Adams. 2010. A conservative immersed interface method for Large-Eddy Simulation of incompressible flows. *J Comput Phys* 229,18, 6300–6317. DOI:http://dx.doi.org/10.1016/J.Jcp.2010.04.040

[3] AVL List GmbH – AVL. 2006. Experimental and CFD technology for preventive reduction of Diesel engine emissions caused by cavitation. Technical Report NNE5-2001-00451.

[4] A. Andriotis, M. Gavaises, and C. Arcoumanis. 2008. Vortex flow and cavitation in diesel injector nozzles. *J Fluid Mech* 610, 195-215. DOI:http:/dx.doi.org/10.1017/S0022112008002668

http://www.aer.mw.tum.de
https://inca-cfd.com

Lagrangian Space-Time Methods for Multi-Fluid Problems on Unstructured Meshes *(STiMulUs)*

Research Institution
University of Trento (via Mesiano, 77 – 38123 Trento)

Principal Investigator
Michael Dumbser

Researchers
Olindo Zanotti and Walter Boscheri

Project Partners
–

LRZ project ID: pr89mo (PRACE project)

Introduction

Several problems and phenomena in engineering as well as in physics are governed by hyperbolic partial differential equations (PDEs), including fluid dynamics, whose conservation laws can be formulated using either an Eulerian approach, where the fluid motion is looked and analyzed from a fixed location, or a Lagrangian approach, in which the observer moves together with a fluid particle.

The main advantage of working in a Lagrangian framework is that material interfaces and contact waves can be precisely identified and located, hence achieving a much better resolution rather than adopting the classical Eulerian formulation. For this reason a lot of research has been carried out in the last decades in order to develop Lagrangian numerical schemes, which can be derived starting directly from the conservative quantities such as mass, momentum and total energy or from the non-conservative form of the governing equations. Lagrangian schemes have been designed and developed in order to compute the flow variables by moving together with the fluid. As a consequence the computational mesh continuously changes its configuration in time, following as close as possible the flow motion by moving with a mesh velocity that must be carefully assigned. Sometimes the flow motion becomes very complex, hence highly deforming the computational elements of the grid, that may be compressed, twisted or even tangled. For such control volumes the mesh size might be drastically reduced, hence leading to very severe CFL stability restrictions on the time step and slowing down the computation. Therefore the challenge of any Lagrangian numerical scheme is to preserve at the same time the excellent properties in the resolution of the fluid flow typically achieved by Lagrangian algorithms together with a good mesh quality without invalid elements. Rezoning techniques are typically used to improve the mesh quality. Our research focuses on the development of finite volume Lagrangian numerical schemes on multidimensional unstructured meshes for fluid dynamic problems, solving the compressible Euler equations for gas dynamics and the ideal classical as well as the relativistic equations for magneto-hydrodynamics. Multi-phase flows are also considered with the seven equation Baer-Nunziato model which governs the interaction between two fluid phases.

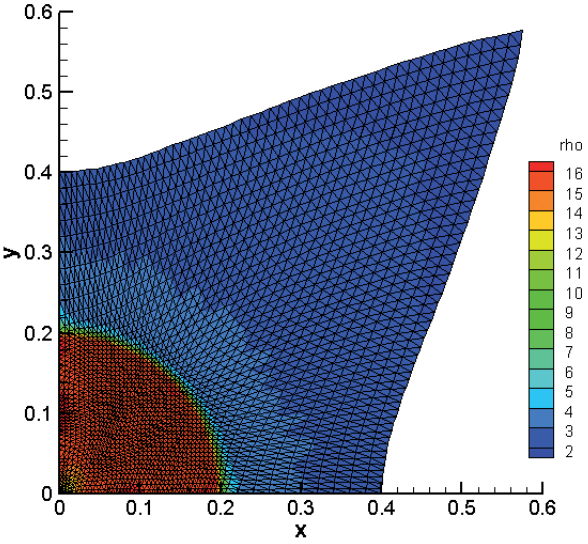

Figure 1: 3rd order density (rho) distribution for the 2D Noh problem. Such test case consists in a diverging shock wave traveling from the origin to the boundaries of the domain, which is filled with gas moving with unity velocity along the radial direction towards the origin.

The numerical algorithms developed in our research group are designed to be high order accurate in space as well as in time, requiring even more information to be updated and recomputed continuously as the simulation goes on.

Due to the above-mentioned procedures and techniques, Lagrangian schemes are typically very demanding in terms of computational efforts. Therefore one should rely on an efficient MPI parallelization of the entire code in order to take advantage from the computational resources of supercomputers like "SuperMUC".

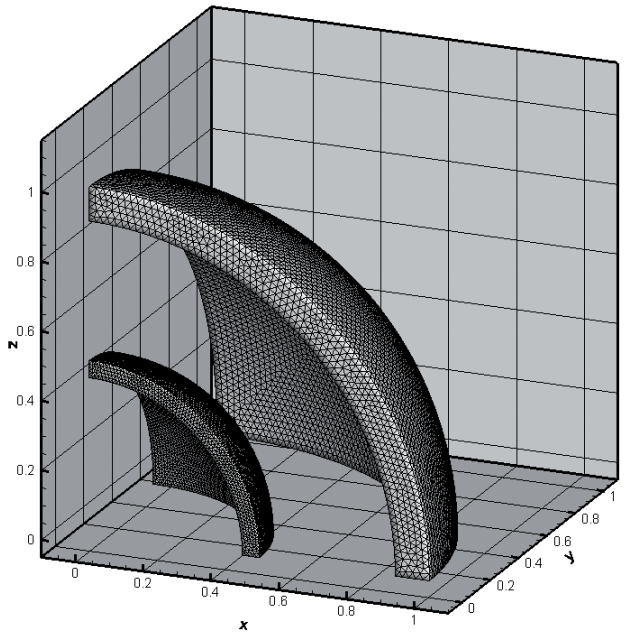

Figure 2: 4th order computational domain for the 3D Kidder problem at the initial (external shell) and final (internal shell) time. The Kidder problem involves an isentropic compression of a shell filled with ideal gas.

Results

PDESol is the name of our code, used for all the simulations that have been run on SuperMUC within the project "STiMulUs". The algorithm is based on its Eulerian version developed by the PI [1]. It is designed to reach arbitrary high order of accuracy, relying on a WENO reconstruction technique for multidimensional unstructured meshes to achieve high order of accuracy in space, while using the local space – time Galerkin predictor on moving meshes to obtain high order accurate schemes also in time. Here, an element – local weak formulation of the governing PDE gives the predicted numerical solution within each control volume. Since such a procedure is carried out locally, i.e. within each element, it can be easily and efficiently parallelized. The mesh motion is computed using a node solver algorithm, that aims at assigning a unique velocity vector to each vertex of the computational grid. In order to keep the algorithm as simple as possible, the mesh motion of each element is constructed by straight edges connecting the vertex positions at the old time level with the new ones at the next time level. A rezoning algorithm is used in some cases to overcome mesh tangling or high element deformations. Our finite volume Lagrangian schemes falls into the category of Arbitrary-Lagrangian-Eulerian (ALE) methods, where the mesh velocity does not have necessarily to coincide with the local fluid velocity, but it can be arbitrarily chosen.

We firstly developed the two-dimensional version of the algorithm on moving triangular meshes for conservative [2] and non-conservative [3] balance laws. In [4] we also considered the MHD equations and finally we have extended the schemes to tetrahedral meshes.

We applied for 3 Millions of CPU-hours at SuperMUC under the PRACE 6th call and for our jobs we typically used a total number of *Nc*=1024 cores. At fixed output times *PDESol* prints only one output file, written by the master node, and *Nc* restart files as checkpoints, needed to carry on the computation from that output time on. For Lagrangian schemes we have to record at each time step not only the values of the physical variables, but also the geometry, i.e. the mesh configuration that has changed w.r.t. the initial computational grid. The storage needed in SCRATCH was less than 5TB for each job, since the same restart files are overwritten at each output time. We perform some classical Lagrangian test cases for hydrodynamics, such as the 2D Noh problem depicted in Figure 1 and the 3D Kidder problem shown in Figure 2. We used at most a total number of control volumes of about 7.2 Millions for running an explosion test case for gas dynamics in three space dimensions, see Figure 3.

On-going Research / Outlook

The research field of the "STiMulUs" project is very challenging but also very promising. The results obtained so far allows us to plan further developments and improvements to our current numerical schemes. We would like to extend to moving curved elements the already existent multidimensional algorithm and then simulate several real world applications, such as complex free surface flows, industrial applications, aerospace engineering as well as hydroelectric and wind energy production systems, etc. We have already applied for a follow-up project in order to continue working on the excellent SuperMUC architecture.

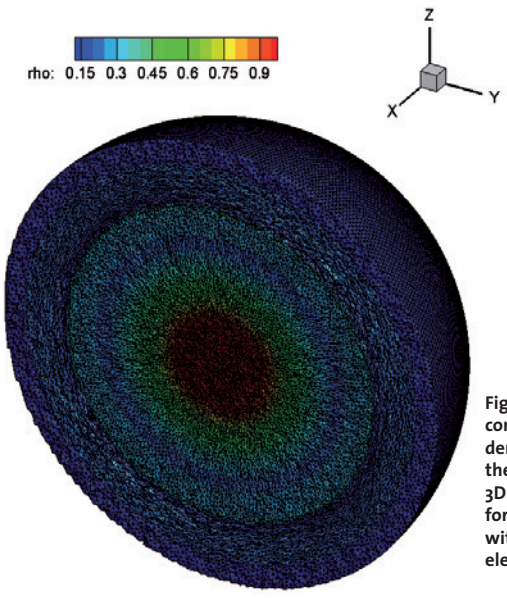

Figure 3: 4th order mesh configuration and density distribution at the final time of the 3D explosion problem for the Euler equations with a total number of elements of 7225720.

References and Links

[1] Dumbser M., Balsara D.S., Toro E.F., Munz C.-D., Journal of Comp. Phys. 227: 8029-8253, 2008.
[2] Dumbser M., Zanotti O.,
[2] Boscheri W., Dumbser M., Commun. Comp. Phys. 14: 1174-1206, 2013.
[3] Dumbser M., Boscheri W., Computers and Fluids 86: 405-432, 2013.
[4] Boscheri W., Dumbser M., Balsara D.S. "High-Order Lagrangian ADER-WENO Schemes on Unstructured Meshes – Application of Several Node Solvers to Hydrodynamics and Magnetohydrodynamics." Submitted to Journal for Num. Meth. In Fluids.

High Energy Physics

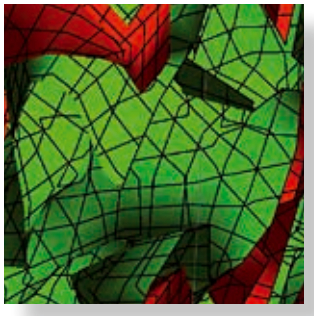

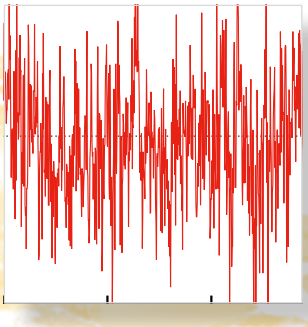

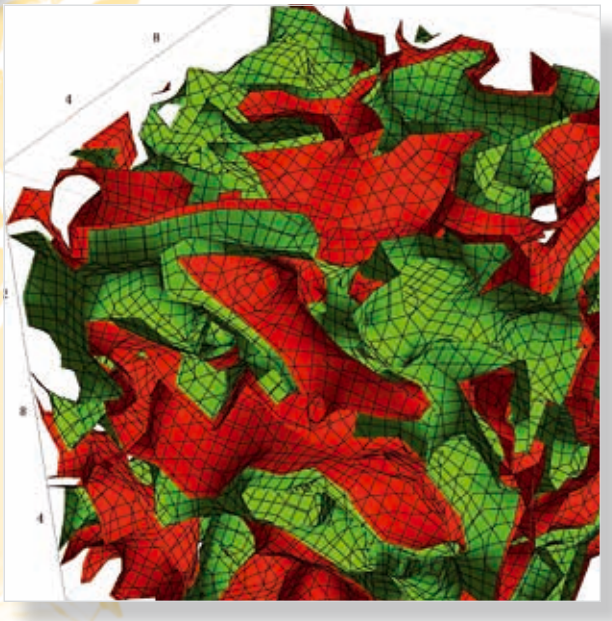

Simulation of $N_f = 2 + 1$ lattice QCD at realistic quark masses

Research Institution
Deutsches Elektronen-Synchrotron DESY

Principal Investigator
Gerrit Schierholz

Researchers
Roger Horsley, Yoshifumi Nakamura, Dirk Pleiter, Paul Rakow, James Zanotti

Project Partners
University of Edinburgh (UK), Riken (Japan), FZ-Julich and University of Regensburg (Germany), University of Liverpool (UK), University of Adelaide (Australia)

LRZ Project ID: h006z

Introduction

In this project we extend previous simulations of $N_f = 2 + 1$ flavors of dynamical fermions [1] close to physical up (m_u), down (m_d), and strange quark masses (m_s) and to large volumes. The overall program is to explore, and quantitatively describe, the physics of light hadron flavors. This includes the hadron spectrum, in particular resonances, hadron structure, as well as precision tests of the Standard Model.

A distinctive feature of our simulations is the way we tune the light and strange quark masses. We have our best theoretical understanding when all three quark flavors have the same masses, because we can use the full power of flavor SU(3). Nature, however, presents us with only one instance of the theory with $2m_s/(m_u+m_d)$ approximately 25. Starting from the SU(3) symmetric point, we are interested in interpolating between these two cases. Our strategy is to keep the singlet quark mass $m=(m_u+m_d+m_s)/3$ fixed at its physical value. We find this choice particularly useful and instructive as we approach the physical point, as both light and strange quark masses are varied over a wide range. SU(3) chiral perturbation theory should also work well in this domain, as the K and eta mesons are lighter than their physical values along our entire trajectory and approach their final values from below. In contrast, the procedure followed by most other collaborations is to first tune the strange quark mass m_s to its physical value and then vary the up and down quark masses. This approach, however, has several drawbacks.

Results

We use the clover action with a single iterated mild stout smearing as described in [2], which we call SLiNC fermions. We are mainly interested in the case of mass degenerate light quarks, $m_u=m_d=m_l$. The SLiNC action has exact flavor symmetry, which facilitates simulations at or close to the physical quark masses and exploring the physics of flavor. Our numerical results obtained so far are at two couplings, β=5.5 which corresponds to a lattice spacing of approximately 0.08 fermi, and β=5.8 which corresponds to approximatly 0.065 fermi.

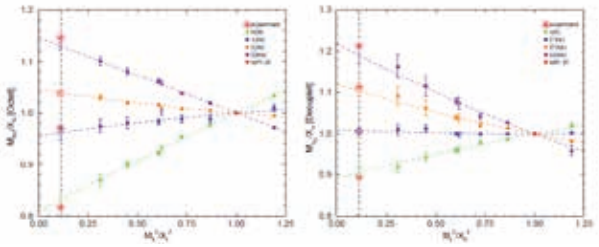

Figure 1: Nucleon octet (left) and decuplet (right) masses as a function of pion mass normalized to the singlet quantities $X_N=(M_N+M_\Sigma+M_\Xi)/3$ and $X_\Delta=(2\,M_\Delta+M_\Omega)/3$.

In Fig. 1 we show a plot of the masses of the baryon octet as well as the decuplet from quark masses just above the SU(3) symmetric point down to the physical point, along the trajectory m = constant. Fan plots are seen with masses radiating from the common point at $m_l=m_s$. Although we have included quadratic terms in the fit, there is really very little curvature in the results. In both pictures the correct ordering of masses is achieved. In particular in the right picture we see that the Lambda-Sigma splitting is correct. The absence of curvature tells us that the Gell-Mann-Okubo mass relations work extremely well all the way from the SU(3) symmetric point to the physical

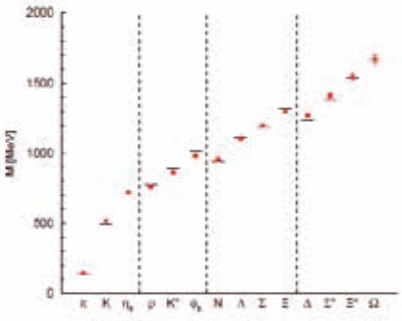

Figure 2: Hadron masses at the physical point.

point. In Fig. 2 we show our final results for the hadron masses at the physical quark masses and compare them with the experimental numbers. The scale has been set by the average mass of the nucleon octet. We find excellent agreement with experimental numbers.

In the context of ongoing dark matter searches, improved knowledge of the strangeness scalar content of the nucleon would lead to more constrained cross sections. Benchmark models show variation of the WIMP-nucleon cross section over an order of magnitude with respect to variation of the strangeness sigma term. As our approach of keeping the singlet quark mass constant in the simulations and using an SU(3) flavor symmetry breaking expansion gives highly constrained fits for hadron masses in a multiplet, this is an advantageous procedure for determining the hyperon sigma terms as it avoids the use of delicate chiral perturbation theory. The slopes from the fan plots (Fig. 1) together with the slope along the SU(3) symmetric line yield the hyperon sigma terms. Results are given in [3].

We have extended our calculation of masses to charm [4]. The charm quark may be kept quenched, as it is reasonable to assume that missing out charm-loop effects is minor. This makes it easy to extrapolate charmonium results to the point where m_u, m_d and m_s are physical. To check that cut-off effects are under control several lattice spacings have to be explored. In the left panel of Fig. 3 we show the pure QCD mass splittings of the pseudoscalar charm mesons. This can then be used in the equivalent baryon octet SU(3) flavor breaking expansion to determine the open charm masses. As an example, in the right panel of Fig. 3 we show a preliminary plot.

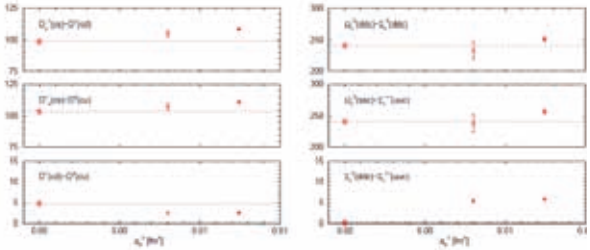

Figure 3: Left panel: the pure QCD mass splittings of the pseudoscalar charm mesons, D^+ ($c\bar{d}$), D^0 ($c\bar{u}$), and D_s^+ ($c\bar{s}$) against a^2 for β=5.50,5.80. The experimental results are given as (red) stars and the horizontal dashed lines are to guide the eye. Right panel: the pure QCD mass splittings of the charm C=1 baryons Σ_c^{++} (uuc), Ξ_c^0 (ddc) and Ω_c^0 (ssc) against a^2 again for β=5.50,5.80.

Outlook

So far most lattice QCD simulations are performed neglecting electromagnetic effects. In order to compute physical observables to high precision, it is important to include and control contributions from QED. We have initiated a similar program, as the symmetry of the electromagnetic current is similar to that of the mass matrix mass $m=(m_u+m_d+m_s)/3$ = constant versus $e_u+e_d+e_s$ = constant = 0. In a follow-up project we shall use this expansion and complement our previous simulations by a fully dynamical simulation of QCD + QED [5].

References and Links

[1] W. Bietenholz et al., Phys. Rev. D 84 (2011) 054509 [arXiv:1102.5300 [hep-lat]].
[2] N. Cundy et al., Phys. Rev. D 79 (2009) 094507 [arXiv:0901.3302 [hep-lat]].
[3] R. Horsley et al., Phys. Rev. D 85 (2012) 034506 [arXiv:1110.4971 [hep-lat]].
[4] R. Horsley et al., PoS LATTICE 2013 (2013) 249 [arXiv:1311.5010 [hep-lat]].
[5] R. Horsley et al., [arXiv:1311.4554 [hep-lat]].

The Chiral Condensate from Lattice QCD with Wilson Twisted Mass Quarks

Research Institution
HISKP (Theorie), Universität Bonn, Nussallee 14-16, 53115 Bonn

Principal Investigator
Carsten Urbach

Researchers
Krzysztof Cichy, Elena Garcia-Ramos, Karl Jansen, Konstantin Ottnad, Falk Zimmermann

Project Partners
NIC DESY

LRZ Project ID: pr63po

Introduction

Symmetries are important concepts in all fields of physics. In particular, symmetries are fundamental for the three forces building the Standard Model of Particle Physics, the electromagnetic, the weak and the strong force: all three forces are described by so-called gauge theories. The underlying gauge symmetry gives rise to the force carriers, so-called gauge bosons, with the photon being the most known example for the electromagnetic interaction.

Symmetries are not only interesting when they are exact, but also when they are broken. This breaking might be either generated by external fields, or dynamically from the theory itself. A well-known example is the magnetisation in ferromagnetic systems. Due to rotational symmetry the magnetisation is expected to be identically zero, however, by applying an external magnetic field, a finite magnetisation can be generated. Moreover, the system dynamically generates a non-zero magnetisation below a certain temperture, the Curie temperature, even without an external field.

Quantum Chromodynamics (QCD), the theory of strong interactions exhibits a similar phenomenon. QCD contains gluons as gauge bosons and quarks as fermionic matter. Chiral symmetry is formally the invariance of QCD in the limit of vanishing quark masses under the exchange of massless left- and right-handed quarks. A non-zero value of the masses of the quarks plays in rough analogy to the ferromagnet the role of an external field. But even at vanishing quark masses chiral symmetry is broken spontaneously leading to a non-zero vacuum expectation value of the chiral condensate S.

QCD is a strongly coupled theory at low energies and, hence, perturbation theory cannot be used to investigate low energy properties of QCD, like chiral symmetry. Therefore, a non-perturbative method needs to be applied, like lattice QCD. In lattice QCD the space-time is discretised with a small but finite lattice spacing a. For finite lattice spacing, QCD can then be solved in Euclidean space-time using Markov-Chain Monte-Carlo methods. However, the discretisation we are using, the so-called Wilson twisted mass formulation of lattice QCD, breaks chiral symmetry at finite lattice spacing values, which makes it necessary to devise special methods to measure the chiral condensate. Such a method was invented by the authors of Ref. [1]. Their so-called *spectral projector* method consists in stochastically evaluating the number of eigenmodes (mode number) of the lattice Dirac operator below some threshold value *M*. In a certain range of *M* values, the dependence of this mode number on M is linear and its slope is proportional to the chiral condensate S. S needs to be renormalised and can, therefore, only be quoted in a given renormalisation scheme at a given scale. We will quote all results in the modified minimal subtraction scheme at a renormalisation scale of 2 GeV. The spectral projector method can also be used to compute the topological susceptibility c, which is a quantity expressing the topological fluctuations of the QCD vacuum.

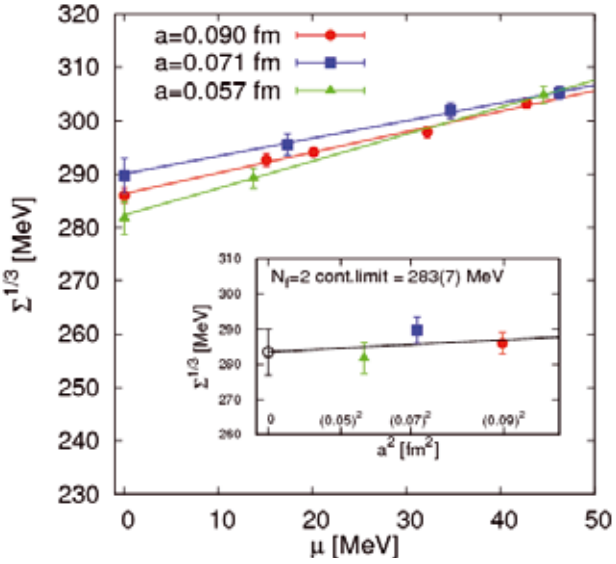

Figure 1: chiral extrapolations of the chiral condensate S as a function of the renormalised quark mass for the 2 flavour ensembles and three values of the lattice spacing. The lines are extrapolations to the chiral limit, linear in the quark mass. Inset: continuum extrapolation of the chirally extrapolated chiral condensate versus the lattice spacing squared.

The simulations are performed at finite values of the lattice spacing, hence the continuum limit has to be performed. Moreover, we simulate at finite values of the quark mass m and, hence, the limit to vanishing quark mass (chiral limit) has to be performed as well.

We have investigated the chiral condensate for QCD with two light flavours (2 flavour) and for QCD with 2 light and a strange and a charm quark (2+1+1 flavours). In both cases we have studied three values of the lattice spacing and a wide range of quark mass values. The lattice spacing a is measured in units of .

Results

We have computed the chiral condensate S for QCD with 2 and 2+1+1 dynamical quark flavours, in both cases for three values of the lattice spacing [2]. The result for the 2 flavour case is shown in Figure 1 and the corresponding 2+1+1 results in Figure 2. It is visible that we control the chiral extrapolation of the renormalised chiral condensate S in the quark mass m and the continuum extrapolation (shown in the inset) very well. The final results are $S^{1/3}$ = 283(14) MeV for the case of 2 flavours and $S^{1/3}$ = 280(12) MeV for 2+1+1 flavours (the reported errors are larger than in Figures 1 and 2, because additional sources of systematic errors were considered, in particular the choice of the range of M values in the mode number computation). This is the first evaluation of the chiral condensate using dynamical up, down, strange and charm quarks. However, within the precision reached we observed no difference in between the 2 flavour and 2+1+1 flavour results. This finding suggests that the influence of the heavier strange and charm quarks is not very large for this observable.

We remark in closing this section that we cannot report in this document here all the results obtained within this project. In particular, let us mention our computation of the topological susceptibility with the spectral projector method [3]. This was also performed for a wide range of lattice spacings and quark masses, with 2 and 2+1+1 dynamical quark flavours. The quark mass dependence of c can be described in the framework of an effective theory, the so-called chiral perturbation theory. This theory predicts that the above mentioned dependence is governed by the chiral condensate (and other low energy constants). Thus, it is possible to extract S in an alternative way. We only mention this alternative extraction leads to a compatible value of S in comparison with the values given above, but the precision of this method is worse than of the direct spectral projector calculation.

On-going Research / Outlook

Lattice QCD is a very computer time demanding scientific application. Only with the computer time made available on supercomputers like SuperMUC significant progress, like the one reported here, can be reached.

We are continuing to evaluate the data produced in this project with the focus on topological properties of QCD.

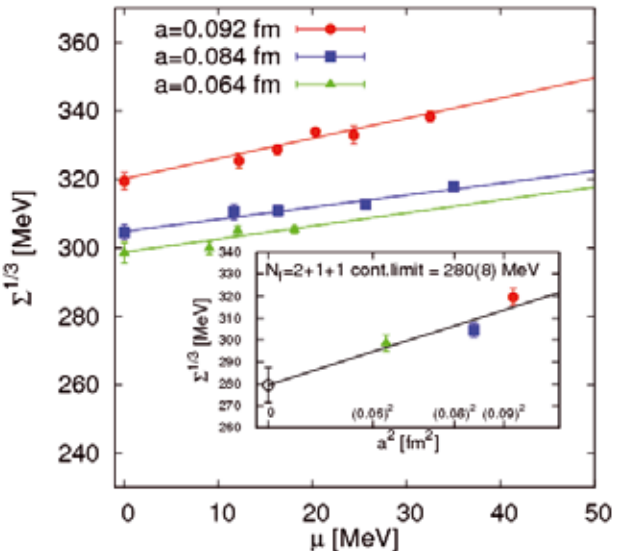

Figure 2: same as Figure 1, but for the 2+1+1 flavour ensembles.

Here we confront the computation of pseudo-scalar flavour singlet meson masses [4] in 2+1+1 flavour QCD with the topological susceptibility in the so-called quenched approximation. The connection is provided by the famous Witten-Veneziano formula, which we are going to check non-perturbatively.

Moreover, the computing resources made available by LRZ are used to reduce the systematic uncertainties in our results even further: in another project we are generating ensembles with physical values of the quark masses, such that a chiral extrapolation is not needed anymore.

References and Links

[1] L. Giusti, M. Lüscher, JHEP **0903** (2009) 013
[2] K. Cichy, E. Garcia-Ramos, K. Jansen, JHEP **1310** (2013) 175
[3] K. Cichy, E. Garcia-Ramos, K. Jansen, JHEP **1402** (2014) 119
[4] C. Michael, K. Ottnad, C. Urbach, Phys. Rev. Lett. **111** (2013) 181602

For the simulation software see
https://github.com/etmc/tmLQCD

Lattice QCD with dynamical up, down and strange quarks

Research Institution
NIC,DESY

Principal Investigator
Stefan Schaefer

Researchers
Coordinated Lattice Simulations (CLS)

Project Partners
HU Berlin,CERN,U Dublin,U Madrid,U Mainz,U Milano,U Münster,U Regensburg,U Roma I, U Wuppertal

LRZ Project ID: pr85we (PRACE project)

Introduction

The parameters of the standard model of particle physics need to be determined from a matching of observables computed within this theory to observables determined in experiments. This project aims at computing some of these parameters at a new level of rigor: the strong coupling constant, the masses of strange and charm quark and also the decay constants of charmed mesons needed to extract matrix elements of the CKM matrix.

This will be achieved by calculations in lattice QCD, which for these observables is the method that delivers the highest level of accuracy. We are therefore generating lattices with the dynamical effects of up, down and strange quarks taken into account in the sea using Wilson fermions where the leading discretization effects have been removed non-perturbatively[1]. To reach precision results, the physics parameters need to be close to the ones realized in Nature. In particular for the masses of the up and down quarks this is a long-standing challenge and only recent years have brought methods with which this regime could be reached. Using specialized techniques for the solution of the linear systems, which account for the largest part of the cost of the simulations, the computational effort to reach the light quark regime has been greatly reduced.

Also, the space-time lattice employed in the simulations needs to be fine, as the continuum limit has to be taken by repeating the computation at several values of the lattice spacing and then extrapolating the lattice spacing to zero. This is very expensive, not only because a constant volume means that the number of points in the lattice – and with it the cost of the computation – rises with the fourth power of the inverse lattice spacing. On top of that we have to cope with the phenomenon of critical slowing down, i.e., that as the latitce spacing a is decreased, the total length of the simulation needs to be increased as a^{-2}.

For the algorithms we use, in particular the Hybrid Monte Carlo algorithm, this dynamical critical exponent, z, is expected to be 2. However, continuum physics poses a particular problem here: in the continuum, field space is separated into disconnected sectors which are identified by the topological charge of the gauge fields. Sampling algorithms based on continuous deformations of the gauge field face a serious problem of ergodicity, with the topological charge effectively freezing on fine lattices.

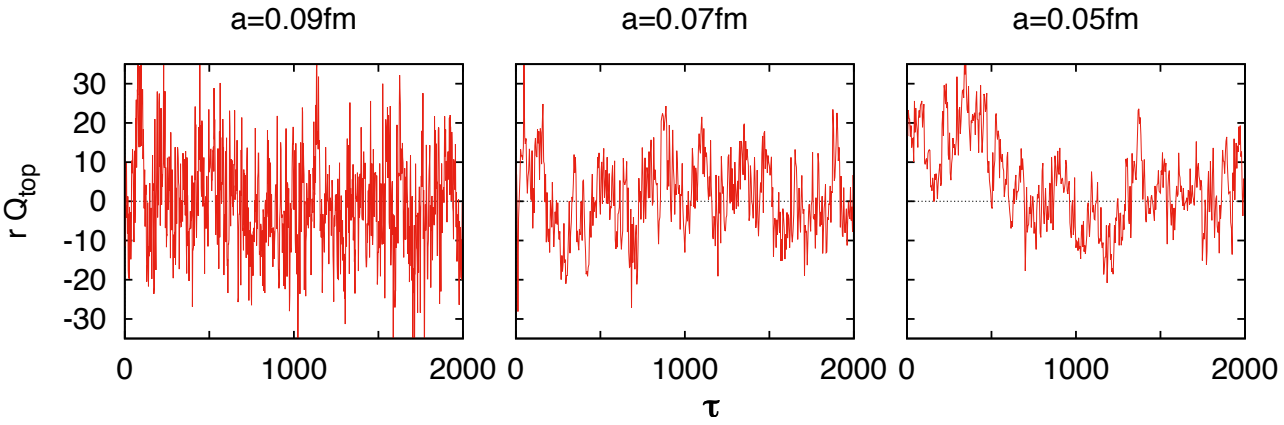

Figure 1: Monte Carlo Time history of the topological charge as a function of the lattice spacing. We show a constant subset of 2000 Monte Carlo time units. The factor r is proportional to the square root of the volume. Critical slowing down is still observed as expected. Clearly, the charge moves well and does not freeze on the finest lattice.

In pure gauge simulations, the critical slowing down due to this mechanism could be shown to occur at least with z=5, but also an exponential behavior is plausible[2]. This has prevented controlled simulations on the fine lattices required for precision physics and in particular the physics of the charm quark which we want to study.

Recently, a solution to the problem has been proposed: by using open boundary conditions in time, the sector formation in the continuum can be avoided without significant impact on the methods used to extract the physics information from these lattices. In this project we use this method for the first time in large scale simulations at small lattice spacing. It is therefore among the first goals to demonstrate that this mechanism also works in simulations with dynamical fermions included.

The simulations are performed as part of the Coordinated Lattice Simulations (CLS) effort[3], where researchers from all over Europe have joined to contribute to this project. Since the generation of the field configurations is the part of lattice simulations which takes the largest computer resources, the generated ensembles will be used in many other projects, the various groups in this effort having interests, e.g, in flavor physics, hadron spectroscopy and hadron structure.

Results

The two highlights of the publicly available openQCD code [4,5], which we are using for the first time in a large scale project for the generation of the the gauge fields, are the open boundary conditions in time and the locally deflated (multigrid) solver for the Dirac equation. The latter eliminates largely the slowing down as the light quark masses approach their physical values. It is described in detail in Ref. [6].

The setup of the Hybrid Monte Carlo implements currently known improvements: Hasenbusch's frequency splitting, fourth order integrators on multiple time scales for the molecular dynamics and twisted-mass reweighting to cure the problem of instabilities due to the explicit chiral symmetry breaking by the Wilson fermions.

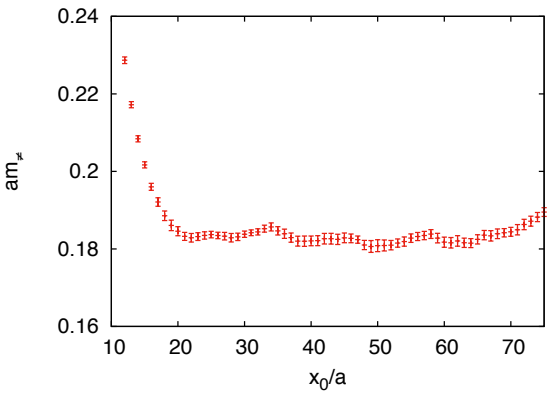

Figure 2: Effective pion mass with open boundary conditions: the ground state can be extracted easily.

The allocation within this PRACE project is the first large scale computer resource dedicated to this setup. It is therefore only possible to show first preliminary results, but so far the proposed algorithmic approach of Ref. [5] has worked well, with the cost of the simulations in reasonable agreement with the time estimates at the start of the project.

As has become clear above, a main improvement over previous calculations are the open boundary conditons which are expected to solve the problem of the critical slowing down. Infact, this project is the first large scale simulation which faces the challenge of approaching the region with a< 0.05fm.

We therefore show the Monte Carlo time history of the charge for three values of the lattice spacing at a pion mass of about 400MeV. Clearly, the topological charge moves freely even on the finest lattice, in contrast to what is observed with periodic boundary conditions.
It is also apparent, that the critical slowing down with the square of the inverse lattice spacing is still present in these simulations and autocorrelation times of the order of 50 time units are observed for the middle lattices. Using the scaling law this translates to 100 units for the finer lattice.

In Figure 2, we also show that the extraction of physics observables, here the pion mass at roughly 400MeV, does not pose any particular problem. This is another confirmation that the approach adopted to solve the problem of the topological tunneling is indeed feasible.

Outlook

This project incorporates many new ingredients. Starting with the action which has been specifically tuned for the current effort, over the many algorithmic innovations to the newly formed group of researchers from all over Europe which are involved in these simulations.

The project is currently underway, with the goal to generate lattices at three different values of the lattice spacing. The parameters are now tuned, the first ensembles have reached target statistics and the others under production. On these ensembles a large variety of physics projects will be carried out. The first targets being the determination of the strong coupling constant and the physics of charm quarks.

The wide range of lattice spacings and quark masses and the availability of the lattices to the large group of reasearches within CLS will certainly lead to many interesting results in the next year, the ground for which are currently being laid during the current investigations.

References

[1] J. Bulava, S. Schaefer, Nucl. Phys. B874 (2013) 188
[2] S.Schaefer, R.Sommer, F.Virotta, Nucl.Phys.B845 (2011) 93-119
[3] https://wiki-zeuthen.desy.de/CLS/
[4] http://luscher.web.cern.ch/luscher/openQCD/
[5] M. Lüscher, S. Schaefer, Lattice QCD with open boundary conditions and twisted-mass reweighting, Comp.Phys.Comm 184 (2013) 519-528
[6] M. Lüscher, Local coherence and deflation of the low quark modes in lattice QCD, JHEP 0707 (2007) 081

Excited state artefacts in calculations of hadron 3-point functions

Research Institution
Institute for Theoretical Physics, Regensburg University

Principal Investigator
Andreas Schäfer

Researchers
G. Bali, S. Collins, B. Gläßle, J. Najjar, R. Rödl, R. Schiel, J. Simeth, W. Söldner, A. Sternbeck

Project Partners
–

LRZ Project ID: pr85xi (Gauss Large Scale project)

Introduction

High energy particle physics experiments, as presently conducted, e.g., at LHC, CERN, Geneva are among the most expensive human research efforts. At LHC protons are collided at very high energy resulting in the production of very many hadrons and a few rare particles, like the Higgs boson, the decay products of which one tries to identify reliably. For any such effort it is crucial to understand well the structure of protons and the interactions between its constituents, quarks and gluons. In addition, investigating hadron structure is also a prominent research area in its own right because QCD is one of the fundamental interactions of the standard model and its non-perturbative aspects are still only little understood. Lattice QCD has the potential to provide this information and in many aspects is complementary to direct experiments which can not address all aspects unambiguously. However, lattice QCD requires to take the combined limit of large volume, small lattice spacing, huge statistics and physical quark masses. The very substantial increase of computing power in recent years has allowed to reach the large volume and large statistics limit and in this project also the physical mass limit. (Other lattice collaborations addressing similar physics questions have reached the same limits in parallel, but this is not a problem, because one needs anyway independent confirmation with several lattice actions to be sure that the remaining artifacts are really under control.) The only limit which could not be reached so far is that of small enough lattice constants, see below.

Let us note that there is a fundamental difference between lattice simulations which calculate known quantities, like masses, which are thus tests of QCD and the ideas of lattice QCD (which are already generally accepted) and lattice calculations for, e.g. Generalized Parton Distributions (GPDs), Transverse Momentum Parton distributions (TMDs), Double Distributions (DDs), Distribution Amplitudes (DAs) etc. all of which parameterize different well defined aspects of hadrons. These are in fact extremely complicated objects, which combine all difficulties of relativistic quantum field theory and extremely non-linear dynamics. They provide information which one either has not yet obtained or more often cannot obtain at all from experiment.

Lattice simulations proceed in two steps. First configurations are generated and than physical observables are analyzed using these ensembles. In this case the ensemble generation took place on our home built computer QPACE. The LRZ projectspr85xi and pr86te concerned exclusively the physics analysis.

Results

The project is intimately connected to project pr86te "Nucleon and meson matrix elements close to the physical point" in the report to which we will discuss additional results. In this report we will rather concentrate on the problem of systematic errors. Most prominently our results show, like other recent result worldwide, that there is one source of error which was underestimated by basically all collaborations in the field so far, namely the admixture of excited states. Lattice simulations of hadronic properties work in the following manner: First the whole formalism of Quantum Field Theory (QFT) is analytically continued to imaginary time, which is referred to as Euclidean time. This is a mathematical well-defined procedure which changes plane waves to factors of the form exp(-Et). If one investigates, e.g., properties of the nucleon one always gets contaminations from all excited states with the same quantum numbers. However, as the masses of these states are larger than that of the ground state nucleon so are their energies and consequently they are exponentially suppressed with respect to the latter. One simply has to propagate the state numerically in Euclidean time sufficiently long to obtain the exact QFT wave function of the nucleon with which one than can calculate physical observables of interest. With previously reached accuracy one thought that this happens rather fast and possible artifacts from this source were assumed to be negligible. However, one has learned meanwhile that this was not the case and that unless special care is devoted to suppressing these contributions lattice QCD calculations on hadron structure

are not really quantitative. We cannot discuss the suppression techniques in detail here as such a discussion would be very technical.

Instead we illustrate the effects for the most important benchmark quantity, <x(u-d)> see below. Unfortunatey we found that even after strongly reducing this kind of artifacts and even at physical quark masses (which we reached in these projects) and for large lattices, for which also finite volume artifacts were found to be absent, a large discrepancy persists. According to present wisdom, this discrepancy can only be attributed to the last known source of errors, namely the finite resolution of the lattice. Thus we can conclude from our results that hadron structure calculations have to be performed with finer lattices than done so far (except for the staggered fermion formulation which has severe fundamental problems). For the standard Wilson fermion formulations this is, however, not possible due to drastically increasing autocorrelation times, without substantial modifications of the formulation of lattice QCD. A promissing suggestion was recently made by Lüscher and Schaefer, introducing open boundary conditions. Thus, while our results still do not giving final answers to many physics questions, as we had hoped that they would, they are helpful to push lattice QCD as such to a higher level of precision.

The momentum fraction carried by quarks in nucleons:
Let us illustrate what was said above for one specific example, namely <x(u-d)> for the proton, which is one of the parameters which characterizes how the momentum of a nucleon is split up between its quarks and gluons. As the exact momentum probability distribution of quarks and gluons inside colliding nucleons is so important, much experimental effort was invested over decades worldwide to pin them down precisely, making especially the difference between the up- and down-quark probability distributions one of the best known quantities in hadron structure physics. Therefore, this is one of the most important benchmarks to test the accuracy of lattice QCD calculations. Here 0<x<1 is the fraction of the nucleon momentum carried by the quark taking part in a reaction and u(x) is, e.g., the probability that an up quark in a nucleon carries the momentum fraction x.

Unfortunately, previous lattice calculations did not reproduce the experimental value or had error bars which were so large that they precluded any clear statement. Fig. 1 shows such earlier results together with the new ones generated within this project as well as the experimental numbers. The plot shows the difference in the mean momentum fraction of the up and down quark in a proton, which is a theoretically especially well defined quantity. The cost of lattice simulations increases rapidly with decreasing quark mass, which is here represented by the resulting pion mass. Therefore, in the past, one usually simulated with unphysically heavy quarks (and thus pions) and then extrapolated the results. Our simulation results are plotted against the pion mass of each simulation, while the experimental points mark the physical pion mass.

One can see that suppressing excited states substantially decreases the value of <x(u-d)> but not sufficiently to obtain good agreement with the experimental values. One also sees that, contrary to expectations the pion mass has no large influence for this quantity. (This is not the case for other quantities.) Finally the two blue points at physical mass were obtained for different (large) volumes. The fact that they agree so well is clear indication that finite volume effects are negligible.

Fig.2 gives a second example leading to the same conclusion. The iso-vector axial vector coupling constant is another parameter characterizing the nucleon which is especially well known. While earlier simulations still left hope for optimism in view of their large statistical and systematic uncertainties, the new Regensburg points show clearly that there is a serious systematic problem. As said above, these results call very clearly for simulations on finer lattices which according to present knowledge are only possible with open boundary conditions.

References and Links

[1] G.S. Bali et al., arXiv:1311.7041
[2] G.S. Bali et al., Phys. Rev. D86 (2012) 054504, arXiv:1207.1110

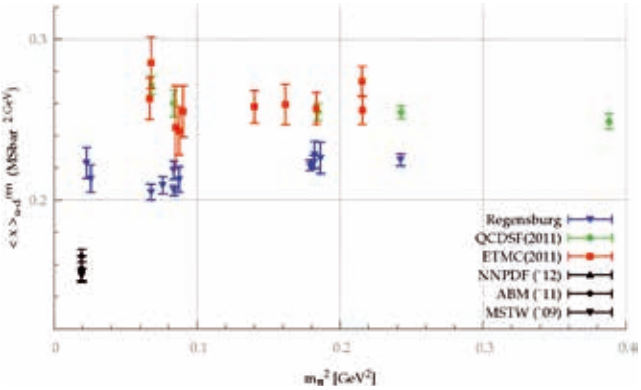

Figure 1: Lattice and experimental results for <x(u-d)> The blue dots are the new results from Regensburg. ETMC (2011) and QCDSF(2011) are earlier lattice results. NNPDF, ABM and MSTW are different fits to experimental data. The error bars and the spread of these points gives a fair assessment for how well this quantity is known experimentally.

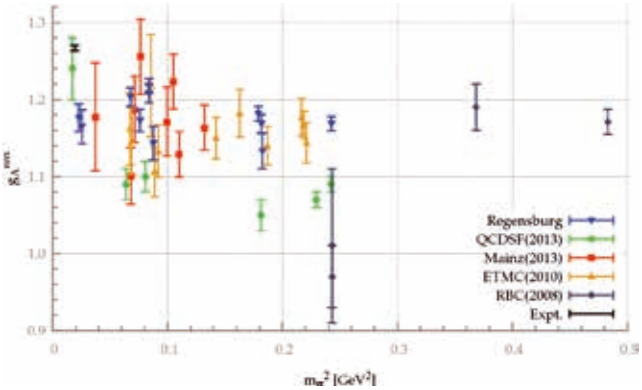

Figure 2: Lattice and experimental results for g_A, the axial vector coupling constant of the nucleon. The blue dots are the new results from Regensburg.

Nucleon and meson matrix elements close to the physical point

Research Institution
Institute for Theoretical Physics, Regensburg University

Principal Investigator
Andreas Schäfer

Researchers
G. Bali, V. Braun, S. Collins, B. Gläßle, J. Najjar, R. Rödl, R. Schiel, J. Simeth, W. Söldner, A. Sternbeck

Project Partners
–

LRZ Project ID: pr86te (Gauss Large Scale project)

Introduction

The introduction to this project is given in the report for project pr85xi "Excited state artifacts in calculations of hadron 3-point functions". We will focus here on the discussion of more results. As explained in the report for pr85xi, we have found clear evidence that present day lattice simulations are still plagued by more severe artifacts than previously assumed. Thus, we will concentrate in this report on applications for which so little is known physics-wise that even lattice results with a possible non-negligible remaining systematic error due to discretization effects are very valuable.

Results

Nucleon Distribution Amplitudes: With the advent of high energy colliders of ever higher luminosity (i.e. number of collisions per second) it became possible to study ever rarer processes, being sensitive to ever more distinct and mathematically well defined aspects of hadron structure. This information is parameterized in terms of new quantities, abbreviated as GPDs, DAs, TMDs, DDs, ... Here we will address Distribution Amplitudes (DAs) which enter the theoretical description of processes in which the final hadronic state is measured completely like *photon+virtual photon → pion or photon+proton → proton*.

Furthermore, we will only discuss the nucleon DA. However we will include in our discussion also the lowest lying negative parity nucleon states. Just like atoms, nucleons, being composite systems, have infinitely many excited states characterized by angular momentum and parity. Today one knows more than 25 such nucleon excitations with spins up to 13/2. One of the puzzles in hadron physics is that among these there are two spin $^1/_2$ negative parity partners of the nucleon with similar mass, N*(1535) and N*(1650) instead of only one as one would expect. The numbers in the brackets give the mass of the states in MeV. In fact, the width of both states is about 150 MeV such that they actually overlap. All of this strongly suggests that their internal wave function should be substantially different and for many years people have developed all kinds of ideas and models for this difference. Some of these models assume, e.g., that one of these two states is rather a 4 quark-1 antiquark bound state than a usual baryon. Obviously, first principle lattice results are very much welcome in this situation. One of the nice features of this project is that the results can be easily visualized. Fig.1 shows the DAs of the nucleon, the N*(1650) and the N*(1535). These depend on the longitudinal momentum fractions of the three quarks in the lowest Fock state contribution to the nucleon wave function. The up-quarks have the momentum fractions 0<x_1,x_2 and the down quark has the momentum fraction x_3. As these three numbers have to add up to one, the corresponding probability distribution can be plotted in the way shown in Fig.1.

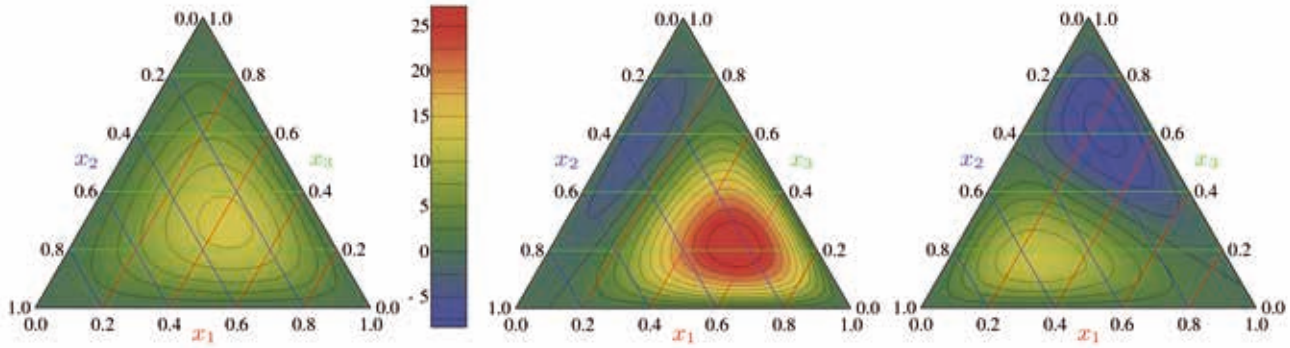

Figure 1: Results for the distribution amplitudes of the nucleon (left), the N*(1650) (middle) and the N*(1535) (right)

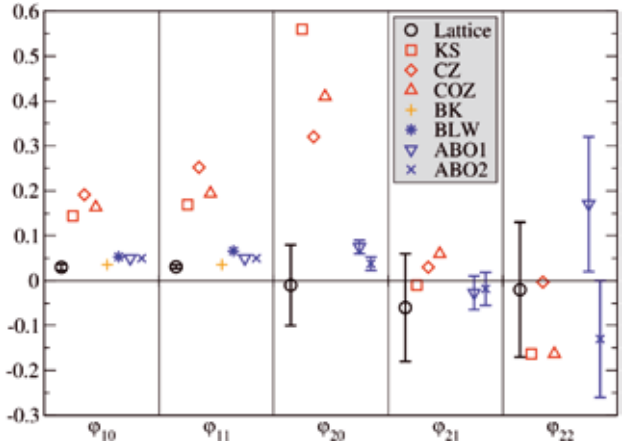

Figure 2: Our lattice results (black) exclude certain models (red) and support others (blue).

One sees that for the ground state nucleon the valence up quark (x_1) carries on average a slightly larger momentum fraction than the two other quarks which split the remaining momentum rather evenly between them. This tendency is much more pronounced for the N*(1650). Both observations are in line with the popular quark-diquark picture of their internal structure. In contrast we find that the DA of the N*(1535) is completely different, actually changing sign (DAs are no probabilities, but amplitudes).

While these plots give a nice intuitive illustration of the relevant physics, one can also quantify the results precisely. This is done in the form of the parameter values for an expansion in certain orthogonal polynomials, see Fig. 2 . Obviously our results (in black) exclude certain models (KS, CZ, COZ) while they are nicely compatible with others (BLW, ABO1, ABO2). It is very unlikely that these qualitative features will change when in future similar calculations are repeated on finer lattices.

Quark-antiquark contributions:
A hadron does not only consist of the minimal number of quarks (this part of the wave function is described by the DAs) but contains also an arbitrary number of quark-antiquark quantum fluctuations. These modify its properties substantially and thus their contribution has also to be calculated. For technical reasons the resulting contributions for any physical observable are called disconnected contributions. The calculation of disconnected contributions is very computer time intensive, but due to the substantial computer resources we could use, we were able to push also such calculations to higher precision. As an example we want to discuss the so-called nucleon sigma term. This term parameterizes the quark contribution to the nucleon mass and enters in many places, also for such exotic topics as the coupling of dark matter candidates to nucleons. Furthermore, its value is very heavily debated with predictions varying by up to a factor 2. We actually calculated it in two independent manners, namely by directly calculating the relevant disconnected contributions and by studying the dependence of the nucleon mass on the pion mass. The results are shown in Fig.3, where the nucleon mass is plotted as function of the pion mass (i.e. the quark masses).The sigma term is the slope of this curve. The results of our direct calculations are shown in blue and are much more precise than what can be obtained from the masses (grey band). Note that the physical mass ratio (green point) is reproduced accurately by our lattice simulation. Our preliminary result for sigma is 31(5) MeV which is close to the lower bound of the values discussed in the literature.

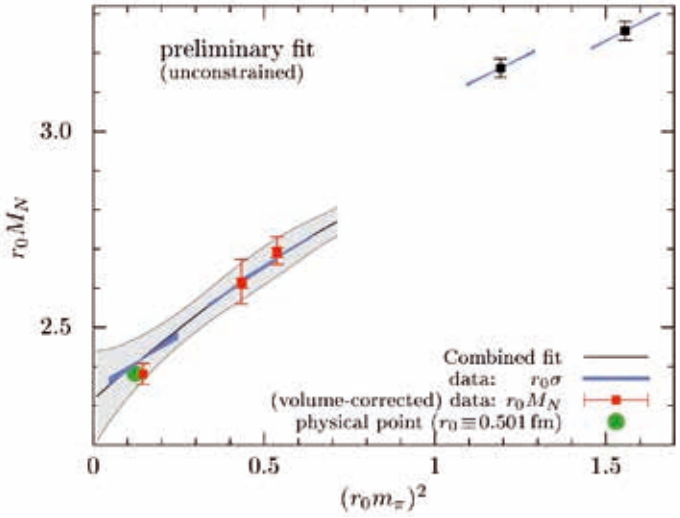

Figure 3: Results for the nucleon sigma term. The slopes obtained from direct calculations of the disconnected contributions (blue) agrees very well with the obtained nucleon and pion masses (grey band).

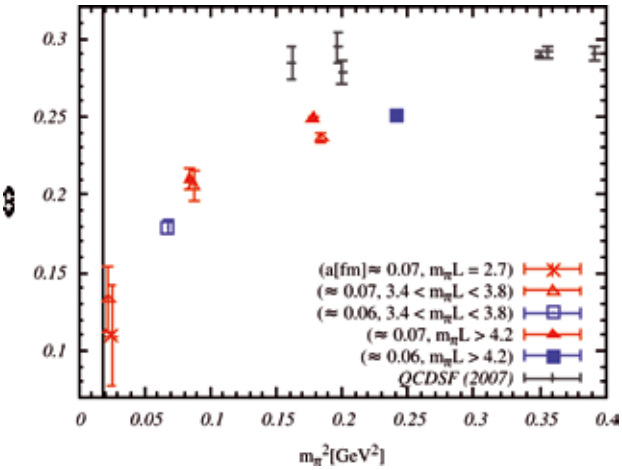

Figure 4: The average momentum fraction carried by a valence quark in a pion. Black are old lattice results from QCDSF. Our new results are plotted in blue and red.

The quark momenta in the pion:
As last example we show the average quark momentum fraction in the pion (which consists of a valence quark and valence antiquark plus gluon and quark quantum fluctuations). This is a very similar quantity as the one discussed in the report for project pr85xi. In this case one observes a very non-trivial dependence on pion/quark mass, such that this is an example for which it was crucial to go to physical masses.

References and Links

[1] R.W. Schiel et al. arXiv:1112.0473
[1] G.S. Bali et al. arXiv:1311.7639

The first two quark generations in fully physical conditions

Research Institution
DESY Standort Zeuthen

Principal Investigator
Karl Jansen

Researchers
A. Abdel-Rehim, Ph. Boucaud, N. Carrasco, A. Deuzeman, P. Dimopoulos, R. Frezzotti, G. Herdoiza, K. Jansen, B. Kostrzewa, M. Mangin-Brinet, I. Montvay, D. Palao, G.C. Rossi, F. Sanfilippo, L. Scorzato, A. Shindler , C. Urbach , U. Wenger

Project Partners
see References and Links

LRZ Project ID: pr86ve (PRACE project)

Introduction

One of the most fascinating phenomenon in nature is the interaction between quarks and gluons as our most fundamental building blocks of matter. A mysterious aspect of this interaction is that, although we observe the binding states of quarks and gluons, e.g. The proton and the neutron, quarks and gluons cannot be detected themselves. The reason is that their binding energy is so strong that they cannot be taken apart. This large binding energy and the corresponding large coupling between quarks and gluons makes it also necessary to employ non-perturbative methods to analyze the theory of describing the quark gluon interaction, quantum chromodynamics (QCD).

Such a non-perturbative method is lattice QCD where the theory is formulated on an Euclidean space time grid with a non-vanishing lattice spacing which in the end has to be sent to zero to recover the continuum theory. In the past, lattice QCD calculations, which are performed on state of the art supercomputers such as SuperMuc, needed to be performed at pion masses which were significantly larger than the experimentally measured one. Having a number of such heavy pion masses available, an extrapolation to the physical pion mass neded to be carried through, which led to a significant systematic error of lattice computations.

Performing lattice QCD calculations at the physical value of the pion mass, as it has been done in this project, offers the exciting possibility of avoiding the rather severe systematic uncertainties related to above mentioned extrapolations. In fact, in particular in the nucleon sector, extrapolations to the physical pion mass belong to the dominant sources of systematic error. Simulations directly at the physical pion mass help therefore dramatically to avoid these uncertainties and to address present discrepancies between experimental/phenomenological results and lattice QCD data in a novel way and allow to shift the focus to other systematic uncertainties as possible sources of these discrepancies.

For this reason, the European Twisted Mass Collaboration (ETMC), which spans across eight countries in Europe, has developed an action which allows such simulations directly at the physical pion mass. The simulations were performed at a lattice spacing of 0.1fm with a linear box extent of 48 lattice points in each of the three space directions and 96 lattice points in the time direction making thus the box size large enough to suppress unwanted finite size effects. The developed action has the nice property of twisted mass lattice QCD (tmLQCD) [1,2] that discretization artefacts are only quadratic in the lattice spacing.

For the simulation on SuperMuc, significant code development effort was invested into the tmLQCD software suite [3] in the form of new 'monomials' for simulations and substantial performance tuning. An overview of this work was presented at the 2013 lattice conference [4,5].

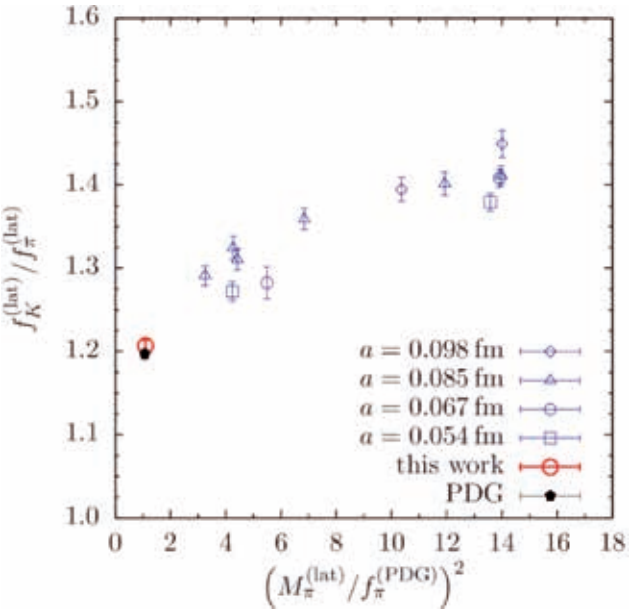

Figure 1: Comparison of the simulation results at the physical point.

Results

The first target observable that has been computed at the physical pion mass has been pion decay constant in units of a scale which is derived from the static potential, r_0=0.5fm. A comparison of the simulation results at the physical point to older ones by ETMC is shown in figure 1. As can be seen the new simulation point (the downward triangle in the figure) hits directly the measured value of the decay constant, indicated by the star. It also confirms the trend of the older data [6] at large pion mass and provides a cross-check that the old extrapolation of ETMC was correct, at least for the case of the here considered pion decay constant.
Another example is the ratio of the Kaon decay constant and the pion decay constant shown in figure 2. Also here the simulations fully reproduce the experimentally measured value. The figure also demonstrate the difficulty of the extrapolation from heavy pion masses: the old data scatter quite a lot and a controlled extrapolation to the physical pion mass has been very difficult.

Besides the so far discussed observables, a number of other quantities has been computed, i.e. the masses of heavier mesons and also their decay constants. All of these measurements at the physical point coincide with their experimental counterparts and also consistency is seen with the old data.

On-going Research / Outlook

The first results which have emerged form this project and which are discussed above are extremely encouraging. They demonstrate that indeed simulations at the physical pion mass are possible with the twisted mass action used in this work. The fact that the pion and the Kaon decay constants are reproduced in these simulations provide very nice evidence that the parameters of the simulations were tuned correctly. Therefore the generated gluon field configurations are very valuable: they can be and are being used to compute further physical observables of interest. To these quantities belong the anomalous magnetic moment of the muon as a prime candidate to discover signs of new physics beyond the standard model. Other quantities are connected to the structure of hadrons such as the axial charge playing an important role in the beta-decays or the average momentum of a quark in a proton which are most important benchmark quantities for lattice calculations of hadronic observables. It is important to realize that for many quantities often also so-called renormalization constants need to be computed. These calculations are carried out in separate simulations and a number of renormalization constants are already available. Thus, through this project on SuperMUC a rich spectrum of physical quantities can be computed which can be directly used to interpret experimental results or to enter phenomenological calculations.

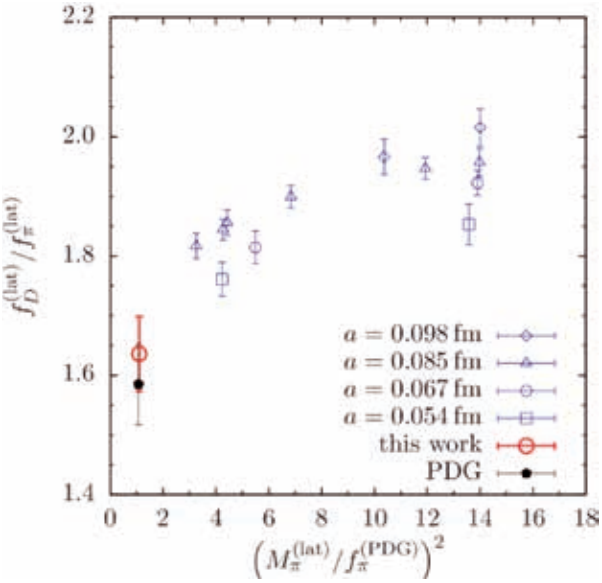

Figure 2: Ratio of the Kaon decay constant and the pion decay constant.

References and Links

[1] R. Frezzotti et al. (ALPHA). JHEP (2001). 08:058. hep-lat/0101001
[2] R. Frezzotti and G. C. Rossi. JHEP (2004). 08:007. hep-lat/0306014
[3] K. Jansen and C. Urbach. Comput.Phys.Commun. (2009). 180:2717–2738. 0905.3331
[4] A. Abdel-Rehim et al. (ETM). In 31st International Symposium on Lattice Field Theory, no. 414 in
[5] A. Deuzeman et al. (ETM). In 31st International Symposium on Lattice Field Theory, no. 416 in
[6] R. Baron et al. (ETM). JHEP (2010). 1006:111. 1004.5284

Projekt Partners

CaSToRC, The Cyprus Institute, 2121 Aglantzia, Nicosia, Cyprus;
Laboratoire de Physique Théorique, Université de Paris XI, 91405 Orsay-Cedex, France;
Departamento de Física Teòrica and IFIC, Univ. de València-CSIC, E-46100 València, Spain;
Albert Einstein Center for Fund. Physics, University of Bern, CH-3012 Bern, Switzerland;
Dip. di Fisica, Università di Roma Tor Vergata and INFN, I-00133 Roma, Italy;
Centro Fermi, Piazza del Viminale 1 I-00184 Rome, Italy;
Institut für Kernphysik, Johannes Gutenberg-Universität, D-55099 Mainz, Germany;
Humboldt Universität zu Berlin, Institut für Physik, Newstonstr. 15, 12489 Berlin, Germany;
Theory Group, Lab. de Physique Subatomique et de Cosmologie, 38026 Grenoble, France;
Deutsches Elektronen-Synchrotron DESY, Notkestr. 85, D-22607 Hamburg, Germany;
Goethe-Universität, Institut für Theoretische Physik, D-60438 Frankfurt am Main, Germany;
INFN -TIFPA, via Sommarive 14 - 38123 Trento, Italy;
IAS, IKP and JCHP, Forschungszentrum Jülich, 52428 Jülich, Germany;
HISKP (Theory), Rheinische Friedrich-Wilhelms Universität Bonn, Germany

Kaon semi-leptonic form factor

Research Institution
Institut für Theoretische Physik, Universität Regensburg

Principal Investigator
Enno E. Scholz

Researchers
Gunnar Bali, Vladimir Braun, Alessio Burello, Benjamin Gläßle, Rudolf Rödl, Wolfgang Söldner

Project Partners
–

LRZ Project ID: pr89ti (PRACE project)

Introduction

In the Standard Model (SM) of particle physics the interactions between the elementary particles are mediated by the strong and electro-weak forces. The strong forces are described by the theory of Quantum Chromodynamics (QCD). QCD forces are mediated by gluons between the quarks, which are the fundamental building blocks of all hadrons, especially the proton and the neutron, and therefore of most matter around us. Six different quark flavors grouped in 3 generations have been observed in Nature (up and down, charm and strange, top and bottom), which differ, e.g., in their masses but also their electric charges. The electro-weak forces are described by another gauge field theory, the electro-weak theory of which for example Quantum Electrodynamics mediating the electric forces via photons is a subgroup. Since the quarks carry electric charges, the electro-weak forces act via photons between different quarks. But there are also the W- and Z-bosons as further force carriers in the electro-weak theory being responsible for more interactions between the elementary particles, also including the leptons (electron, muon, tau and their respective neutrinos).

The eigenstates of the two theories, QCD and electro-weak theory, do not coincide. The electro-weak mixing matrix, commonly referred to as the Cabibbo-Kobayashi-Maskawa (CKM) matrix, describes the mixing between the mass and electro-weak eigenstates of the different quark flavors in the SM. Originally formulated for two generations of quark flavors in 1963 by Cabibbo, later Kobayashi and Maskawa realized that in accordance with the observed violation of charge-parity (CP) symmetry at least a third generation of quark flavors had to be added. The existence of such a third generation was shown by the discovery of the bottom-quark in 1977. Eventually, the completeness of the third generation was verified experimentally with the discovery of the top-quark at Fermilab's Tevatron accelerator in 1995. Over time, the elements of the CKM-matrix have been measured and extracted with increasing precision. They are particularly interesting, because unitarity violations of the matrix may give hints for physics beyond the SM. Particle collider experiments like the Large Hadron Collider (LHC) at CERN or the Belle2 experiments presently are or will in the near future produce improved measurements to determine these matrix elements.

In such experiments decay rates for certain processes involving the elementary particles or bound states of those, like mesons or hadrons, are measured. To extract the CKM-matrix elements from such measurements, one has to know the different contributions of the QCD and electro-weak interactions in these processes. Due to their nature, unlike the electro-weak contributions which can be (at least in principle) calculated analytically order-by-order in a perturbative expansion to the desired precision, for the strong forces such a perturbative expansion is not possible. But it is possible to simulate QCD numerically on a discretized, finite space-time lattice. Basically, one first generates a statistical ensemble of gauge configurations, which sample the correct distribution of the gluon fields according to the QCD action. Then one "measures" the interactions between quarks and the hadronic operators of interest by calculating propagator functions on the generated gauge fields and combine them with certain operators. Numerically this requires the inversion of large sparse matrices to obtain the propagators between certain quarks. These lattice-QCD simulations have matured over the last decades such that by today reliable results from simulations, e.g., for the mass spectrum of the hadrons and certain hadronic matrix elements are available.

Currently, the biggest uncertainty in the first row unitarity relation $|V_{ud}|^2+|V_{us}|^2+|V_{ub}|^2=1$ originates from the CKM-matrix element $|V_{us}|$, which is our motivation to address it in this project. Given the available experimental data, the most precise value for this matrix element can be obtained from the semi-leptonic kaon decay $K\to\pi\, l\, \nu$ (Kl3). From those measurements, one obtains the combination of the matrix element $|V_{us}|$ and the vector form factor f + K π(q2) at zero momentum transfer $q^2=0$. We will extract the form factor for the Kl3-decay from lattice measurements of the matrix element of the weak vector current $V\mu=\bar{s}\ \gamma\mu\ u$ between a kaon and pion state with momenta pi and p f , respectively. The vector current matrix element is related to the semi-leptonic form factors at momentum transfer $q=p_i-p_f$ via

$$\langle\pi(p_f)|V_\mu|K(p_i)\rangle = \\ = f_+^{K\pi}(q^2)\,(p_i+p_f)_\mu + f_-^{K\pi}(q^2)\,(p_i-p_f)_\mu .$$

High precision results for the vector form factor can be obtained from lattice simulations of QCD since leading lattice artifacts are proportional to the kaon-pion mass difference $m_K - m_\pi$ and apply only to the deviation of the form factor from unity in the limit $m_K = m_\pi$. As one is ultimately interested in form factors at zero momentum transfer, it is necessary to reach zero or near zero momentum transfer in the lattice simulations as well. As outlined below, in this study this is achieved by employing so called twisted boundary conditions.

Results

For the analysis Stout-link Non-Perturbative Clover (SLiNC)-fermion gauge configurations with N_f =2+1 flavors are used, which were generated by the QCDSF-collaboration [1, 2] and are available at the ILDG. We used four ensembles with pion masses in the range of approximately 210 to 340 MeV, see Table 1. These ensembles start from the symmetric point at $\kappa_l = \kappa_s$ and in all ensembles the average quark mass $(2m_l+m_s)/3$ has been kept constant. For each of the three ensembles at lattice sizes of 32^3x64 we had around 1800 to 2000 configurations available, while for the ensemble with the lightest pion mass at lattice size of 48^3x96 only 600 configurations were available.

Table 1: SLiNC-ensembles at

κ_l	κ_s	$L^3 \times T$
0.121040	0.120620	32^3x64
0.121095	0.120512	32^3x64
0.121145	0.120413	32^3x64
0.121166	0.120371	48^3x96

To measure the form factor at zero or near zero momentum transfer, we induce additional momentum either to the pion or the kaon state by utilizing twisted boundary conditions in the valence quarks, meaning the boundary conditions are only applied during the calculation of the quark propagators (valence quarks) and were not applied during the generation of the gauge configurations. Applying twist angles θ_k to the spatial directions k to the quark fields

$$\psi(x_k + L) = e^{i\theta_k}\psi(x_k)$$

induces a momentum $|\vec{\theta}|/L$. Here we follow the strategy outlined by the RBC/UKQCD-Coll. [3, 4] for achieving zero momentum by implementing either

$$|\vec{\theta}_K| = L\sqrt{\left(\frac{m_K^2+m_\pi^2}{2m_\pi}\right)^2 - m_K^2}\,, \quad \vec{\theta}_\pi = 0$$

or

$$|\vec{\theta}_\pi| = L\sqrt{\left(\frac{m_K^2+m_\pi^2}{2m_K}\right)^2 - m_\pi^2}\,, \quad \vec{\theta}_K = 0\,.$$

The necessary two- and three-point correlation functions are then calculated with the twists applied accordingly. For the calculation of the three-point correlator the sequential source technique is used. The computations are performed using the publicly available Chroma software package for lattice QCD [5]. The inverter we used and optimized for running on the SuperMUC architecture is a multi-grid domain-decomposition solver. Typically, for the lattice sizes used in this project, we run on partition sizes of 1024 nodes, but scaling of our inverter code would have allowed the use of larger partition sizes as well.

We first started by estimating the pion- and kaon masses from two-point correlators using untwisted fermion fields for each ensemble. From these masses, we determined the twist angles for zero momentum transfer according to the above formulae. In the following step the two- and three-point applying the twist angles were generated and stored to disk. Here we also generated data for additional twist angles leading to small but non-zero momentum transfer. In that way we will be able to interpolate the form factors at several q^2 to zero momentum transfer. The form factor itself can be obtained from suitable ratios of the correlation functions, cf. [3,4].

On-going Research / Outlook

After generating the needed data, we will proceed with the analysis and first results are expected to be presented in forthcoming conferences soon.

We acknowledge the generation of the gauge configurations used in this work by the QCDSF-Collaboration and resources of the SFB-TRR 55 "Hadron Physics from Lattice QCD" [1,2]. The principal investigator is supported by the DFG SFB-TRR 55 and EU grants PITN-GA-2009-238353 (ITN STRONGnet) and PIRG07-GA-2010-268367.

References and Links

[1] W. Bietenholz et al. (QCDSF-Coll.), Phys. Lett. **B690** (2010) 436, arXiv:1003.1114 [hep-lat].
[2] W. Bietenholz et al. (QCDSF-Coll.), Phys. Rev. **D84** (2011) 054509, arXiv:1102.5300 [hep-lat].
[3] P. A. Boyle et al. (RBC-UKQCD-Coll.), J. High Energy Phys. **05** (2007) 016, arXiv:hep-lat/0703005.
[4] P. A. Boyle et al. (RBC-UKQCD-Coll.), Eur. Phys. J. **C69** (2010) 159, arXiv:1004.0886[hep-lat].
[5] R.G. Edwards (LHPC-Coll.), B. Joo (UKQCD-Coll.), *The chroma software system for lattice QCD*, Nucl. Phys. Proc. Suppl. **B140** (2005) 832.

Life and Material Sciences

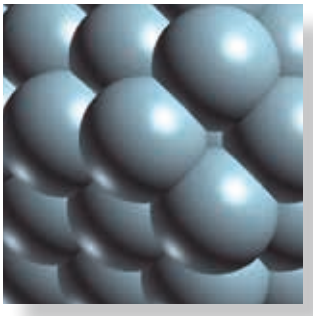

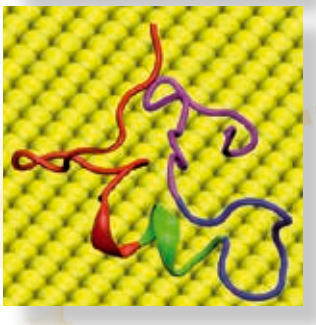

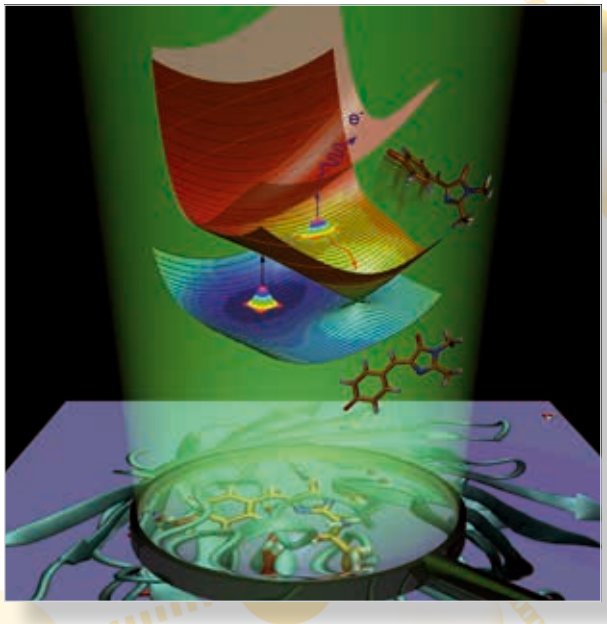

Quantum Monte-Carlo and exact diagonalization studies of correlated electron systems

Research Institution
Institut für Theoretische Physik und Astrophysik, Universität Würzburg, Am Hubland, 97074 Würzburg, German

Principal Investigator
–

Researchers
F. F. Assaad, F. Goth, G. Li, M. Bercx, M. Laubach, J. Werner and W. Hanke

Project Partners
–

LRZ Project ID: h014z

Introduction

Correlated electrons systems are defined by the notion that the whole is more than the sum of its parts. One can mention collective excitations in continuous symmetry broken phases, fractionalization of the electron with elementary charge e and spin $\hbar/2$ into a spinon, carrying spin only, and a holon, carrying charge only, or states which are characterized by global topological quantities. Our overall goal is to study such phenomena in realistic models of correlated electron systems and to understand the emergent quantum many body phenomena. Apart from the intellectual curiosity this line of research will certainly impact material research where correlation effects play a dominant role. The building blocks of the model systems we consider are the electron-electron correlation, spin-orbit coupling and the electron-phonon interaction. These fundamental interactions, lead to a variety of phases including, among others, semi-metals, correlated topological insulators, magnets and superconductors. Our goal is to understand under which conditions these phases occur as well as the nature of the quantum phase transitions between them. The tools we use range from exact diagonalization, which is restricted to very small systems, to quantum Monte Carlo simulations. In the last grant period, we have tackled a number of topics which include studies of i) Topological Kondo Insulators [1] ii) Magnetic impurities in helical edge states [2] iii) Quantum phase transitions between Dirac fermions and an antiferromagnetic Mott insulator [3]. Below we will summarize some of the results we have obtained.

Results

Magnetic impurities on edges of topological insulators.
Quantum Spin-Hall insulators are novel states of matter, which are characterized by an insulating bulk and metallic edge. They have been synthesized in the group of L. Molenkamp at the university of Würzburg. The edge states are helical, meaning that the spin quantization axis is tied to the direction of motion: electrons with spin up (down) move to the right (left). The hallmark of this state, and the reason for which one can experimentally

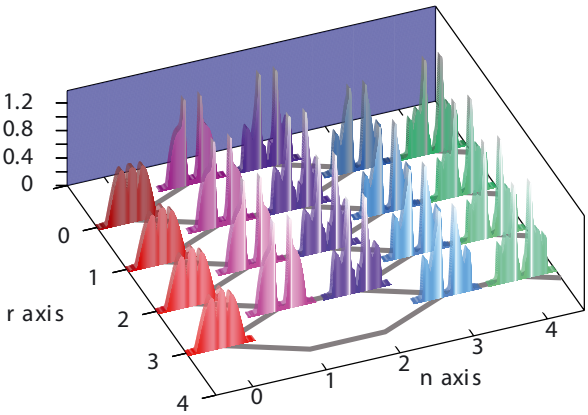

Figure 1: The plot shows the honeycomb lattice of the Kane-Mele model of topological insulators. At each lattice point we attach the local density of states. The magnetic impurity is located at the site r=0 on the edge of the sample. In the local moment regime (top figure) one can see the edge state, and the bulk insulating phase.

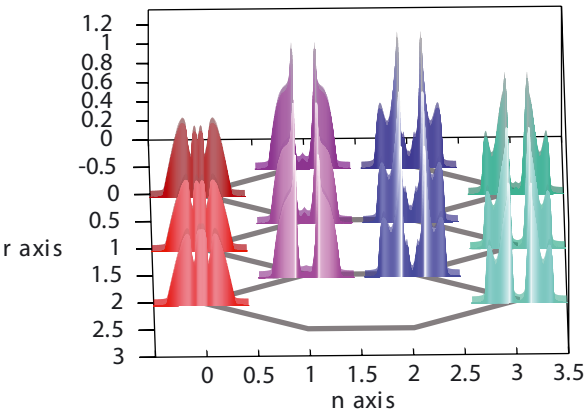

Figure 2: Now below the Kondo temperature one observes a depletion of low lying spectral weight on the edge around the impurity and an increase in the bulk. This images the rerouting of the edge state expected at temperatures below the Kondo scale.

observe it, lies in the fact that it is protected against potential scattering (impurities) due to time reversal symmetry. This is easily seen by noting that inversing the motion of the electron by bouncing of a scalar impurity requires flipping of the spin quantization axis. This is not allowed in the presence of time reversal symmetry.

In fact since the helical edge state is robust, impurities will merely redefine a new boundary and reroute the edge state along this new boundary. The above is valid for a potential scattering center with no internal degree of freedom. In the presence of a magnetic impurity, the situation is much more delicate and dominated by the correlation effects: the Kondo effect. At high temperatures, shown in Figure 1, the magnetic impurity is not screened and – due to the internal spin degree of freedom – acts as a source of backward scattering. Below the so-called Kondo temperature the impurity is screened by the edge state and essentially acts as a potential scattering center. Thereby, one should in our numerical simulations observe a temperature induced rerouting of the edge state. This phenomenon is shown in Figure 2.

The present calculations do not include a detailed understanding of transport phenomena. It is certainly desirable and experimentally relevant to supplement our present study with a detailed temperature analysis of the conductance through the edge state. One can anticipate a suppression of this quantity in the local moment regime – due to the presence of spin-flip scattering – followed by an increase to the unitary limit signaling the rerouting of the edge state around the Kondo cloud.

Fermionic criticality of Dirac fermions.
Another important result obtained in the former grant period is a detailed understanding of the Mott transition from Dirac fermions to an antiferromagnetic Mott insulator. This piece of physics is realized in the Hubbard model on the Honeycomb lattice. The Mott transition is a very old problem, which has continued to capture interest over the years since it is intrinsically a dynamical effect. In two and three dimensions it is a first order transition with a critical endpoint that presumably belongs to the Ising universality class. In the case of the Mott transition of Dirac fermions the transition is continuous and involves a breaking of the SU(2) spin and sublattice symmetries. Field theories of this transitions [4] argue that it belongs to a novel fermionic universality class. The fundamental question is if the field theory of this transition is correct and if we can pin down the critical exponents. A lattice model which we can simulate with quantum Monte Carlo methods and which captures this transition is the Hubbard model on the Honeycomb lattice. We have carried out extensive simulations of this model, and showed that our results can consistently be understood in the framework of the so called Gross-Neveu Yukawa model. Figure 3. shows a data collapse of the magnetization, with exponents compatible with the ε-expansion. We believe that this is an important result. To the best of our knowledge this the only fermionic model one can solve in dimensions higher than one and which shows a correlation driven metal to insulator transition.

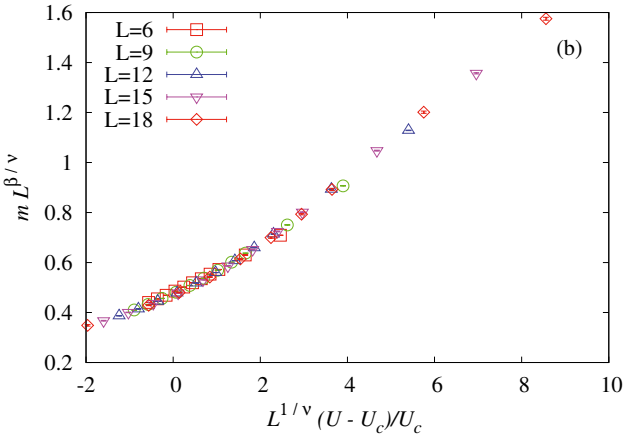

Figure 3: Data collapse of the magnetization for the Hubbard model on the Honeycomb lattice. The exponents are consistent with Gross-Neveu Yukawa universality characterized for example by a very large anomalous dimension η ~ 0.8. (Taken from Ref. [3])

Numerical methods.
Most of our CPU time goes into quantum Monte Carlo simulations. We generically rely on a Feynman path integral formulation to map the quantum many body problem to a classical one with a supplementary (imaginary time) dimension. Depending upon the method, the Monte Carlo time series samples classes of Feynman diagrams (continuous time methods) or Hubbard Stratonovitch fields (auxiliary field methods). In the absence of the so-called negative sign problem (as is the case for the half-filled Hubbard model on the Honeycomb lattice) the computational time scales as βV^3 for auxiliary field methods and $(\beta V)^3$ for continuous time methods. Most of the CPU time is spent in the matrix-matrix multiplication for which we use the BLAS routine zgemm. We use hybrid MPI and OpenMP to achieve optimal parallelization of the Monte Carlo code and typically use 128-256 cores. One important present issue is to determine as best as possible the critical exponents of Gross-Neveu Yukawa criticality. As it stands our lattice sizes are limited to 648 electrons corresponding to 18x18 unit cells of the Honeycomb lattice at half-band filling. It is important to achieve considerably larger lattice sizes so as to pin down universal numbers such as critical exponents. Since the CPU time scales as βV^3 it certainly is a feasible challenge.

References and Links

[1] J. Werner and F. F. Assaad. Phys. Rev. B, 88, 035113, (2013)
[2] F. Goth, D. J. Luitz, and F. F. Assaad. Phys. Rev. B, 88, 075110, (2013)
[3] F. F. Assaad and I. F. Herbut. Phys. Rev. X, 3, 031010, (2013).
[4] I. F. Herbut, V. Juricic, and O. Vafek. Phys. Rev. B, 80, 075432, (2009)

Uranyl Adsorption at Clay Mineral Surfaces

Research Institution
Fachgebiet Theoretische Chemie, Department Chemie, Technische Universität München

Principal Investigator
N. Rösch

Researchers
A. Kremleva, S. Krüger

Project Partners
—

LRZ Project ID: h0351

Introduction

The aqueous and sorption chemistry of actinide elements is of special concern for the assessment of environmental safety with regard to treating and storing radioactive waste of nuclear power plants and other facilities of nuclear industry. In this project the adsorption of solvated actinide ions on clay minerals is studied computationally. Clay minerals are ubiquitous in soils. Clays are used as technical barriers to prevent actinide migration and clay rocks represent a possible host rock formation for the construction of a final repository for highly radioactive waste. Cation adsorption and precipitation is an important mechanism to prevent the transport of actinide ions in the environment. Therefore detailed knowledge of the adsorption chemistry of actinides on clay minerals is of key importance for predicting their behavior and controlling these hazardous elements in the environment.

The well established Vienna Ab Initio Simulation Package (VASP) [1,2] is employed for calculating the electronic structure of periodic bulk and surface models. Surfaces are modeled as repeated slabs, separated by a vacuum layer, to achieve three-dimensional periodicity that allows one to apply the plane-wave band-structure approach to electronic structure. This software is based on MPI for a parallel treatment by distributing bands and coefficients of the wave function representation. For typical calculations with periodic unit cells of 100-200 atoms 64-128 cores can be used efficiently. Larger systems allow a higher degree of parallelization. Test calculations for uranyl adsorbed on montmorillonite, applying models of varying unit cell size, showed efficiencies (referenced to 32 cores) of 78 % on 128 cores and 50% on 256 cores for a model with 200 atoms. This latter value increases to 81 % for a larger unit cell comprising 400 atoms. These results demonstrate a very favorable scaling with increasing systems size. Some types of calculations demanding several electronic structure calculations for various geometries of the same system under study can be parallelized over these geometries. This latter strategy applies to numerical calculations of vibrational frequencies as well as optimization of a chemical reaction path. Dynamical simulations of solvated mineral surfaces present a particular computational challenge because for simulation times of a few ps in the order of 10-100 thousand electronic structure calculations have to be carried out. In optimizations of solvated mineral surfaces, the surface solvation is approximately modeled by adsorption of 1-3 layers of water molecules, while dynamical simulations allow a more realistic treatment of solvation by filling the whole interlayer space of the periodic surface model with water molecules.

Results

Clay minerals show a layered structure at the atomic level, composed of interconnected silica tetrahedra SiO_4 and alumina octahedra AlO_6. In this project the very common class of 2:1 clay minerals has been inspected. This class of clay minerals is built as a central alumina sheet sandwiched between two silica sheets (Figure 1). This basic structure corresponds to the mineral pyrophyllite which exhibits a neutral unit cell. Various other 2:1 clay minerals are derived from this structure by substitutions, inducing permanent negative charges in the mineral layer that are balanced by counter ions (Na^+, K^+, etc.) between the layers.

Clay minerals typically form platelets of micro- to millimeter size. These platelets show predominantly basal surfaces parallel to the mineral layers (Figure 1), exposing chemically saturated silica tetrahedra that show a low reactivity. With respect to metal ion adsorption, edge surfaces oriented (essentially) perpendicular to the minerals sheets (Figure 1) are more reactive as they expose a variety of aluminol, silanol and mixed surface groups for various edge surface orientations. In addition to the

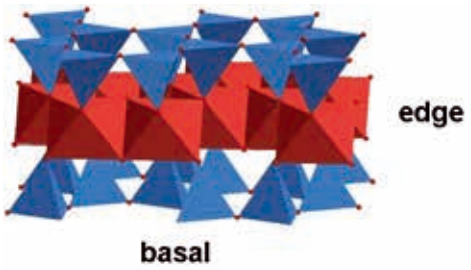

Figure 1: Structure of a layer of the 2:1 clay mineral pyrophyllite, composed of interconnected silica tetrahedra (blue) and alumina octahedra (red), exposing basal and edge surfaces.

negative layer charges resulting from substitutions, the edge surfaces show a variable surface charge depending on the pH of the surrounding aqueous solution, in consequence of adsorption (positive charge, low pH) or release (negative charge, high pH) of solvated protons. In this project, surface structures of pyrophyllite of three common edge surface orientations have been examined. Comparison of bare and solvated surfaces led essentially to the same patterns of surface groups. By means of dynamical simulations we were able to show, in agreement with earlier studies, that some of these surfaces do not show a static distribution of surface groups, but have a dynamical character as protons are easily exchanged between $AlOH_2$ and AlOH surface groups.

In a large survey we studied adsorption of uranyl(VI), UO_2^{2+} on the more important edge surfaces (010), (110), and (100) of pyrophyllite [3]. In agreement with experimental hints we explored preferentially bidentate coordinated uranyl species. These studies have been recently extended to the more important charged 2:1 clay minerals beidellite and montmorillonite which differ from pyrophyllite by substitutions of Si^{4+} by Al^{3+} in the tetrahedral sheet and of Al^{3+} by Mg^{2+} in the octahedral sheet, respectively. These permanent layer charges have been balanced by solvated Na^+ counter ions in the interlayer space. We inspected surface models where these defects are on the surface as well as in subsurface positions. This large set of edge surfaces together with the presence of various possible adsorption sites on each of them resulted in more than 100 adsorption complexes to be optimized. Surprisingly, essentially no changes were found in the structure of the mineral surfaces due to substitutions, even at the surface. Exceptions, besides rare proton exchanges between surface groups, are aqua ligands at surface Al^{3+} centers of the (010) edge surface. These ligands are loosely bound and may be exchanged with the solution or lost in the course of close-by uranyl adsorption. As the surface structures of the minerals compared are rather similar, also the same types of uranyl adsorption complexes have been determined. While the structure of complexes at the same site of different surfaces and minerals is rather similar, the complex formation energies change up to about 100 kJ/mol. The energy differences between various adsorption complexes tend to be wider distributed on pyrophyllite than on the substituted minerals. Notable geometric differences of uranyl adsorption complexes between the minerals inspected are only obtained when adsorption takes place at sites involving a substituted cation directly at the surface. From these results we conclude that the type of surface chemical groups forming various adsorption sites determines the adsorption complexes present. In contrast, surface orientations as well as the specific mineral play only a secondary role. This result agrees with available X-ray absorption fine structure (EXAFS) experiments which provide similar geometric parameters for uranyl adsorption at various clay and related minerals.

EXAFS results for uranyl adsorption on clay minerals showed a slight elongation of the uranyl U-O bond, U-Al/Si distances of about 310 pm and 330 pm and 5-6 U-O equatorial bonds to surface O centers as well as to aqua ligands, which in EXAFS are accessible only in an averaged form. In some experiments this equatorial shell of bonds was resolved into 2–3 shorter and some longer bonds. The short ones were interpreted as bonds to surface O centers while the longer ones have been attributed to bonds to aqua ligands. This interpretation has been extended in our studies. First of all, short as well as long bonds to surface oxygen centers have been calculated. In addition we found in some cases that uranyl complexes transfer a proton of an aqua ligand to the mineral surface, leading to the adsorbate uranylmonohydroxide UO_2OH^+ (Figure 2). For these complexes the U-OH bond was also determined to be short, suggesting another interpretation of the experimentally determined short equatorial U-O contacts.

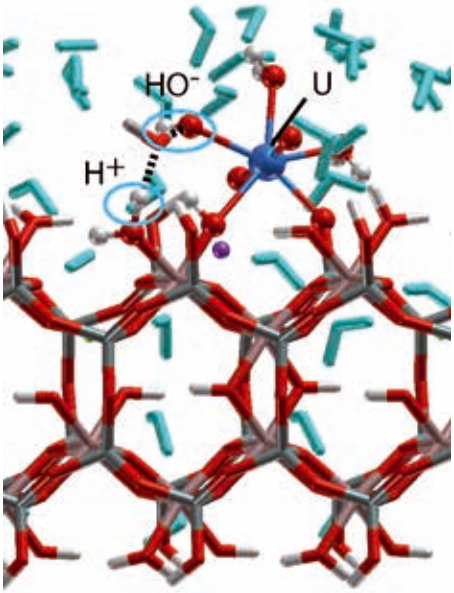

Figure 2: Uranyl UO_2^{2+} adsorbed on a solvated edge surface of the clay mineral pyrophyllite. Proton transfer from an aqua ligand to the surface leads to uranyl monohydroxide UO_2OH^+ as adsorbate.

By comparison of various uranyl adsorption complexes we traced back the variation of lengths of equatorial U-O bonds to the empirical charge of the oxygen centers involved [4]. Thus, a differentiation of bonds to ligands or to the surface by their length is not possible. In addition to our finding of uranylmonohydroxide as a novel adsorbed species, yet to be confirmed experimentally, we calculated for some complexes a reduced equatorial coordination number of 4, instead of the commonly found 5.

Overall we showed that uranyl complexes binding to the same surface groups of various edge surfaces of various minerals are rather similar; several sites may be occupied simultaneously. In addition, the coordination number may be lowered to 4 and hydrolysis on the surface may occur, leading to new adsorbed species. Comparison of optimized geometries and energetic considerations allowed us to suggest probable sites for each surface and mineral. These results provide helpful hints for the con-

struction of thermodynamic models of actinide adsorption at clay mineral surfaces and the interpretation of spectroscopic experiments.

On-going Research / Outlook

This first exemplary survey of actinide adsorption at complex clay mineral surfaces, which provided new insights at the atomic level, will be extended to other pertinent adsorbates like neptunyl NpO_2^+ and more complex minerals like iron-substituted phyllosilicates. In this way we will check if the concepts developed so far can be applied more generally, to support the interpretation of upcoming experiments. An essential facet of these studies will be to account also for the dynamical nature of the mineral/water interface by means of exemplary dynamical simulations.

This work is supported by Bundesministerium für Wirtschaft und Technologie, grant No. 02E11001.

References and Links

[1] Kresse, G., Hafner, J. Phys. Rev. B 47 (1993) 558-561.
[2] Blöchl, P. E., Phys. Rev. B 50 (1994) 17953-17979.
[3] Kremleva, A., Krüger, S., Rösch N., Phys. Chem. Chem. Phys. 14 (2012) 5815-5823.
[4] Kremleva, A., Krüger, S., Rösch, N., Surf. Sci. 615 (2013) 21-25.

Hybrid Density Functional Modeling of Transition Metal Clusters

Research Institution
Fachgebiet Theoretische Chemie, Department Chemie, Technische Universität München

Principal Investigator
N. Rösch

Researchers
T. Soini, A. Nikodem, A. Matveev, A. Genest

Project Partners
—

LRZ Project ID: h0351

Introduction

Catalysis plays a decisive role for a variety of processes in chemical industry. Catalysts facilitate or steer chemical reactions which otherwise would be slow or inefficient due to a large faction of undesired byproducts. Most of the catalysts applied today in industry are heterogeneous catalysts, especially small particles of transition metals, supported on oxides or zeolites. This motivates a considerable scientific effort to study transition metal particles and reactions on their surfaces. In this project we applied for the first time hybrid density functional methods to larger clusters of late transition metals comprising more than 100 atoms. The goal of this project is to examine the performance of various density functionals in the computational determination of properties and chemical behavior of transition metal clusters.

In the fundamental equation of density functional theory, the Kohn-Sham (KS) equation, electronic orbitals and their energies are calculated as eigenvectors and eigenvalues of the density dependent KS operator. These orbitals yield the electronic density. As the KS operator depends in turn on the density, the KS equation has to be solved iteratively (self-consistent field procedure, SCF). While the KS method is exact in principle, the quantum mechanical part of the electron-electron interaction, the density dependence of the so-called exchange-correlation (XC) term, is not explicitly known. Various approximate forms have been suggested. In the simplest formulations, the local density approximation (LDA) and the generalized gradient approximation (GGA), the XC functionals depend on the electronic density and, in addition, its gradients, respectively. More accurate functionals are constructed by also invoking the kinetic energy density of the electrons as variable (meta-GGA) or by including "exact exchange" contributions (hybrid functionals). The largest data sets to be calculated and treated in the Kohn-Sham approach using a local representation are analytic six-dimensional two-electron integrals to construct the Coulomb term of the electron repulsion. For the corresponding "classical" repulsion of electrons these so-called four-center integrals can be simplified by expanding the electron density in an auxiliary representation. For the exact exchange term in hybrid XC functionals, four-center integrals have to be calculated explicitly. For our calculations we used the parallel density functional program ParaGauss [1,2], developed in our group. This software uses Gaussian functions to represent electronic orbitals. Recently ParaGauss has been improved by introducing a new algorithm for the high-performance parallel treatment of the more demanding tasks of the KS approach. A work stealing algorithm without a central steering unit has been implemented [3]. It uses MPI-2 for message passing and replaces the earlier master-worker concept. The new algorithm avoids the bottleneck at the master process for a large number of workers and is applicable to any type of task which can be divided in independent work packages. Initially, these work packages are distributed evenly to the cores used. To equilibrate the computational load, each process which finished its tasks steals untreated tasks of another process and reports back all finished tasks. Thus, each of the parallel processes stays occupied until all tasks have been treated; the resulting load balancing is more favorable than that due to a static distribution [3]. This algorithm has been used to parallelize the calculation of all types of analytic integrals and the numerical evaluation of the XC functionals in ParaGauss.

Results

The new parallelization library has been validated by calculations on metal clusters applying hybrid XC functionals as the analytic four-center integrals needed for the exact exchange part of these functionals are the most demanding tasks of such density functional calculations. As the four-center integrals cannot be stored fully, they have to be recalculated in every SCF cycle. A series of all-electron test calculations of the four-center integrals of medium-sized copper clusters Cu_n, n = 10–22, without exploiting structural symmetry, showed that the new algorithm yields efficiencies above 93% for calculations on 512 cores for all these systems, increasing to 100% for larger systems. Work stealing performed always slightly better than a static distribution of tasks. For Cu_{22} with

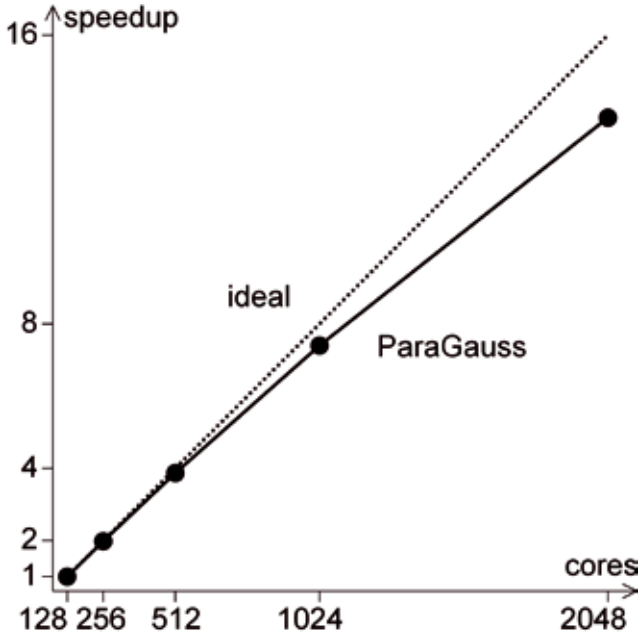

Figure 1: Scaling of a density functional electronic structure calculation of $Pt_{140}(CO)_8$.

work stealing an efficiency above 95% is achieved even on 2048 cores, while a static task distribution yields only 70 %. Models of metal nano particles can be efficiently calculated by choosing spatially symmetric structures and exploiting this symmetry. Full electronic structure all-electron test calculations applying the TPSSh hybrid XC functional including energy derivatives for geometry optimization of Cu_{79} (O_h symmetry) were carried on 512 to 2048 cores. The real time for the calculation of a single geometry dropped from 71 minutes on 512 cores to 26 minutes on 2048 cores, with an efficiency of 92% on 1024 cores and 72% on 2048 cores. This drop of efficiency for 2048 cores for this medium sized calculation is due to a limited scaling of various small tasks of the SCF procedure while the demanding calculation of four-center integrals still yields an efficiency of 96%, demonstrating that the implementation is capable of dealing with larger systems. As a pertinent example of a larger system, treated again with the TPSSh functional, we mention electronic structure calculations using pseudopotentials of the cluster Pt_{140} (D_{4h} symmetry) covered by 8 CO molecules. Test calculations on this system, on 128 to 2048 cores, a very favorable scaling was shown (Figure 1), with an overall efficiency of 86% on 2048 cores.

Our new efficiently parallel implementation of four-center integrals allowed for the first time a comparison of various hybrid XC functionals for larger transition metal clusters which are interesting models of heterogeneous catalysts. The hybrid functionals PBE0, M06 and TPSSh, have been compared to their semi-local congeners PBE (GGA), M06L, and TPSS (both meta-GGA). Cube-octahedral particles of Ni, Pd, and Pt (in O_h symmetry) with 13, 38, 55, 79, and 116 atoms were chosen as test set. Calculated average metal-metal bond lengths and cohesive energies (binding energies per atom) were extrapolated to infinite cluster size to compare the results to the corresponding experimentally known bulk properties. Extrapolated bond lengths are overestimated in general, as is well-known for GGA functionals. Interestingly, TPSSh and TPSS yield better agreement with experiment than PBE, while M06 largely exceeds the PBE results. For TPSSh and TPSS the bulk interatomic distances for Ni (249 pm) and Pd (275 pm) are reproduced within 3 pm; a somewhat larger deviation, 5 pm, was calculated for Pt (exp.: 277 pm). Hybrid functionals underestimate the cohesive energies, in line with the overestimation of bond lengths, while meta-GGA functionals tend to overestimate this property. The known preference of hybrid functionals for high-spin states was confirmed also for the larger transition metal clusters inspected. This finding may also be responsible for a considerable underestimation of ionization potentials of Ni clusters, which are strongly magnetic, while the results for Pd and Pt are similar to GGA results. Overall, TPSSh is the hybrid functional which yields the best results and thus is suggested if a hybrid functional is to be applied in transition metal catalysis studies.

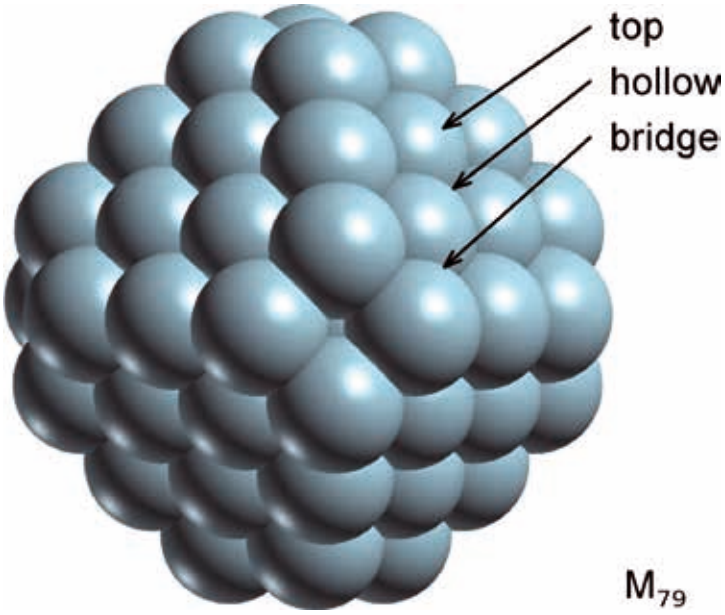

Figure 2: Various types of adsorption sites for CO on the truncated octahedral metal cluster M_{79} as example.

CO is a commonly used test molecule which also plays a key role in many catalytic processes. It was used as adsorbate on Pt clusters to study the performance of various XC functionals when calculating chemical bonding. Here especially the preferred adsorption site of the CO molecule on Pt is of interest, as common density functional methods predict preferred adsorption at hollow sites (Figure 2) in contrast to the experimental finding of top sites on the close-packed Pt(111) surface. This failure of the KS approach is interpreted as a self-energy artifact because the lowest unoccupied molecular orbital of CO, $2\pi^*$, is calculated too low in energy. This failure may be resolved by hybrid DFT methods. Therefore, we calculated CO adsorption at the (111) facets of the cluster model Pt_{79} (D_{4h} symmetry), resulting in the species $Pt_{79}(CO)_8$. In

agreement with other density functional results for surface models, we also find for all GGA, meta-GGA, and hybrid functionals considered that CO adsorption is more stable at hollow sites than at top sites on Pt_{79} (Figure 2). The most preferred site for all methods is the bridge site. The smallest energy difference between hollow and top sites is provided by the TPSSh functional. Calculations with the larger cluster Pt_{140} yield hollow sites as most preferable, showing that the preferred bridge site of Pt_{79} seems to be a feature of smaller clusters. Still, the top site is not preferred on Pt_{140}, in contrast to an extended Pt surface. Interestingly, while current hybrid methods seem to fail in predicting the correct CO adsorption site, we were able to demonstrate that the empirical DFT+U approach is able to resolve this problem, leading to preferred on-top adsorption for CO at Pt_{140} for an appropriate U parameter at the price of slightly underestimating the CO binding energy.

On-going Research / Outlook

Ongoing improvements of the parallel performance of ParaGauss aim at routine applications to transition metal and oxide particles that comprise a few hundred atoms as models in studies of heterogeneous catalytic reactions.

References and Links

[1] Belling, T.; Grauschopf, T.; Krüger, S.; Mayer, M.; Nörtemann, F.; Staufer, M.; Zenger, C.; Rösch N. in: High performance scientific and engineering computing, Bungartz, H.-J., Durst, F., Zenger, C., Eds., Lecture Notes in Computational Science and Engineering, Vol. 8., Springer, Heidelberg, 1999, 439-453.

[2] Belling, T., Grauschopf, T., Krüger, S., Nörtemann, F., Staufer, M., Mayer, M., Nasluzov, V. A., Birkenheuer, U., Shor, A. M., Matveev, A. V.; Hu, A., Fuchs-Rohr, M. S. K., Neyman, K. M., Ganyushin, D. I., Kerdcharoen, T., Woiterski, A., Gordienko, A, Majumder, S, Nikodem, A., Soini, T., Rösch, N., ParaGauss Version 3.1, Technische Universität München, 2013.

[3] Nikodem, A., Matveev, A., Soini, T., Rösch, N., Int. J. Quantum Chem., submitted.

Numerical study of the efficiency of thin film solar cells Research institution

Research Institution
University of Erlangen, Department of Computer Science 10

Principal Investigator
Christoph Pflaum

Researchers
Zhabiz Rahimi, Shuai Yan, Kai Hertel

Project Partners
Fraunhofer Institute of Silicate Research ISC, Department of Material Science 6, The University of Erlangen

LRZ Project ID: h0672

Introduction

There are several ongoing solar cell design projects at the Department of Computer Science 10 of University of Erlangen with cooperation partners from other German industries, research institutes and universities. The common goal of these projects is to analyze and optimize optical properties of thin film solar cells, in order to improve the efficiency of these solar cells. To this end, high frequency Maxwell's equations have to be solved within the solar spectrum wavelength range.

Thin film silicon solar cells are optimized to enhance light absorption. One technique to more efficiently utilize the incident light is increasing the path length of light within a solar cell using textured interfaces. In one approach, a sol-gel derived scattering layer was deposited between glass and ZnO layer, alternative to the commonly used rough TCO substrates [1]. We analyzed the influence of this scattering layer on the external quantum efficiency EQE of solar cell using cell processing and numerical simulations. These surface textures were described by AFM scan data.

Alternatively, nanostructured metal electrodes have been developed and used as transparent electrodes in thin-film solar cells. Solution-processed silver nanowire (Ag NW) films are cost-effective realization of these electrodes. The thin film solar cells manufactured by this process include randomly arranged Ag NW's (see Fig. 1).

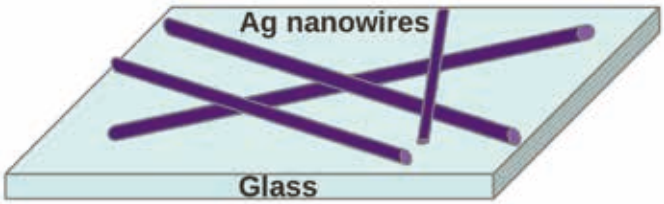

Figure 1: Sketch of Ag NW transparent electrodes.

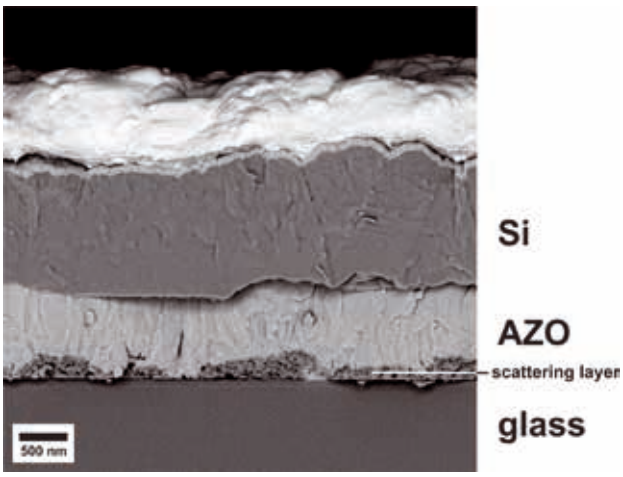

Figure 2: Solar cell structure with SiO_2 scattering layer (Copyright Fraunhofer ISC).

Results

Simulation of thin film solar cell with SiO_2 based scattering layers

We simulated a complete a-Si:H/µc-Si:H tandem solar cell with scattering layers at interfaces of inhomogeneous layers and obtained promising results. The resulting solar cell structure was very large; therefore the high performance computing was required. Our numerical method uses a rigorous full three-dimensional model for optical simulation. We extended and adapted the finite integration technique FIT, so that a thin film solar cell can be precisely calculated. Specially, when interfaces between layers contain random surface roughness. The goal of this work was to simulate effects of a dielectric SiO_2 scattering layer on light trapping and external quantum efficiency EQE inside tandem solar cells shown in Fig. 2, and compare the calculated EQE values with the experiment.

We performed a separate simulation for each wavelength and analyzed the performance of solar cells including layers with textured surfaces. Moreover, the role

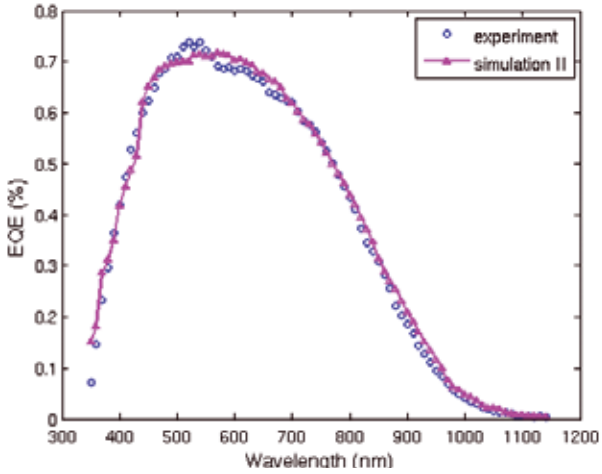

Figure 3: Comparison between measured EQE's for a realistic solar cell shown in Figure 2.

of a p-i-n structure on the accuracy of EQE calculation was studied. The absorbed light was calculated in a-Si:H and µc-Si:H layers separately and combined for the range of light spectrum from 350nm to 1100nm. The external quantum efficiency EQE for each wavelength was computed as the ratio of total solar cell absorbed power to the incoming light power.

An image processing method for approximating interface textures of µc-Si:H layers

We presented an algorithm based on mathematical image processing. This algorithm models changes in texture morphologies of *µc*-Si:H thin films grown on underlying textured AZO surfaces under deposition conditions, where the formation of nano-features is dominant. This algorithm can be used for generating a surface approximation of µc-Si:H layers after plasma enhanced chemical vapor deposition (PECVD) onto surface textured substrates, where data of the textured substrate surface are available as input. We utilized mathematical image processing tools and combined them with an ellipsoid generator approach. The presented algorithm has been tuned for use in thin-film silicon solar cell applications, in which textured surfaces are used to improve light trapping. We demonstrated the feasibility of this method by means of optical simulations of generated surface textures, comparing them to simulations of measured atomic force microscopy (AFM) scan data of both Aluminum-doped zinc oxide (AZO, a transparent and conductive material) and µc-Si:H layers [2].

Simulation of solar cells with nanowires

We studied the properties of Ag NW films and its application as percolation type electrodes for solar cells. Our cooperation partner is Department of Material Science 6, University of Erlangen-Nuremberg. One of our tasks was to simulate the optical properties of NW films using FIT program and calculate the transmission of the films with different surface coverage by Ag NWs. Beside the analysis of the electrical characteristics, we performed tuning of the transparency and conductivity of the film and optimizing their function as transparent electrodes.

We used time harmonic inverse iterative method (THIIM) to solve Maxwell's equation in Ag NW films [3]. Local 2D test has been carried out in order to verify the efficiency and accuracy of the mentioned method for the simulation of optical properties of Ag NW films. Particularly, the plasmonic effect caused by the Ag NW's has been investigated [4]. We have also performed various three-dimensional simulations on SuperMUC cluster for the whole range of light spectrum (up to 160 frequencies) and compared results with experiments as plotted in Figure 4.

On-going Research / Outlook

We have been analyzing optical properties of thin film solar cells in detail using SuperMUC. Current projects running on SuperMUC are the BMBF project SiSoflex und projects in Solarfabrik in ECN (Energy Campus Nürnberg).

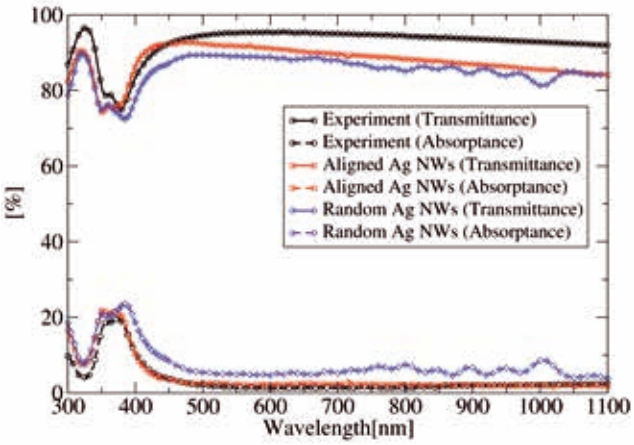

Figure 4: Comparison of simulated and experimental spectra of Ag NW electrodes with similar surface coverage of Ag.

References and Links

[1] Z. Rahimi, M. Mandl, C. Pflaum, H. Stiebig, J. Hüpkes and P. Löbmann, J. Appl. Phys (2014), under review.
[2] K. Hertel, J. Hüpkes, C. Pflaum, Optics Express, Vol. 21, Issue S6, pp. A977-A990 (2013).
[3] C. Pflaum, Z. Rahimi, Numer. Linear Algebra Appl. 18, 653 (2011).
[4] S. Yan, J. Krantz, K. Forberich, C. Pflaum and C. J. Brabec, J. Appl. Phys. 113, 154303 (2013).

Computational studies on porphyrines and related compounds for DSSC

Research Institution
Computer-Chemie-Centrum and Interdisciplinary Center for Molecular Materials, FAU Erlangen

Principal Investigator
Tatyana E. Shubina

Researchers
Timothy Clark, Dmitro Sharapa, Pavlo Dral, Johannes Margraf

Project Partners
—

LRZ Project ID: h0764

Introduction

Computational chemistry has become an indispensable tool for studying properties of known and predicting them for new compounds. Well-known compounds, for example, porphyrins play a central role in living cells and are important for the respiration and regulation processes. It is thus very important and challenging to understand electronic properties of these compounds reliably by quantum-chemical calculations.

On the other hand, porphyrins and related systems recently have found successful application as sensitizers for dye-sensitized solar cells (DSSC).

Photoinduced electron transfer (ET) in electron donor–acceptor conjugates has recently attracted much interest. A major goal of this research is to develop artificial photosynthetic systems that mimic the light-energy conversion processes of natural photosynthesis. The combination of porphyrins and fullerenes as donors and acceptors, respectively, has allowed the rates and efficiencies of charge separation to be maximized while simultaneously minimizing the rates of charge recombination (CR).

Figure 1. Porphyrin–fullerene conjugates *1* and *2* and the fullerene reference C_{60}-ref.

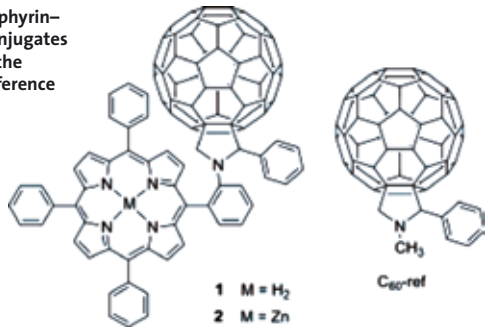

We performed computational studies with *1* and *2*, and the related C_{60}-ref, H_2TPP, and ZnTPP to gain insight into the experimentally observed phenomena. All structures were optimized at the ωB97XD/6-31G(d) level.

As expected, the C_{60} moieties in *1* and *2* behave as electron acceptors. In fact, the LUMO energy of C_{60}-ref matches closely those of both porphyrin–fullerene conjugates. Similarly, the HOMOs in *1* and *2* are located on the porphyrins with HOMO energies that match those of H_2TPP and ZnTPP, respectively. These findings are in excellent agreement with earlier calculations of similar porphyrin–β-oligo-(ethynylenephenylene)–fullerene conju-gates that bear oligo(ethynylenephenylene) (oligo-PPE) bridges.

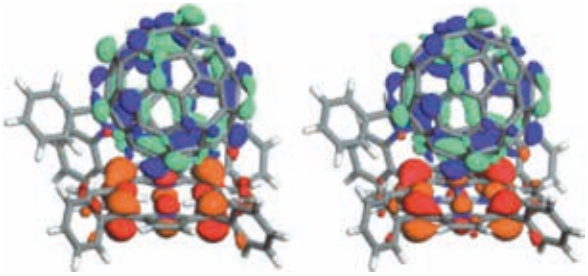

Figure 2. HOMOs (red-orange) and LUMOs (blue-cyan) of *1* (left) and *2* (right) at ωB97XD/6-31G(d) displaying their electron donor–acceptor character.

The calculations confirm the known trends of DFT-based and semi-empirical CI techniques to under- and overestimate the energies of charge-transfer transitions, respectively. The errors are close to equal but in opposite directions. A pragmatic approach would be simply to average the SAOP/TZP and PM6 UNO-CIS transition energies to obtain a closer estimate relative to the experimental results.

As expected, the relative positions of the porphyrins and C_{60} moieties have a large influence on the electron-transfer process. Donor and acceptor are very closely located in *1* and *2*, so it is important to take noncovalent interactions between the porphyrins and C_{60} moieties into account. We have therefore used the ωB97XD functional, which includes dispersion corrections. Indeed, the optimized geometries depend strongly on the level of theory used for the optimization. The calculated distance between donor and acceptor is approximately 3 Å at ωB97XD/6-31G(d), which is in excellent agreement with

that obtained using the MM^+ force field and with experimental distances between nonbonded porphyrins and C_{60} moieties in cocrystallates. The B3PW91 functional, which does not include a dispersion correction, gives an optimized distance between donor and acceptor of more than 4|Å, whereas it is more than 8|Å at PM6.

The two electron donor–acceptor conjugates (*1* and *2*) - one of which features a porphyrin-free base, and one of which features a zinc porphyrin - described here differ fundamentally from those reported to date because of the direct linkers between the carbon of the phenyl ring and the pyrrolidine nitrogen, which results in a completely frozen geometry. This geometrical constraint leads to fast photoinduced electron transfer as evidenced by a decay in just a few picoseconds of the porphyrin singlet excited state. The resulting charge-separated states are long-lived, with lifetimes of 506 ps for *1* and 90 ps for *2*. DFT and semi-empirical UNO-CIS calculations show that the HOMOs and LUMOs are localized on the porphyrin donor and the C_{60} acceptor, respectively, and HOMO–LUMO excitations therefore lead to the charge-transfer states. The energies of frontier orbitals of *1* and *2* correspond to those of the porphyrin and C_{60} references. The presence of zinc in the center of the porphyrin changes its local electronic properties and leads to faster electron-transfer dynamics. Calculated electronic-transition energies and intensities agree reasonably well with the experimental results, which reveals that DFT and semi-empirical UNO-CI methods under- and overestimate the transition energies by the same amount, namely, approximately 0.6 eV in toluene.

Compounds *1* and *2* form an ideal basis for future optimized donor–acceptor conjugates for charge separation, in which other photo- or electroactive moieties can be incorporated.

On-going Research / Outlook

Incentives for DSSCs include various materials and recent progresses considering solid-state devices/substrates flexibility. To this date, record efficiencies reaching 13% have been reported for n-type DSSCs. To go beyond these values, new efficient p-type DSSCs, which complement n-type DSSCs are under intense studies.

In these devices, the chromophore is critical in terms of light harvesting, charge transfer, and charge transport. Many studies are focused on porphyrines- or phthalocyanines-based DSSCs. However, both of those exhibit electron-donating features. On the other hand, similar to porphyrines and phthalocyanines, porphycenes show electron acceptor properties, which should be more useful for the p-type DSSCs.

Time-dependent calculations (TD-DFT) were performed with wB97XD functional with 6–31G(d) basis set using Gaussian 09. The solvent effect (solvent - DMF) was included via SMD solvation model. Molecular orbitals are illustrated in Figure 3. UV-Vis spectra were calculated for the first 30 excited states with the same method (wB97X-D/6–31G(d), DMF). Results are presented in Figure 4.

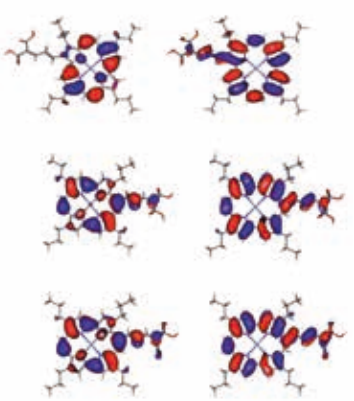

Figure 3. Illustrations of the HOMO (left) and LUMO (right) states top) *P1*, middle) *P2*, and bottom) *P3* (wB97X-D/6–31G(d))

The impact of the position and the nature of the anchor on the molecular and electronic structures of the porphycenes was elucidated through DFTcalculations (see above). While no differences were noted regarding the molecular structures of *P1*, *P2*, and *P3*, their electronic structures are quite different. The highest-occupied molecular orbital (HOMO) topology, for example, reflects in *P2* and *P3* a delocalization of the p-conjugation involving the anchors, that is, via the ethylene bridges – Figure 3. The HOMO of *P1* is, in contrast, nearly exclusively localized at the core of the porphycene with a less than 5 % contribution at the anchor – Figure 3. Hence, electronic coupling to assist hole injection from the valence band of NiO to the HOMO of *P2* and/or *P3* is more effective than the case for *P1*. A common feature of all three porphycenes is a lowest-unocuppied molecular orbital (LUMO) that is totally delocalized - Figure 3. Ideally, the LUMO should be separated from the semiconductor electrode to retard geminate charge recombination.

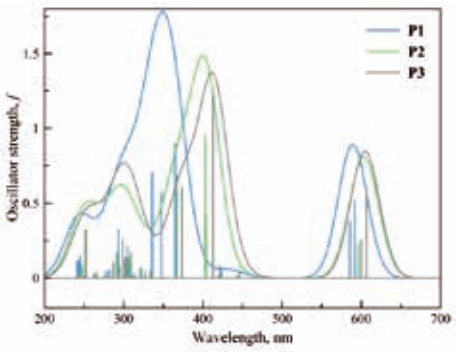

Figure 4. Computed, ωB97XD/6–31G(d) UV-Vis spectra of *P1-P3*

Calculations performed on SuperMUC were done with Gaussian 09 D.01, Orca 3.0.1, Turbomole 6.4 using 1-5 40 cores nodes and 80-160 Gb of RAM. We used theories ranging from HF to CASPT2 with moderate to very large basis sets. CBS and G3-G4 calculations were done also. During calculations performed on SuperMUC approx. 1000-1500 log-files were generated and the same amount of checkpoint files. Total size of generated files is close to 1 Tb (mainly binary/checkpoint files). For the various projects different software was used, such as Gaussian 09, Orca, ADF, MOLPRO, MOLCAS, PSI4, PRIRODA, CFOUR, Dalton installed on LRZ.

References and Links

[1] Ciammaichella, A., Dral, P. O., Clark, T., Tagliatesta, P., Sekita, M., Guldi, D.M. *Chem. Eur. J. 18*, **2012**, 14008-14016
[2] Feihl, S., Costa, R.D., Brenner, W., Margraf, J.T., Casillas, R., Browa, A., Shubina, T.E., Clark, T., Jux, N. Guldi, D.M. *Chem. Comm.*, ***submitted***

Microscopic insights into vibrational dynamics in aqueous solutions

Research Institution
Department of Physical Chemistry II, Ruhr-University Bochum

Principal Investigator
Martina Havenith

Researchers
Matthias Heyden, Gerald Mathias, Martina Havenith

Project Partners
Department of Theoretical Chemistry, Ruhr-University Bochum; Department of Biomolecular Optics, LMU Munich

LRZ Project ID: h1242

Introduction

The properties of water as a liquid and solvent are governed by its extensive hydrogen bond (HB) network. Picosecond lifetimes of water-water HB's dictate the speed limit of dynamic processes involving intermolecular motion, such as diffusion and dipolar relaxations. The ability of solutes to favorably interact with the water HB network divides the world of chemistry into hydrophobic and hydrophilic compounds.

Vibrational spectroscopy is a sensitive probe for H- bonding in liquids in general, but in particular in water and aqueous solutions. The *intermolecular* vibrations in water, e.g. the actual vibrations of the water-water HB's, give rise to characteristic vibrational bands in the far-infrared, including bending and stretching motions of the HB's, around 75 and 200 cm^{-1}, respectively, and librational tumbling of water molecules in their local H-bonding environment at frequencies from 400 to 1000 cm-1. Experimentally, it was shown that the low frequency far-infrared/THz vibrations of the water HB network are subject to long-ranged effects that modify their absorption cross sections in the vicinity of biomolecular solutes. The studies detailed here helped significantly to understand this effect by examining the collective properties and the delocalized character of the HB vibrations in water [1,2] and provided the theoretical basis for a subsequent study on biomolecular systems [3].

In addition, HB's cause significant red shifts of up to several 100 cm^{-1} of the intramolecular vibrational modes, in particular of the O-H stretch vibration. Depending on the particular arrangement of HB's in the vicinity of a water molecule its frequency can range from roughly 3200 to 3700 cm-1.

The absorption cross sections of the intermolecular and intramolecular vibrations depend very strongly on dynamic polarization effects [1], which often expose the limits of simulation methods based on empirical potential energy models. Here, *ab initio* molecular dynamics (aiMD) simulations based on density functional theory (DFT) potential energies are used to study the vibrational spectrum of water and aqueous solutions in unprecedented detail and reveal the effects of correlated vibrational motion, intermolecular polarization effects and the shortcomings of empirical models.

Results

For our simulations we employed the CP2K software package and its QuickStep module for fast and efficient Born-Oppenheimer aiMD simulations with an MPI-parallelized code (www.cp2k.org). The Perdew-Burke-Ernzerhoff exchange correlation functional and a TZV2P basis set were employed to treat systems of 128 water molecules for the neat liquid, and solutions of a single urea molecule in 125 water molecules, at the respective experimental density. In addition hexagonal ice crystals of 96 and 288 water molecules were studied to facilitate the analysis of long-ranged collective vibrational motion detected in the liquid.

Individual simulations exhibited near-linear scaling (89%) on 64 cores. Our simulation protocol further contained implicit parallelization. For the liquids a long single ca-

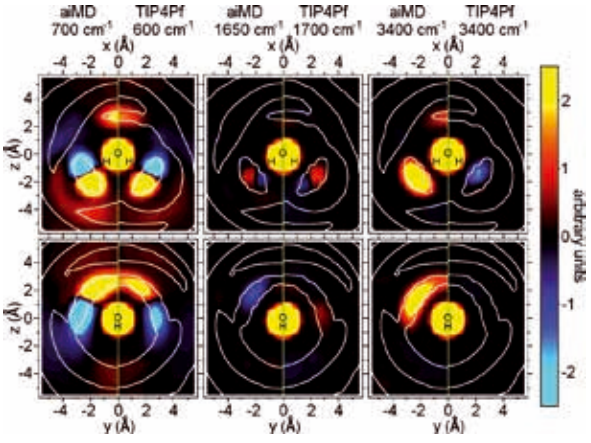

Figure 1: Contributions to the IR cross section from dipolar correlations in the 3D environment of a water molecule from aiMD simulations and simulations with a flexible empirical force field (TIP4Pf). White contours indicate the oxygen density in the 3D environment of the reference molecule [2].

nonical (constant temperature) trajectory (100 ps for water, 160 ps for the solution) was generated at an elevated temperature of 400K to overcome restrictions due to missing nuclear quantum effects in classical simulations on the Born-Oppenheimer potential surface and intrinsic overbinding for water-water HB's in the PBE functional. Uncorrelated snapshots from this trajectory were then used as starting points for microcanical (constant energy) MD simulations of ~20 ps length (16 runs for water, 40 runs for the solution). These were run in parallel using 512 to 1024 cores simultaneously in a single job. For simulations of crystalline ice, 16 independent starting configurations of the proton-disordered crystal were generated directly, which again were simulated in parallel after constant temperature equilibration at 270K for 5 ps.

Both, the system sizes and the overall length of the simulated dynamics, several 100 ps for each system and ~1 ns for the solution, correspond to the current state-of-the-art. The long simulations are required to converge vibrational absorption spectra and to resolve vibrational and dipolar cross correlations as described in references 1&2. In total approximately 3 million CPU hours were used for this project.

With our studies, we were able to provide a full description of the vibrational spectrum in liquid water, including detailed analysis of collective vibrational modes and the contributions to the IR absorption from correlated fluctuations of molecular dipoles. The latter are a consequence of the theoretical connection between the IR cross section and the fluctuations of the system's total dipole moment. Fig.1 shows the three dimensionally resolved contributions to the IR absorption from correlated dipole fluctuations in the environment of a water molecule at 3 selected frequencies, corresponding to librations and the intramolecular bending and OH-stretch vibrations. The results show the presence of positive and negative correlations of the dipolar fluctuations that modulate the total IR absorption, in particular in the first solvation shell. The comparison to simulations with a non-polarizable empirical force field, widely used standard MD simulations (TIP4Pf), indicates the inability of the latter to capture these correlations correctly, even qualitatively, for the intramolecular vibrations [2].

In addition, we analyzed the correlations of the vibrational motion of the atoms in the 3D environment of a water molecule. Here, the comparison between *aiMD* and force field simulations shows, that the non-polarizable force field is able to capture the correlated vibrational motion correctly in the far-infrared region as well as for the OH-stretch. The former region of the spectrum is dominated by long-ranged correlations and collective modes related to sound propagation in water. At the OH-stretch vibration, vibrational motion is, in comparison more localized on single molecules and their neighbours, despite the strong correlations of induced molecular dipoles [1] (apparent for the *aiMD* simulation in Fig. 1). Although the force field does not capture these induced dipoles, this does not seem to affect the collective vibrations. However, this doesn't hold at the bending frequency. Here,

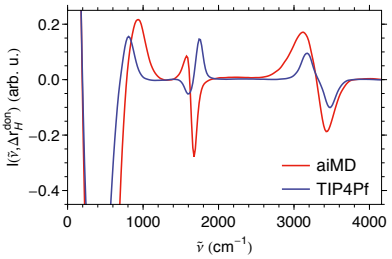

Figure 2: Spectra of the (mass-weighted) cross correlation functions of the atomic velocities of a reference molecule and the hydrogens of its HB donor in aiMD and force field simulations [2].

correlations of vibrational motion are qualitatively incorrect in the force field simulation. This is highlighted in Fig. 2, which displays the Fourier transform of the cross correlation functions between mass-weighted velocities of the reference molecule and hydrogens at the HB donor site. The spectrum shows, as a function of vibrational frequency, whether the vibrational motion of this donor hydrogen are correlated or anti-correlated with the vibrational motions of the reference molecule. At the bending frequency of roughly 1650 cm^{-1}, clearly the correlations observed in the empirical force field simulation are of opposite sign, in addition to the generally reduced strength of the correlations, relative to the *aiMD* reference.

Our results provide us with detailed insights into the vibrational motions in water and aqueous solutions, which are relevant for the interpretation of spectroscopic observations and also provide unique reference data for computationally efficient force field models. Polarizable force field models, for example, which aim to describe the dipolar couplings and spectroscopic properties of water correctly, can therefore be tested against the high quality aiMD simulations carried out on HLRB2 and SuperMUC.

On-going Research / Outlook

Without the infrastructure provided by the LRZ and the HLRB2/SuperMUC, highly accurate aiMD simulation studies that provide detailed microscopic insights into condensed matter, would be computationally prohibitive. Continuing analysis of the aqueous solution trajectories allow us to describe solute-induced effects on the water spectrum at all vibrational frequencies. Further, our data set allows us to develop empirical models that can capture the spectral properties in microscopic detail, ensuring not only that simulated spectra are predicted correctly, but also for the right reasons. Such models are required to allow for similar studies on biomolecular studies. Already now, our comparison between aiMD and empirical models enabled us to carry out a computational study on protein solutions, which focused on the delocalized vibrations in the far-infrared [3], which apart from their exact IR cross section, are correctly reproduced.

References and Links

[1] M. Heyden, J. Sun, S. Funkner, G. Mathias, H. Forbert, M. Havenith and D. Marx. *Proc. Natl. Acad. Sci. USA*, 2010. 107(27), 12068-12073.
[2] M. Heyden, J. Sun, H. Forbert, G. Mathias, M. Havenith and D. Marx. 2012. *J. Phys. Chem. Lett.*, 3. 2135-2140.
[3] M. Heyden and D. J. Tobias. 2013. *Phys. Rev. Lett.*, 111, 218101.

http://www.ruhr-uni-bochum.de/pc2/
http://www.kofo.mpg.de/heyden

THz spectroscopy of solvated biomolecules studied by ab initio molecular dynamics

Research Institution
Lehrstuhl für Theoretische Chemie, Ruhr-Universität Bochum, D-44780 Bochum

Principal Investigator
Dominik Marx

Researchers
Jian Sun, Dominik Marx

Project Partners
Department of Theoretical Chemistry, Ruhr-University Bochum; Department of Biomolecular Optics, LMU Munich

LRZ Project ID: pr23va

Introduction

Solvation of molecules in water is a core topic in molecular sciences and of broad importance to many subdisciplines within chemistry and biology. Based on decades of advances due to spectroscopy in concert with simulation, well-established notions such as interfacial water, solvation water, or so-called "biological water" make clear the point that the properties of water close to solutes might be vastly different from those known from the bulk liquid. Laser spectroscopy in the frequency window from 1 up to about 5 THz, corresponding to roughly 30–200 cm 1 , has been proven recently to be a sensitive tool to probe hydration dynamics. Using THz spectroscopy,"extended dynamical hydration shells" have been detected and shown to feature a distinctly different dynamics compared to bulk water that might extend up to 20 A away from the solute. The pronounced sensitivity of THz spectroscopy to the dynamics of interfacial water is a consequence of a wealth of dynamical processes, such as HB rearrangements and rotational relaxation, that constantly take place in the HB network surrounding solutes.

Lacking much behind, however, is our understanding and, even more so, the assignment of THz spectra of aqueous solutions, which are much broader and less structured than those known from the mid–IR range underlying intra-molecular vibrational spectroscopy. Ab initio molecular dynamics [1,2] has been most successful to decompose IR spectra of solutions into molecular contributions. Yet, despite much progress on understanding the THz response of ions in water, the THz spectrum of a molecule in bulk aqueous solution has never been assigned to our best knowledge. A first step in this direction has been taken recently by dissecting the THz spectrum of the solvent itself, bulk water at ambient conditions, in terms of solvation shell contributions and associated inter-molecular HB modes. [3] THz spectra of aqueous solutions, however, are obviously much more complex than those of the neat solvent.

As the basic building blocks of proteins, amino acids are zwitterionic in ambient water. They feature both anionic and cationic solvation shells, being characteristic from biomolecules to polyelectrolytes, in addition to hydrophobic solvation which can be tuned via their side chains. The vibrational spectra of amino acids, in particular of glycine being the simplest one, have been studied thoroughly using a broad range of experimental and theoretical approaches. [4] While the THz spectra of molecular aqueous solutions still remain terra incognita and, even more, when it comes to assigning these low–frequency vibrational spectra in terms of molecular motion.

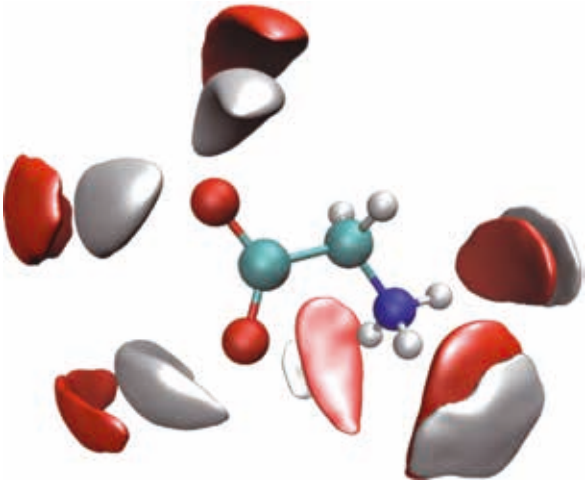

Figure 1: Spatial distribution function of water around solvated glycine, Gly(aq). The red and grey isosurfaces are drawn at a number density of water O atoms of 0.14 Å^{-3} and at 0.19 Å^{-3} for water H atoms, respectively. Note, that there are only three attractor basins at the –COO$^-$ group available for about four and a half hydrogen-bonded water molecules on average, which leads to fast dynamical exchanges compared to the –NH$^+$ group where three basins are available for three donated hydrogen bonds on average. Thus the solvation shell of the –COO$^-$ group is much less well defined than that of the –NH$^+$ group.

Results

AIMD [1] simulations based on the iterative Born–Oppenheimer propagation approach are performed using the Gaussian and plane waves mixed-basis method as implemented in the QUICKSTEP module within the CP2K AIMD simulation package.[2] The spatial distribution function of water around solvated glycine is shown in Fig.1. We find the solvation shell of the $-NH_3^+$ group to be well defined, each of the protons donating a HB to a water molecule. The $-COO^-$ group has roughly four and a half water molecules in the first solvation shell. As Fig.2 shown, intra-molecular glycine THz modes together with rigid–body–like cagemotion, leading to the red line in Fig.2, cannot fully explain the shape of the observed THz domain spectrum. This brings us back to the observation of pronounced solute-solvent coupling, i.e. cross-correlations which are strongly peaked around 200 cm^{-1} according to the green line in Fig.2, that apparently can "fill in" the missing intensity. [5] Based on the observation, we propose a "supermolecular solvation complex" (SSC), which includes a number of n specific interfacial water molecules together with the solute. With this SSC model [5], we were able to unveil three distinct classes of modes of increasing complexity that are all important in the THz regime: (i) intra–molecular low-frequency modes of the solute, (ii) motion of the quasi–rigid solute in its transient solvation cage, and (iii) inter–molecular solute–solvent hydrogen bonding modes that are possibly intimately coupled to suitable intra–molecular solute modes. [5]

Within this general framework, the resulting assignment of the experimental THz spectrum of Gly(aq) turns out to be surprisingly simple: the high-frequency peak at ≈ 320 cm^{-1} is an intra-molecular vibration involving the N-C-C-O angle and thus backbone motion, the lowest frequency feature around 80 cm^{-1} stems from rigid-body-like librational and also rattling motion of the glycine molecule in its own solvation cage, whereas the broader resonance somewhere around 200 cm^{-1} is traced back to inter–molecular glycine-water hydrogen bond stretching motion.

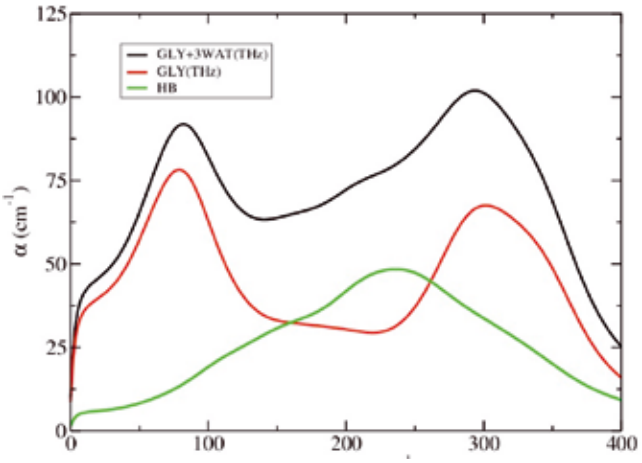

Figure 2: AIMD spectra obtained from the supermolecular solvation complex, Gly(3 H2 O), taking into account only the THz modes. Red line: all modes coming exclusively from glycine motion; Green line: all hydrogen-bonding modes involving the three water molecules; Black line: all THz modes of Gly(3 H2 O). all computed spectra are shown using unscaled absolute intensity units as indicated and no friquency adjustment has been applied.

On-going Research / Outlook

THz spectroscopy as a tool to study (bio)molecular hydration is a rapidly developing field. The focus of this investigation is to understand the measured lineshape of the low–frequency vibrational spectrum of molecules solvated in liquid water. Based on a close interplay of theory and experiment we could show that it is possible to assign THz spectra of molecular solutions in terms of atomic motions thus providing a microscopic picture.

As it is completely out-of-reach to produce trajectories of the necessary quality and length without the use of a facility such as the HLRB2, we are very thankful for the supply of the computational resources. The new generation high performance computer – SuperMUC, allows us to generate much better statistics. Furthermore, it enable us to investigate larger molecules and more complicated systems such as those currently investigated in experiments. While during the process of the project the ongoing experiments observed much larger concentration dependence of the absorption cross section in valine solution than in aqueous alanine, we decided to extend the simulations to the even larger Valine molecule. Such study would not be possible without having accessing to SuperMUC!

References and Links

[1] D. Marx and J. Hutter, Ab Initio Molecular Dynamics: Basic Theory and Advanced Methods (Cambridge University Press, Cambridge 2009).
[2] J. VandeVondele, M. Krack, F. Mohamed, M. Parrinello, T. Chassaing, and J. Hutter, Comput. Phys. Commun. 167, 103 (2005); CP2K code, http://cp2k.berlios.de.
[3] M. Heyden, J. Sun, S. Funkner, G. Mathias, H. Forbert, M. Havenith, and D. Marx, Proc. Natl. Acad. Sci. U.S.A. 107, 12068 (2010).
[4] J. Sun, D. Bousquet, H. Forbert and D. Marx, J. Chem. Phys., 133, 114508 (2010).
[5] J. Sun, G. Niehues, H. Forbert, D. Decka, G. Schwaab, D. Marx, and M. Havenith, J. Am. Chem. Soc. (2014) (accepted).

Simulation of Electron Transfer Processes in Molecular Systems at Surfaces

Research Institution
Friedrich-Alexander Universität Erlangen-Nürnberg, Erlangen, Germany

Principal Investigator
Michael Thoss

Researchers
Pedro B. Coto, Ivan A. Pshenichnyuk, Veronika Prucker, Óscar Rubio-Pons, Susanne Leitherer

Project Partners
Technical University of Munich, Garching, Germany

LRZ Project ID: pr28lo

Introduction

The transfer or transport of electrons (ET) is a key step in many processes in physics, chemistry, biology and technology [1]. Examples range from intramolecular charge transfer in donor-acceptor complexes in solution over ET in sensory proteins or photosynthesis to charge transport processes in solar cells. Among the variety of ET processes, heterogeneous ET in molecular systems adsorbed at semiconductor or metal surfaces have been of particular interest recently. Important applications in which heterogeneous ET plays a fundamental role include photonic energy conversion in organic solar cells (in which photoexcitation triggers the injection of an electron from an excited electronic state of a dye molecule into the conduction band of a semiconductor) and voltage driven charge transport in nano-scale molecular junctions (i.e. molecules which are chemically bound to metal or carbon-based electrodes). Furthermore, understanding ET at the molecule-substrate interface is a pre-requisite for the development of nanoscale molecular devices.

From the theoretical point of view, modelling electron transfer and electron transport at molecule-substrate interfaces requires methodologies that can describe simultaneously a finite system with a discrete energy spectrum, the molecular adsorbate, and an extended system, such as a semiconductor or metal surface or an electrode, with a (quasi-)continuous energy spectrum. Furthermore, the methodologies must be able to describe non-equilibrium effects which are typically present in both heterogeneous ET reactions and voltage driven electron transport processes. Therefore, a proper description of these processes requires, in addition to the detailed characterization of the electronic structure of the system involved in the ET process, a dynamical treatment.

Here, we report recent results on the simulation of heterogeneous ET processes. In particular, we analyze the dynamics of electron injection in a series of short chain nitrile-substituted alkanethiolate self-assembled monolayers (SAM) adsorbed at the Au(111) surface [2] and study voltage-driven charge transport processes in molecular junctions that use graphene as electrode material [3].

Results

The simulations of the ET processes mentioned above have been carried out using a two-step procedure. In the first step, ab initio electronic structure methods are used to determine the electronic structure of the system of interest. This provides important parameters, such as electronic states, energies and donor-acceptor couplings. Specifically, the different systems investigated have been modeled employing periodic density functional theory (DFT) calculations which allows a proper description of their extended nature. We have employed the Vienna ab-Initio Simulation Package (VASP) to solve the Kohn-Sham equations using the projector augmented wave method and a plane wave basis. These calculations strongly benefit from the use of parallel supercomputing environments such as SUPERMUC. In the second step, the parameters obtained from the electronic structure calculations are used to simulate the dynamics of electron injection in heterogeneous ET processes or the current-voltage characteristics in charge transport in molecular junctions employing a model Hamiltonian [2] and non-equilibrium Green's function techniques [3], respectively.

Electron injection dynamics in alkanethiolate SAMs adsorbed at the Au(111) surface
We have simulated the electron injection dynamics in a series of nitrile-substituted alkanethiolate SAM models characterized by having aliphatic spacers of different lengths (-$(CH_2)_2$-, -$(CH_2)_3$-, and -$(CH_2)_4$- , respectively see Fig. 1) adsorbed at the Au(111) surface. In particular, we have considered the injection dynamics from the near-degenerate π_1^* and π_2^* donor states corresponding to the two π^* resonances of the CN group that can be selectively monitored using core-hole clock spectroscopic techniques [4]. For all systems, the most stable adsorption geometry was found to be a fcc bridge-like configuration with the molecules tilted against the sur-

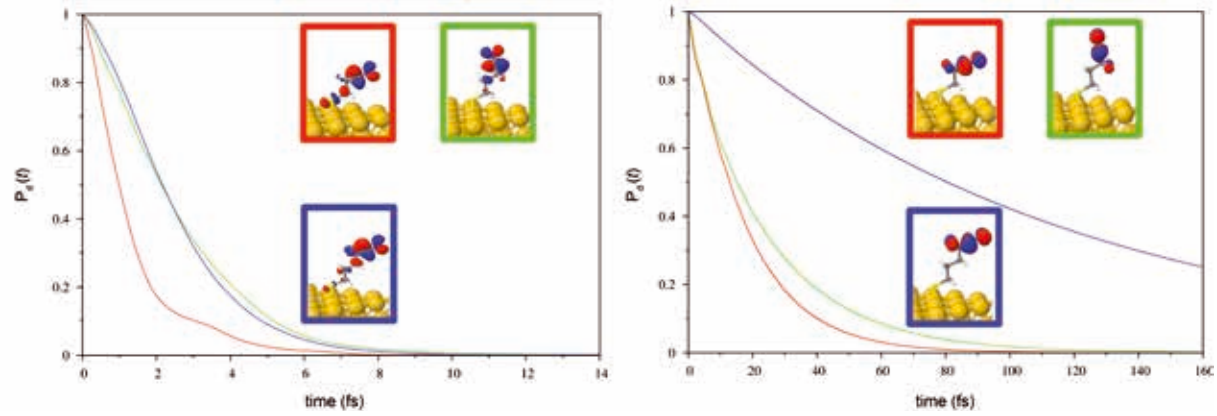

Figure 1: Population dynamics of the (left) and (right) donor states for C2 (red), C3 (green), and C4 (blue). The donor states for the respective systems are also shown.

face normal and the relative orientation of the CN group depending on the number (even or odd) of methylene units in the spacer chain. The simulations of the electron injection dynamics (see Fig. 1) exhibit ultrafast femtosecond ET in all systems with electron injection times that increase with the length of the aliphatic chain for π_1^* ($\tau 1/2$=1.0 fs (C2), $\tau 1/2$= 2.1 fs (C3) and $\tau 1/2$ = 2.2 fs (C4), respectively) and π_2^* ($\tau 1/2$=12.3 fs (C2), $\tau 1/2$=15.1 fs (C3), $\tau 1/2$=80.5 fs (C4), respectively). These results qualitatively agree with the experimental data [4] and can be rationalized in terms of the spatial localization of the donor state and the length of the aliphatic spacer chain.

The π_1^* donor states show faster electron injection times than the corresponding π_2^* states (see Fig. 1). This can be explained on the basis of the spatial localization of the donor states. The π_1^* donor states have a more delocalized character than the corresponding π_2^* states (in particular for C2 and C3, see Fig. 1) with significant contributions at the aliphatic chain and the head group (sulfur atom). This results in a larger coupling to the substrate and therefore in faster electron injection rates. Finally, our results show that in general for both types of donor states the electron injection rate decreases for longer aliphatic spacer groups. This is a consequence of the exponential decrease of the donor-acceptor couplings with the distance between the donor and acceptor moieties.

Charge transport in molecular junctions with graphene electrodes

While most experiments exploring the conduction properties of single-molecule junctions have used metals as material for the electrodes, we have investigated charge transport in a series of molecular junctions with graphene as electrode material. Graphene has several advantages over conventional metals both structural and electronic. On the one hand, graphene is characterized by its rigidity and mechanical stability which allows a more precise control of the molecule-electrode contact geometry than in conventional junctions with metallic leads. On the other hand, it shows excellent electronic properties, in particular, high electron mobility. These factors make graphene a promising material for electrodes of molecular junctions. Our results show that the unique electronic properties of graphene strongly influence the transport in the nanojunctions. In particular, edge states in graphene electrodes with zigzag termination (cf. Fig. 2) result in additional transport channels close to the Fermi energy, which deeply affects the conductance at small bias voltages. Investigating different linker groups as well as chemical substitution, we have also investigated how the transport properties are influenced by the molecule-lead coupling and the energy level lineup [3].

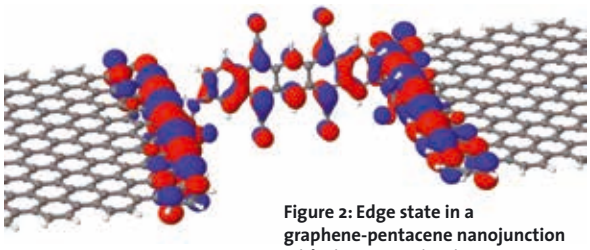

Figure 2: Edge state in a graphene-pentacene nanojunction with zigzag termination.

On-going Research / Outlook

Our on-going research involves the study of photoinduced ET processes in a variety of molecule-surface systems. In addition, we investigate electron transport and photophysical properties of molecular nanocontacts with graphene as electrode material in architectures where two graphene leads are connected by an organic molecule. Due to its particular properties, such as high electron mobility, rigidity, mechanical stability and its optical properties, graphene electrodes may facilitate the optical addressability of the nanocontact for future optoelectronic applications. This project will benefit from the methods developed and the experience acquired in the simulation of electron transfer processes of molecules at metal and semiconductor surfaces.

References and Links

[1] *Electron Transfer: From Isolated Molecules to Biomolecules, Parts I and II*, Adv. Chem. Phys. Vols. 106 and 107, ed. Jortner J. and Bixon M., Wiley, New York, 1999.
[2] Prucker, V., Rubio-Pons, O., Bockstedte, M., Wang, H., Coto, P. B., Thoss, M. 2013. J. Phys. Chem. C. 117, 25334.
[3] Pshenichnyuk, I. A., Coto, P. B., Leitherer, S., Thoss, M. 2013. J. Phys. Chem. Lett. 4, 809.
[4] Kao, P., Neppl. S., Feulner, P., Allara, D. L., Zharnikov, M. 2010. J. Phys. Chem. C 114, 13766.

http://www.thcp.nat.uni-erlangen.de

Nanometer-resolved radio-frequency absorption and heating in bio-membrane hydration layers

Research Institution
Universität Bayreuth

Principal Investigator
Stephan Gekle and Dominik Horinek

Researchers
Miriam Jahn and Christian Schaaf

Project Partners
"Institut für physikalische und theoretische Chemie, Universität Regensburg

LRZ Project ID: pr28xe

Introduction

Radio-frequency (RF) electromagnetic fields are readily absorbed in biological matter and lead to dielectric heating.To understand how RF radiation interacts with macromolecular structures and possibly influences biological function, a quantitative description of dielectric absorption and heating at nanometer resolution beyond the usual effective medium approach is crucial.

We report an exemplary multi-scale theoretical study for bio-membranes that combines i) atomistic simulations for the spatially resolved absorption spectrum at a single planar DPPC lipid bilayer immersed in water, ii) calculation of the electric field distribution in planar and spherical cell models, and iii) prediction of the nanometer resolved temperature profiles under steady RF radiation.

Our atomistic simulations show that the only 2 nanometer thick lipid hydration layer strongly absorbs in a wide RF range between 10MHz and 100 GHz. The absorption strength, however, strongly depends on the direction of the incident wave. This requires modeling of the electric field distribution using tensorial dielectric spectral functions. For a spherical cell model, we find a strongly enhanced RF absorption on an equatorial ring, which gives rise to temperature gradients inside a single cell under radiation. Although absolute temperature elevation is small under conditions of typical telecommunication usage, our study points to hitherto neglected temperature gradient effects and allows to predict thermal RF effects on an atomistically resolved level. In addition to a refined physiological risk assessment of RF fields, technological applications for controlling temperature profiles in nano devices are possible.

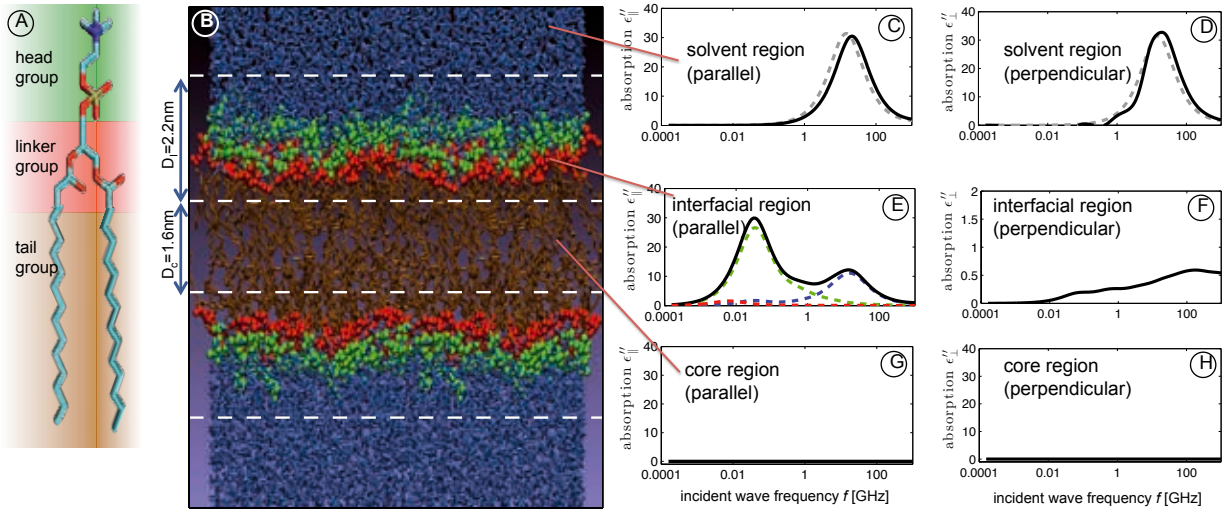

Fig. 1: (A) Chemical structure of a DPPC lipid molecule. (B) Simulation snapshot: 72 DPPC molecules form a bilayer surrounded by water molecules (in blue). Lipid atoms belonging to head, linker, and tail groups are colored in green, red, and brown according to the different background color shades in A. White dashed lines separate the solvent region, the interfacial region, and the bilayer core. (C)+(D) In the solvent region, both the parallel and the perpendicular absorption spectra (solid lines) are similar to a simulated pure bulk water spectrum (dashed lines) with a dominating absorption peak at 15GHz. (E) In the interfacial region the parallel absorption spectrum (black line) shows two peaks at 15 GHz and 30 MHz. The former is due to the water contribution (blue dashed line) while the latter is predominantly due to head groups (green dashed line). The linker groups (red dashed line) hardly contribute. (F) The perpendicular spectrum in the interfacial region is strongly attenuated (note the different scale) and the peak is shifted to significantly higher frequencies. (G)+(H) In the bilayer core there is basically no absorption.

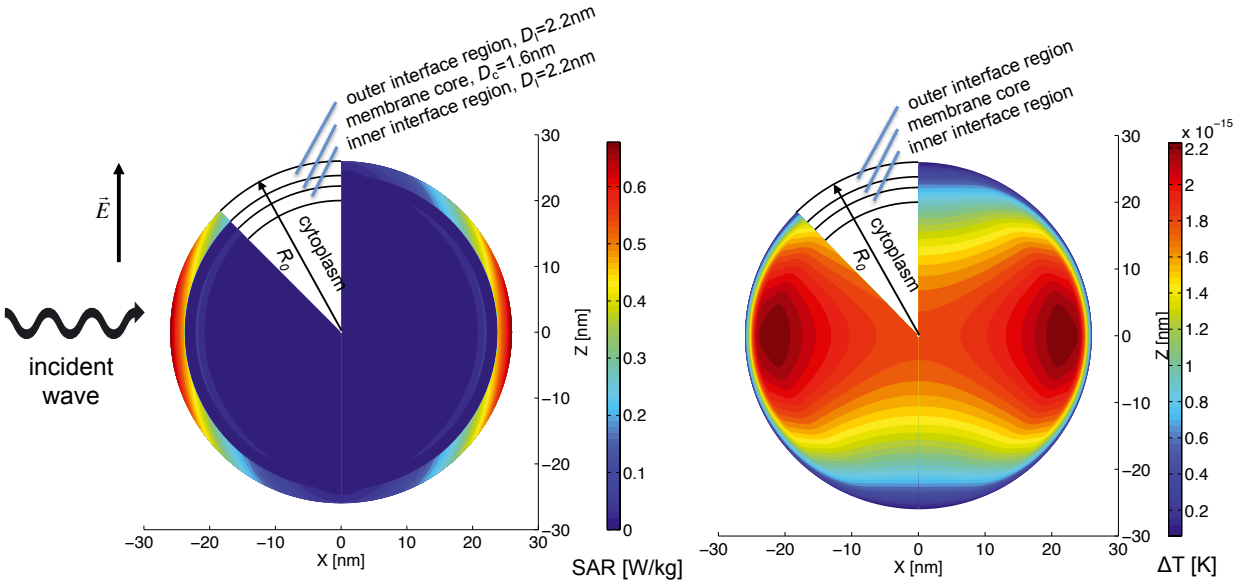

Fig. 2: (A) Specific absorption rates and (B) resulting steady-state temperature distribution for a spherical cell model.

Results

In our Molecular Dynamics (MD) simulations we consider a periodically replicated single dipalmitoylphosphatidylcholine (DPPC) bilayer consisting of 36 lipid molecules per monolayer immersed in 2278 SPC/E water molecules, see Fig. 1 A for the chemical structure of a typical lipid molecule and Fig.1 B for a simulation snapshot. The response of a material to an electromagnetic wave is characterized by the frequency-dependent complex dielectric function. Since our membrane system is anisotropic, the dielectric function is a tensor with two components $\varepsilon_{\parallel}$ and $\varepsilon_{\perp}$ for electric fields parallel and perpendicular to the membrane, respectively [1]. In order to meaningfully distinguish interfacial from bulk effects, we separately analyze the dielectric features in the bilayer core, the interfacial region and the aqueous solvent region, as indicated by broken white lines in Fig. 1 B. We present results for the imaginary part of the dielectric spectrum which is proportional to the spectral absorption power.

Molecular Dynamics simulations are run using the GROMACS package [2] at a temperature of 320K in order to keep the membrane in the fluid state representative of the in vivo situation. Simulations are run in the NVT ensemble starting from a preequilibrated box with a size of 4.597x5.090x6.839 nm^3. These simulation conditions correspond to the ensemble representative of the biological environment, namely constant water chemical potential as described in [3]. The average temperature is fixed at 320 K using a Berendsen thermostat and the integration time step is set to 2 fs. The total simulation time is 6.1 microseconds corresponding to roughly 300,000 CPU hours.

The dielectric absorption spectra thus computed only represent the first step towards a quantitative estimation of the physiologically relevant temperature rise in biological cells as they are exposed to electromagnetic radiation. The second step consisted of a continuum theory to calculate the specific absorption rates (which is non-trivial in a dielectrically anisotropic medium such as a cell membrane). We found that the absorption even for a simple cell shape such as a sphere strongly varies between different points of the membrane as shown in figure 2 A. Next, the specific absorption rates were fed into a heat conduction model. This model consisted of solving numerically the heat conduction equation subject to spatially varying source terms due to the dielectric heating. The result is shown in figure 2 B.

On-going Research / Outlook

Within the DFG-funded Graduiertenkolleg 1640 (”Photophysics of synthetic and biological multichromophoric systems”) located at the University of Bayreuth the suitability of perylen polymers for organic solar cells has been investigated in a joint effort by the groups of Prof. Mukundan Thelakkat in Chemistry and Prof. Jürgen Köhler in Experimental Physics [4]. Our goal using SuperMUC is to determine quantitatively the free energy differences between three different molecular conformations and thereby make predictions about the stability of the molecule in the respective conformations. Umbrella sampling will be used for this investigation. We further want to investigate the folding-unfolding mechanism to find out whether there is a preferred path that the monomers follow in order to fold or unfold.

References and Links

[1] S. Gekle and R. Netz, *J. Chem. Phys.* **137**, 104704 (2012)
[2] B. Hess et al., *J. Chem. Theory Comput.*, **4**, 435 (2008)
[3] E. Schneck et al., *Proc. Nat. Acad. Sci. (USA)*, **109**, 14405 (2012)
[4] F. Spreitler et al., *Phys. Chem. Chem. Phys.*, **14**, 7971 (2012)

Coupled Problems in Computational Modeling of the Respiratory System

Research Institution
Institute for Computational Mechanics, Technische Universität München

Principal Investigator
Wolfgang A. Wall, Michael W. Gee

Researchers
Christian Roth, Mahmoud Ismail, Lena Yoshihara

Project Partners
–

LRZ Project ID: pr32ne

Introduction

Mechanical ventilation is a vital supportive therapy for critical care patients suffering from acute lung diseases in view of oxygen supply. However, pre-existing lung injuries predispose patients to a number of complications which are collectively termed ventilator associated lung injuries (VALI). VALI mainly occurs in the walls of the alveoli, i.e. the small lung compartments constituting the blood-gas barrier. Understanding the reason why alveoli still become damaged or inflamed despite recent developments towards more "protective" ventilation protocols is a key question sought by the medical community. Computational models of the respiratory system can provide essential insights into involved phenomena. In particular, com-putational models offer the possibility to predict data that cannot be measured in vivo such as local alveolar strains and stresses which are relevant for the development and progress of VALI. However, establishing reasonable models is difficult since the lung comprises more than 20 generations of bifurcating airways ending in approximately 500 million alveoli. This complexity inhibits a direct numerical simulation resolving all relevant structures from the onset. Therefore, as a first step, we have developed detailed computational models of distinct parts of the lung, i.e. the tracheo-bronchial and the alveolar region, which will later be combined to one overall "virtual lung" model [1].

Methods

All simulations were performed with our multi-purpose finite element (FE) software platform BACI [2]. BACI has been and is developed within an object-oriented C++ environment. Parallelization is based on domain decomposition methods using MPI. State-of-the-art solution techniques for nonlinear and linear systems of equations as well as for coupling of several physical fields are incorporated in BACI and are continuously developed further in our group. For the imple-mentation of efficient parallel sparse linear algebra operations, BACI makes use of the open-source software framework "Trilinos" (Sandia National Laboratories).

Results

Physiological relevance of computational lung modeling is strongly dependent on the boundary conditions applied in the simulations. Therefore, we considered a motion-tracking algorithm to extract local non-linear lung deformation directly from medical imaging data as the driving force for our simulations (see Figure 1). Our investigation not only mimics displacements in the lung more natu-rally than any of the classical pressure prescribing methods, but also clearly shows the difference in motion between a healthy and a diseased lung.

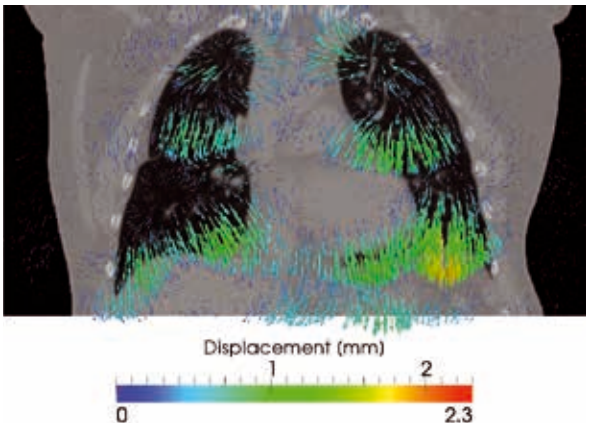

Figure 1: Displacement field of a healthy lung during inspiration; extracted from CT-scans using our motion-tracking algorithm.

As a next step, we coupled nonlinear deformations of lung tissue to a fully resolved four-generation model of the airway tree. The result of this is a volumetrically coupled non-linear fluid-structure interaction problem, which was implemented in a monolithic way [3] utilizing algebraic multi-grid pre-conditioning (see, e.g., [4]). By this method we can show the difference in pressure, airflow, and deformation between natural respiration (Figure 2) and mechanical ventilation. We find that for a given volumetric flow per breath, mechanical ventilation has to happen at a pressure at least five times higher than natural respiratory pressure, to work against the resistance of the ribcage and the respiratory muscles.

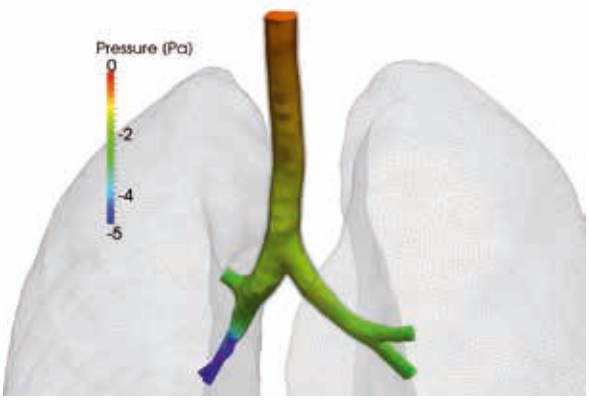

Figure 2: Pressure distribution at 0.2s of inspiration in a healthy four-generation lung model.

To link global lung deformation to quantities that characterise the load, i.e., stress and strain on cellular level, we developed a multi-scale method based on a FE2 approach [3]. Here, we model lung parenchyma on the macro-scale as non-linear continuum, while certain regions of specific interest such as inflammation hotspots are geometrically fully resolved on their micro-scale (see Figure 3). With these methods, we can link ventilation pressure to global lung deformation, and again, global deformation to a load that is persistent on cellular level and suspicious to initiate biological processes responsible for the exacerbation of chronic lung diseases.

Due to limitations on the number of airways visible on CT scans, only a part of the airway tree can be resolved in 3D. For the higher generations of the airway tree, we have established a novel reduced dimensional (reduced-D) model of the entire human lung. The model included the entire respiratory system and the entire pulmonary circulatory system. We have successfully modeled the con-ducting airways and blood vessels using 1D and 0D pipe elements and the acinar regions using 0D Maxwell chamber elements. We have also successfully developed an inter-acinar model that captured the effects of neighboring acini onto each other [5].

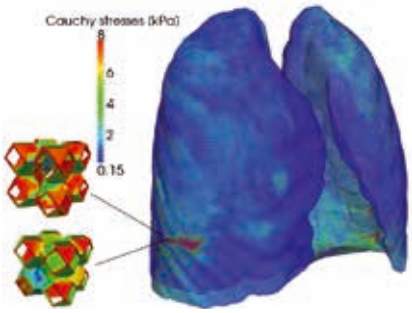

Figure 3: Multi-scale simulation approach showing lung parenchyma modelled as continuum on the macro-scale and two example micro-scale geometries at a strain hotspot in the lower right lung. Stress distribution at the hotspot can be resolved down to cellular level.

By combining the various components of the lung, we investigated the effect of mechanical ventilation on patient specific lung geometries. Figure 4 shows the computational results of ventilating a healthy lung versus ventilating a deceased lung. Briefly, we observed that within the disease lung the baby lung was subjected to an elevated acinar strain, thus being more prone to volutrauma. We also observed that the diseased lung suffered from a significant hypoxia. Furthermore, our model captured local volume competition between neighboring acini, thus suggesting that healthy alveoli within diseased lungs are more likely to collapse.

We have also established a fully stable 3D/reduced-D coupling which guaranteed pressure match at the boundary. Figure 5 shows the pressure distribution at peak inspiration and expiration within a coupled 3D/reduced-D respiratory system. The simulations reproduced the prescribed tracheal pressure. Fur-thermore, the pressure at the coupling boundaries matched perfectly.

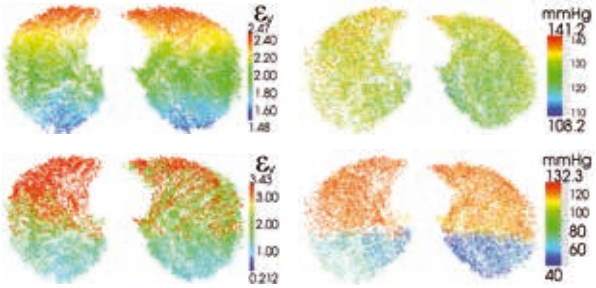

Figure 4: Comparison acinar strain (left) and acinar PO2 (right), for mechanically ventilated healthy lung (top) and diseased Lung (bottom) (Volumetric strain values are taken from [5]).

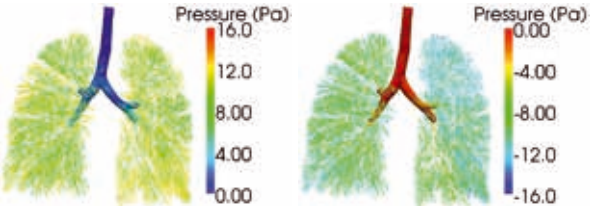

Figure 5: Distribution of pressure within a coupled 3D/reduced-D respiratory system at peak relaxed tidal expiration (left) and peak relaxed tidal inspiration (right) (taken from [6]).

Outlook

Ongoing work is concerned with analyzing different mechanical ventilation profiles and their effects on different lung diseases. In the future, we hope to better understand the aforementioned effects of mechanical ventilation and try to optimize them such that lung damage is minimized while oxygen delivery is maximized for real patients.

References and Links

[1] W. A. Wall, L. Wiechert, A. Comerford, and S. Rausch (2010). Towards a comprehensive computational model for the respiratory system. International Journal for Numerical Methods in Biomedical Engineering 26, 807-827.
[2] W. A. Wall and M. W. Gee (2010). BACI: A parallel multi-physics simulation environment. Technical Report, Institute for Computational Mechanics, Technische Universität München.
[3] L. Wiechert (2011). Computational Modeling of Multi-Field and Multi-Scale Phenomena in Respiratory Mechanics, PhD Thesis, Technische Universität München.
[4] M. W. Gee, U. Küttler, and W. A. Wall (2010). Truly monolithic algebraic multigrid for fluid-structure interaction. International Journal for Numerical Methods in Engineering, 85, 987-1016.
[5] M. Ismail, L. Yoshihara, C. Roth, A. Comerford, W. A. Wall (2014). A comprehensive model of entire human lung incorporating inter-acinar dependencies: Application to spontaneous breathing and mechanical ventilation, in prepara-tion.
[6] M. Ismail, V. Gravemeier, A. Comerford, W. A. Wal (2013). A stable approach for coupling multidimensional cardiovascular and pulmonary networks based on a novel pressure-flowrate or pressure-only Neumann boundary condition formulation. International Journal for Numerical Methods in Biomedical Engineering, in press.

http://www.lnm.mw.tum.de/research/applications/biomedical-respiratory-system/

Importance of Transmembrane Helix Dynamics for the Development of Alzheimer's Disease

Research Institution
Chemie der Biopolymere, WZW, TUM and Physics Department, TUM

Principal Investigator
Christina Scharnagl, Dieter Langosch

Researchers
Alexander Götz, Philipp Hornburg, Hannes Uhrmann

Project Partners
–

LRZ Project ID: pr42ri

Introduction

Integral membrane proteins exhibit conformational flexibility at different structural levels and time scales. Our work focuses on the biophysical basics of the interdependence of transmembrane helix dynamics, helix-helix recognition and helix-lipid interactions. At the same time, we try to understand the impacts of these phenomena on a variety of biological issues, such as membrane fusion, lipid translocation, and intramembrane proteolysis. During the last year, we have mainly investigated the backbone dynamics of the amyloid precursor protein (APP) transmembrane domain (TMD). This TMD is subject to cleavage at various sites by γ-secretase, which ultimately leads to the built-up of peptides that lead to Alzheimer's disease. Since the toxicity of these peptides depends on their size and size depends on the site of cleavage we try to understand how individual cleavage events are influenced by the local and global dynamics of this TMD helix. Fig. 1 shows an overview of steps involved in substrate processing and indicates the role of substrate dynamics as it emerges from our investigations.

Results

Since proteolysis of a helix requires its transient unfolding, we explored the idea that the intrinsic flexibility of a TMD helix by itself would qualify it as a substrate and that mutations within it would change proteolysis via affecting flexibility. To this end, we investigated the amyloid precursor protein TMD helix by molecular dynamics simulations in solution and in a membrane patch. The results reveal a gradient of local backbone dynamics along the monomeric helix which is much more pronounced within a dimerization domain within its N-terminal half than within the actual cleavage region. Dimerization and cleavage domains connect at a di-glycine hinge which is the most dynamic site except the frayed helix termini [1]. Unexpectedly, the local helix dynamics of tested non-substrate TMDs exceeds that of the APP TMD [2]. Finally we tested whether side-chain/main-chain backbonding of both threonine residues within the APP TMD would constrain local backbone dynamics in the free state of the substrate (thus offering the potential of increased dynamics in the enzyme-bound state). Unleash-

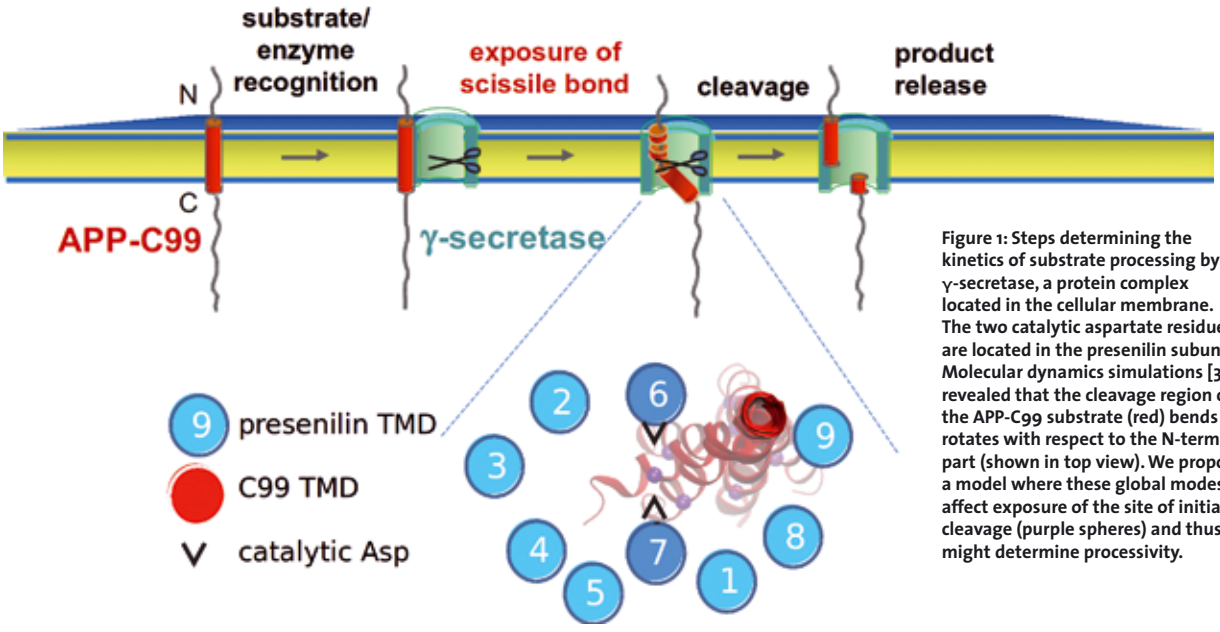

Figure 1: Steps determining the kinetics of substrate processing by γ-secretase, a protein complex located in the cellular membrane. The two catalytic aspartate residues are located in the presenilin subunit. Molecular dynamics simulations [3] revealed that the cleavage region of the APP-C99 substrate (red) bends and rotates with respect to the N-terminal part (shown in top view). We propose a model where these global modes affect exposure of the site of initial cleavage (purple spheres) and thus might determine processivity.

ing both backbonds by mutation to valine does indeed increase local helix dynamics, but not at the site of initial proteolysis. However, the mutations profoundly alter *global* bending and rotational motions at the di-glycine hinge [3] (Fig. 2).

Further, our results reveal significant differences in the overall dynamics of mutant TMDs which are associated with the development of familial Alzheimer's disease. We thus propose that such *global* motions within a substrate TMD helix may affect the way by which it is recognized by the enzyme and/or presented to its catalytic site while the impact of local unfolding on the actual cleavage reaction may be less important for the kinetics and the specificity of cleavage.

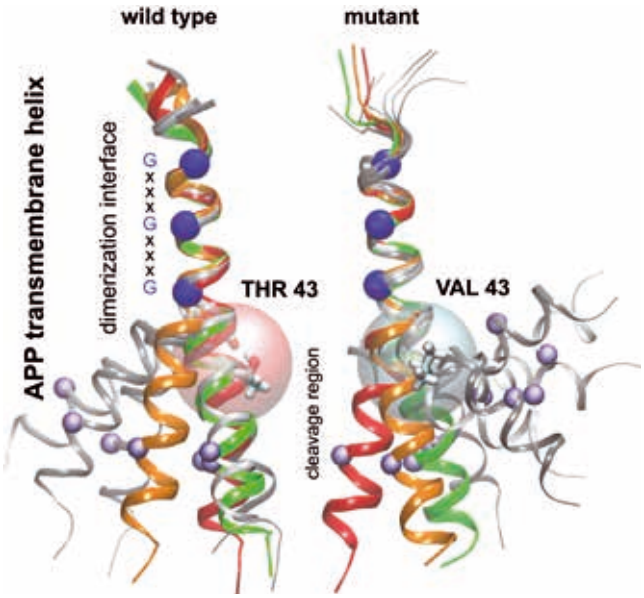

Figure 2: Removing side-chain/main-chain backbonding by mutating the threonine at position 43 profoundly alters amount and direction of helix bending.

On-going Research / Outlook

Our aim is to uncover the structural and dynamical requirements for the proteolytic processing of substrate TMDs by intramembrane proteases. We plan to generate flexibility profiles for a large number of substrates and their disease-associated and neutral variants in order to correlate the dynamic properties of individual residues with their functional importance. Our model systems to be investigated will correspond to point mutants of the APP TMD as well as to the TMDs of the substrates of other intramembrane proteases. In a second project we use MD simulations to answer the question of how peptide/lipid interactions can modulate membrane organization, catalyze lipid translocation and induce protrusion of lipid tails to the membrane surface leading to membrane fusion. Since the impact of helix dynamics depends on lipid composition, we will use comparative analyzes for a variety of model bilayers. All simulations are validated against in-vitro experiments like deuterium/hydrogen exchange, NMR, CD-spectroscopy and functional assays.

In the last year, the introduction of new NAMD versions offering superior scalability greatly accelerated the production of trajectories. Since GPFS is up and working now, SuperMUC's thin nodes allowed us to scale our simulations from 80 to more than 500 cores with output of 25 ns/day (systems with 90000 atoms) and 45 ns/day (30000 atoms), respectively. Compared to HLRB II and the actual Linux Cluster, this is an enormous reduction of the time required for the production of a typical 200 ns trajectory: the wall clock time (including queue time) reduced from 3 months to 2 weeks. However, currently accessible time scales in atomistic MD simulations (hundreds of nanoseconds for individual trajectories) are still far from biologically relevant time scales in global protein dynamics (typically milliseconds). This is a serious problem for sampling the conformational states of TMD helices and the impact of mutations on them. Furthermore, due to the slow rate of lipid diffusion, TMD/lipid interactions and ensuing changes in bilayer properties will not be sampled with sufficient statistical accuracy using current state-of-the art simulations. We intend to solve this issue by running multi-copy simulations (approx. 100-200 ns each, 20-40 replicates) from different starting structures of helices and lipid environment. The use of many short simulations has been reported to be a much more efficient way to sample conformational states as compared to run one simulation for a very long time. The datasets across the multiple simulations will be analyzed using hidden Markov-chain models. Since there are no experimental start structures for the TMDs available, we will setup Monte Carlo sampling and clustering methods to determine a set of approx. 10-20 representative conformations. The production of multiple runs starting from different conformations will greatly benefit from the possibility to run up to 10 jobs per user simultaneously. Since the actual 2.9-version of NAMD scales with 8 to 12 cores/1000 atoms, a single production run needs between 500 and 800 cores. We hope, that the lower limit of cores allowed for a single job on the SuperMUC will not be increased in future, since being forced to run the multiple simulations on the Linux Cluster will make them infeasible.

References and Links

[1] Pester, O., Barret, P., Hornburg, D., Hornburg, P., Pröbstle, R., Widmaier, S., Kutzner, C., Dürrbaum, M., Kapurniotu, A., Sanders, C.R., et al. (2013). The Backbone Dynamics of the Amyloid Precursor Protein Transmembrane Helix Provides a Rationale for the Sequential Cleavage Mechanism of γ-Secretase. J. Am. Chem. Soc. 135, 1317-1329.

[2] Pester, O., Götz, A., Multhaup, G., Scharnagl, C., and Langosch, D. (2013). The Cleavage Domain of the Amyloid Precursor Protein Transmembrane Helix does not Exhibit Above-Average Backbone Dynamics. ChemBioChem 14, 1943-1948.

[3] Scharnagl, C., Pester, O., Hornburg, P., Hornburg, D., Götz, A., and Langosch, D. (2014). Side-Chain to Main-Chain Hydrogen Bonding Controls the Intrinsic Backbone Dynamics of the Amyloid Precursor Protein Transmembrane Helix. Biophys. J. 106, in the press.

http://www.wzw.tum.de/biopolymere/

Scalable simulations of flow in stented intracranial aneurysms

Research Institution
Simulation Techniques and Scientific Computing, University of Siegen

Principal Investigator
Sabine Roller, Jörg Bernsdorf

Researchers
Kartik Jain, Simon Zimny, Harald Klimach

Project Partners
Applied Supercomputing in Engineering, German Research School for Simulation Sciences, Aachen

LRZ Project ID: pr45du (Gauss Large Scale project)

Introduction

An Intracranial Aneurysm (IA) is a weak bulging spot on the wall of a brain artery. Rupture of an aneurysm termed Subarachnoid Hemorrhage (SAH) causes leakage of blood, which can result in paralysis or death of the patient. Nearly 4-5% of the world population is reported to be suffering from un-ruptured IA. Besides several existing options for the treatment of IAs, a novel and minimally invasive endovascular treatment option is the deployment of a flow diverter stent in the parent artery of the aneurysm. A flow diverter stent reduces the wall shear stress (WSS) and increases the residence time of blood inside the aneurysm. These both factors are believed to be the main enhancers in the process of thrombosis i.e. coagulation of blood resulting in clots. With an optimal diversion of the flow, the aneurysm can get completely obliterated in due course by the growing clots. Numerical simulations can provide valuable insights to the clinician for the choice of an optimal design of stents to treat specific patients. Our research work focused on simulations of thrombosis in stented and non-stented patient specific aneurysms and a qualitative comparison of flow properties pre- and post-deployment of stent.

The simulation of flow and thrombosis in realistic geometries of aneurysms is a multi-scale problem and a computationally challenging task that requires a highly scalable end-to-end parallel simulation tool chain. We chose the Lattice Boltzmann Method (LBM) for numerical simulations due to its ease of handling complex boundaries, ease in handling dynamically changing geometries and high scalability on HPC systems. Our research work was complemented by the development of a highly efficient Octree based LBM solver *Musubi* [1], which is part of our simulation framework APES [2].

Results

Our simulation results qualitatively demonstrated the increase in the process of thrombosis inside the aneurysm bulge after the deployment of a stent [3,4]. Figure 1 shows a patient specific IA with a stent deployed in the parent artery.

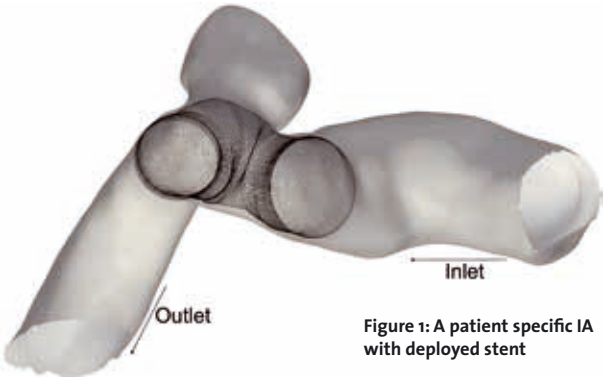

Figure 1: A patient specific IA with deployed stent

Simulations were initially performed on stented and non-stented aneurysms without the initiation of thrombosis for an insight into the flow properties and to serve as a comparison as depicted in figure 2.

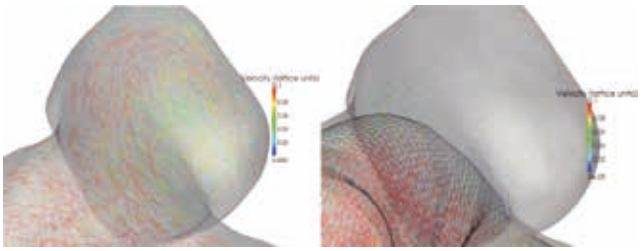

Figure 2: Flow through non-stented and stented IA

The progress of thrombosis with time inside the bulge of the aneurysm is shown in in Figure 3. The thrombosis is initiated on the basis of conditions of low WSS and high residence time inside the aneurysm.

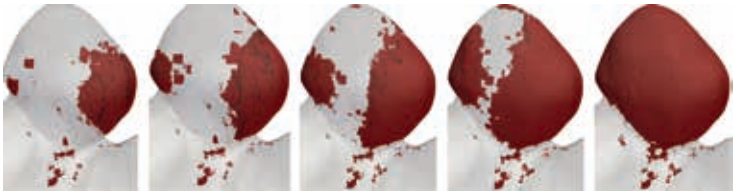

Figure 3: Progression of thrombosis in a stented IA

Simplifications in this model are a Newtonian rheology of the blood and rigid vascular walls. The stent decouples the blood flow from the parent artery to the aneurysm sac resulting in deviated flow properties and an enhanced thrombosis as expected. The time scale of such a simulation increases after the initiation of thrombosis as the artifacts introduced by the changed geometry need to be washed out [3]. The presented simulation was performed on one island of SuperMUC and a single run required around 30 hours of running time in total. Simulations on several other morphologies of aneurysms were performed with meshes consisting of up to one billion elements.

Figure 4 shows the performance map of *Musubi* on up to 4 islands of SuperMUC. We use MLUPS (million lattice updates per second) as a standard unit for performance measurement of LBM simulations, which is plotted against the number of fluid elements per SuperMUC node. *Musubi* exhibits an optimal scaling when the number of elements per core ranges from 2000 to 1 million; thus we regulated the number of used cores according to the problem size to obtain an optimal compute efficiency.

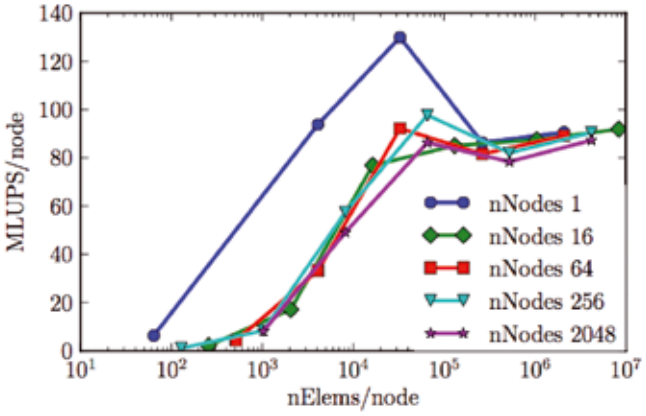

Figure 4: Performance of Musubi on up to 4 islands of SuperMUC

To simulate the largest meshes of 1 billion elements, we used 2 islands. To save disk space, we track only subdomains of interest within the complete geometry in the form of binary files, which are post processed by our framework to obtain visualization files in the VTK format. The largest simulations of one billion elements consume nearly 600 GB of disk space including the post-processed files. The disk consumption scales with the number of simulations and in total, we used nearly 10 TB of disk space on the WORK directory of our project.

On-going Research / Outlook

Our simulation results provided a good insight into the role of the flow diverting stent in the process of thrombosis development in aneurysms. Our detailed resolution of flow phenomena was enabled by the large-scale computations on SuperMUC.

In our ongoing research we are investigating the presence of in-stationary flows inside aneurysms, which resemble a *transition* to turbulence. The presence of such a transitional flow in certain classes of aneurysms can be a potential cause of rupture and we plan to investigate the influence of this flow phenotype on aneurysm rupture. Our previous thrombosis models that were based on flow properties will need some modifications here, as the calculation of flow quantities in a transitional flow is difficult. Our future efforts include the improvement of present simulations by incorporating more complex biological phenomena like moving walls and non-Newtonian blood flow models as well as improvements in the sustained performance and scalability of our simulation framework.

Acknowledgements

The geometries used for these studies were provided by the *THROMBUS* project, funded by the European Commission in the seventh framework program in the area of Virtual Physiological Human (ICT-2009.5.3, PR 269966). Computer resources for this project were provided by the Leibniz Supercomputing Center, Munich under grant *pr-45du*.

References and Links

[1] Hasert, M., Masilamani, K., Zimny, S., Klimach, H., Qi, J., Bernsdorf, J., & Roller, S. (2013). Complex fluid simulations with the parallel tree-based Lattice Boltzmann solver Musubi. *Journal of Computational Science*.

[2] Roller, S., Bernsdorf, J., Klimach, H., Hasert, M., Harlacher, D., Cakircali, M., ... & Zudrop, J. (2012). An adaptable simulation framework based on a linearized octree. In *High Performance Computing on Vector Systems* 2011 (pp. 93-105). Springer Berlin Heidelberg.

[3] Zimny, S., Chopard, B., Malaspinas, O., Lorenz, E., Jain, K., Roller, S., & Bernsdorf, J. (2013). A multiscale approach for the coupled simulation of blood flow and thrombus formation in intracranial aneurysms. *Procedia Computer Science, 18*, 1006-1015.

[4] Jain, K., Zimny, S., Klimach, H., Roller, S. (2013). Thrombosis modeling in stented cerebral aneurysms with Lattice Boltzmann method. *In Proceedings of the 26th Nordic Seminar on Computational Mechanics*

Large-scale Molecular Dynamics in Chemical Engineering

Research Institution
Institute fuer Informatik, Technische Universitaet Muenchen

Principal Investigator
Hans-Joachim Bungartz

Researchers
Wolfgang Eckhardt, Alexander Heinecke

Project Partners
–

LRZ Project ID: pr45ka

Introduction

MD simulation has become a recognized tool in engineering and natural sciences, complementing theory and experiment. Despite its development for over half a century, scientists still quest for ever larger and longer simulation runs to cover processes on greater length and time scales. Due to the massive parallelism MD typically exhibits, it is a preeminent task for high-performance computing.

The simulation code *ls1 mardyn* has been enhanced within the BMBF-funded project IMEMO [1] in order to provide an efficient tool for large-scale MD simulations of phenomena in inhomogeneous systems in chemical engineering. Targeting condensation processes and flow phenomena on the nanoscale, it supports rigid-body electroneutral molecular models composed out of an arbitrary number of Lennard-Jones (LJ) sites, point charges, point dipoles and point quadrupoles. As these scenarios typically require large particle numbers and also show heterogeneous density distributions of particles, see Fig. 1, sophisticated load balancing algorithms have been incorporated into the program to enable good scalability on large processor counts.

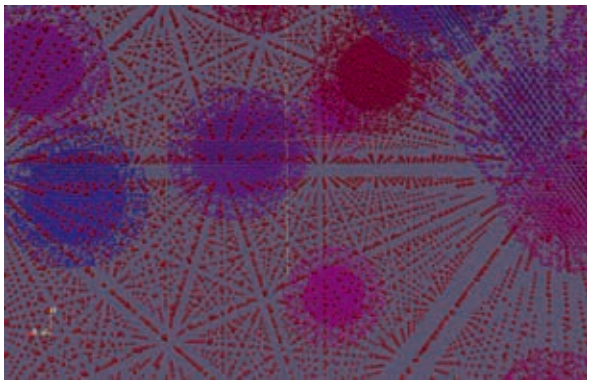

Figure 1: Scenario with a heterogeneous particle distribution as it occurs in the simulation of nucleation.

Results

We optimized our MD code on the micro-architecture level for a specific processor: the Intel Sandy Bridge EP based SuperMUC operated at the Leibniz Supercomputing Centre in Munich. The optimizations targeting SuperMUC include the vectorization for exploiting the new AVX instruction set of the underlying Intel Sandy Bridge architecture, see [2] for details. This results in calculating always four particle interactions with one force calculation kernel call and therefore in drastic reduction of clock cycles. Furthermore, we applied memory optimizations which allow us to reduce the number of bytes needed per particle to 32, please refer to [3]. Due to the utilized LJ potential, we cannot leverage the instruction level parallelism of Sandy Bridge optimally. However, we were able to add a light-weight shared memory parallelization instead which accelerated the code by 12% when using Intel Hyper-Threading Technology on a per core basis.
In order to evaluate the performance of the MD simulation code ls1 mardyn, we executed different tests on SuperMUC. Our test scenario is similar to the initial configuration of nucleation scenarios, where particles are distributed on a regular grid. The single-center Lennard-Jones particles, modeling e.g. Argon, were arranged according to a body-centered cubic lattice, with a number density of $\rho\sigma^3 = 0.78$ in reduced units. The time step length was set to 1 fs.

With respect to strong scaling behavior, we ran a scenario with N=4.8*10^9 particles, which fully utilizes the memory available on 8 nodes (128 cores), as 18 GB per node are needed for particle data. Fig. 2 nicely shows that a nearly perfect scaling was achieved for up to 146,016 cores using 292,032 threads at a parallel efficiency of 42 % comparing 128 to 146,016 cores. To better understand this performance, we investigate the influence of the decreasing particle number per core, as it occurs in this strong scaling experiment, in Fig. 3: here we measured achievable GFLOPS depending on the number of particles simulated on 8 nodes. Furthermore, we show the influence of different cutoff-radii, which determine the number of interactions per molecule, as this parameter

also severely effects the FLOP rate. To make a fair comparison with preceding publications possible, we conducted our runs with a cutoff radius of 3.5 . Already for N=3*10^8 particles, i.e. 2.3*10^6 particles / core (approx. 8% of the available memory) we are able to hit the performance of roughly 550 GFLOPS per 8 nodes, which we also obtained for N=4.8*10^9 (37.5*10^6 particles per core).

Moreover, we performed a weak scaling analysis with 28.25*10^6 molecules per core. This allowed us to perform the, to our knowledge, largest MD simulation to date, simulating 4.125*10^12 particles on 146,016 cores with one time step taking roughly 40s. For this scenario an absolute performance of 591.2 TFLOPS with a speedup of 133,183 X in comparison to a single core was achieved, which corresponds to 9.8% single-precision peak performance efficiency. Further technical details can be found in the PRACE ISC 2013 awarded publication entitled "591 TFLOPS Multi-Trillion Particles Simulation on SuperMUC" [4].

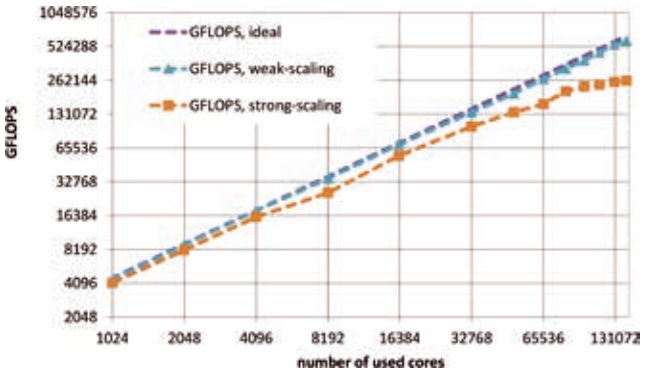

Figure 2a: FLOPS measured for strong and weak scaling experiment.

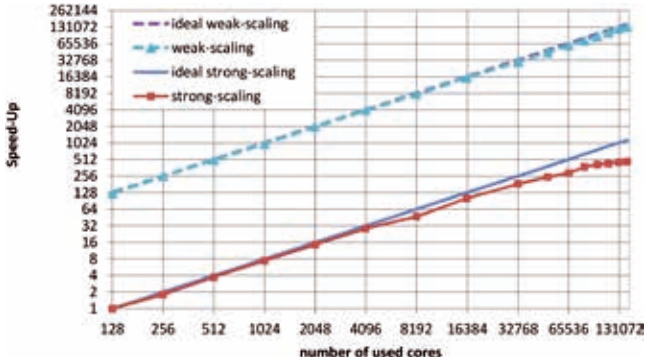

Figure 2b: Speedup for strong and weak scaling experiment. For strong scaling, the speedup is normalized to 128 processes. For weak scaling, the speedup is relative to a single process.

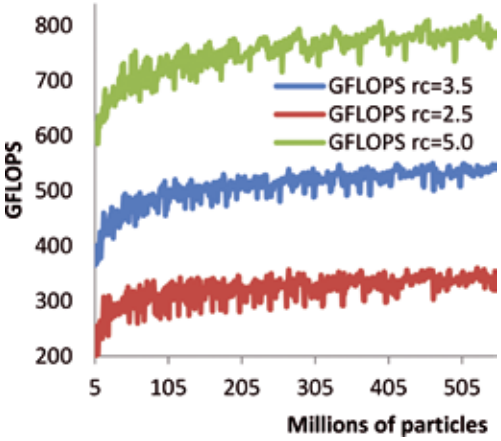

Figure 3: Flop rate on 128 cores in dependence of the number of particles and the cutoff radius (which determines the number of interaction partners of a particle).

On-going Research / Outlook

The current kernel implementation suffers from not fully exploited vector-registers. Increasing the net-usage of vector-registers is subject of ongoing research. The most promising instruction set is currently provided by the Intel Xeon Phi coprocessor which features a full blown gather/scatter implementation. This naturally matches with the second phase of the SuperMUC installation as this phase includes a cluster partition equipped with Intel Xeon Phi coprocessor.

Beside tuning *ls1 mardyn* for better performance on emerging architectures, energy efficiency with focus on the energy to solution ratio is an additional research direction, especially when targeting MD scenarios with millions of time steps. Since SuperMUC is capable of dynamic frequency scaling, it provides an optimal testbed for such activities.

References and Links

[1] C. Niethammer, C. W. Glass, M. Bernreuther, S. Becker, T. Windmann, M. T. Horsch, J. Vrabec and W. Eckhardt: Innovative HPC Methods and Application to Highly Scalable Molecular Simulation (IMEMO). In Inside - Innovatives Supercomputing in Deutschland, Volume 10(1), April 2012.

[2] W. Eckhardt and A. Heinecke: An efficient Vectorization of Linked-Cell Particle Simulations. In ACM International Conference on Computing Frontiers, p. 241–243, May 2012.

[3] W. Eckhardt and T. Neckel: Memory-Efficient Implementation of a Rigid-Body Molecular Dynamics Simulation. In Proceedings of the 11th International Symposium on Parallel and Distributed Computing - ISPDC 2012, p. 103–110. IEEE, Munich, June 2012.

[4] W. Eckhardt, A. Heinecke, R. Bader, M. Brehm, N. Hammer, H. Huber, H.-G. Kleinhenz, J. Vrabec, H. Hasse, M. Horsch, M. Bernreuther, C. Glass, C. Niethammer, A. Bode and H.-J. Bungartz : 591 TFLOPS Multi-Trillion Particles Simulation on SuperMUC. In *International Supercomputing Conference (ISC) Proceedings 2013*, Volume 7905 of Lecture Notes in Computer Science, p. 1–12. Springer, Heidelberg, Germany, June 2013.

Quantum photophysics and photochemistry of biosystems

Research Institution
Department of Physics and Astronomy, Aarhus University, Denmark

Principal Investigator
Anastasia V. Bochenkova

Researchers
Alexander A. Granovsky

Project Partners
Firefly project, Moscow, Russia

LRZ Project ID: pr45vi

Introduction

The interaction of molecules with light is central to vital activity of living organisms and human beings. Photosynthesis, vision in vertebrates, solar energy harvesting and conversion, and light sensing are remarkably efficient processes; and much focus has been on elucidating the role played by the protein environment in their primary events, which occur on a timescale down to sub-picoseconds. Our project deals with computationally demanding simulations of excited-state evolution of photoactive proteins and their light-absorbing molecular units using highly correlated multi-reference methods of quantum chemistry (QC) and their efficient parallel implementation. Such large-scale calculations combined with a high accuracy have been enabled through the PRACE LRZ's SuperMUC infrastructure and the highly tuned and optimized design of the Firefly package [1].

Results

High-level QC methods are required for describing photo-initiated quantum molecular dynamics that involves multiple electronic states. It is challenging to describe electronic fast and efficient de-excitation occurring through so-called conical intersections, where topography around an intersection seam of two degenerate electronic states influences the transition between them. Systems with quasi-degeneracy require multi-reference approaches. The new XMCQDPT2 method [2] is a unique and invariant approach to multi-state multi-reference perturbation theories (PT), allowing an accurate description of large and complex systems; in particular, near the points of avoided crossings and conical intersections. The use of high-performance high-core-count clusters becomes mandatory requirement for predictive modeling of such systems.

Unlike well-established approaches in classical molecular dynamics, QC methods deserve special attention when implementing them on modern computer architectures. Huge data sets of 4-indexed two-electron (2-e) integrals are generated and stored on a disk after their evaluation and intermediate sorting in a two-pass transformation. These data are subsequently used in computationally intensive parts of the code, where most of the computational efforts are due to summation of the individual terms of the PT series. Thus, the QC algorithms inevitably contain different stages, which are I/O intensive (*e.g.,* integral transformation) and computationally intensive (*e.g.,* direct summation of the PT series). The I/O performance is, therefore, of utmost importance. Besides, a theoretical/formulae complexity requires a careful tuning of computationally intensive parts of the code. A straightforward implementation of the summation of the PT series is very inefficient, since at least one or more slow divide operations are required to calculate each individual term of the PT series. Moreover, the summation runs over a large amount of data, involving some combinations of transformed 2-e integrals, thus making such algorithm not processor cache-friendly.

The efficient implementation of the XMCQDPT2 theory within the Firefly package is based on a developed family of the cache-friendly algorithms for the direct summation of the PT series [3], as well as on a so-called resolvent-fitting approach [4], which uses a table-driven interpolation for the resolvent operator, thus further reducing computational costs.

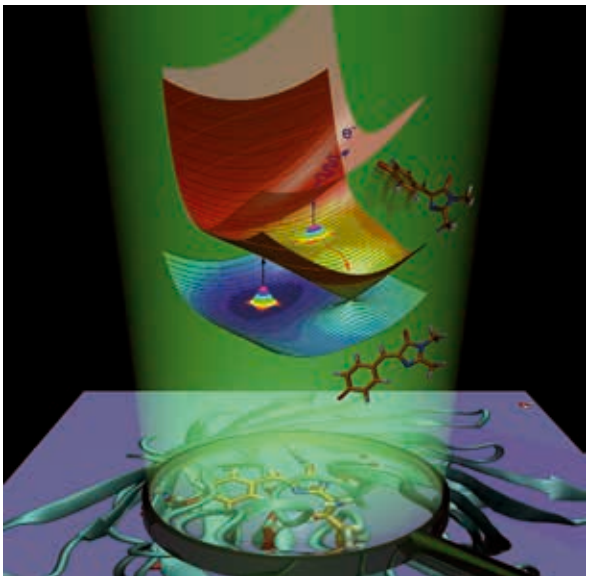

Figure 1: When taken out of the Green Fluorescent Protein, its anionic light-absorbing molecular unit shows a remarkable fundamental interplay between electronic and nuclear excited-state decay channels in the ultrafast photo-initiated dynamics occurring on a pile of potential energy surfaces.

Being executed in its recently developed extreme parallel (XP) mode of operations, Firefly is scalable up to thousands of cores. The XP mode includes a three-level parallelization (MPI process → groups of weakly coupled MPI communicators with parallelization over MPI inside each group → optional multithreading within each instance of a parallel process) and efficient asynchronous disk I/O with real-time data compression/decompression (throughput of up to 5-7 GByte/s).

The Firefly package enables to perform efficient large-scale XMCQDPT2 calculations for systems with up to 4000 basis functions and with large active spaces, which comprise several millions of configuration state functions. Protein and solution environments may also be taken into account using multi-scale approaches. The overall size of model systems may comprise 5000 – 10000 atoms.

The project has the total allocated CPU time of 3 885 000 core-hours, which have entirely been used. The average number of cores used by a single run is 1024 and up to 2944 with at least 24 hours duration. A distributed high-capacity high-bandwidth file system with up to 100 TBytes for temporary storage during a single run is required. The IBM GPFS file system of the LRZ's SuperMUC has been found to be the most sustained to a high load caused by the most I/O intensive parts of the XMCQDPT2 code. The direct benefits from tuning and optimizing the Firefly code have been reaped during the project. The most I/O intensive parts of the code have been redesigned targeting particular large XMCQDPT2 jobs.

The following scientific and technical milestones have been achieved within the project:

- By using excited-state electronic structure calculations of the isolated anionic Green Fluorescent Protein (GFP) chromophore, we have been able to disclose a striking interplay between the electronic and nuclear dynamics that is coupled with a remarkable efficiency in the ultrafast excited-state decay channels of this chromophore (Fig. 1). The energy exchange is found to be fast and, importantly, mode-specific [5]. This finding lays the groundwork for mode-selective photochemistry in biosystems.
- By simulating the photo-initiated early-time nuclear dynamics of the GFP and KFP proteins, their absorption spectral profiles have been retrieved, which appear to be remarkably similar to those of the isolated chromophores [5]. Here, high-frequency stretching modes play an important role defining the spectral widths. Remarkably, they also serve as reaction coordinates in photo-induced electron transfer, which competes with internal conversion mediated by twisting. Many GFP-related proteins prohibit internal conversion, thus possibly directing the decay towards electron transfer; whereas fluorescence may be regarded as a side channel only enabled in the absence of relevant electron acceptors. This finding adds to our understanding of biological evolution and function of light-sensitive proteins.
- We have identified higher electronically excited states of the isolated GFP chromophore anion in the previously unexplored UV region down to 210 nm [6]. By forming a dense manifold, these molecular resonances are found to serve as a doorway for very efficient electron detachment in the gas phase. Being resonant with the quasi-continuum of a solvated electron, this electronic band in the protein might play a major role in the GFP photophysics, where resonant GFP photoionization in solution triggers the protein photoconversion with UV light.
- Computationally, the largest run, ever performed using a highly correlated multi-reference electronic structure theory, has been executed in the XP-mode using 2944 cores with a sustained performance close to 60% of the theoretical aggregate peak performance, *ca.* 40 Teraflop/s. The calculations are aimed at understanding of a wavelength tuning mechanism in the retinal-containing visual proteins, where a single 11-*cis* PSB retinal chromophore is responsible for entire color vision (Fig. 2).

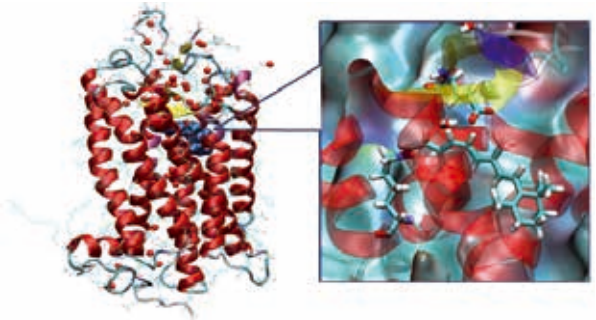

Figure 2: (Left) Dim-light visual pigment Rhodopsin, with the retinal chromophore inside (depicted in blue). (Right) The 11-cis PSB retinal chromophore covalently bound to the protein inside its binding pocket.

On-going Research / Outlook

Our results indicate the existence of efficient electron-nuclear coupling mechanisms in the photoresponse of biological chromophores. These non-adiabatic mechanisms are found to be dual, and, importantly, mode-specific. Numerous ways may be outlined by which the proteins use this electron-to-nuclei coupling to guide the photochemistry and the photophysics that lie behind their functioning. In the future projects, we plan to unravel the details of such non-adiabatic mechanisms, thus enhancing our understanding of the efficiency of light triggered processes in nature. Our findings will ultimately lay the groundwork for mode-selective photochemistry and photophysics in biological systems.

We also expect direct benefits from further tuning and optimizing the Firefly code, aiming at efficient large-scale excited-state and non-adiabatic calculations. This will expand a range of biologically-relevant systems, which will be feasible for high-level *ab initio* calculations, thus further pushing the limits of theory.

References and Links

[1] A.A. Granovsky, Firefly, http://classic.chem.msu.su/gran/firefly/index.html.
[2] A.A. Granovsky, *J. Chem. Phys.* 134 (2011), 214113.
[3] A.A. Granovsky, http://classic.chem.msu.su/gran/gamess/qdpt2.pdf.
[4] A.A. Granovsky, http://classic.chem.msu.su/gran/gamess/table_qdpt2.pdf.
[5] A.V. Bochenkova and L.H. Andersen, *Faraday Discuss.* 163 (2013), 297–319.
[6] A.V. Bochenkova, B. Klaerke, D.B. Rahbek, J. Rajput, Y. Toker, L.H. Andersen, *Phys. Rev. Lett.* (2014), submitted.

Computational electronic spectroscopy of aqueous hydroxide

Research Institution
University of Cambridge

Principal Investigator
Daniel Opalka

Researchers
Daniel Opalka, Michiel Sprik

Project Partners
Institut für Theoretische Chemie, Technische Universität München

LRZ Project ID: pr45wu

Introduction

The solvated hydroxide ion is involved in many biological processes. The absorption of photons by solvated hydroxide ions, for example, is an important source of hydroxyl radicals. The high mobility of hydroxyl radicals and their tremendous oxidation power contribute to much of the damage to DNA through free radicals. In green plants, on the other hand, hydroxyl radicals are involved in the production of energy through photosynthesis. Despite of its simple structure, electronic interactions with surrounding water molecules and embedding into the hydrogen bond network of bulk water make light-induced processes in the solvated hydroxide ion a challenging problem for theory.

Hydrated anions and in particular the hydroxide ion are strongly affected by their fluctuating environment of water molecules. Among the many extraordinary properties of liquid water is the well-known blue-shift of the optical absorption spectrum and ionization potential. The hydroxide ion, as a product of self-ionization in liquid water, is subject to a similar change in its optical properties. This involves more than just hydrogen bonding.

The spectroscopic properties of small anions in aqueous solution are often characterized by charge-transfer to solvent (CTTS) bands. After excitation into a CTTS state an electron is ejected from the solute into a significantly delocalized electronic state of the solvent. In the case of the aqueous hydroxide ion, the CTTS has been measured experimentally at 6.5 eV. As a consequence of the electronic excitation hydroxyl radicals and hydrated electrons are produced which exhibit enormous oxidation and reduction strength, respectively. Similarly, a charge-transfer to the solute may be initiated through absorption of a photon.

Although the electronic structure and electron transfer processes in aqueous solution have attracted much attention in the scientific community, the detailed electronic structure and related microscopic processes have not yet been resolved. From a theoretical perspective, recent advances in the field of many-body perturbation theory and time-dependent density functional theory (DFT) along with the availability of massively parallel computing architectures allow a more detailed characterization of the electronic energy levels of electrolyte solutions and electronic transitions in the condensed phase.

Results

The computation of optical and photoemission spectra requires statistical sampling of the accessible molecular arrangements in a simulation cell. In this project ab initio molecular dynamics has been used to compute trajectories of a cubic simulation cell which contained 1 hydroxide ion and 31 water molecules. The intermolecular forces were computed from DFT. Every trajectory requires appropriate thermalization and typical production runs of 20 ps. The CP2K [1] and Quantum Espresso [2] software which have been employed in this project proved to scale well up to several hundreds of cores although usually 512 or less cores have been used and the calculations were restarted several times. Snapshots were taken from the trajectory for further analysis and the computation of spectra.

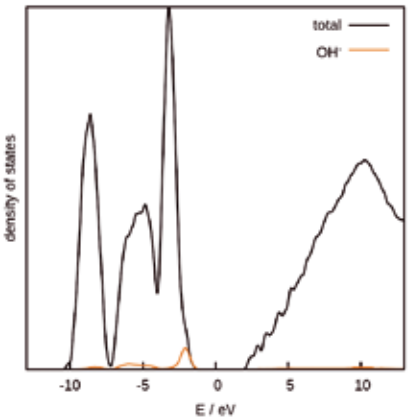

Figure 1: Density of states computed as average from 40 snapshots of an ab initio MD trajectory. The projected density of states at the hydroxide ion corresponds to one ion dissolved in 31 H_2O molecules.

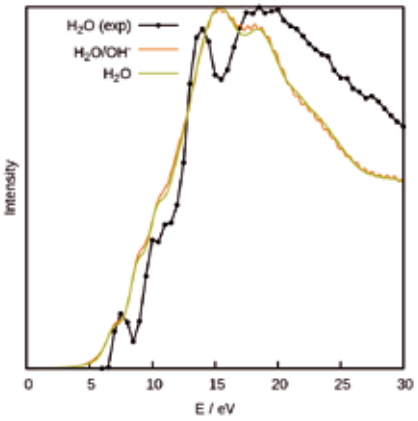

Figure 2: Convoluted absorption spectra computed for a periodic simulation cell of 31 water molecules and 1 and one hydroxide ion. Experimental data is shown for comparison.

The density of states (DOS) and the projected DOS to the solute in Fig. 1 provide a first approximation to electronic states of the solution. The positions of the highest occupied (HOMO) and lowest unoccupied molecular orbitals (LUMO) of the solvated hydroxide ion and, analogously for the solvent, the valence band maximum

(VBM) and conduction band minimum (CBM). The edge of the valence band of water appears close to the HOMO of the hydroxide ion in agreement with experimental results. The gap between between CBM and VBM (4.1 eV), however, is significantly underestimated (experiment: 8.7 eV).

A more appropriate description of the fundamental band gap and the relative position of the HOMO of the solute and the VBM of the LUMO is obtained from the quasi-particle equations of many-body perturbation theory. Within the G_0W_0 approximation the first-order correction to the molecular orbital energies is computed with a non-local self-energy correction. The central object required for the solution of the quasi-particle equations is the dielectric matrix and thus the polarizability to determine the screened Coulomb interaction of the electrons. In the present work we have used an implementation within the Quantum Espresso software collection [2,3]. From 40 samples of a MD trajectory the position of the HOMO of OH^- has been determined 0.7 eV above the VBM of the solvent. The computed ionization potential from the degenerate of the $2p_\pi$ state of the hydroxide ion was found at two slightly different energies due to the asymmetric solvent environment. The band gap of the solvent has been found at 8.1 eV.

Optical absorption spectra have been computed following the same strategy. We used time-dependent density-functional perturbation theory to compute the absorption spectrum for the aqueous hydroxide ion. The absorption spectrum has been computed over a wide range of frequencies with a Liouville-Lanczos approach as implemented in the turboTDDFT software [2,4]. Fig. 2 shows the spectra computed with the HSE hybrid functional together with the experimental spectrum of pure water. While the broad absorption band is in agreement with the experimental data, no absorption band can be assigned to the solute from the low-resolution spectrum. In order to identify the CTTS from the hydroxide ion to the solvent molecules the first 20 transitions have been computed in a separate calculation. A recently implemented Davidson algorithm for the computation of selective eigenvalues of the Liouvillian super-operator has been employed for these calculations [2,5]. The code provides efficient load and memory distribution and scales well beyond the system size in the present work. Typical simulations for the periodic simulation cell including 95 atoms and an excess charge have been performed on 512 to 1024 cores.

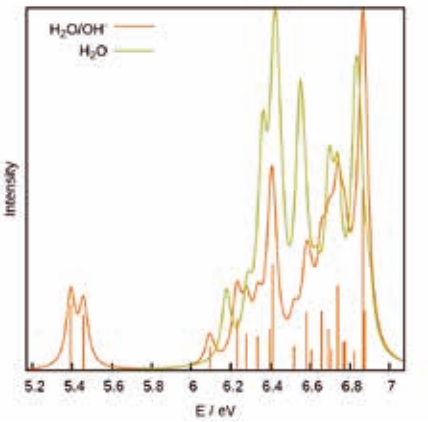

Figure 3: Absorption spectrum for the lowest 20 electronic transitions computed from a periodic simulation cell of 32 water and 31 water and one hydroxide ion.

On-going Research / Outlook

The description of CTTS in aqueous solutions remains a challenging problem in computational chemistry. Recent developments in the field of MBPT and time-dependent DFT and the availability of efficiently parallelized implementations provide the basis for further work on molecules with solvation shells beyond the current limitations. In particular the electronic structure and spectroscopy of solvated radicals which contain at least one unpaired electron represents an important problem. The simplest example of such a system is the solvated electron which is created as a product in the photolysis of liquid water or from excitation of a solute into a CTTS state. Its diffuse structure and genuine quantum mechanical behavior require a consistent description of the electronic structure of both the solute and solvent.

References and Links

[1] CP2K, http://www.cp2k.org
[2] Quantum Espresso, http://www.quantum-espresso.org/
[3] Y. Ping et al., Chem. Soc. Rev. 42, 2437-2469 (2013)
[4] Malcioglu et al., Comput. Phys. Commun., 182, 1744-1754 (2011)
[5] X. Ge et al., arXiv:1402.0486 [physics.chem-ph]

Theoretical investigation of photo-catalytic water splitting

Research Institution
Chair for Theoretical Chemistry, TU Munich

Principal Investigator
Karsten Reuter

Researchers
Harald Oberhofer, Daniel Berger

Project Partners
–

LRZ Project ID: pr58ba

Introduction

Oxide surfaces – such as TiO_2 or ZnO – have long been known to possess the ability to split water if irradiated by light. Unfortunately, the yields are small and most of the reactive surfaces only work with highly energetic UV-light. In order to make the process of water splitting viable for large scale application one therefore has to either find new materials or surfaces or introduce co-catalysts, like e.g.~small clusters of coinage metals which have shown much promise in experiments.

Our project was mainly concerned with the formulation of methods to investigate the mechanisms involved in the water splitting process and finding promising new catalyst materials. Due to the size of the involved systems and the need to accurately describe not only structures but also chemical reactions we exclusively used methods based on Density Functional Theory. Apart from data analysis and simulation control scripts using the python ASE[1] frameworks all simulations were either performed with the FHI-aims[2] or CASTEP[3] DFT packages.

Results

Computational screening of co-catalysts
We formulated a theoretical approach for the screening of viable catalyst/co-catalyst combinations [4]. At the same time we were able to show that DFT beyond the GGA level is necessary to achieve even qualitatively correct results. Looking at Au clusters up to 55 atoms (see below) this means the fully non-local treatment of up to 4345 electrons in a sufficiently large basis. For this we employed the numeric atomic orbital all-electron code FHI-aims [2], which shows excellent parallelisation and near linear scaling with system size. It is very well suited for use on architectures such as SuperMUC due to a customised scalapack implementation which at its heart has the highly efficient ELPA [5] eigenvalue solver.

Non-local exchange calculations for such a large number of heavy atoms is not only expensive in terms of CPU time but also with regards to memory consumption. Additional optimisation of the code was necessary to reduce the memory necessary per core below the 1.5 Gb available on SuperMUC thin nodes.

Additionally, we implemented a solid state embedding scheme based on the QM/MM approach which allows us to even go beyond hybrid DFT functional accuracy [6]. With our embedding approach we can also study surface and solvent effects acting on the Au-clusters. As this approach effectively eliminates the need for periodic boundary conditions, QM/MM surface calculations show the same parallel efficiency as vacuum runs with only a minimal overhead due to the polarisation of the MM region.

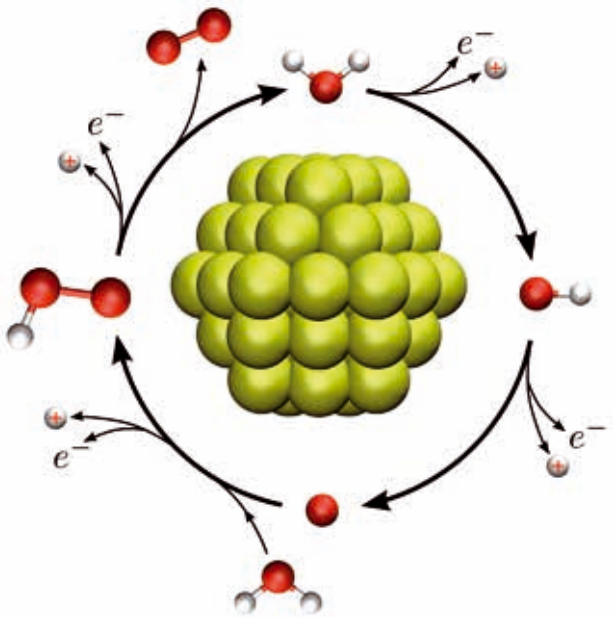

Figure 1: Schematic of a water oxidation reaction via proton coupled electron transfer on a gold nano-particle. Colour coding of the depicted atoms is as follows: red=O, white=H, yellow=Au

For this part of the project we used about three quarters of our available CPU-time (3M CPU hours). The number of files generated was small (<5-7 files per run where only

one file needs to be stored as output). Yet, for the largest clusters checkpointing files on SCRATCH did reach significant sizes of up to ~100 Gb. As these are only relevant in case of a crash or wall-time overrun no permanent storage of checkpoint files is necessary. Number of CPU's per job depended strongly on the size of the system at hand. Small jobs were typically conducted on up to 256 cores, while for the large ones we used up to 4096 cores. Average job size was around 512 cores.

A new thin film phase of ZnO
Together with the experimental group of Prof. Wöll at the Karlsruhe Institute of Technology we studied the formation of ZnO mono-, di- and tri-layers on Copper surfaces [7]. Such systems are relevant for chemical applications, as they allow direct coupling of a chemically active oxide with a metal, and can be produced relatively easily by oxidising brass surfaces. Using CO as a probe molecule we were able to show the existence of a before unknown thin film phase of ZnO, which is structurally situated halfway between the already known graphitic and Wurtzite phases. An example of the new phase is depicted in Figure 2 below.

In order to rule out any polarisation and finite size effects calculations had to be performed on a 5x5 Cu surface unit cell mirrored around the centre of the simulation box. As calculations were performed with the pseudopotential based plane-wave code CASTEP[3] such large box sizes were rather costly. In order to compare with experiment we calculated the harmonic vibration frequency spectrum and the transition dipole for the adsorbed CO molecule, on every unique adsorption site. Vibrational analysis was performed via the method of finite differences with the ASE[1] python framework. CASTEP parallelises well on SuperMUC architecture especially regarding reciprocal space sampling over k-points.

In total we used approximately 1M CPU hours for this project. Due to the nature of our implementation of the Tkatchenko Scheffler van der Waals correction a large number (~300 per run) of temporary files were generated on scratch. Yet again, only the actual output files containing energies and frequencies were retained for later use. Here, memory limitations were not an issue. On average we again used used around 512 cores per run. Calculation of the transition dipole moments was performed in a post-processing step on a workstation.

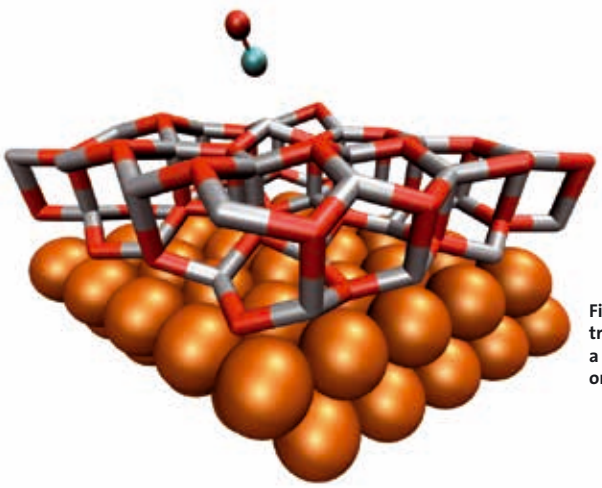

Figure 2: CO adsorbed on double layered ZnO in the transitionary phase between graphitic and Wurtzite on a Copper substrate. Colour coding of the depicted atoms is as follows: red=O, blue=C, silver=Zn, orange=Cu

Outlook

Calculations for projects such as the this are extremely costly due to the large size of the systems involved and the level of theory necessary to gain meaningful results. Only with a supercomputer such as SuperMUC were these calculations even possible. During the two years run-time of our project, progress was hindered by frequent breakdowns and longer outages of services at SuperMUC. These, which in part can be attributed to the newness of the system, added up to a total of not much less than 10% downtime over the course of our project. Additionally, SuperMUC policy to completely eliminate access to project data at the very day the project ends seems curiously strict, at least compared to other large supercomputing centres, as it essentially prohibits users from running jobs during the last days of their allotted project time.

Nevertheless, the results outlined above represent only the beginning of our research into more effective water splitting catalysts. With the computational infrastructure (i.e. QM/MM and embedding) we implemented, we are now in the position of being able to use beyond hybrid-DFT accuracy methods on realistic systems. In addition, we can directly study the influence of photo-generated charges on the water splitting reaction, thus going beyond the currently standard proton-coupled electron transfer mechanisms. In future work we will plan to study TiO_2 based water splitting, with regards to the influence of surface defects as well as surfaces nano-patterned with coinage metal clusters. Special focus will be put on photo-generated charges and pathways including charged intermediates, not accessible to periodic boundary calculations. Finally, in another project, we aim to calculate free energy barriers – and thus rates – for the water splitting reaction, accounting for nuclear quantum effects of the proton at the same time.

References and Links

[1] https://wiki.fysik.dtu.dk/ase/
[2] https://aimsclub.fhi-berlin.mpg.de/
[3] http://www.castep.org/
[4] H. Oberhofer and K. Reuter; J. Chem. Phys. 139 044710 (2013)
[5] T. Auckenthaler, V. Blum, H.-J. Bungartz, T. Huckle, R. Johanni, L. Krämer, B. Lang, H. Lederer, and P.R. Willems; Parallel Comput. 37 783 (2012)
[6] D. Berger, AJ. Logsdail, H. Oberhofer, MR. Farrow, CR A. Catlow, P. Sherwood, AA. Sokol, V. Blum, and K. Reuter; *in preparation*
[7] V. Schott, H. Oberhofer, A. Birkner, M. Xu, Y. Wang, M. Muhler, K. Reuter, C. Wöll; Angew. Chem. Int. ed. 52 11925 (2013)

Role of Interfacial Water in the Formation of Specific, Transient, and Non-Specific Protein-Protein Interactions

Research Institution
Center for Bioinfromatics, Saarland University

Principal Investigator
Volkhard Helms

Researchers
Ozlem Ulucan, Siba Shanak

Project Partners
–

LRZ Project ID: pr58go

Introduction

The large part of all proteins interacts with others for proper biological activity. In these cases, the proteins bind in very specific orientations. However, due to common diffusional motion, proteins constantly collide with other molecules where they form non-specific interactions that exhibit very short life times. So far little is known how these two kinds of contacts differ.

It is widely appreciated that water molecules play a crucial role in governing the structure, stability, dynamics, and function of biomolecules. However, the exact range of processes mediated by water is not well understood. The properties of the confined water are difficult to predict and may be very different from those of bulk water[1].

Using the Barnase: Barstar, Cytochrome c: Cytochrome c peroxidase, and the N-terminal domain of enzyme I: Histidine-containing Phosphocarrier protein-protein complexes, we have started this project by investigating the formation of specific complexes and the role of water upon complexation of those pairs.

Results

We conducted two different sets of molecular dynamics simulations for the three protein-protein complexes in explicit solvent. All interactions were modeled by the Amber force field FF99SB-ILDN[2] and water molecules were modelled by the TIP3P[3] water model. To mimic physiological conditions 100 mM NaCl was added, including neutralizing counterions. All simulations were carried out using the GROMACS[4] package, version 4.5.4 First, we combined umbrella sampling and the weighted histogram analysis method to characterize the one dimensional binding free energy surface of the three systems. The initial configurations for umbrella sampling were generated by translating one of the protein partners along the z-axis up to 3 nm distance between the surfaces of the two proteins, while keeping the other one fixed. For each system we simulated 40 ns-long 25 umbrella sampling windows on overage. The one-dimensional free energy profiles of protein-protein association were found to be downhill (see Figure 1). Using these one-dimensional free energy profiles, the computed standard free energies of binding are in good agreement with the experimental values (see Table 1).

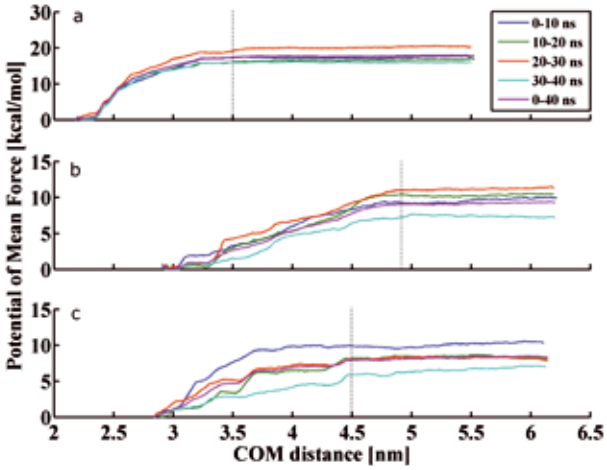

Figure 1: Potential of mean force calculated from different time intervals. a) Barnase: Barstar. b) Cytochrome c: Cytochrome c peroxidase c) N-terminal domain of enzyme I: Histidine-containing Phosphocarrier.

Subsequently, we performed a second set of MD simulations for the three protein-protein systems to characterize the density and the tetrahedral order parameter[5] of the interfacial water localized between the two protein interfaces. The starting configurations were obtained in the same way as previously mentioned for the umbrella sampling simulations. Additionally, harmonic position restraints were applied to the backbone atoms of the proteins to maintain their interfacial distance and a fixed relative orientation. The interfacial distance was varied between 0.35 and 5.0 nm, resulting in 12 different initial configurations. Each simulation was 20 ns long. The snapshots for analysis were collected every 0.25 ps. The results are provided in Figure 2. As seen in the figure the density and the orientational order parameter of

	$\Delta W(\frac{kcal}{mol})$	$\Delta G_{PMF}(\frac{kcal}{mol})$	$\Delta G_v(\frac{kcal}{mol})$	$\Delta G°(\frac{kcal}{mol})$	$\Delta G°_{exp}(\frac{kcal}{mol})$
BN:BS	-15.2	-15.7	-2.5	-18.2	-19.6 [6]
CC:CCP	-6.6	-7.9	-2.6	-10.5	-8.8 [7]
EIN:HPR	-5.6	-6.4	-2.7	-9.1	-7.8 [8]

Table 1: Standard free energies of binding for the BN:BS, CC:CCP and EIN:HPr complexes computed from full windows(40 ns).The calculated values; ΔW, ΔG_{PMF} and ΔG_v stand for the PMF depth, the free energy change of binding between the bound and unbound section of the PMF and the free energy of change from the unbound volume to the standard state volume, respectively. $\Delta G°_{exp}$ values stand for the corresponding experimental values.

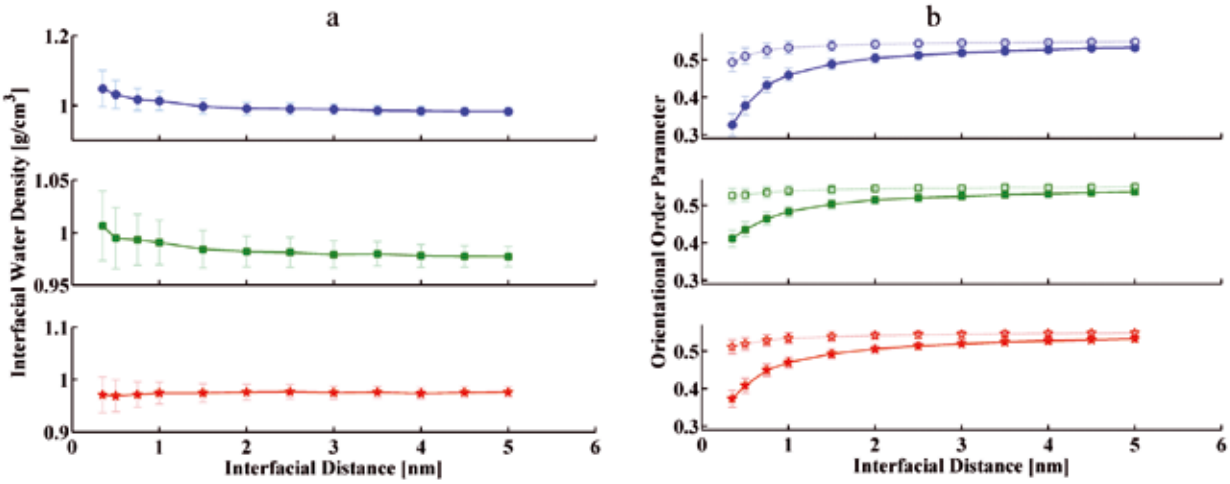

Figure 2: Density (panel a) and orientational order parameter (panel b) of the interfacial water for the three systems; Barnase: Barstar (blue circles), Cytochrome c: Cytochrome c peroxidase (green squares) and N-terminal domain of enzyme I: Histidine-containing Phosphocarrier (red stars). In panel b, the solid symbols are the orientational order parameter when only including neighboring water molecules. The open symbols stand for a modified orientational order parameter of the interfacial water molecules when considering their four closest water oxygens or interfacial protein atoms (O and N) within a 3.5 Å distance cutoff

confined water deviate noticeably from the bulk values at close separation of the confining proteins.

In general, we used 320-480 cores for each umbrella sampling job depending of the system size. For the interfacial water simulations we used 160-320 cores per a job). In total, the used CPU-time is about 4.8 million core hours which is 1/3 of the total granted time. The overall storage that we used for this project is about 23 TB.

On-going Research /Outlook

The work reported here contains the first part of our project. It has been completed recently and submitted to the *Journal of Chemical Theory and Computation*. In the second part of the project we are comparing currently the binding processes of specific complexes, transient intermediates, and non-specific complexes on the example of the same protein systems as stated in our project proposal.

References and Links

[1] P. Ball, "Water as an active constituent in cell biology," *Chemical Reviews*, vol. 108, pp. 74-108, Jan 2008.

[2] K. Lindorff-Larsen, S. Piana, K. Palmo, P. Maragakis, J. L. Klepeis, R. O. Dror, et al., "Improved side-chain torsion potentials for the Amber ff99SB protein force field," *Proteins-Structure Function and Bioinformatics*, vol. 78, pp. 1950-1958, Jun 2010.

[3] W. Jorgensen, "Transferable intermolecular potential functions for water, alcohols, and ethers. Application to liquid water," *J. Am. Chem. Soc*, vol. 103, pp. 335-340, 1981.

[4] D. Van Der Spoel, E. Lindahl, B. Hess, G. Groenhof, A. E. Mark, and H. J. Berendsen, "GROMACS: fast, flexible, and free.," *J Comput Chem*, vol. 26, pp. 1701-18, Dec 2005.

[5] J. R. Errington and P. G. Debenedetti, "Relationship between structural order and the anomalies of liquid water," *Nature*, vol. 409, pp. 318-321, Jan 18 2001.

[6] G. Schreiber and A. R. Fersht, "INTERACTION OF BARNASE WITH ITS POLYPEPTIDE INHIBITOR BARSTAR STUDIED BY PROTEIN ENGINEERING," *Biochemistry*, vol. 32, pp. 5145-5150, May 18 1993.

[7] H. K. Mei, K. F. Wang, S. McKee, X. M. Wang, J. L. Waldner, G. J. Pielak, et al., "Control of formation and dissociation of the high-affinity complex between cytochrome c and cytochrome c peroxidase by ionic strength and the low-affinity binding site," Biochemistry, vol. 35, pp. 15800-15806, Dec 10 1996.

[8] A. Ginsburg, R. H. Szczepanowski, S. B. Ruvinov, N. J. Nosworthy, M. Sondej, T. C. Umland, et al., "Conformational stability changes of the amino terminal domain of enzyme I of the Escherichia coli phosphoenolpyruvate : sugar phosphotransferase system produced by substituting alanine or glutamate for the active-site histidine 189: Implications for phosphorylation effects," *Protein Science*, vol. 9, pp. 1085-1094, Jun 2000.

Interface impurities and defects in complex oxide heterostructures

Research Institution
Institute of Physics, University of Augsburg

Principal Investigator
Thilo Kopp

Researchers
Natalia Pavlenko

Project Partners
–

LRZ Project ID: pr58pi

Introduction

Novel electronic phases at the interfaces of correlated complex oxide heterostructures can be very different from the properties of bulk matter and are of fundamental importance and technological potential for multifunctional electronic devices. Recent experimental studies demonstrate that the high mobile carrier densities at the interfaces of band insulators $LaAlO_3$(LAO) and $SrTiO_3$(STO) can be produced from two different sources: (i) electronic reconstruction due to the polar charge transfer and (ii) charge carriers provided by oxygen vacancies. The oxygen defects are also considered as a central mechanism for magnetic polarization in these systems and for a recently discovered nanoscale electronic separation between superconducting and ferromagnetic states. In this context, the tuning of the electron carrier density by the control of the interfacial microstructure and defects as well as the theoretical exploration of the electronic state of the defect-rich heterointerfaces are central issues which open a direction for further investigations of complex oxide interfaces.

In the present project, the inhomogeneous electronic states and magnetic properties at the interfaces of the polar-nonpolar heterostructures of $LaAlO_3$ and $SrTiO_3$, with oxygen defects have been studied by density functional theory. The influence of defects has been modelled through incorporation of oxygen vacancies into the structures. The main goals of the proposed modeling are (i) achieving an understanding of the inhomogeneous microscopic states of quantum electron liquids stabilizing near the polar-nonpolar heterointerfaces of LAO/STO-type, (2) exploration of the mechanisms of the interfacial magnetism and (3) investigation of the influence of electron-phonon interactions and structural disorder induced by defects in the emergence of novel electronic states at the interfaces. The project is aimed to address the unresolved problems including generation of heterointerfaces with predictable transport characteristics. In this way, the project is expected to advance the generation of novel nanoscale devices that use the striking properties of quantum systems to surpass the limits of today's electronics.

Special implementations of the DFT approach like the linearized augmented plane wave method (LAPW) implemented in the all-electron full-potential WIEN2k package [1] and pseudopotential Quantum Espresso (QE) package [2], are applied for the first-principles studies of the interface electronic states in structures containing oxygen defects. In these implementations, the electronic properties of the heterointerfaces are modelled by the calculations of the electronic structure for specially selected computer-generated supercells. As a result, the electronic structure, electronic orbital occupancies and magnetic polarization of the supercells can be analyzed with atomic resolution. The calculated valence and conducting charge density profiles as well as the structural atomic distortions due to defects and polarization fields near the interface allow to explore different interface reconstruction mechanisms.

In this project, we explore the electronic structure of the first titanate surface/interface layers considering different configurations and concentrations of oxygen vacancies. We find that in contrast to the bulk stoichiometric $SrTiO_3$, each local atomic configuration with vacancy contains missing hybridization links which strongly influence the local energies of d orbitals of the nearest Ti atoms. The vacancy-induced orbital reconstruction at titanate interfaces leads to a shift and partial occupation of the vacancy-directed Ti e_g-orbitals and to the formation of local magnetic moments due to a magnetic splitting of hybridized e_g and $3d_{xy}$ states. Our calculations of $SrTiO_3$-surfaces and LAO/STO interfaces demonstrate the universal character of the orbital reconstruction of titanates due to surface/interface oxygen vacancies.

We also performed the studies of the electronic states of heterostructures with the oxygen-reduced LAO overlayers. We find that the oxygen defects in the LAO overlayer produce local electronic states of a mixed sp character which are redistributed between the surface AlO_2 and interface TiO_2 layers resulting in the confinement of electrons in the parallel, surface and interface 2D layers with different effective masses. We obtain that for small concentrations of oxygen vacancies $c_v \leq 1/8$ at the AlO_2

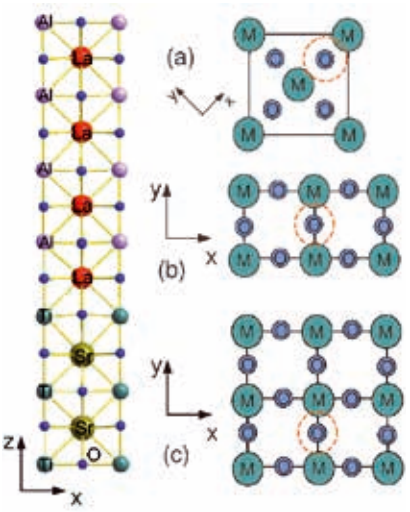

Figure 1: Schematic view of the $SrTiO_3/LaAlO_3$ heterostructure. The supercell contains a 4 uc thick $LaAlO_3$ layer deposited on a 2.5 uc thick $SrTiO_3$ slab. The full supercell consists of two symmetric parts of the depicted structure and a vacuum layer of 13Å. The structures on the right side show M_nO_{2n} (M=Ti, Al)-plaquettes (a) with one eliminated O(2a,a) atom (dimerized vacancy), (b) with eliminated O(0.5a,0.5a) (chained vacancy) and (c) with eliminated O(0.5a, 0.25a), generated for the study of the systems with O-vacancies. The position of an O-vacancy is identified by a red dashed circle.

surface, the vacancy released electrons are transferred to the LAO/STO interface and compensate the interface polar-discontinuity, which also leads to an insulating surface state. In view of these findings, we explore the oxygen defects at the LAO-surface as a possible source for the two-dimensional electronic liquid state at the LAO/STO interfaces.

Results

In the studies of the electronic structure of titanate surface/interface multilayers with defects[3-5], we analyze a number of supercells with different local atomic configurations near oxygen defects, which corresponds to different concentrations of oxygen vacancies (Fig.1). We find an important orbital reconstruction of the local 3d-electronic states of Ti atoms close to the oxygen vacancies. For instance, for the configuration with vacancy stripes (shown in Fig.1(b)), the obtained orbital reconstruction leads to a strong "splitting" of the $3d_{3z^2-r^2}$ and $3d_{x^2-y^2}$ states (Fig.2(a)) with the $3d_{3z^2-r^2}$ being almost completely occupied with close to 2 electrons and the $3d_{z^2-y^2}$ almost completely empty and at very high energies above the Fermi level E_F.

The two-dimensional character of the magnetic ordering at the interface is confirmed by our extensive calculations of the supercells in which the oxygen vacancies residing at the LAO/STO interface and in more distant layers from the interface TiO_2-layers. Our studies of the LAO/STO heterostructures with surface oxygen defects reveal their key role in the generation of the two-dimensional electronic state at the interface, in particular due to a transfer of the electron charge from the surface to the interface by the LAO polar field. This important finding allows to shed light on the mechanisms of the interface electronic reconstruction and has been obtained in a combination with the photoemission (ARPES) studies of the LAO/STO-interfaces.

The scientific results of the project require extremely demanding supercomputer simulations which include: (i) realistic mechanisms of surface and interface electronic and ionic reconstruction; (ii) superlattice and surface geometric relaxation and optimization; (iii) numerically consuming spin-polarized calculations of electronic structure with the inclusion of strong local correlations for d-electrons in transition metal oxides; (iv) the post-processing calculations required to analyze the electronic states of the interfaces (band structure calculations with initially generated **k**-point grid and given number of bands, calculations of Fermi surfaces which also require generation of a high-density **k**-point grid, performed using the programs bands_FS.x and kvecs_FS.x which are parts of the QE-package). For the superlattices of $LaAlO_3$/$SrTiO_3$ containing up to 120 atoms in a supercell, a single run of GGA+U includes typically from 100 to 150 iteration steps until the final convergence with respect to the electronic charge and total energy could be reached. With up to 512 cores used each run of the parallel k-points calculations, each converged GGA+U run usually requires up to 3,000-4,500 CPU hours. In addition, in each superlattice, the relaxation of the interface distances could be achieved by performing up to 10 single GGA runs which required about 8,000-10,000 CPU hours. Due to a wide range of superlattices analyzed in our project ($LaAlO_3$/$SrTiO_3$-bilayers with different sizes ranging from 20 to 120 atoms), such computationally demanding calculations already required about 3,000,000 CPU hours.

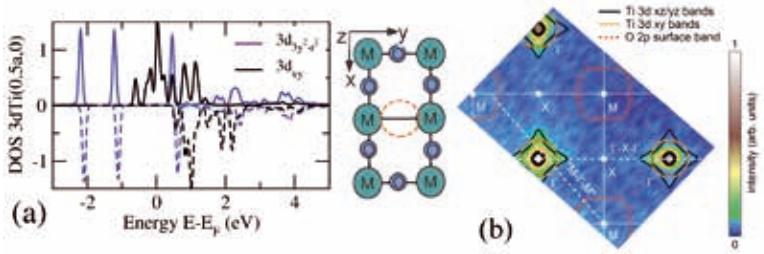

Figure 2(a) Electronic density of states of a system with interface oxygen defects and (b) calculated and measured Fermi surface of LAO/STO heterostructure.

On-going Research / Outlook

The scientific progress of the project has been achieved mainly due to the computation facilities available within SuperMuc. The current research of the project pr58pi is directed on the studies of the effect of pressure on the electronic and magnetic states at the oxide interfaces, which is a direct extension of the computational studies performed during 2013.

References and Links

[1] P. Blaha et al., WIEN2K, An Augmented Plane Wave+Local Orbitals Program for Calculating Crystal Properties, ISBN 3-9501031-1-2 (TU Wien, Austria, 2001)
[2] P. Giannozzi et al.,J.Phys.: Condens.Matter 21, 395502 (2008).
[3] N. Pavlenko, T. Kopp, E.Y. Tsymbal, G.A. Sawatzky, and J. Mannhart, Phys.Rev.B 85, 020407(R) (2012); N. Pavlenko, T. Kopp, E.Y. Tsymbal, J. Mannhart, and G.A. Sawatzky, Phys.Rev.B 86, 064431 (2012).
[4] G.Berner, M.Sing, H.Fujiwara, A.Yasui, Y.Saitoh, A.Yamasaki, Y.Nishitani, A.Sekiyama, N.Pavlenko, T.Kopp, C.Richter, J.Mannhart, S.Suga, and R.Claessen, Phys.Rev.Lett. 110, 247601 (2013).
[5] N.Pavlenko, T.Kopp, and J.Mannhart, Phys. Rev. B 88, 201104(R)(2013).

Reconstructing Phylogenetic Trees from Whole Genomes and Transcriptomes

Research Institution
Heidelberg Institute for Theoretical Studies

Principal Investigator
Alexandros Stamatakis

Researchers
Andre Aberer, Tomas Flouri, Fernando Izquierdo-Carrasco, Alexey Kozlow

Project Partners
1KITE consortium www.1kite.org

LRZ Project ID: pr58te

Introduction

Phylogenetic tree reconstruction strives to infer the evolutionary relationships among a set of organisms (species, frequently also denoted as taxa) based on molecular sequence data. Recent advancements in sequencing technology, in particular the emergence of so-called next generation sequencers, have generated an avalanche of sequence data, that now makes it possible to use whole transcriptomes and even genomes of a large number of species for tree reconstruction. Tree inference under the maximum likelihood (ML) criterion is a widely used, but compute-intensive method for this task. Our goal is to test and improve the scalability of our ML-based tree reconstruction software as well as to empirically assess the quality of the results in the context of two large-scale collaborative phylogenetic analysis projects:

The 1K insect transcriptome project studies the transcriptomes (i.e., the expressed parts of the genome) of 1,000 insect species encompassing all recognized insect orders on the planet. The project aims to establish the first robust backbone tree for insects. Similarly, the goal of the second project is to infer a phylogeny of a representative sample of bird genomes.

Results

Bird phylogeny
The bird genome analyses have been completed and we expect the respective manuscript to be submitted to Science within the next 1-2 months. As originally planned, these runs only required a relatively small fraction of the CPU time we had originally applied for.

Insect phylogeny
We have already assembled the data for all 1000 insect transcriptomes. This data is available now to conduct the large-scale production runs. The production runs to analyze the 100 insect transcriptome dataset will be completed by the end of 2013. We will submit a manuscript on this initial 100 species insect transcriptome tree within the next 1-2 months. Apart from the Maximum Likelihood based inferences with ExaML (see below), we have also conducted some preliminary tests with a program called DPPDIV that infers divergence times on trees. A divergence times inference program transforms the relative times on a phylogeny that represent the mean substitution rate per site (per nucleotide in the sequence) to real times (in years).

The original DPPDIV [1] (Dirichlet Process Prior Divergence estimator) code that we used for inferring divergence times has been adapted and parallelized by our group using a novel high performance library (phylogenetic likelihood library, see: http://www.libpll.org/). By integrating our library with DPPDIV, we achieved an improvement of run times of up to a factor of 300 [2]. In 2014 we expect to execute comprehensive analyses on the 1000 transcriptome dataset using our ExaML code.

Computational Research
The computational objectives as initially stated are as follows: The data analysis on SuperMUC will be conducted using MPI-based codes for reconstructing phylogenetic trees that have been developed in our group, namely the new Exascale Maximum Likelihood (ExaML) code we have developed. The code has been published [3] and is available as open-source code. ExaML executes up to 3.2 times faster than the previous RAxML-Light software we developed because of the more efficient parallelization and communication scheme, while implementing exactly the same tree search algorithm. One of our group members (A.J. Aberer) participated in the extreme scaling workshop at LRZ in summer 2013.

ExaML at the SuperMUC Extreme Scaling Workshop

As a prerequisite to the SuperMUC extreme scaling workshop, we successfully demonstrated that ExaML scales linearly up to 4,096 processes (see Figure 1) for a bird genome dataset which is among the largest empirical datasets currently available. We then analyzed a dataset that is one order of magnitude larger than the dataset used in Figure 1 and determined the scaling behavior on up to 32,768 processes.

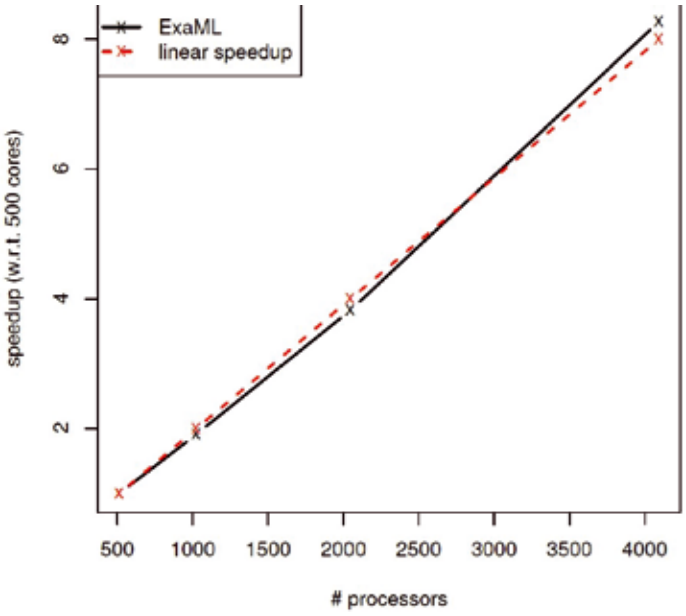

Figure 1: Scalability of ExaML on 4096 cores for the bird genome dataset

Here, we identified sub-optimal scaling with respect to the the reference run (4K processes). During the workshop, a second run revealed that with 32K processes, reading and processing the input file already consumed 33% of the total runtime (15 min).

The respective input file is a pre-processed binary data file with a size of 16 GB. We thus tried to improve start-up efficiency of ExaML. We modified the data distribution scheme, such that, each process reads larger contiguous blocks (measure 1). Furthermore, we modified the code to directly read input data from the file into the target data structures without the use of intermediate buffers (measure 2).

Measure 2 reduced the initialization time by a factor of 2. However, measure 1 did not improve the start-up time. We assume that the bottleneck is the high number of disk accesses that are performed by all processes simultaneously. We intend to address this issue in 2014.

On-going Research / Outlook

In the first year we were able to complete the production level runs on an initial 100 insect transcriptome dataset and on the bird genome dataset using our new open-source ExaML code on the SuperMUC. We expect to submit papers about these two analyses to high quality journals within the next 1-2 months. The inference of the 1000 insect transcriptome tree has been delayed due to technical issues and the sheer size as well as complexity of the project. In the consortium there are over 40 partners involved. However, the collection of the samples, molecular sequencing of the data, and dataset assembly has been completed now, such that we can initiate the analyses in early 2014.

At the technical level, we have identified several problems and challenges and also developed and released several new codes for large-scale evolutionary analyses of molecular sequence data on supercomputers We have released, a new, scalable, and *checkpointable* code for maximum likelihood based phylogenetic inference called ExaML. The code deploys a radically new parallelization approach and scales linearly up to 4096 cores. Scalability beyond this point is currently limited by the file I/O during the program start-up phase. However, we are confident that this issue can be addressed in a relative straight-forward way by using MPI parallel I/O routines. It is thus mainly an issue of further software development.

Using the ExaML code base and the new parallelization scheme, we also started developing ExaBayes, a Bayesian program for phylogenetic inference. We are testing its scalability and stability on SuperMUC at present. In accordance with the tradition of our lab, we will soon make it available to the community as open-source code. To date, it is the only Bayesian inference program that scales on Supercomputers and that is able to analyze datasets as large as the insect or bird datasets we use here.

Furthermore, the ExaBayes framework can be used to design a scalable Bayesian divergence times estimation tool from scratch. Despite the substantial speedup we attained by integrating our phylogenetic likelihood library into an existing program (DPPDIV), the performance gains are not sufficient to analyze our datasets. Note that, the phylogenetic likelihood library also uses the old master-worker parallelization scheme, that, as we have shown in the past, does not scale well beyond 1000 cores. Divergence time estimation represents an important step in the phylogenetic analysis pipeline.

Overall, we have been able to identify performance bottlenecks in the codes and also developed new, scalable codes. Furthermore, we have identified the needs for further research and development of tools that allow for large-scale molecular data analysis on supercomputers. The project is highly exploratory, since it is the first that attempts to infer and post-analyze such huge molecular datasets in an evolutionary context. At the end of 2014 we expect to have released at least two open source codes for supercomputers (ExaML & ExaBayes) published two high quality papers (bird tree and 100 insect transcriptomes) and have completed the analyses on the 1000 insect transcriptome dataset.

References and Links

[1] Heath, T.A., Holder, M.T., and Huelsenbeck, J.A. 2011. A Dirichlet process prior for estimating lineage-specific substitution rates. *In Molecular Biology and Evolution*, doi: 10.1093/molbev/msr255

[2] Darriba, D. Aberer, A.J., Flouri, T., Heath, T.A., Izquierdo-Carrasco, F. and Stamatakis, A. 2013. Boosting the performance of Bayesian divergence time estimation with the Phylogenetic Likelihood Library. In Proceedings of IPDPS 2013, Boston, USA.

[3] Stamatakis, A. and Aberer A.J. 2013. Novel Parallelization Schemes for Large-Scale Likelihood-based Phylogenetic Inference. In Proceedings of IPDPS 2013, Boston, USA.

http://www.exelixis-lab.org
https://github.com/stamatak/ExaML

Methanol Synthesis over Cu/ZnO from *ab initio* molecular dynamics

Research Institution
Lehrstuhl für Theoretische Chemie, Ruhr-Universität Bochum

Principal Investigator
Dominik Marx

Researchers
Johannes Frenzel, Luis Martínez-Suárez

Project Partners
1KITE consortium www.1kite.org

LRZ Project ID: pr63ce

Introduction

Heterogeneous catalysis is essential to industrial produc-tion of all sorts of bulk chemicals and goods. The im-provement, development, and design of more efficient catalysts in terms of turnover (selectivity) and energy reduction is highly demanding. Therefore, it is most im- portant to get adequate handle on physical and chemical processes on the molecular scale taking places at cata-lytic surfaces under reaction conditions.

One example is the synthesis of methanol which is of great importance not only for bulk chemical industry but also gives a clean liquid fuel in a future "Methanol economy" [1]. Starting from syngas (a mixture of CO_2, CO and H_2) modern methanol synthesis is performed by the ICI process which requires temperatures of 513-533 K and pressures of 5-10 Mpa to enhance the thermodynamically limited yield. In spite of extensive experimental and theoretical studies in the last decades, the reaction pathway(s) involved in CO_2 reduction over ZnO supported copper nanocatalysts is still under debate. The experimental identification of different intermediates, as well as the fact that the process must necessarily include at least three hydrogenation steps and one deoxygenation step gives evidence to a complex reaction network. Herein, the most important point are the severe environmental conditions which cause morphological changes, so-called strong metal-support interactions (SMSI) of the nano- structured Cu catalyst material dispersed on a ZnO ma- trix and stabilized by Al_2O_3. Rationalizing the synergistic structure-reactivity relationships of Cu and ZnO, the particular function of ZnO, and the nature of the active site are subject to contradictory mechanisms which have been proposed. While some of these effects may be present at the same time under these extreme reaction conditions experimental insight turned out to be very elaborate. On the one hand the surface structure of Cu/ZnO and, hence, the active site may be created *in-situ* under elevat-ed temperature, high pressure and reactive gas phase (syngas) of the catalytic process, but on the other hand it may also depend on the actu-al preparation of the catalyst.

From the simulations' point of view the catalytic processes at surfaces are an extremely chal-lenging system. Its inter- actions can not be parametrized in terms of force fields. It has been show that electronic effects at the Cu/ZnO interface promote methanol formation from CO_2. Chemical reactions involve bond breaking and for-mations which request the accurate modeling of the electronic structure. Furthermore, pressure and tempera-ture effects in terms of fluctuation of the nuclei can not be neglected at the outset when computing such processes. A computational scheme is necessary which integrates all these aspects.

Over the recent years, we developed such an efficient multi-step computational scheme with advanced ab initio molecular dynamics (AIMD) at its heart, and success-

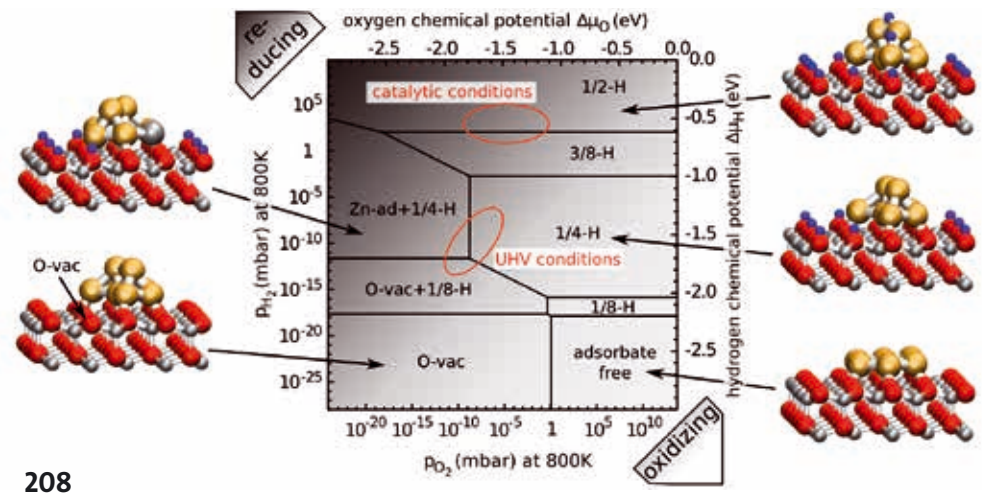

Fig. 1 Phase diagram of Cu_8/ZnO(000 1) supported nanocatalysts. The structures are in thermodynamic equilibrium with hydrogen and oxygen reservoirs which control the chemical potentials ΔμH and $\Delta\mu_o$. Zinc, oxygen, hydrogen and copper atoms are represented in gray, red, blue and cyan colors, respectively. This figure was adapted from Ref. [4].

fully applied to the high temperature and high pressure variant of methanol synthesis from CO and H_2 over the less com- plex bare ZnO catalyst [2,3].

Results

By performing advanced ab initio molecular dynamics (AIMD) simulations we obtained an atomistic understand- ing of the chemical species and mechanistic insight in the heterogeneous catalytic process of methanol synthesis from syngas over a ZnO supported Cu nanocatalyst. The free energy landscape of chemical reactions from CO_2 and H_2 to give methanol is computed in the first place by using ab initio metadynamics for computational hetero- geneous catalysis. Employing *ab initio* electronic structure calculations at density functional theory level it is further shown that driven by morphological and electronic changes complex electronic charge transfer processes across the metal-support interface explain the enhanced reactivity toward CO_2 at conditions of the industrial metha-nol synthesis [4]. With the calculation of a refined thermo-dynamic phase diagram we obtain further atomistic in-sight in the morphological changes and redox state de-pendent reactivity of Cu/ZnO, which are subject SMSI, depending on temperature and pressure [4].

These results for once more demonstrate our multi-step computational scheme [3] to be powerful, complementary, and general approach which is able to "synthesize" meth-anol *in silico* by unveiling an unexpectedly complex reaction network with a manifold of chemical species and a rich landscape of interconnecting reaction pathways including the identification of important side reaction, e.g. the water gas shift reaction (WGSR) and reverse WGSR.

The AIMD simulations were carried out with CPMD a DFT-based molecular dynamics code. An ultrasoft plane wave basis set with a 25 Ry energy cutoff and pseu- dopotentials were used for the description of the electro- nic structure were used. The Kohn-Sham equations of DFT were propagated in an extended Lagrangian scheme. This computationally demanding part of the cal-culation is assigned to processor groups (PGr), which require a high band width/low latency interconnect. Within a PGr parallelization is realized via MPI for inter-node communication and either MPI or OpenMP/Vector proces- sing for intra-node parallelization. At this level of parallel- ization the allocation of 160 cores allowed for the highest speedup, because one FFT-plane could be assigned to each core while the speedup breaks down if FFT planes are assigned to several cores. The CPMD propagation of a singleCu_8/ZnO(000 1) catalyst system required 8.9 core·min per step on SuperMIG and 6.1 core·min per step on SuperMUC, i.e., fully utilizing 4 nodes and 10 nodes, respectively. There exist another level of paral-lelization which is the multiple walker extension to the metadynamics simulation. Walkers interact in building up the biasing potential and this interaction requires negligible communication effort. Such, the algorithm parallelizes intrinsically with respect to the number of replicas (walk- ers) of the total system allowing for some tenths of walk- ers. However, in our metadynamics exploration

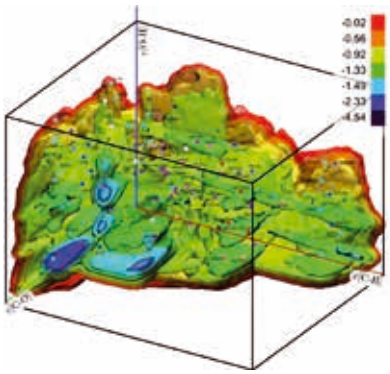

Fig. 2 Three dimensional free energy surfaces generated by ab initio metadynamics propagating the chemical transformations from CO_2 and H_2 to give methanol over the reduced 1/2 H ML covered Cu_8/ZnO(000 1) catalyst surface. Collective variables are the coordination numbers of carbon to hydrogen in the system (c[C–H]), oxygen to hydrogen in the system (c[O–H]), and carbon to all oxygen of the surface layer of ZnO(000 1) (c[C–O]). Relative free energies ΔF (in eV) are provided according to the color scale. Analysis of the AIMD trajectory underlying the metadynamics yield the individual chemical species which are indicated by labels being set at the geometric center of species occurrence.

simula- tions of the free energy surface for the CO_2 hydrogenation to give methanol over Cu_8/ZnO(000 1) (see Fig. 2) we only used five to ten walkers, because best performance to queue waiting time was reached on both super computer systems. In total our project has consumed five million core hours total since project starting. Typically 160 or 800 cores were used per job. The overall storage needed in SCRATCH and PROJECT was 4.4 TiB and 10 GiB, respectively, which distributed over approximately 150,000 files.

We note that after migrating from HLRB-II (SGI Altix 4700) to superMIG our project was easily transferred and could efficiently utilize this machine and, thus, became the largest project on it in the year 2012.

On-going Research / Outlook

The overview on the reaction network allows the selection of reaction channels inherent to low free energy paths. Restricting to only one channel decreases complexity and allows to sample a larger number of individually tailored reaction variables by individual metadynamics simulations which can be computed run in parallel jobs. The obtained paths of minimum free energies will allow very detailed kinetic and thermodynamic information to allow for pro- found conclusions on the overall mechanism of methanol synthesis on Cu/ZnO. This automated computational approach in the framework of accelerated AIMD is to the best advantage especially in those cases where it is difficult to get a handle on state-of-the-art approaches, i.e. optimizing immense numbers of static structures prior mapping interconnecting minimum energy pathways, carefully narrowing down transition states, and finally estimate thermodynamic corrections by virtue of harmonic analysis.

References and Links

[1] G. A. Olah, A. Goeppert, and G. K. Surya Prakash, Beyond Oil and Gas: The Methanol Economy (Wiley-VCH, Weinheim, Germany, 2006).
[2] J. Kiss, J. Frenzel, N. N. Nair, B. Meyer, and D. Marx, J. Chem. Phys. 134, 064710 (2011).
[3] J. Frenzel, J. Kiss, N. N. Nair, B. Meyer, and D. Marx, Phys. Status Solidi B 250, 1174 (2013).
[4] L. Martínez-Suárez, J. Frenzel, D. Marx, and B. Meyer, Phys. Rev. Lett. 110, 086108 (2013).

http://whww.theochem.rub.de/research/marx
http://www.ruhr-uni-bochum.de/solvation

Magnetism of free and deposited magnetic molecules

Research Institution
Universität Bielefeld, Fakultät für Physik

Principal Investigator
Jürgen Schnack

Researchers
Michael Czopnik, Oliver Hanebaum, Christian Heesing, Martin Höck, Henning-Timm Langwald, Jörg Ummethum

Project Partners
School of Chemistry, Manchester University, School of Chemistry, University of Edinburgh

LRZ Project ID: pr63fa

Introduction

Magnetic molecules are an interesting and growing class of new materials with prospective applications as nextgeneration storage devices or magnetic refrigerants to name just a few applications. They usually contain paramagnetic ions, which are held together by chemical ligands which also mediate the magnetic exchange interactions between the magnetic moments of the ions.

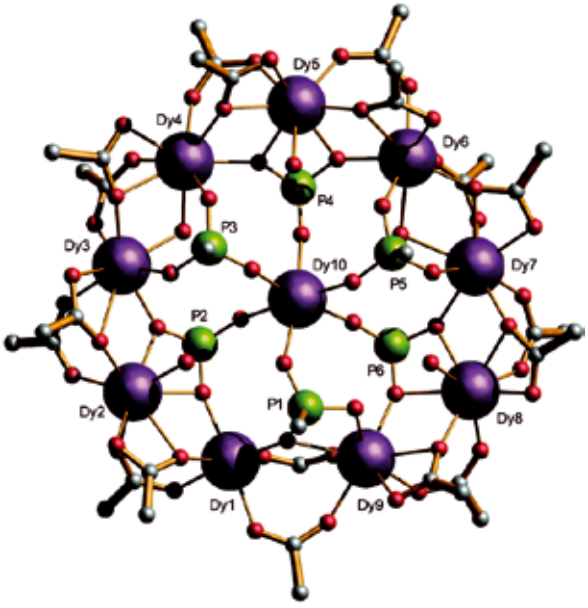

Figure 1: Structure of the magnetic molecule $[Ln_{10}(O_2CtBu)_{18}(O_3PtBu)_6(OH)(H_2O)_4]$ (Ln ions, Dy or Gd, large purple spheres) [1].

Figure 1 shows as an example the structure of a recent magnetic molecule that comprises nine Lanthanide ions in a disk-like structure [1]. Although such molecules are of finite size, and the magnetic degrees of freedom (often only the spins) constitute just a subsystem, the related Hilbert spaces can assume huge dimensions. This renders a treatment based on a numerically exact diagonalization of the relevant Hamiltonian virtually impossible. We therefore resort to powerful approximations developed for many-body quantum systems. Among them we mainly employ the Finite-Temperature Lanczos Method (FTLM), which belongs to the Krylov space methods, the Density Matrix Renormalization Group (DMRG) method as well as the Numerical Renormalization Group (NRG).

Magnetic molecules are very often well-described by the following Hamiltonan

$$\hat{H} = -2 \sum_{i<j} J_{ij} \hat{\boldsymbol{s}}_i \cdot \hat{\boldsymbol{s}}_j + \sum_i \hat{\boldsymbol{s}}_i \cdot \mathbf{D}_i \cdot \hat{\boldsymbol{s}}_i + \mu_B B \sum_i g_i \hat{s}_i^z \,. \quad (1)$$

Here the first term (Heisenberg term) describes the mutual interaction between spins at sites i and j with strength J_{ij}; it determines whether spins want to align in a parallel fashion (ferromagnetic) or in an antiparallel fashion (antiferromagnetic). The second term is called single-ion anisotropy; it models local preferential directions. The third term (Zeeman term) accounts for the interaction with an external magnetic field.

Results

The main focus of our numerical investigations during the past two years was on interesting spin systems with large Hilbert spaces. Here we further improved our FTLM code. We were able to reach record dimensions when modeling a new magnetic molecule which contains 12 Gd ions of spin s=7/2 each. Such a system possesses a Hilbert space of the huge dimension of $(2s+1)^N$=68.719.476.736, which even when exploiting symmetries, leads to very large Lanczos vectors of up to 109. But thanks to our openMP parallelization and to the fact that we evaluate matrix elements on the fly, we could evaluate the magnetic observables of this molecule [2].

A key reason to investigate gadolinium-based magnetic molecules is given by their promising magnetocaloric properties, which allow sub-Kelvin magnetic

refrigeration [3]. To this end the magnetic entropy of the substances needs to be calculated which again is done by means of FTLM or numerically exact diagonalization in the case of smaller molecules. Figure 2 shows as an example the curves of constant entropy (isentropes) for a molecule where six Gd ions occupy the vertices of a distorted octahedron. From such thermodynamic relations Carnot processes can be constructed and cooling rates can be evaluated. One can for instance estimate the final temperature when running down an isentrope in an adiabatic process. Figure 2 demonstrates that indeed sub- Kelvin temperatures can be reached [4].

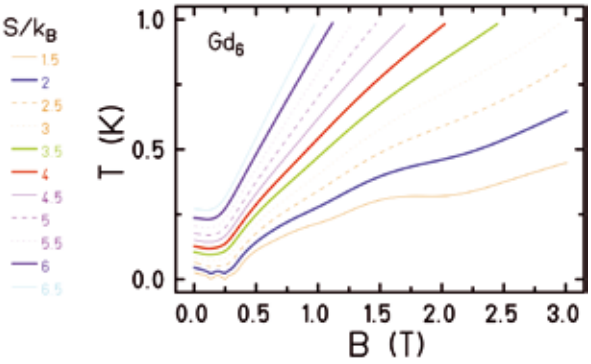

Figure 2: Theoretical isentropes for a magnetic molecules containing six Gd ions positioned at the vertices of a distorted octahedron [4].

Another important direction of our research efforts concerns the modeling of deposited magnetic molecules. In experiment these molecules are placed on metallic substrates and interact with the electrons of the conduction band. We model such systems as singleimpurity single-channel Kondo systems by means of NRG [5]. In a first step we investigated how the exchange interaction with the metal's electrons modifies the magnetic properties of a single deposited anisotropic spin. We could show that for an easy-axis anisotropy the impurity magnetization is stabilized at a value, which depends on the anisotropy for cases when the thermal energy is smaller than the Zeeman energy, which is assumed to be smaller than the anisotropy energy. In the case of hard-axis anisotropy, the magnetization curves can feature steps, which are modified due to fieldinduced pseudo-spin-1/2 Kondo effects [5].

Using our openMP-parallelized DMRG and Dynamical DMRG code we could interpret Inelastic Neutron Scattering results on a new 18-membered Fe(III)-based spin ring. For this purpose we evaluated the dynamical spin-spin correlation function, which is a measure for the amount of neutron scattering at a certain energy and wave vector [6].

Outlook

An important extension of (1) is provided by a more general interaction term. In the following Hamiltonian this is taken care of by replacing the isotropic exchange Jij in (1) by a 3x3 matrix

$$\underset{\sim}{H} = -2 \sum_{i<j} \underset{\sim}{s}_i \cdot \mathbf{J}_{ij} \cdot \underset{\sim}{s}_j + \sum_i \underset{\sim}{s}_i \cdot \mathbf{D}_i \cdot \underset{\sim}{s}_i + \mu_B B \sum_i g_i \underset{\sim}{s}_i^z \,. \quad (2)$$

Such an interaction matrix can account for anisotropic as well as antisymmetric (Dzyaloshinskii-Moriya) exchange and also for dipolar interactions. Anisotropic interactions have attracted increased interest recently due to the fact that such interactions may enhance Single-Molecule Magnet properties, i.e. barriers for magnetization reversal [7]. Chemically, this means that the usual 3d-elements are replaced by 4d- or 5d-elements such as osmium or ruthenium.

Another research direction concerns the investigation of more complex deposited spin systems such as the two hypothetical arrangements shown in Figure 3. In such scenarios it is possible that the coupling screens a part of the deposited spin system to a certain degree depending on the exchange coupling to the substrate as well as on temperature and field. In our investigations we try to find out under which circumstances the strong coupling case leads to a practically decoupled residual spin system that behaves as if it was free, i.e. not coupled to the surface.

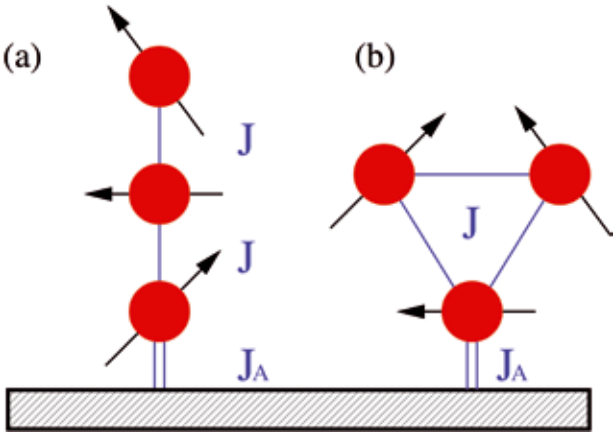

Figure 3: Sketch of deposited molecules, which interact with a metallic substrate.

References and Links

[1] K.H. Zangana, E.M. Pineda, E.J.L. McInnes, J. Schnack, R.E.P. Winpenny, Chem. Commun. **50**, 1438 (2014)
[2] Yong Zheng, Qian-Chong Zhang, La-Sheng Long, Rong-Bin Huang, A. Müller, J. Schnack, Lan-Sun Zheng and Zhiping Zheng, Chem. Commun. **49**, 36 (2013)
[3] T.N. Hooper, J.Schnack, S.Piligkos, M. Evangelisti, E.K. Brechin, Angew. Chem. Int. Ed. **51**, 4633 (2012)
[4] J. Schnack, C. Heesing, Eur. Phys. J. B **86**, 46 (2013) [5] M. Höck, J. Schnack, Phys. Rev. B **87**, 184408 (2013)
[6] J. Ummethum, J. Nehrkorn, S. Mukherjee, N. B. Ivanov, S. Stuiber, Th. Strässle, P. L. W. Tregenna- Piggott, H. Mutka, G. Christou, O. Waldmann, J. Schnack, Phys. Rev. B **86**, 104403 (2012)
[7] V. Hoeke, A. Stammler, H. Bögge, J. Schnack, T. Glaser, Inorg. Chem. **53**, 257 (2014)

Li deintercalation in Li_2FeSiO_4: The influence of interfaces

Research Institution
Universität Ulm, Institut für Theoretische Chemie

Principal Investigator
Axel Groß

Researchers
Nicolas Hörmann

Project Partners
Helmholtz Institute Ulm (HIU) Electrochemical Energy Storage

LRZ Project ID: pr63fo

Introduction

In this part of the project pr63fo, structures and processes at electrochemical interfaces are studied using first-principles electronic structure calculations. However, in contrast to most of the other studies performed in this project, no metal/water interfaces are addressed that are occuring in electrocatalysis. Rather, interfaces are considered that are relevant for electrochemical energy storage in Li batteries. Before, however, addressing the electrode/electrolyte interface, which is the ultimate goal, relevant bulk deintercalation behavior needs to be understood. We are currently preparing a separate project proposal for LRZ.

Although widely used in everyday mobile electronic devices, a general understanding of electrochemical energy storage in Li batteries is still in its infancy. The prototypical cathode material LiFePO4 e.g. exhibits huge performance improvements upon size reduction, that can indeed not only be understood by "trivial size effects". Several years of fundamental research have suggested several mechanisms, which can be understood taking into account spinodal decomposition, elastic strain, surface and interface energies and nonequilibirum, nonlinear kinetics (for an overview see e.g. [1,2]).

Our work focuses on determining and evaluating relevant descriptors from ab-initio calculations [3] in a comprehensive approach for the relatively new and promising intercalation material Li_2FeSiO_4. Also the electrode electrolyte interface shall be examined in the future. Our studies are performed by DFT calculations, which is widely used in physics and chemistry.

Results

Similarly as $LiFePO_4$, Li_xFeSiO_4 phase separates into one phase with high and one with low Li content upon deintercalation. At low temperatures, these phases are $LiFeSiO_4$ and Li_2FeSiO_4 for x>1. The open circuit voltage (OCV) of such an electrode with respect to Li^+/Li metal anode was found to be 3.12 V [3], in agreement with experiment. Initial work on LRZ computers has been dedicated to study polar surfaces of Li_2FeSiO_4 which has already been published [4].

In the subsequent work we were specifically interested in the interface properties of the $LiFeSiO_4/Li_2FeSiO_4$ phase boundaries, as well as in defect statistics and the role of localized polarons. As these studies need high accuracies and large unit-cells with up to 256 atoms, it is especially the high computational resources of the LRZ that enabled these calculations. The calculations were performed with the periodic DFT package VASP, using PAW pseudopotentials and the PBE exchange-correlation functional. To improve the description of the transition metal d electrons, we used the GGA+U approach, with U_{eff} = 4 eV for Fe. Relative energies are converged to about 2 meV/atom. Calculations of single defects and polarons were performed in 2x2x2 unit-cells which corresponds to 12x11x10 Å^3 or 128 atoms respectively (see Fig. 1). The (010) interface was described within a 1x8x1 supercell with according number of atoms. Test calculations in larger cells were also performed.

The bottleneck to most intercalation materials used in Li batteries is getting Li into and out of the electrode.

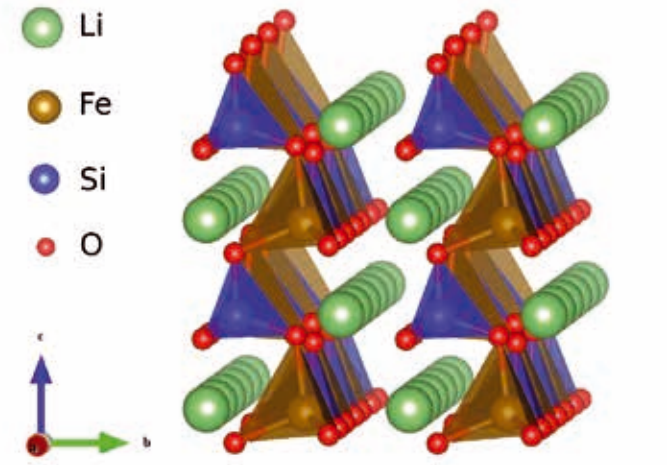

Figure 1: 2x2x2 supercell of Li_2FeSiO_4

Whereas this is described by diffusion through the surface and inside the bulk for solid solution forming electrodes, additional phenomena occur in phase separating materials. The simplest understanding to describe this deintercalation is as a nucleation and growth process, where the formation of a delithiated phase inside the filled cathode costs additional energy due to coherency strain and interface creation. The subsequent delithiation proceeds then via a movement of the domain boundary through the solid. Studies on LiFePO4 have shown that the equilibrium boundary alignment can be understood by minimizing strain energy [2,5]. On the other hand, phase boundaries cost energy proportional to their surface area which essentially influences the nucleation rate. To our knowledge this has not yet been studied rigorously by ab-initio means for any battery compound. To understand elastic energy contributions the elastic properties have to be analyzed. Fig. 2 illustrates the anistropy of elastic energy due to coherency depending on boundary alignment, indicating that interface alignment perpendicular to <110> is favorable.

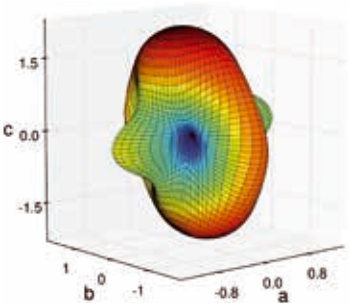

Figure 2: Directionality of strain energy of coherent $LiFeSiO_4/Li_2FeSiO_4$ interfaces

We have also developed a method to calculate interface energies with less computational demand than current approaches. Calculating correct interface energies necessarily relies on correct reference energies of two unequal slabs that are subsequently joined together. Whereas current approaches utilize slabs in vacuum, we dare to use respective bulk cells. The underlying assumption is simple elasticity theory, assuming that planar interfaces lead to homogeneous elastic strains in the two materials according to an energy minimum principle. The necessary elastic properties are determined from bulk calculations. The approach allows to calculate interface energies depending on local strain. The computational demand is immensely reduced rendering e.g. large scale screening possible.

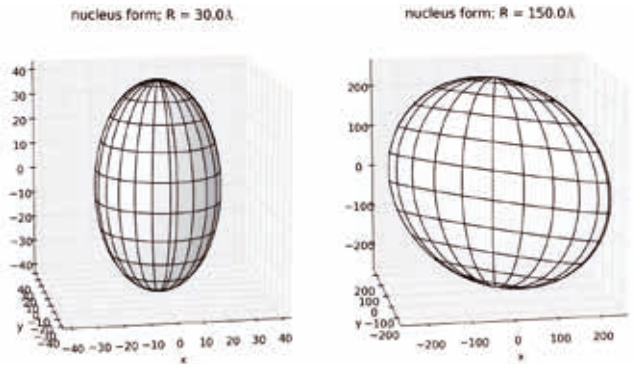

Figure 3: Size dependence of $LiFeSiO_4$ ellipsoidal precipitates including strain and interface energies.

With the first results for the (010) $LiFeSiO_4/Li_2FeSiO_4$ interface energy (approx. 6 meV/Å²) we can calculate the form and energy cost of ellipsoidal $LiFeSiO_4$ domains inside a Li_2FeSiO_4 matrix. The effects of strain become apparent in the size dependent shape changes of the precipiate (see Fig. 3).

These calculations allow to determine the critical nuclei and relate nucleation rate with applied overpotential. Although absolute numbers have to be taken with care (see e.g. [1]), we are currently evaluating how they relate to qualitative performance predictions, a necessary knowledge for promoting e.g. computational material discovery.

Furthermore we studied the energetics of localized polarons, which showed strong binding indicating that only concerted Li^+-e^- motion is realized at room temperature, putting typical multicomponent charge transport into perspective. Details will be published as soon as possible.

Computational and storage demands of these studies are rather high, especially due to post-processing on certain output files of VASP. The typical size of these outputs is 2.7 Gb. The necessary storage capacity for all the results described above is approx. 150 Gb, before analysis. Often numerical convergence could only be achieved after subsequent continuation jobs of 48 h calculation time. Calculations were mainly performed in parallel on 4-8 fat nodes each with 40 cores which pays respect to parallel scaling studies of a colleague (Tanglaw Roman), which indicate performance reduction for >160 core jobs.

On-going Research / Outlook

As stated in the introduction we will apply for a separate project to cover the studied phenomena in more detail, also for related compounds to investigate trends. Furthermore we want to study nucleation at surfaces which has not been done at all for battery materials, where especially the electrolyte might have an influence.
Also the mobility of localized polarons as well as the various influences (or not) of polaronic local charges on the ionic conductivity shall be assessed.

References and Links

[1] R. Malik et. al. 2013. A Critical Review of the Li Insertion Mechanisms in LiFePO4 Electrodes. *J. Electrochem. Soc.* 160, A3179-A3197
[2] M.Z. Bazant. 2013. Theory of Chemical Kinetics and Charge Transfer based on Nonequilibrium Thermodynamics. *Accounts of Chemical Research*. 46, 5 1144-1160.
[3] N.G. Hoermann and A. Gross. 2013. Stability, composition and properties of Li2FeSiO4 surfaces studied by DFT. J. *Solid State Electrochem.* doi: 10.1007/s10008-013-2189-x
[4] N.G. Hoermann and A. Gross. 2014. Polar surface energies of iono-covalent materials: Implications of a charge transfer model tested on Li2FeSiO4 surfaces. *Chem. Phys. Chem.* Accepted.
[5] A.G. Khachaturyan. 2008. Theory of structural transformations in solids. *Dover Publ.*

Role of the Exchange Mechanism in Lithium Self-Diffusion Processes

Research Institution
Institute for Theoretical Chemistry, University of Ulm

Principal Investigator
Tanglaw Roman

Researchers
Markus Jäckle

Project Partners
Helmholtz Institute Ulm for Electrochemical Energy Storage

LRZ Project ID: pr63fo

Introduction

With the increased demand for high-capacity batteries, the anode materials lithium and magnesium are of great interest, both from a fundamental as well as from a technological point of view.[1][2] As far as the performance and safety of these materials are concerned, it has to be noted that magnesium does not exhibit dendrite growth which for lithium electrodes is one of the main obstacles as these dendrites might lead to short-cuts which destroy the battery.[3][4]

On a microscopic level, metallic growth consists of atomic deposition and subsequent diffusion processes. In order to contribute to a deeper understanding of the differences between magnesium and lithium with respect to dendritic growth, in this project the adsorption of metal atoms and little clusters and diffusion processes on both metals have been studied. In particular the role of the exchange-mechanism[5][6] in the self-diffusion has been addressed based on DFT calculations using the Vienna-Abinitio-Simulation-Package (VASP)[7] together with an automatic search routine for transition states, the Nudged-Elastic-Band (NEB) method.[8]

Results

In the initial phase of the project, the technical parameters for the optimized performance of the VASP code on the SuperMUC were determined. This concerned both the convergence of the electronic self-consistent field (SCF) cycle as well as the convergence of the geometry determination in the structure optimization and in the transition state search routine.

Adsorption properties were mapped out by evaluating the potential energy surface of adatoms on the metallic substrates. The NEB method is based on the calculation of several configurations between the initial and the final state of a given process which are called images. Formally, these images are connected by springs and the energetic minimum with respect to this "nudged band"

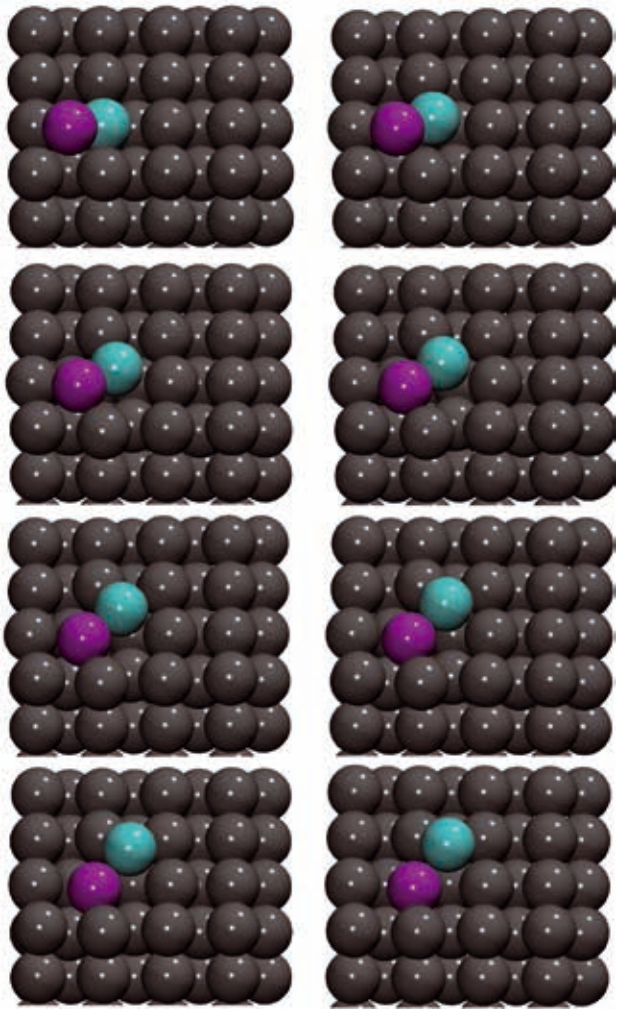

Figure 1: Different relaxed states along the minimum energy path for a self-diffusion process involving the exchange mechanism on a lithium(001)-surface; purple atom being a lithium atom which initially adsorbed in the hollow-position and the turquoise one being a lithium surface-atom in the top position.

is determined yielding the minimum energy path (MEP). These images can be calculated independently leading to a very good scaling of the NEB method on parallel computers.

The DFT-NEB calculations for the diffusion-process via the exchange-mechanism were performed by employing 8 images, the corresponding states along the minimum energy path (MEP) are illustrated in Fig. 1. It turned out that on Li the exchange-mechanism is slightly less favorable than the traditional hopping mechanism.

Furthermore, according to our calculations self-diffusion on magnesium is much more facile than self-diffusion on lithium. Fast diffusion leads to smooth surfaces so that our results give a first hint why dendrite growth occurs on lithium but not on magnesium.

On-going Research / Outlook

The determination of minimum energy paths with the NEB method is very well suited for the SuperMUC because of its good scalability. Self-diffusion on flat metal surfaces still corresponds to a relatively simple process. In order to model dendrite growth, self-diffusion on more complex substrates such as stepped surfaces or islands has to be studied. This makes not only the determination of the minimum energy path more complex, also the calculations for each image become more demanding due to the enlarged size of the unit cell that has to be used in the periodic DFT code. This makes the SuperMUC even more suitable for this project.

Because of the increasing demand for computer power in this particular topic, it is planned to submit an extra LRZ proposal for computer time for battery related projects. The corresponding proposal is in preparation.
As a mid-term goal of this particular project, the simulation of growth processes on a macroscopic time scale and a mesoscopic length scale using a kinetic Monte-Carlo (KMC) algorithm is envisioned. This multi-scale project requires as a first step and input for the KMC simulations the determination of all possible diffusion processes for complex surface structures based on DFT calculations. The implementation of an adequate KMC code has already begun.

Acknowledgments

I want to thank Dr. Tanglaw Roman for his support. I also want to thank Dr. Sung Sakong, Dr. Fernanda Juarez, Florian Gossenberger and Nicolas Hörmann for their support. Also I would like to thank the LRZ for supporting this sub-project through the sharing of CPU-time.

Last, but not least, I want to thank Reinhold Bader for his suppport regarding the memory-management issues which was well appreciated.

Figure 1 was created using the Visual Moleculard Dynamics (VMD) viewer, which is available free of charge.[9]

References and Links

[1] G. Girishkumar, B. McCloskey, A. C. Luntz, S. Swanson and W. Wilcke, J. Phys. Chem. Lett. **1**, 2193 (2010).
[2] H. D. Yoo et al., Energy Environ. Sci. **6**, 2265 (2013).
[3] Y. S. Cohen, Y. Cohen and D. Aurbach, J. Phys. Chem. B. **104**, 12282 (2000); N. Nishikawa et al., J. Electrochem. Soc. **157**, A1212 (2010)
[4] D. Aurbach, Y. Cohen and M. Moshokovich, Electrochem. Solid-State Lett. **4**, A113 (2001); Q. S. Zhao and J. L. Wang, Electrochim. Acta 56, 6530 (2011).
[5] G. L. Kellogg and P. J. Freibelman, Phys. Rev. Lett. **64**, 3143 (1990).
[6] A. Gross, *Theoretical Surface Science: A Microscopic Perspective,* Springer-Verlag, 2nd edition, 2009, 246.
[7] http://www.vasp.at
[8] /http://theory.cm.utexas.edu/henkelman/research/saddle
[9] http://www.ks.uiuc.edu/Research/vmd/

Ab initio description of the isomerization dynamics of adsorbed molecular switches

Research Institution
Department Chemie, Technische Unversität München, Germany

Principal Investigator
Karsten Reuter

Researchers
Reinhard Maurer

Project Partners
–

LRZ Project ID: pr63ya

5

Introduction

A key goal of molecular nanotechnology is to stimulate a controlled conformational change in functional molecules adsorbed on well defined substrates. Molecular switches, that is, molecules that are reversibly switchable between two or more meta-stable states, present ideal building blocks for future molecular devices. However, very often one consequence of metal surface adsorption is the loss of switching function, such as is the case for the prototypical molecular switch azobenzene (Fig. 1) adsorbed to coinage metal surfaces (Ag(111), Au(111)). Here, overly strong coupling to the surface is believed to drastically reduce the lifetime of the excited states and might even modify the energy landscape of the corresponding isomerization motion. In addition to the electronic coupling, steric hindrance might prevent molecular motion. An approach to lift off the molecule by derivatizing it with bulky spacer groups has led to the successful switching of tetra-*tert*-butyl-azobenzene (TBA) on Au(111). This success led to a formulation of a novel substrate-mediated photoisomerization mechanism, very different from the gasphase case, that might explain the experimentally observed spectroscopic properties. In general, a basic understanding of the mechanisms underlying molecular switching on metal contacts is currently still absent, but is obviously an important prerequisite to the design of functioning devices and simultaneously a chance to investigate the basic properties of such interesting surface chemical bonding scenarios.

First-principles modelling based on Density-Functional Theory (DFT) represents a valuable method to gain such understanding. On the basis of a model characterising the structural properties of azobenzene and its derivative TBA on coinage metal surfaces [1], we proposed a detailed investigation of the mechanistic properties of these systems. The objective of this investigation was an *ab-initio* based parameter-free description and rationalization of molecular functionality at solid surfaces. This included the following goals:

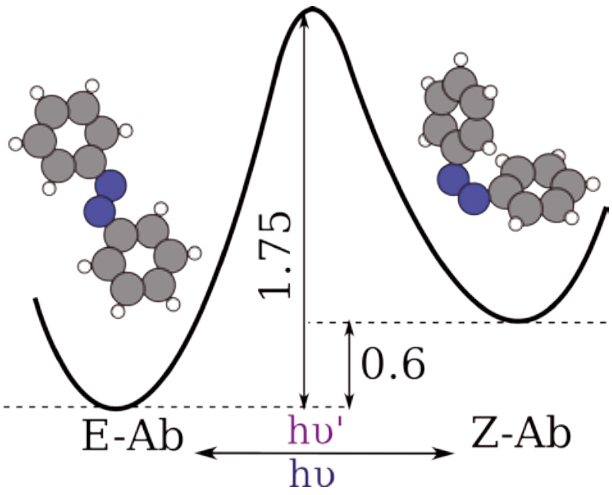

Figure 1: Trans and Cis isomer of the azobenzene molecule, superimposed on a schematic reaction path. Shown energy values are in eV.

Molecular function heavily depends on the ground state stability of the two meta-stable states. A preliminary step to the investigation of excited state properties must be a full understanding of the ground state energetics of azobenzene derivatives on coinage metal surfaces including transition state structures. The chosen methodology has to be evaluated throughout the study, to yield consistent quality geometries and energetics in the ground state, including an account of dispersion interactions and a reasonable description of excited state properties, while allowing a maximum of computational efficiency.

In the next step a systematic investigation of the possible excited state pathways and involved regions of the excited state potential energy surfaces is conducted. This includes possible pathways and states known from the gasphase dynamics, but also resonances, due to the metal electronic states. This can only be achieved if a highly efficient excited-state methodology is at hand

Results

We have initially conducted an assessment of the principal performance of the ΔSelf-Consistent-Field-Density-Functional Theory (ΔSCF-DFT) method, which we have chosen as an efficient approach to electronic excited states. Investigating the lowest lying excited states of gasphase azobenzene [2] along main isomerization pathways, we find that the overall description of the excited state behavior by ΔSCF-DFT is in very good agreement with higher level techniques such as Time Dependent DFT (TD-DFT) or wave function based approaches. Similar isomerization paths as for the isolated azobenzene molecule were subsequently calculated for azobenzene adsorbed on Ag(111) and Au(111). These geometries were calculated via constrained optimization techniques and quadratic synchronous transit (QST) transition state searches (Fig. 2) employing the CASTEP program package [3].

The CASTEP code is written in modular FORTRAN 90 language and solves the electronic eigenvalue problem by expanding the wave-function in a plane wave basis set, while representing the rapidly varying part close to the atomic nucleus with a pseudopotential. Due to periodicity, the eigenvalue problem can be solved independently at different points in momentum-space. This property is extensively used in the parallelisation scheme of CASTEP resulting in excellent scaling properties on SuperMUC. The therewith calculated ground state isomerization pathways of metal-adsorbed azobenzene alone already allow the rationalization of the loss of switching function for azobenzene and derivatives on a Ag(111) surface on the level of a loss of bistability - the main prerequisite to molecular switching [4].

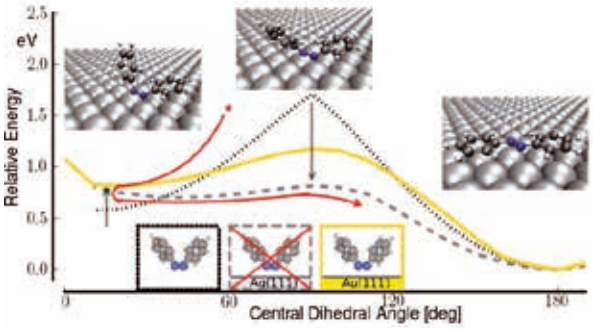

Figure 2: Groundstate energetics of the isomerization between trans and cis azobenzene in gasphase (black), adsorbed to a Ag(111) surface (grey), and adsorbed to a Au(111) surface (yellow)

All calculations up to this point were done on the assumption of a low coverage limit. Through close collaboration with the experimental group of Prof. Stefan Tautz (FZ Jülich) we could show, however, that lateral adsorbate-adsorbate interactions in more dense adlayers can significantly influence the adsorbate geometry and also the entailed energetics. Detailed normal incidence X-ray standing wave (NIXSW) measurements on azobenzene adsorbed on Ag(111) have in fact revealed that adlayers prepared at 210 K show strongly distorted structures, compared to a low coverage flat adsorption geometry of Azobenzene [5]. We performed dispersion corrected DFT calculations with our current setup on a variety of different coverages and find an energetically favorable geometry at intermediate coverage that nicely matches the experimentally found geometry, therefore also validating the high accuracy of our computational approach. This sidetrack study showed that a complete analysis of possible isomerization pathways also has to take into account the full parameter-space of complexity, including the coverage situation, but also effects due to molecular functionalization. Similar ground state mappings as we have done for azobenzene therefore have been conducted for its derivative, the TBA molecule.

With a detailed understanding of the ground-state energetics that crucially determine the molecular function, we approached in the next step the description of excited states. We have therefore implemented into CASTEP a modified ΔSCF-DFT [6] scheme, which enables a highly efficient calculation of excited states for metal-surface adsorbate molecules on the basis of static DFT. With this methodology we are able to accurately reproduce spectroscopic properties of organic/inorganic adsorbate-substrate complexes with significantly reduced computational cost when compared to Time-Dependent DFT or Many-Body Perturbation Theory. A series of excited state energy curves along important degrees of freedom has revealed that the energetics do in fact point to a strongly modified isomerization mechanism of adsorbed azobenzene when compared to the gasphase case.

On-going Research / Outlook

We are currently employing the above mentioned approach to systematically map the ground- and excited-state enegetics along degrees of freedom that are relevant to photo-induced isomerization. The corresponding energetics will be used for a full dynamical simulation of the transient switching mechanism. The computing time on SuperMUC was essential in establishing our current understanding of the switching process. Up to date a total of 5,5 Mio. CPUh have been used in this study with a temporary peak hard disk usage of 6 Terabyte. Owing to the favorable scaling properties of the CASTEP code our computations are ideally suited for the infrastructure provided by SuperMUC and the planned system upgrade will enable us to perform detailed investigations on larger derivatives of azobenzene, tackling questions related to molecular functionalization or coadsorbate effects.

References and Links

[1] McNellis, Meyer, and Reuter, Phys. Rev. B 80, 205414 (2009)
[2] Maurer, Reuter, J. Chem. Phys. 135, 224303 (2011)
[3] CASTEP: http://www.castep.org/
[4] Maurer, Reuter, Angew. Chem. Int. Ed. 48, 12009 (2012)
[5] Mercurio, Maurer, Liu, Hagen, Leyssner, Tegeder, Meyer, Tkatchenko, Soubatch, Reuter, Tautz, Phys. Rev. B 88, 035421 (2013)
[6] Maurer, Reuter, J. Chem. Phys. 139, 014708 (2013)

The chemistry of porphyrins adsorbed on metallic surfaces

Research Institution
TUM, Department of Molecular Nanoscience and Chemical Physics of Interfaces

Principal Investigator
Wilhem Auwärter

Researchers
Marie-Laure Bocquet, Tangui Le Bahers, Marie Lattelais, Torsten Houwaart

Project Partners
Laboratoire de Chimie, ENS de Lyon, France

LRZ Project ID: pr85la

Introduction

The mechanism for binding oxygen to metalloporphyrins is a vital process for oxygen breathing organisms. Understanding how small gas molecules are chemically bound to the metal complex is also important in catalysis or the implementation of chemical sensors. For investigating these binding mechanisms, porphyrin rings with a central cobalt or iron atom are supported on copper or silver surface, leading to non-planar deformation –a saddle geometry-. In 2011, the collaborative team in ENS Lyon and TUM have deciphered, how the poisonous carbon monoxide gas attaches to one type of supported metal-porphyrin, by means of detailed Scanning Tunneling Microscopy experiments complemented by density functional theory calculations [1]. Indeed, two CO molecules dock between the central metallic atom and the two opposite nitrogen atoms of the macrocycle (see figure 1). Hence the paired ligand assumes the position of the rider on a saddle.

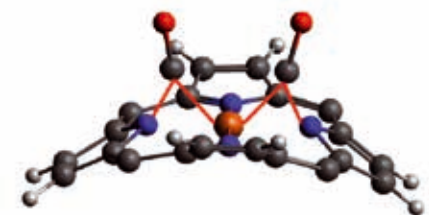

Figure 1: DFT model of dicarbonyl bonding at saddle-shaped cobalt tetraphenyl-porphyrins anchored on well-defined coinage metal substrates like Cu and Ag. The Ag(111) surface considered here and the phenyl substituants have been removed form clarity.

The idea of the simulation project is to tentatively generalize at the single molecule level an anomalous binding mode for CO molecule –called the rider mode- onto cobalt porphyrins adsorbed on well-defined surfaces. The straightforward generalization has been initially scheduled: -to test the binding of other gaseous molecules like NO and O_2 or solid particles like Fe adatoms; to try other metal porphyrins like Fe porphyrin and to model other "weaker" but planar substrates like epitaxial graphene on Cu and graphene on Ir.

Results

Fe adatom- CoTPP:
In conjunction with high-resolution STM images acquired after Fe deposition (TUM in Barth's group), Co adatom is shown to bind in a bisector position from two Co-N directions (see figure 2). 4 positions are equivalent in the deformed porphyrin macrocycle and Fe is switching easily between these four equivalent sites in the macrocycle (fluxional ligand even at low temperature). We have estimated the activation energy barrier for the two diffusion paths between equivalent adsorption sites through Nudged Elastic Band (NEB) calculations. In addition DFT shows that the Fe adatom keeps part of its magnetism and even induces some magnetism in the Co center. This finding fits nicely XMCD measurements (collaboration with MPI, Stuttgart) that evidence a ferromagnetic coupling between Co central metal and Fe ligand atom is evidenced by XMCD measurements (coll. MPI, Stuttgart). [1]

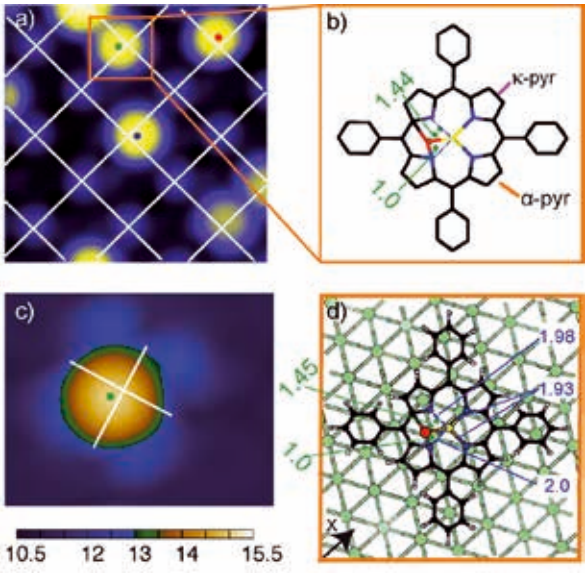

Figure 2: a) High-resolution STM image revealing a minute off-center adsorption of the Fe atoms on the porphyrin lattice. (I = 0.1 nA, V_b = -0.1 V, 55.4 Å x 55.4 Å). b) Schematic model extracted from the STM data. c) Simulated constant-current STM image based on the structure shown in d) (V_b = -0.2 V, 32 Å x 25 Å). The given distances are relative to the bare Ag substrate and the overall corrugation amounts to 5 Å. d) DFT optimized Fe/Co-TPP complex on Ag(111) in a 11x5sqrt(3) cell. The four Co-N distances are quoted. Green, black, blue, white, yellow and red balls depict respectively Ag, C, N, H, Co and Fe atoms.

Ongoing Research (preliminary modelling results)

CO and O_2 onto FeTPP :
Two gaseous adducts have been successfully found to fix onto surface-confined Fe porphyrins (see figure 3). For CO ligation, the configuration is different from the rider case exhibited by CoTPP: the dual CO molecules do not bind opposite N atoms from down-facing pyrroles but only the Fe center and adopt tilted positions, as already seen for metallic Fe adatoms onto metal surfaces. Somehow the CO pair decouples Fe from the macrocycle. For O_2 molecules, we found after many trials a similar way to bind two molecules when the inherent magnetism of O_2 is forced to be quenched. Again the adsorption configuration resembles the "rider" mode but the O_2 molecules do not bind linearly the metal center. Unexpectively Co porphyrins don't stand the two O_2 molecules the same way than Fe porphyrins, which is still puzzling to us.

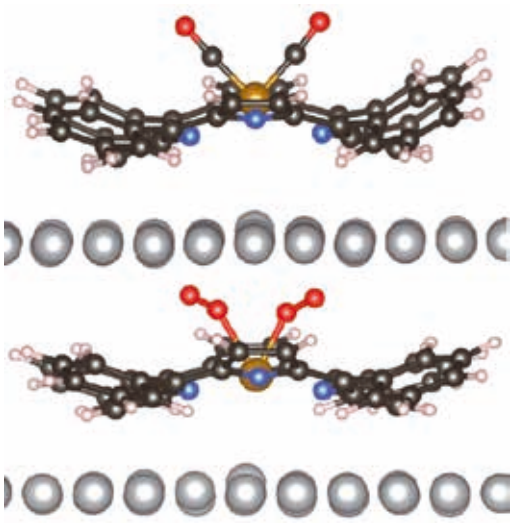

Figure 3: DFT models of (top) 2 CO molecules and (bottom) 2 O_2 molecules onto FeTPP/Ag(111). Ag atoms are represented by grey balls.

FeP on graphene/Cu(111) :
The theoretical study of the physisorption of FeP on graphene and copper supported graphene (lattice-matched, atop-fcc) showed that for both surfaces the molecule-substrate interaction is weak. The adsorption energy of FeP is about 0.8-0.9 eV on freestanding graphene, where as it is 0.5 eV on copper supported graphene, when dispersion is accounted for the top copper-layer. Similarly the adsorption distance is respectively 3.3-3.4 Å on pristine graphene and 3.1-3.3 Å on graphene-covered metal.

Because of the weakness of the interaction on copper supported graphene the porphine molecule will be too mobile to be properly investigated by low temperature STM. This is one obstacle to propose this system for an STM investigation. Hence we propose to anchor covalently Fe porphine to epitaxial graphene via concerted reversible cycloadditions and/or irreversible dehydrogenations. It is expected that the products, if any, will stay immobile on the surface for proper STM characterization prior and after introduction of gaseous ligands. In this research direction we have found two possible products (not shown): the first resulting from a cycloaddition between a patch of graphene and a pyrrole group and the second resulting from a double dehydrogenation of two opposite pyrrole groups. More modelling work is needed to reveal other grafting possibilities on epitaxial.

For all the described DFT modelling we used the VASP code with typically 512 cores per job. Typically the biomimetic molecules require very large supercell (2 to 3 nm) to avoid spurious interactions between adjacent cells and spin-polarized calculations. Since they are on condensed phase, the metallic slab is a large lateral dimension to accommodate the large molecule. Typically there are about 350 metallic atoms and 80 light atoms for a given adsorption system. A fine optimization of one interfacial geometry (including the spin) requires the following characteristics: Nb steps : 350 ; Hour/step : 0.21 ; Nbr Procs : 512 (thin nodes); Total 0,03763 million hour. The largest generated file (WAVECAR file) is around 4 Gbytes.

In this project, we have been granted in june 2013 2 millions of hours so that we could optimized in SuperMUC roughly 50 guessed adsorption structures among the three different topics summarized above.

It is noticeable that we have experienced problems to run onto the fat nodes after their integration into the SuperMUC infrastructure. In contrast previous SuperMIG nodes worked perfectly for the same type of adsorption systems. However, the provided resources on SuperMUC have heavily needed for these large-scale calculations because the results are generated very fast in time, albeit consuming a lot of CPU hours (see above). This type of research could not be conducted on clusters from local mesocenters because they would require months for structural optimizations and some of them are untractable because of the large memory requirements.

Outlook

In the future, we need to comfort all the preliminary results described in the on-going research section in order to complete the scheduled project. It seems that we have succeeded in our attempt to generalize the rider ligation (see figure 3). However our study on a graphene-based substrate has encountered some bottlenecks. But our grafting proposal seems a promising way to immobilize the porphyrins before characterizing their ligation to gaseous species. A continuation proposal will be submitted, which takes into account the realistic amount of computed time per interfacial system.

References and Links

[1] "Cis-dicarbonyl binding at cobalt and iron porphyrins with saddle-shape conformation", K. Seufert, M.L. Bocquet, W. Auwarter, A. Weber-Bargioni, et al. Nature Chemistry 2011, 3, 114-119.
[2] "Changing the magnetic moment of a Metalloporphyrin by site-selective positioning of Fe atoms", S. Vijayaraghavan, W. Auwärter, et al., to be submitted.

Ab initio modelling of the adsorption in *giant* Metal-Organic Frameworks

Research Institution
Department of Chemistry, University of Torino, Italy

Principal Investigator
Bartolomeo Civalleri

Researchers
Matteo Ferrabone, Roberto Orlando, Guillaume Maurin

Project Partners
Institut Charles Gerhardt, Université de Montpellier 2, France

LRZ Project ID: pr85qu (PRACE project)

Introduction

Metal-Organic Frameworks (MOFs) are a new class of materials that in the last decade has seen a paramount growth and are expected to play a huge impact in the development of next-generation technologies [1]. They consist of inorganic nodes (i.e. a metal ion or a cluster) connected through organic ligands that act as linkers to form a porous three-dimensional framework. The combination of different nodes and linkers makes MOFs very versatile materials with interesting and promising applications in many fields, including [1]: gas adsorption, catalysis and photo-catalysis, drug delivery, sensing, nonlinear optics.

The structural versatility and permanent porosity of MOFs has determined, in recent years, their emerging success for gas capture, storage and separation [2] over well-established microporous materials such as zeolites. So far, the target of *ab initio* modeling of the adsorption in MOFs has been small-to-medium size frameworks (e.g. MOF-5) and their interaction with small molecules (e.g. H_2, CO_2 and CH_4).

This project focuses on the *ab initio* modeling of the adsorptive capacity of the so-called giant MOFs [2] because of the very large size of the pores and the corresponding huge surface area. Among giant MOFs, the most representative one is probably MIL-100 [2]. It is comprised of trimeric units of a trivalent atom (e.g. Al, Sc, V, Mn, Cr, Fe) octahedrally connected with 1,3,5-BTC (benzene-1,3,5-tricarboxylic acid). It ideally crystallizes in a non-primitive cubic lattice (Space group: Fd-3m, a=72.9 Å and V=388000 Å^3) with 2788 atoms in the primitive cell (which is the one adopted for calculation). MIL-100 has a framework topology that resembles the zeolite MTN, with a unique hierarchical system of three types of cages of different dimensions from micro- (6.5 Å) to meso-pores (25–30 Å). Its surface area of 3340 $m^2 g^{-1}$ is three times larger than the values measured for the MCM-41 inorganic mesoporous materials.

Among the hottest topics in MOFs research in recent years, it has been their application in clean energy and environmental protection, most significantly as storage media for gases such as hydrogen and methane, and carbon dioxide capture [3]. An important consideration in maximizing the uptake of gases within porous MOF crystals is to increase the number of adsorptive sites within a given material. In this respect, the structure of MIL-100 is characterized by the presence of a large number (i.e. more than 200) of coordinatively unsaturated (CUS) metal atoms which are exposed at the inner surface of the pores. Interestingly, an isoreticular family of MIL-100-type MOFs have been obtained in which Cr is substituted by other trivalent metals like Al, Sc, V, Mn and Fe. CUS play a crucial role to determine the extraordinarily adsorptive properties of these MOFs, thus greatly enhancing the uptake of gases, such as CO_2 and CH_4. Here, we would like to study the adsorption of CO_2 in isoreticular MIL-100 with different metals (e.g. Al, Fe).

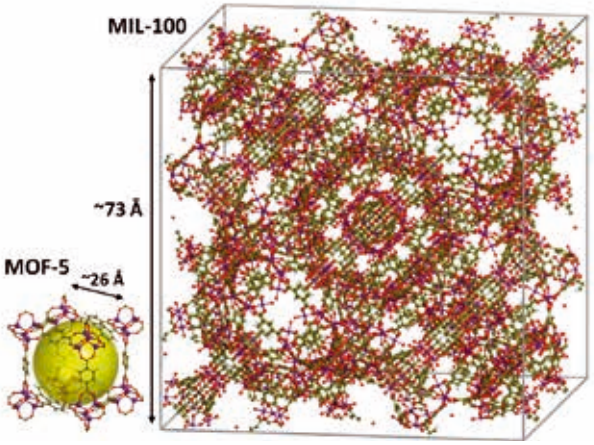

Figure 1: Comparison between the crystallographic unit cells of the giant MIL-100 (10880 atoms) and MOF-5 (424 atoms)

Beyond the fundamental interest to investigate this giant MOF in interaction with small molecules, there is a considerable interest in the adsorption of drugs for application in drug delivery [4]. Several drugs suffer from important drawbacks such as poor solubility and/or stability in the biological aqueous media, often resulting in short half-lives, low bio-availabilities, and limited bypass-

ing of biological barriers. MOFs nanoparticles have been recently proposed to circumvent these drawbacks [4]. For instance, MIL-100 is able to adsorb 350 mg g^{-1} of ibuprofen more than MCM-41 under the same conditions. These differences were attributed to the pore sizes and structural effects, particularly the accessible dimensions of the windows of the cages in the solids. Highly challenging drugs, such as the antitumoral busulfan (Bu), widely used in chemotherapy regimes for leukaemias, and the antiviral azidothimidine-triphosphate (AZT-TP), an anti-HIV compound, have also been recently entrapped into nanoparticles of different porous iron(III)-based MOFs, because of their nontoxicity. Among them, MIL-100(Fe) has been shown to be a very promising nanovector system for those molecules for his large payload and its specific interaction between the Fe (CUS) and the drugs that is expected to retard the release. Here, we intend to investigate the specific interaction of Bu with the open metal site.

Results

Giant MOFs, with thousands of atoms in the unit cell, represent a tremendous challenge for current *ab initio* calculations. To our knowledge, this is the first time that a fully periodic *ab initio* approach is applied to such exceptionally highly porous and large MOFs. The use of Tier-0 computer resources provided by PRACE, such as the SuperMUC HPC system, is essential to tackle this challenging problem. The periodic *ab initio* code CRYSTAL is used for the calculations [5,6]. It computes the electronic structure of periodic systems within Hartree-Fock, density functional theory (DFT) or various hybrid approximations and uses atom-centered Gaussian functions.

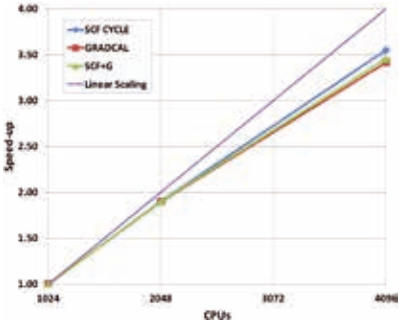

Figure 2: Running time scaling with the number of computing cores for MIL-100(Al)-N (2720 atoms) on the SuperMUC HPC system. See text for further details.

To the purpose of the project, the code has been optimized to be efficient and low memory consuming for the very large systems under investigation and to reach a better scaling on more than 1000 cores [5]. Figure 2 shows the scaling of the code for MIL-100(Al)-N, a model system in which a nitrogen atom substitutes the oxygen at the center of the inorganic unit. It consists of a unit cell containing 2720 atoms without symmetry. Calculations have been carried out by using the massive parallel (MPP) version of the code with the B3LYP method combined with an all-electron basis set of 44604 basis functions. The speed-up (t_n/t_{1024}, n=nr. CPUs) refers to the wall-clock time required for a SCF^+G calculation run with 1024 cores. SCF represents a single cycle of the calculation of the total energy of the system, while G corresponds to the evaluation of the forces. Both are then important steps in more complex calculations like the relaxation of the crystalline structure. Overall, a very good scalability is reached with the speed-up being 3.45 (86%) with 4096 cores.

Along with benchmark calculations, current results include the prediction of the basic properties of the examined system. We have investigated the structural features of the isoreticular MIL-100(M) family with different metal atoms (M) in the structure. So far, we have optimized the structure of MIL-100 with M=Al and Sc. MIL-100(Cr) and MIL-100(Fe) have also been investigated. The two transition metals present unpaired electrons and this makes calculations more complicated, although still affordable. Experimental data show that iron is in a high spin state and there is an antiferromagnetic coupling among the atoms. Computed results confirm that a ferromagnetic interaction that tends to align the spin vectors in a parallel fashion is not favored. While a ferrimagnetic solution, in which an antiferromagnetic interaction is present, is more stable.

On-going Research / Outlook

As stated above, the project is still on-going, but present results are very promising. Starting with the optimized structure of MIL-100(Al), we will extend the study to model the interaction of CO_2 on the adsorption sites which is one of the main objective of this study. To this purpose, a multilevel theoretical approach will be used that combines periodic and cluster calculations. This will allow us to go beyond periodic DFT results by using post-SCF techniques on cluster models and obtain a better prediction of the adsorption energies. For MIL-100(Fe), we will start investigating the specific interaction of Bu with the open metal site. This is an extraordinary challenge for *ab initio* modeling (about 4000 atoms without symmetry). The atomistic details provided by these *ab initio* calculations will allow us, for the first time, to understand the interaction forces acting between key drugs in the pharmaceutical field and an innovative drug carrier (MIL-100) to an unprecedented level of accuracy.

In perspective, as a by-product, structural data, energies and forces obtained from these very challenging calculations will be used to refine existing force fields to study the dynamics of adsorbed molecules within the pores of MIL-100. They will be then employed to run classical MD and GCMC simulations.

References and Links

[1] Special issue on "Metal-Organic Frameworks". 2012. Guest Editors: H.-C. Zhou, J.R. Long and O.M. Yaghi. *Chem. Rev.* 112, 673–1268.
[2] G. Férey, et al. 2004. A Hybrid Solid with Giant Pores Prepared by a Combination of Targeted Chemistry, Simulation, and Powder Diffraction, *Angew. Chem., Int. Ed.* 43, 6296.
[3] K. Sumida, et al. 2012. Carbon Dioxide Capture in Metal-Organic Frameworks. *Chem. Rev.* 112, 724.
[4] P. Horcajada, et al. 2010. Porous metal-organic framework nanoscale carriers as a potential platform for drug delivery and imaging, *Nature Mater.* 9, 172.
[5] R. Dovesi, R. Orlando, A. Erba, C.M. Zicovich-Wilson, B. Civalleri, et al. 2014. CRYSTAL14: A Program for the Ab Initio Investigation of Crystalline Solids. *Int. J. Quantum Chem.* DOI: 10.1002/qua.24658.
[6] http://www.crystal.unito.it

Investigation of the adsorption of free-base porphine on coinage metal surfaces

Research Institution
Department Chemie, Technische Universität München, Germany

Principal Investigator
Karsten Reuter

Researchers
Christoph Scheurer, Katharina Diller, Reinhard Maurer, Moritz Müller

Project Partners
–

LRZ Project ID: pr85za

Introduction

The adsorption of organic molecules on metal surfaces offers a wide range of possible applications on both the macroscopic scale and the nanoscale, ranging from heterogeneous catalysis over solar cells and organic light emitting diodes (OLEDs) to molecular switches on surfaces. In order to tailor the functionality of the adsorbate-substrate systems to specific requirements, it is necessary to use classes of versatile molecules which can be tuned accordingly. Porphyrins, which always consist of an aromatic tetrapyrrole macrocycle and sometimes of additional substituents and/or a metal center, fulfill this prerequisite due to their intrinsic optical and electronic properties and conformational flexibility. Many porphyrin compounds occur naturally, for example chlorophyll, which is responsible for photo-synthesis, or hemeproteins, which transport respiratory gases in the blood of mammals. Nowadays also a myriad of artificial species is available as building blocks and functional units for applications such as chemosensors or nano-catalysts, but also for medical applications like anti-cancer and anti-HIV drugs. Because of their photophysical properties, porphyrins are extensively studied as components in OLEDs [1] and organic solar cells [2]. As the functional properties of porphyrins can be tuned by adsorption on (solid) surfaces, porphyrin-metal interfaces are ideal to explore prototype anchored coordination complexes and general aspects of surface-confined coordination chemistry.

Surprisingly, while the larger, substituted porphyrins have been investigated extensively, only a small number of studies is dedicated to the adsorption of the basic unit of all porphyrins, the free base porphine (2H-P, Figure 1), on metal surfaces. This is insofar surprising as the study of 2H-P as a prototypic tetrapyrrole system can be expected to give valuable insights for the adsorption behavior and electronic structure not only of the 2H-P itself, but of the whole molecule class of porphyrins. Different from the behavior of larger porphyrins on Cu(111) and Ag(111), scanning tunneling microscopy (STM) experiments of 2H P on these substrates reveal a repulsive interaction between molecules, which leads to isolated molecules in the low-coverage regime [3, 4]. This repulsion was assigned to be the consequence of an electron transfer from the substrate to the molecule, i.e., a (partial) filling of the LUMO of the 2H-P. However, open questions remain which cannot be answered by the experiments at this point. The observed electron transfer to the LUMO is only very weak on Ag(111), but far stronger on Cu(111). With experiments alone, it cannot be explained why these different interactions with the respective surfaces seemingly lead to the same repulsion between adjacent porphines. Therefore simulations of those systems are crucial for the understanding of both the molecule-molecule and the molecule-substrate interaction.

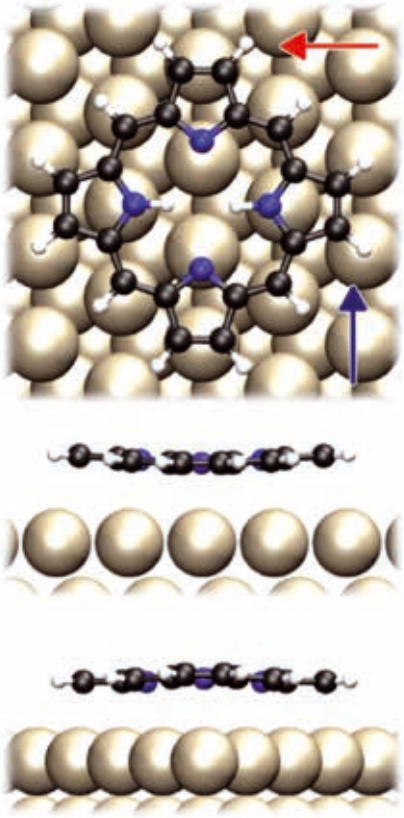

Figure 1: Top and side views (along red and blue arrows) of free-base porphine (2H-P) adsorbed on Ag(111). Black: carbon, blue: nitrogen, white: hydrogen, gray: silver

Results

All our calculations were performed using density functional theory (DFT). The porphine molecule consists of 20 carbon and four nitrogen atoms (Figure 1). During the work on this project we studied the adsorption on (5x5), (6x6) and (7x7) Ag(111) and Cu(111) surface slabs to simulate different molecular coverages. At present, systems of such size can only be treated by DFT with local or semi-local exchange and correlation (xc) functionals (PBE in our case). As current approximations to the xc functionals do not properly account for dispersive forces which are crucial for the description of molecular adsorbates such as the porphyrins, we additionally employed a semi-empirical correction which accounts for the long-range van-der-Waals interaction. In such an approach, pair-wise potentials are added a posteriori to the DFT description, in order to improve the description of adsorption energetics and geometries. We were using the implementation within the CASTEP 6.0.1 package [5]. This code is written in FORTRAN 90 and is very widely used in the context of adsorption studies. As implemented in CASTEP, the electronic eigenvalue problem is tackled by expanding the wave-function in a plane wave basis set, with the rapidly varying part close to the atomic nuclei represented by smooth pseudopotentials. The periodic boundary conditions enable the calculation of the wave-function in Fourier space, where then all possible momenta or k-vectors have to be taken into account in order to correctly represent the density. This amounts to solving the generalized eigenvalue problem underlying these calculations independently at different positions in k-space and then generating the electronic density from this set of wave-functions. This is a basic ingredient of the parallelization scheme in CASTEP. The minimal communication between calculations at different k-vectors ensures almost ideal scaling in this respect. Further parallelization is achieved by density and band partitioning. For this project the number of k-points ranged from 4 to 16, depending on the calculation being a geometry optimization or a high accuracy total energy evaluation. The size of the investigated systems required highly parallelized calculations, typically running on 32 nodes and employing 512 CPUs per run. Up to now, 1.8 Mio. CPUh have been used on this project, with a temporary hard disk usage of 3.4 Terabyte in the PROJECT directory.

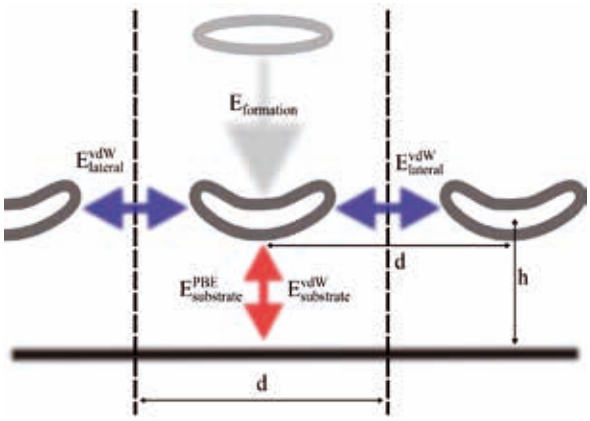

Figure 2: Energy contributions which determine the self-assembly behavior of adsorbed molecules. All terms were accessed separately within this project.

In a first step, dispersion-corrected DFT was used to identify favorable adsorption sites and geometries of 2H P on Cu(111) and Ag(111) for the three surface slabs (5x5), (6x6) and (7x7). For all coverages our determined structures agree excellently with those derived from STM and near-edge X-ray absorption fine-structure (NEXAFS) spectroscopy experiments [3, 4].

The energy contribution associated with the deformation of the molecule upon adsorption is one of the energy terms contributing to the total adsorption energy (gray arrow, Fig. 2). To explain the repulsive behavior observed in the STM measurements, we followed two routes: One was the investigation of the possible charge transfer effects that were predicted from the experimental results. To this end we compared the information obtained from different methods (partial charge partitioning, density difference evaluation and projected density of states evaluation) and were able to confirm the experimental predictions. The second route (on-going research) investigates the coverage-dependent energy contribu-tions, with special focus on (i) lateral interactions between molecules dominated by van-der-Waals forces (blue arrows, Fig. 2), (ii) interactions between the adsorbates and the metal surfaces (red arrow, Fig. 2) which are influenced by the observed charge transfer.

On-going Research / Outlook

Our current research focuses on finalizing the analysis of the determined energy contributions and their role in the self-assembly of the prototypic 2H-P molecules. Identifying the exact mechanisms which determine the repulsive behavior of the porphines on Ag(111) and Cu(111) is expected to give us the ability to predict the assembly behavior of other (larger, substituted) porphyrins. A second branch of the project deals with the simulation of X-ray spectroscopy data. Generally, a detailed assignment of experimentally derived spectroscopic signatures is crucial for the interpretation of many systems of interest in surface science and often relies on *ab-initio* based spectroscopic simulations. While the typically employed approach consists of neglecting the effect of the underlying substrate, experience shows that especially for the stronger interacting Cu(111) substrate, these effects play a crucial role and have to be accounted for. We currently work on including the surface in our calculations, thus improving both the description of the system at hand, as well as the general methodology.

References and Links

[1] M. A. Baldo, D. F. O'Brien, Y. You, A. Shoustikov, S. Sibley, M. E. Thompson, and S. R. Forrest, *Nature* 395, 151–154 (1998).
[2] A. Yella, H.-W. Lee, H. N. Tsao, C. Yi, A. K. Chandiran, M. Nazeeruddin, E. W.-G. Diau, C.-Y. Yeh, S. M. Zakeeruddin, and M. Gratzel, *Science* 334, 629–634 (2011)
[3] F. Bischoff, K. Seufert, W. Auwärter, S. Joshi, S. Vijayaraghavan, D. Écija, K. Diller, A. C. Papageorgiou, S. Fischer, F. Allegretti, D. A. Duncan, F. Klappenberger, and J. V. Barth, *ACS Nano* 7, pp 3139–3149 (2013)
[4] K. Diller, F. Klappenberger, F. Allegretti, A. C. Papageorgiou, S. Fischer, A. Wiengarten, S. Joshi, K. Seufert, D. Écija, W. Auwärter, and J. V. Barth, *J. Chem. Phys.* 138, 154710 (2013)
[5] S. J. Clark, M. D. Segall, C. J. Pickard, P. J. Hasnip, M. I. J. Probert, K. Refson, and M. C. Payne, *Z. Kristallogr.* 220, 567 (2005), http://www.castep.org

http://www.th4.ch.tum.de/

Electrophysiology: Atomistic modeling

Research Institution
CNRS- Université de Lorraine, Nancy France

Principal Investigator
Mounir Tarek

Researchers
Lucie Delemotte, Marina Kasimova, Vincenzo Carnevale

Project Partners
Temple University, Philadelphia, PA, USA

LRZ Project ID: pr86ba (PRACE project)

Introduction

Excitable cells produce electrochemical impulses mediated by the transport of ions across their membrane through proteins pores called ion channels. The most important family of channels propagating an electrical signal along the cell surface is the voltage-gated ion channel (VGCs) family. VGCs are essential physiological effectors: they control cellular excitability and epithelial transport. A myriad of genetic mutations found in the genes encoding their subunits cause channel malfunction. These so-called channelopathies have been incriminated in a variety of diseases, including, among others, epilepsy, pain syndromes, migraines, periodic paralyses, cardiac arrhythmias, hypertension and hypotension [1]. Contemporary research will benefit from new insights into the minute details of VGC function, paving the way to a fine understanding of function disruption by specific mutations and to new pharmacological strategies to mitigate channel malfunction.

What are the key molecular level elements of channel function? How are these modulated? How do specific genetic mutation affect them? In this project, we *implement molecular modeling strategies that will allow us to predict VGCs activation-deactivation kinetics ab initio* and to retrieve current/voltage relationships from computational data, which can be directly compared to electrophysiology recordings.

Our goal is to provide a proof of principle for a VGC of known crystal structure: the Kv1.2 voltage-gated potassium channel (see Fig. 1). As other VGCs, gating of this channel is regulated by changes in the polarization state of the membrane: the tetrameric pore gate of Kv1.2 opens and closes following activation or deactivation of its voltage-sensing domains (VSD). Recently, we proposed a model of the Kv1.2 VSD activation using molecular dynamics (MD) simulations that agrees with a large body of experimental data [2,3]. This model involves 5 VSD states: α (activated), β, γ, δ (three intermediate) and

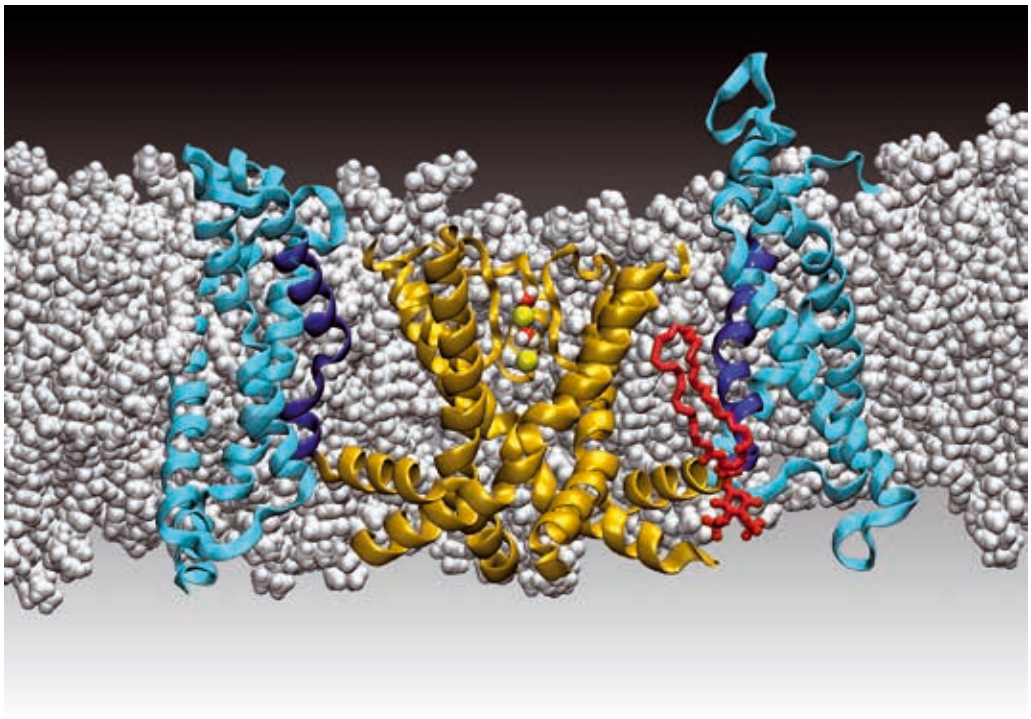

Figure 1: Kv1.2 voltage gated ion channel embedded in its membrane. Are highlighted the central pore domain (gold) encompassing the selectivity filter (2 potassium ions and water molecules), 2 peripheral voltage sensor domains (cyan) including the S4 ubiquitous helix (blue) and a nearby PIP2 lipid (red).

ε (resting), each characterized by a specific salt bridge network between the S4 helix positive charges (R1, R2, R3, R4, K5 and R6) and negative countercharges belonging to of the VSD or the neighboring lipid headgroups. The salt bridge rearrangement during individual transitions is accompanied by the transmembrane translation of S4 in a screw-like motion.

Results

We have designed a procedure to estimate the free energy landscape of VSD activation and uncover the kinetics of channel gating. This will allow us to (i) confirm the thermodynamic stability of the 5 states and (ii) determine the minimum energy transition pathway linking them. To enhance the sampling of the configurational space and to recover the energetic landscape of the process, we have used multidimentional metadynamics. This protocol relies heavily on the determination of the collective variables that best describe the process and enable efficient biasing of the configurational sampling. Here, we have designed a minimal set of collective variables that combine the two main molecular determinants of activation: 1- the binding and unbinding of the S4 gating charges to/from binding sites and 2- their spatial translation. Such a choice has enabled us to produce the multi-dimensional free energy surface (FES) of two of the four transitions linking the Kv1.2 VSD conformations, enabling us to gain unprecedented molecular insight into the molecular mechanism at work. Fig. 2 reports the results for the γ/δ transition, in which the first collective variable describes the transition of R2 and the second the transition of R4. In a next step, we have investigated how this free energy landscape is modified i) by the mutation of key residues and ii) by a change in the lipid environment. The mutations we have considered to test the procedure target residues belonging to the central hydrophobic region of the VSD, which acts as a barrier for the passage R2 in the γ/δ transition and have all been characterized by electrophysiology experiments.

In I173F and I230T, the kinetics of activation and deactivation are enhanced despite the opposite nature of the mutation: I173F introduces a bulky, aromatic residue in the barrier region while I230T introduces a supplementary polar residue. In agreement with these experimental findings, we found that for the γ/δ transition of I230T and I173F, the barrier for R2 transfer is significantly lowered. The characterization of the process at a molecular level highlights important differences: while I230T provides an increased solvation of the upper VSD water crevice, I173F creates a supplementary cation-π interaction that lubricates the passage of R2 across the hydrophobic barrier. Thus, the results obtained so far corroborate the mutagenesis experiments and provide a molecular interpretation usually hard to extract from the electrophysiology results. Following the same protocol, we have studied the effect of PIP2, a negatively charged lipid that hampers activation of the channel. We show that the δ state is significantly stabilized by the presence of PIP2 through specific protein/lipid salt bridges.

In summary, using Kv1.2 as a prototype, we have demonstrated that the framework we have designed enables us to bridge microscopic features extracted from MD simulations with macroscopic data extracted from electrophysiology measurements providing an insight that is unattainable by other experimental techniques.

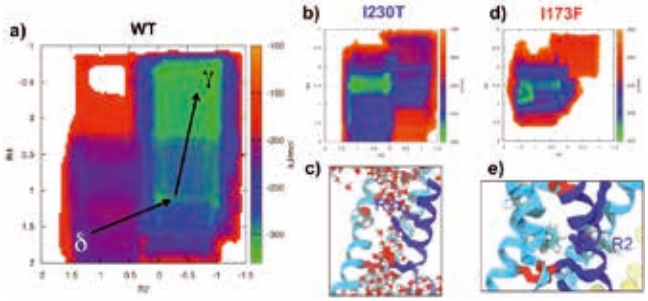

Figure 2: Free energy landscape for the γ/δ transition. Two collective variables, representing the displacement of R2 and R4, respectively, describe the process. A) FES for the WT, showing a degenerate minimum free energy pathway linking γ and δ. b) FES for I230T c) Increased solvation of the upper crevice. T230 is represented as VdW spheres and water molecules in cpk representation, d) FES for I173F e) zoom on the barrier region showing the transfer of R2 between F173 and a conserved Phe residue of S4.

Computational Strategy

To design the best protocol to evaluate the Kv1.2 activation kinetics we explored several options and chosen the best one providing fast and accurate estimates of the FES of this complex process. We have chosen to use GROMACS4.6 [4], coupled to PLUMED2 [5] that allows one to use up to 50 multiple walkers (8192 processor) without a loss of performance. A large fraction of our effort has been dedicated to the determination of a minimal set of collective variables that not only describes the molecular process but also enables us to efficiently sample conformations. After trying out several implementations of path collective variables, we realized that the dynamics of the process was best described by several collective variables, each describing the transfer of a single charge along the activation pathway (see results).

Ongoing Research

The total amount of computing time used for this study exceeds 32 M CPU-Hours. We are now generating the complete set of free energy surfaces for the 4 transitions for the WT and the mutants. Further discretization of the Smoluchowski equation will enable us to retrieve the kinetic constants associated with each transition and taken together will enable to reconstruct the electrophysiology curves ab initio.

References and Links

[1] FM. Ashcroft, From molecule to malady, Nature 440 440-447 (2006).
[2] Delemotte, L., Tarek, M. et al. *Proc. Natl. Acad. Sci. USA*. 108:6109-6114 (2011).
[3] Tarek, M. and Delemotte, L. *Acc. Chem. Res*. 46: 2755-2762 (2013)
[4] http://www.gromacs.org/
[5] http://www.plumed-code.org/

http://www.lrz.de/services/compute/supermuc

The allosteric effect of the SH2 domain on Abl kinase activation

Research Institution
Centro Nacional de Investigaciones Oncologicas (CNIO)

Principal Investigator
Francesco L. Gervasio (CNIO, now UCL)

Researchers
Nicole Dolker (CNIO); Ludovico Sutto (UCL); Giorgio Saladino (UCL); Silvia Lovera (UCL)

Project Partners
University College London (UCL)

LRZ Project ID: pr86ga (PRACE project)

Introduction

Protein kinases are involved in the regulation of most cellular pathways. Correspondingly, their dysregulation is related to an important number of human diseases. Protein kinases share a common canonical catalytic domain, consisting of a number of highly conserved motifs, which have to undergo substantial conformational changes to be catalytically active. In many kinases the interaction with other domains or proteins triggers full activation.

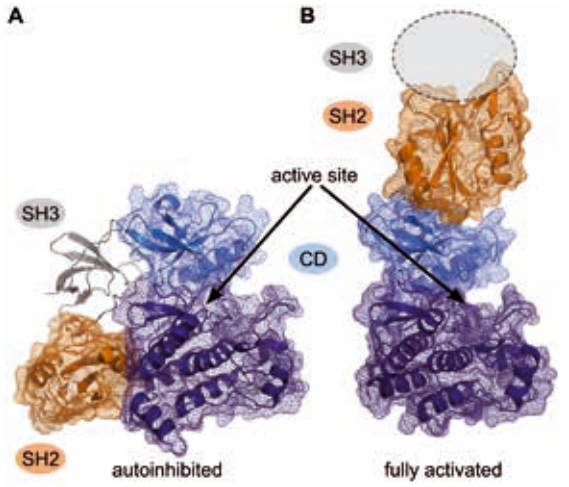

Figure 1: Structure of Abl kinase in the autoinhibited (A) and fully activated "top-hat" (B) conformations.

The Abelson tyrosine kinase (Abl) is of special interest because of its importance as an anti-cancer drug target. The fusion protein BCR-Abl leads to over-activation of Abl, causing chronic myeloid leukemia (CML). Recently a number of ATP-competitive Abl inhibitors, first and foremost Imatinib, have been approved for the treatment of CML. The treatment is very effective, but a significant proportion of patients relapse due to drug resistance-causing mutations. As most of the mutations are located around the active site, it has been proposed that inhibitors that bind to allosteric (remote) sites might overcome the resistance problem.

Unfortunately, the knowledge on allosteric regulation of kinases is still limited. A more detailed understanding of allosteric effects on the activation of Abl and other bio-medically important protein kinases is, therefore, of paramount importance for the rational design of new drugs.

In the case of Abl, both auto-inhibition and full activation are allosterically regulated by the interactions of the catalytic domain with the Src Homology 2 (SH2) domain During activation, the complex formed by the catalytic domain, the SH2 and the SH3 domain, has to undergo a major reordering (Figure 1). The mechanism by which SH2 in the "top-hat" position allosterically activates the catalytic output is not known.

In this project, we studied the activation of the catalytic domain by the SH2 domain.

Methods

In this project, we studied the activation of the catalytic domain of the Abl kinase by the SH2 domain. In order to obtain quantitative data on the thermodynamics and kinetics of Abl activation in the presence of the SH2 domain, we used molecular dynamics simulations (MD). In classical MD, atoms are represented by rigid spheres, and interactions between them are described by simplified models (Figure 2). Integration of Newton's equations of motion then yields a trajectory for the system.

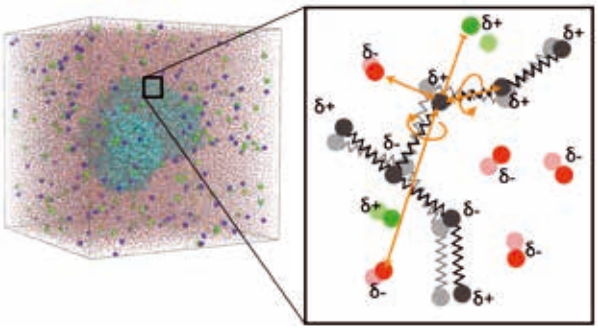

Figure 2: Schematic representation of molecular dynamics simulations.

On a large supercomputer, unbiased MD simulations of complex systems, such as the Abl-SH2 complex, can be expanded in the range of µs to give insight into the dynamics of the system. However, in order to analyze the energetics of proteins motions, the corresponding conformational space has to be sampled exhaustively, which exceeds the accessible time span by orders of magnitude. This difficulty can be overcome by the use of enhanced sampling methods. In the current project, we used parallel tempering metadynamics (PTmetaD). PTmetaD is an extremely efficient and intrinsically parallel method for the calculation of the free energy of a system as a function of one or more collective variables (CVs), which have to be chosen carefully to represent the conformational changes under investigation correctly. Additionally, a number of replicas are run in parallel at different temperatures, and an exchange of coordinates between replicas at adjacent temperatures is attempted at regular intervals to enhance the conformational sampling. All calculations were carried out with the GROMACS4.5 molecular dynamics package and the PLUMED-plugin for free energy calculations.

Free energy calculations are computationally expensive. An average job in this project was run on 4000 CPUs, taking up a total of over 1 mio core hours. However, these simulations do not need to run continuously. For easier data management they were split into shorter consecutive runs with a walltime of 24 h each.

To validate the computational results we designed a set of mutants expected to decouple the SH2 domain from the kinase domain and measured their catalytic activity experimentally in collaboration with the group of Prof. Giulio Superti-Furga at CeMM in Vienna. Finally, we expanded our findings on the allosteric regulation of the kinase domain to other, therapeutically relevant kinases, including the FGFR, EGFR and FES.

Results

The combination of molecular dynamics simulations with experiments in vitro and in vivo has shown how the SH2 domain in the "top-hat" conformation changes the dynamics of the catalytic domain of the Abl kinase. Based on the molecular dynamics simulations, we could identify several residues that are key to the interplay between catalytic and SH2 domain (Figure 3).

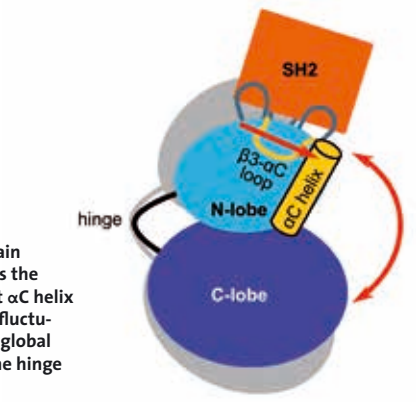

Figure 3: The SH2 domain stabilizes and positions the catalytically important αC helix and channels thermal fluctuations into productive global movements, such as the hinge motion.

The picture that has emerged from our studies is that the SH2 domain stabilizes and repositions the loops that form the binding site, which, in turn, interact with the surrounding loops, modifying the flexibility of a number of catalytically important structural motifs highly conserved in protein kinases, such as the P-loop, the αC helix and the activation loop. The β3-αC loop preceding the αC helix plays a key role as a lever, transmitting the signal from the SH2 domain-binding site towards the catalytic motifs in the kinase domain.

Moreover, the SH2 domain modifies the opening and closing of the N-and C-lobes upon the active site (hinge motion). Our model is supported both computationally and experimentally by a number of mutants that change the interaction between the catalytic domain and the SH2 domain without disrupting the domain-domain interface. Introduction of glycine or proline residues in the β3-αC loop weakened and stiffened the lever respectively. The glycine mutant lowered the effect of the SH2 domain, while the proline mutant activated the kinase domain maintaining the activating effect of the SH2 domain.

Stiffening the hinge with a proline residue decreased substantially the activity of the free CD, which cannot be rescued in the CD-SH2 construct. The hinge motion is involved in the rate-determining step of the phospho-transfer reaction in most kinases.

To understand how general are these findings were, we also studied the activation of other kinase domain by allosteric effectors. In the epidermal growth factor receptor we have found that oncogenic mutations far from the active site change the dynamics of the domain substantially. In the fibroblast growth factor receptor we have studied the mode of action of a novel allosteric inhibitor, leading to more potent derivatives that will proceed to clinical trials.

On-going Research / Outlook

It will be interesting to investigate whether other SH2 domain-containing kinases undergo Abl-like motions and interactions depending on SH2 domain engagement. The discovery of the allosteric coupling of catalytically active residues in Abl with SH2 binding may instruct both the strategies aiming at the development of small molecules interfering with the SH2-kinase interface but also conformation-depending kinase inhibitors.

References and Links

[1] C. Herbert, ..., F.L. Gervasio* et al. Molecular mechanism of SSR128129E, an extracellularly acting small molecule allosteric inhibitor of FGF receptor signaling, *Cancer Cell,* 23, 489-501, 2013.

[2] J. Juraszek, G. Saladino, T. Van Erp, F.L. Gervasio* Efficient numerical reconstruction of protein folding kinetics with partial path sampling and path-like variables. *Phys Rev Lett*, 110, 108106, 2013.

[3] L. Sutto & F.L. Gervasio* The effect of oncogenic mutations on the conformational free energy landscape of EGFR kinase Proc Natl Acad Sci USA, 110, 10616-10621, 2013.

[4] N. Dölker, M. Górna, A.S. Torralba, F.L. Gervasio, and G. Superti-Furga. *The SH2 domain regulates c-Abl kinase activity by a cyclin-like mechanism and impairment of the hinge motion* submitted for publication.

All-atom simulations of the Amyloid-beta peptide interacting with gold

Research Institution
Center S3, CNR Institute of Nanoscience, Modena, Italy

Principal Investigator
Luca Bellucci, Stefano Corni

Researchers
Rosa Di Felice (S3 & USC, Los Angeles, USA), Giovanni Bussi (SISSA, Trieste, Italy)

Project Partners
Leibniz Supercomputing Centre

LRZ Project ID: pr86ge (PRACE project)

Introduction

The increasing technological importance of nanomaterials naturally raises the concern for possible toxic effects when they accidentally contact living organisms. Such effects will likely involve the interactions of nanomaterials with the protein arsenal of the body. On the other hand nanoparticles (NPs) have been proposed for innovative diagnostic and therapeutic approaches, applications that define the emerging field of theranostic (therapy+diagnostic) nanomedicine.

Understanding the interaction mechanisms between biomolecules and inorganic surfaces are of paramount importance to rationalize the behavior of this new generation of nanoscale-based systems. The molecular adsorption on solid surfaces/NPs involves many dynamical steps, from the initial recognition of the molecule by the surface to the equilibrium conformational rearrangement of the adsorbed molecule. To analyze the adsorption process, therefore, it is necessary to investigate the dynamical behavior of the system: this is, in most case, hard to be directly sorted out from experimental data alone. The rationalization of the behavior of such heterogeneous systems represents one of the major challenges in the interdisciplinary field of nanotechnology.

Specific aspects can be successfully investigated by using computational techniques. Among them, molecular dynamics (MD) simulations provide the "natural" tool to perform a variety of studies that aim at the structural and dynamical description of the adsorption process. However, the mere use of MD does not guarantee a suitable conformational sampling of such systems and more advanced techniques to enhance the sampling (e.g. metadynamics or Replica-Exchange-MD) are mandatory.

By exploiting recently developed classical force-field (FF) parameters that describe the interaction of proteins with gold surfaces in water, e.g. GolP [1], in advanced MD techniques, it is possible to study the adsorption process of proteins on a gold surface at the atomistic level.

Starting from the computational tools developed and validated so far [2], the research within this project was designed to study the interaction between the gold surface and the intrinsically unstructured protein β-Amyloid.

β-amyloid is a short peptide of 42 amino acids (Aβ42), whose inclination to aggregation triggers the formation of fibrils and plaques observed in the Alzheimer's disease. Au NPs are among the most versatile and easy-to-use NPs, and are currently being tested as imaging contrast agents, absorptive heating systems and as dual imaging and therapeutic agents. Our simulations shed light on how and why the interaction with Au modifies the conformational ensemble of Aβ42 and therefore provide microscopic insights on the NP role in modifying the fibrillation propensity of Aβ42.

Results

The project "All-atom simulations of the Amyloid-β peptide interacting with gold" (AmyGo) has generated the required data to clarify the conformational ensemble of Aβ42 in water and attached to a large, bare Au NP.

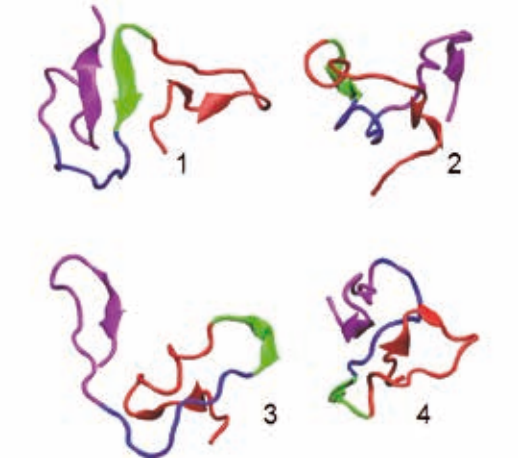

Figure 1. Examples of conformations found during the T-REMD.

Classical MD simulations were performed with GROMACS in conjunction with the PLUMED plugin [3], using the GolP FF.

Within AmyGo, we performed a preliminary extensive Temperature Replica Exchange MD simulation (T-REMD) for the Aβ42 peptide in water (300ns per replica, 64 replicas, in a simulation box large enough to prevent image interactions even in the fully extended conformation). The conformational ensemble is complex (Figure 1) and contains some infrequent but considerably populated structures with high β-sheet content, which may be fibrillation-prone conformations.

We then simulated, with statistical significance (128 realizations, at least 20 ns each), the binding process of Aβ42 to Au(111), i.e., the events that lead from the peptide in solution to the peptide adsorbed on the surface. Analyzing all the MD trajectories, we observed that the Aβ quickly adsorbed on the gold surface. In all cases, the adsorbed peptide remained trapped to the gold surface during the rest of the simulation, without substantial conformational rearrangement. We identified the preferential Au-binding sites. We also reconstructed a kinetic picture of the process, not available in the REMD simulations.

Because of the large number of degrees of freedom and the different kinds of interactions in the system under study (i.e. protein-protein, protein-gold, protein-water etc.), the conformational sampling of the system is elusive to straight MD. To bypass this limitation, we employed the Hamiltonian-Temperature-Replica Exchange MD (HT-REMD) as implemented in PLUMED. The HT-REMD technique is a variant of the well-known T-REMD. In HT-REMD, N copies of the system (replicas) run concurrently at different temperatures and scaled Hamiltonians in different portions of the system (i.e. scaling the potential interactions between gold and the adsorbed protein). On one hand, scaling the specific gold-protein potential in the modified-Hamiltonian replicas, it is possible to decrease the high energy barriers due to the interactions between the surface and the peptide. On the other hand, with the use of high temperatures it is possible to accelerate the crossing of the energy barriers of the whole system. Exchanges of the configurations of neighboring replicas are attempted at fixed intervals, and are accepted or rejected by means of a Metropolis test so as to ensure the correct thermodynamic ensemble. The HT-REMD protocol, therefore, represents an efficient solution to improve the sampling of heterogeneous systems where the interactions among the various species can be very different in intensity.

Starting from relevant structures found in the T-REMD trajectory in solution, we performed a statistically significant HT-REMD simulation of Aβ42 on Au(111).

We could run approx. 100 ns for each of the 128 replicas (i.e., an aggregated simulation time of approx. 12 μs). Visual inspection (Figure 2) and cluster analysis of the trajectory confirm that the conformational ensemble is strongly perturbed by the presence of the surface.

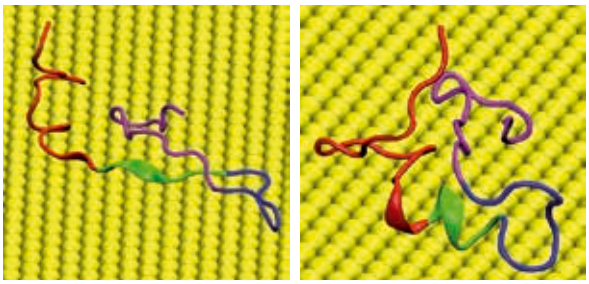

Figure 2. Examples of *Aβ42* conformations on Au(111) obtained from the HT-REMD simulations (water not shown for clarity). The secondary structure element (helix and β-sheet) are shown with cartoon representation. The conformational ensemble on gold is modified with respect to the ensemble in water.

On-going Research / Outlook

The AmyGo results described above give us a detailed characterization of the conformational ensemble in solution. The effect of inorganic materials on the propensity of polypeptides to aggregate is a subject of current intense research, but its microscopic comprehension is still very limited. Thanks to our simulations, for the important case of Aβ42 on Au, we are now in the position of understanding at the atomistic level the effect of the surface on the conformational ensemble of the polypeptide.

We have shown that a HT-REMD protocol can be fruitfully applied to such class of problems. This opens the way to similar simulations of other systems, to gain insight on the possible different behaviors.

Thanks to the Peta-scale facilities and the unconventional HT-REMD computational protocol, which here we validated for AmyGo attached to a Au NP, the investigation of the effects of inorganic surfaces and nanoparticles on the Aβ42 conformational landscape can be extended further. In particular, functionalized gold surfaces and nanoparticles are promising candidates to be studied with this approach.

References and Links

[1] Francesco Iori, Rosa Di Felice, Elisa Molinari and Stefano Corni, 2009. An atomistic force-field to describe the interaction of proteins with Au(111) surfaces in water, *J. Comput. Chem.*, 30,9 (Jul 2009), 1465–1476.

[2] Luca Bellucci, Giorgia Brancolini, Arrigo Calzolari, Oliver Carrillo Parramon, Stefano Corni, and Rosa Di Felice, 2012. Proteins and Peptides at Gold Surfaces: Insights from Atomistic Simulations, *ACS Symposium Series, Proteins at Interfaces III State of the Art*, 1120,10,(Dec 2012), 229–250.

[3] www.plumed-code.org

Mesoporous silica for drug delivery: a quantum mechanical simulation

Research Institution
Department of Chemistry, University of Torino (Italy)

Principal Investigator
Piero Ugliengo

Researchers
Massimo Delle Piane, Marta Corno

Project Partners
Alfonso Pedone – Dep. Chemistry, University of Modena and Reggio Emilia

LRZ Project ID: pr86le (PRACE project)

Introduction

The mechanisms of interaction between solid excipients and drugs are based on surface chemistry related phenomena. Consequently, understanding the physico-chemical features of surfaces is a fundamental step to describe and predict the strength of these interactions. The results can shed light on how the nature of the excipient can affect the properties of a drug formulation.

Among the most important inorganic materials, silica based ones play a key role, because they are chemically inert, structurally robust, easy to prepare and characterize. Considering this class of materials, ordered mesoporous structures have attracted a lot of interest in the last decades.. Among silica-based mesoporous materials, MCM-41 is one of the most studied. In 2001 it was firstly proposed as a drug delivery system, with ibuprofen as a model drug.

In this project, this drug molecule was studied in interaction with an accurate model of MCM-41, providing structures and interaction energies for the adsorption of ibuprofen with this material of unprecedented quality. Simulation of a variety of physical observables (infrared and NMR spectra) represents a key point in order to validate the results by comparison with experimental data.

Results

The chemical systems that are investigated in this project are made up of hundreds atoms in the form of a crystalline material. To study such systems with the state-of-the-art methods chosen for this project (ab-initio DFT calculations, using hybrid functionals) High Performance Computing (HPC) is the method of choice. These simulations was completed in a feasible time only by exploiting the thousands of processors available on the SuperMUC machine (20 million CPU hours have been awarded – 1024-2048 cores was the average run during the project). A previously designed [1] realistic model of the MCM-41 mesoporous silica material was chosen as the starting point for this PRACE project (Figure 1). It was validated against many experimental results. Particularly, the computational resources available in this project made possible the ab-initio simulation of its infrared spectrum, focusing on the OH stretching region, that resulted in a remarkable agreement with the experiment.

All modeling was done with and without introducing an empirical correction for dispersion (since DFT calculations are known to miss the correct description of London forces). This last point reflected our intention to highlight the role of these forces in such complex systems.

By mapping the electrostatic potential of the MCM-41 pore walls, we sampled the potential energy surface of the drug-silica system by docking the ibuprofen molecule on 6 different spots on the pore walls. The obtained structures showed the formation of broad H-bond networks between the surface silanols (SiOHs) and the COOH carboxyl functionality of the molecule, with a significant deformation of the pore walls, with respect to the bare mesoporous material as the pore surface adapts itself to accommodate the incoming molecule. Inclusion of the dispersive vdW forces produced a dramatic change in all structures: ibuprofen came significantly closer to the surface and in some cases this influenced the geometry of the strong, directional H-bond interactions. This results are in accordance with our previous experience in modeling the adsorption of drugs on amorphous silica

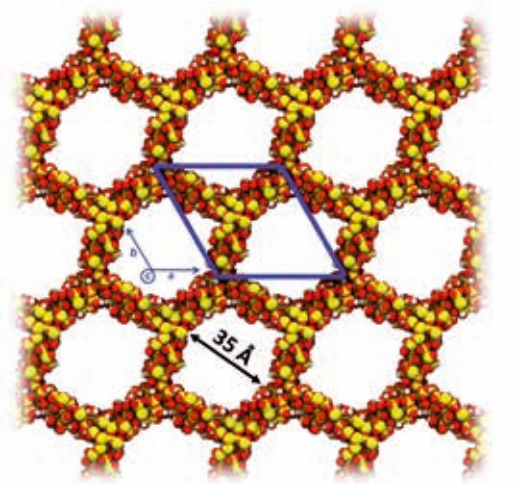

Figure 1: The MCM-41 mesoporous silica model. Unit cell drawn in blue. 579 atoms in 42x42x12 Å unit cell (drawn in blue).

surfaces and demonstrate once again that dispersion cannot be neglected in this kind of systems [2].

As a subsequent step the drug loading of the mesoporous material was gradually increased, up to 7 ibuprofen molecules per unit cell, resulting in an almost complete coverage of the pore walls (Figure 2).

We decided to investigate whether the adsorption of ibuprofen on the pore walls of MCM-41 follows a Langmuirian model. That is, if also in a complex system of this kind, with a molecule interacting with an amorphous scaffold, all the adsorption sites are equivalent and multiple adsorption events are independent from each other. To answer this question, we had to shift the analysis to an energetic point of view, accurately computing the interaction energies. This study showed that interaction energies of ibuprofen in all the cases were very similar (from a minimum of -91 kJ/mol to a maximum of -122 kJ/mol, including dispersion), despite evident discrepancies in the geometrical features of the adsorption. This demonstrates a very weak dependence on the adsorption site. Furthermore, when in "high loading", the average interaction energy per ibuprofen molecule (-106 kJ/mol) was found to be almost identical to the arithmetic average of the "single loading" cases, indicating an almost complete independence between the adsorption events. Comparison of these results with the ones obtained without accounting for dispersion interactions showed that their contribution to the total interaction energy varies between 54% and 70%, depending on the model: dispersion is indeed the driving force of the adsorption.

Given the amorphous nature of the MCM-41, experimental results can only provide average structural information. This, in turn, has made very difficult their interpretation. Our simulations can indeed help experimentalists to explain what they observe. For example, by computing the infrared spectra of our models, we obtained a clear indication that the observed broadness of the experimental C=O band may be due to slightly different adsorption situations. Furthermore, simulation of the NMR chemical shifts of ibuprofen in interaction with MCM-41, provided extremely useful information to interpret the solid state MAS-NMR data, that represent at the moment one of the most important way to directly investigate the drug/MCM-41 system.

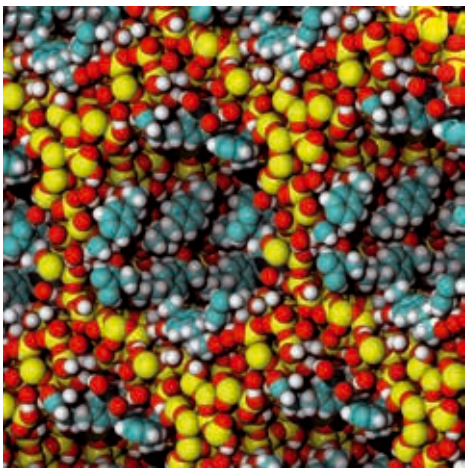

Figure 2: "High loading" model: MCM-41 in interaction with seven ibuprofen molecules adsorbed on the pore walls. Structure cut to show the inside of the pores.

In the last part of the project, we performed a molecular dynamics simulation of the "high loading" structure, at room temperature, to check the stability of the interaction and to investigate the drug mobility. From the technical point of view, the molecular dynamics simulations were run through the well-established VASP and CP2K codes. The NMR chemical shifts were computed with the QuantumESPRESSO code. As regards static calculations (that represented the great majority of the project), the CRYSTAL code [3], developed at the University of Torino, was employed. Particularly, this PRACE project saw a continuous synergy between the modeling team and the CRYSTAL developers to keep enhancing the efficiency and stability of the code. This cooperation resulted in a much improved code that will provide advantages well beyond the specific scientific area of this project.

As far as we know, these simulations represent the state of the art, with respect to the modeling of silica-based materials. We have demonstrated that the evolution of HPC architectures and the continuous advancement in the development of more efficient computational chemistry codes have been able to take the Density Functional Theory approach (even in its more accurate hybrid guise) out of the realm of "small" chemical systems. This opens the path to the accurate ab-initio simulation of complex chemical problems (in material science and beyond) without many of the simplifications that were necessary in the recent past.

On-going Research / Outlook

Our research in the field will follow multiple paths, in parallel. First of all, further analysis of the huge amount of data obtained in this year of calculations will be necessary and we will run more simulations (particularly molecular dynamics) to better investigate scientific questions that remained unanswered. Secondly, an interesting point of debate in the study of ibuprofen confinement in mesoporous silica concerns the physical state of this molecule in the system. In particular, it is still not clear if the majority of the drug population is in interaction with pore walls or in a free state and, in this case, if it is as a free molecule or in a dimeric form. We aim to simulate the adsorption of ibuprofen dimers on silica surfaces to shed light on this important point.

Finally, the team is already active in modeling the functionalization of silica-based materials with acidic and basic substituents, closing the gap between the simulated system and the real industrial application of MCM-41 and similar mesoporous silica materials as a drug carrier.

References and Links

[1] Ugliengo, P., Sodupe, M., Musso, F., Bush, I. J., Orlando, R. and Dovesi, R. Realistic Models of Hydroxylated Amorphous Silica Surfaces and MCM-41 Mesoporous Material Simulated by Large-scale Periodic B3LYP Calculations. *Adv. Mater.*, 20, 23 (Dec. 2008), 4579-4583.

[2] Delle Piane, M., Corno, M. and Ugliengo, P. Does Dispersion Dominate over H-bonds in Drug-Surface Interactions? The Case of Silica-Based Materials as Excipients and Drug-Delivery Agents. *J. Chem. Theory Comput.*, 9, 5 (May 2013), 2404-2415.

[3] http://www.crystal.unito.it

Collective proton tunneling in hexagonal ice

Research Institution
Ruhr-Universität Bochum, Lehrstuhl für Theoretische Chemie

Principal Investigator
Dominik Marx

Researchers
Christof Drechsel-Grau and Dominik Marx

Project Partners
–

LRZ Project ID: pr86ru

Introduction

Ice crystals, solid water, consist of oxygen (O) and hydrogen (H) atoms forming water (H_2O) molecules and display diverse structures as a function of temperature and pressure. The structure of crystalline ices exhibits a long-range order of oxygen atoms, whereas the positions of the hydrogen atoms can be arranged either regularly (proton-ordered structure) or disorderly (proton-disordered structure). Two neighboring oxygen atoms accommodate exactly one hydrogen atom, and the three sites form a hydrogen bond connecting two water molecules. In proton-ordered ice structures, the hydrogen atom can occupy only one site along a hydrogen bond. In contrast, proton-disordered ice structures allow for two possible hydrogen sites along a hydrogen bond: O-H—O and O—H-O. The proton order of ice structures has profound consequences for the proton motion, and this research aims at deepening our understanding of the relation between structure and dynamics.

Figure 1: Schematic initial (left) and final (right) state of the transfer of six protons (black) in the proton-ordered six-ring (O: red; H: white; hydrogen bond: blue).

Dynamics in ice arises from proton transfer along a hydrogen bond (D-H—A → D^-—H-A^+): a proton (H^+), the positively charged nucleus of a hydrogen atom, is transferred from the oxygen atom it is bonded to (proton donor D=OH) to the neighboring oxygen atom in the hydrogen bond (proton acceptor A=H2O). Proton transfer thus leads to two charge defects, a negatively charged hydroxide ion (D^-=OH^-) and a positively charged hydronium ion (H-A^+=H_3O^+). The charge separation not only requires energy to reach the final state, but it is also associated with a large barrier separating the initial and the final state, thus rendering proton transfer unfavorable in proton-ordered and proton-disordered ice structures. However, proton-disordered ice crystals such as ordinary (hexagonal) ice allow for the transfer of several protons, collective proton transfer, which can lead to a final state without charge defects for six transferred protons (Fig. 1). Although a barrier to proton transfer remains, the energy difference between the initial and final state is substantially lower for collective proton transfer because no charges are separated, thus increasing the likelihood for the system to be in the final state.

Whereas the likelihood of finding the system in the final state compared to the initial state, a static quantity, depends on the energy difference between the two states, the speed with which the system proceeds from the initial to the final state (time-dependent motion) depends on the barrier, arising from the energy penalty associated with breaking bonds, separating the two states. Because the hydrogen atom and the proton are very light, classical laws are insufficient to describe its motion. Therefore, a quantum-mechanical description of the nuclei is required. In a classical description of the proton motion, the proton must hop over the barrier to transfer from the donor to the acceptor. The laws of quantum mechanics, however, also allow particles to move through the barrier. This classically forbidden process is called tunneling, and its likelihood increases with decreasing width of the barrier, mass of the tunneling particle, and temperature.

This study is motivated by recent neutron scattering experiments that detected proton motion in proton-disordered ice crystals from temperatures close to the melting point down to 5 K [1]. These experiments are puzzling because they required neither high pressure, which reduces the hydrogen-bond distance and thus decreases the barrier width, nor specific salts, which introduce excess defects that facilitate proton transfer. The experimental data have been interpreted schematically in terms of the simulta-

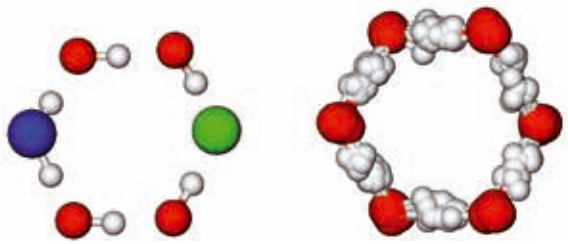

Figure 2: Representative transition-state structures at high (left) and low (right) temperature (O: red; H: white; hydronium ion: blue; hydroxide ion: green).

neous tunneling of six protons in a proton-ordered water hexamer (six-ring) embedded in a proton-disordered ice crystal. Herein, we investigate the role of quantum fluctuations to elucidate the mechanism of collective proton transfer in ordinary ice. In particular, we show that proton transfer proceeds via hopping at high temperature and via collective proton tunneling at low temperature [2].

Results

Special techniques and resources are required to describe proton transfer because this process involves the breaking and making of bonds. Moreover, because the barrier to proton motion is high, proton transfer is a rare event, and its occurrence has to be enforced by appropriate sampling techniques. To meet these particular requirements, we employed density functional theory and molecular dynamics simulations, which can describe changing bonding patterns and sample the positions and velocities of the ice crystal, respectively [3]. The transfer from the initial to the final state was induced by constraining a variable that involved the positions of all six protons along their respective hydrogen bonds. This procedure enabled us to study the correlated proton motion along the transition and to sample positions of low probability. The above methods describe nuclei as point particles evolving according to the laws of classical mechanics at high temperature (300 K). These "classical" (ab initio molecular dynamics) simulations were compared to "quantum" (ab initio path integral) simulations at low temperature (50 K), in which each nucleus was described by a necklace of 32 beads allowing for the representation of the quantum spread of each atom, to study the role of quantum fluctuations for correlated proton motion.

The mechanism of a chemical reaction can often be inferred from the structures found at the transition state (energy maximum in classical processes) separating the initial and final state. Our analysis of the sampled structures at the transition state, located halfway between the initial and final state, reveals large qualitative differences between the high-temperature (classical) and the low-temperature (quantum) regime (Fig. 2). In the former case, three protons have been transferred via classical single-particle hopping from their donors to their acceptors, leading to a defect pair consisting of a hydronium ion and a hydroxide ion at opposite ends of the proton-ordered six-ring. In contrast, in the latter case, the transition state is characterized by the collective transfer of all six protons

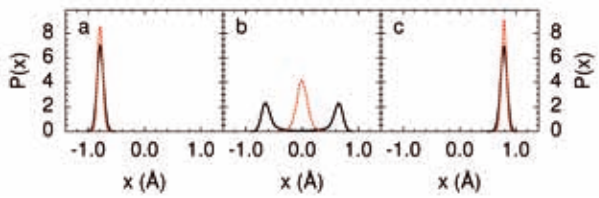

Figure 3: Distribution of the variable x enforcing the tran-sition from the initial (a) via the transition (b) to the final (c) state at low (black) and high (red) temperature (x is the average of the difference between the D-H and H-A distance over all hydrogen bonds in the proton-ordered six-ring). Delocalization of protons over structures resembling the initial and final state shows collective tunneling at low temperature (b).

from the initial to the final state and back. The distributions of the proton positions (Fig. 3) demonstrates that the protons must move simultaneously, which also explains why essentially no defect is observed at low temperature. The analysis of the proton motion further showed that the proton transfer at 50 K proceeds via tunneling: the six protons move simultaneously through the barrier [2]. Hence, in spite of relatively long hydrogen-bond distances, the spread of the quantum particles at low temperature becomes so large that tunneling through the barrier can occur. The results obtained and insights gained from this study thus provide a rationalization of the experimental evidence for proton motion in ice at low temperature.

The results obtained herein would not have been possible without the efficient CPMD program package and the use of high-performance computing platforms. In particular, our in-house version of the CPMD code was modified to allow for constraining the variable including the positions of all six protons relative to their respective hydrogen-bond donors and acceptors required for inducing the transition from the initial to the final state. The CPMD program is known for its excellent scaling on various high-performance computing platforms owing to its distributed-memory design for the computation of the energies and forces acting on the nuclei, which is based on pseudopotentials and a plane-wave expansion of the valence Kohn-Sham orbitals. In addition, each bead of the quantum simulations is essentially independent of the other beads, thus leading to an intrinsic parallelization of the program as a function of the number of beads. Each of the 32 beads could be parallelized over 16 cores, resulting in a total of 512 cores per job. The total amount of data generated was about 5 TB. The data generated based on the allocated resources of 2.95 million cpu hours on SuperMUC have been analyzed and will lead to at least two additional publications.

On-going Research / Outlook

As mentioned above, the results and insights obtained regarding the qualitative differences in collective proton motion at high and low temperature would not have been possible without the resource allocation on SuperMUC by LRZ. Ongoing research on collective proton transfer in ice crystals is in progress and will be disseminated shortly. The path integral approach for investigating quantum fluctuations has proven successful in providing crucial insight into fundamental quantum processes and is suitable for high-performance computing platforms. This methodology has great potential to unravel chemical and physical processes in complex systems involving many more electrons, thus allowing for the efficient use of more cores per bead.

References and Links

[1] L. Bove, S. Klotz, A. Paciaroni, and F. Sacchetti. 2009. Phys. Rev. Lett., 103, Article 165901, 4 pages.
[2] C. Drechsel-Grau and D. Marx. 2014. Phys. Rev. Lett. In press.
[3] D. Marx and J. Hutter. 2009. Ab initio molecular dynamics: Basic theory and advanced methods. Cambridge University Press, Cambridge, UK.

http://www.theochem.rub.de
http://www.cpmd.org

Phase transition based control of friction at the nanoscale

Research Institution
Empa Swiss Laboratories for Material Science and Technology

Principal Investigator
Carlo Pignedoli

Researchers
Andrea Benassi

Project Partners
Institute for Practical Computation, LMU Munich

LRZ Project ID: pr89mi (PRACE project)

Introduction

The ability to control and manipulate frictional forces at the nanoscale is extremely important for technology, being closely tied to progress in transportation, manufacturing, energy conversion, and lubricant consumption, impacting on innumerable aspects of our health and environment. In recent years a lot of effort has been devoted to gain control of friction at both the macroscopic and microscopic scale. However, most of the employed techniques cannot be straightforwardly extended to the nanoscale, where a flexible and almost cost-free way to dynamically tune friction forces is still lacking.

The flexibility of selected physical properties of the sliding bodies, necessary to actuate a dynamical control of friction, might be provided by the occurrence of a phase transition. A few evidences of this possibility can already be found in literature, and are related to the development of atomic force microscopy (AFM), a quickly improving experimental tool that allows to study, using nanosized oscillating tips, surface properties by sampling contact and non-contact forces down to the atomic scale. The transition to a superconducting state strongly alters the properties of the electronic degrees of freedom and thus the way the energy is dissipated through them. As a result the non-contact dissipation of a tip oscillating close to a $NbSe_2$ surface has been found to undergo a strong drop crossing the critical temperature T_c for the onset of superconductivity [1]. Oppositely polarized domains in a ferroelectric medium give rise to very different energy dissipation when perturbed with an AFM tips both in contact and non-contact mode, and this effect has been used for long time to image domains and to study the their dynamics at surfaces [2] but never exploited in the converse way, i.e. to tune dissipation and friction.

Recently Benassi and coworkers demonstrated the possibility to control nanofriction by switching the order parameter of a structural phase transition [3]. Friction force microscopy (FFM) experiments on a model ferro-distortive substrate have been simulated, showing a non-monotonic behavior of friction as a function of the substrate temperature, broadly peaking at T_c. Besides this unusual feature (stick-slip friction of a single contact on ordinary substrates is known to decrease monotonically unless multiple slips occur), below T_c, the frictional response is found to depend strongly on the substrate distortive order parameter: different values of the substrate distortion can give rise to a very different friction force. Acting now with an external stress field the distortive order parameter of the substrate can be changed reversibly and dynamically, increasing or decreasing the frictional properties of the substrate.

The goal of our PRACE project was to identify a real material hosting a structural phase transition in a range of parameters accessible to the standard experimental techniques. To this aim, a practical structural phase transition to look at is the rotational melting occurring near 260 K in pristine C_{60} molecular crystals (aka Fullerite). Such first order phase transition leads from an ordered structure with locked fullerene at low temperatures, to an angular disordered phase with almost freely rotating fullerenes at high temperatures. Recent measurements have indicated a sharp drop of tip adhesion and of AFM sliding friction in connection with this bulk transition [4], see figure 1 (a). However the explanation given for this strong frictional drop is in open contradiction with thermodynamics, as it is immediately visible from a comparison with the cohesive energy of the Fullerite crystal available in the literature. Despite the great importance that the measured frictional drop can have in the control of friction, no theoretical explanation or simulation data are available for the tribological properties of this system.

Results

Using classical molecular dynamics we simulated the pull-off and sliding friction experiments in presence of the rotational melting phase transition. We started reproducing the bulk and surface rotational melting transition, to this aim the potential by Sprik et al. [5] proved to be best solution. This potential is constituted by a Lennard-Jones short range term plus a long range coulombic

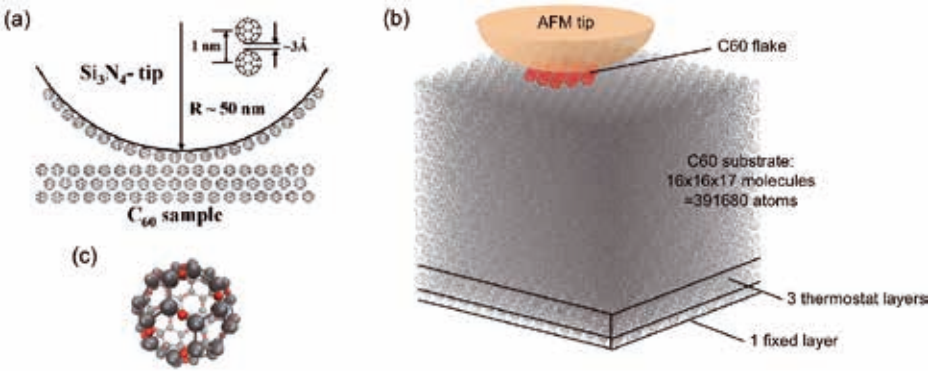

Figure 1: (a) Sketch of the sliding experiment, adapted from reference [4]. (b) Simulation box showing the Fullerite bulk hosting the phase transition, the surface and the C_{60} flake attached to the silicon nitrate tip. (c) C_{60} molecule interaction centers, C atoms in gray, double bond centers in red.

interaction. Every C_{60} molecule is treated as a rigid body with 90 interaction centers placed on every carbon atom and on every double bond, to mimic the charge delocalization, see figure 1 (c). Finite size effects are known to inhibit the occurrence of the phase transitions thus, to have a satisfactory description of rotational melting, we need to work with large systems, our typical simulation box contains more than 4.000 fullerenes corresponding to ~400.000 atoms. As we simulate pull-off and sliding friction experiments we act with an external driving force on the systems. The work done by this force increases the internal energy and, in order to reach a steady state and to prevent the system from blowing up, the excess energy must be disposed off with a thermostat.

As demonstrated in reference [6], a good thermostatation procedure, which does not interfere with the simulated non-equilibrium phenomena, requires the thermostat to be applied far away from the sliding region (fullerite surface) and to have a large portion of solid between them in order to favor the thermalization of the excess energy before reaching the bottom of the simulation box. The simulation box details are given in figure 1(b).

After the characterization of the phase transition we simulated pull-off and sliding friction experiments. In our reference experiment the tip was coated by a monolayer of C_{60} molecules thus, instead of simulating the full silicon nitrate tip, we simply slide or pull the red C_{60} flake of figure 1 (b) which is in direct contact with the Fullerite surface. While the order of magnitude of pull-off and friction forces is the same as in the experiments, the drop at the critical point is much smaller than the measured one, namely only 20% instead of a factor two. After investigations along different lines we concluded that the only way to produce such a huge drop in both the pull-off and friction forces is through a rotation of the C_{60} flake modifying its degree of commensurability with respect to the surface. When the tip approaches the surface at $T > Tc$ the C_{60} flake attached to the tip will more likely contact the surface in an incommensurate configuration. This results in a small friction and pull-off force. Conversely, when the tip approaches the surface at $T < Tc$ the molecules are not rotating and the surface is ordered, this allows the C_{60} flake to rotate and get in registry with the substrate. In this configuration pull-off and friction forces can increase by an order of magnitude. In conclusion, the phase transition, i.e. the rotation of the C_{60} molecules, is not directly responsible for the drastic change in the frictional properties of the Fullerite surface, it rather triggers a change in the contact geometry between the tip and the surface. The possibility to control the contact geometry, the commensurability and thus the frictional properties of a surface through the occurrence of phase transitions deserves further investigation being of great potential impact in the field of nanomanipulation.

The molecular dynamics simulations have been performed with the LAMMPS code [7] an open source state of the art code specifically designed for HPC purposes. The typical production run required 4096 cores for 24 hours.

On-going Research / Outlook

New experiments to probe the dissipation of Fullerite across its rotational melting transition with non-contact AFM are ongoing at Empa, in the group of professor H.J. Hug. From the theoretical side new simulations will be carried out to understand how to promote or inhibit the occurrence of the phase transition thus gaining a dynamical control of the friction coefficient, this could be in principle achieved applying an external pressure. Interesting is also the perspective of tailoring the critical temperature by filling the fullerenes with molecules or increasing the number of carbon atoms per molecule.

The results of this activity will be soon published on peer reviewed international journals and presented in many invited contributions at international conferences on friction, dissipation and manipulation at the nanoscale.

References and Links

[1] M. kisiel, E. Gnecco, U. Gysin, L. Marot, S.Rast, E. Meyer, *Nat. Mater.* **10**, 119 (2011)
[2] A.K. Taganstev , L.E. Cross and J.Fousek "Domains in Ferroic Crystals and Thin Films" Springer (NY) (2010)]
[3] A. Benassi, A. Vanossi, G.E. Santoro, E. Tosatti *Phys Rev Lett.* **106**, 256102 (2011)
[4] Q. Liang, H. Li, Y. Xu, X. Xiao *J. Phys. Chem. B* **110**, 403 (2006)
[5] M. Sprik, A. Cheng, M.L. Klein *J. Phys. Chem.* **96**, 2027 (1992)
[6] A. Benassi, A. Vanossi, G.E. Santoro, E. Tosatti *Phys. Rev.* B **82**, 81401 (2010)
[7] http://lammps.sandia.gov/

More info about our research on nanoscale friction and dissipation at: https://sites.google.com/site/benassia/

A Gating Mechanism of Pentameric Ligand-Gated Ion Channels

Research Institution
Institut de Sciences et d'Ingiénerie Supramoléculaires, Strasbourg, France

Principal Investigator
Marco Cecchini

Researchers
Nicolas Calimet, Siddharth Malik

Project Partners
–

LRZ Project ID: pr89te (PRACE project)

Introduction

Pentameric ligand-gated ion channels (pLGICs) mediate intercellular communication in the brain by converting a chemical signal into an ion flux through the postsynaptic membrane. They are multimeric membrane proteins where each subunit consists of an extracellular (EC) domain and a transmembrane (TM) ion pore region. The agonist binding site is located at the boundary between subunits in the EC domain. The ion pore is formed by the transmembrane helices M2, which delineate an axial ion channel (Fig. 1). The topologically distinct EC and TM domains are allosterically coupled to each other [1].

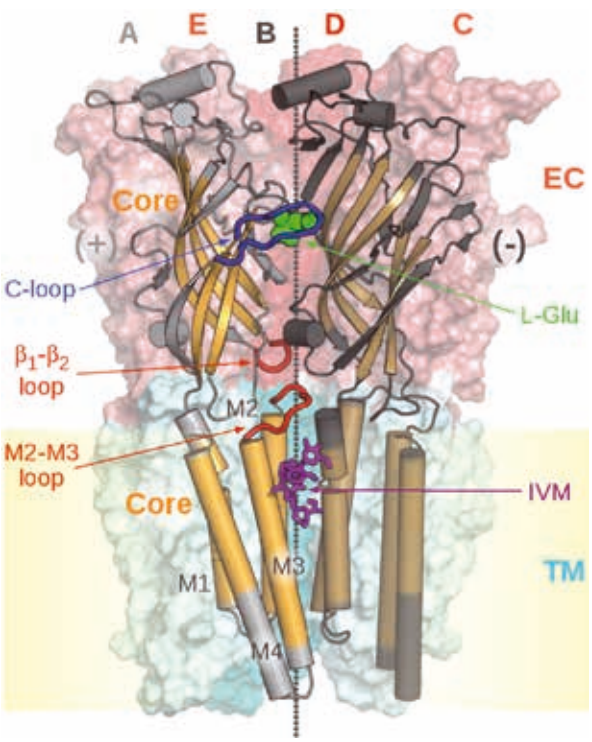

Figure 1: Topology of pLGICs as visualized by the crystal structure of GluCl. Side view of the homopentamer with the five-fold pseudosymmetry axis (gray spheres) that runs perpendicular to the membrane (yellow box). The front A and B subunits are shown in cartoon representations (light and dark gray). The endogenous agonist L-glutamate (green spheres) and the allosteric agonist ivermectin (IVM, magenta sticks) bind at the subunits interface in the EC and TM domain, respectively.

The 3D structure of pLGICs is known for the most part at atomic resolution. Prokaryotic homologues (GLIC & ELIC) have provided complete structures for both the active (A) and the resting (R) state of the channel. Also, the structure of the first eukaryotic channel (GluCl) was recently crystallized in complex with the endogeneous neurotransmitter and the allosteric agonist ivermectin (IVM) [2]. Despite the increasing availability of high-resolution structures, the mechanism of gating ions in pLGICs has remained elusive. Here, we present atomistic molecular dynamics (MD) simulations of the GluCl channel simulated with and without IVM. The relaxation of GluCl induced by the removal of IVM captures a sequence of structural events which elucidate the link between agonist unbinding from the TM domain and ion-channel closing. Based on these results, a general mechanism of activation/deactivation is proposed.

Results

Relaxation of GluCl with IVM removed
The structural relaxation of GluCl induced by the removal of IVM was investigated by sub-μs atomistic MD simulations with an explicit treatment of the solvent and membrane environment. Analysis of the time series (Fig. 2) of several observables shows that, in the absence of IVM, GluCl evolves to a more twisted conformation approaching that of ELIC, which still exhibits an open channel akin to GLIC.

Importantly, the twisting of the receptor results in the enhanced mobility of the pore-lining helices, which dynamically re-orient in the radial direction and shrink the ion pore. Thus, the simulation of GluCl with IVM removed captures the early stages of the transition from open to closed providing structural details of the gating reaction.

Ion gating
A more detailed analysis at the subunit level [3] reveals that the mechanism of pore closing involves four sequential events (Fig. 3).

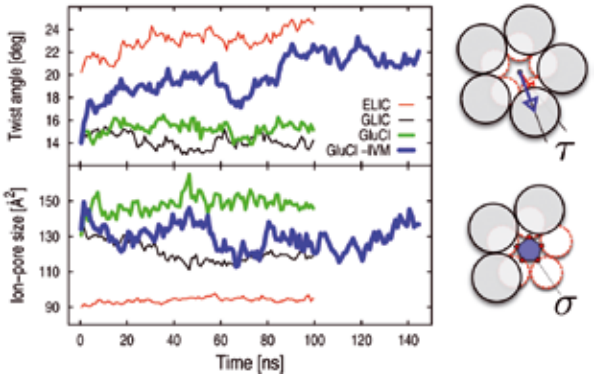

Figure 2: Time dependence of two structural/functional observables used for characterizing activation in pLGICs. The time series of the global twist of the receptor (τ) and the size of the ion pore (σ) are shown for the prokaryotic channels ELIC (red) and GLIC (black), and for the eukaryotic GluCl with (green) and without (blue) IVM. On the right-hand side, a schematic representation of the observables is given.

The transition consists of a global quaternary change (*twisting*) followed by tertiary relaxation of both the EC and TM domains with the *outward tilting* of the β-sandwiches providing a structural communication pathway between the neurotransmitter site and the ion pore. In this scenario, the global twisting would contribute to the allosteric coupling by "locking" the ion channel into an open-pore conformation. Key to translate the repositioning of the EC/TM interfacial loops into opening/closing of the channel is the structural coupling between the M2 and M3 helices. Interestingly, this result provides an interpretation for the "locally-closed" structure of GLIC [4]. Also, the occurrence of a large reorientation of the β-sandwiches on ion channel's deactivation has been recently confirmed by the X-ray structure of GLIC at pH=7 [5]. Overall, the gating mechanism emerging from our simulations assigns a primary role to receptor twisting, which mediates the structural communication between the orthosteric site and the ion pore in pLGICs.

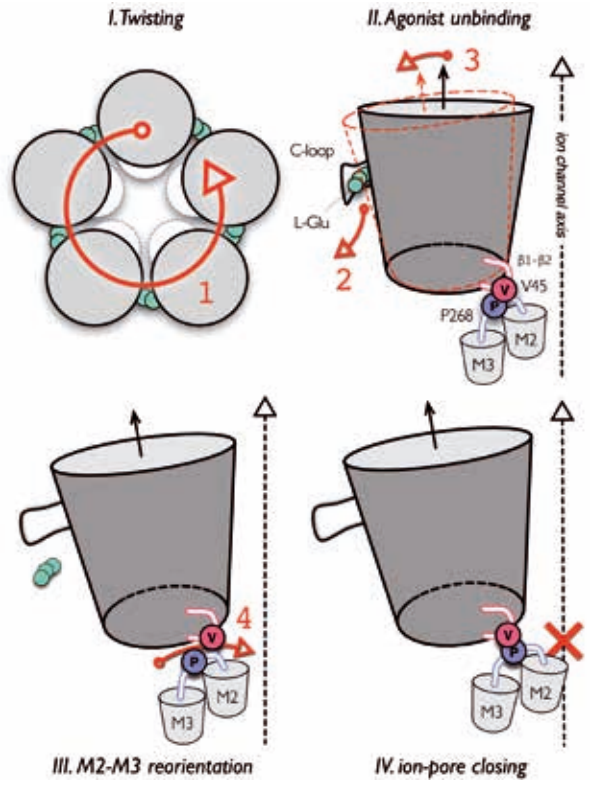

Figure 3: Model of the allosteric mechanism for gating ions in pLGICs. The simulation of GluCl with IVM removed shows that the closing of the ion pore (red cross) involves four sequential events (large red numbers). The process is initiated by a global transition to a twisted conformation of the receptor (1). The spontaneous unbinding of L-Glu from the orthosteric site is the next step (2). Agonist unbinding results in an outward tilting of the β-sandwiches in the EC domain, which lifts the β1- β2 loop into the up position (3) and opens the way to the passage of the bulky side chain of the conserved P268 (on the M2-M3 loop) in the direction of the ion pore (4).

Benefits from running on SuperMUC

The MD simulations were conducted on all-atom representations of the full-length pLGIC pentamers (GluCl with or without ivermectin, ELIC, GLIC) embedded in a lipid bilayer and solvated in a water box, for a total of about *200,000 atoms* each. Typical simulation runs of ~55 ns/day could be attained using *2048 CPU* cores and a custom build of the highly-scalable NAMD 2.9 package optimized for the host platform (as per our PRACE Preparatory Access 2010PA1153). In particular, given the major role of the quaternary twist in the proposed allosteric model of gating in pLGICs, we were able to assess that this event is repeatedly found over multiple independent MD simulations on the μs timescale. The amount of sampling required for this model validation (which is worth about *10 millions CPU* core hours as well as terabytes of storage) would not be possible without the level of performance and scalability offered by SuperMUC.

On-going Research / Outlook

One key result of our explicit solvent/membrane MD simulations is that binding of ivermectin stabilizes the active state of GluCl by preventing the twisting of the receptor in the direction of the resting state. Importantly, this observation suggests that LGICs function could be regulated by chemical events solely affecting the twisting transition. For a proof of concept, we are currently developing an efficient simulation setup to estimate the barrier(s) preventing the ion channel opening when IVM is bound. This approach, which is based on umbrella sampling of the twisting reaction, will enable to quantify the allosteric modulation by IVM binding. Moreover, free energy simulations based on the systematic fragmentation of ivermectin will determine which portions of the allosteric agonist are involved in its activity and help identifying the minimum pharmacophore required for GluCl activation. Running these atomistic free energy simulations obviously requires millions of CPU core hours.

References and Links

[1] Changeux J.P. & Taly A. (2008) *Trends in Molecular Medicine* **14**(3)93-102.
[2] Hibbs R.E. & Gouaux E. (2011) *Nature* **474**(7349), 54-60.
[3] Calimet N., Simoes M., Changeux J.P., Karplus M., Taly A. & Cecchini M. (2013) *Proc. Natl. Acad. Sci. USA.* **110**(42):E3987-96.
[4] Prevost M.S., Sauget L., Nury H., Van Renterghem C., Huon C., Poitevin F., Baaden M., Delarue M. & Corringer P.J. (2012) *Nature Structural & Molecular Biology* **19**, 642-649.
[5] Sauguet L., Shahsavar A., Poitevin F., Huon C., Menny A., Nemecz A., Haouz A., Changeux J.P., Corringer P.J. & Delarue M. (2014) *Proc. Natl. Acad. Sci. USA.* **111**(3):966-71.

Molecular Dynamics Simulation of Protein-Protein Complex Formation in a Crowed Environment

Research Institution
Lehrstuhl für Molekulardynamik, Physik-Department T38, TU München

Principal Investigator
Martin Zacharias

Researchers
Aliaksei Krukau, Rainer Bomblies, Alexander Knips, Florian Kandzia, Guiseppe La Rosa, Katja Ostermeir, Fabian Zeller

Project Partners
Leibniz Rechenzentrum, München

LRZ Project ID: pr89tu (PRACE project)

Introduction

The process of protein-protein complex formation is of fundamental importance for a better understanding of a variety of biological processes. In a cellular environment the high concentration of surrounding proteins can influence the association process between proteins. Aim of the research project was to simulate the formation of specific and non-specific protein-protein complexes and to investigate the effect of additional protein molecules (crowding) on complex formation in atomic detail. The project also involved methodological advancements to accurately calculate the free energy profiles of biomolecular interactions. So far protein association has been studied mostly using simplified coarse-grained protein models without an explicit inclusion of solvent molecules. Alternatively, Brownian Dynamics simulations using rigid partner proteins can also be used to study protein-protein association and encounter [1]. However, such techniques largely neglect the conformational flexibility of proteins and often approximate the aqueous environment poorly. Both conformational adaptation of protein partners and hydration effects are of critical importance for protein-protein interactions and need to be accounted for accurately in order to realistically simulate and understand complex formation events. In the present study atomistic Molecular Dynamics (MD) simulations of proteins in the presence of explicit solvent and ions were used.

As a model system the complex formation of two well known small proteins, Colicin E9 (E9) and the Immunity protein 9 (Im9), known to form very specific high-affinity complexes [2, see Fig. 1]. The E9 protein is a DNA hydrolyzing enzyme and Im9 is a high-affinity protein inhibitor that blocks the E9 activity upon binding. Both proteins consist of ~100 residues and structures of the complex and the isolated partners are known [2]. Specific binding of protein partners may occur directly from the separate fully solvated unbound states of the partner molecules. However, it is also possible that the process involves several intermediate states (encounter complexes) and initial non-specific binding followed by diffusion on the protein surfaces towards the specific complex structure. Since in MD simulations each protein molecules is flexible it will be possible to also directly investigate conformational changes associated with binding events at an unprecedented resolution in time and space. In addition, the role of solvent and dehydration (de-wetting) during binding can be studied at a high level of detail during multiple binding events. The simulation model system contained multiple proteins and allowed studying whether the crowding environment in a cell (high protein density) has a direct influence on the association of protein molecules.

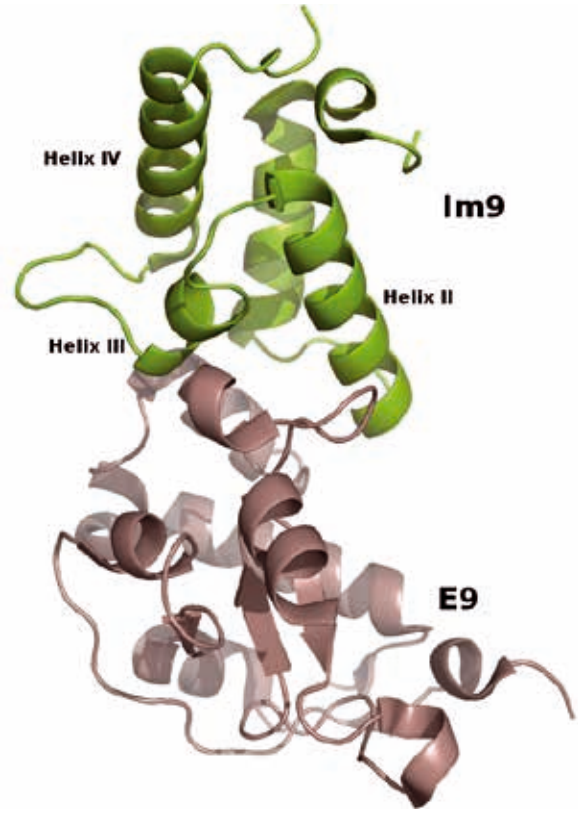

Figure 1: Crystal structure of the complex between colicin E9 (red cartoon) and Immunity protein Im9 (green cartoon) protein (protein data bank entry 1EMV).

Results

The simulations can help to answer several fundamentally important questions on the mechanism of protein-protein complex formation. How do transient non-specific encounter complexes look like? Do they still have a wet (solvated) or partially dry interface structure? This question is also related to the possibility of anomalous diffusion that may play a role for protein-protein binding in an in vivo situation.

Are there intermediates on the path towards a specific protein-protein complex? Does the complex formation process involve the diffusion of proteins on the surface of the partner (initially bound at a nonspecific site) before reaching the native binding site? Are there trapped incorrectly bound states competing with specific binding? These questions cannot be answered accurately using simpler coarse-grained protein models or rigid protein partners and a rough implicit description of the surrounding solvent.

MD simulations of multiple copies of the colicin E9 and Im9 protein were started from random initial placements in simulation box which contained up to 27 copies of each protein. The simulation system also contained surrounding explicit water molecules and ions (200 mM) resulting in a total number of atoms of $1.2 \cdot 10^6$. The mean distance of ~3-5 nm between proteins corresponded to a dense protein solution similar to the crowed environment of a cell. After equilibration of the simulation system several production runs using the GROMACS software [3] were performed resulting in an aggregate simulation time of almost 1 us (990 ns). This was possible due to the excellent scaling of the program for the large simulation system on multiple cores. Typically, between 512-2048 cores were used.

During the simulations multiple association and dissociation events were observed. This included formation of specific contacts (contacts that are observed in the native protein-protein complex) and non-specific contacts. During the aggregate simulation time ~25% of the E9 and Im9 pairs formed transient complexes. The great majority of association events corresponded to non-specific binding events with a mean number of contacts that corresponded to ~30% of the number of contacts observed in the native specific complex. A contact is here defined as a minimum distance between two residues in two proteins of < 0.625 nm. This cutoff includes also transient association events that contain interfacial hydration layers. Around 10% of the transient complexes included specific contacts (that also occur in the native protein complex). The analysis of the transiently formed complexes is still ongoing and requires the design of new tools to systematically investigate the large number of possible protein-protein encounters.

Besides of the study of protein-protein interactions using unrestrained MD simulations new methods to extract the change in free energy upon biomolecular association were developed employing the parallel computing

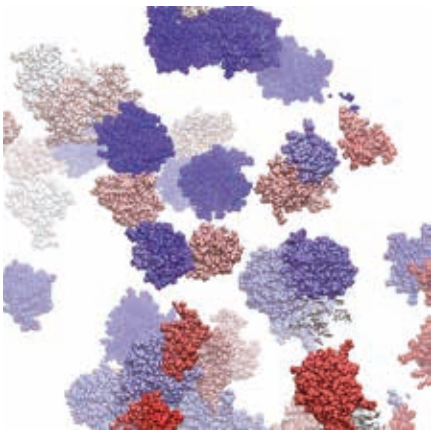

Figure 2: Molecular dynamics simulation snapshot of a colicin E9 and Im9 protein solution (van der Waals presentation and individual colors for each protein) indicating multiple transient association events.

capabilities of SuperMUC. The method is based on the well-established Umbrella sampling approach to induce the dissociation or association of two binding partners along a distance coordinate. In such simulations accurate convergence of calculated free energy changes is difficult to achieve and one obtains usually different numbers for the association and dissociation processes. By allowing exchanges between neighboring umbrella sampling windows and by adding a potential that offsets the free energy change along the reaction coordinate in an iterative process we were able to achieve very rapid convergence of calculated free energy changes along the separation coordinate [4]. This method is well suited to systematically study non-specific versus specific binding for pairs of proteins.

On-going Research / Outlook

In our ongoing research we currently design tools to systematically analyze the transient association events observed during the MD-simulations of the colicin E9 and Im9 proteins. The main goal is to characterize the types of transient contacts. Are these contacts mainly electro-statically driven and involve interfacial waters or do they involve mostly nonpolar hydrophobic protein-protein contacts? Another interesting issue is the role of conformational adaptation during transient complex formation. Of particular interest is also the diffusion of proteins on the surface of the protein partners. The ongoing and future analysis is also focused on the question of the time range for the transient interactions which likely requires longer simulation times. It is planned in the future to perform more extensive simulations possibly on even larger systems. The binding affinity of long-lived transient complexes will be investigated using umbrella sampling simulations (indicated above) and will be compared to the native binding mode. This will help to relate the strength of non-specific association to the affinity of protein-protein binding in a native complex.

References and Links

[1] Gabdoulline RR, Wade RC. Brownian dynamics simulation of protein-protein diffusional encounter. Nature Methods.14 (1998) 329-41.
[2] Papadakos G, Wojdyla JA, Kleanthous C. Nuclease colicins and their immunity proteins. Quart. Rev. Biophys.114 (2011) 1-47.
[3] http://www.gromacs.org/
[4] Zeller F, Zacharias M Adaptive Biasing combined with Hamiltonian Replica Exchange to improve umbrella sampling free energy simulations. J ChemTheo Comput 10 (2014) 703-710.

Extreme Scaling on SuperMUC

Extreme Scaling of Real World Applications to more than 130,000 Cores on SuperMUC

In July 2013, the Leibniz Supercomputing Centre (LRZ) organized the first workshop to test extreme scaling on SuperMUC, a 3 PFLOP/s system with Intel Sandy Bridge CPU cores in its thin node islands. The workshop has been attended by groups from 12 international projects, whose codes have already proven to scale up to 4 islands (32,768 cores). During the workshop, the participants tested the scaling capabilities of their codes up to the whole system.

In addition to the participants, application experts from LRZ, Intel and IBM were on site to resolve issues and to assist in performance optimization. New techniques such as fast startup were successfully tested and helped to reduce the startup time by a factor of 2-3. At the end of the workshop, 6 codes successfully ran on the full machine, 4 codes managed to run on half of the system, and 2 applications ran on 4 islands.

With a peak performance of 3 PFLOP/s (=10^{15} Floating Point Operations per second), SuperMUC is one of the fastest supercomputers in the world (ranked no. 4 in the TOP500-list in June 2012) and (at the time of writing) is still the fastest pure x86 supercomputer without accelerators. The network interconnect between the nodes allows for perfectly linear scaling of parallel applications.

SuperMUC consists of 18 Thin Node Islands (Intel Sandy Bridge EX) and one Fat Node Island (Intel Westmere EX). Each Island contains more than 8,192 cores.

All compute nodes within an individual island are connected via a fully non-blocking Infiniband network (FDR10 for the Thin Nodes, QDR for the Fat Nodes). Above the island level, the high speed interconnect enables a bi-directional bi-section bandwidth ratio of 4:1.

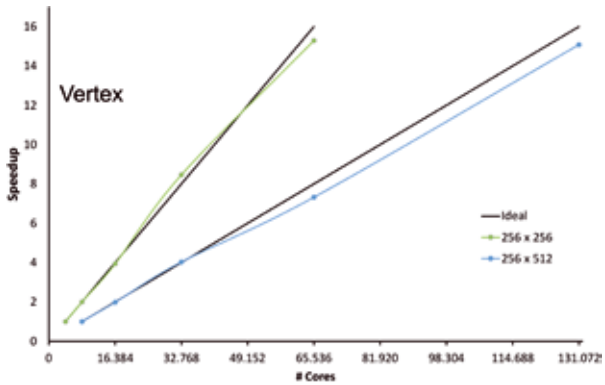

Figure 1. Vertex: Neutrino-radiation hydrodynamics code, simulates from first principles the physical processes during the evolution of a supernova explosion (Image reprinted from ref. [1]).

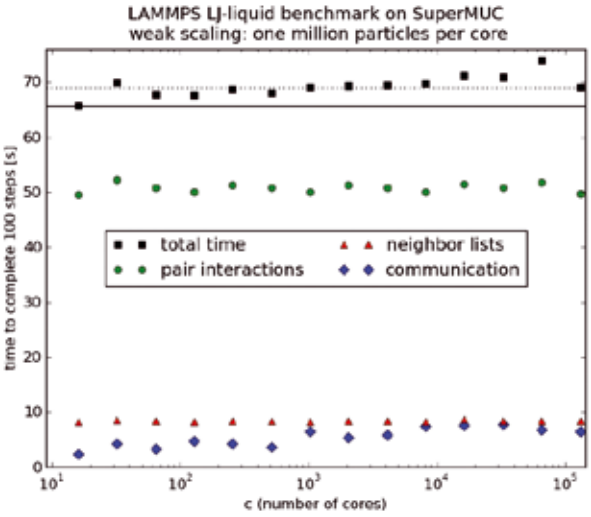

Figure 2. LAMMPS: Classical molecular dynamics code (image reprinted from ref. [2]).

Results

SuperMUC has a theoretical peak performance of 3.185 PFLOP/s for the 18 thin node islands. Running the **LINPACK** benchmark, we measured 161 TFLOP/s on one island, 2.56 PFLOP/s on 16 islands, and 2.897 PFLOP/s on the full machine (18 islands). LINPACK was run with IBM-MPI. The following real world applications ran successfully on SuperMUC. Absolute performance numbers are given where available. Listed in brackets after the application name are the maximum number of islands the application ran on:

APES (8 islands):

A suite of solvers for problems common in engineering applications. It is based on a common mesh representation library TreElM, and provides besides the solvers a mesh generation and post-processing tool. Currently there are mainly two different solvers developed within APES to implement two different numerical methods: Musubi and Ateles. Musubi implements a Lattice-Boltzmann scheme and can deal with various models. Besides the main incompressible Navier-Stokes model it is also capable of propagating passive scalars and multiple species in liquid or gas mixtures. It is mainly used for flow simulations that involve complex geometries, e.g. the flow through a channel filled by some obstacles for the simulation of electrodialysis. Another is the flow of blood through aneurysms and the simulation of the clotting effects. Ateles is a high-order discontinuous Galerkin solver that is currently mainly deployed for the simulation of linear conservation laws, like the Maxwell equations.

BQCD (16 islands):
Hybrid Monte-Carlo program for simulating lattice QCD with dynamical Wilson fermions. BQCD managed to achieve 10 TFLOP/s on one island (8,192 cores) and 27 TFLOP/s on 16 islands (131,072 cores). BQCD was run with Intel-MPI.

CIAO (8 islands):
Second order, semi-implicit finite difference code, used in combustion research. CIAO was run with IBM-MPI.

ExaML (4 islands):
Exascale Maximum Likelihood (ExaML) MPI application for inferring evolutionary trees of a set of species under the maximum likelihood criterion. It is an implementation of the popular RAxML search algorithm for partitioned multi-gene or whole-genome datasets.

ICON (4 islands):
ICOsahedral Nonhydrostatic general circulation model is a joint development of the Max Planck Institute for Meteorology in Hamburg, and the Deutscher Wetterdienst. ICON is a next generation earth system model designed to simulate multiple scales of the atmosphere processes, enabling both climate simulations and numerical weather predictions. It provides the option to run locally nested highly refined resolutions, allowing simulations at a very fine scale. ICON is a non-hydrostatic global model with a local zoom function.

GROMACS (8 islands):
Molecular dynamics code [1]. GROMACS achieved 98 TFLOP/s on one island, 154 TFLOP/s on two islands, and 223 TFLOP/s on four islands. GROMACS was run with both IBM-MPI and Intel-MPI. The reported performance numbers were measured with IBM-MPI.

LAMMPS (16 islands):
Classical molecular dynamics code. LAMMPS achieved 5.6 TFLOP/s on one island and 90 TFLOP/s on 16 islands. LAMMPS was run with IBM-MPI [2].

Nyx (16 islands):
N-body and gas dynamics code (astrophysics). Nyx was run with IBM-MPI.

P-Gadget3-XXL (16 islands):
Highly optimized and fully MPI parallelized TreePM-MHD-SPH code for simulating cosmological structure formation. In its current version it also allows for an effective OpenMP parallelization within each MPI task (IBM-MPI).

SeisSol (8 islands during the worksop, 18 islands during special block operation period in the winter 2013/14):
High-order (5th or 6th order for production runs) discontinuous-Galerkin-based solver for dynamic rupture and seismic wave. During the workshop, SeisSol could only be scaled up to 32,000 cores due to limitations of reading large unstructured meshes (see the results given in Fig. 5). Following the workshop, SeisSol's mesh input component was redesigned. After some further optimizations, simulations using mesh sizes of close to 100 million grid cells were executed on the full SuperMUC during two extreme scaling periods in winter 2013/14. SeisSol achieved a sustained performance of around 1.1 PFLOP/s [13] (see Fig. 6).

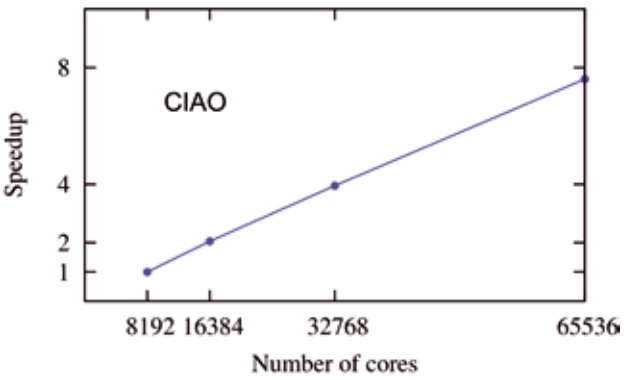

Figure 3. CIAO: Second order, semi-implicit finite difference code (combustion research, image reprinted from ref. [2]).

Vertex (16 islands):
Neutrino-radiation hydrodynamics code, simulates from first principles the physical processes during the evolution of a supernova explosion. Vertex achieved 15 TFLOP/s on one island and 250 TFLOP/s on 16 islands. Vertex was run with IBM-MPI.

walBErla (16 islands):
A massively parallel software framework for simulating complex flows with the lattice Boltzmann method (LBM).

Regarding the application performance, we observed that hybrid programs (MPI+OpenMP) on SuperMUC are still slower than pure MPI programs (e.g. GROMACS), but applications scale to larger core counts (e.g. VERTEX). Core pinning needs a lot of experience by the programmer. Parallel

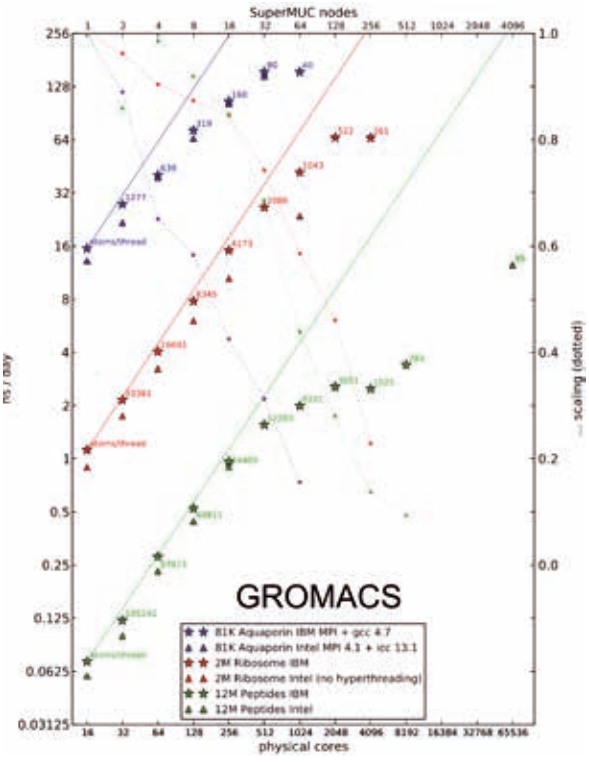

Figure 4. GROMACS: Molecular dynamics code (Image reprinted from ref. [3]).

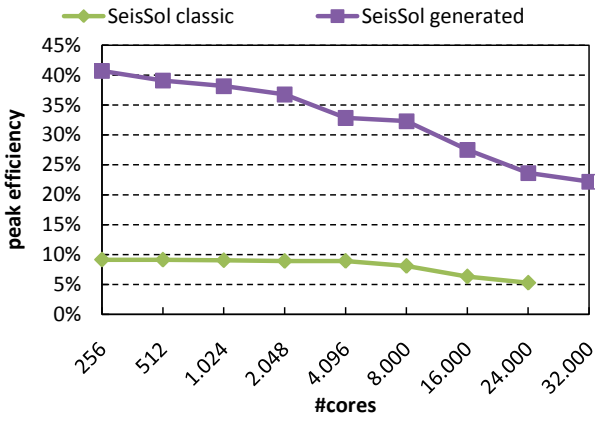

Figure 5. SeisSol strong scaling for the LOH.1 benchmark (unstructured mesh with 7 Mio tetrahedral grid cells), which was chosen as setup for the Extreme Scaling workshop (image reprinted from ref. [4].

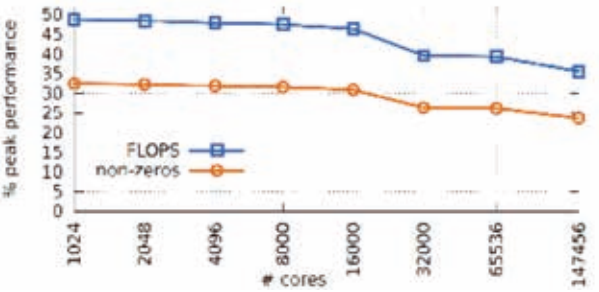

Figure 6. Strong scaling of a seismic-wave simulation for the stratovolcano Mount Merapi using SeisSol on an unstructured tetrahedral mesh with 99 Mio grid cells [13]. Given is the achieved percentage of peak performance also considering the nominal value with matrix padding ("non-zeros"). On 147,456 cores, the simulation achieved a sustained performance of 1.13 PFLOPS in the scaling tests, and 1.09 PFLOPS throughout a 3-hour run under production conditions (image reprinted from ref. [4]).

I/O still remains a challenge for many applications, both with regard to stability and speed. Several stability issues with GPFS were observed for very large jobs due to writing thousands of files in a single directory. This will be improved in the upcoming versions of the application codes.

Conclusion and Outlook

Ten out of twelve projects were able to generate scaling curves up to 8 or 16 islands. From the preliminary data the following FLOP/s rates have been obtained: 250 TFLOP/s for VERTEX on 16 and 223 TFLOP/s for GROMACS just 4 islands. The measured FLOP/s rates for the complete application codes correspond to 10% or more of the peak performance of SuperMUC. These results obtained in a short workshop can definitely compete with results reported from other TOP10 supercomputers such as the K-computer and the Blue Waters system. They demonstrate the usability of SuperMUC for real world applications.

In the block operation periods following the workshop, all the participants could further work on the scaling and performance of their applications, which led to the remarkable results from Seissol. This software achieved more than 30% of the peak performance on SuperMUC and will be further optimized by the developers.

References and Links

[1] Towards Petaflops Capability of the VERTEX Supernova Code. Andreas Marek, Markus Rampp, Florian Hanke, Hans-Thomas Janka. In: Advances in Parallel Computing, Vol. 25 (2014) 712-721. Parallel Computing: Accelerating Computational Science and Engineering (CSE). Editors: Bader, M., Bode, A., Bungartz, H.-J. , Gerndt, M., Joubert, G.R., Peters, F. ISBN print 978-1-61499-380-3, ISBN online 978-1-61499-381-0. DOI 10.3233/978-1-61499-381-0-722

[2] Extreme Scaling Workshop at the LRZ. Momme Allalen, Gurvan Bazin, Christoph Bernau, Arndt Bode, David Brayford, Matthias Brehm, Jürg Diemand, Klaus Dolag, Jan Engels, Nicolay Hammer, Herbert Huber, Ferdinand Jamitzky, Anupam Kamakar, Carsten Kutzner, Andreas Marek, Carmen Navarrete, Helmut Satzger, Wolfram Schmidt, Philipp Trisjono. In: Advances in Parallel Computing, Vol. 25 (2014) 691-697. DOI 10.3233/978-1-61499-381-0-691

[3] Scaling of the GROMACS 4.6 molecular dynamics code on SuperMUC. Carsten Kutzner, Rossen Apostolov, Berk Hess, and Helmut Grubmüller. In: Advances in Parallel Computing, Vol. 25 (2014) 722-727. DOI 10.3233/978-1-61499-381-0-722.

[4] Accelerating SeisSol by Generating Vectorized Code for Sparse Matrix Operators. Alexander Breuer, Alexander Heinecke, Michael Bader, Christian Pelties. In: Advances in Parallel Computing, Vol. 25 (2014) 347 – 356. DOI 10.3233/978-1-61499-381-0-347

[5] Extreme Scaling of Lattice Quantum Chromodynamics. David Brayford, Momme Allalen, Volker Weinberg. In: Advances in Parallel Computing, Vol. 25 (2014) 698-702. DOI 10.3233/978-1-61499-381-0-698

[6] End-to-end Parallel Simulations with APES. Harald Klimach, Kartik Jain, Sabine Roller. In: Advances in Parallel Computing, Vol. 25 (2014) 703 – 711. DOI 10.3233/978-1-61499-381-0-703

System Description

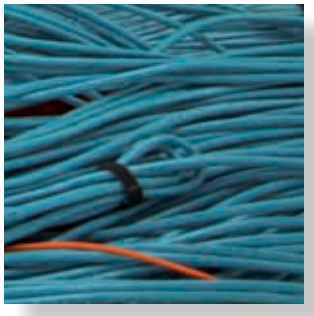

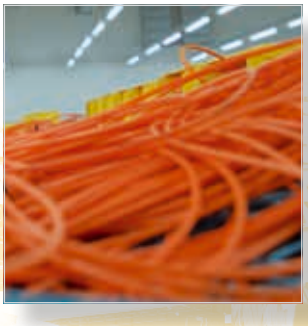

SuperMUC Petascale System (Phase 1)

SuperMUC is the new supercomputer at Leibniz-Rechenzentrum (Leibniz Supercomputing Centre) in Garching near Munich (the MUC suffix is borrowed from the Munich airport code). With more than 155,000 cores and a peak performance of more than 3 Petaflop/s (=10^{15} Floating Point Operations per second), SuperMUC is one of the fastest and most energy efficient supercomputers in the world.

System purpose and target users

SuperMUC strengthens the position of Germany's Gauss Centre for Supercomputing in Europe by delivering outstanding compute power and integrating it into the European High Performance Computing ecosystem. With the operation of SuperMUC, LRZ acts as a European Centre for Supercomputing and a Tier-0 centre of PRACE, the Partnership for Advanced Computing in Europe. SuperMUC is available to German and European researchers to expand the frontiers of science and engineering.

System highlights

- 155,656 processor cores in 9,400 compute nodes
- More than 300 TB RAM
- Infiniband FDR10 interconnect
- 4 PB of NAS-based permanent disk storage
- 10 PB of GPFS-based disk storage for scratch and work areas
- More than 30 PB of tape archive capacity
- Powerful visualization system
- High energy efficiency through warm water cooling

Energy Efficiency

SuperMUC uses a new, revolutionary form of warm water cooling developed by IBM. Active components like processors and memory are directly cooled with water that can have an inlet temperature of up to 40 degrees Celsius. The "High Temperature Liquid Cooling" together with very innovative system software promises to cut the energy consumption of the system, eliminiating the need of additional chillers. In addition, all LRZ buildings are heated re-using this energy.

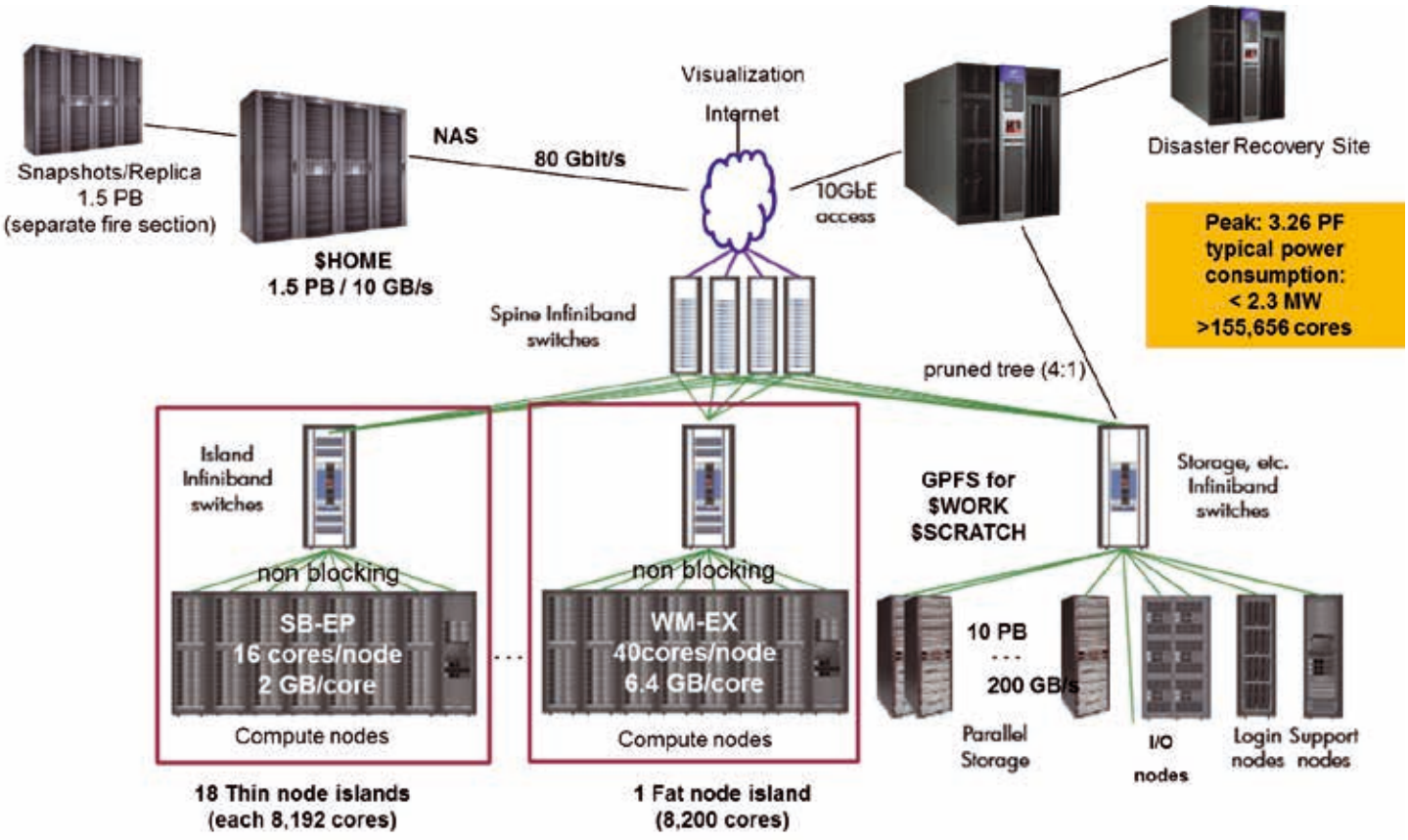

Figure: Schematic view of SuperMUC

Technical data

Installation Date	**2012**	**2011**
Item	**Thin Node Islands**	**Fat Node Island**
System	IBM System x iDataPlex	BladeCenter HX5
Processor Types	Sandy Bridge-EPIntel Xeon E5-2680 8C	Westmere-EX Intel Xeon E7-4870 10C
Number of Islands	18	1
Nodes per Island	512	205
Processors per Node	2	4
Cores per Processor	8	10
Cores per Node	16	40
Logical CPUs per Node (Hyperthreading)	32	80
Nodes per Island	512	205
Total Number of nodes	9216	205
total Number of cores	147,456	8200
Peak Performance [PFlop/s]	3.185	0.078
Linpack Performance [PFlop/s]	2.897	0.065
Total size of memory [TByte]	288	52
Memory per Core [GByte] (typically available for applications)	2 (~1.5)	6.4 (~6.0)
Size of shared Memory per node [GByte]	32	256
Bandwidth to Memory per node [Gbyte/s]	102.4	136.4
Latency to local memory [ns (cylces)]	~ 50 (~135)	~70 (~170)
Latency to remote memory [ns (cylces)]	~ 90 (~240)	~120 (~200)
Level 3 Cache Size (shared) [Mbyte]	20	24
Level 2 Cache Size [kByte]	256	256
Level 1 Cache Size [kByte], Associativity	32@ 8 way	32
Level 3 Cache Bandwidth and Latency (shared) [byte/cycle]	1 x 32 @ 31 cycles	1 x 32
Level 2 Cache Bandwidth and Latency [byte/cycle] Latency is much longer, if data are also in L1 or L2 of other core.	1 x 32 @ 12 cycles	1 x 32
Level 1 Cache Bandwidth and Latency [byte/cycle] Latency is much longer, if data are also in L1 or L2 of other core.	2 x 16 @ 4 cycles	2 x 16
Level 3 Cache line Size [Byte]	64	64
Electrical power consumption of total system [MW]	< 2.3	
Network Technology	Infiniband FDR10	Infiniband QDR
Intra-Island Topology	non-blocking Tree	
Inter-Island Topology	Pruned Tree 4:1	
Bisection bandwidth of Interconnect [TByte/s]	35.6	
Filesystem for SCRATCH and WORK	IBM GPFS	
File System for HOME	NetApp NAS	
Size of parallel storage [Pbyte]	10	
Size of NAS user storage [PByte]	1.5 (+ 1.5 for replication)	
Aggregated bandwidth to/from GPFS [GByte/s]	200	
Aggregated bandwidth to/from NAS storage [GByte/s]	10	
Login Servers for users	5	
Service and management Servers	12	
Batchsystem	IBM Loadleveler	
Archive and Backup Software	IBM TSM	
Capacity of Archive and Backup Storage [PByte]	> 30	

Why "warm" water cooling?

Typically, water used in data centers has an inlet temperature of approx. 16 degrees Celsius, and, after leaving the system, an outlet temperature of approx. 20 degrees Celsius. To cool down water to 16 degrees Celsius requires complex and energy-hungry cooling equipment. At the same time there is hardly any use for the warmed-up water as it is too cold to be used in any technical process.

SuperMUC allows an increased inlet temperature. It is easily possible to provide water having up to 40 degrees Celsius using simple "free-cooling" equipment as outside temperatures in Germany hardly ever exceed 35 degrees Celsius. At the same time the outlet water can be made quite hot (up to 70 degrees Celsius) and re-used in other technical processes – for example to heat buildings or to produce cold air by adsorption cooling.

By reducing the number of cooling components and using free cooling, LRZ expects to save several millions of Euros in cooling costs over the 5-year lifetime of the system.

System Configuration Details

LRZ's target for the architecture is a combination of a large number of powerful compute nodes with moderate memory and a peak performance of several hundred GFlop/s each (thin nodes), and a small number of fat compute nodes with large shared memory. The network interconnect between the nodes allows for perfectly linear scaling of parallel applications up to the level of more than 8,000 tasks (non-blocking fat tree network topology).

SuperMUC consists of 18 Thin Node Islands and one Fat Node Island. Each Island contains more than 8,192 cores. All compute nodes within an individual Island are connected via a fully non-blocking Infiniband network (FDR10 for the Thin nodes / QDR for the Fat Nodes). Above the Island level, the high speed interconnect enables a bi-directional bi-section bandwidth ratio of 4:1 (intra-Island/inter-Island, pruned tree network).

System Software

SuperMUC uses following software components:
- Suse Linux Enterprise Server (SLES)
- System management: xCat from IBM
- Batch processing: Loadleveler from IBM
- MPI from IBM and from Intel

From the user side a wide range of compilers, tools and commercial and free applications is provided. Many scientists also build and run their own software.

Storage Systems

SuperMUC has a powerful I/O-Subsystem which helps to process large amounts of data generated by simulations.

Home file systems

Permanent storage for data and programs is provided by a 16-node NAS cluster from Netapp. This primary cluster has a capacity of 2 Petabytes and has demonstrated an aggregated throughput of more than 10 GB/s using NFSv3. Netapp's Ontap 8 "Cluster-mode" provides a single namespace for several hundred project volumes on the system. Users can access multiple snapshots of data in their home directories.

Data is regularly replicated to a separate 4-node Netapp cluster with another 2 PB of storage for recovery purposes. Replication uses Snapmirror-technology and runs with up to 2 GB/s in this setup.

Storage hardware consists of >3,400 SATA-Disks with 2 TB each protected by double-parity RAID and integrated checksums.

Work and Scratch areas

For highest-performance checkpoint I/O IBM's General Parallel File System (GPFS) with 10 PB of capacity and an aggregated throughput of 200 GB/s is available. Disk storage subsystems were built by DDN.

Tape backup and archives

LRZ's tape backup and archive systems based on TSM (Tivoli Storage Manager) from IBM are used for or archiving and backup. The have been extended to provide more than 30 Petabytes of capacity to the users of SuperMUC. Digital long-term archives help to preserve results of scientific work on SuperMUC. User archives are also transferred to a disaster recovery site.

Visualization and Support systems

SuperMUC is connected to powerful visualization systems: the new LRZ office building houses a large 4K stereoscopic powerwall as well as a 5-sided CAVE artificial virtual reality environment.

Extension of the system

In the summer of 2014, LRZ will start user operation of an additional compute island called SuperMIC (MIC stands for Many Integrated Cores), consisting of 32 compute nodes with dual socket Intel Ivy Bridge processors. Each compute node has two Intel Xeon Phi accelerator cards (Knights Corner). Additionally, users will get access to a new remote visualization cluster, called SuperRVS. Eight dedicated nodes with dual socket Intel Sandy Bridge EP, 128 GByte RAM and NVIDIA Tesla K20Xm cards have been installed and will allow users to interactively analyze and visualize their data.

The biggest upgrade of the system, however, will begin in early 2015 with the installation of SuperMUC Phase 2, which will double the peak performance of the system to approx. 6.4 PFlop/s. The attached file systems will also be enhanced and users will benefit from higher bandwidths.

In this book, the Leibniz Supercomputing Centre (LRZ) reports on the results of numerical simulations performed between 2012 and 2014 on the SuperMUC petascale system. The papers were selected from the review reports of projects that have used the supercomputer.

SuperMUC began user operation on July 20th, 2012. Its architecture is an IBM System x iDataPlex with a theoretical peak performance of more than 3 PFLOP/s. The machine consists of 18 Thin Node Islands (with Intel Sandy Bridge EP) and one Fat Node Island (with Intel Westmere EX). Each Island contains more than 8,192 cores.It was ranked no. 4 in the TOP500-list at the time of installation.

The articles provide an overview of the broad range of applications that require high performance computing to solve the challenging scientific problems. For each project, the scientific background is described, along with the results achieved and the methodology used.

ISBN 978-3-9816 675-0-9
www.lrz.de